UNIVERSITY OF SOUTHAMPTON

FACULTY OF MEDICINE

Cancer Sciences Unit

Volume 1 of 1

Fc: Fc gamma receptor interactions in anti-PD-1 monoclonal antibody therapy and their role in anti-tumour immunity against neuroblastoma

by

Júlia Moreno Vicente

Thesis for the degree of Doctor in Philosophy

September 2020

UNIVERSITY OF SOUTHAMPTON

ABSTRACT

FACULTY OF MEDICINE

Cancer Sciences

Thesis for the degree of Doctor of Philosophy

Fc: Fc gamma receptor interactions in anti-PD-1 monoclonal antibody therapy and their role in anti-tumour immunity against neuroblastoma

Júlia Moreno Vicente

Programmed cell death (PD)-1 is an inhibitory co-receptor expressed on activated T cells that plays an important role in down-regulating anti-tumour immunity. Monoclonal antibodies (mAbs) that block PD-1 have shown encouraging results in advanced adult cancers, but objective responses are limited to a subset of tumours and patients. Recent studies highlight the importance of the Fc domain of anti-PD-1 mAbs with their anti-tumour activity. Therefore, the aim of this work was to study the role of Fc: Fc gamma receptor (FcγR) interaction in anti-PD-1 therapy, together with the potential application of these mAbs in neuroblastoma, a childhood cancer that bears a particularly poor prognosis.

In vitro characterisation of three anti-PD-1 isotypes (mouse IgG1, IgG2a and IgG1-N297A) was performed to confirm binding and functional activity of these mAbs. To investigate the effect of Fc: FcγR interactions in vivo, antigen-specific T-cell responses were studied with the OT-I transfer model and endogenous responses to the model antigen ovalbumin. Anti-tumour activity and modulation of immune populations in the tumour microenvironment (TME) was assessed in an immunogenic model (MC38) as well as in murine neuroblastoma models.

Results showed that an anti-PD-1 mAb that lacked FcγR binding (IgG1-N297A) was optimal at expanding anti-CD40 stimulated antigen-specific responses of both transgenic OT-I and endogenous T cells. In the context of cancer, both IgG1 and IgG1-N297A mAbs improved survival and increased immune infiltration in MC38, although the IgG1-N297A mAb induced a more profound activation of immune cells within the TME. In contrast, preferential engagement of activating FcγRs by anti-PD-1 IgG2a caused phagocytosis of activated T cells in vitro and abrogated therapeutic activity in vivo. A similar trend in therapeutic efficacy and phenotypic changes across anti-PD-1 isotypes was observed in neuroblastoma tumours. In view of the limited efficacy as a monotherapy in this model, anti-PD-1 mAbs were combined with tumour-targeting anti-GD2 mAbs and immune-modulatory cyclophosphamide with the aim to increase T-cell infiltration and the CD8: Treg ratio. Despite improved outcomes, the triple combination schedule was not sufficient to stop tumour growth, and hence other schedules or therapeutic strategies may be required.

Taken together, these results support an important role for Fc:FcγR interactions in the therapeutic activity of anti-PD-1 mAbs, highlighting the detrimental effect of engaging of activating FcγR. Future work should focus on defining the role of the inhibitory FcγR in modulating anti-PD-1 mAb therapy. Furthermore, anti-PD-1 mAbs were also able to modulate the neuroblastoma TME, albeit to a lesser degree. Due to the cold nature of these tumours, combinatorial approaches that increase immune infiltration and activation will likely be required to enhance the efficacy of these mAbs.

Table of Contents

Table of Tables

Table of Figures

List of Accompanying Materials

Academic Thesis: Declaration Of Authorship

I, **Júlia Moreno Vicente** declare that this thesis and the work presented in it are my own and has been generated by me as the result of my own original research.

Fc: Fc gamma receptor interactions in anti-PD-1 monoclonal antibody therapy and their role in anti-tumour immunity against neuroblastoma.

I confirm that:

1. This work was done wholly or mainly while in candidature for a research degree at this University;
2. Where any part of this thesis has previously been submitted for a degree or any other qualification at this University or any other institution, this has been clearly stated;
3. Where I have consulted the published work of others, this is always clearly attributed;
4. Where I have quoted from the work of others, the source is always given. With the exception of such quotations, this thesis is entirely my own work;
5. I have acknowledged all main sources of help;
6. Where the thesis is based on work done by myself jointly with others, I have made clear exactly what was done by others and what I have contributed myself;
7. None of this work has been published before submission.

Signed:

Date: 2nd September, 2020

Acknowledgements

Firstly, I would like to thank my supervisors Dr Juliet Gray and Professor Stephen Beers for their support and guidance throughout this project, and particularly for their help in the preparation of this thesis. Also to Professor Mark Cragg for his help during the first year of lab rotations and all of his suggestions and comments during lab meetings.

I would like to thank and acknowledge Ian C. Mockridge, who produced the data shown in Figure 3.2 and assisted me with all SPR experiments. I would also like to extend my gratitude to the other members of the production team in the Antibody and Vaccine Group: Dr Claude Chan, Chris A. Penfold, Jinny H. Kim and Dr Tanya Inzhelevskaya. This work would have not been possible without their incredible work to produce the huge amount of antibodies I used throughout these 4 years!

A huge thanks goes to Steven Booth, who was always there to make me laugh with his controversial comments and to give me a hand whenever I needed (as well as to give me the best tips to work efficiently!). Thanks to the BRF staff Lisa Dunning, Sam Martin and Nick Hudson for always taking care of all my mice. In particular, I can't thank enough the help (also emotional) provided by Vikki English. Thank you so much, not only for spending all that time teaching me, but also for all the good moments and loud laughs that we had in the PCU and outside!

I would like to thank everyone in the Antibody and Vaccine Group for making these challenging four years some more enjoyable ones. Especially, I would like to thank Charys, Franzi, Anna, Osman, Russell, Kam, Martin and Anne for providing the much needed mental support in and outside the lab.

On a personal note, I would like to thank Dr Richard Stopforth, whose mental and scientific support throughout these 4 years was incalculable. I would have not made it passed my transfer without his encouraging words and scientific advice on backing up and endnote libraries.

Finalment, vull agrair a la meva família i als meus amics tot el suport que m'han donat des de la distància. En especial al meu pare Angel, a la meva mare Victoria i al meu germà David - no ho hagués pogut fer sense vosaltres!! Gràcies per sempre creure en mi. I per acabar, vull dedicar tota aquesta feina a les persones que ja no estan aquí per poder celebrar-ho amb mi, però que sempre viuran dins meu allà on vagi.

Definitions and Abbreviations

A/I	Activating/ inhibitory ratio
ADCC	Antibody dependent cellular cytotoxicity
ADCP	Antibody dependent cellular phagocytosis
AF	Alexa Fluor
ALL	Acute lymphoblastic leukaemia
ALK	Anaplastic lymphoma kinase
AMP	Adenosine monophosphate
APC	Antigen presenting cell
ATP	Adenosine triphosphate
BMDMs	Bone marrow-derived macrophages
bMMRD	Biallelic mismatch repair deficiency
BSA	Bovine serum albumin
CAR	Chimeric antigen receptor
CD	Cluster of differentiation
CDC	Complement dependent cytotoxicity
CDRs	Complementarity determining regions
CFSE	5-6-Carboxyfluorescein diacetate succinimidyl ester
cGAMP	Cyclic GMP-AMP
cGAS	GMP–AMP Synthase
C_H	Constant heavy chain
CHO	Chinese hamster ovary
C_L	Constant light chain
CPM	Cyclophosphamide
CSF1R	Colony stimulating factor 1 receptor
CTL	Cytotoxic T lymphocyte
CTLA-4	Cytotoxic T lymphocyte antigen 4
DAMPs	Damage-associated molecular patterns
DCs	Dendritic cells
Degly	Deglycosylated
DMEM	Dulbecco's Modified Eagle's Medium

DMSO	Dymethyl sulfoxide
EDTA	Ethylenediaminetetraacetic acid
EFS	Event free survival
EGFR	Epithelial growth factor receptor
EMA	European Medicines Agency
EOMES	Eomesodermin
ER	Endoplasmic reticulum
EWS	Ewing sarcoma
Fab	Fragment antibody binding
Fc	Fragment crystalizable
FCS	Foetal calf serum
FcγRs	Fc gamma receptors
FcRn	Neonatal Fc receptor
FDA	Food and Drug Administration
FoxP3	Forkhead box protein 3
FSC	Forward scatter
GD2	Disialoganglioside 2
GlcNAc	N-acetylglucosamine
GM-CSF	Granulocyte macrophage colony stimulating factor
GMP	Guanosine monophosphate
GSK-3	Glycogen synthase kinase 3
GTP	Guanosine triphosphate
HAMA	Human anti-mouse antibody
HER2	Human epidermal growth factor receptor 2
HIF-1	Hypoxia-inducible factor 1
HIV	Human immunodeficiency virus
HL	Hodgkin's lymphoma
HLA	Human leukocyte antigen
HMGB1	High-mobility group box 1 protein
HPLC	High Performance Liquid Chromatography
IC	Immune complex
ICD	Immunogenic cell death

IDO	Indoleamine 2,3-dioxygenase
IFN	Interferon
Ig	Immunoglobulin
IHC	Immunohistochemistry
IL	Interleukin
Ip	Intraperitoneal
IRF	Interferon regulatory factor
ITAM	Immunoreceptor tyrosine based activating motif
ITIM	Immunoreceptor tyrosine based inhibitory motif
ITSM	Immunoreceptor tyrosine based switch motif
IV	Intravenous
kDa	Kilodaltons
KIRs	Killer Ig-like receptors
LAG-3	Lymphocyte-activation gene-3
LB	Lysogeny broth
LCMV	Lymphocytic Choriomeningitis virus
LM	Listeria monocytogenes
LPS	Lipopolysaccharide
mAb	Monoclonal antibody
MAGE	Melanoma antigen-encoding gene
MAPK	Mitogen-activated protein kinase
M-CSF	Macrophage colony stimulating factor
MDSCs	Myeloid derived suppressor cells
MFI	Median fluorescence intensity
MHC-I	Major histocompatibility complex class I
MHC-II	Major histocompatibility complex class II
MIC-A/B	MHC-I chain related molecules A/B
mIgG	Mouse IgG
MyD88	Myeloid differentiation factor 88
MW	Molecular weight
NB	Neuroblastoma
NF-kβ	Nuclear factor kappa beta

NICE	National Institute for Health and Care Excellence
NK	Natural killer
NSCLC	Non small cell lung cancer
OS	Overall survival
PAMPs	Pathogen-associated molecular patterns
PBMCs	Peripheral blood mononuclear cells
PBS	Phosphate buffered saline
PCR	Polymerase chain reaction
PD-1	Programmed cell death -1
PD-L1/2	Programmed cell death ligand ½
PDX	Patient derived xenograft
PFS	Progression free survival
PI3K	Phosphoinositide 3-kinase
PK C	Protein kinase C
PMA	Phorbol 12-myristate 13-acetate
PNGase	Peptide-N-Glycosidase F
P/S	Penicillin-streptomycin
RA	Retinoic acid
RBCLB	Red blood cell lysis buffer
RMS	Rhabdomyosarcoma
RPMI	Roswell Park Memorial Institute
RT	Room temperature
RU	Resonance units
S.D	Standard deviation
SDS-PAGE	Sodium Dodecyl Sulphate-Polyacrylamide Gel Electrophoresis
SEM	Standard error of the mean
SHP	Src-homology 2 domain-containing tyrosine phosphatase
SHIP	SH2-domain-containing inositol polyphosphate 5 phosphatase
SIOPEN	International Society of Paediatric Oncology Europe Neuroblastoma
STING	Stimulator of interferon genes
SSC	Side scatter
SPR	Surface plasmon resonance

S1PR1	Sphingosine 1-phosphate receptor 1
TAA	Tumour associated antigens
TAMs	Tumour associated macrophages
TAP-1/2	Transporter associated with antigen processing-1/2
Tbet	T-box transcription factor TBX21
TBK1	TANK-binding kinase 1
TCR	T-cell receptor
TDLN	Tumour-draining lymph node
TGF-β	Transforming growth factor beta
Th	T helper cell
TH-MYCN	Tyrosine hydroxylase-MYCN
TILs	Tumour infiltrating lymphocytes
TIM-3	T cell immunoglobulin- and mucin-domain-containing molecule-3
TLR	Toll-like receptor
TME	Tumour microenvironment
TNF	Tumour necrosis factor
TNFRSF	Tumour necrosis factor receptor super family
TRAIL	TNF-related apoptosis-inducing ligand
Treg	Regulatory T cell
TRIF	TIR domain-containing adaptor-inducing IFN-β
V_H	Variable heavy chain
V_L	Variable light chain
WT	Wild type

Chapter 1: Introduction

1.1 Cancer immunology and the tumour microenvironment

1.1.1 Cancer immunology

Cancer is considered to be a global epidemic disease, with incidence and mortality rates rapidly increasing in the past decades in both developed and developing countries. The World Health Organisation estimates that 18.1 million people had cancer in 2018, of which 9.6 million succumbed to the disease (1). Cancer is a complex disease that arises from a progressive transformation of normal cells into malignant counterparts. It is a multistep process that involves genetic and epigenetic modifications that ultimately endow pre-malignant cells with the essential capabilities to sustain tumour growth. These fundamental characteristics, known as hallmarks of cancer, were first described by Hanahan and Weinberg, and comprised six biological traits: acquired autonomy to growth and mitogenic signals; insensitivity against growth arrest signals; ability to evade apoptosis; ability of self-renewal; ability to sustain angiogenesis; and potential to invade other tissues and metastasise (2). In a revised version of the hallmarks of cancer, the authors proposed the evasion of immune destruction to be an emerging hallmark for malignant transformation and growth. Furthermore, the tumour-promoting role of inflammation was addressed, highlighting how immune cells can contribute to either tumour surveillance or tumour progression depending on the specific context (3).

These changes were incorporated following a renewed interest and public acceptance of the immunoediting theory (4). This theory postulated that the host immune system is capable of surveying against cancer cells at an early stage of development, recognising and eliminating emerging malignant cells. However, due to the intrinsic genome instability of malignant cells, rare variants may arise that can evade elimination and enter an equilibrium phase. At this stage, immune cells prevent tumour expansion but also exert a selective pressure that favours the outgrowth of less immunogenic clones, sculpting the immunogenicity of the tumour. Progression to the escape phase is supported by the editing process, which may lead to reduced immune recognition or development of resistance mechanisms against the immune attack; but it may also reflect the formation of an immunosuppressive environment that supports tumour growth (4). In line with this,

the tumour microenvironment (TME), which is defined as the highly complex and heterogeneous environment surrounding a tumour, is known to comprise a plethora of cell populations that bear specialised functions. Within the TME, cancer cells build a large network of interactions with other cells from the host to ultimately support and promote tumour progression. Together with specific cell types, numerous pathways have emerged as pivotal for immune evasion, being shared across different tumour types. Amongst these, immune checkpoint molecules have aroused a great interest due to their powerful immunosuppressive role and the profound impact that their therapeutic targeting has shown in some advanced cancers (5-9).

1.1.2 Immune cell populations in the TME

Although many immune cell populations, as well as non-immune cell types (endothelial cells, cancer-associated fibroblasts, stromal cells), co-inhabit the TME (3), this introduction will focus on three major immune subsets: Natural killer (NK) cells, tumour-infiltrating lymphocytes (TILs) and infiltrating populations of a myeloid origin.

1.1.2.1 Natural killer cells (NKs)

NK cells are large lymphocytes of the innate immune system with a significant ability to induce cytotoxic killing of target cells without the need for antigen-specific recognition. Although this enables a rapid response and elimination of infected or transformed cells, NK cells have traditionally been considered to lack immunological memory (10). Their cytotoxic ability is finely regulated by a dynamic balance of activating and inhibitory signals delivered through a large repertoire of NK receptors that recognise ligands at the surface of infected or transformed cells (11). Under homeostatic conditions, inhibitory receptors such as NKG2A and inhibitory Killer Ig-like receptors (KIRs), recognise self major histocompatibility (MHC) class I molecules expressed on the surface of autologous cells, thereby preventing NK-cell mediated killing. On the other hand, activating receptors such as NKG2D or NKp30 engage ligands expressed on the surface of cancer cells such as MHC-I chain-related protein (MIC)-A/B and B7-H6, respectively, thereby delivering activating signalling to NK cells (11). The lack of interactions between the inhibitory receptors with their putative MHC-I ligands licenses NK cell cytotoxicity in the presence of additional activating signal such as dendritic cell (DC)-derived stimulatory cytokines (i.e interleukin (IL)-12, IL-15). Once activated, NK cells can mediate lysis of tumour cells through direct cytotoxic activity or

through the binding of CD16 receptor to antibody-opsonised target cells (10), which will be explained in further detail in section 1.2.2. Cytotoxic mechanisms include the release of lytic molecules such as perforin and granzymes, but also contact-dependent apoptosis mediated by members from the tumour necrosis factor receptor superfamily (TNFRSF) such as Fas-L and TNF-related apoptosis-inducing ligand (TRAIL) (12).

1.1.2.2 Effector T cells

T cells are lymphocytes that develop in the thymus and comprise the cellular arm of the adaptive immune system. T cells recognise processed antigens in the context of an MHC molecule through their T-cell receptor (TCR) and co-receptor molecules (i.e CD8, CD4) (13). They can be divided into two major functionally distinct subpopulations based on whether they recognise peptides in complex with MHC class I or class II molecules. CD8 T cells bind to MHC-I molecules, which are present in all nucleated cells, and function as cytotoxic effector cells. On the other hand, CD4 T cells are known as T helper (Th) cells and interact with MHC-II molecules present in antigen presenting cells (APCs) such as DCs, macrophages or B cells (13). These Th cells secrete cytokines and express co-stimulatory molecules that are essential for the regulation and orchestration of immune responses. Depending on the nature of the antigen and environmental cues, CD4 T cells can be polarised towards Th1 cells by IL-12 or skewed towards a Th2 response by IL-4. Th1 cells are capable of inducing pro-inflammatory responses defined by the production of interferon gamma (IFN-γ) and activation of phagocytes and cytotoxic T cells; alternatively, Th2 cells are characterised by the production of anti-inflammatory cytokines (IL-4/IL-5) and B-cell stimulation (14). Besides this Th1/Th2 paradigm, alternative subsets of helper T cells have been identified in the recent decades, including IL-17- or IL-9-producing CD4 helper T cells, named Th17 and Th9, respectively. Although their role in cancer is less clear, these distinct Th subsets have been shown to take part in the pathogenesis of autoimmune disease, chronic inflammation and allergy (15).

T cells play a critical role in tumour eradication through the production of immunostimulatory cytokines and cytotoxic molecules. As a result, the presence of TILs correlates with increased survival in a range of solid cancers. Findings from a recent large-scale study in colorectal cancer provide evidence that high density of CD3 or CD8 TILs exhibited a better prognostic value than the standard classification based on tumour histopathology (16, 17). This study is in line with similar work in other tumour types, where high intratumoural CD3 or CD8 T cells

correlated with better prognosis, as these TIL populations presumably reflect ongoing anti-tumour immunity (18).

1.1.2.3 Regulatory T cells (Tregs)

Regulatory T cells are a subset of CD4 T cells involved in the maintenance of self-tolerance and prevention of autoimmunity (19). During thymic development, the initial positive selection of functional T cells that can recognise self-MHC is followed by a negative selection process. In this process, T cells that interact with self-peptides in the context of MHC with an intermediate-to-high affinity evolve as naturally occurring Tregs, and exit the thymus to participate in the maintenance of central tolerance. Alternatively, different subsets of Tregs can arise from naïve CD4 T cells in the periphery, contributing to the maintenance of peripheral tolerance (19). In cancer, Tregs are considered to be one of the main immunosuppressive cell types owing to their ability to down-regulate proliferation and activation of effector T cells in a range of cancers. It is now widely recognised that tumour-derived factors attract Tregs to the tumour site or induce the conversion of effector CD4 T cells within the TME (20). In addition, secretion of chemokines such as CCL22 by tumour-infiltrating CD8 T cells can also promote Treg accumulation at the tumour site in a CCR4-dependent manner (21).

Their immunological effects are mediated through various mechanisms, including soluble factors such as IL-10 and transforming growth factor (TGF)-β, or contact-dependent inhibition by the up-regulation of immunosuppressive receptors such as Cytotoxic T-lymphocyte Antigen (CTLA)-4. In addition to direct inhibition of tumour cytotoxicity, Tregs can have a profound effect on other immune subsets within the TME such as macrophages or DCs, inducing dysfunctional and immunosuppressive phenotypes to further suppress anti-tumour immunity (22). Therefore, due to the potent suppressive role of Tregs in anti-tumour immunity, a low intratumoural CD8: Treg ratio was found to be predictive of poor prognosis in numerous cancers (18, 23).

1.1.2.4 Tumour-associated macrophages (TAMs) and myeloid cells

Macrophages are tissue-resident myeloid cells that can arise from two main sources. A large proportion of macrophages arise during embryonic development, and migrate very early on to a particular tissue. However, macrophages can also develop from circulating monocytes in the blood, which undergo final differentiation into macrophages after recruitment (24). Under normal conditions, macrophages are involved in the maintenance of tissue homeostasis via the

clearance of apoptotic cells and production of growth factors. However, they also display a broad range of pathogen recognition receptors that make them powerful effector cells, which can mediate phagocytosis of target cells or pathogens and produce of pro-inflammatory cytokines. Besides their important role in phagocytosis, macrophages also function as APCs, coordinating innate immunity with antigen-specific immune responses (24).

Macrophages are phenotypically highly plastic cells which, upon activation can adopt distinct morphological and functional characteristics depending on the nature and context of the activation stimuli (24). In cancer, the presence of immunoregulatory cytokines (IL-10, IL-4/IL-13, TGF-β) within the TME predominantly polarises TAMs towards an immunosuppressive M2-like phenotype, as opposed to M1-skewed macrophages that have pro-inflammatory roles and promote anti-tumour immunity (25, 26). M2-like TAMs can secrete soluble factors and express surface immunosuppressive molecules that induce T-cell dysfunction, reducing T-cell proliferation and cytotoxicity (27, 28). Although this M1/M2 dichotomy has been widely used in an attempt to define phenotypically distinct subsets of TAMs, it confers a rather simplistic model that may not reflect the complex spectrum of phenotypes that co-inhabit within the TME. Nevertheless, high levels of TAM infiltration often correlate with poor prognosis, and numerous studies suggest that these cells can promote tumour growth, metastasis and confer resistance to different forms of anti-cancer therapy (26).

Other tumour-infiltrating myeloid cells include granulocytes, activated DCs and monocytes, together with an immunosuppressive myeloid population referred to as myeloid-derived suppressor cells (MDSCs). This subset of cells comprises immature myeloid precursors of monocytic and granulocytic origin that may further mature into TAMs (26).

1.1.3 Immune checkpoints

Immune checkpoints are molecules involved in the maintenance of homeostasis and peripheral tolerance to self-antigens, limiting T-cell activation to prevent autoimmune responses. However, tumours can benefit from the function of immune checkpoints, such as the inhibitory co-receptors CTLA-4 and programmed cell death (PD)-1, to suppress anti-tumour immunity (9, 29, 30). In this section, focus will be given to the inhibitory effects mediated by the PD-1 pathway. In light of the relevance of the co-expression of multiple checkpoint molecules in cancer,

however, examples of other inhibitory receptors and their ligands have been summarised in Figure 1.1 (31).

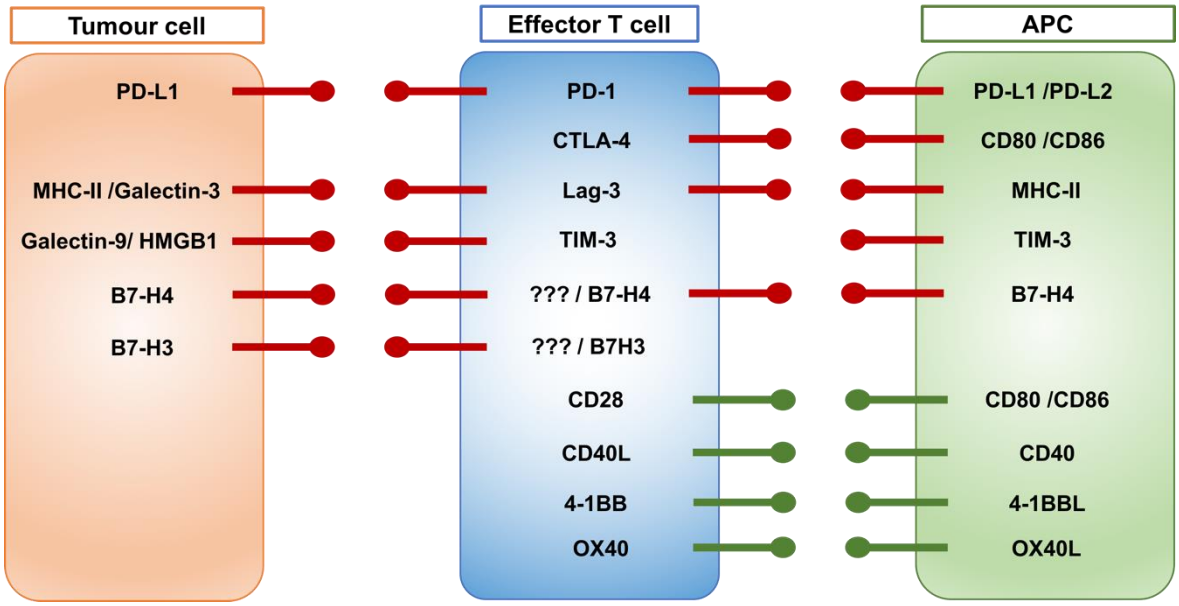

Figure 1.1 Immune checkpoint and co-stimulatory receptors and their ligands. The activation status or tolerance towards a tumour associated antigen is determined by the balance between activating and inhibitory signals delivered to effector T cells and APCs by tumour cells or other immune cells in the TME. Inhibitory co-receptors that down-regulate the activation status of effector T cells include: PD-1, CTLA-4, LAG-3 (Lymphocyte-activation gene-3), TIM-3 (T cell immunoglobulin- and mucin-domain-containing molecule-3) and ligands of the B7 superfamily (B7-H3, B7-H4), receptors for which remain unknown. Whilst all the inhibitory receptors engage ligands that are expressed on the surface of tumour cells, the majority can also engage their cognate ligands on APCs or suppressive myeloid cells in the TME (31). On the contrary, co-stimulatory receptors that promote activation of T cells include CD28, 4-1BB or OX40; but also include ligands for co-stimulatory receptors found on APCs, such as CD40L.

1.1.3.1 The PD-1 inhibitory signal

PD-1 is a member of the B7 co-stimulatory receptor family, and consists of an immunoglobulin-like extracellular domain, a transmembrane domain and a cytoplasmic tail responsible for the transduction of the intracellular signal (32, 33). PD-1 is absent on naïve and memory lymphocytes, but largely expressed on activated T and B cells (34) where it acts as a negative regulator of immune responses by inhibiting proliferation and effector functions. Early seminal studies provided evidence of this by highlighting the important role of PD-1 in maintaining peripheral tolerance and preventing autoimmunity. In mice, PD-1 deficiency accelerates autoimmune predisposition by lowering the threshold for T-cell

activation, leading to the induction of different forms of autoimmune disorders depending on the genetic background of the particular mouse strain. As such, PD-1 deficiency was shown to accelerate the onset and frequency of type I diabetes (35, 36) and lead to the development of Lupus-like disease, caused by augmented activation and proliferation of PD-$1^{-/-}$ CD8 T cells (37). Together with these, PD-L1 expression on both APCs and peripheral tissues, such as parenchymal cells in pancreatic islets, contributed to tissue-specific peripheral tolerance and protected against type I diabetes by ligating PD-1 on immune cells (38). Whilst the aforementioned studies provide evidence of the involvement of PD-1 in peripheral tolerance, subsequent work also showed the influence of PD-1 deficiency on tumour growth. Some of the first reports proved that lack of PD-1 expression on T cells led to an increase in IL-2 and IFN-γ secretion that enabled T-cell driven tumour rejection in vivo (39). Furthermore, growth of myeloma cells was suppressed in PD-1 deficient mice, whilst overexpression of PD-L1 on tumour cells markedly enhanced their tumorigenesis, supporting the potent immunosuppressive role of PD-1/PD-L1 interaction in cancer (40).

Besides the well-recognised immunosuppressive role that PD-1 has on T cells, recent reports suggest that the majority of myeloid populations might also express PD-1. In vitro, stimulation with the Toll-like receptor (TLR)-4 ligand lipopolysaccharide (LPS), up-regulated PD-1 in over 50% of bone marrow-derived macrophages (BMDMs), but this was completely blocked by nuclear factor (NF)-kB inhibition (41). In a Listeria monocytogenes (LM) model, PD-1 was up-regulated on splenic DCs after infection and blockade of programmed cell death ligand 1 (PD-L1) increased IL-12 production, suggesting that PD-1 signalling inhibits cytokine production by DCs (42). In cancer, both myeloid progenitors and M2-like TAMs were found to express PD-1, and its expression was associated with impaired maturation and phagocytosis (43, 44). Thus, although PD-1 has been traditionally considered to be a specific inhibitory receptor for lymphocytes, it is becoming more clear that it can be expressed in myeloid cells where it also exerts inhibitory function.

As illustrated in Figure 1.2, the intracellular cytoplasmic tail of PD-1 contains an immunoreceptor tyrosine-based inhibitory motif (ITIM) and an immunoreceptor tyrosine-based switch motif (ITSM) (32). In T cells, TCR stimulation leads to Lck activation, which in turn triggers the phosphorylation of both ITIM and ITSM motifs of PD-1. Phosphorylation occurs at the two tyrosine residues Y223 and Y248 in the ITIM and ITSM motifs, respectively. These two phosphorylated residues can then

act as a docking site for the recruitment of the two Src-homology 2 domain-containing tyrosine phosphatase (SHP)-1 and SHP-2 (45). Despite phosphorylation of both ITIM and ITSM motifs, mutagenesis studies highlighted the prominent role of ITSM in PD-1 function. These studies showed that mutation of Y248F in the ITSM motif but not Y223F in the ITIM was sufficient to abrogate PD-1 intracellular signalling (32, 46). Likewise, recruitment and activation of SHP-2 was found to be essential to induce T-cell suppression (32, 46). Together with this, it has also been found that ligand binding is indispensable for PD-1-mediated inhibition. Upon ligation with its ligands, PD-1 translocates to and accumulates in TCR-CD28 microclusters at the immune synapse. However, in the absence of ligand binding, PD-1 remains diffusely distributed in the membrane (46, 47). Furthermore, although SHP-2 was recruited in the absence of ligand binding, only PD-1 engagement was able to block T-cell activation (48), and the extent of SHP-2 recruitment was dependent on the strength of TCR stimulation (49).

PD-1 has a direct inhibitory effect on T cells by reducing the phosphorylation of CD3 ζ -chain and its downstream molecules, thereby blocking the activation of proximal signal molecules associated to the TCR (45, 46). Recruitment of PD-1 to the immunological synapse reduced the TCR sensitivity to cognate antigens, increasing the threshold for the minimum number of MHC-peptide-TCR complexes required to trigger calcium signals (49). Nevertheless, recent studies propose that T-cell inhibition is largely induced by the effect that PD-1 has on CD28 co-stimulation within the TCR-CD28-PD-1 clusters (33, 45-47). These studies demonstrated that many of the downstream pathways activated by CD28 are sensitive targets of PD-1 inhibition. For instance, CD28-induced activation of phosphoinositide 3-kinase (PI3k), Akt or protein kinase (PK)-C pathways was down-regulated by PD-1 signalling, together with a decrease in glucose metabolism that led to impaired proliferation (33, 45, 46, 48). Of note, only minimal levels of surface PD-1 were required to inhibit human CD4 T-cell function. Whilst mRNA and protein expression of PD-1 peaked at 48h after stimulation, the inhibitory effects on IL-2 expression could be detected as early as 2 hours post-stimulation (48).

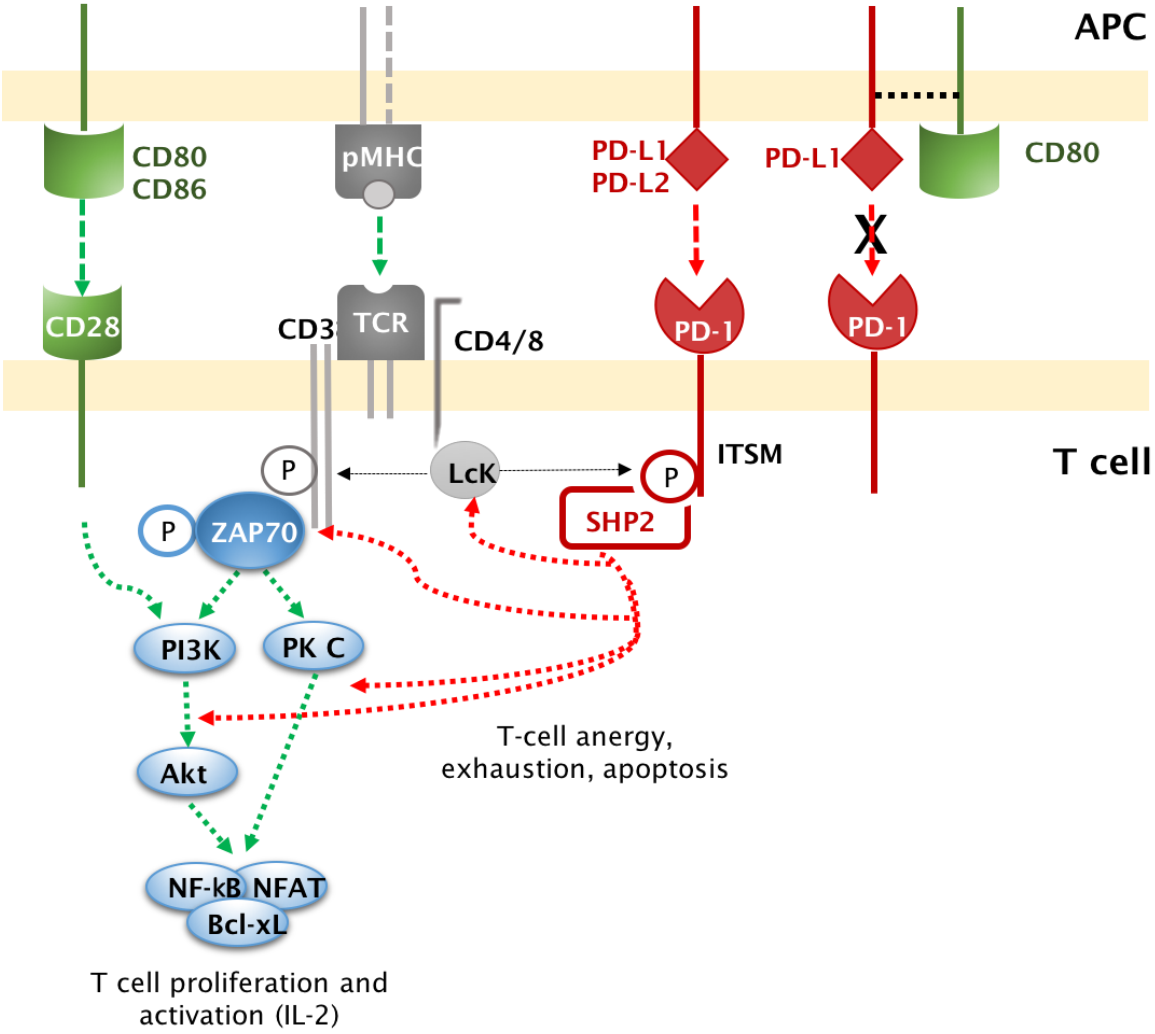

Figure 1.2 Intracellular downstream events upon PD-1/PD-L1 engagement. Binding of the TCR with peptide-MHC complex activates Lck, which phosphorylates the intracellular CD3 and ζ -chains of the TCR complex. This phosphorylated site recruits ZAP70, which becomes phosphorylated by Lck and in turn phosphorylates LAT, a transmembrane protein that acts as a docking site for downstream effectors including the PI3K/Akt and PK C pathways. These pathways are also activated through the co-stimulatory signal downstream CD28. The intracellular cascade downstream TCR and CD28 molecules leads to the mobilisation of calcium ions and the activation of transcription factors such as NFAT, NF-kβ or the pro-survival Bcl-xL. These events culminate in the proliferation and activation of effector functions (cytokine production) of lymphocytes. Ligation of PD-1 by PD-L1/2 translocates this receptor to TCR-CD28 microclusters, where Lck phosphorylates the ITSM motif on PD-1 cytoplasmic tail. Recruitment of SHP2 phosphatase triggers the dephosphorylation of multiple molecules downstream the TCR and CD28, reducing T-cell proliferation and effector functions. High levels of CD80 on APCs can block PD-1:PD-L1 binding by sequestering PD-L1 molecules in cis. Adapted from Ostrand-Rosenberg S. et al. (2014) (50).

Importantly, T-cell functions are differentially affected by PD-1 inhibition, consistent with the various effects that PD-1 has on the aforementioned signalling pathways. Inhibition of T-cell proliferation, along with tumour necrosis factor (TNF)-α and IL-2 production are the most sensitive functions, followed by the impairment of IFN-γ production. However, only T cells expressing high to intermediate levels of PD-1, such as those found in chronically activated or exhausted T cells, are sensitive to loss of cytotoxic activity (49). Of note, PD-1 signalling activates a negative feedback loop whereby SHP-2 dephosphorylates the PD-1 intracellular tail. As a consequence, continuous TCR signalling and Lck kinase activity was required to sustain PD-1-mediated inhibitory signalling (46, 47), suggesting that chronic antigen exposure is a prerequisite to induce profound T-cell inhibition through PD-1.

1.1.3.2 Regulation of PDL-1/2 expression and function

PD-L1 and PD-L2, the two ligands of PD-1, are found on numerous activated immune cell types. PD-L1 has a broad expression pattern and is found on several immune cells such as macrophages, monocytes, DCs, NK cells, B and T cells, as well as other stromal cells like activated vascular endothelial cells (51-54). In contrast, PD-L2 expression is reported to be restricted to immune cells, mainly activated macrophages and DCs, and its role in immune evasion is less clear. To date, most studies suggest that PD-L2 could also dampen tumour immunity in a similar way to PD-L1 by inhibiting T cell proliferation and cytokine secretion (53, 55, 56).

PD-L1 expression is often described as an adaptive immune resistance mechanism that tumour cells can acquire to down-regulate anti-tumour immunity (29). To date, there is extensive evidence supporting that cancer cells from different tumour types can up-regulate PD-L1 expression in response to different pro-inflammatory molecules and cytokines that are present in the TME. Cytokines that are normally released during the course of an immune response, such as IFNs or TNF-α, are potent drivers of PD-L1 expression in tumour cells (21, 57-59). Thus, IFN-γ produced by activated CD4 T helper cells and other immune cells at the TME can drive the up-regulation of PD-L1 on tumour cells, thereby suppressing immune responses. Additionally, tumour cells may constitutively express PD-L1 at the cell surface. Dysregulation of multiple intracellular pathways has been described to be involved in the constitutive expression of PD-L1 on tumour cells. For instance, oncogenic activation of the mitogen-activated protein kinase (MAPK) pathway up-regulated PD-L1 expression in melanoma and non-small cell lung cancer (NSCLC)

(60, 61). Similarly, activation of the PI3K/Akt pathway, frequently caused by loss or inactivating mutations of the tumour suppressor PTEN, led to constitutive PD-L1 expression on cancer cells (62). This could be driven by Akt-induced activation of nuclear factor NF-kB, which was found to up-regulate PD-L1 at the transcriptional level (63). Another stimulus that can up-regulate PD-L1 on tumour cells include hypoxia-inducible factor (HIF)-1α, which can bind to a hypoxia response element at the PD-L1 promoter region and activate PD-L1 transcription (64).

Although initial reports focused on PD-L1 expression on tumour cells, multiple studies highlight that host-derived PD-L1 on tumour infiltrating immune cells may also play a critical role in immunosuppression. Some authors propose that both tumour and host PD-L1 expression contribute to immunosuppression in a non-redundant manner (65), while others indicate that myeloid PD-L1 plays a dominant role. For instance, whilst PD-L1 expression on sarcoma cells was transiently up-regulated by a peak in IFN-γ secretion, TAMs presented constant higher levels (66). Likewise, expression of PD-L1 on APCs was sufficient to inhibit T-cell anti-tumour immunity in vivo; however, treatment with anti-PD-L1 mAbs improved survival and this effect was dependent on the recruitment of newly primed T cells from secondary lymphoid organs (67, 68).

More recently, the expression of PD-L1 on T cells has also aroused interest. In a similar fashion to PD-1, PD-L1 up-regulation on T cells responds to antigen presentation and inflammatory cues in the TME. Diskin B et al. found that specific ablation of PD-L1 on T cells, which accounted for 30% of PD-L1+ cells in the tumour, decreased tumour growth in a pancreatic cancer model. Ligation of PD-1 by PD-L1 expressed on T cells inhibited neighbouring T cells but also polarised macrophages towards an M2-like phenotype, which led to decreased co-stimulatory receptor expression and antigen presentation (69). Overall, the aforementioned studies provide evidence of the broad expression that PD-1 receptor and its ligands have in the TME, together with the multiple pathways that drive PD-1/PD-L1 up-regulation and lead to impaired anti-tumour immunity, thereby supporting the clinical impact of PD-1 targeting mAbs.

1.1.3.2.1 Alternative functions of PD-L1

A small number of studies propose that PD-L1 may bind to alternative receptors to PD-1. Blockade of the trans-interaction between CD80 and PD-L1 enhanced T-cell expansion and prevented anergy (70), although the impact of CD80/PD-L1 interaction on T-cell activation appeared to be less compared to that of PD-1/PD-

L1 (70, 71). However, new evidence points to a novel and more complex role of PD-L1 in regulating immune responses. In a human immunodeficiency virus (HIV) setting, PD-1 blockade increased CD69 expression and IFN-γ production on memory T cells but had the opposite effect on naïve T cells when co-cultured with DCs. This suggests that PD-L1 expressed on DCs has different roles at the priming and the effector phase (72). In cancer, CD80 expression on APCs has been shown to disrupt the interaction between cis-PD-L1 and PD-1 on T cells, limiting the inhibitory signal at an early stage of T-cell activation (73). Another work suggested that sequestration of CD80 by PD-L1 could be disrupted by PD-L1 blocking mAbs, and this would enable the interaction between CD80 and CD28, enhancing CD28 downstream signalling (74).

However, a study by Zhao Y. et al. postulates that cis-interactions between PD-L1 and CD80 can also attenuate CD80-CTLA-4 binding. Disruption of PD-L1-CD80 interactions by anti-PD-L1 mAbs reduced this attenuation and CTLA-4 became the dominant suppressive mechanism of T-cell activation. The authors also suggested that due to the monomeric interaction between CD28 and CD80, CD28-mediated signalling was more resistant to CD80 sequestration by PD-L1 as opposed to CTLA-4, which binds CD80 homodimers (75). Therefore, the role of PD-L1 at an early phase of anti-tumour responses is highly complex and it likely involves contrasting functions depending on expression levels and co-expression of other receptors.

1.1.4 Generation of anti-tumour responses

As mentioned previously, evasion of anti-tumour immunity has emerged as a pivotal trait in cancer development. Effective anti-tumour immune responses generally rely on the stimulation of antigen-specific cytotoxic CD8 T cells and Th1 cells, and their capacity to destroy tumour cells and generate immunological memory. DCs are key players in initiating and orchestrating anti-tumour responses owing to their role as professional APCs and their unique ability to stimulate naïve T-cell responses. In the context of cancer, immature DCs at the tumour site can take up and process tumour antigens (Figure 1.3 point 1). Immature DCs can uptake peptides from dying tumour cells through phagocytosis, macropynocytosis or receptor-mediated endocytosis. Typically, such extracellular products are internalised into endocytic vesicles that follow a process of acidification to become phagolysosomes. In these, active proteases degrade extracellular antigens into peptide fragments (76). These vesicles will eventually fuse with other cytosolic vesicles originated in the endoplasmic reticulum (ER) that contain MHC-II molecules

and will travel to the plasma membrane to display extracellular antigens in the context of MHC-II. However, peptides obtained from phagocytosis can also be presented on MHC-I molecules by a process called cross-presentation, which enables the generation of CD8 T-cell responses (76, 77). Certain subsets of DCs can perform cross-presentation in a more efficient way. The transcription factor Batf3 has been shown to be required in both mice and humans for successful cross-presentation and subsequent CD8 T-cell tumour cytotoxicity (78). Despite being a minor subpopulation of tumour-associated myeloid cells, Batf3-dependent CD103+ DCs were the only cell type able to carry tumour associated antigens (TAA) to tumour-draining lymph nodes (TDLNs) and mediate cross-presentation to CD8 T cells, leading to the generation of CD8 T-cell responses (79).

Besides antigen uptake, DCs also require a danger signal to initiate maturation, which can take different forms (Figure 1.3 step 1). On the one hand, pathogen-associated molecular patterns (PAMPs) can be recognised by pathogen pattern recognition molecules such as TLRs expressed on DCs. TLR ligands include the microbial cell-well component LPS, single and double stranded RNA, and CpG DNA motifs (80). Once engaged, TLRs trigger the activation of both NF-kβ and IFN regulatory factor (IRF) pathways via adaptor molecules like myeloid differentiation factor 88 (Myd88) and TIR domain-containing adaptor-inducing IFN-β (TRIF), which ultimately lead to DC maturation and secretion of pro-inflammatory cytokines (81). Alternatively, damage-associated molecular patterns (DAMPs) associated with tissue damage, such as cytosolic DNA, can be sensed by cyclic guanosine monophosphate (GMP)-adenosine monophosphate (AMP) synthase (cGAS). In the presence of guanosine triphosphate (GTP) or adenosine triphosphate (ATP), cGAS can produce cGAMP (cyclic GMP-AMP). In turn, cGAMP can bind to the ER membrane-associated stimulator of interferon genes (STING). Following binding, STING forms a complex with TANK-binding kinase 1 (TBK1) and traffics to endolysosomal compartments, where TBK1 is able to phosphorylate target transcription factors. As such, STING activation also leads to an NF-kB-dependent pro-inflammatory response and an IRF-3 dependent type I IFN response that promotes immune activation (82).

These pro-inflammatory stimuli induce a change in the chemokine receptor profile of immature DCs, thereby up-regulating CCR7, which enables DCs to mature and traffic to TDLNs (Figure 1.3 step 2). Likewise, naïve T cells follow a chemokine gradient through CCR7 signalling and reach secondary lymph nodes via high endothelial venules (83). Optimal T-cell priming by DCs requires an antigen-specific

signal, which is mediated by the interaction of the TCR with the MHC-antigen complex; and a second co-stimulatory signal, normally provided by the interaction between CD80/86 on APCs with the co-stimulatory receptor CD28 present in T cells (76, 84). These interactions induce an up-regulation of CD25 and IL-2 production by T cells, which are important in modulating early proliferation and differentiation of these cells (13). The interaction between CD80/86 on DCs and CD28 on CD4 T cells also up-regulates CD40L on CD4 T cells. This molecule is required to provide CD4 T-cell help to license DCs, as the interaction between CD40: CD40L up-regulates additional co-stimulatory molecules (CD80/86, CD40, 41BB-L) at the surface of APCs that in turn provide further co-stimulation to naïve CD8 T cells (76, 85). Other co-stimulatory signals are involved in T-cell activation, such as the TNFSF member CD70 expressed on DCs that binds to the constitutively expressed CD27 on naïve T cells (Figure 1.3 point 3) (76).

Together with these, a third signal is provided by the specific pattern of cytokines present during activation, which modulates the type of T-cell response (Figure 1.3 step 3). Production of IL-12 by DCs results in the development of Th1 responses, which lead to the release of IFN-γ and IL-2 (86). These cytokines promote proliferation and differentiation of CD8 T cells into active cytotoxic lymphocytes. Also, they help to suppress Th2-mediated anti-inflammatory responses, further polarising T-cell immunity towards a Th1 response (14).

When priming occurs, T cells start to proliferate and undergo clonal expansion and differentiation (Figure 1.3 step 4). After expansion, activated T cells exit the TDLNs through efferent lymphatic vessels owing to the up-regulation of sphingosine 1-phosphate receptor 1 (S1PR1) and the loss of CCR7 expression (Figure 1.3 step 5) (83, 87). The CXCR3: CXCL9/10 chemokine axis is especially involved in recruiting CD8, Th1 and NK cells to the tumour site. Together with these, there is a recruitment of additional circulating innate effectors like monocytes and neutrophils to the local inflammation site (88).

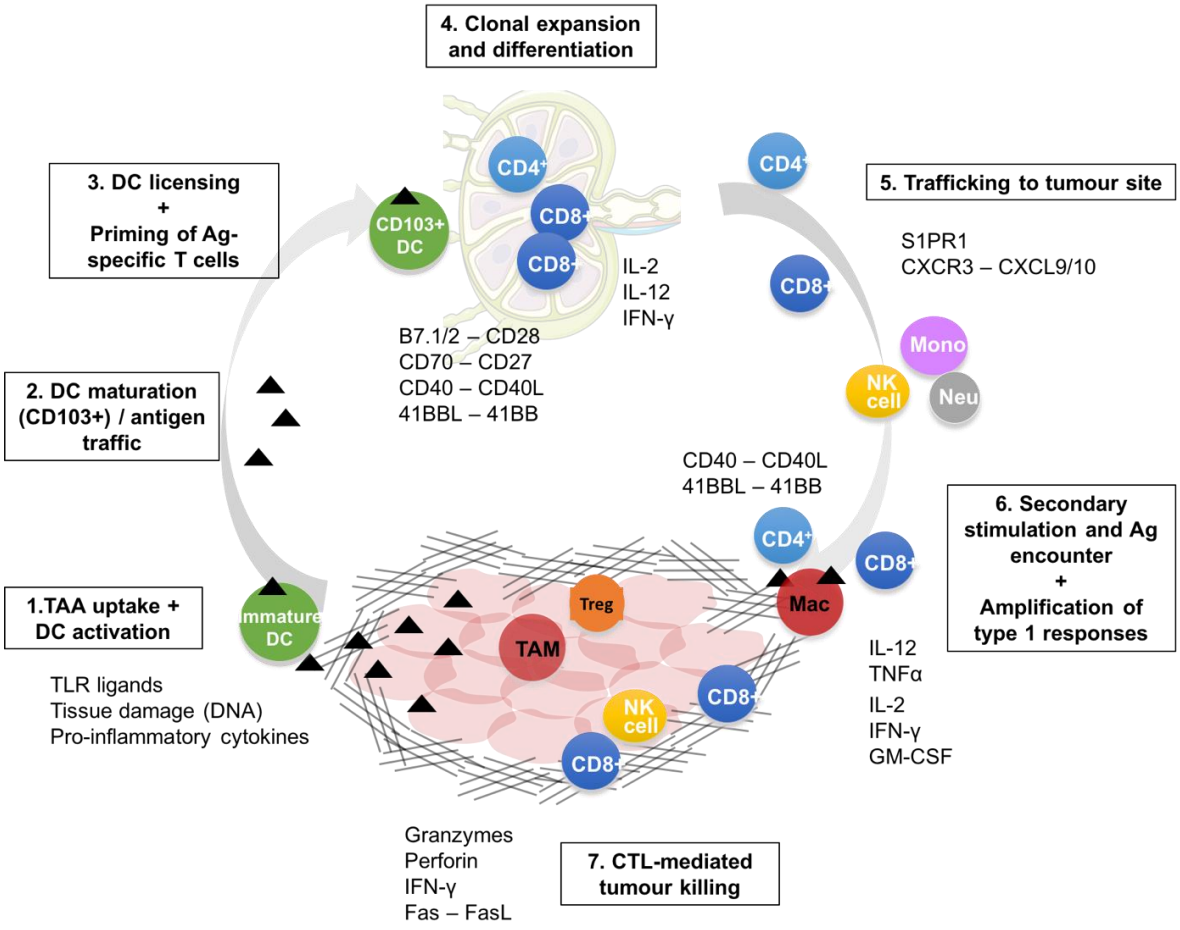

Figure 1.3 Generation of effective anti-tumour immunity.
Apoptotic or necrotic tumour cells release DAMPs (ATP, high-mobility group box 1 protein; HMGB1) or DNA into the stroma that can be taken up or recognised through TLR signalling by DCs. Following antigen uptake and activation, DCs mature and traffic to lymph nodes, where they encounter naïve T cells and cross-present cognate antigens to CD8 T cells. Bidirectional signalling through co-stimulatory molecules and cytokines between DCs, CD4 and CD8 T cells leads to DC licensing and T-cell expansion and differentiation. Activated T cells and other circulating innate cells traffic to the tumour site following chemotactic gradients and encounter antigen presented by macrophages at the tumour bed. Crosstalk between macrophages and T cells further amplifies the Th1 response and activates cytotoxic CD8 T cells, which induce tumour cell death through cell-cell contact (Fas: FasL) or soluble factors (granzymes, perforin) (13).

At the tumour site, secondary encounter with APCs, such as macrophages, displaying TAA, will result in further immune activation. In turn, activation of M1 macrophages by Th1 cells through IFN-γ and CD40L increases the intracellular killing ability of these cells and their expression of CD80/86, MHC-II and CD40, amongst others (89). In addition, Th1 cells produce granulocyte-macrophage colony-stimulating factor (GM-CSF) that stimulate monocytes in bone marrow and IL-2 for additional activation of cytotoxic CD8 T cells (CTLs) (Figure 1.3 step 6).

When CTLs finally encounter tumour cells bearing its cognate antigen, they release cytotoxic granules that contain a range of cytotoxic molecules (i.e perforin, granzyme B), thereby causing tumour cell death; or induce cell death through direct contact via Fas: FasL interaction (Figure 1.3 step 7) (13, 90).

1.2 Monoclonal antibody therapy

Cancer immunotherapy aims to empower the patient's own immune system to combat cancer, by both enhancing the recognition and the efficient elimination of cancer cells. Several immunotherapeutic modalities exist, amongst which monoclonal antibodies (mAbs) are the most widely used largely thanks to their high antigen-specificity, the broad range of effector mechanisms that they can elicit, and the ease with which they can be manufactured compared to other cellular therapies. Immunotherapies have traditionally been divided into two main arms depending on the involvement of the host's immune system. Active approaches such as checkpoint blockers or immunostimulatory mAbs aim to stimulate the host's immune response against cancer, ultimately leading to the generation of immunological memory. Passive immunotherapies, such as mAbs that target TAA, interact directly with tumour cells, marking them for clearance by innate immune effector cells, but do not rely on stimulating adaptive immunity to exert their therapeutic effects (91). Because of this, they are not typically believed to induce immunological memory, although some recent evidence argues against this view (see 1.2.3.1). Although therapeutic mAbs can be engineered to target a wide range of molecules, to date their structure and function largely recapitulates that of natural antibodies produced by plasma cells in the body.

1.2.1 Antibody structure

Antibodies, also known as immunoglobulins (Ig), are Y-shaped molecules that consist of a dimer of two heavy and light chains, with interchain disulphide bonds connecting the two heavy chain. The variable region of the antibody is made up by the N-terminal domain of both variable heavy (V_H) and light (V_L) chains, while the constant region is formed of the constant domains of the heavy (C_H) and light (C_L) chains (see Figure 1.4). These two structurally differentiated parts endow antibodies with their two main functions. The variable region bears the antigen-binding site and complementarity-determining regions (CDRs), therefore dictating each antibody molecule's specificity. On the other hand, the constant region

determines the effector function of an antibody via recruitment of effector cells and molecules (92).

Digestion of antibodies by proteases has been widely used to study antibody structure, and has generated the most currently used terminology to define different parts of the molecule. Proteolytic cleavage by papain at the hinge region that links the two heavy chains gives two identical fragments that contain the antigen-binding activity (Fab; fragment antigen binding). The remaining fragment containing C_{H2} and C_{H3} is known as fragment crystallisable (Fc) and interacts with effector cells and complement molecules. This Fc region differs between Ig isotypes and subclasses. Alternately, enzymatic digestion by pepsin gives a single fragment where the two Fab arms remain linked, named $F(ab')_2$ (92).

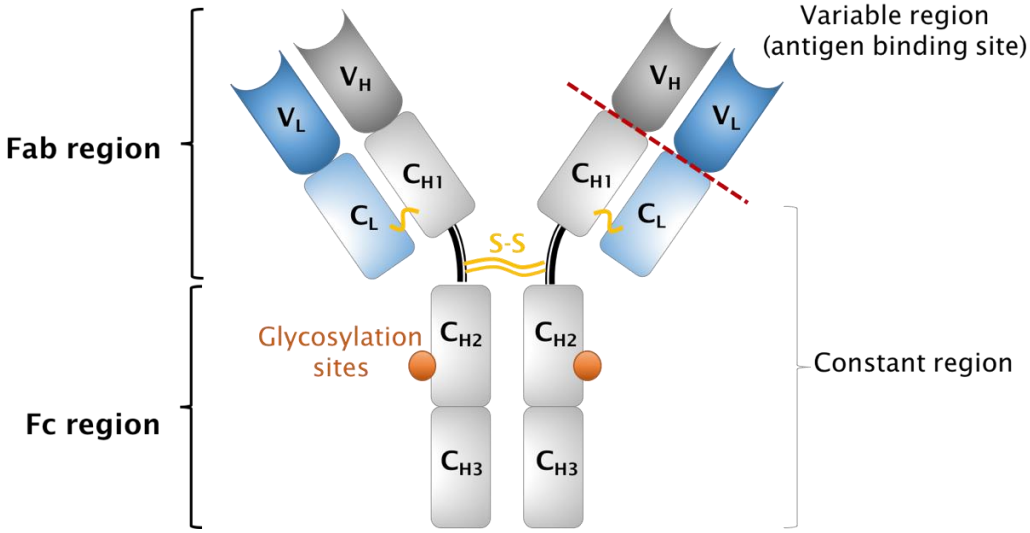

Figure 1.4 Immunoglobulin G structure.
IgG antibodies are large molecules (150 kDa) made of four polypeptide chains. IgGs are formed of two identical class γ heavy chains linked to each other by disulphide bonds (yellow) at the hinge region; and two light chains, bound to the core heavy chains by additional disulphide bonds. The variable region of IgGs contains the antigen binding site, which confers the specificity of the IgG. In contrast, the constant region is less variable and determines the IgG subclass. Within the constant region, the Fc of IgG bears a highly conserved N-glycosylation site (orange) at residue 297 that is essential for IgG-mediated effector functions.

1.2.1.1 IgG isotype and subclasses

Depending on the type of C region, antibodies can be classed into 5 different isotypes, namely IgM, IgD, IgA, IgE and IgG, with different structure and properties. IgG is the most abundant isotype in humans, and is found predominantly in blood and extracellular fluids. It is formed of two light chains with a variable and a

constant domain, and two heavy chains with a variable and 3 constant domains (see Figure 1.4). Disulphide bonds link together domains C_L and C_{H1} at the Fab region, whilst domains C_{H1} and C_{H2} at the heavy chain are linked by a flexible region named the hinge. Disulphide bonds further link the two heavy chains at this hinge region. The hinge provides a degree of free movement of the two Fab arms, allowing the two antigen binding sites to bind epitopes within a range of distances. Monomeric IgGs are hence bivalent molecules in terms of antigen binding, thanks to which they display high avidity interactions (92).

In humans, antibodies of the IgG isotype have 4 different subclasses (IgG1, 2, 3 and 4), each of them carrying specialised functions and properties. Similarly, there are 5 subclasses of mouse IgGs, namely IgG1, 2a/b/c and IgG3 (92, 93). The presence of carbohydrate chains attached at the N297 residue is indispensable for the effector functions of IgGs. As displayed in Figure 1.5, the core structure of this glycan is formed of N-acetylglucosamine (GlcNAc) and mannose residues, which can be further extended by sialic acid and galactose, or modified by fucosylation of the core glycan structure (92). The composition of the carbohydrate side chain influences the quaternary structure of the Fc region, and hence the antibody effector function. As such, the presence of glycan chains favours an open conformation of the Fc region, allowing the interaction with Fc-γ receptors (FcγRs) found on immune effectors (94). In line with this, absence of glycosylation at N297 has been found to abolish the effector function of IgG antibodies, further illustrating the importance of these carbohydrate chains (95, 96). Depending on the type of mutation and IgG isotype backbone, the extent at which the effector functions are abrogated varies. This is important in the design of Fc-null engineered mAbs, and will be further discussed in section 1.3.2.

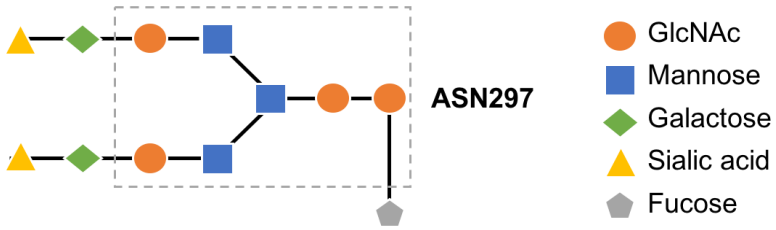

Figure 1.5 N-glycosylated carbohydrate side chain.
N-linked glycosylation consists of the attachment of oligosaccharides to the nitrogen atom of the asparagine (Asn) residue at the position 297 within the Fc region of IgGs. Composition of this carbohydrate side chain alters IgG binding to FcγRs and hence the antibody-mediated effector functions. Adapted from Vidarsson G. et al. (2014) (92).

1.2.2 Antibody function

Antibodies have a key role in immunity, contributing in three main ways: neutralisation, complement activation and opsonisation. Antibodies can neutralise the damaging effect of pathogens and toxins by binding to their surface and preventing them from entering cells. Although the neutralisation of pathogens is accomplished through the Fab portion of the antibody, it is the Fc region that endows these molecules with their main effector functions. Once antibodies are bound to a pathogen surface via the Fab region, immune effector cells expressing Fc gamma receptors (FcγRs) can interact with the available Fc region and target the pathogen for elimination. Depending on the type of cell and FcγR, antibodies can induce antibody-dependent cell cytotoxicity (ADCC) or phagocytosis (ADCP). Alternatively, opsonising mAbs might activate the classical pathway of the complement by interacting with the complement molecule C1q in a process termed complement-dependent cytotoxicity (CDC). Triggering of the complement cascade increases in turn the number of chemokines and complement molecules opsonising the pathogens, which will further recruit more immune effectors to the site of infection (97). The effector mechanisms activated by the Fc region are influenced by the isotype and subclass of antibody. Whilst IgG isotypes are potent activators of the Fc-mediated effector pathways, other antibody classes like IgE or IgA have more specialised roles. IgE plays an important role in allergy via the sensitisation of mast cells, while IgA participates in the first line of pathogen neutralisation in the epithelium (97).

1.2.3 Therapeutic antibodies

Therapeutic mAbs are high affinity molecules that can be designed to target a wide range of antigens. In cancer, therapeutic mAbs have traditionally been targeted to tumour antigens, with the ultimate goal of inducing tumour cell death. Similar to naturally secreted antibodies, the anti-tumour activity elicited by these mAbs can be induced through direct and indirect mechanisms (Figure 1.6). Direct effects are mediated by the Fab portion of the mAb, and involve blockade of growth factors or the transduction of pro-death signals through the engagement of molecules such as CD20 on tumour cells (98). Direct tumour-targeting mAbs against death receptors such as Fas and TRAIL may also require FcγR cross-linking to transduce pro-death signals (99, 100). On the other hand, therapeutic mAbs that induce cell death by indirect mechanisms rely on the recruitment of FcγR-expressing immune cells or complement molecules (101). In contrast to mAbs targeting tumour

antigens, immunomodulatory mAbs target molecules that are generally expressed on immune cells, with the aim of directly stimulating the immune system against cancer.

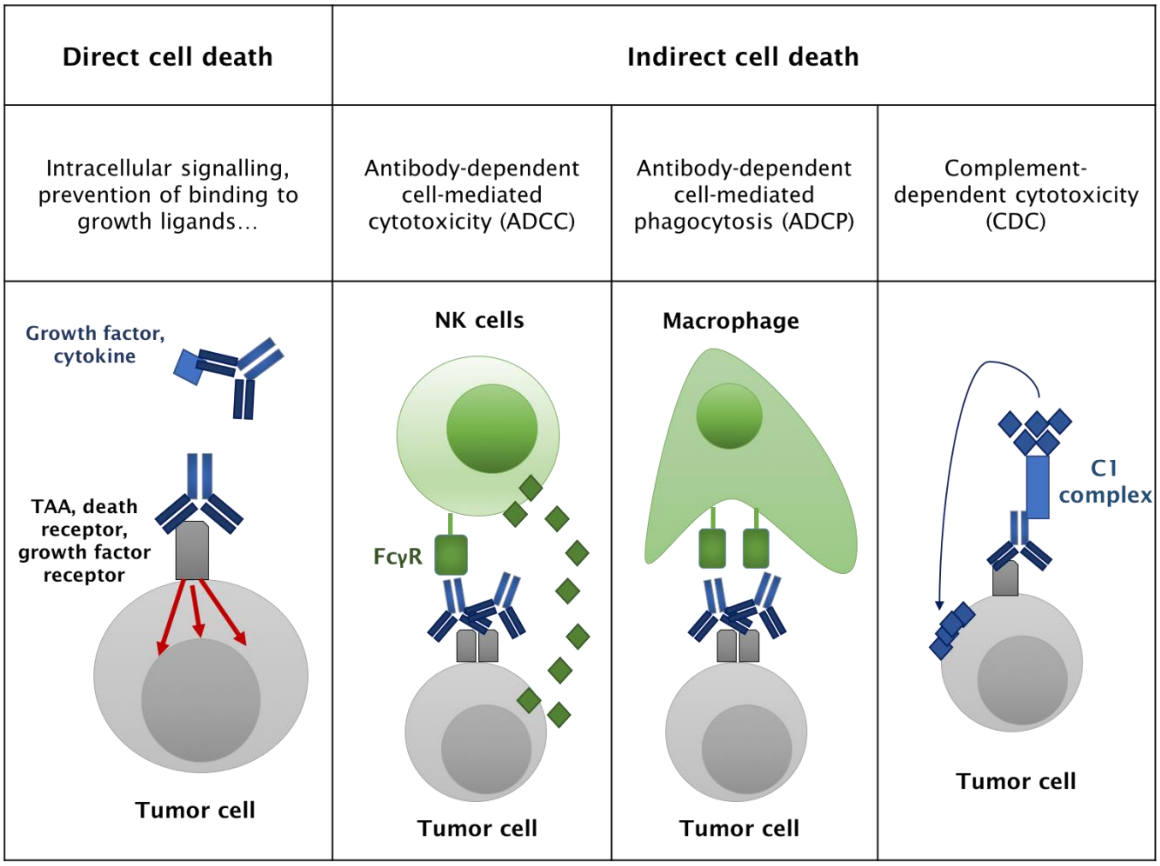

Figure 1.6 Antibody-mediated effector mechanisms.
MAbs targeting tumour antigens can elicit cell death by direct or indirect mechanisms. Direct cell death can be induced by delivering pro-death intracellular signals or by blocking proliferative signals through growth factor receptors. Indirect cell killing may involve the recruitment of immune effector such as NK cells, which can induce ADCC by releasing cytotoxic granules containing perforin and granzymes. Alternatively, recruitment of phagocytes or complement molecules may lead to ADCP or CDC, respectively, ultimately resulting in tumour cell lysis.

1.2.3.1 Direct tumour-targeting mAbs

The majority of therapeutic mAbs approved for clinical use in cancer are classed as direct tumour-targeting mAbs. These mAbs are designed to target tumour cells directly, being raised against TAA that are usually over-expressed on the tumour tissue and absent or minimally expressed on healthy cells. Targets for these mAbs include CD20 on B cell malignancies, human epidermal growth factor receptor (HER)-2 in breast cancer or the epithelial growth factor receptor (EGFR) in colorectal or lung carcinomas. Whilst direct tumour-targeting mAbs have traditionally been thought to act predominantly through direct binding effects, either by blocking

proliferative signals or directly triggering cell death, it is now widely recognised that their therapeutic activity also relies in part on antibody-dependent mechanisms (CDC, ADCC and ADCP) (97). Furthermore, recent evidence suggests that direct tumour-targeting mAbs could also promote a "vaccinal" effect in vivo, thereby inducing adaptive responses that could provide long-term anti-tumour immunity (102, 103). These findings ultimately point to the fact that the distinction line between types of therapeutic mAb may be more diffuse than it was initially thought, and that similar mechanisms might govern some of their anti-tumour activity.

1.2.3.2 Immunomodulatory mAbs

Immunomodulatory mAbs include therapeutic antibodies targeting molecules with immune-related functions. There are two main classes of immunomodulatory mAb, depending on the type of target molecule. Immunostimulatory mAbs target co-stimulatory receptors, whereas checkpoint inhibitors are mAbs against co-inhibitory receptors generally expressed at the T-cell surface. Whilst the goal of immunostimulatory mAbs is to directly trigger immune cell activation, the latter group acts by blocking inhibitory interactions that hinder immune activation. Although both types of immunomodulatory mAbs have been shown to elicit potent anti-tumour immunity in vivo (104, 105), to date, checkpoint inhibitors have had a more extensive translation into clinical practice.

1.2.3.2.1 Immunostimulatory mAbs

Immunostimulatory mAbs often target co-stimulatory receptors on the surface of immune cells that are key for their activation and function. In T cells, these mAbs act agonistically, providing the co-stimulatory signal to prevent anergic responses that would otherwise be triggered by the single interaction between MHC-peptide complex and the TCR alone. These co-stimulatory receptors include CD27, OX40 and 4-1BB amongst other molecules. Agonistic mAbs to these receptors have been shown to augment anti-tumour immunity in various tumour models, enhancing survival and expansion of functional CD8 effector T cells (106-108). Alternatively, immunostimulatory mAbs can target receptors on APCs such as macrophages or DCs, to aid maturation and activation. One example is CD40, a member of the TNFRSF constitutively expressed on APCs. Interaction with its trimeric ligand CD40L on activated helper CD4 T cells results in activation and licensing of APCs, which in turn up-regulates additional MHC and co-stimulatory molecules, and promotes secretion of pro-inflammatory cytokines to augment adaptive immune responses (76, 85). Agonistic mAbs targeting CD40 can mimic the interaction with its natural

ligand and have been shown to trigger cytotoxic T cell responses against tumour models in vivo (109, 110).

1.2.3.2.2 Checkpoint blocking mAbs

As introduced in section 1.1.3, immune checkpoint molecules have well-known immunosuppressive functions that tumours benefit from to dampen anti-tumour immunity. The aim of blocking such inhibitory receptors with mAbs is to unleash endogenous anti-tumour T cell responses, eradicating tumours and establishing immunological memory (111). The mechanism and clinical success of mAbs blocking PD-1 in cancer therapy are reviewed in more detail in section 1.3.

1.2.4 Fc-*γ* receptors in mAb therapy

The choice of isotype of a therapeutic mAb is of critical importance to determine its effector mechanism due to the fact that each isotype displays a specific binding pattern to different types of FcγRs. FcγRs are transmembrane glycoproteins that belong to the immunoglobulin superfamily and have a key role in regulating immune activation. The FcγR system is composed of a set of activating receptors and a sole inhibitory receptor, and the balance between activating and inhibitory signalling pathways can set a threshold for cellular activation. This is of special importance to myeloid cells, which express both activating and inhibitory FcγR receptors, as it directs immunity towards a tolerogenic or an immunogenic response in the context of antibody engagement (101).

1.2.4.1 FcγR expression

In both human and mouse, Fc regions from the different isotypes bind to specific FcγRs on myeloid cells with varying affinities. The ratio of affinities for the activating versus the inhibitory receptor of each IgG subclass (A/I ratio) is used as a general measure to determine the ability of a given antibody to trigger effector responses in vivo (112). Isotypes with higher A/I ratios are more effective at triggering ADCC and ADCP, whereas low A/I often translate into suppression of FcγR-mediated effector functions. Despite having a similar set of FcγRs, with multiple activating and a single inhibitory FcγR, human and murine systems are not exactly the same. The differential pattern of expression and binding affinity for IgG isotypes increases the complexity of translating the results from the murine system into the human one. Therefore, it is important to understand the similarities and

differences between both systems, in order to better translate findings from in vivo models.

1.2.4.1.1 Human FcγRs

There are 5 main functional FcγRs in humans (I, IIa/b, IIIa/b), each of which has a characteristic pattern of cellular expression and binding affinity to IgG isotypes, as summarised in Table 1-1. In addition, cross-over events between FcγRIIa and FcγRIIb genes are postulated to be the origin of a hybrid product that conforms the third isoform of this receptor, namely FcγRIIc (Table 1-1). Although it is not clear whether FcγRIIc bears a functional role, its expression has been reported in approximately 20% of individuals on monocytes/ macrophages, granulocytes and NK cells (113-115).

In terms of antibody binding, IgG1 and IgG3 bind to the high affinity receptor, hFcγRI, whilst IgG2 only binds to low affinity receptors, including FcγRIIa/b and IIIa. IgG4 was initially described as a neutral IgG isotype, but it has been found that this isotype can still bind to activating FcγRs including FcγRI, IIa and IIIa, together with the inhibitory FcγRIIb. Therefore, IgG1 and IgG3 are the most pro-inflammatory subclasses and have the highest A/I ratios, whilst IgG2 and IgG4 present low A/I ratios and are less effective at triggering FcγR-mediated effector responses (112). The majority of immune effectors express more than one FcγR, which enables the fine-tune regulation of immune responses triggered by different IgG subclasses. As such, monocytes, macrophages, DCs and neutrophils co-express several activating FcγRs as well as the inhibitory FcγRIIb. This is however not the case for B cells or NK cells, which only express FcγRIIb and FcγRIIIa, respectively (101).

Table 1-1 Function and expression pattern of human FcγRs.

Receptor	FcgR I (CD64)	FcgR IIa (CD32)	FcgR IIb (CD32b)	FcgR IIc (CD32c)	FcgR IIIa (CD16a)	FcgR IIIb (CD16b)
Structure	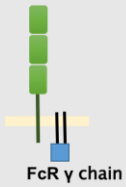					
Binding affinity	**High** 1) IgG1= IgG3 2) IgG4	**Low to medium** 1) IgG1 2) IgG3 3) IgG2 4) IgG4	**Low to medium** 1) IgG1= IgG3 = IgG4 2) IgG2	**Low to medium** 1) IgG1 2) IgG3 3) IgG2 4) IgG4	**Low to medium** 1) IgG3 2) IgG1 3) IgG4 4) IgG2	**Low to medium** 1) IgG1 2) IgG3
Cell type	Monocytes Macrophages Neutrophils Dendritic cells	Monocytes Macrophages Neutrophils Dendritic cells	Monocytes Macrophages Neutrophils Dendritic cells B cells	Monocytes Macrophages Neutrophils NK cells	Monocytes Macrophages Dendritic cells NK cells	Neutrophils
Function	Activating	Activating	Inhibitory	Activating	Activating	Activating

Adapted from Nimmerjahn F. and Ravetch JV. (2008) (101).

1.2.4.1.2 Mouse FcγRs

To date, 4 different FcγRs have been described in mice (Table 1-2): FcγRI, II, III and IV. Murine FcγRI is a high-affinity receptor for the IgG2a isotype only, presenting low affinity for IgG2b, IgG3 and no binding activity to IgG1 (112). Whilst FcγRII and FcγRIII are low-affinity receptors for all mouse IgGs, FcγRIV only binds to IgG2a/b with medium affinity (112, 116). Hence, IgG2a and IgG2b bind to all activating FcγRs and are the most potent inducers of effector responses, as reflected by their higher A/I ratios (70 and 7, respectively) compared to IgG1 (0.1). Of note, these A/I ratios represent the ratio of the calculated affinity of activating FcγRIII (for IgG1) or FcγRIV (for IgG2a/b) to that of the inhibitory FcγRII receptor (112). Importantly, a significant enhancement of IgG1-mediated effector activity was observed in mice lacking the inhibitory FcγRII receptor, indicating that the a priori reduced A/I ratio of this isotype can be increased by preventing FcγRII binding (112).

In terms of normal FcγR expression patterns in mice, the majority of cells from the myeloid lineage (monocytes, macrophages and DCs) express all activating FcγRs as well as the inhibitory FcγRII, whilst neutrophils primarily express FcγRIII and FcγRIV. In contrast, B cells and NK cells exclusively express FcγRII and FcγRIII, respectively.

Hence, ADCC mediated by NK cells is completely dependent on the activating FcγRIII receptor in mice (101, 117).

Table 1-2 Function and expression pattern of mouse FcγRs.

Receptor	FcgR I	FcgR II	FcgR III	FcgR IV
Structure			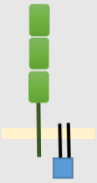	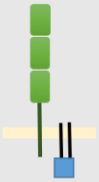
Binding affinity	**High or low** 1) IgG2a 2) IgG2b 3) IgG3	**Low to medium** 1) IgG1 2) IgG2b 3) IgG2a = IgG3	**Low to medium** 1) IgG2b 2) IgG2a 3) IgG1	**Low to medium** 1) IgG2a 2) IgG2b
Cell type	Monocytes Macrophages Dendritic cells	Monocytes Macrophages Neutrophils Dendritic cells B cells	Monocytes Macrophages Neutrophils Dendritic cells NK cells	Monocytes Macrophages Neutrophils Dendritic cells
Function	Activating	Inhibitory	Activating NK cell cytotoxicity (ADCC)	Activating

Adapted from Nimmerjahn F. and Ravetch JV. (2008) (101).

1.2.4.2 FcγR signalling

To prevent deleterious activation by soluble antibodies, most FcγRs interact with monomeric mAbs with low affinity. As an exception, FcγRI is the only high-affinity receptor (10^{-8}–10^{-9}M), capable of binding to monomeric IgG (93). However, the binding of multiple FcγRs by opsonising mAbs or immune complexes (ICs) results in a high-avidity interaction capable of delivering the activating signalling required for the activation of immune effectors. Upon cross-linking by ICs or high-affinity mAbs, immunoreceptor tyrosine-based activating motifs (ITAMs) present in activating FcγRs or their adaptor molecules become phosphorylated by members of the SRC family of kinases (i.e LYN). As detailed in Figure 1.7, these phosphorylated sites can in turn activate an intracellular signalling cascade that will eventually lead to the activation of the cell, which may translate in cell degranulation and ADCC, cytokine production or ADCP (118). Some human and all murine activating FcγRs lack the intrinsic ability to signal and rely on adaptor molecules, generally the Fc receptor common gamma chain (119) for their

expression at the cell surface and to deliver the intracellular signal. Alternatively, three human FcγRs have been described that do not require this Fc common gamma chain. Whilst FcγRIIIb is anchored to the plasma membrane by a glycolipid chain that lacks a cytoplasmic signalling domain, FcγRIIa/c contain an ITAM signalling motif within their cytoplasmic tail (101).

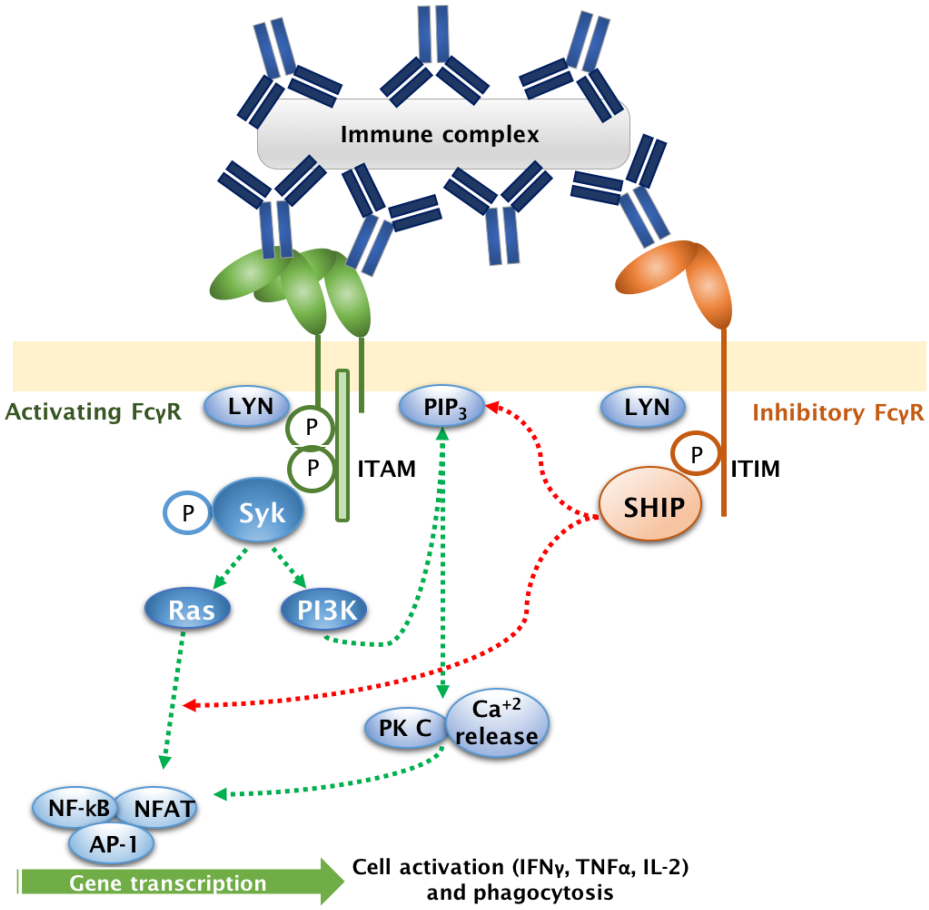

Figure 1.7 Activating and inhibitory FcγR intracellular signal.
Target cells or pathogens are bound by antibodies and form immune complexes (ICs). The cross-linking of several activating FcγR by ICs triggers the activation of kinases of the SRC family, such as Lyn. These kinases phosphorylate tyrosine residues on FcγR ITAMs, which then act as a docking site for kinases of the SYK family. Syk phosphorylation and activation results in the subsequent activation of Ras and MAP kinase pathways, which ultimately lead to the activation of immune cells by activating multiple transcription factors (NF-kB, NFAT or AP-1). These events trigger effector functions such as phagocytosis and cytokine release. Similarly, ICs induce the activation and phosphorylation of the inhibitory FcγR at the ITIM motifs. This phosphorylation recruits SHIP phosphatases, which suppresses intracellular mediators downstream of activating FcγRs to ultimately result in a decrease of effector functions. Adapted from Nimmerjahn F. and Ravetch JV. (2008) (101).

In contrast, the inhibitory FcγR carries an ITIM in its cytoplasmic tail. Upon receptor cross-linking, phosphorylation of the ITIM motif by the kinase LYN leads to the

recruitment of SH2-domain-containing inositol polyphosphate 5 phosphatases (SHIP) molecules, which interfere with the activating FcγR signals by catalysing the dephosphorylation of downstream molecules, thereby resulting in impaired effector functions (120). Hence, binding of the inhibitory FcγR increases the activation threshold of the cell and reduces cell proliferation, phagocytosis and degranulation (121).

1.2.4.2.1 Regulation of FcγR expression

The expression of FcγRs is controlled by multiple environmental cues. Whilst pro-inflammatory mediators such as LPS or IFN-γ upregulate the expression of activating FcγRs on myeloid cells (112, 122, 123), other cytokines such as IL-4, IL-10 or TGF-β have the opposite effect, increasing FcγRIIb expression and down-regulating the expression or function of its activating counterparts (116, 124-126). Nevertheless, cytokines may have different effects depending of the immune effector type. As an example, IL-4 has been shown to decrease FcγRI expression on human blood monocytes but not DCs (127). Furthermore, tumours are characterised by hypoxic environments due to their rapid and uncontrolled growth. Studies from our laboratory have shown that hypoxia can lead to an up-regulation of the inhibitory FcγRIIb (128). Therefore, expression of FcγRs is dynamic and largely influenced by the tumour milieu, which may have important implications for the therapeutic activity of mAbs.

1.2.4.3 Role of Fc: FcγR interaction in mAb therapy

As more evidence is compiled, the dominant role that Fc: FcγR interactions have in mAb-based immunotherapies becomes clearer. As mentioned in section 1.2.3.1, numerous studies have demonstrated that direct tumour-targeting mAbs require functional activating FcγRs to have therapeutic activity. In a study by Clynes and Ravetch (2000), anti-HER2 mAbs were shown to engage both the activating FcγRIII and the inhibitory FcγRIIb on myeloid cells. Whilst tumour control was lost by abrogating engagement of activating FcγRs, the interaction with the inhibitory receptor impaired the cytotoxic ability of these mAbs, and mice deficient in FcγRII showed complete arrest of tumour growth (121). Similarly, activating FcγRIV was essential for the macrophage-mediated ADCP of HER-positive cancer cells in vivo (129), whilst all the activating FcγRs participated in the depletion of lymphoma cells by anti-CD20 mAbs (130).

In contrast to direct tumour-targeting mAbs, some immunostimulatory mAbs require engagement with the inhibitory FcγR in order to deliver their agonistic activity (131). Anti-CD40 mAbs engineered as a murine IgG1 resulted in expansion and activation of antigen-specific CD8 T cells, whilst IgG2a and a mutant lacking FcγR binding lacked this adjuvant effect. Similar results were found in a tumour model, where the anti-tumour effect of anti-CD40 mAbs was lost in FcγRII$^{-/-}$ mice (132). Conversely, other immunostimulatory mAbs targeting receptors on the surface of T cells have shown very different FcγR requirements. A comprehensive study on anti-4-1BB mAbs showed that these were able to enhance anti-tumour responses via the two effector mechanisms; while IgG2a engaged activating FcγRs on macrophages and triggered depletion of regulatory T cells, the Fc portion of IgG1 cross-linked the receptor by binding to FcγRII, thus delivering the co-stimulatory signal to CD8 effector T cells (133). Similarly, recent studies highlight the ability of anti-OX40 IgG2a mAbs to deplete intratumoural Tregs. This effect was dependent on activating FcγRs and correlated with tumour regression (134). In these two cases, IgG2a isotypes act as direct targeting mAbs to deplete immunosuppressive cell populations within the TME, rather than providing co-stimulatory signals.

Likewise, checkpoint inhibitors targeting CTLA-4, which is highly expressed on activated Tregs, have shown similar results both in preclinical models and ex-vivo. In two in vivo studies using colorectal carcinoma and melanoma models, anti-CTLA-4 exhibited enhanced anti-tumour immunity as a murine IgG2a form, but not when given as an IgG1 isotype or an Fc-null variant (IgG1-D265A). This effect was driven by the selective deletion of CTLA-4+ Tregs through FcγRIV engagement. (135, 136). In agreement with this, one study suggested that the human IgG1 anti-CTLA-4 mAb Ipilimumab was able to bind FcγRIIIa ex vivo on monocytes from melanoma patients, thereby eliciting ADCC of Treg (137). Moreover, response to Ipilimumab in melanoma patients was associated with the FcγRIIIa high-affinity polymorphism, further supporting the involvement of activating FcγRs in anti-CTLA-4 mAb therapy (138). Despite targeting another checkpoint pathway, the isotype requirements for mAbs targeting PD-1/ PD-L1 are considered to differ from those mentioned above, and will be discussed in further detail in section 1.3.2.

All together, it is clear that the choice of isotype is a critical step for mAb immunotherapy, and this is likely due to the broad expression of FcγRs on immune cells and their pivotal role in regulating innate and adaptive immune responses. The desired effector functions will depend on the type of target and mAb, i.e

immunostimulatory and checkpoint blocking mAbs may benefit from isotype variants that lack the ability to engage activating FcγRs, whereas direct tumour-targeting mAbs may take advantage of isotypes that trigger ADCC and ADCP, further enhancing the cytotoxic potential of the therapy. The specific requirements of mAb therapy are yet to be elucidated, but will likely vary across tumour types with different TME, target molecules and time course of the disease.

1.3 Anti-PD-1 mAbs in cancer

As summarised in section 1.1.3.1, interaction between PD-1 and PD-L1 is a potent mechanism used by cancers to inhibit anti-tumour immunity. Numerous studies in murine tumour models have demonstrated the capability of PD-1 blockade to promote tumour regression and prolong animal survival in a wide range of histologically distinct tumours, generating a robust immunological memory mediated by memory T cells (40, 139, 140). PD-1 blocking mAbs trigger a polyclonal expansion of tumour-specific cytotoxic T cells that are able to target cancer cells and lead to the regression of established and metastatic tumours (141, 142). As opposed to direct targeting strategies (e.g anti-CD20 mAbs), this polyclonal response potentially minimises the rise of antigen-loss tumour variants that can escape immune attack. In line with these studies, further research using ex vivo human cells showed an enhanced T-cell proliferation and cytokine production in response to PD-1 or PD-L1 targeting mAbs (143, 144).

Such studies paved the road to assess safety and efficacy of these agents in clinical trials, in which blockade of the PD-1 pathway led to remarkable clinical results in a variety of cancers, most notably metastatic melanoma (objective response of 28-40%) and NSCLC (objective response rates of 18-36%) (6-8, 30, 145, 146). These results culminated in the U.S Food and Drug Administration (FDA) approval of two PD-1 blocking mAbs, Pembrolizumab and Nivolumab, for the treatment of metastatic melanoma and NSCLC, respectively. As summarised in Table 1-3, the anti-PD-1 mAbs Cemiplimab and Sintilimab were more recently approved to be used in cutaneous squamous-cell carcinoma and Hodgkin's lymphoma (HL), respectively (147, 148). In addition, three other drugs that inhibit the pathway by blocking PD-L1 (Atezolizumab, Avelumab, Durvalumab) have been approved to be used in NSCLC, bladder cancer and Merkel-cell carcinoma, respectively (111, 149, 150). To date, the number of clinical studies underway is already surpassing the 1000, and

the list of cancers with FDA approval currently includes an increasing number of solid carcinomas (renal, head and neck, stomach, bladder, liver) and HL.

Table 1-3 FDA approved mAbs targeting PD-1/ PD-L1 pathway.

Drug	Target	Isotype	Approval
Nivolumab	PD-1	IgG4-S228P	Melanoma, NSCLC, SCLC, Head and neck, renal cell, urothelial, colorectal, hepatocellular, HL
Pembrolizumab	PD-1	IgG4-S228P	Melanoma, NSCLC, SCLC, Head and neck, renal cell, urothelial, colorectal, Merkel-cell, gastric, cervical, oesophageal, hepatocellular, HL.
Cemiplimab	PD-1	IgG4-S228P	Cutaneous squamous cell carcinoma
Sintilimab	PD-1	IgG4-S228P	HL (China)
Tislelizumab	PD-1	IgG4	Conditional approval for HL (China) Phase III in solid cancers (NSCLC, hepatocellular, etc)
Durvalumab	PD-L1	IgG1- Fc null (triple-mutant domain)	Urothelial carcinoma
Atezolizumab	PD-L1	IgG1-N297A	Bladder cancer, triple-negative breast cancer, NSCLC
Avelumab	PD-L1	IgG1	Gastric & Merkel-cell carcinomas
*Accurate as of August 2020.			

Despite its unequivocal success, PD-1 blockade is not effective in all cancers, nor in all patients within a responsive tumour type. Of those who initially respond, acquired resistance will further reduce the overall percentage of patients benefiting from this immunotherapy. Understanding the biology that underlies the differences between responsive and non-responsive tumours is fundamental to predict response to immunotherapy and design effective combinations for those patients that fail to respond to monotherapy with anti-PD-1 mAbs.

1.3.1 Immune responses to PD-1/ PD-L1 blockade

To date, one of the main focuses of preclinical investigations has been to study the precise T-cell populations that preferentially respond to PD-1/ PD-L1 blockade. Following acute antigen exposure, the majority of effector T cells die during the contraction phase, while a small percentage (5-10%) remain to form long-lived memory T cells. These cells are maintained via homeostatic proliferation (IL-7/ IL-15) and can rapidly proliferate and differentiate into effector-like T cells upon

secondary challenge (151, 152). During chronic antigen exposure, T cells acquire an altered differentiation state termed exhausted phenotype, which involves loss of function (IL-2 production, proliferation, cytotoxic killing) and up-regulation of inhibitory co-receptors (PD-1, LAG-3) (153).

Originally, exhausted T cells were considered to be terminally differentiated because of their low proliferative capacity and their overall stable transcriptional profile. In a Lymphocytic Choriomeningitis virus (LCMV) model of chronic infection, effector T cells were initially re-invigorated by anti-PD-L1 mAbs but eventually became re-exhausted if antigen exposure persisted (154). However, in the same LCMV model, T cells that presented a typical exhausted phenotype were able to re-expand in vivo and mount effective secondary responses despite high PD-1 expression (155). This evidence supported the contention that a fraction of exhausted T cells retained the ability to proliferate and differentiate into effector cells. Furthermore, two different populations of exhausted T cells were defined on the basis of the transcription factors eomesodermin (EOMES) and T-box transcription factor 21 (T-bet), which regulate CD8 T-cell effector and memory differentiation (153). Whilst PD-1-high, EOMES-high CD8-T cells were terminally differentiated and had limited proliferative capacity, the PD-1-int, T-bet-high CD8 population retained in vivo proliferation. This second subset acted as a progenitor pool, giving rise to PD-1-high, EOMES-high cells (156).

In the context of cancer, two distinct exhausted PD-1+ CD8 T-cell subsets with differential abilities to respond to PD-1 therapy have also been described, based on the expression of the transcription factor Tcf1. Terminally differentiated, Tcf1 negative TILs had restricted proliferative capacity, produced more effector molecules (granzymes, IFN-γ) and were more cytotoxic. In contrast, progenitor exhausted Tcf1+ TILs showed homeostatic self-renewal and were also able to give rise to terminally exhausted Tcf1 negative cells in a process that required TCR stimulation. Blockade of PD-1/ PD-L1 preferentially expanded Tcf1+ TILs, increasing the numbers of progenitor exhausted TILs but also the conversion of progenitors to terminally exhausted CD8 T cells (157-159). Treatment with the S1PR1 inhibitor FTY720 did not alter tumour growth or the percentages of Tcf1 subsets, further supporting the idea that Tcf1+ cells self renew and also give rise to Tcf1 negative TILs within the TME. This was also the case after checkpoint inhibitors, suggesting that this treatment induced proliferation of TILs rather than de novo priming and recruitment of T cells from TDLNs (158). Nevertheless, the possible contribution of peripherally expanded effector T cells that infiltrate the

tumour bed cannot be ruled out. As a recent study pointed out, local expansion of memory-like TIL clones and infiltrative process of effector T cells from blood may represent two mechanisms that have independent contributions to clinical responses (160).

Other studies have given more focus to the surrounding cell types and environmental cues in the TME that drive an effective anti-tumour immune responses in response to PD-1/ PD-L1 blockade. Several studies published in recent years found that TIL proliferation and tumour clearance in response to PD-1/ PD-L1 blockade was dependent on the activation of intratumoural Batf3+ (CD103+) DCs (79, 161, 162). In a study by Salomon H. et al., anti-tumour responses were seen in B16 tumours after treatment with Flt3L, which induced mobilisation of DC precursors from bone marrow, and the TLR3 agonist Poly:IC. Therapeutic activity was dependent on Batf3+ DCs, type I IFNs and the cross-presentation of TAA by DCs to T cells in TDLNs. Because DCs up-regulated PD-L1 upon activation, the anti-tumour response was further enhanced with anti-PD-L1 mAbs (79). Following a similar approach to activate DCs, another work determined that release of IFN-γ by CD8 TILs after PD-1 blockade could be sensed by intratumoural Batf3+ DCs. These, in turn, produced and secreted IL-12 that licensed CD8 TILs and enabled tumour-cell killing (162). Alternatively, another proposed mechanism emphasised the role of CXCL9 secretion by CD103+ DCs to mediate the recruitment of CXCR3-expressing CD8 T cells after PD-1 blockade (161). In agreement with previous studies, therapeutic activity of anti-PD-1 mAbs was not altered when lymphocyte egress from TDLNs was blocked (161, 162), demonstrating that tumour control is likely driven by expansion of Tcf1+ TILs. Although these studies highlight different mechanisms of action, it is clear overall that Batf3+/CD103+ DCs and Tcf1+ CD8 TILs have a significant role in orchestrating effective anti-tumour immunity in response to PD-1 blockade.

1.3.2 Role of the Fc region in anti-PD-1/ PD-L1 mAbs

At present, clinically approved anti-PD-1 mAbs are designed as human or humanized IgG4 isotypes bearing the S228P mutation, which prevents Fab-arm exchange with host IgG4 antibodies (163). Anti-PD-1 mAbs are believed to act predominantly through ligand blockade, in a FcγR-independent manner, and therefore the human IgG4 isotype was chosen due to its low engagement of FcγRs to reduce the potential depletion of PD-1+ effector CD8 T cells. Nevertheless, binding to both activating and inhibitory FcγRs has been noted with IgG4-ICs in

vitro (93) and in vivo (128, 164). These demonstrate that IgG4 mAbs retain the ability to bind FcγR, and imply that anti-PD-1 mAbs may still be able to engage FcγR in vivo, which could impact their therapeutic efficacy.

The first evidence of the modulation of anti-PD-1 mAb efficacy by FcγR engagement was provided by Dahan R. et al. (2015). In this study, the authors showed that engagement of activating FcγRs by anti-PD-1 mAbs led to the depletion of intratumoural CD8 T cells and to poor anti-tumour immunity. Although not fully investigated, the authors suggested that interactions with the inhibitory FcγRII were also detrimental to the efficacy of anti-PD-1 mAbs (104). In another recent report, a novel human IgG4-S228P anti-PD-1 mAb cross-linked FcγRI in macrophages and caused a small increase in the phagocytosis of PD-1+ cells. In contrast, the IgG4 counterpart did not bind FcγRI and had no effect in phagocytosis. These results translated into an increased CD8 infiltration and reduced tumour growth of a xenograft skin cancer model by IgG4 but not IgG4-S228P anti-PD-1 mAbs (165). Therefore, this study suggested that the S228P mutation, which was initially introduced to prevent Fab-arm exchange, may enhance binding to activating FcγR in anti-PD-1 mAbs, thereby limiting their efficacy.

As a result of the previous study, the novel anti-PD-1 mAb Tislelizumab was engineered into a humanised IgG4 without the S228P mutation (Table 1-3). In a comparative ex vivo study, although Tislelizumab, Nivolumab and Pembrolizumab demonstrated production of IFN-γ and proliferation of TILs cultured with tumour spheroids from colorectal cancer patients, the amount of IFN-γ and the activation of TILs was significantly higher with Tislelizumab compared to the other two mAbs (166). However, it has not been proven that the S228P mutation per se decreases the efficacy of other clinically approved anti-PD-1 mAbs. Furthermore, although the in vivo half-life of IgG4-S228P and IgG4 anti-PD-1 mAbs did not seem to differ in the preclinical study (165), the authors did not specifically address the potential fab-arm exchange that could occur in vivo and how this could undermine efficacy. Hence, the removal of this point mutation might not be the best approach to produce Fc-null variants of anti-PD-1 mAbs. Alternatively, other research indicates that multiple mutations might be required to completely abrogate FcγR engagement of IgG4 mAbs. As an example, addition of the point mutation L235E in IgG4-S228P mAbs further reduced binding to activating and inhibitory FcγR and showed no ADCC of EGFR-expressing target cells (167). Overall, what these studies highlight is that Fc engineering of PD-1 blocking mAbs confers a novel approach to enhance the therapeutic efficacy of these mAbs.

In line with the previous reports detailed above, one study described a link between FcγRs and hyperprogression (HP) in response to PD-1 blockade (168). HP is a phenomenon that has recently been characterised and accepted as a separate clinical outcome, which has been reported in 9-29% of patients after anti-PD-1 mAb therapy (169). Although the definition of HP varies, it defines a paradoxical rapid and extensive outgrowth of cancer that was not seen before anti-PD-1 therapy, but was secondary to it (169). Interestingly, in a study by Russo G.L. et al., Nivolumab as an intact IgG but not as a $F(ab)_2$ induced accelerated tumour growth in NSCLC patient-derived xenografts (PDX) harbouring EGFR mutations (168). This study associated HP to tumour-infiltrating macrophages and suggested that it was FcγR-mediated. Although another study linked HP to an increase in Treg proliferation and suppression following PD-1 blockade (170), both mechanisms might not be mutually exclusive; instead, both could potentially contribute to resistance to anti-PD-1 mAbs.

Due to the preferential expression of PD-L1 in cancer cells and tumour-infiltrating myeloid cells, the Fc requirements of mAbs targeting PD-L1 are considered to be opposite to those of PD-1 blocking mAbs. Initial reports by Dahan R. et al. proposed that anti-PD-L1 mAbs required the engagement of activating FcγRs to deliver effective anti-tumour activity in the colorectal MC38 and B16 melanoma tumour models in vivo. The therapeutic effect was partly due to the FcγRI-dependent reduction of CD11b+ myeloid populations at the TME, which correlated with an increase in CD8 T cells (104). Similarly, the efficacy of Avelumab in mediating cancer cell lysis correlated with the level of expression of PD-L1 on cancer cells, which determined the extent of NK-mediated ADCC through CD16 ligation (171). In line with this, engineered afucosylated anti-PD-L1 mAbs enhanced lysis of PD-L1+ cancer cells and induced stronger activation of CD8 T cells compared to parental or Fc-null anti-PD-L1 mAbs. This effect was proposed to be driven by the improved binding to FcγRIIIa by afucosylated mAbs (172). In contrast, a recent study claimed that the therapeutic activity of anti-PD-L1 mAbs in the MC38 model was independent on FcγRs. However, the authors found that murine IgG2a was more effective than IgG1 or IgG2a-D265A mAbs in CT26 model, where treatment with IgG2a decreased PD-L1+ macrophages at the tumour site (173). Altogether, these studies suggest that anti-PD-L1 mAbs are likely to act as direct targeting mAbs, with PD-L1 expression on tumour cells functioning as a target antigen, in addition to checkpoint blockers, contrary to anti-PD-1 mAbs. Hence, targeting of PD-L1 may benefit from enhanced FcγR-mediated effector functions, whilst the

engineering of anti-PD-1 mAbs into Fc-null variants could provide improved efficacy.

1.3.3 Predictive biomarkers of response to PD-1 blockade

Given that PD-1 blocking antibodies are only effective in a minority of patients and tumours, the search for biomarkers to accurately predict response to this immunotherapy has aroused great interest. To date, there is no single biomarker of response to PD-1 blockade. Although concurring traits of responsive cancers have been identified, the study of most of these require a tissue biopsy from the tumour, which may not be available in some tumour types or patients.

1.3.3.1 PD-L1 expression in tumour

Detection of PD-L1 expression on tumour cells by immunohistochemistry (IHC) was one of the earlier biomarkers identified to potentially predict response to PD-1 blockade, with the rationale that therapeutic blockade of PD-1 would only be effective if the inhibitory PD-1/PD-L1 axis was active within the tumour. In favour of this, tumour PD-L1 positivity has been reported to correlate with improved objective response rates compared to PD-L1 negative tumours in many adult cancers (174). Nevertheless, durable and complete responses to PD-1 blockade have been seen in PD-L1 negative tumours, and thus the absence of PD-L1 expression is not necessarily indicative of unresponsiveness to therapy (6, 30, 175). In addition to tumour expression, PD-L1 positivity on tumour-infiltrating myeloid cells has also been correlated with responses to checkpoint inhibitors (68) and some studies suggest that it might be a better prognostic marker than tumour PD-L1.

Besides the variability on PD-L1 expression across tumour types and patients, there are technical difficulties in terms of detection by IHC. Use of different detection antibodies or thresholds for positivity may help explain the differences seen across studies. Furthermore, a recent study proposed that the abundant glycosylation of PD-L1 affects its detection. Increased signal intensity was achieved by enzymatic deglycosylation of tumour samples, and this led to an improved detection of PD-L1 and a better prediction of the therapeutic efficacy of PD-1/PD-L1 blockade (176).

1.3.3.2 Mutational burden

Tumour mutational burden, and more specifically the extent of non-synonymous mutations, which potentially generate novel epitopes to be displayed by MHC

molecules, has been shown to correlate with response to PD-1 blockade (177, 178). This highlights the importance of neoantigens in dictating therapeutic anti-tumour immune responses. The strong relationship between mutational load and PD-1 responsiveness was first suggested by the fact that biallelic mismatch repair deficient (bMMRD) tumours were more responsive to PD-1 blockade as compared to non-bMMRD, irrespective of the tumour type. This is thought to be driven by the large number of somatic mutations that bMMRD cancers bear due to biallelic defects of the DNA mismatch repair system, which gives rise to an increased number of potential neoantigens (179). Besides its role in primary response to PD-1 blockade, the specific mutational landscape of a tumour has been demonstrated to be important in acquired resistance to immunotherapy in adult cancers. In a study by Anagnostou et al., the analysis of relapsed tumours from patients that had initially responded to PD-1 blockade revealed a loss of 7 to 18 putative mutation-associated neoantigens compared to pre-treatment counterparts (180).

1.3.3.3 Immune contexture

The dynamic nature of cancer and the interactions between tumour and stromal cells dictate the spatial organisation of immune populations within the TME. As reviewed by Fridman WH et al., a dense intratumoural lymphocyte infiltrate is a common characteristic of tumours with favourable prognosis, as opposed to an absent or peritumoural immune infiltrate (181). Recent studies are shedding some light on the value of immune infiltrates in determining responsiveness to PD-1 blockade. Two different studies in melanoma patients have found that the best predictive value of response to therapy were pre-treatment biopsies displaying co-localisation of CD8 T cells and PD-L1 expressing TAMs or tumour cells at the invasive margin (141, 182). During the responsive phase to therapy, tumour regression was driven by intratumoural proliferation of CD8 T cells, which were restricted back to the invasive margin at the time of tumour relapse, supporting the importance of intratumoural immune infiltrates in the therapeutic activity of anti-PD-1 mAbs (141).

1.4 Immunotherapy for paediatric cancers: Neuroblastoma

Cancer remains the second leading cause of death in children after traumatic injuries, with an estimated 1800 new cases per year occurring in children and adolescents in the United Kingdom (183). Despite advances in conventional treatments such as surgery, chemotherapy or radiation, outcomes for some

childhood malignancies remain poor. Moreover, tumours that are refractory to conventional therapies or relapse after initial treatment still represent a major challenge for paediatric oncology. Following the breakthrough of immunotherapy to treat adult cancers (30), this approach has emerged as a promising alternative in the treatment of childhood malignancies thanks to the numerous advantages that it can offer over conventional therapies. Amongst these, the more specific targeting of cancer cells is of great importance as it has the potential to reduce treatment-related side effects, which is critical in paediatric patients to improve the long-term quality of life of survivors (184).

Paediatric cancers differ from those in adults in many ways, bearing unique biological traits that need to be considered carefully when assessing the potential translation of immunotherapy into childhood cancers. Firstly, adult cancers are most frequently from an epithelial origin. Chronic exposure to environmental insults contributes to continued DNA damage, which favours the development of cancer (185). This origin often results in chronic inflammation and increased number of mutations compared to childhood malignancies. These, in contrast, generally arise from genetic abnormalities of cells of an embryonic or mesenchymal origin and have a shorter pre-neoplastic period, leading to lower mutational load (186, 187). Furthermore, paediatric tumours present with faster kinetics than most adult tumours, exhibiting a rapid growth that could potentially outpace the efficacy of strategies such as immunotherapy, which rely on relatively slow and complex immune modulation. Another factor that may potentially impact the translation of immune-based therapies into paediatric patients is that many of them undergo very intensive multi-modal therapy as first line and salvage therapies, and are therefore likely to be very heavily pre-treated by the time they are considered for early phase trials of immunotherapies. Despite these unfavourable features, remarkable success has been achieved in children with neuroblastoma (NB) and acute lymphoblastic leukaemia (ALL) after treatment with direct tumour-targeting mAbs and chimeric antigen receptor (CAR)-T cells, respectively (188, 189). These studies provided proof of concept that immunotherapeutic approaches can also be effective in paediatric cancers

1.4.1 PD-1 blockade in paediatric cancers

Until now, immunotherapy for childhood cancers has focused on direct tumour-targeting approaches of a single TAA, which can lead to the eventual rise of antigen-loss tumour variants. On the other hand, the stimulation of endogenous

anti-tumour immunity by checkpoint inhibitors may result in the expansion of a broader repertoire of antigen-specific T cells, thereby reducing antigen-loss tumour variants and potentially benefiting a larger proportion of patients. Furthermore, this approach could lead to the generation of immunological memory, which could be more beneficial for childhood patients to reduce the risk of relapse. Therefore, and following the success achieved in adult cancers, there is a lot of interest in the potential translation of PD-1 blockade into paediatric oncology.

As discussed in section 1.3.3, there are various biomarkers that can help to predict response to PD-1 blockade. In order to evaluate the potential application of this therapy in childhood cancers, it is essential to understand how these biomarkers differ in the paediatric population. Notably, paediatric cancers are generally known to carry fewer neoantigens and be less immunogenic than adult malignancies, with the notable exception of a small proportion of hypermutated paediatric tumours (190). Recent studies indicate that the frequency of mutations in childhood cancers is overall 14 times lower than in adult cancers (i.e 0.02-0.49 mutations per Mb), with significantly fewer mutated genes per tumour (187). Relapsed tumours, however, harbour significantly more mutations than primary tumours, and mutational burden increases with age (187). Furthermore, the repertoire of genetic mutations and epigenetic alterations in childhood cancers differs from that of adult tumours even in tumours with similar histology (191). However, it is important to note that responses to checkpoint inhibitors have been reported in adult cancers with a similar level of mutational burden (i.e breast cancer) (192, 193), evidencing the role of other factors in determining clinical responses.

Likely due to their lower immunogenicity, paediatric malignancies generally present low TIL infiltration and are hence described as immunologically cold tumours (194). In two cohorts of paediatric patients with solid tumours, low levels of TILs were described in most paediatric cancers, with metastatic sites generally harbouring larger infiltration of CD8 T cells (195, 196). A further insight into the type of immune infiltrate revealed that, in paediatric cancers, these are scattered within the tumour and are predominantly formed of TAMs that accumulate in areas of necrosis, with lower frequencies of DCs or lymphocytes as compared to many adult malignancies (196, 197).

In view of the role of PD-L1 expression as a response biomarker in adult cancers, a number of studies have assessed PD-L1 expression in paediatric cancers. However, the results of these are very discordant, and hence difficult to interpret. Some studies report high expression levels across a broad range of paediatric

malignancies (198, 199), whereas other studies report very low expression levels (200, 201). Of note, PD-L1 expression is dynamic and responds to environmental cues in the TME such as cytokines or cell-to-cell interactions (58). Hence, expression may change during the course of treatment or disease progression, making it difficult to draw strong conclusions from the result of a single biopsy.

1.4.1.1 Clinical experience of PD-1 blockade to date

Despite the growing number of clinical trials assessing PD-1 blockade in childhood cancers (Table 1-4), single agent studies in most tumour types have shown little therapeutic activity. Administration of Pembrolizumab showed no clinical efficacy in a cohort of 5 paediatric patients with progressive primary brain tumours (202), or in a larger cohort of 121 children screened for PD-L1-positive tumours (16 central nervous system; 5 lymphomas; 45 advanced solid tumours) where only 4 partial responses were reported (203). Similarly, Nivolumab as a monotherapy did not show anti-tumour activity in 20 patients with Ewing sarcoma (EWS) and osteosarcoma (204). In a study by Geoerger et al., which included 74 paediatric patients (12 osteosarcoma, 11 EWS; 11 NB; 10 rhabdomyosarcoma (RMS); 10 non-RMS soft tissue sarcoma; 6 Wilm's tumour; 5 HL; 1 non-HL lymphoma; and 8 other tumour types), partial responses were seen in only 2 HL and 1 atypical rhabdoid tumour after monotherapy with the PD-L1 blocking mAb Atezolizumab (203).

Although over 300 children have been treated with PD-1 blocking antibodies, significant clinical activity to single agent therapy has only been shown in paediatric HL and a few other case-report studies of EWS and bMMRD glioblastoma. In HL, adult phase I trials of Nivolumab and Pembrolizumab showed durable disease control, achieving an overall response rate of 83% and 65%, respectively (205, 206). Despite previous autologous stem cell transplant and targeted therapy, complete responses were seen in more than 15% of the patients (207). Similarly, Pembrolizumab achieved an overall response rate of 69% and a complete response of 22% in a phase II trial (208). Classical HL tumours treated with conventional therapies show strong PD-L1/2 expression due to frequent copy number alterations in the PDL1/2 locus, which is further increased in relapsed tumours after PD-1 blockade (209-211). This may contribute to the high rate of response to PD-1 blockade in HL tumours despite not having a particularly high mutational burden compared to other cancers (192). Although the number of paediatric patients with HL treated with checkpoint inhibitors is limited, preliminary results from single agent studies appear similar to the adult experience (212, 213).

Results from two more recent phase I/II trials evaluating PD-1 blockade in children or young adults with various solid tumour histologies (EWS, RMS, osteosarcoma, NB, melanoma) showed few or no objective responses (214, 215). In line with the previous findings, these studies also reported 60% objective responses in HL patients. Of note, PD-L1 positivity was part of the entry criteria of one of these trials, but as a consequence of the disappointing results, it was concluded that PD-L1 positivity was not sufficient as a predictive biomarker of response (215).

Paediatric MMRD glioblastoma is potentially favourable for checkpoint inhibition in that it exhibits a higher mutational load and increased predicted number of neoantigens compared to sporadic gliomas and other childhood cancers (216). In a case report, two children with bMMRD glioblastoma refractory to conventional therapies were treated with Nivolumab and showed remarkable reductions in tumour burden followed by durable remission (190). In another case report, a heavily pre-treated patient presenting with recurrent metastatic EWS achieved sustained remission after 9 cycles of Pembrolizumab (217).

Table 1-4. Ongoing clinical trials with PD-1/PD-L1 blockade as a monotherapy in childhood malignancies.

Drug	Target	Study phase	Age	Cancer types	Study ID
Nivolumab	PD-1	Phase II	>1 yr	GBM	NCT02550249
	PD-1	Phase I/II	1-18 yrs	bMMR deficient tumours	NCT02992964
	PD-1	Phase I/II	1-21 yrs	Solid tumours	NCT02901145
	PD-1	Phase I/II	1-40 yrs	Sarcoma, Solid tumours	NCT03465592
	PD-1	Phase I/II	12 mo – 18 yrs	Hypermutated cancers	NCT02992964
Pembrolizumab	PD-1	Phase II	1-29 yrs	bMMR deficient brain tumours excluding HGG, DIPG	NCT02359565
	PD-1	Phase I/II	0.5-17 yrs	Melanoma, solid tumours, lymphoma (PD-L1+, progressive)	NCT02332668
	PD-1	Phase II	>14 yrs	NK/T-cell lymphoma	NCT03107962
	PD-1	Phase II	>12 yrs	Bone and soft tissue sarcoma	NCT02301039
	PD-1	Phase II	>12 yrs	Bone and soft tissue sarcoma	NCT03092323

Drug	Target	Study phase	Age	Cancer types	Study ID
	PD-1	Phase I/II	6 mo – 17 yrs	Solid tumour, HL	NCT02332668
Atezolizumab	PD-L1	Phase I/II	0-30 yrs	Solid tumours	NCT02541604
	PD-L1	Phase II	>6 yrs	Metastatic Alveolar Soft Part Sarcoma	NCT03141684
Durvalumab	PD-L1	Phase I	1-17 yrs	Solid tumours, lymphoma, CNS tumours	NCT02793466
Avelumab	PD-L1	Phase I/II	<18 yrs	Lymphoma, relapsed or refractory solid tumours	NCT03451825
	PD-L1	Phase II	12- 49 yrs	Osteosarcoma	NCT03006848
*Accurate as of August 2020. Glioblastoma (GBM); bialelic mismatch repair (bMMR); diffuse intrinsic pontine glioma (DIPG); high-grade glioma (HGG); central nervous system (CNS).					

1.4.1.2 Combination strategies

The poor results from single agent studies highlight the need to design rational combinations of therapies to maximise the clinical benefit of PD-1 blockade in paediatric cancers. In view of the poor immunogenic nature of childhood malignancies, the combination of anti-PD-1 mAbs with cytotoxic therapies (radiotherapy, chemotherapy) (178, 218), or direct tumour-targeting immunotherapies holds great promise owing to their ability to reduce tumour burden and potentiate the release of tumour neoantigens (219). As summarised in Table 1-5, there are already multiple trials testing some of these combinations in childhood cancers, as well as other combinatorial approaches involving dual checkpoint blockade, which has led to significant clinical results in adult patients.

Table 1-5 Ongoing clinical trials of combination therapies including PD-1/PD-L1 blockade in childhood malignancies.

Drug	Target	Study phase	Age	Cancer types	Study ID
Nivolumab +Ipilimumab	PD-1 CTLA-4	Phase I/II	1-30 yrs	Solid tumours, sarcomas	NCT02304458

Drug	Target	Study phase	Age	Cancer types	Study ID
	PD-1 CTLA-4	Phase II	6 mo -21 yrs	High grade primary CNS tumours	NCT03130959
Nivolumab +Relatlimab	PD-1 LAG-3	Phase II/III	>12 yrs	Melanoma	NCT03470922
Nivolumab +Blinatumomab ± Ipilimumab	PD-1 CD19/CD3 CTLA-4	Phase I	>16 yrs	CD19-positive precursor B-lymphoblastic leukaemia	NCT02879695
Nivolumab + Brentuximab	PD-1 CD30	Phase II	5-30 yrs	Classic HL	NCT02927769
	PD-1 CD30	Phase I/II	>15 yrs	Non-HL	NCT02581631
Nivolumab + EBV virus specific T cells	PD-1 EBV-ST cells	Phase I	>12 Kg	EBV-positive lymphomas	NCT02973113
Nivolumab + Dinutuximab +131-I mIBG	PD-1 GD-2 RT	Phase I	1-18 yrs	Neuroblastoma	NCT02914405
Nivolumab +CPM ± radiotherapy	PD-1 CT RT	Phase I/II	<18 yrs	Solid tumours	NCT02813135
Nivolumab + Stereotactic radiosurgery	PD-1 RT	Phase I	>15 yrs	Chordoma	NCT02989636
Nivolumab + BMS-986205	PD-1 IDO1	Phase III	>12 yrs	Advanced melanoma	NCT03329846
Nivolumab + Azacytidine	PD-1 CT	Phase I/II	1-30 yrs	AML	NCT03825367
Nivolumab + K27M peptide	PD-1 Peptide vaccine	Phase I/II	3-21 yrs	DIPG, glioma	NCT02960230
Nivolumab + CT ± radiotherapy	PD-1 CT RT	Phase I/II	3-18 yrs	High-grade glioma	NCT04267146
Nivolumab ± Azacytidine ± surgery	PD-1 CT Surgery	Phase I/II	>39 yrs	Osteosarcoma	NCT03628209
Nivolumab + CPM/ Capecitabine/ Vinblastine	PD-1 CT	Phase I/II	4-18 yrs	Solid tumour Lymphoma	NCT03585465

Drug	Target	Study phase	Age	Cancer types	Study ID
Nivolumab + Entinostat	PD-1 HDAC inhibitor	Phase I/II	6-21 yrs	CNS, solid tumours	NCT03838042
Pembrolizumab + ABVD/ COPDAC	PD-1 CT	Phase II	3-25 yrs	Classical HL	NCT03407144
Pembrolizumab + Doxorubicin	PD-1 CT	Phase II	>12 yrs	Soft tissue sarcoma	NCT03056001
Pembrolizumab + Decitabine +Radiotherapy	PD-1 CT RT	Phase I	12 mo – 40 yrs	Relapsed and refractory solid tumours or lymphoma	NCT03445858
Pembrolizumab + Aldesleukin	PD-1 IL-2	Phase II	>15 yrs	Stage III/IV melanoma	NCT02748564
Pembrolizumab + iC9-GD2	PD-1 GD2 CAR-T cell	Phase I	All ages	Relapsed/ refractory Neuroblastoma	NCT01822652
Durvalumab + Tremelimumab	PD-L1 CTLA-4	Phase II	>16 yrs	Advanced rare tumours	NCT02879162

*Accurate as of August 2020. Chemotherapy (CT); Cyclophosphamide (CPM); Radiotherapy (RT); Central nervous system (CNS); Epstein Barr virus (EBV); Hodgkin's lymphoma (HL); Diffuse intrinsic pontine glioma (DIPG).

1.4.1.2.1 Chemotherapy

Cytotoxic chemotherapy is still the first line of treatment in most childhood cancers. Chemotherapy may cause temporary functional impairments in the immune system by depleting immune cells and inducing myelosuppression (220, 221). Nevertheless, the idea that chemotherapy-induced immunosuppression would diminish the efficacy of immunotherapy has been challenged by recent findings. Several studies report a combined additive effect, although the precise mechanism of action is not well-defined (222-227). Chemotherapy has been reported to modify the local TME in various ways, such as depleting Tregs, increasing antigen cross-presentation via neoantigens release or inducing immunogenic cell death (ICD) (222, 223). Chemotherapy-induced ICD is proposed to lead to the exposure of calreticulin and heat-shock proteins on the surface of dying cells, and the release of ATP and high-mobility group box 1 protein (HMGB1) into the extracellular matrix, amongst others. Once these DAMPs are released and

sensed by neighbouring immune cells, they are suggested to act both in the innate and adaptive arms of immunity to coordinate anti-tumour responses (223).

In regards to PD-1 blockade in adults, the combination of Nivolumab and platinum-based chemotherapy increased overall survival in patients with NSCLC in a non-randomised clinical trial (224). Additional preclinical studies showed that chemotherapeutic drugs sensitised tumours lacking immune infiltration to checkpoint inhibition, and promoted CD8 T cell-driven anti-tumour immunity (225). The mechanism underlying this combined effect might be related to the up-regulation of PD-L1 that some types of chemotherapy like paclitaxel induce in tumour cells (227). Alternatively, the decrease in Treg numbers induced by metronomic low doses of cyclophosphamide (CPM) could be driving the synergy with anti- PD-1/ PD-L1 mAbs in some tumour models (226, 228). Because of their relatively low levels of intracellular ATP, which is needed for the detoxification of CPM, Tregs are more susceptible to low doses of this chemotherapeutic agent than conventional effector T cells (229). Overall, there is a clear rationale for combining cytotoxic therapies with anti-PD-1 mAbs (Figure 1.8), although the specific mechanism of synergy may vary depending on the type of chemotherapy.

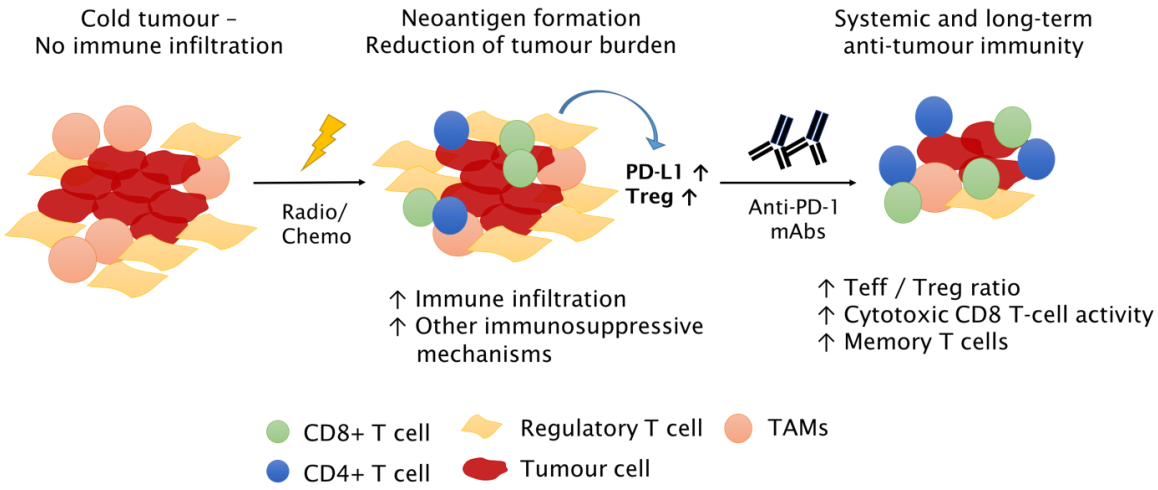

Figure 1.8 Rationale for combining chemo/ radiotherapy with PD-1 blockade. Treatment with cytotoxic agents can turn cold tumours into more immunogenic, hot tumours, by triggering neoantigen release, as well as reducing tumour burden. Nevertheless, these treatments lead to the up-regulation of alternative immunosuppressive mechanisms such as PD-L1, thereby inhibiting tumour-infiltrating immune cells. In this context, treatment with anti-PD-1 mAbs could release the inhibition and lead to increased infiltration of cytotoxic CD8 T cells and a more effective and long-lasting anti-tumour immunity.

Paediatric cancers are extremely sensitive to chemotherapy, which can lead to clinical responses in the majority of children, even in the context of relapsed

tumours. To accelerate the translation into childhood oncology, immunotherapy should perhaps aim to enhance the efficacy of these existing treatments to achieve greater efficacy with lower doses. This way, the toxic side effects derived from the intensive chemotherapeutic regimens could also be reduced.

1.4.1.2.2 Direct targeting mAbs

Combination of PD-1 blockade with immunotherapies that directly target tumour cells could provide a similar synergistic effect to that of cytotoxic therapies, promoting tumour cell death and antigen release (219). In solid tumours, the efficacy of direct tumour-targeting mAbs or CAR-T cells is generally dampened due to the presence of a dense immunosuppressive TME and the rise of antigen loss tumour variants, limiting the therapeutic activity of such treatments as a monotherapy (189, 230). Despite little preclinical evidence in paediatric cancers, a study in NB described an up-regulation of PD-1/ PD-L1 following therapy with direct targeting mAbs, supporting the combination of both approaches (231) for NB patients.

1.4.2 Neuroblastoma

Neuroblastoma is the most common extra-cranial solid malignancy of childhood, accounting for 6-8% of childhood cancers and over 15% of all paediatric cancer deaths (232). NB is an embryonic tumour that originates from sympathetic neural crest cells and displays a broad spectrum of clinical behaviour (232). Despite their high heterogeneity, NB tumours harbour recurrent somatic mutations that have prognostic value and help to stratify treatment intensity. Genomic amplification of MYC-N, which occurs in 20-30% of NB and over 40% of metastatic tumours, is strongly associated with advanced disease and poor outcome (233). MYC-N is normally expressed in the neural crest, participating in the regulation of differentiation and survival of developing neural cells, and its ectopic expression has been shown to be sufficient to drive NB tumorigenesis (234, 235). This strong association enabled the use of MYC-N gene status to form part of the clinical risk stratification system, together with age at diagnosis or tumour histopathology (232). Other genetic markers include activating mutations or gene amplifications of the anaplastic lymphoma kinase (ALK) gene, which are seen in approximately 10% of primary NB lesions (236, 237).

Amongst neuroblastoma patients, over 50% of children are classified as high-risk due to either metastatic disease at the time of diagnosis or the presence of MYC-N

amplification (232). The standard therapy for high risk NB includes induction chemotherapy, surgical excision of the primary tumour, followed by consolidation therapy comprising radiotherapy and intensive myeloablative chemotherapy with autologous bone marrow transplant (232). Providing a state of minimal residual disease can be achieved, patients are then treated with 13-cis retinoic acid (RA) as a maintenance therapy to induce terminal differentiation of neuroblastoma cells (Figure 1.9) (232). Following approval in 2015, the first mAb-based immunotherapy was introduced as part of the maintenance therapy for high-risk NB, and is now considered a standard component of treatment. This is reviewed in more detail in section 1.4.2.1.2.

Despite this aggressive treatment, which generally involves toxic side effects that limit the further intensification of these current regimens, long-term survival remains poor, with a three-year progression free survival (PFS) of only 30 - 40% in high-risk patients (238, 239). Therefore, there is a clear need for more effective and less toxic approaches to treat patients with high-risk NB.

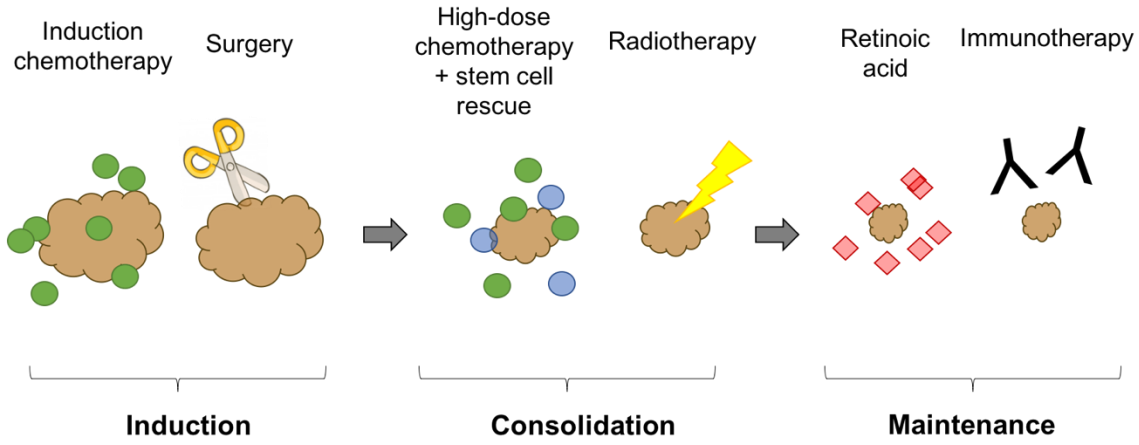

Figure 1.9 Schematic diagram of the current standard of care treatment for NB patients.
High-risk neuroblastoma includes patients presenting with metastasis or whose tumours have unfavourable biological features (e.g. MYCN amplification). The current treatment approach comprises induction multi-agent chemotherapy (incorporating rotating triplets of chemotherapeutic agents such as cisplatin, doxorubicin, cyclophosphamide and etoposide, amongst others), to reduce tumour burden and metastasis, followed by surgery of the primary mass. Consolidation therapy consists of myeloablative chemotherapy with autologous hematopoietic stem cell transplant, followed by targeted radiotherapy to the primary tumour bed. Oral cis-retinoic acid is given as a maintenance therapy, with the aim of promoting differentiation of residual neuroblastoma cells. More recently, anti-disialoganglioside (GD)2 antibodies led to further improvement in event-free survival and are now included as standard care for high-risk neuroblastoma patients.

1.4.2.1 The immune response to neuroblastoma

Numerous studies have demonstrated the presence of cellular and humoral anti-tumour immunity in patients with NB. The first evidence came from a study by Hellstrom IE et al. in 1968, who showed that blood lymphocytes and serum from NB patients reacted against autologous and allogenic tumour cells, inhibiting the in vitro formation of tumour colonies (240). Thereafter, several TAA were identified in multiple studies, reinforcing the idea of a natural anti-tumour immunity in these patients. These TAA included peptides from members of the melanoma antigen-encoding gene (MAGE) family, tyrosine hydroxylase and the MYC-N oncoprotein (241-245). Regarding the functional relevance of these TAA in the immunity against NB, antigen-specific T cells generated against the human MYC-N-derived peptide S9K were able to trigger MHC-I dependent cytotoxicity of MYC-N amplified NB cells (244). Likewise, vaccination with tyrosine hydroxylase DNA in vivo was able to induce T-cell dependent anti-tumour immunity and improve survival in mice with NXS2 NB tumours (245).

In a similar study by Coughlin CM et al., circulating T cells were detected in the blood of NB patients that were specific for the TAA survivin, an inhibitor of apoptosis that is widely expressed in NB (246). Although these tumour-specific T cells were incapable of infiltrating the tumour bed and exerting effective anti-tumour activity, they retained their functionality and were able to react against autologous NB cells in vitro (247). In preclinical studies, DNA vaccination with high affinity MHC-I-restricted peptides from survivin was sufficient to eradicate NB tumours in 50% of mice. Of these, over 80% also showed a reduction in tumour growth upon rechallenge (248), supporting the functional capabilities of survivin-specific T cells against NB.

1.4.2.1.1 Mechanisms of immune evasion

The above studies provide evidence of a natural, tumour-specific immunity in NB. However, the clinical manifestation and progression of the disease highlights the ability of cancer cells to avoid immune recognition and sustain tumour growth. It is widely established now that tumours can display a large array of mechanisms to evade immune attack. The majority of NB cells often present loss or downregulation of classic MHC-I molecules, which is often linked to a weak or absent mRNA level of molecules in the antigen processing machinery, such as transporter associated with antigen processing (TAP)-1 and TAP-2 (249-251). Although this lack of self MHC-I molecules in NB cells can dampen T-cell mediated immunity, it would

presumably make these cells more susceptible to NK-cell mediated killing. Nevertheless, NB tumours have also been shown to downregulate MIC-A and MIC-B proteins. These molecules are ligands for the activating receptor NKG2D present in both T and NK cells, thereby impairing NK cell-mediated cytotoxicity. Soluble MIC-A was also found in most patients' sera and was able to reduce NK-mediated killing of NB cells and decreased NKG2D expression in peripheral blood lymphocytes (252, 253). In a similar way, NB cells express non-classical human leukocyte antigen (HLA) molecules such as HLA-E and HLA-G, which are ligands for the inhibitory NKG2A receptor found on NK cells and T lymphocytes (254, 255). High expression of HLA-E inhibited NK cell-mediated cytotoxicity in vitro and in vivo, and promoted invasion and metastasis by inducing IL-10 and TGF-β secretion from NK cells (254).

As highlighted in section 1.1.2, the presence of immunosuppressive cell populations in the TME is an additional mechanism that has long been purported to dampen anti-tumour immunity in virtually all cancers. In NB, both immunosuppressive cytokines and cells have been found in blood from high-risk patients (256, 257). Whilst clinical evidence is limited, in vivo models have demonstrated the critical role that immunosuppressive regulatory T cells play in NB tumours, as depletion of these cells has been shown to enhance anti-tumour immunity after vaccination (257). Similarly, expression of inhibitory ligands on the surface of NB cells has been reported and can further limit anti-tumour immunity. As such, the inhibitory molecule B7-H3 was detected in the bone marrow of high-risk NB patients and was capable of down-regulating NK cell-mediated cytotoxicity (258). Moreover, expression of the inhibitory ligand PD-L1 has also been described in NB (259), but its inhibitory role will be discussed in more detail in sections 1.4.1 and 1.4.2.2.

Besides the recognition of a specific tumour antigen, engagement of co-stimulatory molecules is also required to induce an effective activation of T cells. These co-stimulatory receptors are sparse on NB cells and are likely to be limited in APCs due to the predominantly non-inflammatory and immunosuppressive tumour milieu (260, 261). For instance, gangliosides derived from murine NB cell lines impaired maturation of DCs and decreased the expression of the co-stimulatory receptors CD80/86 and CD40, as well as IL-12 production (261). Modulation of the co-stimulatory signal mediated by agonistic mAbs proved to have a therapeutic effect in preclinical in vivo models. In these studies, mAbs targeting the co-receptor 4-1BB or CD40 resulted in 60% survival in the Neuro2a murine model (262). Overall,

the aforementioned preclinical studies highlight the presence and relevance of a suppressive TME that can be targeted to achieve a better therapeutic efficacy in NB patients.

1.4.2.1.2 Immunotherapy: clinical experience targeting GD2

Despite the compiled evidence of anti-tumour immunity against NB-specific TAA, only one immunotherapy has been approved to be used in the clinical practice. Immunotherapy with mAbs directed against the disialoganglioside GD2 aim to specifically target tumour cells to trigger cytotoxic killing. GD2 is a glycolipid largely expressed on the surface of tumours of neuroectodermal origin, such as NB and melanoma (263). Importantly, this antigen is ubiquitously expressed by all NB tumours regardless of the stage, while its expression in normal human tissue is restricted to neurons, skin melanocytes and peripheral sensory nerve fibre, making it a good target for immunotherapy (264, 265).

One of the first anti-GD2 mAbs, the murine 14.18 antibody, was initially developed as an IgG3 isotype, but further reports indicated that the isotype-switch variant 14G2a (murine IgG2a) displayed increased effector functions by human cells (266, 267). In order to prevent human anti-mouse antibody (HAMA) responses against murine anti-GD2 mAbs (268) and increase effector functions, the chimeric Ch14.18 construct was developed, consisting of variable regions of the murine 14G2a mAb and constant regions of heavy and light chains from a human IgG1 antibody (269). In a pivotal randomised phase III trial, combination of the anti-GD2 mAb Dinutuximab (Ch14.18/SP2/0) with IL-2 and GM-CSF significantly improved 2 year event-free survival (EFS) and overall survival (OS) in patients with high-risk NB (189). This notable success culminated with the FDA approval in 2015 of this anti-GD2 mAb for the maintenance treatment of high-risk NB patients. A comparable anti-GD2 mAb cloned into Chinese hamster ovary (CHO) cells instead of murine hybridoma cells (dinutuximab beta, Ch14.18/CHO) (270) was later approved by the European Medicines Agency (EMA) and the National Institute for Health and Care Excellence (NICE) in the UK.

The major mechanism of action of anti-GD2 mAbs is proposed to be ADCC of GD2-expressing NB cells by NK cells, granulocytes and monocytes/macrophages (266, 267, 270, 271). In the presence of Ch14.18, both human peripheral blood mononuclear cells (PBMCs) and isolated NK cells were able to mediate efficient lysis of NB cells. Interestingly, the ability of granulocytes from both healthy donors and NB patients to mediate NB lysis appeared to be superior than PBMCs, and was

further augmented by addition of GM-CSF (271). In line with these findings, the stimulatory cytokines IL-2 and GM-CSF were included as part of the treatment schedule in the pivotal phase III clinical trial to enhance anti-GD2 mAb effector functions by NK cells and granulocytes/ monocytes, respectively (189). Nevertheless, subsequent studies conducted by the International Society of Paediatric Oncology Europe Neuroblastoma (SIOPEN) group established that co-administration of IL-2 did not improve EFS, but led to increased toxicity (272). Finally, although CDC has also been suggested to play a role in the anti-tumour activity of anti-GD2 mAbs (266, 267), complement activation is thought to contribute to antibody-induced neuropathic pain in NB patients. Because of this, the humanised hu14.18 mAb, which is currently in clinical testing, was engineered with the point mutation K332A at the Fc region with the aim of reducing complement activation and limit toxicity (273).

Despite the initial success of this immunotherapy, an update on the initial study by Yu A et al. (2010) described a reduction in the difference in PFS and OS between standard therapy and immunotherapy at 4 years compared to that of the preliminary results observed after 2 years (Figure 1.10) (274). This limited long-term efficacy highlights the need for a combination strategy that can provide long-term immunity, and hence potential combinations that could synergise with anti-GD2 therapy are currently being sought. For instance, TGF-β, which was found in blood and bone marrow in NB patients, decreased activating receptors on NK cells such as NKG2D and NKp30. In vitro inhibition of TGF-β rescued the expression of activating receptors and the cytotoxic ability of NK cells towards NB. Further in vivo studies indicated that the combination of TGF-β inhibitors and anti-GD2 therapy could extend survival in xenograft models compared to mAbs alone (275). In other studies, combination of anti-GD2 mAbs with chemotherapeutic drugs (topotecan and doxorubicin) induced efficient killing of NB cells in vitro and improved survival in syngeneic and human NB cell lines in vivo (276, 277).

Alternatively, immunomodulatory drugs that can boost T-cell responses could synergise with innate immune activation by anti-GD2 mAbs. As such, recurrent NXS2 tumours following therapy with anti-GD2-IL-2 immunoconjugates had increased expression of MHC-I molecules compared to primary tumours (278). This fact could enhance NB recognition and targeting by cytotoxic T cells. Hence, blocking the inhibitory PD-1 pathway in parallel with boosting immune responses against GD2 could lead to the generation of T-cell memory and may reduce tumour recurrence.

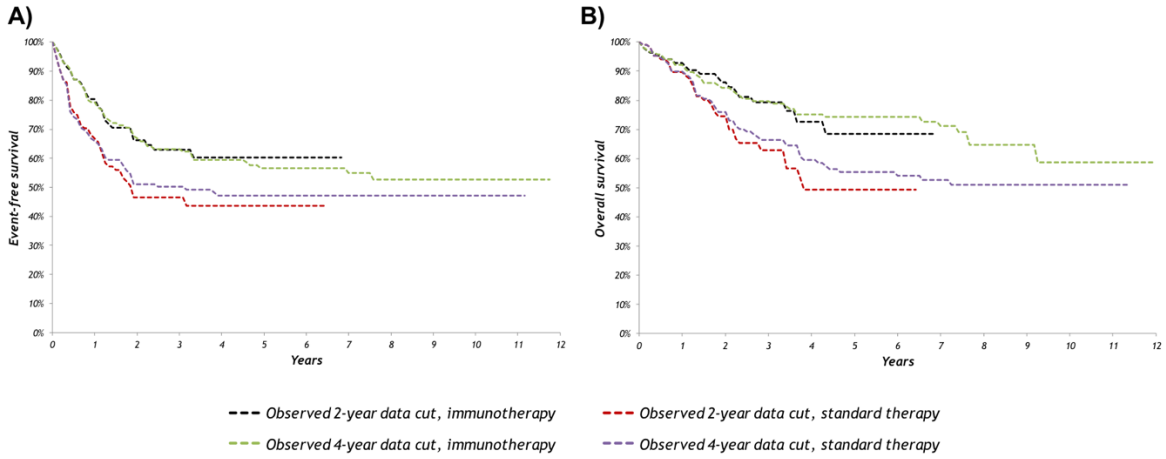

Figure 1.10 Observed PFS (A) and OS (B) in the primary 2-year and updated 4-year data analysis.
Comparison of the progression-free survival (A) and overall survival (B) data for the updated, 4-year analysis (March 2014), and the original 2-year analysis (June 2009) (274).

1.4.2.2 PD-1 blockade in neuroblastoma

1.4.2.2.1 Expression of PD-1/PD-L1 and correlation with outcome

As discussed in section 1.4.1, detection of PD-L1 expression by IHC on paediatric cancers is variable, depending on the study design but also in the tumour type. As summarised in Table 1-6, PD-L1 expression has been described in NB cells (up to 70%) and immune infiltrates (24%), although not all studies differentiate between immune cell- or tumour cell-associated expression. Importantly, PD-L1 has been found to be inducible in NB cells upon IFN-γ exposure in vitro and in vivo (Table 1-6). This implies that despite an initial lack of expression, PD-L1 could be up-regulated at the TME after immune cell activation and release of IFN-γ, leading to T-cell inhibition by PD-1 and therapeutic blockade with mAbs. In terms of PD-1, expression of this molecule has been reported to range between 16 – 40% in NB TILs or bone marrow infiltrates, although the number of studies is limited.

Table 1-6 Summary table of the expression of PD-1 and PD-L1 in NB.

Study	PD-1	PD-L1	Tissue
Zuo S., (2019) (279)	-	35% PD-L1 expression	IHC from NB patients
Majzner R.G., (2017) (198)	-	14% PD-L1 expression	IHC from NB patients
	-	24% PD-L1+ TAICs (amongst TAICs+ tumours)	IHC from NB patients
Melaiu O., (2017) (280)	16% TILs	34% PD-L1+	IHC from NB patients at diagnostic
Dondero A., (2016) (259)	-	Inducible upon IFN-γ exposure	In vitro culture of cell lines
	-	Inducible upon IFN-γ intratumoural injection	Subcutaneous SH-SY5Y NB cell line in vivo
	-	Inducible upon IFN-γ exposure	BM-derived neuroblasts from high-risk NB
	40% in CD3+ cells 2% in NK cells	-	Lymphocyte infiltration in BM from high-risk NB
Aoki T., (2016) (195)	-	No expression in tumour or immune infiltrates	IHC from NB patients
Chowdhury F., (2015) (199)	20-30% PD-1+ CD8+ TILs	72% PD-L1+ tumours	IHC from high-risk NB
Boes M., (2015) (281)	-	Baseline + inducible upon PolyI:C exposure	In vitro culture of cell lines

*Accurate as of August 2020. IHC (immunohistochemistry); TAICs (tumour-associated immune cells); TILs (tumour-infiltrating lymphocytes); BM (bone marrow).

Similar to many adult tumours, a high CD3 infiltration correlated with better outcome in NB patients (Table 1-7). Loss or down-regulation of MHC-1 molecules is a frequent event in NB tumours, thereby hindering T-cell immunity (249, 251). Expression of MHC molecules in tumour cells also correlated with better prognosis in NB, as these MHC+ tumour cells can be targeted by CD8 T cells through MHC-peptide: TCR interaction. In terms of PD-L1, whilst some studies found no correlation or a negative association between PD-L1 expression and clinical outcome, most suggested that PD-L1 correlated with poorer outcomes (Table 1-7). In a recent study, the average numbers of tumour-infiltrating CD8 and CD45RO tended to be lower in patients where pre-treatment samples were classed as PD-L1 positive (279). Also in this study, relapse was seen in 6/6 (100%) patients displaying PD-L1 positivity in post-chemotherapy biopsies, whilst only 3/9 (33%) patients with

PD-L1 negative biopsies exhibited tumour recurrence. Despite the small population size of this study, the presented results support that PD-1/ PD-L1 pathway could be actively inhibiting the proliferation of TILs before and after chemotherapy (279).

Table 1-7 Correlation of PD-1/ PD-L1 with outcome in NB.

Study	Expression	Correlation
Zuo S., (2019) (279)	PD-L1+ sample (trend)	Poor outcome
Srinivasan P., (2018) (282)	PD-L1+ and CD3+ infiltration	Low/ intermediate risk tumours
Majzner R.G., (2017) (198)	PD-L1+ sample (trend in PD-L1+ tumours)	Poor outcome
Melaiu O., (2017) (280)	HLA+ tumour or CD3+ density	Better outcome
	PD-L1+ regardless of HLA status compared to HLA ^{high} or PD-L1 ^{low}	Poor outcome
	PD-L1+ tumour density	No correlation
	PD-1+ TILs	No correlation
Dondero A., (2016) (249)	PD-L1 gene expression of primary tumours	No correlation
Chowdhury F., (2015) (199)	PD-L1+ expression/ PD-L1+ and PD-1+ CD8 high	Better outcome
*Accurate as of August 2020.		

1.4.2.2.2 Preclinical studies

Preclinical studies addressing the efficacy of checkpoint inhibitors in paediatric cancers are limited, and most of the evidence supporting the inhibitory activity of PD-1/ PD-L1 pathway comes from the study of protein expression of such molecules on tumour biopsies. Nevertheless, some studies have assessed the therapeutic activity of anti-PD-1 or anti-PD-L1 mAbs in murine models of NB. In a study by Srinivasan P. et al., PD-L1 blockade achieved 40% long-term survival as a monotherapy and 60% when combined with anti-CTLA-4 mAb. The N2a cell line was shown to be sensitive to IFN-γ and up-regulated PD-L1 in vitro and in vivo. In contrast, the more aggressive and less immunogenic counterpart (AgN2a) presented decreased CD3 infiltration compared to N2a and did not up-regulate PD-L1. Similarly, low- and intermediate-risk NB tumours had significantly higher CD3 and PDL1 expression compared to high-risk NB tumours (282). Thus, this work implies that aggressive NB tumours might be less immunogenic and less susceptible to PD1/ PD-L1 blockade.

Likewise, other studies indicate that monotherapy with anti-PD-1 mAbs has a rather poor therapeutic activity, but postulate that it can be combined with other immunotherapies and achieve synergistic effects. As such, addition of a depleting anti-CD4 mAb in combination with PD-1 blockade had a 100% curative rate in a mouse model of disseminated NB, perhaps suggesting that CD4+ Tregs are a key factor in limiting therapeutic activity of anti-PD-1 mAbs (283). Reduction of MDSCs through a selective colony stimulating factor 1 receptor (CSF1R) inhibitor also achieved tumour rejections in a spontaneous NB model when combined with anti-PD-1 mAbs. This combination re-polarised intratumuoral myeloid cells and facilitated T-cell recruitment to the tumour site (284, 285). Alternatively, treatment of 9464D tumours in vivo by STING-activating nanoparticles resulted in increased CD8 T-cell infiltration, reduced Tregs and increased therapeutic activity, which was further augmented with the combination of anti-PDL1 mAbs (286).

Following the FDA approval of anti-GD2 mAbs, the combination of this immunotherapy with PD-1 blockade is a promising and feasible strategy for high-risk NB patients. To date, only one study has assessed such combination. Siebert N. et al. reported that both NB cells and monocytes/ granulocytes from PBMCs up-regulated PD-L1 during ADCC conditions triggered by anti-GD2 mAbs. This was paralleled with an up-regulation of PD-1 on lymphocytes, all together indicating that PD-1-PD-L1 interaction could be an active resistance mechanism after anti-GD2 mAb therapy. Albeit to a low extent, addition of PD-1 blockade increased tumour cytotoxicity in vitro. In vivo, the addition of PD-1 blockade did not increase OS (80%) compared to monotherapy with anti-GD2 mAbs (90%), probably due to the already maximal therapeutic effect of the monotherapy (231).

Whilst the dual combination of anti-GD2 and anti-PD-1 mAbs offers great promise, it is conceivable that the prominent immunosuppressive cell populations at the TME could dampen the overall success of these therapies. In line with this, a triple combination approach is already being tested in the MiNivAN trial (NCT02914405), which aims to improve long-term survival in patients with NB by combining Nivolumab, anti-GD2 mAbs and targeted molecular radiotherapy (131-I mIBG). The rationale for this combination was initially based on preclinical data suggesting a synergy between immune- and tumour-targeting mAbs with radiotherapy, with the latter promoting a more favourable immune microenvironment through suppression of Tregs (287). Therefore, in this current work, pre-clinical studies were performed to assess these dual and triple combinations, with the ultimate aim

of inferring potential mechanisms of action and resistance, as well as obtaining clinically relevant information to inform the design of future clinical trials.

In summary, there is now sufficient evidence to suggest that PD-1/ PD-L1 interaction might be a key mechanism driving T-cell inhibition in adult and paediatric cancers. PD-1 blockade may have limited efficacy as a monotherapy in NB, and it is more likely to achieve therapeutic effects when combined with other forms of cytotoxic or immunomodulatory therapies. Hence, understanding the effect of anti-PD-1 mAbs in anti-tumour immunity and assessing different combinatorial regimens in preclinical models is important to establish the potential translation of PD-1 blockade into NB.

1.5 Hypothesis, aims and objectives

Recent studies highlight the impact of the Fc domain of anti-PD-1 mAbs on their anti-tumour activity. These studies suggest that anti-PD-1 isotypes lacking the ability to engage activating FcγR on TAMs are desired to prevent phagocytosis of PD-1-expressing T cells (104). Neuroblastoma has an extensive presence of TAMs (284) and expression of PD-1 and its ligand has been reported in the neuroblastoma TME (198, 199), but single agent anti-PD-1 therapy does not appear to have clinical efficacy in paediatric cancers (202, 214, 215). Therefore, it is important to study how different anti-PD-1 isotypes regulate anti-tumour immunity against neuroblastoma and explore combinatorial approaches that enhance the therapeutic activity of these mAbs.

1.5.1 Hypothesis

The hypothesis of this current work is that therapeutic checkpoint blockade can be achieved in neuroblastoma by optimising anti-PD-1 isotype and combining with other immunomodulatory therapies to induce more effective and long-term responses.

1.5.2 Aims and objectives

The overall aim is to determine the most optimal anti-PD-1 mAb isotype and investigate potential combination therapies in neuroblastoma models. To achieve this, the specific objectives of this project are as follows:

- Characterise three murine anti-PD-1 isotypes, namely mIgG1, mIgG2a and mIgG-N279A, in terms of their in vitro binding profile and ligand blocking capacity.
- Understand the role of anti-PD-1 isotype in modulating T-cell responses in vitro.
- Study the ability of different anti-PD-1 isotypes to enhance both endogenous and OT-I antigen-specific T-cell responses in vivo.
- Investigate the in vivo immune effects and anti-tumour activity of anti-PD-1 mAbs as a monotherapy in solid tumour models including MC38 and neuroblastoma.
- Explore the combination of an optimal anti-PD-1 isotype with cyclophosphamide and anti-GD2 mAbs in vivo in both 9464D and spontaneous TH-MYCN models of neuroblastoma, mirroring the schedule followed in the MiNivAN trial.

Chapter 2: Materials and methods

2.1 Animals

Animals were maintained by the Biomedical Research Facility (University of Southampton; Establishment licence 70/2906 XDA2EEF13) in accordance with Home Office regulations. All procedures were approved by the local ethics committee and performed in accordance with the Animals (scientific procedures) Act 1986 as set out in project licence (P81E129B7) and personal licence (PIL I510F102C).

Wild type C57BL/6 inbred mice were supplied by the Biomedical Research Facility (University of Southampton). Females (8 -12 weeks of age) were used in all experiments. All therapies were delivered by intra-peritoneal (Ip) injection using sterile needles.

2.1.1 OT-I Transgenic mice

TCR transgenic C57BL/6 mice, referred to as OVA-TCR-I (or OT-I), present $H2K^b$ restricted $OVA_{257-264}$ specific CTL clones (288). Detection of these cells by flow cytometry can be performed by staining with $H2K^b$-SIINFEKL tetramer, which selectively binds to OVA-specific T cells. OT-I mice were supplied by the Biomedical Research Facility (University of Southampton). Females (8 -14 weeks of age) were used as source of spleens for OT-I adoptive transfer experiments.

2.1.2 TH-MYCN Transgenic mice

TH-MYCN transgenic mice were first developed by Weiss WA. et al., (235). These mice are transgenic for the MYC-N gene, which is transcriptionally controlled by a tyrosine hydroxylase (TH) promoter that induces expression in neuroectodermal tissue to mimic presentation in human neuroblastoma. Whilst homozygous mice develop tumours at an early developmental stage, heterozygous mice may develop tumours at a later point, allowing the full development of the immune system before tumour presentation. Because of this, only heterozygous mice that presented with tumour after the first 6 weeks of life were used in experiments.

2.1.2.1 Genotyping of heterozygous TH-MYCN

Genotyping of TH-MYCNs was performed by amplification and detection of the MYCN gene in DNA samples. Ear tips from 1-2 months old mice were lysed and used to obtain DNA. Tips were transferred into polymerase chain reaction (PCR) tubes and mixed with 2.5 µl proteinase K (Thermo Scientific) and 100 µl of tail lysis buffer (50 mM Tris, 12.5 mM MgCl2, 0.5% Tween). Samples were incubated in a S1000 Thermocycler (BioRad) for 18 h at 55 ˚C followed by 1 h at 70 ˚C before being transferred to 4 ˚C. DNA samples (1 µl) were transferred to a fresh PCR tube together with the DNA of a positive control mouse. Samples were mixed with a PCR master mix containing 18 µl MiliQ water; 5 µl GoTaq 5x Buffer (Promega); 0.5 µl dNTPs (10 mM, Promega); 1 µl of each TH-MYCN reverse and forward primers (Sigma-Aldrich, see sequence below) and 0.3 µl GoTaq G2 DNA (Promega) enzyme. Samples were then run in the S1000 Thermocycler (see Table 2-1 for PCR settings) and loaded into an agarose gel (see 2.3.2). Gels were imaged in BioRad Gel Doc XR using Quantity One software.

Primer sequences:

- **MYCN_RT_F1:** CGACCACAAGGCCCTCAGTA
- **MYCN_RT_R1**: CAGCCTTGGTGTTGGAGGAG

Table 2-1 PCR settings for the genotyping of TH-MYCN transgenic mice.

Temperature (˚C)	Time	Number of cycles
92	2 minutes	-
92	15 seconds	x30
66	15 seconds	
72	30 seconds	
4	Standing	

2.1.2.2 Tumour monitoring

All heterozygous mice were palpated for tumours twice a week by trained animal technicians to check for abdominal/ paraspinal masses. Once tumours were detected, tumour growth was monitored and animals were treated when tumours reached 10 mm. Endpoint was determined by technicians when tumour-bearing mice presented with large tumour burden or animal welfare was compromised. In case of tumour clearance after therapy, tumour presentation and animal health was monitored for another 4 months before mice were culled.

2.2 Cell culture

2.2.1 Culture of cell lines

Cells used in this report are summarised in Table 2-2. All cell culture media was supplemented with 10% foetal calf serum (FCS), 100 U/ml penicillin-streptomycin (P/S) (Life Technologies), 2 mM L-glutamine (Life Technologies) and 1 mM pyruvate (Life Technologies) unless otherwise stated. Cells were cultured at 37°C and 5% CO_2 and passaged 2-3 times per week. Typically, cells were first washed with PBS. Adherent cells were then detached using sterile cell scrappers. Regarding tumour cell lines, adherent MC38 cells were dissociated by incubating with Trypsin-EDTA (ethylenediaminetetraacetic acid; Thermo Fisher) for 5 minutes at 37°C. Alternatively, 9464D cells were detached with TrypLE Express (Thermo Fisher), which contains cell-dissociation enzymes, by incubating cells for 5 minutes at 37°C. In both cases, enzymatic reaction was stopped by adding twice the volume of culture media. Following dissociation from flasks, cells were pelleted at 450 xg for 5 minutes, re-suspended in culture media and seeded in new flasks. Routinely, passaged cells were counted using a CellDrop Cell Counter (DeNovix).

Table 2-2 List of cell lines and culture conditions.

Cell line	Origin and cell type	Culture media	Properties	Specific information
HEK293F	Human embryonic kidney	Freestyle 293F media (Life Technologies)	Non-adherent	Culture in shaking at 8% CO2 @ 130 rpm
CHO-K1	Hamster ovary	RPMI 1640 (Thermo Fisher)	Adherent	-
CHO-K1-PD-L1	Hamster ovary	RPMI 1640 (Thermo Fisher)	Adherent	+ 10 µg/ml puromycin
RAW 264.7	Mouse monocyte/ macrophage	DMEM-high glucose (Thermo Fisher)	Adherent	-
J774A.1	Mouse monocyte/ macrophage	DMEM-high glucose (Thermo Fisher)	Mostly adherent	-
9464D	Mouse NB	RPMI 1640 (Thermo Fisher)	Adherent	+ 1.8 µl 2-β Mercapto-ethanol + 0.1 mM non-essential aminoacids No P/S

Lan-1	Human NB	RPMI 1640 (Thermo Fisher)	Semi adherent	No L-glutamine/ pyruvate
MC38	Mouse colorectal carcinoma	RPMI 1640 (Thermo Fisher)	Adherent	-
DMEM = Dulbecco's Modified Eagle's Medium; RPMI = Roswell Park Memorial Institute.				

2.2.2 Cell freezing and thawing

An average of 2-5 x10^6 cells were frozen using CryoTube vials (Thermo Fisher) in 1ml of culture medium containing 10% dimethyl sulfoxide (DMSO). For RAW 264.7 and J774A.1, medium was replaced for FCS containing 10% DMSO. For transfected CHO-K1, cells were frozen in medium in the absence of selection. For cell thawing, cells were rapidly transferred to pre-warmed media after initial thawing in a 37°C water bath for 1 minute. Cells were centrifuged at 450 xg for 5 minutes to remove any excess of DMSO and resuspended in fresh culture medium.

2.3 Molecular Biology

All DNA was quantified using a NanoDrop Spectrophotometer (ND-1000; V3.5.2 software); A260/280 ratios were used to assess the degree of protein contamination. DNA and glycerol stocks were stored at -20˚C.

2.3.1 Polymerase Chain Reaction (PCR)

Mouse CD274 cDNA (pCMV6-Entry vector) plasmid (OriGene) was amplified using PCR. Typically, 25 µl reaction mixtures contained the following: 2.5 µl of 10x buffer, 0.5 µl dNTPs (10mM, Promega), 1 µl DNA polymerase (Promega), 1 µl of 5' and 3' primers (100 ng/µl, OriGene), 1 µl cDNA template (100 ng) and 18 µl water. PCR reactions were performed on PTC-200 Peltier Thermal Cyclers (MJ Research), involving 25-30 cycles that consisted in serial incubation steps: 30 seconds at 95˚C (denaturation); 10 seconds at 60˚C (annealing); 1 minute per kb at 72˚C (extension) followed by 10 minutes at 72˚C (final extension).

2.3.2 Agarose gel electrophoresis

DNA fragments were separated according to size using agarose gel electrophoresis. Typically, 0.7 g UltraPure™Agarose (Invitrogen) was dissolved in

1X TAE buffer (40 mM Tris base, 20 mM acetic acid and 1 mM EDTA in distilled water). Agarose mix was supplemented with GelRed™ (Biotium) to enable the binding of DNA. Samples were mixed with 6x Orange DNA loading dye (Thermo Fisher) and loaded into agarose gels alongside a DNA size control (O-GeneRuler 1kb, ThermoFisher). Gels were typically run at 120-140V using a PowerPac-300 power supply (BioRad) and visualised using a Bio-Rad UV Transilluminator Imaging System and Quantity One® software (BioRad).

2.3.3 DNA digestion and extraction

Vector plasmids were digested using restriction enzymes in a 20 µl reaction mix, typically containing 2 µl 10x Multicore buffer (Promega); 1 µl EcoRI enzyme (Promega); 1 µl NheI enzyme (Promega); 1.5 µl pCI-Puro vector (1 µg); and 14.5 µl distilled water. Samples were incubated 1 hour at 37˚C and ran in an agarose gel (see 2.3.2) or amplified by PCR.

DNA bands of interest were excised from agarose gels with a scalpel and DNA was extracted using the QIAEX II Gel Extraction Kit (QIAGEN) as per manufacturer's instructions. Briefly, 1 ml of QX1 solubilisation buffer (7 M $NaPO_4$, 10 mM NaAc, pH 5.3) and 10 µl of QIAEX II solution beads were mixed with the excised gel bands and incubated for 10 minutes at 50˚C. Samples were washed with QX1 buffer followed by two washes with PE buffer (10 mM Tris-HCl, 80% ethanol, pH 7.5). Pellet was dried for 10 minutes and DNA was eluted in 20 µl TE buffer (10 mM Tris-HCl, 1 mM EDTA pH 8.0). Samples were incubated 10 minutes at 50˚C, pelleted and the supernatant containing DNA was collected.

2.3.4 DNA ligation

Cloning of mCD274 into pCI-Puro vector was performed using the Quick-fusion cloning kit (Biotool). Briefly, a 10 µl reaction was assembled, containing 1 µl fusion enzyme; 2 µl fusion buffer; 55ng of pCI-Puro (6 µl) and 20 ng of CD274 (1 µl) in a 2:1 molar ratio of insert:vector. Ligation mix was incubated at 37˚C for 30 minutes and kept on ice until transformation.

2.3.5 Plasmid transformation and bacterial cell culture

Plasmid transformations were performed by heat-shock method. DNA (100 ng) was added to JM109 *E.coli,* (Promega) at a ratio of 1 µl DNA: 10 µl of bacteria. The mix was then incubated for 30 minutes on ice, followed by 35-45 seconds in a 42˚C

water bath and another 2 minutes on ice. Next, 500 µl of S.O.C. medium (2% tryptone, 0.5% yeast extract, 10 mM NaCl, 2.5 mM KCl, 10 mM $MgCl_2$, 10 mM $MgSO_4$, 20 mM glucose; Invitrogen) was added, and bacterial cultures were incubated in a 37˚C shaking incubator (MaxQ 6000, ThermoScientific) for 1 hour. Cultures were plated on agar plates supplemented with selection antibiotic (50 µg/ml kanamycin or 100 µg/ml ampicillin) and incubated at 37˚C overnight. On the following day, individual colonies were picked and grown in 10 ml Lysogeny broth (LB) medium containing the appropriate selection antibiotic. Cultures were grown at 37˚C in a shaking incubator overnight and subsequently used for small-scale DNA purification. If a large-scale protein purification was to be performed, 10 ml of bacterial culture were added to conical flasks containing 100 ml LB cultures with appropriate antibiotic, and grown overnight at 37°C in a shaking incubator.

2.3.6 Small-scale plasmid purification (Miniprep)

DNA from 10 ml bacterial cultures of selected colonies was purified using the QIAprep® Spin Miniprep Kit (QIAGEN). Briefly, 10ml cultures were pelleted at 3220 xg for 5 minutes and mixed with equal amounts of P1 resuspension buffer (50 mM Tris-Cl, pH 8.0; 10 mM EDTA; 100 µg/ml RNase A) and P2 lysis buffer (200 mM NaOH, 1% SDS). After 5 minutes, 350 µl of neutralising P3 buffer (3 M potassium acetate, pH 5.5) was added to stop the reaction. Lysates were centrifuged 10 minutes at 15870 xg and supernatants were transferred to QIAprep2.0 spin columns, pelleted and washed three times with PE buffer to remove any residual buffer. Purified DNA was then eluted in 50 µl of EB buffer (10 mM Tris-Cl, pH 8.5).

2.3.7 DNA sequencing

Purified DNA from Miniprep was sequenced externally (Source BioScience) according to the traditional Sanger DNA sequencing method. Following confirmation of successful cloning, selected colonies were expanded in conical flasks containing 100 ml LB cultures with appropriate selection antibiotic, and grown overnight at 37°C in a shaking incubator prior to large-scale plasmid purification. In parallel, glycerol stocks were prepared by pelleting 10 ml bacterial cultures and resuspending with glycerol at a 1:1 ratio.

2.3.8 Large-scale plasmid purification (Maxiprep)

To purify sufficient amount of plasmid to be used in transfections, HiSpeed® Plasmid Maxi Kit (QIAGEN) was used as per manufacturer's instructions. Briefly, 100

ml bacterial cultures were pelleted at 3220 xg for 15 minutes and bacterial cultures were lysed as described in 2.3.6. Cell lysates were then transferred to a QIAFilter Cartridge and filtered with a a pre-equilibrated HiSpeed Tip column. DNA was washed with QC buffer (1 M NaCl; 50 mM MOPS, pH 7.0; 15% isopropanol), eluted with buffer QF (1.25 M NaCl; 50 mM Tris· Cl, pH 8.5; 15% isopropanol) and precipitated with isopropanol. The isopropanol-DNA mixture was filtered with a QIAprecipitator module, with a second wash step adding 2 ml of 70% ethanol. Finally, DNA was eluted from the module in 1 ml of TE buffer.

2.4 Transfection of plasmid DNA

2.4.1 Transient transfection in HEK293F cells

HEK293F cells (10^6 cells/ml in small conical flasks) were transfected with 5-10 µg plasmid DNA using the lipid-based 293Fectin™ Transfection Reagent (Invitrogen) at a 1:1 ratio of DNA:transfection reagent. Typically, DNA and transfection reagent were pre-diluted in equal amounts of Opti-MEM® I medium (Gibco) and incubated 5 minutes at room temperature (RT) before mixing. Mixtures were incubated at room temperature for 20-25 minutes to allow the formation of DNA-lipid complexes, and then added drop-wise to cells. Cells were incubated at 37˚C and 8% CO_2 in a shaking incubator for 24 hours.

2.4.2 Stable transfection of adherent cell lines

Three different liposome-based methods of transfection were used to stably transfect mCD274 DNA plasmid into the adherent cells lines RAW264.7, J774.A1 and CHO-K1. For all the methods, adherent cells were harvested using trypsin-EDTA (Lonza) on the day before transfection, resuspended in fresh culture medium and plated in 6-well plates. To reach a 60-80% confluence, RAW264.7 and J774.A1 cells were plated at $2x10^6$ cells/ well, whilst CHO-K1 were seeded at $3x10^5$ cells/well due to their faster proliferation rate.

After transfection, cells were subcloned in flat-bottomed, 96-well plates and selected in the presence of 1 µg/ml puromycin (InvivoGen) for RAW264.7 and J774.A1, or 10 µg/ml for CHO-K1. Growth of single colonies was monitored for 3-4 weeks and positive colonies were screened for CD274 expression by flow cytometry. Stable cell pools were sorted via fluorescence activated cell sorting (see 2.8.3) and frozen at early passages.

2.4.2.1 GenePORTER® Transfection Reagent (Genlantis)

DNA plasmid (4 µg/well) and 20 µl of GenePorter transfection reagent were diluted in Opti-MEM® I medium to a final volume of 500 µl. Diluted DNA was added to each GenePorter reagent Eppendorf at 1:1 ratio, mixed and incubated 15 minutes at RT. Culture medium was removed from wells before the DNA;transfection reagent mix was added drop-wise to cells. Plates were incubated 4 hours at 37˚C and 5% CO_2 before adding 1 ml of growth medium supplemented with 20% FCS. Cells were then incubated at 37˚C and 5% CO_2 for 2-3 days.

2.4.2.2 Lipofectamin®2000 Reagent (Invitrogen)

DNA plasmid (3.5 µg/well) and two different concentrations of lipofectamin reagent (6 and 9 µl) were diluted in Opti-MEM® I medium to a final volume of 150 µl. Diluted DNA was added to each lipofectamin reagent Eppendorf at 1:1 ratio, mixed and incubated 5 minutes at RT. Mixtures were added drop-wise to cells and plates were incubated at 37˚C and 5% CO_2 for 2-3 days.

2.4.3 FuGENE®HD Transfection Reagent (Promega)

DNA plasmid (2 µg/well) was diluted in Opti-MEM® I medium to a final volume of 100 µl. FuGENE reagent was pre-warmed at RT and added to DNA solution at different ratios of FuGENE reagent (µl):DNA (µg) (4:1. 3:1, 3:2). FuGENE:DNA mixture was incubated 15 minutes at RT before being added drop-wise to cells, which were then incubated 2 days at 37˚C and 5% CO_2.

2.5 Antibodies

In-house antibodies were purified on Protein A columns with purity assessed by electrophoresis (Sebia hydragel K20 system) and lack of aggregation determined by High Performance Liquid Chromatography (HPLC). Details of the in-house monoclonal antibodies used are listed below.

Table 2-3 List of in-house monoclonal antibodies used.

Name	Target	Isotype
Rat EW1-9	Mouse PD-1	Rat IgG1
Rat EW1-9	Mouse PD-1	Deglycosylated – Rat IgG1
Mouse EW1-9 m1	Mouse PD-1	Mouse IgG1

Mouse EW1-9 m2a	Mouse PD-1	Mouse IgG2a
Mouse EW1-9 m1N297A	Mouse PD-1	Mouse IgG1-N297A
14.G2a	Human/ mouse GD2	Mouse IgG2a
3-23M1	Mouse CD40	Mouse IgG1
JG1.1A	Human CD137	Rat IgG1
145-2C11	Mouse CD3	Hamster IgG
KT3	Mouse CD28	Rat IgG2a
GK1.5	Mouse CD4	Rat IgG2a
2.4G2	Mouse FcγR II, III	Rat IgG2b
AT10 m2a	Human CD32	Mouse IgG2a
AT10 m1	Human CD32	Mouse IgG1
AT10 m1N297A	Human CD32	Mouse IgG1-N297A
OKT3	Human CD3	Mouse IgG2a
Nivolumab (5C4)	Human PD-1	Human IgG4
Nivolumab (5C4)	Human PD-1	Human IgG4-FALA
AT171.2	Anti-ChiLob7/4	Human IgG4

2.5.1 Dialysis and quantification of antibodies

Antibodies were buffer-exchanged in endotoxin-low phosphate-buffered saline (PBS; 0.12 M NaCl (sodium chloride); 24 mM Na2HPO4 (disodium hydrogen phosphate); 5.8 mM KH2PO4 (potassium dihydrogen phosphate) in distilled water) using 10 kDa Slide-a-lyzer® Dialysis cassettes (Thermo Fisher). Typically, antibodies were dialysed in 1 L of PBS and left to stir for 1-2 hours, with 3-5 buffer exchanges per dialysis. Mouse antibodies were quantified with a NanoDrop Spectrophotometer, using a molar extinction coefficient of 1.45.

2.5.2 Antibody conjugation

Rat EW1-9 antibody was conjugated with Alexa Fluor®488 using the Protein Labelling Kit (Invitrogen). Briefly, antibodies were dialysed into PBS and adjusted to a concentration of 2 mg/ml. Protein was mixed with Alexa Fluor®488 reactive dye on a magnetic stirrer for 1 hour at RT in the dark. In parallel, purification column was loaded with resin and primed with PBS. Protein mixture was loaded into the

column and eluted with 1X elution buffer, carefully collecting the protein fraction and removing any excess dye.

2.5.3 Deglycosylation of antibodies

Rat EW1-9 was enzymatically deglycosylated using PNGase F (peptide:N-glycosidase F; Promega), that cleaves oligosaccharides from N-linked glycoproteins. PNGase F was mixed with antibody at a ratio of 200 µg of antibody: 1 µl of enzyme and incubated at 37°C overnight (~16 hours). Deglycosylation was confirmed using SDS-PAGE (see 2.5.4). Following confirmation, residual enzyme was removed by dialysing antibodies in PBS using a Pur-A-Lyzer Maxi (50 kDa) Kit (Sigma-Aldrich).

2.5.4 Sodium dodecyl sulfate polyacrylamide gel electrophoresis (SDS-PAGE)

Sodium dodecyl sulfate polyacrylamide gel electrophoresis (SDS-PAGE) is used to separate proteins according to size. To confirm the successful deglycosylation of rat EW1-9, 10-well BOLT™ 10% Bis-Tris Plus Gel (Invitrogen) were used to separate proteins ranging from 15 to 260 kDa. Briefly, 4 µg of wild-type and deglycosylated EW1-9 antibodies were diluted in miliQ water with either reducing or non-reducing dye a 1:4 ratio in a final volume of 16 µl. Mixtures were incubated 15 minutes at 95°C and run alongside 5 µl of a pre-stained protein standard (Novex®Sharp, Invitrogen). Gels were run in 20X MOPS-SDS Running buffer (1 M MOPS, 1 M Tris base, 2% SDS and 20 mM EDTA) at 200V for 30 minutes. Next, gels were incubated with Coomassie stain (0.1% Coomassie R250 (ThermoFisher); 10% acetic acid; 40% methanol) for 40 minutes at RT on a rocket, and distained with destaining buffer (20% methanol, 10% acetic acid in 1L distilled H_2O) (3-4 washes of 30 minutes).

2.6 Cell-based assays

2.6.1 Magnetic bead purification of mouse T cells

Mouse T cells or CD8 T cells were purified using the Pan T Cell Isolation Kit II or the CD8 Isolation Kit (Miltenyi Biotec) respectively, as per manufacturer instructions. Briefly, mouse spleens were harvested and mechanically dissociated into single-cell suspensions. Typically, 10^7-10^8 cells were pelleted at 450 xg for 5 minutes and resuspended in 40 µl of MACs Buffer (PBS; pH 7.2, 0.5% BSA (bovine serum albumin); 2 mM EDTA) per 10^7 cells. When working with higher numbers

($>10^7$), reagent volumes were scaled up accordingly. Cell suspensions were incubated 5 minutes at 4°C with 10 µl of Biotin-Antibody cocktail and washed with 30 µl of MACs Buffer, followed by a 10-minute incubation with 20 µl of Anti-Biotin MicroBreads at 4°C. For the magnetic bead separation, LS Columns (Miltenyi Biotec) were placed in suitable MACS magnetic separators and primed with 3 washes of 1 ml MACs Buffer. Labelled cell suspensions were then applied into the columns and the flow-through containing purified T cells was collected. Columns were finally rinsed with 3 washes of 1 ml MACs Buffer and flow-through was collected. Routinely, T cell and CD8 purity was confirmed by flow cytometry using APC-labelled anti-mCD3 mAb (Thermo Fisher, clone 17A2) or anti-mCD8 mAb (Thermo Fisher, clone 53-6.7) as detailed in section 2.8.1.

2.6.2 Stimulation of mouse T cells

To elucidate the kinetics of PD-1 expression in murine T cells, splenocytes or CD3+ purified T cells (2.6.1) were incubated for 24, 48 or 72 hours in the presence of soluble or plate-bound anti-CD3 (145-2C11, in-house) at different concentrations. Cells were harvested and stained to look at the surface expression of PD-1 by flow cytometry (see section 2.8.1 and Table 2-4).

2.6.3 Harvest and culture of bone marrow-derived macrophages

Murine bone marrow was harvested from the femur and tibia of wild-type C57BL/6 mice using a 20 ml syringe and 25 gauge needle, and washed in 20 ml of RPMI1640 media supplemented as detailed in section 2.2. Cells were counted and cultured at $4x10^6$ cell/well in 6-well plates in RPMI1640 media supplemented with 20% L929 conditioned media as a source of macrophage colony-stimulating factor (M-CSF) (see below). Bone marrow cells were cultured 6-8 days to differentiate into BMDMs, after which morphology was assessed with a CKX41 Olympus microscope connected to Cell B software (Olympus). Culture conditions were as described in section 2.2, with media washes on days 4, 6 and 8. For BMDM skewing, cells were stimulated for 24 or 48 hours with the following reagents: LPS (50 ng/ml, Sigma-Aldrich), IFN-γ (20 ng/ml, Peprotech), IL-4 (20 µg/ml, Peprotech) IL-13 (5 µg/ml, Peprotech). BMDMs were harvested by first washing twice with 1 ml sterile PBS followed by incubation with 1 ml of trypsin (15 minutes at 37°C) and a 15-minute incubation on ice. Then, BMDMs were gently detached using scrappers and stained for flow cytometry analysis or used in co-culture assays.

The murine L929 cell line (ATCC) was cultured in supplemented RPMI 1640 as described in section 2.2. Once confluence was reached, supernatants were collected and sterile filtered using Millex 0.22 µm PES membrane filters (Thermo Fisher) and stored at -20°C until required. L929 supernatant contains macrophage-colony stimulating factor (M-CSF) required to induce BMDM differentiation into macrophages during in vitro culture (289).

2.6.4 Binding curves

HEK293F cells were transiently transfected with a plasmid carrying murine PD-1 as detailed in section 2.4.1. Routinely, PD-1 expression was assessed by flow cytometry as detailed in section 2.8.1 to confirm the successful transfection. HEK293F cells expressing PD-1 ($2x10^5$) were incubated 30 minutes at 4°C in 96-well plates with the parental rat EW1-9 or the mouse isotypes IgG1, IgG2a or IgG1-N297A at concentrations detailed in figure legend. Plates were centrifuged for 5 minutes at 450 xg and cells were washed with PBS to wash away any unbound antibody. Cell suspensions were stained with APC-labelled anti-rat or PE-labelled anti-mouse secondary antibodies as described in section 2.8.1 to indirectly detect the amount of EW1-9 antibody bound to the cell surface. Cell autofluorescence was subtracted and data is shown as mean fluorescence intensity (MFI) at each concentration as a percentage of maximum binding.

2.6.5 Competition binding assay

HEK293F cells transfected with PD-1 (see section 2.4.1) were incubated with different concentrations of mouse EW1-9 antibodies (5, 2.5, 1.25, 0.625, 0.312, 0.078 µg/ml) for 30 minutes at 4°C in 96-well plates. Next, a constant amount of 1 µg/ml of Alexa Fluor®488-conjugated rat EW1-9 was added to wells and incubated 45 minutes at 4°C. Cells were harvested, transferred to 3 ml tubes and washed before acquisition on FACSCanto™. Cell autofluorescence was subtracted and data is shown as mean fluorescence intensity (MFI) of the rat EW1-9 antibody relative to the concentration of competitive mouse isotypes.

2.6.6 CFSE proliferation assays

CFSE (5-6-Carboxyfluorescein diacetate succinimidyl ester) Cell division tracker (BioLegend) consists of a fluorescent dye commonly used to indirectly measure lymphocyte proliferation. CFSE can passively diffuse into cells and covalently couple with intracellular molecules. Following each cell division, CFSE fluorescence will

progressively be halved, which enables the visualisation of cell subsets in different cell cycle divisions. Typically, cell suspensions were centrifuged for 5 minutes at 450 xg and resuspended in 1 ml of PBS at 10^7 cells/ml in a 50 ml tube. To stain, a final working concentration of 1 µM CFSE (5 mM stock solution) was pre-diluted in 5 µl PBS and placed at the side of the 50 ml tube. Cells were mixed with CFSE dye by inverting the tube, and were incubated for 10 minutes at RT in the dark. To stop the reaction, tubes were washed with 50 ml of culture medium containing 10% FCS and cell suspensions were resuspended and counted before use in in vitro assays.

2.6.7 ^{3}H-Thymidine incorporation assays

The ^{3}H-thymidine incorporation assay is another method to measure cell proliferation in vitro. Incorporation of the radioactive nucleotide ^{3}H-thymidine into new strands of DNA during cell division provides a means of measuring the proliferative capacity of cultured cells during the last 16 hours of culture. Typically, 1 microcurie/ well of radioactive ^{3}H-thymidine (Perkin Elmer) was diluted in culture media and 20 µl of the diluted solution were added into each well. Plates were incubated for 16 hours at 37˚C and 5% CO_2. Following incubation, cells were lysed using a harvesting system and transferred to filter plates (Opti-plate-96, Perkin Elmer). After a 2-hour incubation to air-dry the plates, 40 µl/ well of scintillation fluid (Perkin Elmer) were added and a scintillation β-counter was used to measure the DNA radioactivity recovered from the cells.

2.6.8 Suppression assay with recombinant proteins

Round-bottomed 96 well-plates were coated with 0.1, 1 or 5 µg/ml anti-CD3 mAb (in-house), diluted in 50 µl of PBS. An irrelevant huDR3-huFc and mPD-L1-huFc recombinant proteins (R&D Systems) were plated together with anti-CD3 mAb at 1 or 5 µg/ml. Plates were incubated overnight at 4°C to allow the proteins to bind the well's surface. On the following day, mouse CD8 T cells were purified as detailed in section 2.6.1. PBS was carefully removed from 96 well-plates with a multichannel pipette and wells were washed with PBS before adding the CD8 T-cell suspension at $4x10^4$ CD8 T cells/ well. Appropriate mAbs (anti-mPD-1 EW1-9 mAbs or irrelevant anti-huCD32 AT10 mAbs) were added at a working concentration of 5 µg/ml. For positive controls, 2.5 µg/ml of anti-mCD28 mAb (in-house) was also added, whilst negative controls comprised CD8 T cells alone. Following 3.5 days of culture at 37°C, radioactive ^{3}H-thymidine (see 2.6.7) was added to wells to measure cell proliferation during the last 16 hours of culture.

2.6.9 Cross-linking assay

The cross-linking assay was developed on the basis of the suppression assay previously detailed (2.6.8) but with the addition of mFcγR II to provide cross-linking of soluble mAbs. Briefly, enzymatic deglycosylation of anti-CD3 mAb (in-house) was achieved by PNGase F digestion (see 2.5.3) and confirmed by SDS-PAGE gel (see 2.5.4). Round-bottomed 96 well-plates were coated with 50 µl containing 0.1, 1 or 5 µg/ml deglycosylated anti-CD3 mAb plus 1, 2.5 or 5 µg/ml or recombinant proteins (mPD-L1-huFc, huDR3-hu-Fc or huLILRB3-huFc) depending on the assay. Next, 1, 2.5 or 5 µg/ml of mFcγR II recombinant protein (R&D Systems) was added in 50 µl of PBS dilution; depending on the assay, mFcγR II was added immediately after anti-CD3/Fc proteins or following an overnight incubation. In both cases, mFcγR II protein was incubated overnight at 4°C.

On the following day, mouse CD8 T cells were purified as detailed in section 2.6.1. PBS was carefully removed from 96 well-plates with a multichannel pipette and wells were washed with PBS before adding the CD8 T-cell suspension at $4x10^4$ CD8 T cells/ well. Appropriate mAbs (anti-mPD-1 EW1-9 mAbs or irrelevant anti-huCD32 AT10 mAbs) were added at a working concentration of 5 µg/ml. For positive controls, 2.5 µg/ml of anti-mCD28 mAb (in-house) was also added, whilst negative controls comprised CD8 T cells alone. Following 3.5 days of culture at 37°C, radioactive ^{3}H-thymidine (see 2.6.7) was added to wells to measure cell proliferation during the last 16 hours of culture.

2.6.10 Phagocytosis assay

BMDMs were harvested and differentiated as detailed in 2.6.3. On the day before the assay, BMDMs were harvested from 6 well-plates with 1 ml of trypsin (15 minutes at 37°C) and gentle scrapping with cell scrappers on ice. After centrifugation at 450 xg for 5 minutes, cells were resuspended in RPMI plus 20% L292 at $5x10^5$ cell/ml. 100 µl of cell suspension was added in flat-bottomed 96 well-plates and incubated overnight at 37°C in the absence or presence of 2 ng/ml IFN-γ and 50 ng/ml LPS. Media of wells was changed on the day of the assay to complete RPMI before co-culture with the T cells.

Primary mouse T cells were harvested and purified (see 2.6.1), and PD-1 expression was up-regulated by incubating T cells with 5 µg/ml of plate-bound anti-mCD3 mAb (145-2C11) for 48h prior to the assay. On the day of the assay, T cells were harvested using a multichannel pipette and resuspended in 1 ml to perform CFSE

staining (see 2.6.6). CFSE-labelled T cells were resuspended at $2.5x10^6$ cell/ml and 100 µl of cell suspension were transferred into a U-bottomed 96 well-plate to opsonise with 50 µl of mEW1-9 mAbs at 5 µg/ml. After a 30-minute incubation on ice, the 150 µl of cell suspension was added to 96 well-plates with BMDMs and incubated for 1 hour at 37˚C in the dark to allow phagocytosis of the target T cells. Next, 10 µl of pre-diluted APC-labelled anti-F4/80 mAb were added into wells and incubated for 15 minutes at RT. Finally, wells were washed twice with PBS and FACS wash buffer, and cells were scrapped with a pipette tip. Samples were run on a FACSCalibur™ flow cytometer to elucidate the percentage of double positive cells and analysed using FCS Express V3.

2.6.11 Peripheral blood mononuclear cell isolation

Leucocyte cones were obtained from healthy volunteers (National Blood Services) and human PBMCs were isolated using Lymphoprep density gradient medium (STEMCELL technologies). Briefly, leukocyte cone contents were diluted into a final volume of 50 ml with PBS supplemented with 2mM EDTA. Next, 25 ml of diluted blood was carefully layered onto two 50 ml falcons containing 12.5 ml of Lymphoprep at RT. Samples were centrifuged for 20 min at 800 xg (RT and with no brake). The interphase layer containing PBMCs was then removed using a Pasteur pipette and transferred into a fresh 50 ml tube. PBMCs were subsequently washed 3 times by diluting the sample to a final 50 ml volume with PBS supplemented with 2mM EDTA and centrifuged for 5 min at 300 xg (RT). Following the last wash, PBMCs were counted using a CellDrop Cell Counter (DeNovix) and used for subsequent assays.

2.6.12 Human suppression assay

To design a suppression assay with human T cells, isolated PBMCs (2.6.11) were used as a source of effector cells. Following the last wash, 1-2 x 10^7 PBMCs were transferred into a fresh 15 ml conical tube. After centrifugation at 450 xg for 5 minutes, PBMCs were resuspended in 1 ml of PBS and cells were labelled with 2.5 µM CFSE as detailed in section 2.6.6. For the optimisation of the assay, the kinetics of PD-1 expression on human T cells were assessed by pre-coating round-bottomed 96 well-plates overnight at 4°C with 50 µl of anti-hCD3 mAb (OKT3; in-house) at a range of concentrations, as detailed in figure legends. Next, 1, 2.5, 5 or 10 µg/ml of recombinant proteins (huPD-L1-huFc or mFGFR2b-huFc; R&D Systems) were added in the appropriate wells and incubated overnight at 4°C.

On the following day, PBS was carefully removed from 96 well-plates and CFSE-labelled human PBMCs were added at $5x10^4$ cells/ well and incubated at 37°C and 5% CO_2 in the presence or absence of relevant human antibodies (anti-ChiLob7/4 AT171.2, 5C4 IgG4 or 5C4 IgG4-FALA; in-house). Cells were harvested after 24, 48 or 72h and run in FACSCanto™ flow cytometer (BD Bioscience) following staining with flow cytometry mAbs: Pacific Blue-labelled anti-huCD8 (BioLegend); APC-labelled anti-huPD-1 (Thermo Fischer); PerCP-labelled anti-huCD3 (BioLegend) or APC-labelled anti-huCD4 (BioLegend).

2.7 In vivo studies

2.7.1 Antibody half-life

To assess the in vivo half-life of anti-PD-1 mAbs, 8-12 weeks-old wild-type C57BL/6 females were injected Ip with 250 µg of appropriate mAbs. Blood withdrawal (20 – 50 µl) was performed 1h, 24h, 48h, 7 and 14 days after Ip. Blood samples were incubated 2-3 hours at RT to allow the blood to clot. Samples were centrifuged at 2200 xg for 5 minutes, and then serum was removed using a pipette and transferred to a fresh tube. Serum samples were stored at -20 °C until used.

To be able to detect murine anti-PD-1 mAbs from serum, HEK293F cells were transiently transfected with a plasmid encoding mouse PD-1 as detailed in section 2.4.1. Next, $5x10^4$ cells were plated in round-bottomed 96 well-plates and incubated 30 minutes on ice with the specified serum dilutions or a known dilution range of anti-PD-1 mAbs, as detailed per figure legend. Plates were washed with PBS to remove unbound antibody and stained with APC-labelled anti-rat or PE-labelled anti-mouse secondary antibodies for 30 minutes on ice in the dark. Cell suspensions were washed again in FACS buffer and run in FACSCalibur™ flow cytometer to obtain MFI values. Percentage of maximum binding is shown relative to the highest MFI value from the corresponding standard curve. To elucidate the concentration in serum of murine EW1-9 mAbs, the equation from the linear range of the standard curve was used to extrapolate concentration values.

2.7.2 Adoptive cell transfer: OT-I model

To set up adoptive OT-I cell transfer experiments, spleens from 8-14 weeks old OT-I transgenic females were harvested and single-cell suspensions were prepared using cell strainers. Spleen cells were stained with PE-conjugated H2Kb-SINFEKEL tetramer, CD8 and CD62L antibodies and run on a FACSCalibur flow cytometer to

calculate the frequency of naïve OVA-specific CD8 T cells. Typically, 8-12 weeks-old wild-type C57BL/6 females were injected intravenously (IV) with $0.5x10^6$ OT-I CD8 T cells. On the following day, mice were immunised with 5 mg of OVA (Sigma-Aldrich) ± therapy (as detailed in specific figure legends) according to treatment group, and bled on days 3, 5, 7, 14 and 21 after treatment.

To perform a rechallenge, mice were bled between days 40 and 60 after initial immunisation in order to confirm that the levels of OT-I cells were below 10% of all CD8 T cells. Mice were then treated with 30 nM SIINFEKL peptide (Sigma-Aldrich) and bled on days 3, 7 and 21 after rechallenge. Routinely, 50 µl of blood were collected and immediately mixed with 5 µl heparin to avoid clotting. Blood was stained with $H2K^b$-SIINFEKL tetramer, CD8, CD62L, CD44 and PD-1 antibodies and incubated 20-30 minutes at RT in the dark. Next, 1 ml of 1x Red blood cell lysis (RBCL) buffer (Sigma-Aldrich) was added and incubated for 1-2 minutes. Cells were pelleted at 490 xg for 5 minutes and washed with 3 ml of FACs buffer prior to acquisition in a FACSCanto flow cytometer.

2.7.3 Syngeneic 9464D neuroblastoma model

The murine 9464D cell line was derived from a spontaneous TH-MYCN tumour (see section 2.1.2) and was kindly provided by Dr Rimas Orentas, NIH. 9464D cells were cultured in vitro at low passages as described in section 2.2. On the day of inoculation in wild type C57BL/6 mice, cells were washed twice in 10 ml of PBS and counted using an hemocytometer. Routinely, cell viability was assessed using Trypan Blue dye (Sigma-Aldrich) and confirmed to be >80% before challenging the mice. Thereafter, $5x10^5$ 9464D cells were subcutaneously inoculated on the right flank in C57BL/6 female mice aged 8-10 weeks at start of every experiment. Typically, 5 mice were used in each group unless otherwise stated in specific figure legends. Once tumours were palpable, growth was monitored 3 times/week using calipers,

2.7.3.1 Survival studies

For experiments in which therapeutic activity of mAbs was assessed, mice were randomly allocated to treatment groups when tumours were first palpable or reached 5x5 mm, with similar average sizes across treatment groups. Control mice were dosed with PBS alone or irrelevant isotypes following the same schedule as treatment groups. Mice were monitored/measured three times per week and culled when tumours reached a humane endpoint of 15x15 mm.

Administration schedules are detailed in figure legends of individual experiments. For antibody treatments, mAbs were diluted in sterile PBS to the appropriate concentration and administered Ip in up to 300 µl. When cyclophosphamide (CPM; Sigma-Aldrich) was administered, CPM crystals were weighted in a bijou up to the appropriate dose depending on the weight of mice. Typically, 20 – 100 mg/kg doses were prepared in sterile PBS and CPM was dissolved with vortexing. Once prepared, CPM doses were immediately injected Ip in 200 µl volume.

2.7.3.2 Calculation of blood counts

Typically, 30-40 µl of blood was withdrawn from mice and collected in the presence of 5 µl of heparin. Total volume was measured using a calibrated pipette. Next, 5 µl were used to count the total number of blood cells using a CellDrop Cell Counter (DeNovix). The remaining blood sample was stained for flow cytometry analysis (see 2.8.1) with the following markers: CD45, CD8 and CD4. To calculate total blood counts, the volume of heparin (5 µl) was subtracted to the total volume measured with the pipette. Then, the subtracted volume (blood) was divided by the total volume (blood plus heparin) to obtain the dilution factor specific for each sample. The number of counts obtained from the cell counter were then multiplied by the dilution factor to obtain the total number of cells per ml of blood. The percentage of CD8 and CD4 T cells obtained in flow cytometry was used to calculate the total counts of CD8 and CD4 T cells per ml of blood.

2.7.4 Syngeneic MC38 colorectal carcinoma

The murine colorectal carcinoma cell line MC38 was cultured in vitro at low passages as described in section 2.2. On the day of inoculation, cells were washed twice in 10 ml of PBS and counted using a haemocytometer. Routinely, cell viability was assessed using Trypan Blue dye (Sigma-Aldrich) and confirmed to be >80% before challenging the mice. Then, $5x10^5$ MC38 cells were subcutaneously inoculated on the right flank in C57BL/6 female mice aged 8-10 weeks at start of every experiment. Growth was monitored 3 times/week and tumours were measured using calipers.

For survival experiments, animals received 3 doses of 200 µg of appropriate antibodies on days 8, 12 and 15 after tumour inoculation. Average size of treatment groups at the start of the therapy was 7x7 mm. Animals were culled when tumours reached a humane endpoint of 15x15 mm. In the case of tumour clearance, animals were re-challenged 100 days post tumour inoculation. A group

of naïve mice were inoculated with MC38 alongside re-challenged mice, and tumour growth was monitored as detailed above.

2.7.5 Immunophenotyping of subcutaneous tumours and spleens

For immunophenotyping purposes, mice were treated when tumours reached 7x7 mm to enable sufficient tissue sample to be processed and stained. In 9464D-bearing mice, tumours and spleens were harvested 3 days after treatment with rat EW1-9 parental and deglycosylated. In both 9464D and MC38 models, therapy with murine anti-PD-1 isotypes was administered as 3 doses of 200 µg on days 1, 5 and 8 after tumours reached 7x7 mm. Then, 24 hours after the last dose, tumours and spleens were harvested and processed as follows.

Tumours were first dissected into small pieces on a petri dish using scalpels and transferred to universal tubes. Then, 1 ml of 1 unit/ml Liberase TL and 1 µl DNase (Roche) were added to each tube to aid the digestion of the tissue. Samples were incubated on a shaking incubator at 37°C for 15 minutes, after which 20 ml of media containing 10% FCS were added to each tube to stop the enzymatic digestion. Tumour and spleen samples were passed through a cell strainer with the help of a 5 ml syringe plunger to obtain single-cell suspensions, and then transferred to a 15 ml tube. Cells were pelleted at 490 xg for 5 minutes and resuspended in 5 ml PBS before counting. Spleens were mechanically disaggregated and passed through a cell strainer to obtain single-cell suspensions. Cell suspensions were transferred to 50 ml falcon tubes, pelleted at 490 xg for 5 minutes and resuspended in 10 ml of PBS for counting. Tumour and spleen cells were resuspended at 10^7 cells/ml in order to add 100 µl of cell suspension containing 10^6 cells in each 3 ml tube to stain for flow cytometry. To stain for T cell markers, spleen and tumour cells were incubated with 10 µg/ml of 2.4G2 antibody (in-house) for 15 minutes on ice, in order to block non-specific binding of staining antibodies. For all the panels, a master mix with all the staining antibodies was prepared and cells were stained as detailed in section 2.8.1 and 2.8.2.

2.8 Flow cytometry analysis of cell-surface molecules

Flow cytometry enables the study of different cell populations and the expression levels of an antigen of interest. Typically, up to 10^6 cells were stained and acquired using FACSCanto™ or FACSCalibur™ flow cytometers (BD Bioscience), and data was analysed using BD FACSDiva™ Software or FCS Express V3 (De Novo Software),

respectively. When looking at the expression of a relevant marker, fluorochrome- and isotype-matching antibodies were used as a control at the same concentration as the test antibody. Fluorochrome-conjugated antibodies used for flow cytometry analysis are listed below.

Table 2-4 List of antibodies used for flow cytometry

Target	Fluorochrome	Clone	Isotype
Rat IgG-Fc	APC	Polyclonal	Goat $F(ab')_2$
Mouse IgG-Fc	PE	Polyclonal	Goat $F(ab')_2$
mCD3	APC	17A2	Rat IgG2b, kappa
mCD4	eFluor 450	GK1.5	Rat IgG2b, kappa
mCD8a	APC	53-6.7	Rat IgG2a, kappa
mCD8a	PerCP-Cyanine5.5	53-6.7	Rat IgG2a, kappa
mCD45.2	PE-Cyanine7	104 RUO	Rat IgG2b, kappa
NK1.1	BV510	PK136	Mouse IgG2a, kappa
FoxP3	PE	FJK-16s	Rat IgG2a, kappa
CD11c	eFluor 450	N418	Armenian hamster IgG
Ly-6C	PerCP-Cyanine5.5	HK1.4	Rat IgG2c, kappa
Ly-6G	PE-Cyanine7	RB6-8C5	Rat IgG2b, kappa
CD11b	PE	M1/70	Rat IgG2b, kappa
MHC-II I-A/I-E	V500	M5/114.15.2	Rat IgG2b, kappa
F4/80	APC	Cl:A3-1	Rat IgG2b
mPD-L1/CD274	PE	MIH5	Rat IgG2a, lambda
Isotype	PE	eBR2a	Rat IgG2a, kappa
mCD25	APC	PC61.5	Rat IgG1, lambda
Isotype	APC	G0114F7	Rat IgG1, lambda
mPD-1/CD279	APC	RMP1-30	Rat IgG2b, kappa
Isotype	APC	eB149/10H5	Rat IgG2b, kappa
mPD-1/CD279	PerCP-eFluor 710	RMP1-30	Rat IgG2b, kappa
Isotype	PerCP-eFluor 710	eB149/10H5	Rat IgG2b, kappa
mPD-1/CD279	PE-Cyanine7	J43	Armenian hamster IgG
Isotype	PE-Cyanine7	eBio299 Arm	Armenian hamster IgG

mOX40/CD134	APC	OX-86	Rat IgG1, kappa
mLAG-3/CD223	APC	eBioC9B7W	Rat IgG1, kappa
Isotype	APC	eBRG1	Rat IgG1, kappa
EOMES	Alexa Fluor 488	Dan11mag	Rat IgG2a, kappa
LAMP-1/mCD107a	Alexa Fluor 488	eBio1D4B	Rat IgG2a, kappa
Isotype	Alexa Fluor 488	eBR2a	Rat IgG2a, kappa
T-bet	APC	4B10	Mouse IgG1, kappa
Isotype	APC	MOPC-21	Mouse IgG1, kappa
IFN gamma	APC	XMG1.2	Rat IgG1, kappa
Isotype	APC	eBRG1	Rat IgG1, kappa
TIM3/CD366	FITC	RMT3-23	Rat IgG2a, kappa
Isotype	FITC	eBR2a	Rat IgG2a, kappa
Ki67	FITC	16A8	Rat IgG2a, kappa
Isotype	FITC	RTK2758	Rat IgG2a, kappa
CD44	FITC	IM7	Rat IgG2b, kappa
Isotype	FITC	eB149/10H5	Rat IgG2b, kappa
CD62L	APC-Cyanine7	MEL-14	Rat IgG2a, kappa
Isotype	APC-Cyanine7	RTK2758	Rat IgG2a, kappa
CD62L	Pacific Blue	MEL-14	Rat IgG2a, kappa
Isotype	Pacific Blue	RTK2758	Rat IgG2a, kappa
CD49a	Alexa Fluor 488	HM-a2	Armenian hamster IgG
MHC-I (H-2K^{b}/H-2D^{b})	FITC	28-8-6	Mouse IgG2a, kappa
Isotype	FITC	MOPC-173	Mouse IgG2a, kappa
huCD3	PerCP	OKT3	Mouse IgG2a, kappa
huCD4	APC	OKT4	Mouse IgG2b, kappa
huCD8a	Pacific Blue	SK1	Mouse IgG1, kappa
huPD-1	APC	J105	Mouse IgG1, kappa

2.8.1 Surface staining

Routinely, 100 µl samples containing approximately 10^6 cells were stained in 5 ml tubes for 30 minutes at 4 °C in the dark, and washed with 3 ml of FACS buffer (PBS

+ 1% (w/v) BSA + 0.025% (v/v) sodium azide). Tubes were centrifuged at 490 xg or 450 xg for 5 minutes, supernatants were discarded and pellets were dissociated in the remaining volume (~100 µl) prior to acquisition.

2.8.2 Intracellular staining

Intracellular staining was performed to detect intracellular factors or cytokines using the Forkhead box protein 3 (FoxP3)/ Transcription factor buffer set (eBioscience™) according to manufacturer's instructions. Briefly, after staining for surface markers, 3 ml tubes were washed with 3 ml FACS buffer and pelleted at 490 xg for 5 minutes. Pellets were dissociated and mixed with 300 µl of FoxP3 Fixation/ Permeabilisation working solution, previously prepared by mixing 1 part of FoxP3 Fixation/ Permeabilisation Concentrate with 3 parts of FoxP3 Fixation/ Permeabilisation Diluent. Samples were incubated overnight (~16 hours) at 4˚C in the dark. On the next day, 1 ml of 1X Permeabilisation buffer (1 part of 10X Permeabilisation buffer with 9 parts of distilled water) was added to each tube, and cells were pelleted at 490 xg for 5 minutes. Following dissociation of the pellets, cells were stained with intracellular markers and incubated 45 minutes at 4˚C in the dark. Then, cells were washed with 1 ml 1X Permeabilisation buffer followed by a wash with 3 ml of FACS buffer, and stored at 4˚C until samples were acquired.

To perform intracellular staining of IFN-γ, 2-2.5 x 10^6 unstained cells were cultured in 2-2.5 ml complete RPMI in 12 well-plates at 37°C for 6 hours in the presence of 50 ng/ml phorbol 12-myristate 13-acetate (PMA; Sigma-Aldrich), 1 µg/ml ionomycin (Sigma-Aldrich) and 1 µl/ml of Golgi Plug (BD Bioscience). Then, cells were transferred to 15 ml tubes and centrifuged at 490 xg for 5 minutes. Cells were re-suspended in 100 µl of FACS buffer, incubated 10 min at RT with the blocking 2.4G2 antibody and surface and intracellular stained as detailed in sections 2.8.1 and 2.8.2.

2.8.3 Fluorescence-activated cell sorting

Transfected colonies were sorted using a FACSAria-II flow cytometer (BD Biosciences) to select specific expression levels of the antigen of interest. To prepare cells for sorting, cells were opsonised with an antigen-specific fluorochrome-conjugated antibody for 30 minutes at 4°C in the dark. Cells were washed and resuspended in culture medium. After sorting on the desired populations, cells were collected in FACS tubes containing FCS, washed in growth

medium and plated in a single well of a flat-bottomed, 96-well plate with selection medium supplemented with Ciprofloxacin (Sigma-Aldrich) for the first 24 hours. Cells were gradually expanded in selection medium and frozen at early passages.

2.9 Surface Plasmon Resonance (SPR) analysis

Antibodies were characterised by Surface Plasmon Resonance (SPR), which is an optical method that can be used to detect protein: protein interactions by immobilising recombinant proteins on a metal film and measuring the increase in refractive index upon binding of a soluble analyte (290). For all SPR analyses, a BIAcoreT100 analyser and a His Capture Kit (GE Healthcare Life Sciences) were used. Briefly, anti-His mAbs were immobilised at 5000 resonance units (RU) to the flow cells of CM5 sensor chips by standard amine coupling according to the manufacturer's instructions. Soluble analytes were flowed over as described in each specific experiment. Following each cycle, regeneration of the surface was carried out with 10 mM Glycine pH1.5 for 1 min to completely remove analytes from the surface of the chip. Binding of proteins was measured as an increase in RUs from baseline and results plotted as sensograms.

2.9.1 Binding kinetics and affinity

His-tagged mouse PD-1 recombinant protein (R&D Systems) was captured onto the chip (2000 RU) and soluble murine anti-PD-1 antibodies were injected through the flow cells at 100, 20, 4, 0.8, 0.16 nM in HBS-EP+ buffer (10 mM Hepes, 150 mM NaCl, 3 mM EDTA, 0.005% Tween-20; GE Healthcare Life Sciences) at a flow rate of 30 µl/min. Blank flow cell (HBS-EP+ buffer) was automatically subtracted from all curves. Bivalent fitting model was used to calculate Ka/Kd values (291).

2.9.2 FcγR binding profile

His-tagged recombinant proteins (R&D Systems) of the four mouse FcγRs (I, II, II, IV) were captured onto the chip (1000 RU) and soluble murine anti-PD-1 antibodies were injected through the flow cells at 500, 166.7, 55.5, 15.5, 6.2 nM in HBS-EP+ buffer at a flow rate of 30 µl/min. Blank flow cell (HBS-EP+ buffer) was automatically subtracted from all curves.

2.9.3 Blocking of PD-L1/2

His-tagged mouse PD-1 recombinant protein was captured onto the chip (2000 RU) and soluble murine anti-PD-1 antibodies were injected at a flow rate of 100 µl/min and 100 µg/ml to saturate the chip. HBS-EP+ buffer was injected as a negative control. Fc-recombinant PD-L1 or PD-L2 protein (25 µg/ml ; R&D Systems) or HBS-EP+ buffer were next injected at 25 µl/min.

2.10 Statistical analysis

All statistical tests were performed using GraphPad Prism 7 Software. Graphs show mean ± standard deviation (S.D) unless otherwise stated. Statistical differences between two samples were assessed by unpaired two-tailed T tests unless otherwise stated. When more than two groups were compared, statistical differences were assessed by one-way ANOVA test unless otherwise stated. Survival differences were analysed by Log Rank tests. Differences were considered statistically significant when $p < 0.05$.

Chapter 3: In vitro characterisation of murine anti-PD-1 mAbs

3.1 Chapter introduction

Recent studies highlight the importance of the interaction between FcγRs and the Fc domain for the anti-tumour activity of anti-mouse PD-1 (hereafter referred to as anti-PD-1) mAbs (104). In order to study the specific requirements of anti-PD-1 mAbs in the context of anti-tumour immunity, mAbs with the same PD-1 epitope specificity but distinct Fc regions were generated in-house. The parental anti-PD-1 mAb EW1-9 rat IgG1 was raised in-house by Dr. Emily Williams (University of Southampton) using conventional immunisation and hybridoma technologies (117). In order to avoid the generation of anti-rat antibody responses in our murine models, murine EW1-9 mAbs were generated by Dr. Claude Chan using standard recombinant approaches to change the Fc domain from rat IgG1 to mouse IgG1 or mIgG2a. Additionally, mIgG1 was further modified by site-directed mutagenesis at the 297 residue (EU numbering (292)) in the C_{H2} region to express the N297A mutation. These mouse Fc regions were selected because of their differential FcγR engagement selectivity, as illustrated in Figure 3.1. Whilst mIgG1 binds the inhibitory and only one low-affinity activating FcγRs, thereby bearing low A/I ratio (A/I=0.1), mIgG2a binds multiple activating FcγRs, including the high-affinity receptor, resulting in a high A/I ratio (A/I=69) as calculated by Nimmerjahn and Ravetch (112). Furthermore, the asparagine (N) to alanine (A) substitutions at residue 297 of the N-linked glycosylation site has been shown to reduce binding to FcγRs and abrogate effector functions (95, 96), and was chosen for its almost null FcγR engagement. In this first chapter, the binding properties of the three murine anti-PD-1 isotypes were characterised, as well as their ability to block PD-1 and their downstream effect on T-cell stimulation in vitro.

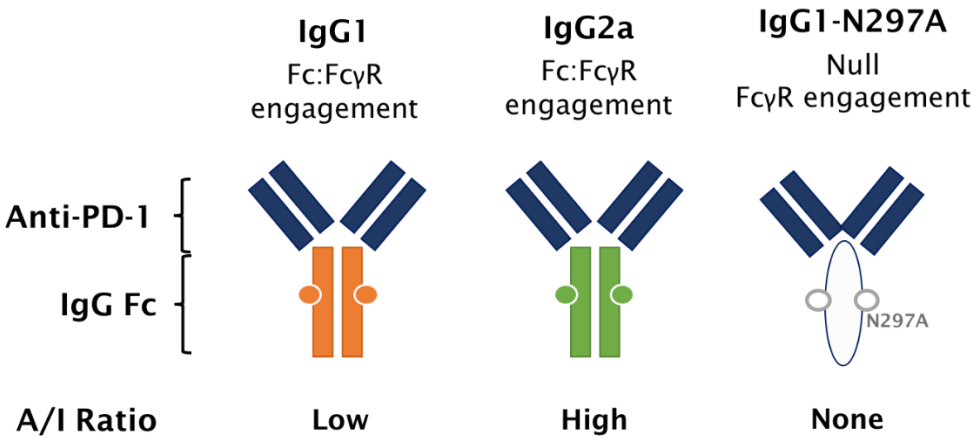

Figure 3.1 Distinct subclasses of murine anti-PD-1 mAbs.
All three antibodies retained the same epitope specificity, but their Fc regions were engineered to have distinct FcγR engagement patterns and thus differential ability to trigger effector mechanisms. Whilst mIgG1 binds the low-medium affinity activating FcγRIII as well as the inhibitory FcγRII (low A/I ratio), mIgG2a preferentially binds activating FcγRs with high affinity, yet retaining binding to FcγRII (high A/I ratio). On the contrary, mIgG1-N297A has impaired FcγR engagement (null A/I ratio) (112).

3.2 In vitro characterisation of murine anti-PD-1 mAbs

3.2.1 Murine FcγR binding pattern

The first step to characterise the different engineered murine anti-PD-1 isotypes was to confirm their FcγR binding pattern. To this end, a SPR assay was designed (Figure 3.2 A) in which anti-His antibodies were captured onto the dextran matrix of a CM5 sensor chip. His-tagged mouse FcγRs fusion proteins were injected in different flow cells and captured onto the chip by anti-His antibodies. Subsequently, murine and rat anti-PD-1 mAbs were flowed over the chips and their binding was measured as detailed in figure legend (Figure 3.2). The change in mass on the chip is represented in the sensorgrams as a deflection of the curve. As shown in Figure 3.2 B, mIgG1 displayed a very similar binding pattern to the parental rat antibody, only binding FcγRII and III with low affinity. Mouse IgG2a isotype bound with higher affinity to the activating FcγRI and IV, whilst showing a low affinity for the inhibitory FcγRII and activating FcγRIII. On the contrary, mutation of the 297 residue abrogated any FcγR interaction with the Fc of the antibody under these conditions. Hence, these results confirmed that the three murine engineered anti-PD-1 mAbs had the expected FcγR binding pattern, with mIgG2a displaying a higher A/I ratio than mIgG1, and mIgG1-N297A lacking FcγR binding ability.

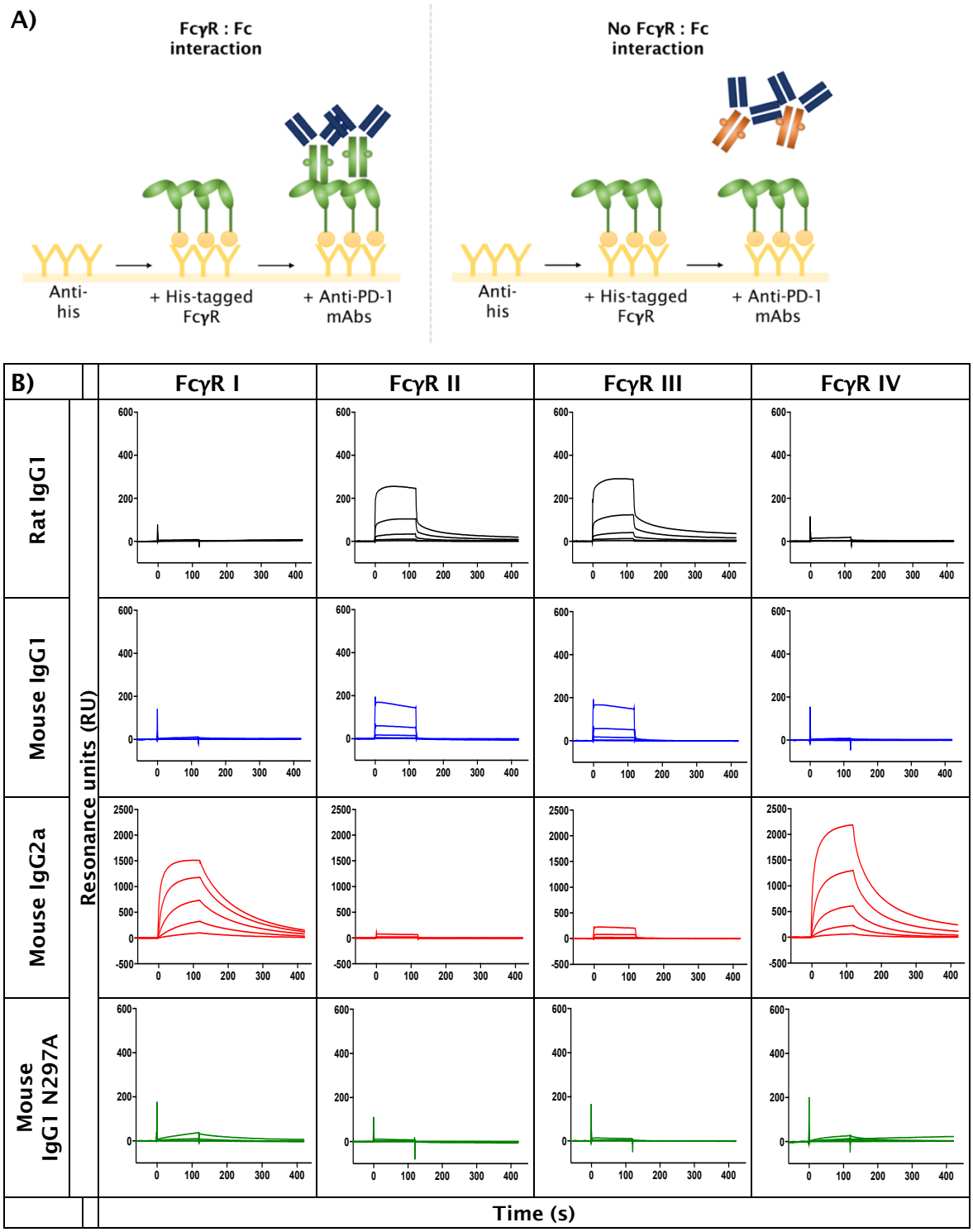

Figure 3.2 FcγR engagement by anti-PD-1 (clone EW1-9) mAbs.
A) Schematic representation of SPR analysis. (B) Sensograms showing binding of anti-PD-1 mAbs mIgG1, mIgG2a, mIgG1-N297A and the parental rat IgG1 to mouse FcγRs. Recombinant anti-His antibodies were immobilised at 5000 resonance units (RU) onto CM5 sensor chips by standard amine coupling. His-tagged mouse FcγRs (I, II, II, IV) were then captured onto the chip at 1000 RU. Soluble anti-PD-1 mAbs were injected through the flow cells at 500, 166.7, 55.5, 15.5, 6.2 nM in HBS-EP+ buffer at a continuous flow rate during 120 seconds. Buffer was then flowed over for another 300 seconds to allow the bound FcγRs: mAbs complexes to dissociate. Finally, the surface was regenerated to remove any remaining complexes but maintaining His-tagged FcγRs on the surface of the chip. This sequence was repeated with the various anti-PD-1 mAb isotypes and concentrations.

3.2.2 Ability to block PD-1/PD-L interaction

Next, the ability of murine anti-PD-1 mAbs to bind PD-1 and block the interaction between PD-1 receptor and its ligands was confirmed. For this, a His-tagged recombinant PD-1 protein was captured onto the sensor chip by anti-His antibodies (Figure 3.3 A). Then, soluble murine anti-PD-1 antibodies or buffer alone were flowed over the chip, followed by PD-L1 and PD-L2 recombinant proteins. Interaction with PD-1 in the presence or absence of anti-PD-1 mAbs was detected on the sensograms. As displayed in Figure 3.3 B, both ligands were able to bind to PD-1 in the absence of blocking antibodies (black lines). Addition of all murine anti-PD-1 mAbs abolished the interaction, indicating that these mAbs can effectively block PD-1: PD-L1/2 interaction.

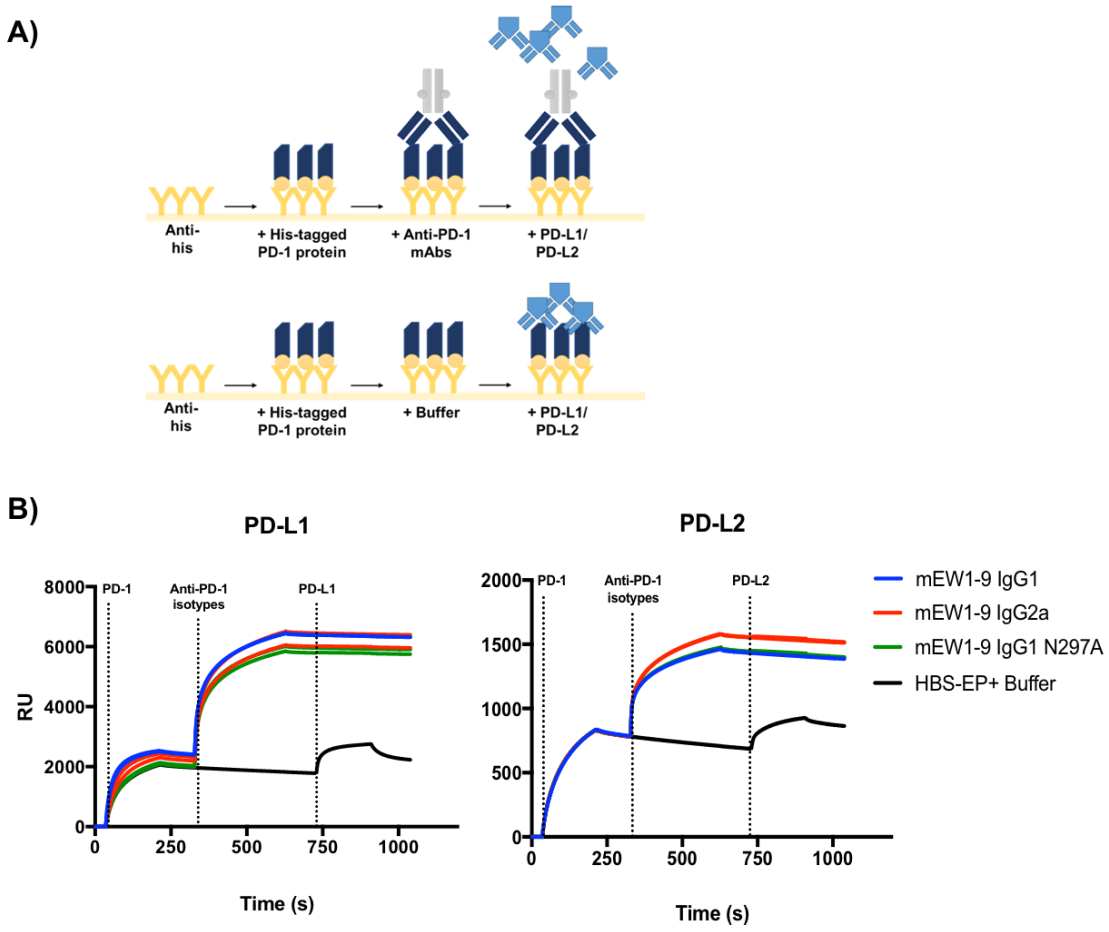

Figure 3.3 Ability of murine anti-PD-1 mAbs to block ligand interaction.
A) Recombinant anti-His antibodies were immobilised at 5000 RU onto CM5 sensor chips, and His-tagged mouse PD-1 recombinant protein was captured onto the chip at 2000 RU. Murine anti-PD-1 mAbs (100 μg/ml) or HBS-EP+ buffer were injected into the flow cell until saturation was reached. Lastly, Fc-recombinant PD-L1 or PD-L2 proteins were injected at a continuous flow rate during 200 seconds. Buffer was flowed to allow dissociation of protein: protein complexes prior to surface regeneration at the end of each cycle. Each anti-PD-1 mAb or control buffer were run in duplicate cycles. B) Results were plotted as sensograms, showing mass (RU) across time (s).

In order to study which immune populations express PD-1 within the TME, simultaneous detection of PD-1 expression during treatment with therapeutic anti-PD-1 mAbs was required. Hence, the ability of the anti-PD-1 clone RMP1-30, frequently used in flow cytometry analysis, to bind PD-1 in the presence of the EW1-9 clone, was assessed. As shown in Figure 3.4 A, detection by flow cytometry of surface PD-1 on transfected HEK293F cells was equivalent in the absence or presence of murine EW1-9 antibody clones, yet undetectable with an irrelevant fluorochrome-labelled antibody. These results were confirmed by SPR following a similar approach to that of Figure 3.3. However, in this case, the RMP1-30 mAb was injected instead of PD-L1/2 proteins (Figure 3.4 B) in the presence (blue line) or absence (black line) of EW1-9 rat anti-PD-1 mAb bound to PD-1. Similar to the results from flow cytometry, RMP1-30 mAb had the ability to bind PD-1 even in the presence of therapeutic anti-PD-1 antibody, and thus indicated that this clone could be used in subsequent flow cytometry studies.

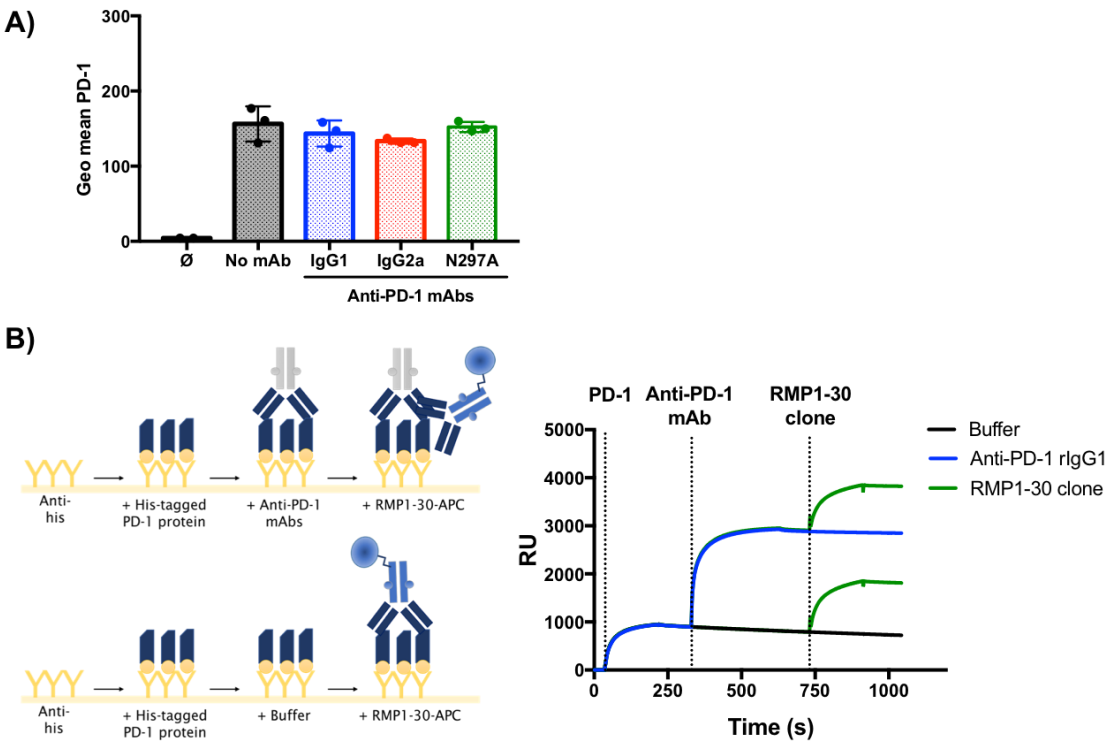

Figure 3.4 Binding of RMP1-30 clone to PD-1 in the presence of anti-PD-1 mAbs. A) HEK293F cells were transiently transfected with a plasmid encoding mouse PD-1 protein. Cells were incubated with murine anti-PD-1 mAbs (EW1-9 clone) prior to staining with RMP1-30. Detection was performed by flow cytometry. Experiment performed once with triplicates. Bars represent mean MFI ± SEM. B) Recombinant anti-His antibodies were immobilised at 5000 RU onto CM5 sensor chips by standard amine coupling, and His-tagged mouse PD-1 recombinant protein was captured onto the chip (2000 RU). Saturating concentrations (100 µg/ml) of murine antibodies or HBS-EP+ buffer were injected into the flow cell before RMP1-30 mAb (25 µg/ml) was injected. B) Results were plotted as sensograms, showing mass (RU) across time (s).

3.2.3 Binding kinetics and avidity

Therapeutic mAbs are usually characterised by medium-to-high binding affinities (10^{-7} – 10^{-12} K_D) (293, 294). In contrast to monovalent affinities, the avidity of mAbs takes into account the bivalent binding to the target molecule (92). To confirm an equivalent avidity of the murine anti-PD-1 mAbs, binding kinetic studies were performed. Similar to previous assays, mouse PD-1 protein was immobilised onto a CM5 sensor chip and a range of concentrations of the murine anti-PD-1 mAbs were injected into the flow cells in different cycles. From the binding curves obtained, a fitting model was applied to calculate the predicted avidity of murine mAbs (291). The similar binding curves (Figure 3.5 A) together with the similar K_D values used to calculate the avidity (Figure 3.5 B) confirmed that all three murine anti-PD-1 mAbs had a comparable high avidity towards mouse PD-1.

A)

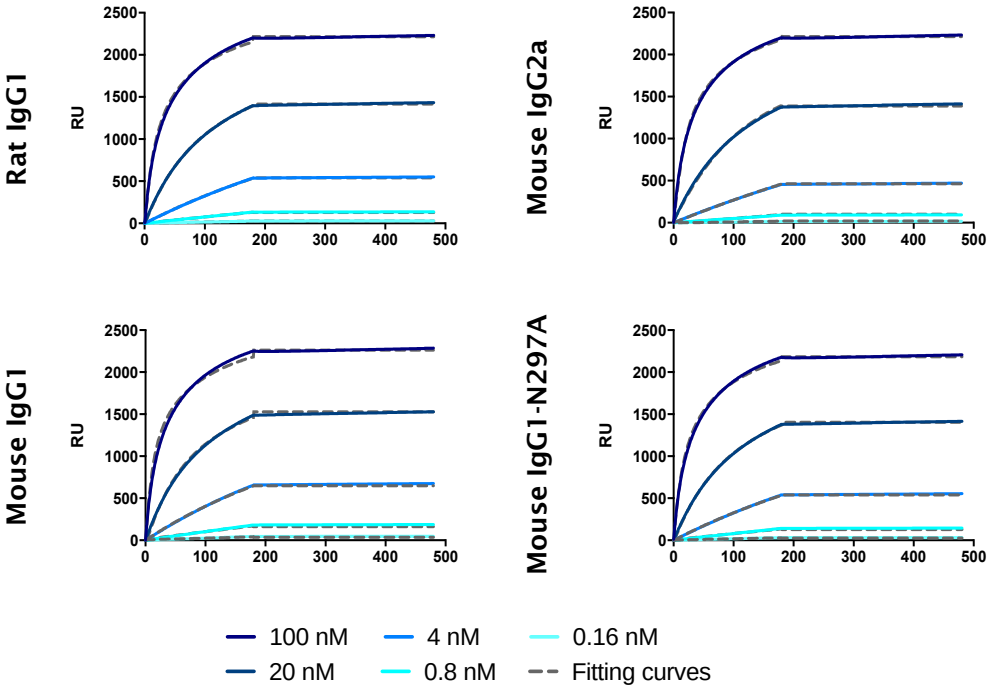

B)

EW1-9 Abs	K_{on}	K_{off}	K_D (K_{off}/K_{on})
Rat IgG1	1.8×10^{5}	1.06×10^{-7}	5.88×10^{-13}
Mouse IgG1	2.4×10^{5}	8.86×10^{-7}	3.69×10^{-12}
Mouse IgG2a	2.4×10^{5}	7.3×10^{-8}	3.22×10^{-13}
Mouse IgG1-N297A	1.9×10^{5}	4.5×10^{-7}	2.36×10^{-12}

Figure 3.5 Binding kinetics and avidity of rat and murine anti-PD-1 mAbs. Recombinant anti-His antibodies were immobilised at 5000 RU onto CM5 sensor chips by standard amine coupling, and His-tagged mouse PD-1 recombinant protein was captured onto the chip (2000 RU). A range of concentrations of murine and rat anti-PD-1 mAbs (100, 20, 4, 0.8, 0.16 nM) were then injected into the flow cells during different cycles preceded by regeneration of the chip surface. A) Results were plotted as sensorgrams, showing mass (RU) across time (s). B) A bivalent fitting model (291) was applied to the binding curves data to calculate association (K_{on}) and dissociation (K_{off}) constants. K_D values calculated from K_{on} and K_{off} represent the predicted avidity of mAbs towards murine PD-1 protein.

3.2.4 Binding kinetics on cell-based assays

Once the ability of murine anti-PD-1 mAbs to bind PD-1 was confirmed by SPR, their comparable binding to PD-1 expressed at the cell surface was established. Since T cells up-regulate PD-1 upon activation, these cells were initially used as targets to detect binding of murine anti-PD-1 mAbs. To start, the kinetics of PD-1 up-regulation on murine T cells upon in vitro stimulation were established. T-cell activation through antigen recognition can be mimicked with mAbs targeted at the

CD3: TCR complex (295, 296). Nevertheless, immobilisation of anti-CD3 mAb on plastic is an essential requirement to cross-link CD3 molecules and stimulate T cells in the absence of accessory cells (295, 296). In light of these, murine T cells were purified from splenocytes and incubated in the presence of 1 or 5 µg/ml (34, 297) of soluble or plate-bound anti-CD3 mAb for up to 72 hours. PD-1 expression was then assessed by flow cytometry as exemplified in Figure 3.6 A. Results showed that maximal expression of PD-1 was reached after 48 hours of stimulation with 5 µg/ml plate-bound anti-CD3 mAb, in both CD4 and CD8 T-cell subsets (Figure 3.6 B). In agreement with previous publications, soluble anti-CD3 mAb was unable to cross-link and stimulate T-cell activation and PD-1 expression (295, 296).

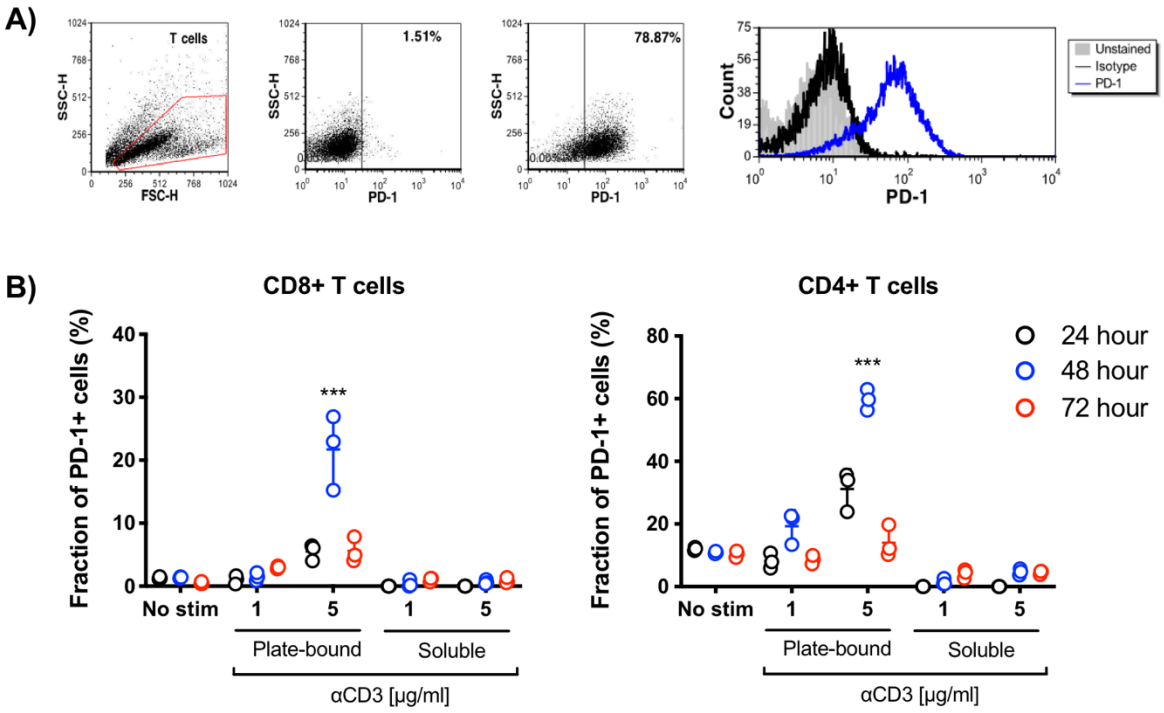

Figure 3.6 PD-1 induction on in vitro stimulated murine T cells.
T cells were purified by negative selection using a pan T-cell isolation Kit. T cells were cultured in U-bottomed 96 well-plates with 1 or 5 µg/ml of soluble or plate-bound (incubated overnight at 4ºC) anti-CD3 mAb. After 24, 48 or 72 hours of incubation, T cells were harvested and stained for PD-1 expression (clone RMP1-14). A) Example of gating strategy followed to calculate the percentage of T cells expressing PD-1 according to an isotype control. Histograms exemplify the up-regulation of PD-1 upon T-cell stimulation. B) Graphs show the percentage of PD-1 positive CD8 and CD4 T cells across time points. Experiment was done once with triplicates. Bars represent mean ± SEM, ***p<0.001.

Taking these results into account, an in vitro assay was designed to assess the binding ability of murine anti-PD-1 mAbs. Purified T cells were stimulated for 48 hours with 5 μg/ml of plate-bound anti-CD3 mAb, harvested and incubated with a range of concentrations of murine and rat anti-PD-1 antibodies. In order to detect binding by flow cytometry, secondary anti-rat or anti-mouse Fc fluorochrome labelled antibodies were used as appropriate. However, consistent results were not obtained with this method probably due to the transient and relatively low PD-1 expression on in vitro activated T cells. Hence, another approach was sought and transient transfection of HEK293F cells with mouse PD-1 was performed. Following plasmid transformation into E. Coli, large-scale protein purification was carried out to obtain mouse PD-1 protein for subsequent transfections. As shown in Figure 3.7 A-B, successful transfection of PD-1 into HEK293F cells resulted in a high percentage of PD-1 positive cells, which expressed higher levels of PD-1 compared to in vitro activated T cells (Figure 3.6 A). Transfected HEK293F cells were then incubated with different concentrations of anti-PD-1 mAbs and stained with secondary antibodies for subsequent flow cytometry analysis (Figure 3.7 C).

Results evidenced that all murine anti-PD-1 mAbs bound to cell-surface PD-1 in a similar manner to the parental rat antibody (Figure 3.7 D). To further confirm that murine anti-PD-1 isotypes had comparable binding affinities for cell-surface PD-1, a competition assay was developed. For this, a similar approach to that of the binding curves (Figure 3.7 D) was used. This time, however, transfected HEK293F cells were incubated with 1 μg/ml of the rat anti-PD-1 with different concentrations of each murine isotype. To simplify the assay and prevent the use of a secondary detection antibody, rat anti-PD-1 mAb was pre-labelled with Alexa Fluor (AF)-488. As shown in Figure 3.7 E, detection of rat anti-PD-1-AF488 decreased as the concentration of murine isotypes increased. At 1 μg/ml of all murine isotypes, 50% of rat anti-PD-1 mAb binding was inhibited, indicating that the three murine mAbs compete in an equivalent manner with the parental rat anti-PD-1 mAb.

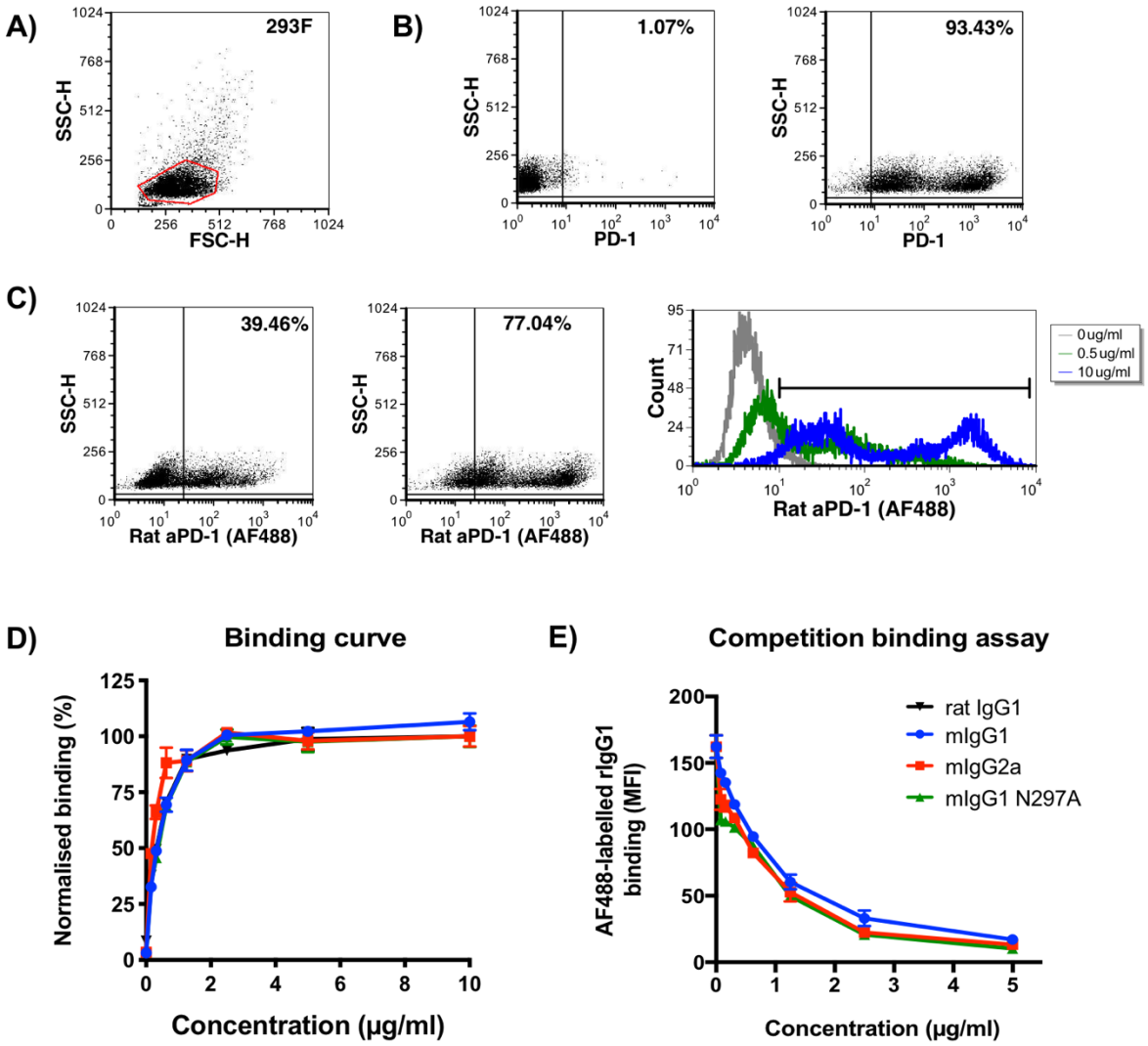

Figure 3.7 Binding curve and competition binding assay.
HEK293F cells were transiently transfected with a plasmid encoding mouse PD-1 protein. Cells were gated on FSC-SSC (A) and PD-1 expression was confirmed respective to a matched isotype control (B). D) Transfected cells were incubated with a two-fold dilution curve from 10 µg/ml of anti-PD-1 mAbs and cell suspensions were stained with APC-labelled anti-rat or PE-labelled anti-mouse secondary antibodies. Graph shows the normalised binding of mAbs at each concentration as a percentage of the maximum binding (MFI value) obtained in the standard curve. C, E) Transfected cells were incubated with different concentrations of murine antibodies (5, 2.5, 1.25, 0.625, 0.312, 0.078 µg/ml) in the presence of 1 µg/ml of AF488-conjugated rat anti-PD-1 mAb. Graph (E) shows MFI of the rat antibody relative to the concentration of competitive mouse isotypes. Representative experiment of two. Bars represent mean ± SEM of triplicates.

3.2.5 In vivo half-life

Once the in vitro binding characterisation was performed, the in vivo half-life of murine anti-PD-1 mAbs was investigated. This was important to be able to assure that any therapeutic difference in vivo would be due to differential FcγR binding patterns and not because of differences in bioavailability. In the clinical setting, 10 mg/kg of the humanised anti-PD-1 mAb Pembrolizumab have been used to treat patients with advanced cancer (7), which is equivalent to doses of 200-250 µg in mice. In line with this, therapeutic doses of anti-PD-1 mAbs in pre-clinical studies are typically of 200-250 µg (104, 165). Therefore, wild-type mice were injected with a singe dose of 250 µg of either parental rat antibody or murine isotypes to study the in vivo half-lives of these mAbs. Blood samples were taken at different time points after injection, and serum was collected and frozen down. To be able to determine the specific concentration of our murine anti-PD-1 mAbs in mouse serum, a similar in vitro assay to that of the binding curve (Figure 3.7 D) was designed, which involved the transient transfection of HEK293F cells with mouse PD-1 to enable specific binding of anti-PD-1 mAbs.

To optimise the assay, PD-1+ cells were harvested 24 hours after transfection and incubated with a serial dilution of serum from the different time points, alongside a standard curve. Opsonised cells were then stained with secondary anti-rat or anti-mouse Fc mAbs, and percentage of maximal MFI (normalised binding) was plotted from flow cytometry values (Figure 3.8 A-C). To be able to infer serum concentration from MFI values, a serum dilution of 1 in 10.000 was chosen for subsequent assays, as these MFIs were in the linear range of the standard curve (B). This was then performed for all the time points and mAbs. As shown in Figure 3.8 D, there was a slight increase in binding after the 1 hour bleed, but this was seen across antibody isotypes and it could be due to the fact that antibodies were delivered by intra-peritoneal injection, and hence their maximal presence in blood was delayed. Despite a larger variation at earlier time points (up to 24 hours after injection), both rat and murine antibodies displayed similar half-lives in vivo. Furthermore, the equation from the linear range of the standard curve (B) was calculated and the concentration of murine mAbs was determined. The parental rat anti-PD-1 mAb was not included in this analysis because its secondary antibody was labelled with a different fluorochrome and hence a separate linear equation was needed.

As shown in Figure 3.8 E, the three murine anti-PD-1 isotypes displayed similar values across time points and the concentration decreased in a similar fashion over time, suggesting that there was no difference in antibody half-life in vivo.

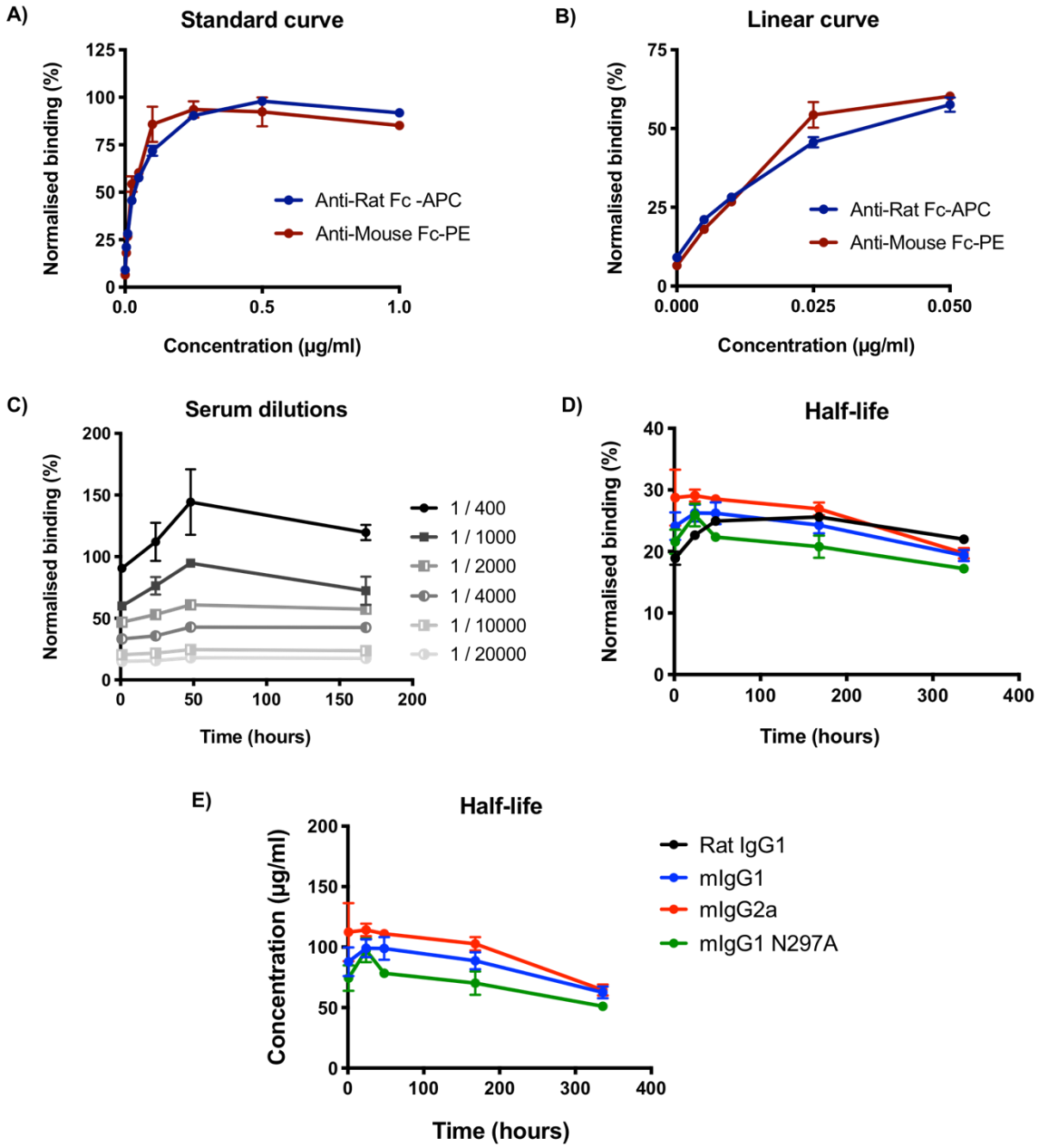

Figure 3.8 In vivo half-life of murine anti-PD-1 mAbs.
Mice were injected (Ip) with 250 µg of mAbs and bled after 1h, 24h, 48, 7 and 14 days to collect serum. PD-1 expressing HEK293F cells were incubated 30 minutes on ice with a three-fold dilution curve from 1 µg/ml of anti-PD-1 mAb (A,B); with the specified serum dilutions (C); or with a 1/10.000 serum dilution from the different time points (D,E). Cell suspensions were stained with APC-labelled anti-rat or PE-labelled anti-mouse secondary antibodies and run in flow cytometry. Graphs show normalised binding at each concentration (A) or time point (B-C) as a percentage of the maximum binding (MFI value) obtained from the standard curve (A-C). Otherwise, the concentration of murine mAbs in serum is shown (D). Experiments were performed once. Bars represent mean ± S.D, 3 mice per treatment group.

3.3 Development of a suppression assay

After confirming equivalent binding and PD-1 blocking ability, the function of murine mAbs with differential FcγR engagement was determined in vitro. Due to the inhibitory activity of PD-1 (45, 46), it was hypothesised that murine anti-PD-1 mAbs would be able to release such inhibition and enhance T-cell proliferation. Thus, a suppression assay was designed based on the co-culture of activated murine T cells with adherent cells expressing PD-L1. Taking into account that PD-L1 has been demonstrated to be expressed in macrophages (298), bone marrow was harvested and BMDMs from wild-type mice were differentiated in vitro for 7 days in the presence of M-CSF (289). To confirm differentiation prior to functional assays, morphological assessment of cells (i.e non-round cells with processes; (299)) was carried out as illustrated in Figure 3.9. BMDMs were then stimulated with various stimuli combinations in order to test if the expression of PD-L1 could be up-regulated on these cells, with the ultimate aim to use PD-L1 expressing BMDMs in co-culture assays with murine T cells. Flow cytometry analysis (Figure 3.10 A) revealed that, whilst the pan-macrophage marker F4/80 (300) remained constant across treatments (B), PD-L1 expression was up-regulated in BMDMs by pro-inflammatory stimuli such as IFN-γ and LPS (C). In parallel, concurrent up-regulation of CD40 was noted with the same pro-inflammatory signals (D).

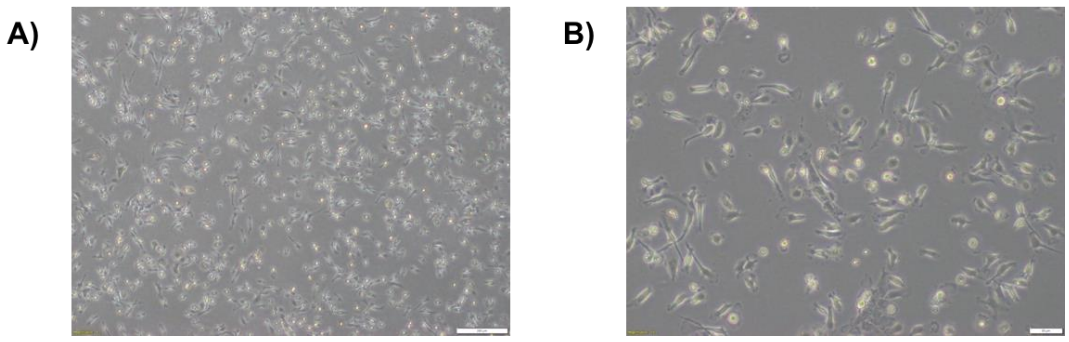

Figure 3.9 Morphology of in vitro differentiated BMDMs.
Murine bone marrow was harvested from the femur and tibia of wild-type C57BL/6 mice and cells were cultured at $4x10^6$ cell/well in 6-well plates in the presence of L929 conditioned media containing M-CSF. Bone marrow cells were cultured 6-8 days to differentiate into BMDMs. Morphology was assessed with a CKX41 Olympus microscope connected to Cell B software (Olympus) and images taken with 4X (A) and 10X (B) objectives.

Expression of co-stimulatory molecules by activated macrophages, such as CD40, can lead to a potent stimulation of T-cell responses (76, 85). Moreover, cis-interaction on APCs between PD-L1 and CD80, which is often up-regulated upon macrophage activation by LPS/IFN-γ (298), can further reduce the inhibitory effect of PD-L1 on T cells (73). Therefore, in these circumstances of strong T-cell activation, PD-L1-mediated inhibition might be insufficient to decrease T-cell proliferation, preventing any beneficial effect of anti-PD-1 mAbs. Taking this into account, a stable cell line expressing PD-L1 was generated to avoid the use of activated macrophages in the co-culture.

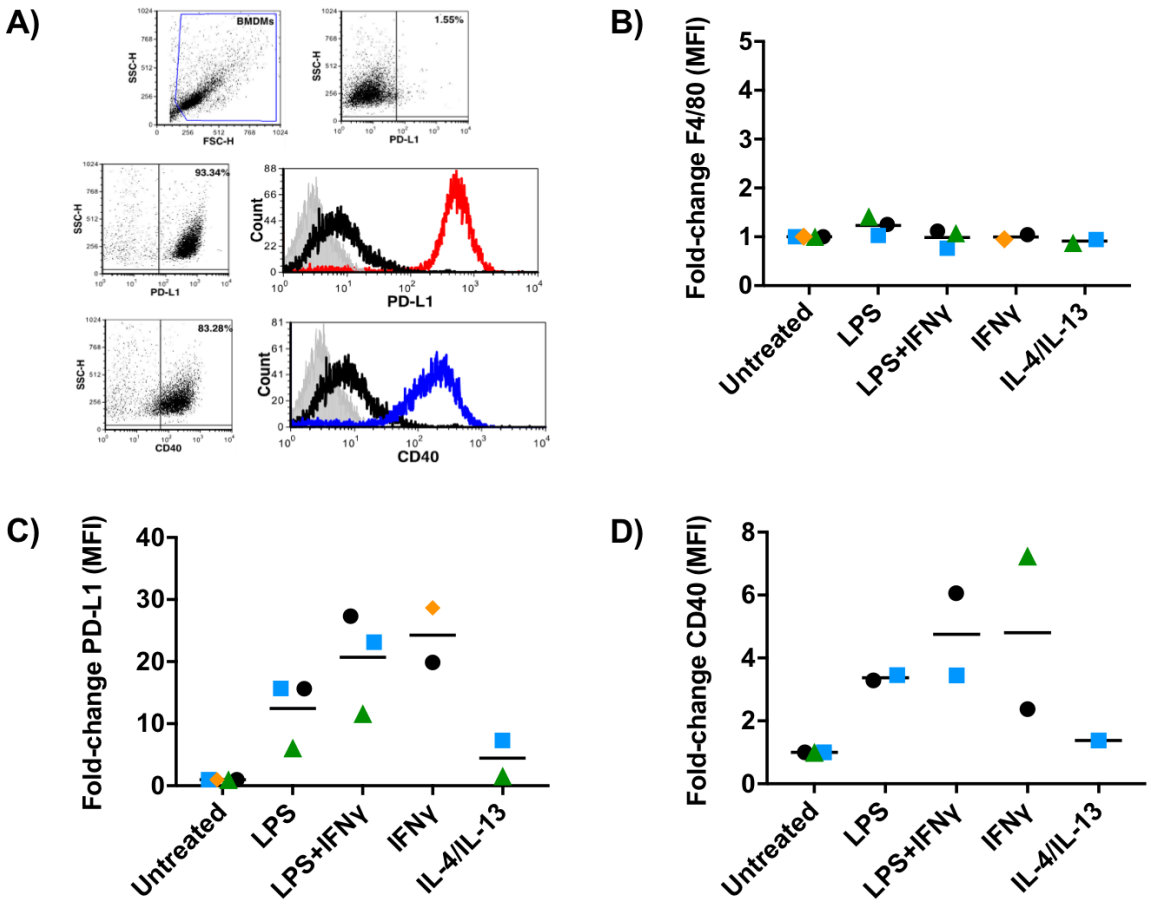

Figure 3.10 Expression of PD-L1 and CD40 on BMDMs.
BMDMs were differentiated in 6-well plates for 6 to 8 days before stimulation. 24 hours after treatment, BMDMs were mechanically detached from the wells and the expression of several markers was analysed by flow cytometry. A) Cells were gated by FSC-SSC and expression of PD-L1 and CD40 was assessed according to the same, matched isotype control. Representative histograms show the overlap between unstained cells (grey), isotype control (black) and CD40 (blue) or PD-L1 (red) expression in LPS-treated BMDMs. B-D) Summary plots of the fold-change MFI of stimulated BMDMs relative to non-treated BMDMs for each donor. Expression of F4/80 (B), PD-L1 (C) and CD40 (D) are shown. Coloured dots represent each BMDM donor and black bars indicate the mean of the replicates.

In order to achieve a stable transfection, mouse PD-L1 (CD274) was cloned into the pCI-Puro vector, which carried a selection gene that conferred resistance to puromycin and enabled the selection of transfected cells with this antibiotic (Figure 3.11 A). Following bacterial transformation, the purified pCI-Puro-PD-L1 plasmid contained the desired PD-L1 insert, as checked by restriction enzyme analysis (B).

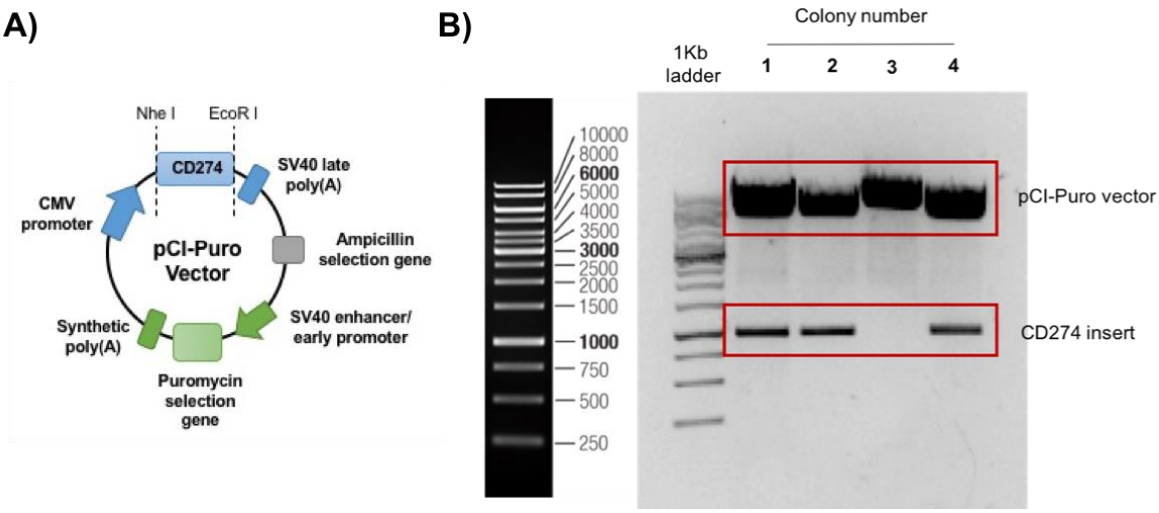

Figure 3.11 Generation of pCI-Puro-PD-L1 plasmid.
A) Diagram of the pCI-Puro-PD-L1 construct generated. The original pCI-Puro plasmid was initially made by Dr. Claude Chan (University of Southampton). Following ligation of pCI-Puro and PD-L1 DNA, bacterial cultures were transformed with the fusion plasmid and colonies were picked. B) The presence of pCI-Puro-PD-L1 plasmid was assessed on colonies after small-scale purification of DNA. Colonies 1, 2 and 4 were sent to sequence. A single positive colony was then grown to perform large-scale DNA purification and obtain sufficient DNA content to perform subsequent transfections.

First, a transient transfection of pCI-Puro-PD-L1 was performed using HEK293F cells to confirm that PD-L1 protein could be expressed at the cell surface. As shown in Figure 3.12, transfection of HEK293F cells achieved a high expression of PD-L1 compared to non-transfected cells, as assessed by flow cytometry. This confirmed the ability of mammalian cells to express murine PD-L1 after transfection with pCI-Puro-PD-L1 plasmid.

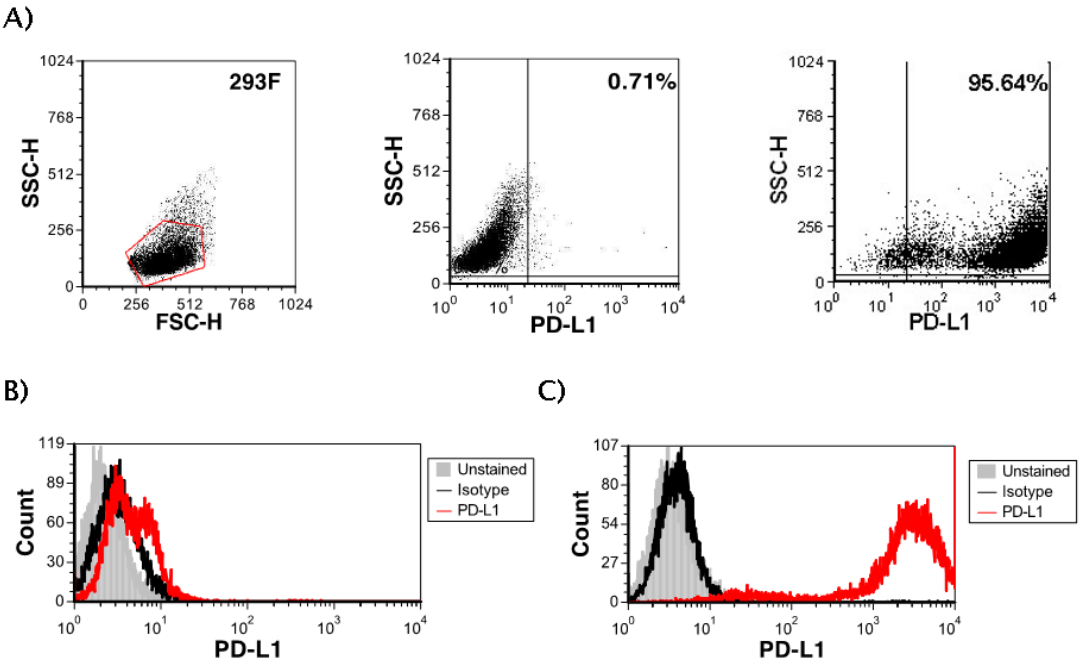

Figure 3.12 Transient transfection of pCI-Puro-PD-L1 in HEK293F cells.
pCI-Puro-PD-L1 DNA was transiently transfected in soluble HEK293 cells and protein expression was checked 2-3 days post-transfection. Dot plots (A) and histograms (B-C) show the cell surface expression of PD-L1 relative to isotype controls in non-transfected (B) and transfected (C) cells.

With the ultimate goal to study the involvement of FcγRs in PD-1 blockade therapy, the two murine myeloid cell lines RAW264.7 and J774A.1 (which express mouse FcγRs) were transfected with pCI-Puro-PD-L1 plasmid. Although numerous methods and reagents were tried (summarised in 2.4.2), all attempts to stably transfect PD-L1 on myeloid cell lines were unsuccessful. This could be due to their inherent ability as macrophage cell lines to take up and sample the surrounding environment (301). Endocytosis of foreign DNA plasmids would lead to their degradation and prevent their integration into the cell DNA. In agreement with this, lipid-based transfection methods used in primary macrophages or cell lines generally yield poor transfection efficiency and a transient expression, which is largely lost after 24 hours (301). As a surrogate model, stable transfection was performed in adherent CHO-K1 cells. Transfected cells were selected with puromycin and positive colonies were evident after 3 weeks post-transfection as illustrated in Figure 3.13 A. Transfected colonies were screened for PD-L1 expression and colonies with different levels of PD-L1 were sorted by FACs to have homogeneous populations. Cell lines expressing the empty vector, high PD-L1 or very high PD-L1 levels (Figure 3.13 C) were grown and stocks frozen down to be used in subsequent in vitro studies.

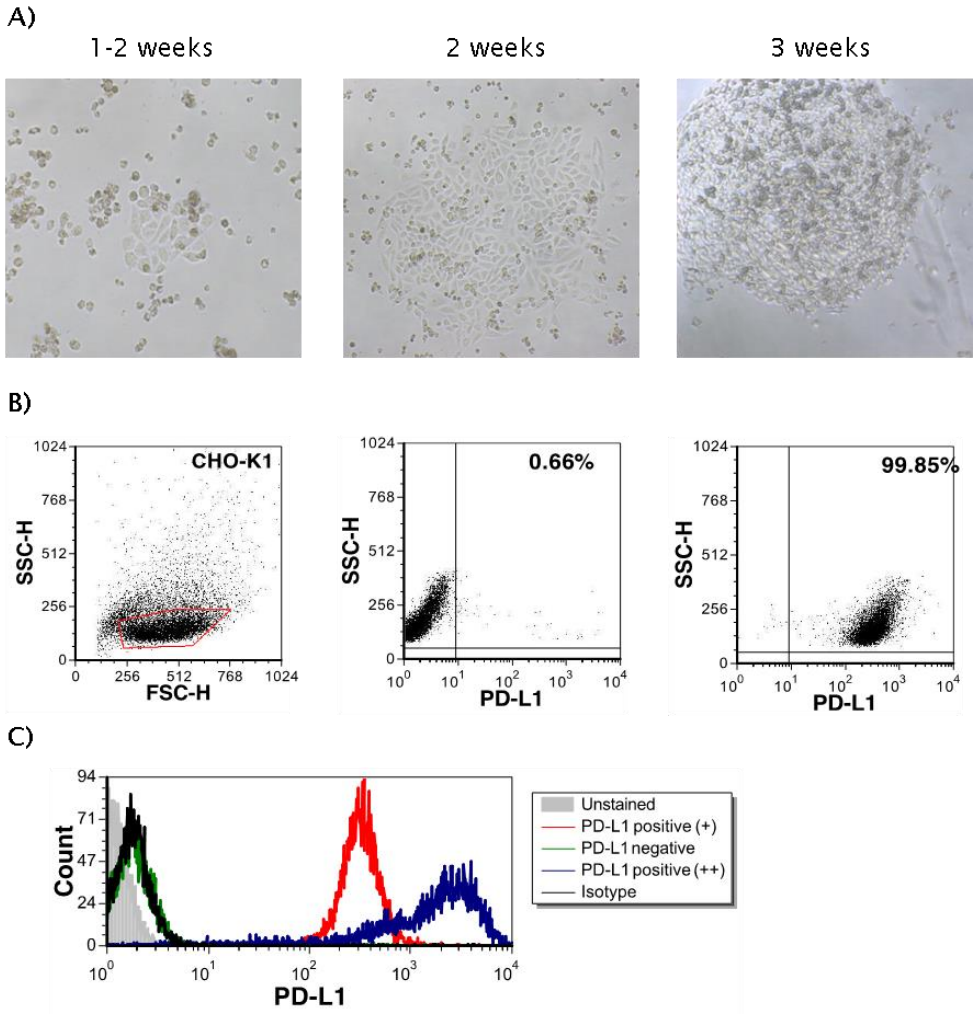

Figure 3.13 Stable transfection of pCI-Puro-mCD279 in CHO-K1 cells.
Adherent CHO-K1 cells were transfected with pCI-Puro-PD-L1 plasmid. After two days, cells were cultured in 96 well-plates in the presence of 10 µg/ml of puromycin to select for positive clones. A) Representative pictures of positive clones at different times post-transfection, illustrating the growth of transfected cells in isolated colonies. B) After 3 weeks, wells with positive colonies were screened for PD-L1 surface expression by flow cytometry. An example of high PD-L1 expression is shown. C) Transfected cells expressing PD-L1 were sorted into three distinct populations, which carried an empty vector (green) or expressed high (red) and very high (blue) levels of PD-L1. From this point, the three populations were cultured as different cell lines, in the presence of 10 µg/ml of puromycin throughout the culture period.

Once the generation of a PD-L1-expressing cell line was achieved, purified mouse T cells were co-cultured in the presence of CHO-K1 cells expressing PD-L1 (CHO-PD-L1) or CHO-K1 cells carrying the empty vector (CHO-Ø). To trigger T-cell activation and PD-1 up-regulation in the first instance, anti-CD3 and anti-CD28 mouse mAbs were added in the co-culture. Although different cell densities and concentrations of the anti-CD3/CD28 mAbs were tried, a robust T-cell activation was not consistently obtained. This was probably due to the inability of soluble

antibodies to crosslink and signal through the TCR/CD28 clusters. Therefore, we opted to use beads carrying mouse anti-CD3/CD28 mAbs to stimulate T-cell proliferation. Stimulatory beads can induce strong activating signals that may overcome PD-1 inhibition. To overcome this, several ratios of bead: T cell were initially tested to establish the required level of suboptimal stimulation. However, the maximal degree of inhibition observed on T-cell proliferation by PD-L1 expressing CHO-K1 cells was very limited, even at the lowest ratio of beads. Alternatively, a range of CHO-K1: T-cell density ratios was carried out. Nevertheless, the rapid proliferation of CHO-K1 cells resulted in a fast exhaustion of the culture medium, despite different lengths of co-culture (2 to 4 days) being tried. This fact limited T-cell proliferation, especially at higher densities of CHO-K1, thereby confounding the effect of PD-L1 inhibition. Overall, no consistent effect of PD-L1 in T-cell proliferation was achieved with the aforementioned co-culture system.

3.3.1 Suppression assay with recombinant Fc proteins

As an alternative to the co-culture of PD-L1 expressing cells, recombinant proteins were used to mimic the presence of PD-L1 and limit the effect of other cell–cell interactions. Recombinant mouse PD-L1 was purchased in the form of homodimers with the Fc region of human IgG1 antibodies, leading to a mPD-L1-huFc recombinant protein. To provide cross-linking of recombinant proteins and anti-CD3 mAb, 96 well-plates were coated overnight at 4 degrees with the relevant proteins and cells were added on the following day. It is important to note that anti-CD3 mAb and mPD-L1-huFc may compete for binding to the plastic surface, thereby reducing the amount of anti-CD3 mAb bound, which would in turn reduce T-cell proliferation per se. Hence, the irrelevant huDR3-huFc recombinant protein was used at the same concentration as mPD-L1-huFc as a control to account for the potential reduction in anti-CD3 mAb binding to the wells.

To assess cell proliferation, two methods –CFSE staining and ^{3}H-thymidine incorporation– were carried out side by side in multiple assays to determine the most sensitive method. Whilst CFSE dilution did not show any significant differences across conditions, the measurement of thymidine incorporation was able to detect subtle differences and was therefore used in subsequent assays. Furthermore, to prevent the potential suppressive effect of Tregs in the culture, purified CD8 T cells were used in the suppression assay as opposed to total CD3+ cells.

To start, a titration of plate-bound recombinant Fc proteins and anti-CD3 mAb was performed to determine the optimal combination. The duration of the assay was kept to a total of 4 days, with the addition of ^{3}H-thymidine at the last 16 hours before cell harvest. As shown in Figure 3.14 , whilst 0.1 μg/ml of anti-CD3 mAb was not sufficient to trigger proliferation of purified CD8 T cells, 1 and 5 μg/ml lead to T-cell proliferation. In most combinations, culture with irrelevant huDR3-huFc showed increased CD8 proliferation compared to mPD-L1-huFc, which suggested that the recombinant PD-L1 was able to inhibit CD8 T-cell proliferation through PD-1 interaction and not due to less anti-CD3 binding. Nevertheless, the combination of 1 μg/ml of anti-CD3 plus 5 μg/ml of plate-bound recombinant Fc proteins appeared to give the biggest window of inhibition between irrelevant huDR3-huFc and mPD-L1-huFc proteins and was therefore chosen for subsequent assays.

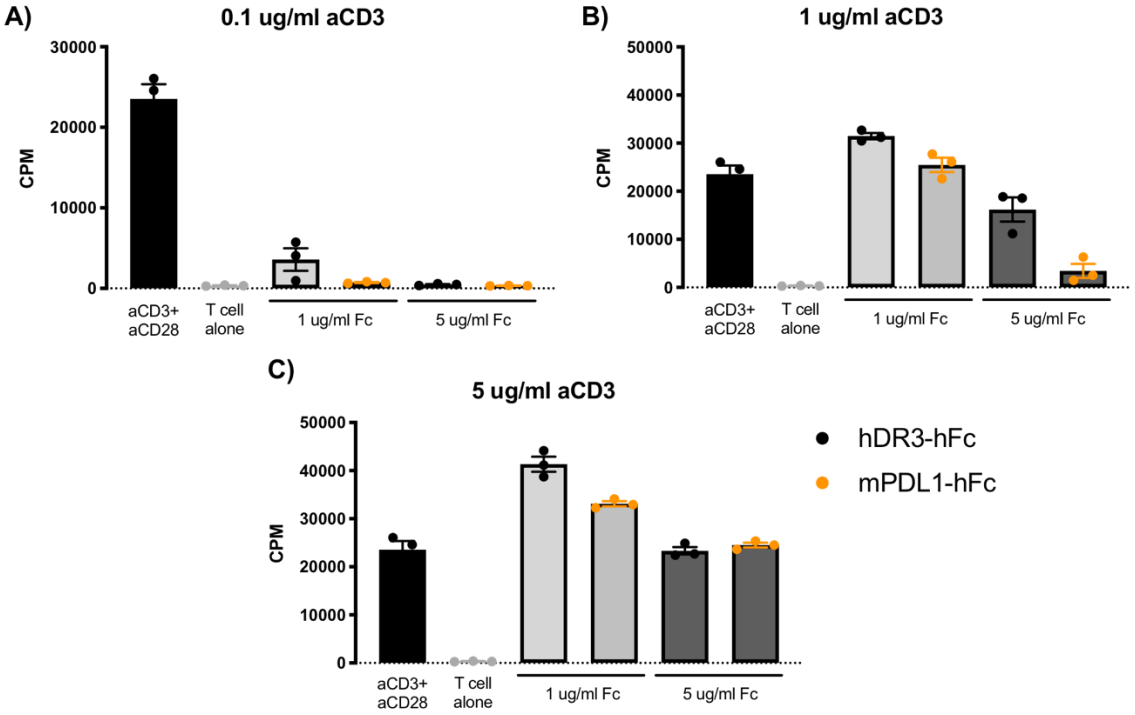

Figure 3.14 Titration of recombinant Fc proteins and anti-CD3 mAbs.
Anti-CD3 mAb and recombinant Fc proteins were plated at different concentrations in 96 well-plates overnight at 4ºC. On the following day, spleens form C57BL/6 mice were harvested and single cell suspensions were obtained. CD8 T cells were purified by magnetic isolation and plated at 4x10^{4} cells/ well for 4 days at 37ºC. ^{3}H-thymidine was added on day 3 and cells were harvested on the following day. DNA radioactivity was measured with a scintillation beta-counter. Graphs show the results for CD8 T cells cultured in the presence of 0.1 μg/ml anti-CD3 mAb plus 1 or 5 μg/ml of Fc proteins (A); 1 μg/ml anti-CD3 mAb plus 1 or 5 μg/ml of Fc proteins (B); or 5 μg/ml anti-CD3 plus 1 or 5 μg/ml of Fc proteins (C). Black bars represent positive controls, where CD8 T cells were cultured with 1 μg/ml anti-CD3 mAb plate-bound plus 2.5 μg/ml anti-CD28 mAb. Negative controls indicate CD8 T cells alone. Black dots indicate huDR3-huFc whilst orange dots represent mPD-L1-huFc. Experiment was done once in triplicates. Bars show mean ± SEM.

Next, the ability of murine anti-PD-1 isotypes to release PD-1-mediated inhibition of CD8 T-cell proliferation was assessed. As shown in the schematic Figure 3.15 A, CD8 T cells were cultured in the presence of plate-bound irrelevant huDR3-huFc or mPD-L1-huFc with 1 μg/ml of anti-CD3 mAb plus anti-PD-1 mAbs or irrelevant isotypes. As expected, irrelevant antibodies were unable to rescue T-cell proliferation in the presence of mPD-L1-huFc, whereas anti-PD-1 mAbs increased proliferation (Figure 3.15 B-D, filled bars). However, in the presence of irrelevant recombinant Fc protein, there was no difference between irrelevant and anti-PD-1 mAbs, indicating that the effect was specific to PD-1: PD-L1 interaction (Figure 3.15 B-D, white bars). Importantly, the three anti-PD-1 isotypes released PD-1 inhibition to a similar extent, indicating that the different isotypes did not affect the ability of these mAbs to release T-cell proliferation in the presence of PD-L1.

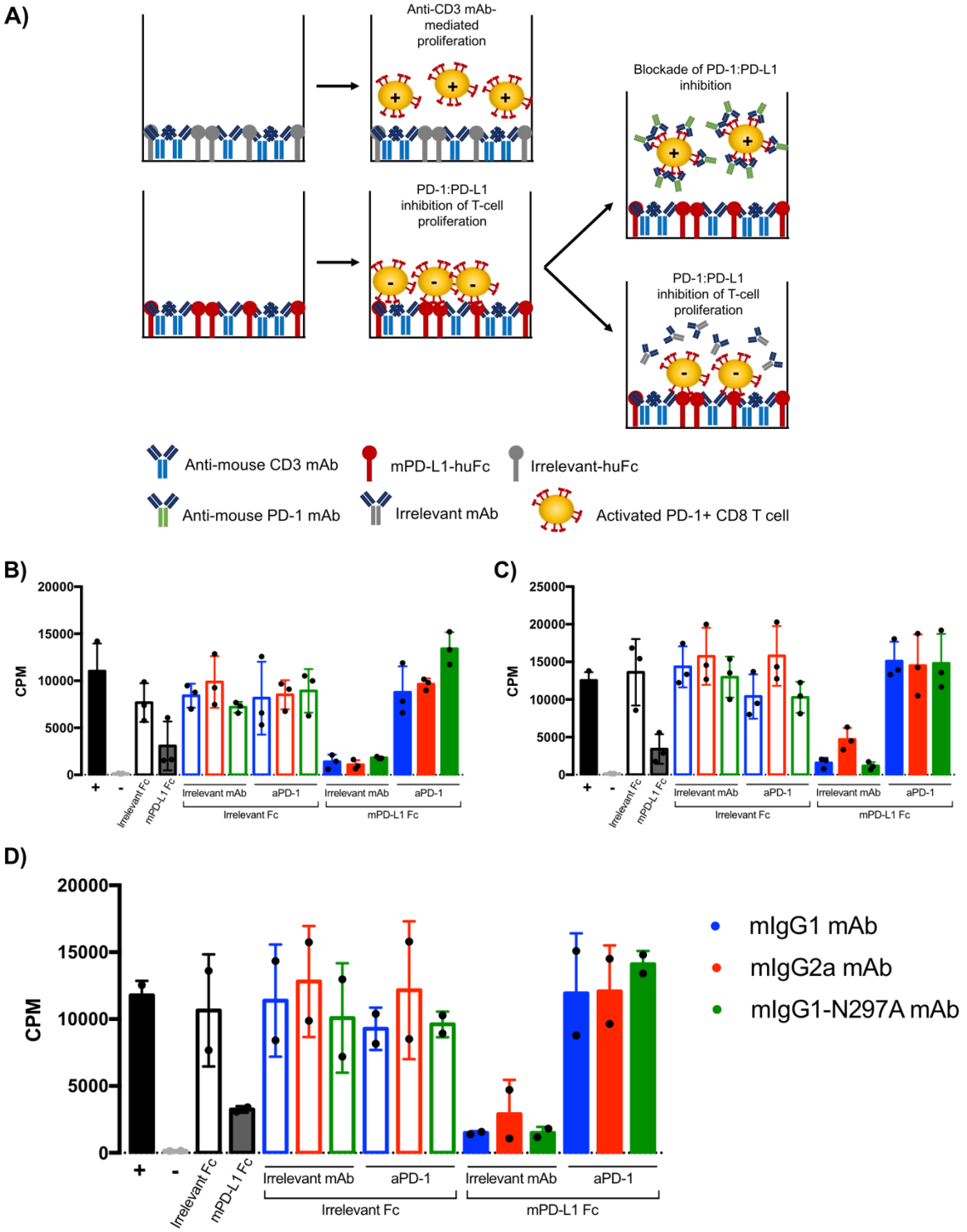

Figure 3.15 Suppression assay with mouse anti-PD-1 isotypes.
A) Schematic representation of the suppression assay. B-D) Anti-CD3 mAb (1 μg/ml) and recombinant Fc proteins (5 μg/ml) were plated on 96 well-plates overnight at 4ºC. On the following day, CD8 T cells purified from C57BL/6 mice were plated at 4x104 cells/ well for 4 days at 37ºC. In appropriate wells, irrelevant or anti-PD-1 isotypes were added at 5 μg/ml together with CD8 T cells. ^{3}H-thymidine was added on day 3 and cells were harvested on the following day to measure DNA radioactivity with a scintillation beta-counter. Black bars represent positive controls, where CD8 T cells were cultured with 1 μg/ml anti-CD3 mAb plate-bound plus 2.5 μg/ml anti-CD28 mAb. Negative control wells included CD8 T cells alone. Experiment was performed twice (B and C) in triplicates. Combined means from both experiments are shown in D. Bars show mean ± S.D.

3.4 Effector mechanisms of murine anti-PD-1 mAbs

In all the experiments shown above, the three murine anti-PD-1 isotypes displayed similar results in terms of biochemical characterisation and ability to release T-cell suppression. This was expected because, in spite of their distinct Fc region, they all bear the same F(ab) regions, which determine binding to PD-1 and the functions that derive from blocking PD-1: PD-L1 interaction. Nevertheless, the primary focus of this work is to elucidate the role of different Fc regions in anti-PD-1 therapy, and hence the effect of engaging activating, inhibitory or no FcγRs by anti-PD-1 mAbs was studied in vitro.

3.4.1 Anti-PD-1 mAb-mediated phagocytosis by BMDMs

In the TME, it is believed that anti-PD-1 mAbs predominantly bind activated T cells that express high levels of PD-1. However, the TME is known to be rich in activated myeloid populations that express a range of activating FcγRs that can lead to effector mechanisms such as ADCC and ADCP (101). Whilst those effector mechanisms are desirable in the setting of a direct-tumour targeting mAb (302), engagement of activating FcγR by anti-PD-1 mAbs could lead to the deletion of PD-1 expressing T cells in the TME. Considering the profound effect that this could have on anti-tumour immunity, the first step was to study the effect of engaging activating FcγRs by anti-PD-1 mAbs.

To this end, a phagocytosis assay was carried out in vitro to investigate the potential phagocytosis of activated T cells by myeloid cells (Figure 3.16 A). For this, BMDMs were differentiated in vitro for 6 days and re-plated into 96 well-plates the day before performing the assay, in the presence of LPS. In parallel, purified T cells were stimulated for 48h to up-regulate PD-1 expression. On the day of the assay, CFSE-labelled T cells were opsonised with anti-PD-1 mAbs and co-cultured with BMDMs, which were subsequently stained with F4/80 to perform flow cytometry analysis. As exemplified in Figure 3.16 B, double positive cells represented the percentage of phagocytosis, as F4/80-labelled BMDMs acquired CFSE staining after phagocytosis of CFSE-labelled T cells. Results showed that the positive control, an antibody that targeted a largely expressed T-cell antigen such as CD4, increased phagocytosis compared to its irrelevant isotype (black bars) (Figure 3.16 C). In a similar way, anti-PD-1 mIgG2a increased phagocytosis compared to its matching irrelevant isotype. In contrast, anti-PD-1 mIgG1 or mIgG1-N297A did not increase phagocytosis of T cells compared to their matched irrelevant controls.

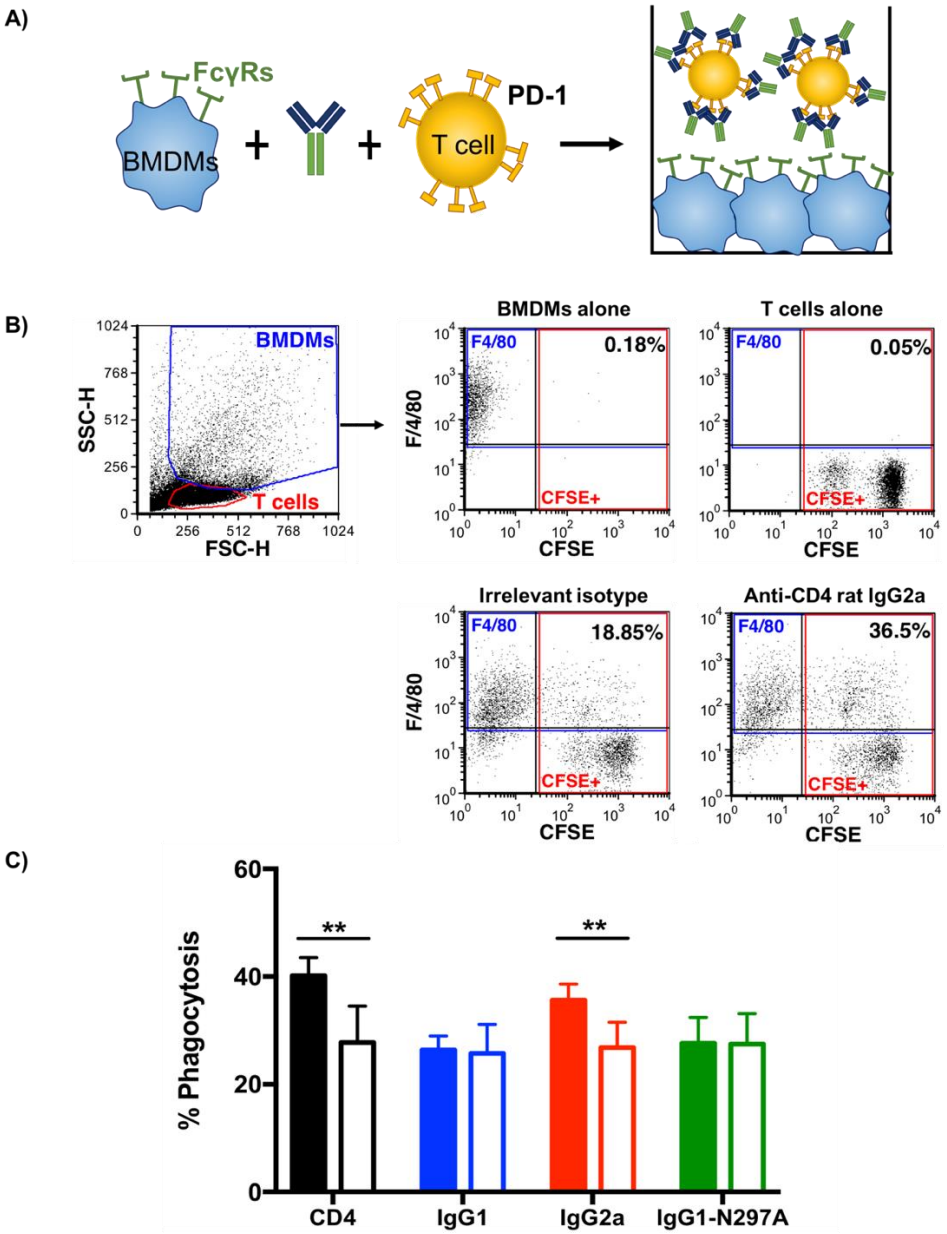

Figure 3.16 Phagocytosis assay with mouse anti-PD-1 isotypes.
A) Schematic diagram of an in vitro phagocytosis assay. BMDMs were harvested and differentiated in vitro for 6 days. The day prior to the assay, BMDMs were re-plated at $5x10^4$ cell/well in the presence of 50 ng/ml LPS and incubated overnight at 37˚C. Primary mouse T cells were harvested, purified and incubated for 48 hours with 5 µg/ml of plate-bound anti-mCD3 mAb. On the day of the assay, T cells were stained with CFSE and opsonised with 5 µg/ml anti-PD-1 or irrelevant isotypes for 3o minutes on ice. Opsonised T cells ($2.5x10^5$ cell/well) were co-cultured with BMDMs for 1 hour at 37˚C and then BMDMs were stained with APC-labelled anti-F4/80 mAb for 15 minutes at RT before analysis by flow cytometry. B) Example plots showing the gating strategy followed to obtain the percentage of double positive events (percentage of phagocytosis). C) Percentage of phagocytosis calculated per condition. Filled bars correspond to relevant mAbs whilst clear bars correspond to irrelevant isotype controls. Experiment performed twice in triplicates. Bars show mean ± S.D. Student T-test, **p<0.01.

Overall, engagement of FcγRs by anti-PD-1 mAbs caused increased phagocytosis of T cells in vitro, since mIgG2a, which has a high A/I ratio, showed the biggest increase whilst mIgG1-N297A did not induce phagocytosis. These findings support the idea that engagement of activating FcγRs by anti-PD-1 mAbs could be detrimental to the therapeutic potential of these mAbs, as it could lead to the phagocytosis of activated PD-1+ TILs, which have been described to be essential for the efficacy of PD-1 blockade (157-159). Furthermore, it is important to note that physiological levels of PD-1 on activated primary T cells were enough to lead to the phagocytosis of such cells after opsonisation by anti-PD-1 mAbs, indicating that this phenomenon could also take place in vivo at the TME.

3.4.2 Optimisation of murine cross-linking assay

Once the prejudicial impact of engaging activating FcγRs was established in vitro, we sought to explore whether engagement of the inhibitory FcγRII could also modulate the therapeutic activity of anti-PD-1 mAbs. Generally, immunostimulatory mAbs targeting TNFRSF members such as CD40 or 4-1BB require the engagement of FcγRII via their Fc region to induce cross-linking and deliver their stimulatory signalling through their target receptor (131-133). Besides TNFRSF members, engagement of FcγRII might be able to modulate the agonistic activity of other therapeutic mAbs. As such, binding of FcγRII by anti-PD-1 mAbs could provide agonistic inhibitory signalling through PD-1 receptors at the T-cell surface, leading to T-cell suppression.

To be able to elucidate the impact of FcγRII binding in anti-PD-1 therapy, a murine cross-linking assay was attempted. Similar to the suppression assay (Figure 3.15), 96 well-plates were coated with a combination of anti-CD3 mAb, recombinant Fc proteins and mouse FcγRII protein. However, both anti-CD3 mAb (hamster IgG) and recombinant proteins (disulphide-linked homo-dimers with a human IgG1 Fc) could also bind mFcγRII and lead to undesired interactions that would affect the outcome of the assay. To tackle this, enzymatic deglycosylation of anti-CD3 mAb to prevent binding to mFcγRII and a two-step sequential coating, with mFcγRII being coated one day after anti-CD3 and Fc proteins, were attempted. Nevertheless, due to the complexity of the assay and the time constrains, the effect on T-cell proliferation of mFcγRII engagement by anti-PD-1 mIgG1 versus mIgG1-N297A could not be evaluated, and further development of this assay was abandoned.

3.4.3 Optimisation of human suppression and cross-linking assays

Of note, it is important to highlight that there is no human IgG isotype that has an equivalently low A/I ratio to that of mIgG1, as all human isotypes are able to bind the high-affinity huFcγRI. Because of this, even if anti-PD-1 mIgG1 had shown decreased T-cell proliferation in the presence of high levels of mFcγRII, this effect may not be reflective of what could happen in the human system with clinically approved anti-PD-1 mAbs. Therefore, in vitro suppression and cross-linking assays were attempted using human cells and mAbs to try and elucidate the potential effect that huFcγRIIb engagement by clinically approved mAbs could have on T cells. To this end, human anti-PD-1 IgG4 Nivolumab (clone 5C4) was engineered as an Fc null variant bearing the FALA mutation (303) to enable the comparison between IgG4 and an Fc null mAb.

To start, the kinetics of proliferation and PD-1 expression of human CD8 and CD4 T cells were established in vitro. CFSE-labelled PBMCs were cultured with different concentrations of plate-bound anti-huCD3 mAb for 24, 48 and 72 hours to stimulate T-cell proliferation and PD-1 up-regulation. As shown in Figure 3.17 A,B, maximal proliferation, which was reached after 72 hours, was already achieved at the lowest concentration of anti-huCD3 mAb (25 ng/ml) in both CD4 and CD8 T-cell subsets. Despite the absence of proliferation at 24 or 48 hours, PD-1 expression was detected throughout the culture and peaked at 48 hours (Figure 3.17 C,D). Although some variability was noted at 24 hours, the three concentrations of anti-huCD3 mAb up-regulated PD-1 to a similar extent. As a result of these findings, the duration of the suppression assay was set to 72 hours to allow sufficient PD-1 up-regulation and inhibition of T-cell proliferation.

A number of experiments were conducted in an attempt to develop and optimise a human suppression assay with huPD-L1-HuFc and irrelevant Fc protein. However, unfortunately no consistent T-cell proliferation and inhibition by PD-1: PD-L1 interaction was achieved, and the further development of the assay had to be abandoned because of time constraints.

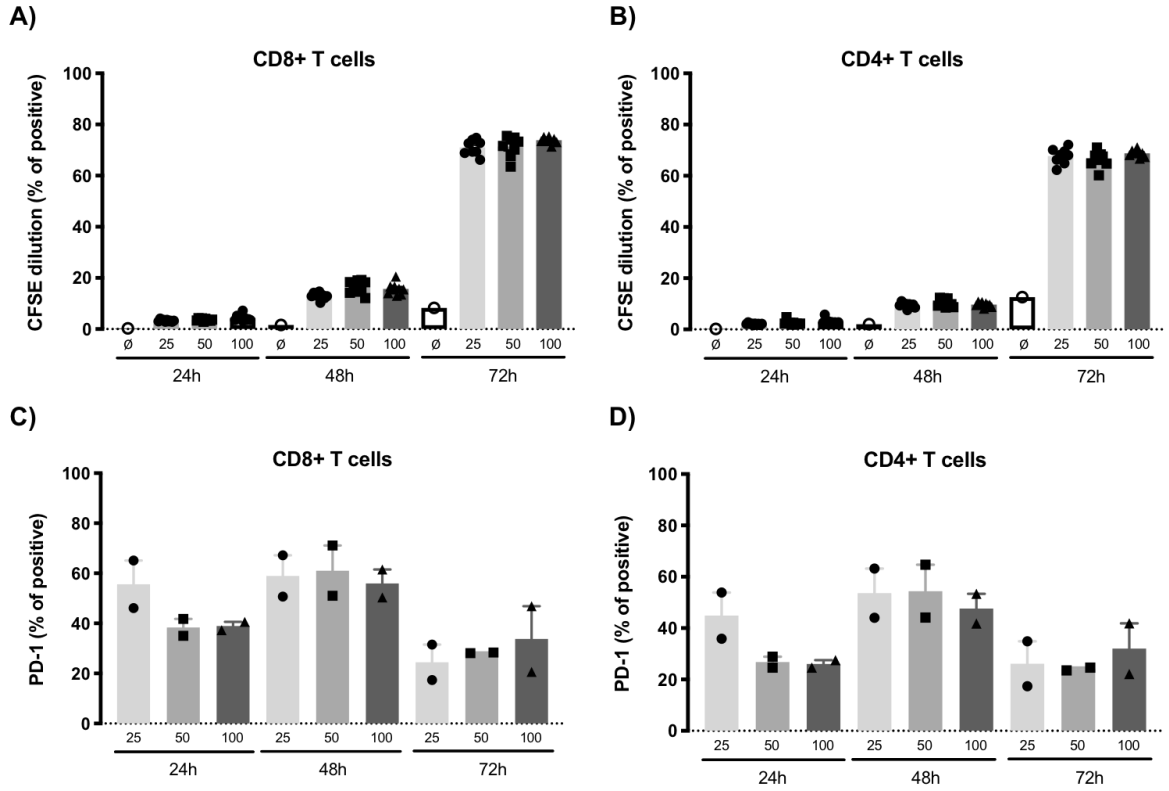

Figure 3.17 Proliferation and PD-1 expression on human T cells upon stimulation with plate-bound OKT3.
Round-bottomed 96 well-plates were coated with 25, 50 or 100 ng/ml anti-huCD3 mAb (OKT3) overnight at 4ºC. On the following day, PBMCs were isolated from leucocyte cones (see 2.6.11) and 1-2 x10^7 cells were labelled with CFSE (see 2.6.12). Cells were harvested after 24, 48 or 72 hours of culture and stained with anti-CD3, anti-CD8 and anti-PD-1 labelled mAbs. A-B) Proliferation of CD8 (A) and CD 4 T cells (B) shown as percentage of CFSE dilution. C-D) Expression of PD-1 on CD8 (C) and CD4 T cells (D) shown as percentage of positive relative to an isotype control. Experiment performed once, in 2-6 technical replicates.

3.5 Chapter discussion

To study the impact of FcγR engagement on PD-1 blockade therapy, three murine anti-PD-1 antibodies were generated that possessed different FcγR binding pattern. As a prerequisite to study their effector functions, the ability of these mAbs to bind murine FcγRs was confirmed. In agreement with previous reports, mIgG1 showed binding to a sole low-affinity activating FcγR and the inhibitory FcγRII, thereby bearing low A/I ratio. On the contrary, mIgG2a had a high A/I ratio, displaying high affinity for activating FcγRs. This suggests that this mAb will be able to trigger activation of FcγRs and mediate potent ADCC/ADCP (112). As previously described, the N297A mutation abrogated the ability of anti-PD-1 antibodies to bind to any murine FcγR (Figure 3.2) (96). Nevertheless, it was critical to confirm this, as other reports showed that N297A mutations on an mIgG2a background may still show residual binding to FcγRIII and IV, as determined by SPR (96).

Nivolumab and Pembrolizumab were the first two mAbs targeting PD-1 that were approved by the FDA for the treatment of melanoma and NSCLC (6, 30). These mAbs directly occupy part of the PD-L1 binding site, but also induce conformational changes that are incompatible with PD-L1 binding. However, Pembrolizumab interacts with a larger surface area of PD-1 and shares more residues with the PD-L1 binding site compared to Nivolumab (293). This is thought to be key in the differences of affinity that these two mAbs present. Whilst Pembrolizumab binds with a very high affinity (Kd=27pm), Nivolumab presents a lower binding affinity (Kd=1.45nM), albeit higher than the affinity between PD-1 and PD-L1 (293, 294). When the binding properties of murine anti-PD-1 mAbs were assessed by SPR, these antibodies were found to bind to mouse PD-1 in a similar fashion, as illustrated by their similar binding kinetics and comparable dissociation rates (Figure 3.5). Nevertheless, a direct comparison between the affinity of clinically approved anti-PD-1 mAbs and murine EW1-9 mAbs could not be made, as the experimental set up in the current work measured avidity, rather than affinity. In order to be able to make these comparisons, a better experimental analysis would be required, and could involve the capture of EW1-9 mAbs to the chip and addition of soluble PD-1 recombinant protein to achieve monovalent interactions, thereby allowing the calculation of affinity constants.

In agreement with the SPR data, binding of murine anti-PD-1 mAbs to cell-surface PD-1 showed equivalent binding curves across isotypes (Figure 3.7 D). Likewise, the three isotypes competed with the parental rat antibody with similar ability in

vitro (Figure 3.7 E). Importantly, the modification of the Fc region did not alter the ability of anti-PD-1 antibodies to efficiently block the interaction of PD-1 with its two ligands, PD-L1 and PD-L2 (Figure 3.3). This agrees with the fact that most of the residues in PD-1 that interact with PD-L1 are also involved in the binding of PD-L2 (304).

Furthermore, the three murine isotypes showed similar in vivo half-life (Figure 3.8). This is important, as it indicates that the therapeutic efficacy will not be affected by the in vivo availability of the antibodies. One of the main factors that determine the half-life of therapeutic antibodies is the neonatal Fc receptor, FcRn. This receptor is involved in the recycling of IgG antibodies to maintain homeostatic levels in serum, and mutations that increase FcRn affinity can enhance antibody persistence (305). Although some initial studies suggested that deglycosylated mAbs had a lower affinity for FcRn (306), others found no difference in the relative in vivo clearance or FcRn affinity of aglycosylated IgG (307). Moreover, neither human IgG1-LALA or huIgG1-N297A isotype variants significantly affected pharmacokinetics in cynomolgus monkeys compared to wild type isotypes (308), in agreement with the findings in our murine anti-PD-1 mAbs.

In order to confirm the ability of our anti-PD-1 mAbs to block PD-1 signal and release T-cell proliferation, a suppression assay was developed. To note, it was first established that PD-1 expression on mouse T cells peaked 48 hours after in vitro stimulation with anti-CD3 mAbs (Figure 3.6), consistent with previous reports (34). Because of this, the length of the suppression assay was set to 3-4 days to leave sufficient time for anti-PD-1 mAbs to have effect. In the first instance, various methods were tried utilising different PD-L1-expressing cells in the co-cultures. However, neither stimulated BMDMs, cell lines from the myeloid lineage or stably transfected CHO cells provided the right extent of PD-L1-derived inhibition in vitro. In view of this, plate-bound recombinant proteins were used, despite them not providing the most physiological setting. Following this approach, all three murine anti-PD-1 mAbs were shown to be able to release PD-1-mediated inhibition of T-cell proliferation to a similar extent (Figure 3.15). This was consistent with the previous data on SPR, where anti-PD-1 mAbs could block PD-1: PD-L1 interaction equivalently.

Cumulative evidence in the last decades supports the important role of ADCP mediated by myeloid cells, such as macrophages, in the anti-tumour activity of direct tumour-targeting mAbs (302). This process is initiated by the engagement of activating FcγRs on the surface of macrophages by the Fc region of mAbs. The

intracellular cascade that occurs downstream FcγRs leads to effector functions such as cytokine secretion or phagocytosis (101). To investigate if murine anti-PD-1 mAbs could trigger phagocytosis in vitro, an assay was developed by combining BMDMs, activated and PD-1-expressing primary mouse T cells and murine anti-PD-1 mAbs. Murine IgG2a, which preferentially binds activating FcγRs, was the only Fc variant that induced an increase in phagocytosis compared to its irrelevant control (Figure 3.16). This is in agreement with previous reports, where mAbs bearing a high A/I ratio were shown to induce phagocytosis and deplete target cells (133, 138, 309). Notably, physiological expression of PD-1 on activated primary T cells was sufficient to trigger phagocytosis following opsonisation with anti-PD-1 mAbs. These results propose that phagocytosis of T cells could also occur in vivo, and supports the premise that engagement of activating FcγRs by anti-PD-1 mAbs may be detrimental to their therapeutic activity. In agreement with this, a novel human IgG4-S228P anti-PD-1 mAb cross-linked huFcγRI in macrophages and caused a small increase in phagocytosis of PD-1+ cells (165). Although these were transfected cells and not primary human T cells, this study showed that the clinically approved anti-PD-1 isotype can also lead to phagocytosis of target cells despite a lower A/I ratio.

Human IgG4 presents little or no binding to FcγRIIb as monomers, but it can bind FcγRIIb in the form of IgG4 ICs (93). Moreover, because of its low A/I ratio, IgG4, is more likely to engage the inhibitory FcγRIIb than other antibody isotypes. To date, it has been well described how immunostimulatory mAbs targeting TNFRSF members require the interaction of FcγRIIb to deliver their agonistic signal (132, 133). Besides TNFRSF receptors, engagement of FcγRIIb on monocytes by anti-CD28 mAb was shown to enable cross-linking of the mAb, which was sufficient to deliver its superagonistic activity (128). Hence, the possibility exists that FcγRIIb cross-linking of anti-PD-1 mAbs could lead to PD-1 signalling and inhibition of T cells. In fact, PD-1 can act as a monomer, in contrast to many co-stimulatory receptors that need multimerisation. Early after T-cell stimulation and before large numbers of PD-1 molecules are expressed on the T-cell surface, the inhibitory signal mediated by PD-1 ligation can be detected (33). This suggests that minimal cross-linking would be required to induce inhibition via PD-1 signalling, and further supports the potential detrimental effect of anti-PD-1 mAbs cross-linking by FcγRIIb.

Although significant effort was made to develop murine and human assays to elucidate the role of the inhibitory FcγR in anti-PD-1 mAbs, full optimisation was unfortunately not achieved. In terms of the murine assay, the quantity of plate-bound FcγRII needed to provide sufficient cross-linking would need to be

determined prior to testing the engagement of anti-PD-1 mAbs. To do this, soluble anti-CD3 mAb could be used in the presence of a titration of plate-bound Fc proteins and FcγRII to establish the minimum amount of plate-bound protein required in these conditions for a mAb to deliver agonistic signals. Then, plate-bound anti-CD3 mAb and Fc proteins could be combined with the required amount of FcγRII to investigate any differences in T-cell proliferation with anti-PD-1 mIgG1 versus mIgG1-N297A. Moreover, rather than assessing T-cell proliferation, phosphorylation of intracellular messengers downstream the TCR and CD28 could be studied by flow cytometry or western blot. PD-1 signalling can reduce phosphorylation of Akt and glycogen synthase kinase (GSK)-3 in human CD4 T cells (33). Hence, the phosphorylation status of these proteins could also be investigated following culture with FcγRII and anti-PD-1 mIgG1.

In parallel, it would be interesting to establish the ability of both human Nivolumab IgG4 and IgG4-FALA variants to release T-cell suppression and investigate any potential differences arising from FcγR binding. As a result of a mixed PBMC culture, both activating and inhibitory FcγRs are present and could modulate T-cell proliferation. To specifically interrogate the role of the inhibitory FcγRIIb, PBMCs could be pre-cultured at high-density prior to the assay, as it has been shown that human FcγRIIb can be up-regulated in monocytes under high-density cultures, favouring cross-linking and signalling of agonistic mAbs (128, 310). Furthermore, if any differences were noted between huIgG4 and huIgG4-FALA after high-density cultures, specific blockade of FcγRIIb with anti-huFcγRII mAbs may restore T-cell proliferation, and would thereby confirm that engagement of FcγRIIb was detrimental to anti-PD-1 therapy. Interestingly, a recent study associated hyperprogression after anti-PD-1 therapy to tumour macrophages and suggested that it was FcγR mediated, as whole IgG Nivolumab but not $F(ab)_2$ induced accelerated tumour growth in NSCLC patient-derived xenografts (PDX) (168). Although the authors proposed that FcγRIIb was the cause of HP in this study, no direct proof was demonstrated, and hence both activating and inhibitory FcγRs could be implicated. This would agree with the findings and hypotheses presented in this current chapter, where both activating and inhibitory FcγRs could be detrimental to anti-PD-1 mAb therapy by different mechanisms.

Overall, the pertinent contribution of each Fc-mediated mechanism, either phagocytosis or cross-linking, will likely depend on the relative expression of activating and inhibitory FcγRs at the TME. Due to the immunosuppressive nature of the TME, expression of FcγRIIb may be up-regulated at the tumour site prior to

immunotherapy (121, 311, 312); however, following an initial immune activation induced by anti-PD-1 mAbs, activating FcγRs could be up-regulated. In the former scenario, cross-linking of PD-1 could diminish the efficacy of anti-PD-1 mAbs, but as inflammation progresses and a larger number of activated T cells are recruited, up-regulation of activating FcγRs may favour phagocytosis of effector T cells.

Chapter 4: In vivo characterisation of murine anti-PD-1 antibodies

4.1 Chapter introduction

Although in vitro studies are informative in allowing us to investigate the effect of single interactions on T-cell proliferation and function, they are limited in terms of how closely they reflect the complex environment of in vivo systems. It is thus important to ascertain the properties and function that murine anti-PD-1 mAbs may have in vivo, to have a more accurate picture of the role of anti-PD-1 isotype in generating anti-tumour immunity.

In cancer, the TME is extremely complex and exhibits numerous mechanisms of immunosuppression. To avoid the confounding issues potentially introduced by the presence of such a highly immunosuppressive environment, the murine anti-PD-1 isotypes were first tested in vivo using a vaccination setting with the model antigen ovalbumin together with agonistic anti-CD40 mAb and the OT-I cell transfer model. This model can be used to monitor antigen-specific T-cell responses in blood, enabling the characterisation of T-cell subsets during the course of an immune response. Thus, the magnitude of CD8 T-cell expansion in the presence of different anti-PD-1 isotypes may inform about the ability of these mAbs to release T-cell inhibition.

Secondly, to begin to elucidate how the choice of isotype would alter the efficacy of anti-PD-1 mAbs in cancer, the colorectal cancer model MC38 was used. This murine cell line was chosen owing to its immunogenic nature and its known sensitivity to anti-PD-1 therapy, which would maximise the potential to observe any differences in activity across anti-PD-1 isotypes. Therefore, in this chapter we established the in vivo activity of anti-PD-1 mAbs in a vaccination and an immunotherapy-sensitive tumour model settings, and investigated the type and magnitude of the immune response induced by each of the antibody isotypes.

4.2 OT-I transfer model

The OT-I transfer model is based on the adoptive transfer of ovalbumin specific CD8 T cells from transgenic OT-I mice (313). OT-I CD8 T cells include a population that bear a high-affinity TCR for the MHC-I specific SIINFEKL peptide derived from ovalbumin. Expansion and phenotype of SIINFEKL-reactive OT-I cells can be serially monitored through tetramer staining after administration of active immune interventions (288). In order to transfer an equal number of SIINFEKL-reactive OT-I cells into recipient mice, splenic OT-I cells were stained for the CD8 marker and an MHC-I tetramer carrying the OT-I cognate epitope. Hence, double-positive cells shown in Figure 4.1 represent the CD8 T cells that are specific for the ovalbumin peptide. The expression of the marker CD62L was also assessed to obtain the percentage of naïve OT-I CD8 T cells. An equal number of 10^5 tetramer+, CD62L+ OT-I CD8 T cells was then transferred to recipient mice at the start of each experiment.

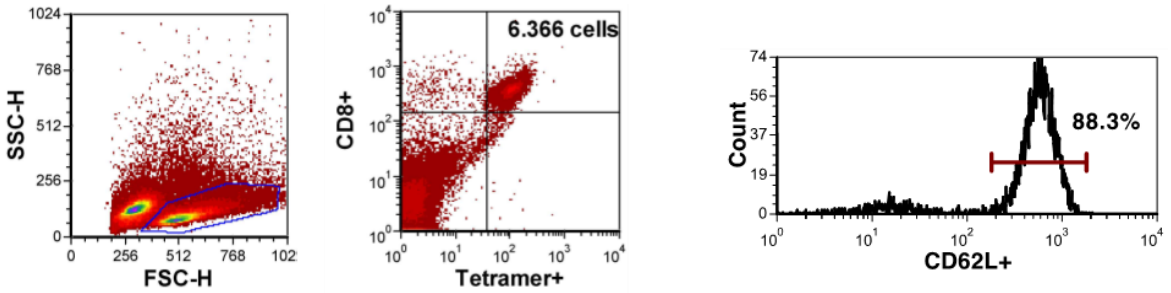

Figure 4.1 OT-I set-up gating strategy.
Single-cell suspensions of OT-I splenocytes were obtained from OT-I transgenic mice and stained for flow cytometry analysis. From the lymphocyte gate, double-positive cells for CD8 and tetramer were gated and the percentage of CD62L+ cells was checked. At the start of OT-I transfer experiments, an equal number of CD8+Tet+CD62L+ cells were injected IV into aged- and sex-matched wild type C57BL/6 mice.

One day post OT-I transfer, mice were administrated with ovalbumin and the appropriate antibodies as per treatment group, to trigger antigen-specific expansion of OT-I cells. To assess primary responses, the percentage of Tet+ OT-I cells in blood and their phenotype were monitored on days 3, 5, 7, 14 and 21 after treatment. As illustrated in Figure 4.2, doublets were excluded from the initial lymphocyte gate (A) and CD8 T cells were divided into two subsets according to tetramer staining. Tetramer positive (Tet+) cells corresponded to the expanded OT-I population specific for the high affinity SIINFEKL, whilst tetramer negative CD8 T cells represented OT-I cells with specificities other than SIINFEKL, which are

generally lower affinity. In this setting, endogenous responses from recipient mice were fully blocked after transferring 10^5 OT-I T cells, as shown in previous studies (313).

To explore the nature of T-cell responses, the phenotype of both tetramer positive and negative CD8 T-cell subsets was assessed according to the expression of CD44, CD62L and PD-1, using isotype controls (Figure 4.2 B-C) as a reference. Resting T cells are characterised by the expression of the lymph-node homing receptor CD62L and low expression of CD44. Upon encounter with the cognate antigen, naïve T cells expand and differentiate into memory T cells, which are subdivided in central memory (CD62L+CD44+) or effector (CD62L-CD44+) T cells, exhibiting distinct functional properties (152). Central memory T cells are a long-lived subset of memory cells that home to lymph nodes, where they proliferate in a homeostatic fashion. They bear little effector capacity but can give rise to secondary effector T cells upon antigen re-encounter. In contrast, effector T cells (CD44+CD62L-) are short-lived cells that preferentially home to the tissue, have a higher proliferation rate and can rapidly mediate effector functions (152). In regards to PD-1 expression, up-regulation on T cells upon antigen encounter and co-stimulatory signals can provide evidence of an activated T-cell phenotype (34).

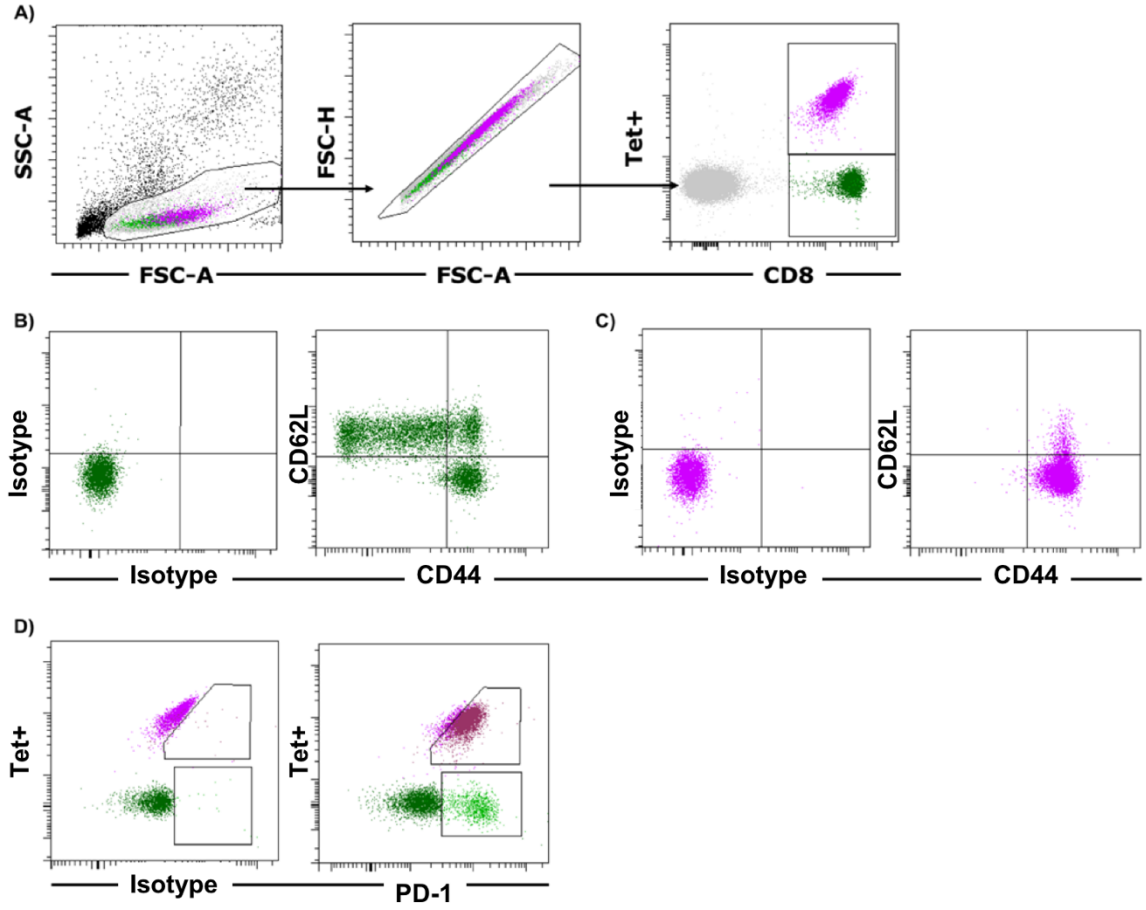

Figure 4.2 Representative example of the gating strategy followed in OT-I transfer experiments.
A) Lymphocytes were gated according to FSC-SSC plot and doublets were excluded. Expression of CD8 and tetramer staining were used to gate on SIINFEKL-specific CD8 T cells (double positives) and ovalbumin-reactive CD8 T cells with a different epitope specificity (tetramer negative). B-C) Percentage of CD62L+, CD44+ or double positives was calculated in Tet negative (B) and Tet positive (C) CD8 T cells. D) Percentage of PD-1+ cells, obtained by subtracting isotype values from stained samples.

4.2.1 OT-I response upon treatment with anti-CD40 mAbs

Following T-cell activation, up-regulation and ligation of PD-1 leads to dephosphorylation of intracellular mediators downstream both TCR and co-stimulatory receptors such as CD28, thereby reducing T-cell activation (45-47). Despite administration of ovalbumin, the OT-I TCR cognate antigen, it was hypothesised that the lack of co-stimulatory signals would prevent sufficient T-cell activation to synergise with anti-PD-1 mAbs. This was confirmed in a preliminary OT-I transfer experiment, where PD-1 blockade was unable to expand OT-1 responses in the presence of ovalbumin alone (see Appendix A, Figure 6.2).

In order to try and enhance the effects of anti-PD-1 mAbs on OT-I expansion, concurrent administration of checkpoint inhibitors and agonistic anti-CD40 mAbs was investigated. This was performed on the basis that CD40 agonists would induce sufficient activation of OT-I cells to up-regulate surface PD-1, thereby rendering T cells susceptible to PD-1 mediated inhibition and subsequent release by PD-1 blockade. Agonistic anti-CD40 mAbs can bind to CD40 expressed on APCs and induce their activation in a similar fashion to the natural ligand, CD40L. Activated APCs can in turn secrete cytokines such as IL-12 that promote Th1 responses (86), leading to the release of IFN-γ and CD8 T-cell activation with subsequent PD-1 up-regulation. In support of this, agonistic anti-CD40 mAbs up-regulated PD-1 on both CD8 and CD4 TILs from MC38 tumours (314). Importantly, CD40 agonists also led to an IFN-γ dependent up-regulation of PD-L1 on tumour-infiltrating monocytes and macrophages (314), further suggesting that these mAbs could favour the inhibitory effect mediated by the PD-1/ PD-L1 pathway and the subsequent release by PD-1 blockade.

To test whether PD-1 blockade could enhance T-cell responses, a suboptimal T-cell stimulation was required. To find a suboptimal dose of agonistic anti-CD40 mAb that was capable of inducing PD-1 expression, a range of concentrations were tested across two different OT-I experiments. As displayed in Figure 4.3 B, mice treated with both 50 and 100 µg of anti-CD40 mAb showed maximal expansion of Tet+ OT-I cells and similar kinetics. A concentration as low as 25 µg was sufficient to achieve the same maximal level of Tet+ CD8 T-cell expansion as the positive control (100 µg), despite the OT-I response contracting faster. Whilst 2.5 µg showed limited enhancement, 10 µg seemed to deliver good Tet+ CD8 expansion but without reaching maximal. In terms of PD-1 expression, both Tet+ and negative CD8 subsets demonstrated PD-1 expression, albeit with different kinetics (Figure 4.3 C,D). Results showed that up-regulation of PD-1 on Tet+ CD8 T cells was already maximal on day 3 after treatment and was reached even with lower doses of anti-CD40 mAb (Figure 4.3 C). This indicates that PD-1 levels were not dose-dependent and thus suggested that treatment with murine anti-PD-1 mAbs at lower doses of anti-CD40 could potentiate OT-I expansion by blocking PD-1. On the other hand, 100 µg of anti-CD40 mAb appeared to also activate a small percentage of CD8 T cells specific for non-SIINFEKL antigens, as PD-1 levels increased in the tetramer negative population at day 7 (Figure 4.3 D), compared to ovalbumin alone or in combination with lower doses of anti-CD40 mAb. Overall, based on its ability to induce suboptimal expansion of Tet+ OT-I cells compared to higher doses, 10 µg of anti-CD40 mAb was chosen for subsequent experiments.

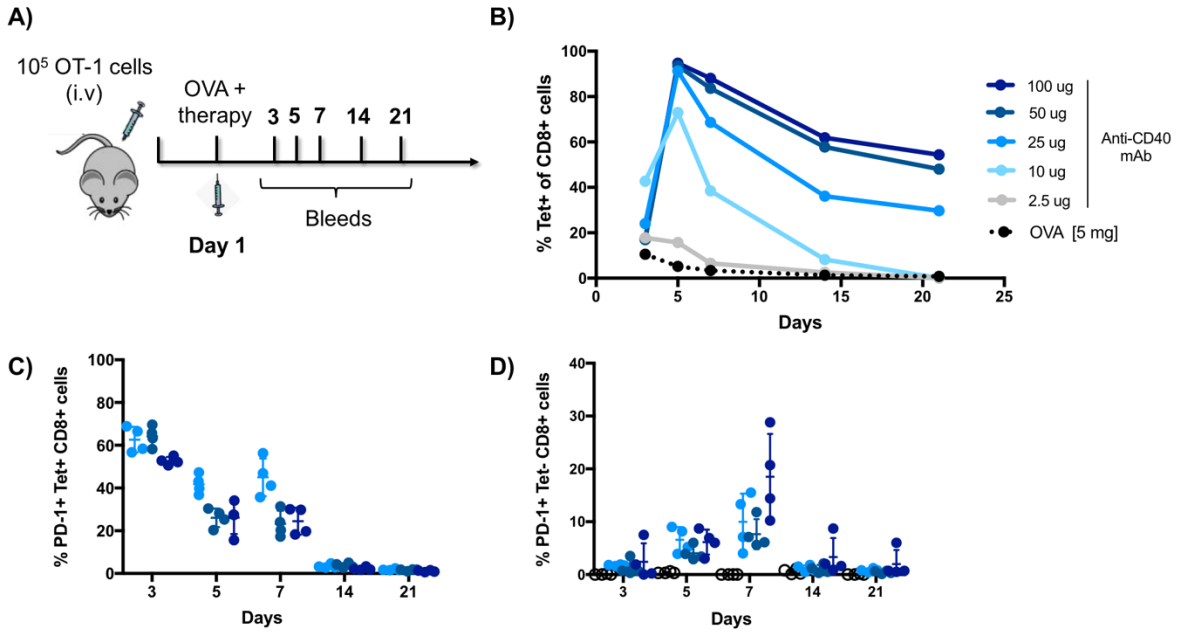

Figure 4.3 OT-I primary response after therapy with a titration of anti-CD40 mAb plus ovalbumin.
A) Schematic summary of the experiment. One day after OT-I adoptive transfer, a titration of anti-CD40 mAb (2.5 – 100 µg) was given Ip in combination with 5 mgs of ovalbumin. C-D) Percentage of Tet+ (C) and tetramer negative CD8 T cells expressing PD-1. Due to the low percentage of Tet+ CD8 T cells in the ovalbumin control group, PD-1 expression was not shown for this group. Bars represent mean ± S.D. Experiment performed once, N=4 mice per group.

4.2.2 Enhancement of primary OT-I responses by anti-PD-1 mAbs

To test the ability of murine anti-PD-1 mAbs to enhance OT-I responses, mice were immunised with ovalbumin in combination with anti-PD-1 isotypes and 10 µg of anti-CD40 mAb. As shown in Figure 4.4 (B,C), at the peak of the response (day 5), mIgG1-N297A enhanced Tet+ OT-I expansion compared to the other two murine isotypes and the group treated with irrelevant mAbs. As the immune response decreased, all murine isotype groups contracted with similar kinetics although mIgG1-N297A still showed enhanced Tet+ CD8 expansion compared to the other anti-PD-1 isotypes and irrelevant group at day 7 (Figure 4.4 D) and compared to mIgG2a and irrelevant groups at day 14 and 21 (Figure 4.4 E,F). As expected, mice in the positive control group (100 µg of anti-CD40 mAb) showed increased Tet+ OT-I expansion from day 5, whilst animals treated with ovalbumin alone did not significantly up-regulate OT-I responses (Figure 4.4).

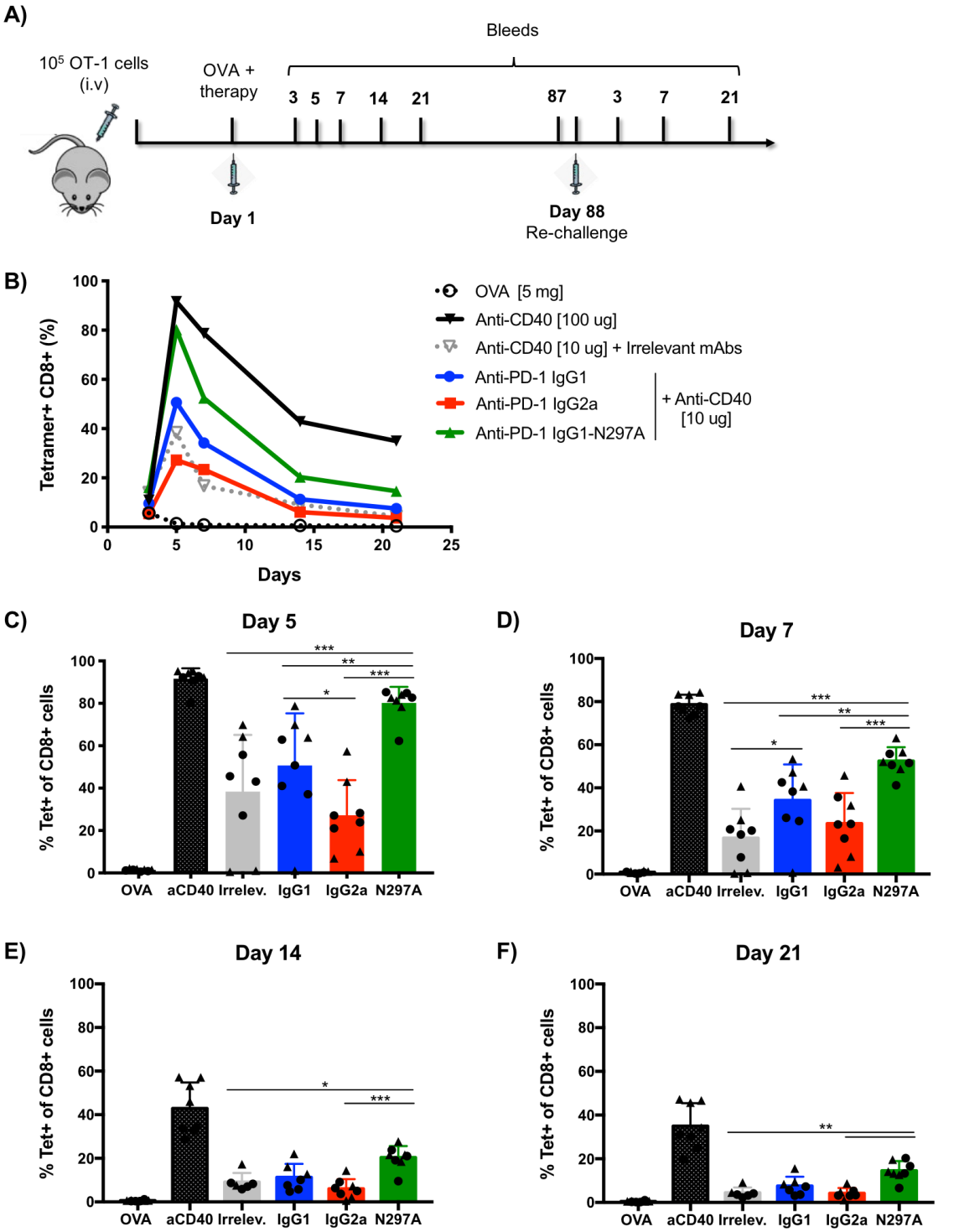

Figure 4.4 Primary OT-I response after administration of murine anti-PD-1 mAbs in combination with anti-CD40 mAb.
A) Schematic diagram of the schedule and timelines of the assay. B) Kinetics of OT-I expansion represented as Tet+ CD8 T cells as a percentage of total CD8 T cells. A baseline dose of 5 mg ovalbumin was given alone (negative control) or in combination with 100 µg of anti-CD40 mAb (positive control). For treatment groups, 10 µg of anti-CD40 were given in addition to 250 µg of murine isotypes or a combination of irrelevant AT10 mAbs (mIgG1, mIgG2a and mIgG1-N297A). C-F) Percentage of Tet+ OT-I cells on days 5 (C), 7 (D), 14 (E) and 21 (F). Experiment performed twice, N=8 mice per group. Triangles correspond to the first experiment whilst circles correspond to the second. Bars represent mean ± S.D, ***p<0.001, **p<0.01, *p<0.05 (One-way ANOVA).

Due to technical issues, expression of PD-1 in the anti-PD-1 mIgG1, mIgG2a and mIgG1-N297A groups was only assessed in the second experiment. Despite some variability in control groups, anti-PD-1 mIgG1-N297A displayed the highest up-regulation on Tet+ CD8 T cells at the peak of the response (Figure 4.5 A), followed by mIgG1 and finally mIgG2a. Interestingly, in the tetramer negative CD8 subset, IgG1-N297A was the only anti-PD-1 isotype that triggered an increase in percentage of PD-1 positive cells compared to the irrelevant control group (Figure 4.5 B). Concurrent with the peak in Tet+ CD8 T-cell expansion, PD-1 expression was higher in the mIgG1-N297A group on days 5 and 7, suggesting that this antibody could also activate other lower-affinity T-cell clones.

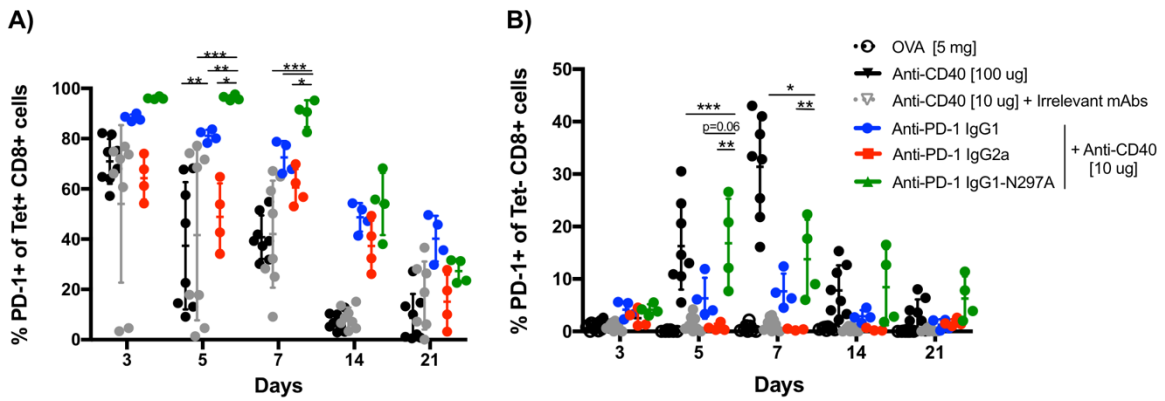

Figure 4.5 Expression of PD-1 during primary OT-I expansion.
A) Percentage of Tet+ CD8 T cells expressing PD-1. Due to the low percentage of Tet+ CD8 T cells in the ovalbumin control group, PD-1 expression was not shown for this group. B) Percentage of tetramer negative CD8 T cells expressing PD-1. Experiment performed twice, N=8 mice for OVA, anti-CD40 100 µg and irrelevant groups (AT10 mIgG1, mIgG2a, mIgG1-N297A); N=4 mice for anti-PD-1 mIgG1, mIgG2a and mIgG1-N297A groups. Graphs show mean ± S.D, ***p<0.001, **p<0.01, *p<0.05 (One-way ANOVA).

Besides the expansion of Tet+ OT-I cells, the expression of surface markers on T cells can give important information about the nature of the immune response triggered. According to the expression of CD62L and CD44, the percentage of effector Tet+ OT-I cells peaked at day 5 and 7 after therapy (Figure 4.6 B,C) in most treatment groups, indicative of the expansion and differentiation of naïve T cells due to antigen encounter. With the exception of ovalbumin-treated mice, all groups presented similar high percentages of effector CD44+ T cells (>80%) from day 7, which persisted throughout the primary response at the expense of CD44+CD62L+ T cells that remained lower than 20% (Figure 4.6 C-E). However, both positive control and anti-PD-1 mIgG1-N297A groups appeared to display faster kinetics in effector T-cell expansion at the early time points (Figure 4.6 A,B).

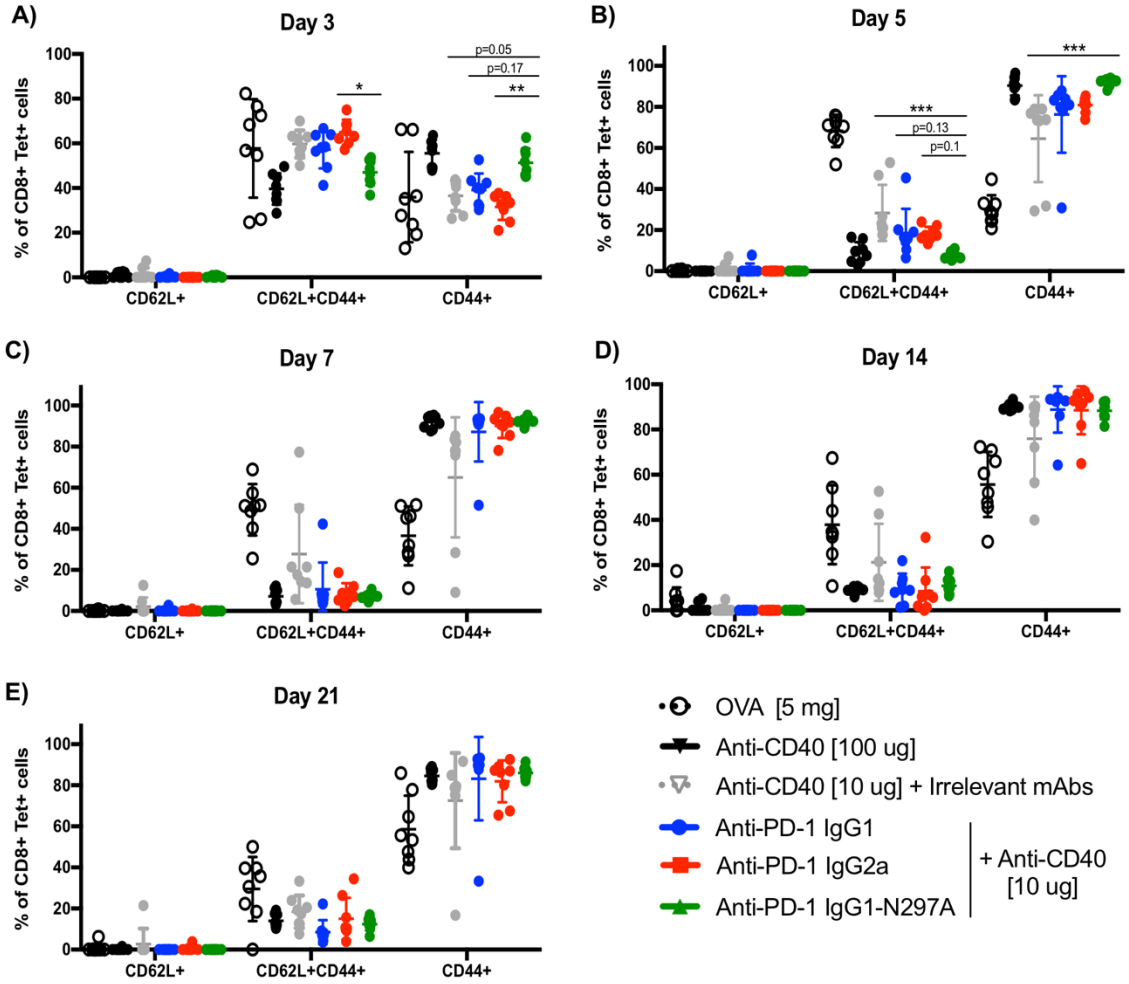

Figure 4.6 Phenotype of tetramer positive OT-I responses during the primary response.
A-E) Graphs represent the percentage of naïve (CD62L+), effector (CD44+) and central memory (CD62L+CD44+) T cells within Tet+ CD8 T cells on days 3 (A), 5 (B), 7 (C), 14 (D) and 21 (E) after treatment with anti-CD40 and anti-PD-1 mAbs. Experiment performed twice, N=8 total mice per group. Bars represent mean ± S.D, ***p<0.001, **p<0.01, *p<0.05 (One-way ANOVA).

In contrast, the majority of OT-I cells in the tetramer negative population were naïve, with ovalbumin-treated mice showing the highest percentage at the peak of the response (Figure 4.7 B,C). However, some changes in the subsets of memory T cells were observed. All groups treated with murine anti-PD-1 mAbs and the positive control showed a similar distribution of T-cell percentages on day 3 (A). However, mice in both the positive control and anti-PD-1 mIgG1-N297A groups expanded a higher percentage of effector CD8 T cells at the peak of the response compared to mice treated with irrelevant, mIgG1 or mIgG2a anti-PD-1 mAbs. This increase in effector T cells was likely driven by a reduction in naïve CD8 T cells that was observed in parallel at day 5 and 7 (Figure 4.7 B,C) and coincided with the up-regulation of PD-1 expression mentioned previously (Figure 4.5 B). Taken together,

these results suggest that anti-PD-1 mIgG1-N297A could induce bystander activation of lower affinity T-cell clones, which led to increased number of effector T cells expressing PD-1.

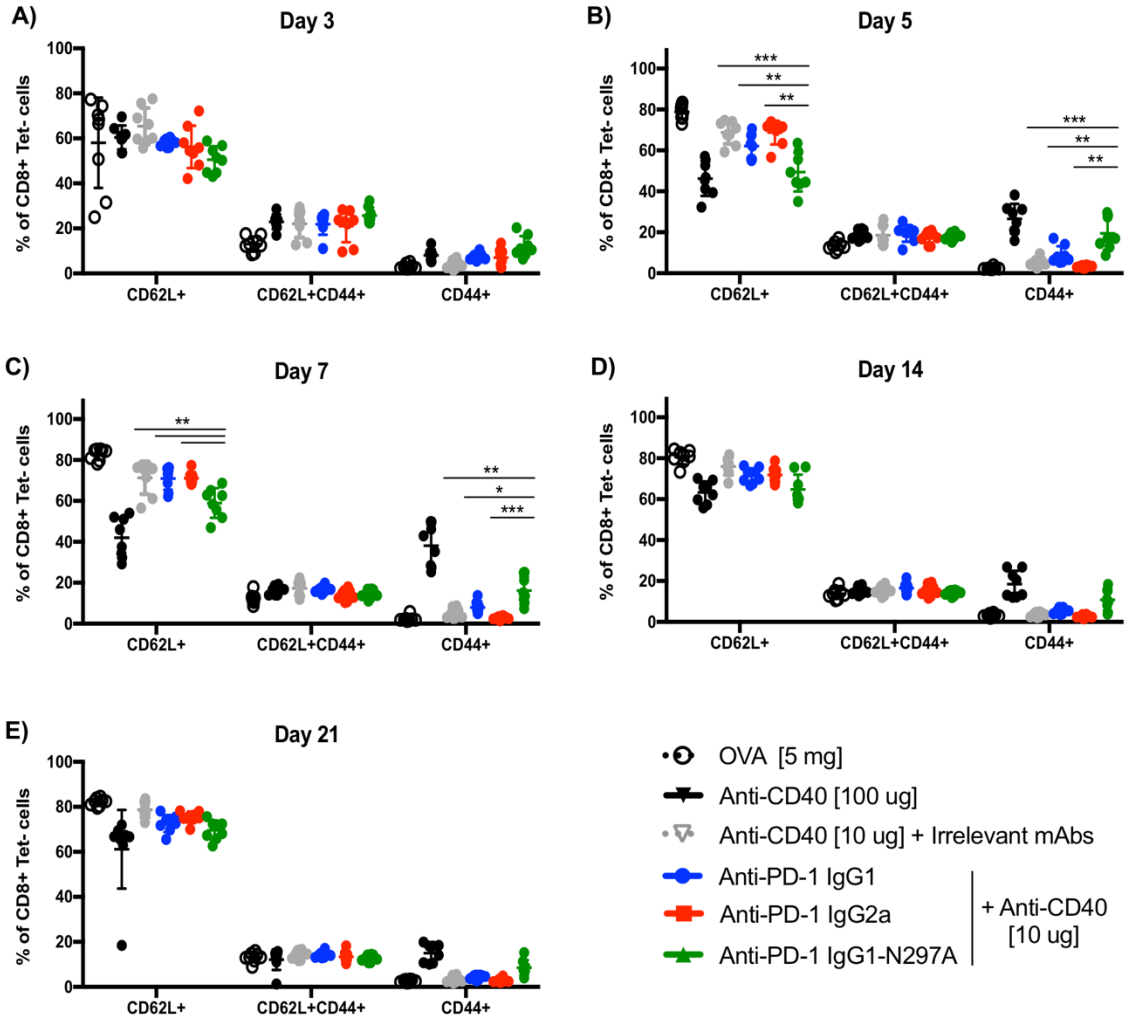

Figure 4.7 Phenotype of tetramer negative OT-I responses during the primary response.
A-E) Graphs represent the percentage of naïve (CD62L+), effector (CD44+) and central memory (CD62L+CD44+) T cells within tetramer negative cells on days 3 (A), 5 (B), 7 (C), 14 (D) and 21 (E) after treatment with anti-CD40 and anti-PD-1 mAbs. Experiment performed twice, N=8 mice per group. Bars represent mean ± S.D, ***p<0.001, **p<0.01, *p<0.05 (One-way ANOVA).

4.2.3 Enhancement of memory OT-I responses by anti-PD-1 mAbs

In order to achieve long-lasting anti-tumour immunity, it is essential not only to mount strong immune responses, but also to be able to generate immunological memory that can prevent tumour relapse. Thus, differences in secondary responses following initial combination treatments were investigated. To perform this, mice where OT-I expansion had contracted to less than 10% of total CD8 T cells were re-challenged with SIINFEKL peptide. Of note, the baseline phenotype according to CD62L and CD44 expression was equivalent across groups both in Tet+ (see Appendix A, Figure 6.3 A) and tetramer negative (see Appendix A, Figure 6.4 A) CD8 T-cell subsets. Despite some variability across experimental replicates (Figure 4.8 A,B), anti-PD-1 mIgG1-N297A showed increased OT-I expansion compared to the irrelevant control and the other two anti-PD-1 isotypes throughout the secondary response (Figure 4.8 C-F). Whilst mIgG2a showed no expansion of OT-I cells, anti-PD-1 mIgG1 increased the percentage of Tet+ OT-I cells at the peak of the secondary response (E). This enhancement may reflect the small increase on OT-I expansion observed on day 7 of the primary response (Figure 4.4 C,D).

In terms of PD-1, expression levels rapidly increased in all three anti-PD-1 treatment groups and irrelevant controls in the Tet+ population after re-challenge (Figure 4.8 G). Although the overall magnitude of the secondary response with anti-PD-1 mIgG2a was limited, the fact that this isotype showed up-regulation of PD-1 could indicate that the small numbers of expanded memory OT-I T cells may remain functional and become activated upon re-challenge. In contrast, PD-1 expression remained very low within the tetramer negative CD8 T cells, with no clear differences observed across groups (Figure 4.8 H). In a similar way, the frequencies of different T-cell subpopulations, as defined by CD62L and CD44 expression, did not vary amongst treatment groups. Effector CD44+ Tet+ CD8 T cells rapidly peaked in a similar fashion across groups after re-challenge (see Appendix A, Figure 6.3). Nevertheless, mice in the mIgG1-N297A group displayed a faster expansion of effector T cells from central memory T cells compared to the other groups (see Appendix A, Figure 6.3 B). As expected due to their different epitope specificity, the majority of tetramer negative T cells remained naïve after re-challenge with SIINFEKL and did not expand nor changed phenotype (see Appendix A, Figure 6.4).

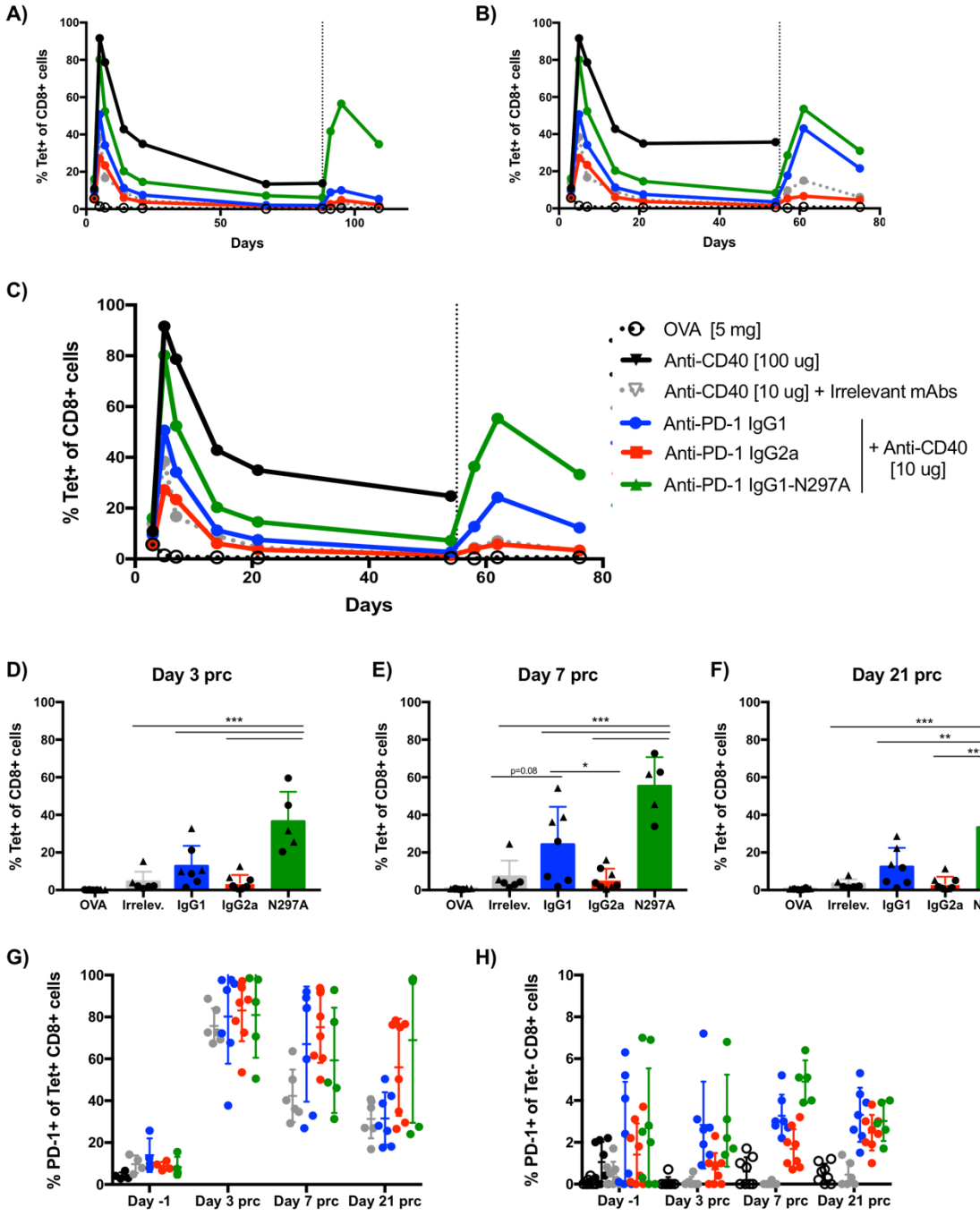

Figure 4.8 Memory OT-I response after re-challenge with SIINFEKL peptide. A-C) Kinetics of OT-I expansion after re-challenge in the first (A) and second (B) experiments as well as the combined results (C). Prior to re-challenge, percentage of OT-I T cells in blood was assessed and re-challenge was only performed if the levels were below 10%. Re-challenge was performed with SIINFEKL peptide IV and blood was withdrawn on days 3, 7 and 21 after re-challenge. D-F) Percentage of Tet+ OT-I cells on days 3 (D), 7 (E) and 21 (F) after re-challenge. G-H) Percentage of PD-1 expression in Tet+ (G) and tetramer negative (H) CD8 T cells. Due to the low percentage of Tet+ CD8 T cells in the ovalbumin control group, PD-1 expression was not shown for this group. Experiment performed twice, N=4-7 mice per group (triangles indicate values from experiment 1 and circles from experiment 2). None of the mice treated with 100 µg of anti-CD40 mAb were able to be re-challenged due to persistent high levels of Tet+ OT-I T cells. Bars represent mean ± S.D, ***p<0.001, **p<0.01, *p<0.05 (One-way ANOVA).

4.3 Endogenous anti-OVA response to anti-PD-1 mAbs

The OT-I transfer model provides a very useful tool to investigate antigen-specific T-cell responses, but the high affinity of the OT-I T-cell TCR for their cognate antigen may create an artificial model. To validate the previous findings in a more physiological setting, it was investigated whether these results could be recapitulated in the context of an endogenous response to ovalbumin, without an adoptive transfer.

4.3.1 Endogenous response upon treatment with anti-CD40 mAbs

Similar to OT-I transfer experiments, the ability of 10 and 100 μg of anti-CD40 mAb to induce expansion of ovalbumin-reactive T cells was first confirmed (Figure 4.9). In the case of an endogenous response to ovalbumin, 100 μg of anti-CD40 mAb only expanded an average of 10% Tet+ CD8 T cells, whereas the lower dose of 10 μg only showed a minimal increase (Figure 4.9 B,C). There was also a delay in the peak of the response, which was maximal at day 7 (B) whilst it peaked on day 5 during OT-I responses (Figure 4.4 B). In view of this slower kinetics, day 5 bleeds were not performed in subsequent endogenous response experiments.

Expression of PD-1 was high in Tet+ CD8 T cells with both doses of anti-CD40 mAb (Figure 4.9 D), suggestive of the potential for Tet+ responses to be augmented by anti-PD-1 mAbs. Moreover, the percentage of tetramer negative CD8 T cells expressing PD-1 was also increased at both doses, although there was a larger increase with the higher dose of anti-CD40 mAb (Figure 4.9 E). This up-regulation presented similar kinetics to those seen in OT-I experiments (Figure 4.3 D). Although the overall levels of CD8 expansion were notably lower, these results recapitulated those from OT-I experiments, and hence these two doses of anti-CD40 mAb were used in subsequent experiments.

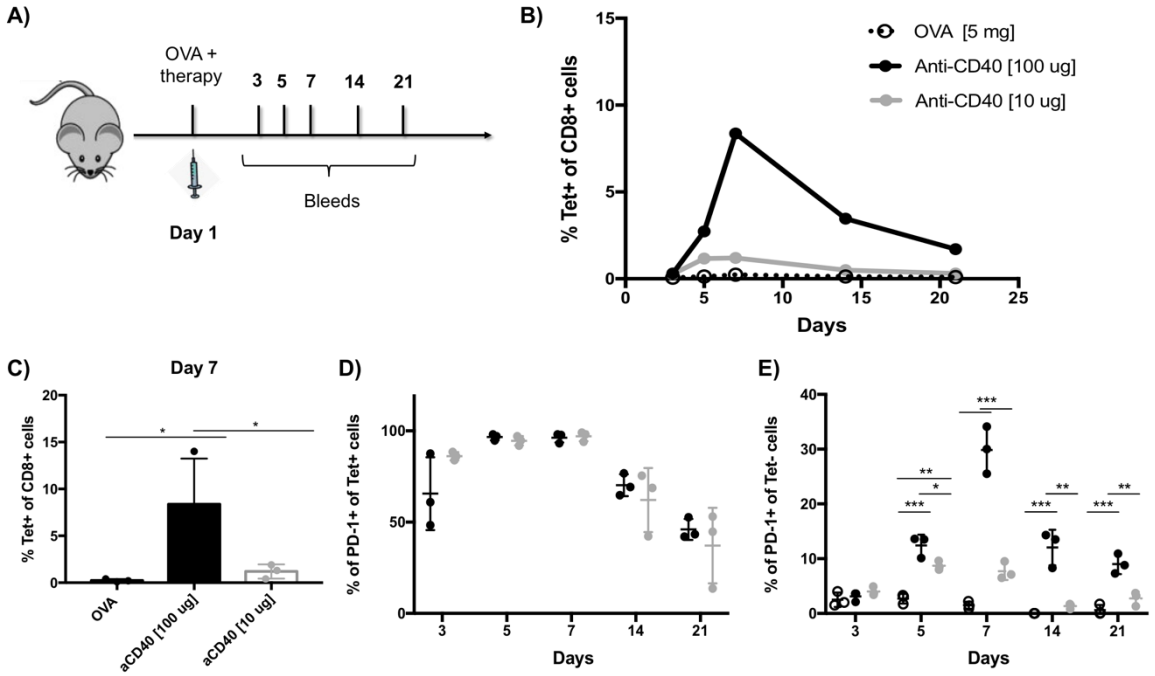

Figure 4.9 Endogenous response to ovalbumin plus anti-CD40 mAb.
A) Schematic summary of the experiment. After initial challenge with ovalbumin plus antibody treatments, animals were bled on days 3, 5, 7, 14 and 21 and blood was processed as previously described. The gating strategy followed was detailed in Figure 4.2. B) Kinetics of Tet+ CD8 T-cell expansion. C) Percentage of Tet+ CD8 T cells at day. D-E) Percentage of Tet+ (D) and tetramer negative (E) CD8 T cells expressing PD-1. Due to the low percentage of Tet+ CD8 T cells in the ovalbumin control group, PD-1 expression was not shown for this group. Bars represent mean ± S.D. Experiment performed once. N=3 mice per group, *p<0.05 (One-way ANOVA).

4.3.2 Enhancement of endogenous response by anti-PD-1 mAbs

Next, anti-PD-1 mAbs were combined with 10 μg of anti-CD40 mAb and endogenous responses to ovalbumin were assessed. As shown in Figure 4.10 B, only the mIgG1-N297A isotype enhanced Tet+ CD8 expansion and increased the percentage of Tet+ CD8 T cells at the peak of the response (Figure 4.10 C), albeit with large variability. This is consistent with the expression of PD-1 in Tet+ CD8 T cells, which was maximal only in mice treated with 100 μg of anti-CD40 mAb and the mIgG1-N297A anti-PD-1 group (Figure 4.10 D). Interestingly, up-regulation of PD-1 was also noted in the tetramer negative subset (Figure 4.10 E) in the same two groups, recapitulating the results from the OT-I transfer experiments and pointing to a broader activation of T cells. Nevertheless, no differences were observed in terms of the phenotype of expanded Tet+ CD8 T cells, either at the peak of the response (Figure 4.10 F) or at other time points (see Appendix A, Figure 6.5). No differences were found within the tetramer negative subset neither (see Appendix A, Figure 6.6 A-C) except for a slight rise in effector T cells in both the

positive control and anti-PD-1 mIgG1-N297A groups on day 7 (Figure 4.10 G). Although this was not statistically significant, this possible increment agrees with the expansion seen in OT-I experiments (Figure 4.7 B,C). Taken together, these results endorsed the findings that mIgG1-N297A is the optimal anti-PD-1 isotype for releasing PD-1 restricted T-cell responses in vivo.

To investigate whether the changes observed during the primary T-cell expansion translated into a differential ability to drive memory responses, the same protocol used for OT-I transfer re-challenges was followed (see 2.7.2). However, the levels of remaining Tet+ CD8 T cells at the end of the primary endogenous response were found to be insufficient to mount detectable memory responses in any of the treatment groups other than the positive control (see Appendix A, Figure 6.8 A). This might be related to the fact that the levels of T-cell expansion achieved during the primary response were very low and hence not enough to be maintained for a secondary response. Accordingly, no changes were seen in PD-1 expression or T-cell phenotype amongst groups (see Appendix A, Figure 6.8 B-J) and hence, the potential differences in memory responses triggered by anti-PD-1 isotypes could not be assessed.

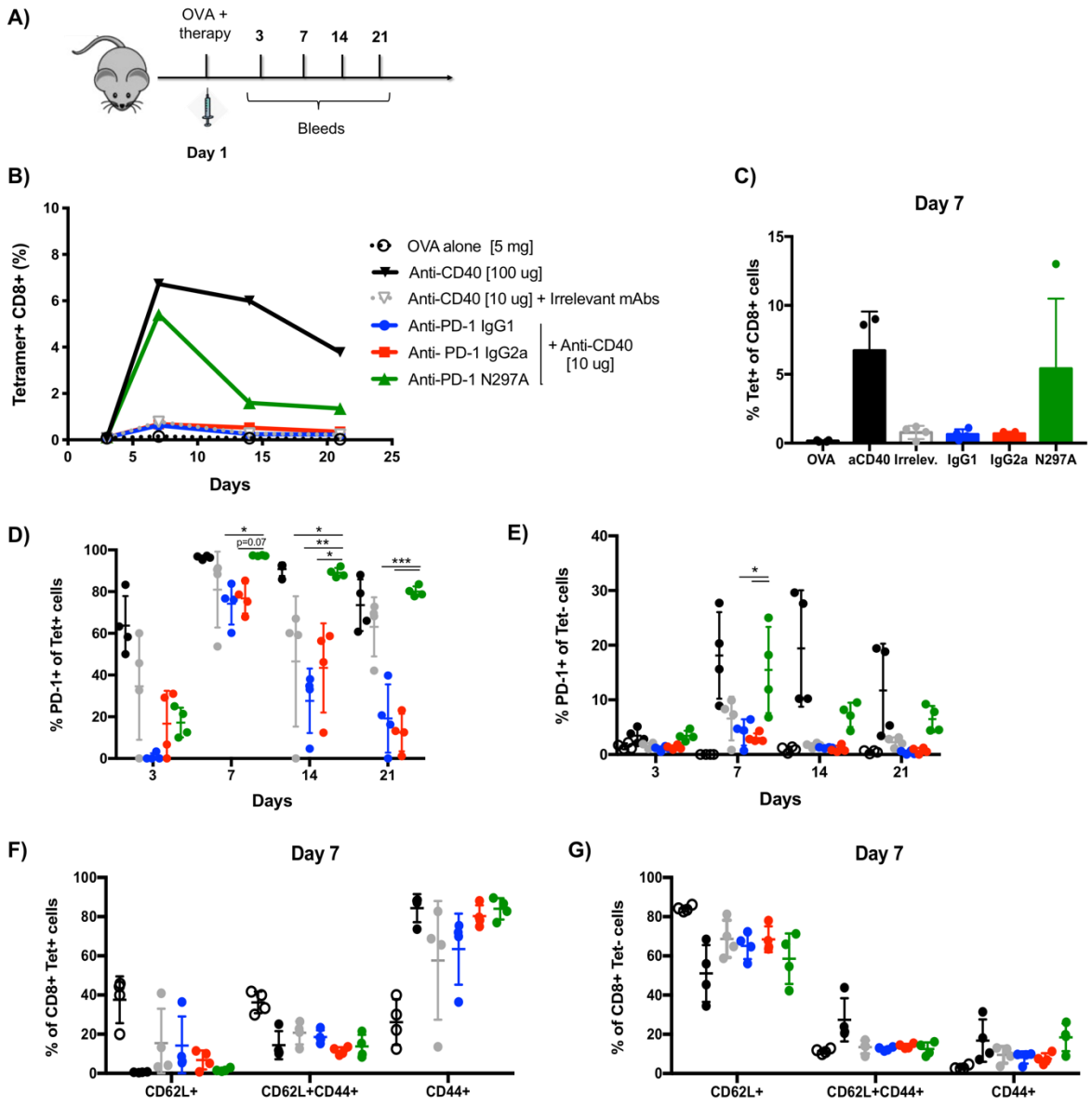

Figure 4.10 Enhancement of endogenous anti-OVA responses by anti-PD-1 mAbs.

A) Schematic diagram of the timelines of the assay. B) Kinetics of the endogenous response represented as percentage of tetramer+ CD8 amongst all CD8 T cells at each time point. A baseline dose of 5 mg ovalbumin was given alone (negative control) or in combination with 100 µg of anti-CD40 mAb (positive control). For the treatment groups, 10 µg of anti-CD40 were given in addition to 250 µg of murine isotypes or a combination of irrelevant mAbs. C) Percentage of Tet+ CD8 T cells on day 7. D-E) Expression of PD-1 in Tet+ (D) and tetramer negative (E) CD8 T-cell subsets. Due to the low percentage of Tet+ CD8 T cells in the ovalbumin control group, PD-1 expression was not shown for this group. F-G) Phenotype of Tet+ (F) and tetramer negative (G) CD8 T cells on day 7 according to CD62L and CD44 staining. Experiment performed once, N=4 mice per group. Bars represent mean ± S.D, ***p<0.001, **p<0.01, *p<0.05 (One-way ANOVA).

As mentioned before, the levels of Tet+ CD8 T-cell expansion achieved by the highest dose of anti-CD40 mAbs during an endogenous response to ovalbumin were relatively low (Figure 4.10 B) compared to the maximal expansion observed in OT-I experiments (Figure 4.4 B). To investigate if anti-PD-1 mIgG1-N297A could further enhance T-cell responses at the highest dose of the anti-CD40 mAb adjuvant, mice were treated with 100 µg of anti-CD40 mAb plus irrelevant or anti-PD-1 mAb. Similar to the previous results, addition of anti-PD-1 mAb appeared to increase Tet+ CD8 T cells at the peak of the response (Figure 4.11 B,C). Up-regulation of PD-1 in Tet+ CD8 T cells was already maximal in the anti-CD40 group alone (D), and no differences were observed throughout the response. Furthermore, both treatment groups showed expansion of CD44+ Tet+ CD8 T cells to a similar extent and with similar kinetics (see Appendix A, Figure 6.7).

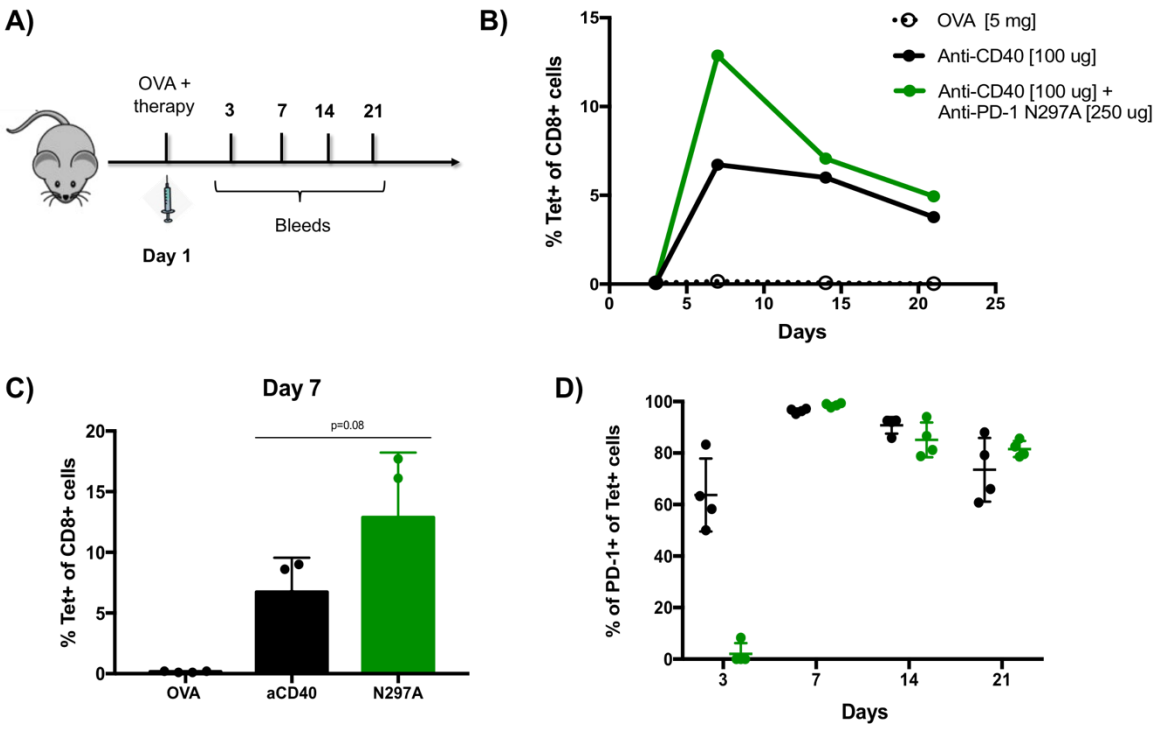

Figure 4.11 Expansion of Tet+ CD8 T cells by anti-PD-1 mIgG1-N297A during an endogenous anti-OVA response.
A) Schematic diagram of the timelines of the assay. B) Expansion of Tet+ cells amongst all CD8 T cells at each time point. A baseline dose of 5 mg ovalbumin was given alone; in combination with 100 µg of anti-CD40 mAb plus irrelevant mAb; or in combination with 100 µg of anti-CD40 mAb plus 250 µg of anti-PD-1 mIgG1-N297A. C) Percentage of Tet+ CD8 T cells on day 7. D) Percentage of PD-1 expressing Tet+ CD8 T cells. Due to the low percentage of Tet+ CD8 T cells in the ovalbumin control group, PD-1 expression was not shown for this group. Experiment performed once, N=4 mice per group. Bars represent mean ± S.D, $p>0.05$ (One-way ANOVA).

Interestingly, a significant expansion of tetramer negative CD8 T cells by anti-PD-1 treatment was noted (Figure 4.12 A,B). This expansion was accompanied by an increase in PD-1 expression (Figure 4.12 C) and correlated with the clear expansion of tetramer negative CD44+ CD8 T cells (Figure 4.12 D-F) observed from day 7 to 21 after treatment administration. This expansion appeared to be driven by the priming and activation of naïve T cells, which experienced a sharp drop in the anti-PD-1 mAb group at day 7 (Figure 4.12 D), whilst there was no difference in the percentage of central memory T cells between the OVA control and anti-PD-1 mAb groups. Likewise, no differences were noted at the earliest time point (day 3), indicating that the changes observed were secondary to the immunisation (see Appendix A, Figure 6.6 D). These changes were restricted to the primary response, as no major differences were observed after re-challenge with SIINFEKL peptide (see Appendix A, Figure 6.9). However, this could again be a reflection of low levels of T-cell activation during the primary response; although some individual mice displayed up to 15% Tet+ cells during the primary response, it may be that a more potent activation signal is required to expand enough primary T cells to mount robust memory responses.

Overall, the results from OT-I transfer experiments were corroborated in the more physiological setting of an endogenous response to ovalbumin, depicting anti-PD-1 mIgG1-N297A as the optimal mAb to enhance activation and expansion of both high and lower-affinity CD8 T-cell responses.

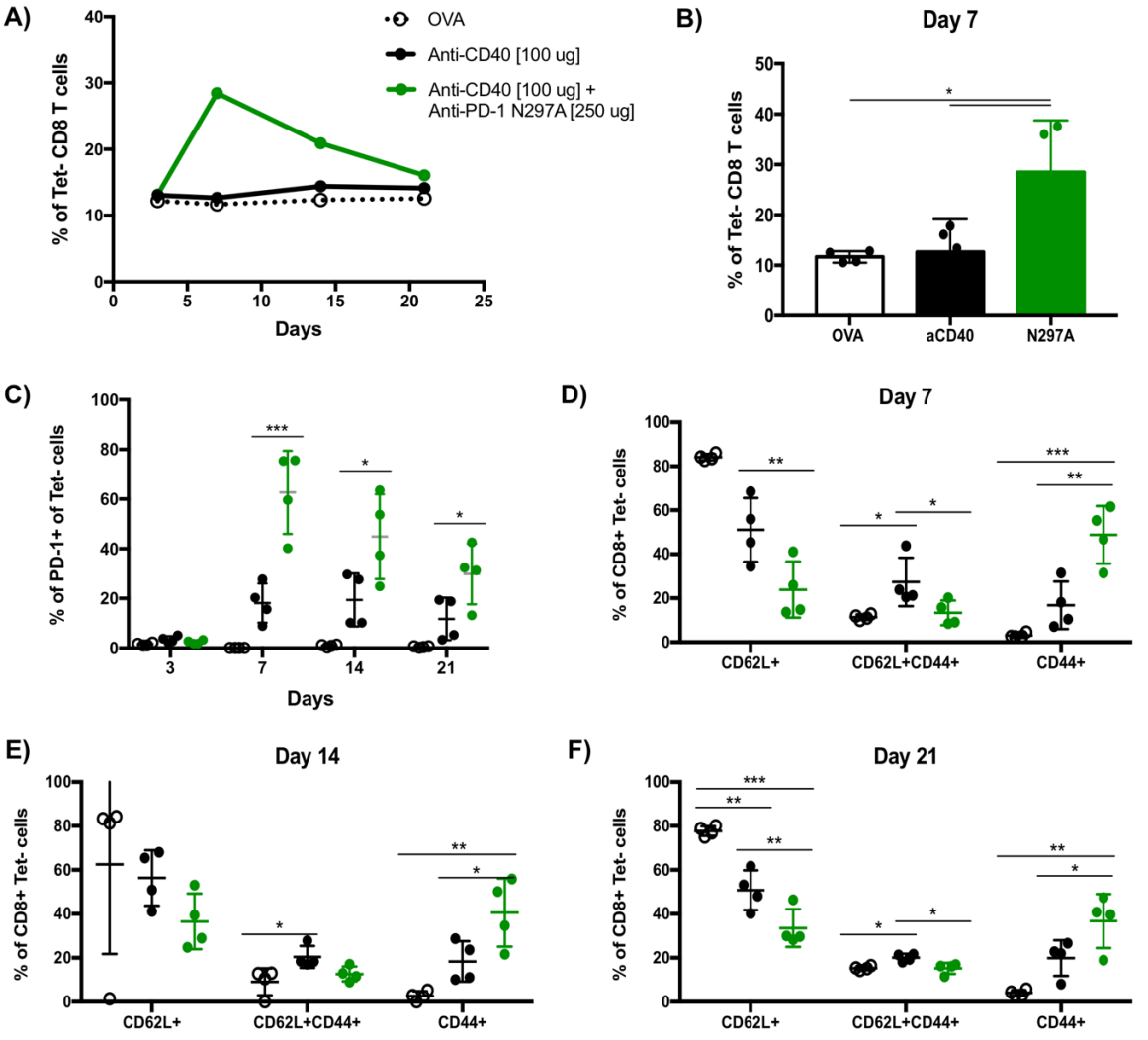

Figure 4.12 Expansion of tetramer negative CD8 T cells by anti-PD-1 mIgG1-N297A during an endogenous anti-OVA response.
A) Expansion of tetramer negative cells amongst all CD8 T cells at each time point. A baseline dose of 5 mg ovalbumin was given alone; in combination with 100 µg of anti-CD40 mAb plus irrelevant mAb; or in combination with 100 µg of anti-CD40 mAb plus 250 µg of anti-PD-1 mIgG1-N297A. B) Percentage of tetramer negative CD8 T cells on day 7. C) Percentage of PD-1 expressing tetramer negative CD8 T cells. D-F) Phenotype of tetramer negative CD8 T cells on day 7 (D), day 14 (E) and day 21 (F) according to CD62L and CD44 staining. Experiment performed once, N=4 mice per group. Bars represent mean ± S.D, ***p<0.001, **p<0.01, *p<0.05 (One-way ANOVA).

4.4 Therapeutic effect of anti-PD-1 isotypes in MC38 model

One of the best characterised syngeneic tumour models on a C57BL/6 background is the colorectal adenocarcinoma cell line MC38. This model is known to be sensitive to PD-1 blockade and numerous studies have demonstrated that monotherapy with checkpoint inhibitors has a therapeutic effect in in vivo models using this cell line, making it ideal to assess differences between anti-PD-1 isotypes (161, 315). Also, the initial study performed by Dahan R. et al. on the effect of Fc: FcγRs interactions in PD-1 blockade was based in the MC38 cell line. In this study, two rat anti-PD-1 mAb clones were engineered into murine IgG1, IgG2a and the Fc-null IgG1-D265A isotypes (104), equivalent to the three isotypes used in the current work. Hence, using the MC38 cell line as a first assessment of the in vivo efficacy of our anti-PD-1 isotypes provided us with a known sensitive model as well as a good comparison with the previously published literature.

Firstly, the therapeutic effect of the three murine isotypes was investigated. As illustrated in Figure 4.13 A, three doses of 200 µg of anti-PD-1 or irrelevant mAbs were delivered at days 8, 12 and 15 after tumour inoculation, when tumours were established (average size of 7x7 mm at the time of first dosage). Results evidenced a clear difference in the efficacy of the murine anti-PD-1 mAbs; both mIgG1 and mIgG1-N297A provided effective long-term therapy in the majority of mice, with no significant difference in outcome between mice treated with either of the two mAbs. In contrast, outcomes of mice treated with anti-PD-1 mIgG2a were not significantly different from mice treated with control mAb (Figure 4.13 B-G). These results clearly highlighted the role of mAb Fc and FcγRs in this model in dictating the therapeutic efficacy of anti-PD-1 therapy, and indicated that the engagement of activating FcγRs by mIgG2a could completely abrogate the effect of PD-1 blockade.

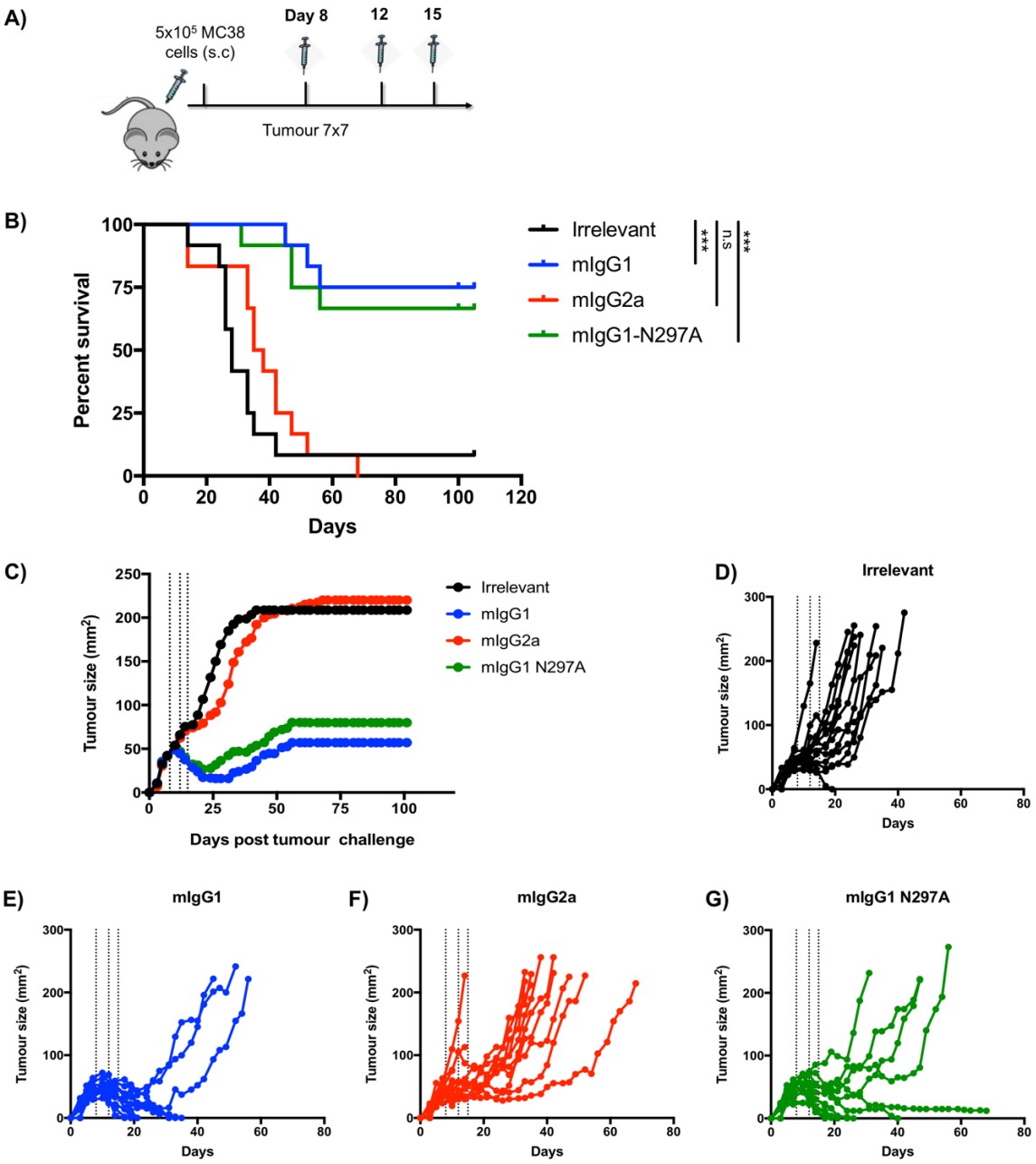

Figure 4.13 Monotherapy with anti-PD-1 isotypes in MC38 model.
A) C57BL/6 mice were subcutaneously inoculated with 5x10^5 MC38 cells and tumour growth was monitored 3 times/week. Mice received 3 Ip doses of 200 µg of irrelevant mAbs (AT10 mIgG1, mIgG2a and mIgG1-N297A) or anti-PD-1 mIgG1, mIgG2a and mIgG1-N297A mAbs, on days 8, 12 and 15 after tumour inoculation. B) Survival curves showing the percent of mice alive at each time point after tumour inoculation. Animals were culled when tumours reached a humane endpoint of 15x15 mm. C-G) Tumour growth curves showing the mean at each time point (C) or growth curves for each individual mice treated with irrelevant mAbs (D), anti-PD-1 mIgG1 (E), anti-PD-1 mIgG2a (F) and anti-PD-1 mIgG1-N297A (G). Tumour size was calculated as length x width and growth was monitored 3 times/week using calipers. Experiment performed twice, N=12 mice per group. Log-rank (Mantel-Cox) Test, ***p<0.001.

In order to limit the risk of tumour relapse, the induction of long-term anti-tumour immunity is a key goal for immunotherapy. To study the generation of immunological memory by anti-PD-1 mAbs, mice that had cleared primary MC38 tumours were subsequently re-challenged with the same cell line 100 days after the first inoculation. As shown in Figure 4.14 B-D, the majority of survivors were able to reject the re-challenge, except for one mouse treated with anti-PD-1 mIgG1 that developed a tumour. Importantly, all naïve mice that were challenged alongside the re-challenged groups developed tumours (Figure 4.14 A), demonstrating that the MC38 cells used for the re-challenge retained the ability to grow in vivo. Therefore, treatment with anti-PD-1 mIgG1 or mIgG1-N297A not only led to approximately 70% of complete responses, but also induced long-term immunological memory in the majority of mice.

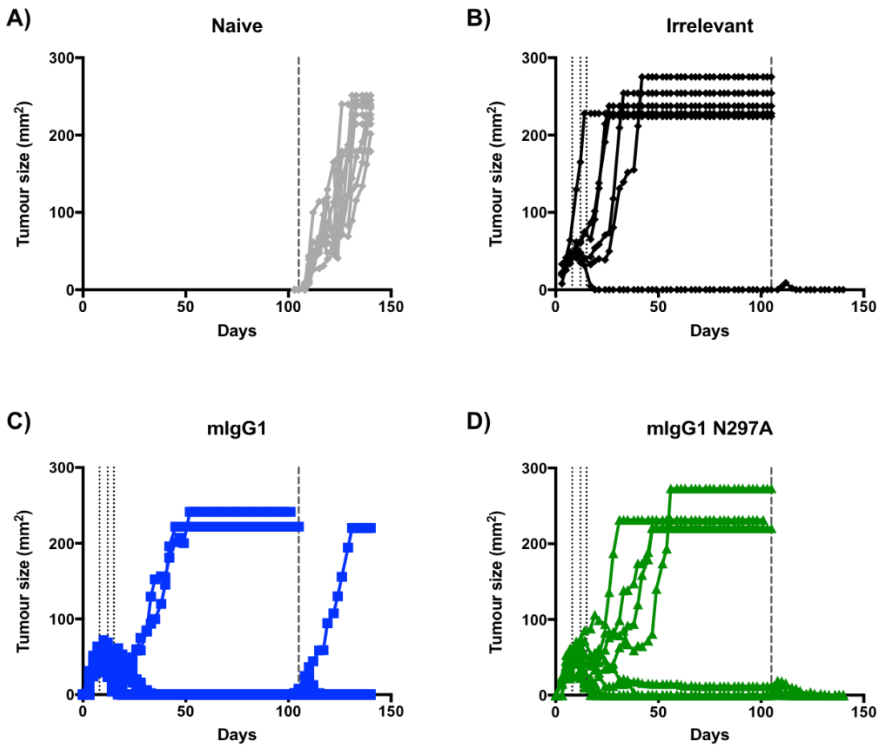

Figure 4.14 Re-challenge with MC38 after anti-PD-1 therapy.
In the case of tumour clearance after initial challenge, mice were subcutaneously re-challenged with $5x10^5$ MC38 cells 100 days post tumour inoculation. A group of age- and sex-matched naïve mice were inoculated with MC38 alongside re-challenged mice, and tumour growth was monitored as detailed in Materials and Methods. Experiment performed twice, N=10 mice in naïve group; N=1 mouse in irrelevant group; N=9 mice in anti-PD-1 mIgG1 group; and N=8 mice in anti-PD-1 mIgG1-N297A group.

4.5 Immunophenotyping of MC38-bearing mice after therapy with murine anti-PD-1 mAbs

Besides cancer cells, the TME comprises a range of immune cells that influence tumour evolution. The composition of innate and adaptive immune cells within the TME can offer important insights into the immunogenic nature of the tumour, and has been used to predict patient outcome in human cancers (16). Furthermore, changes in the TME upon therapeutic interventions can reflect responsiveness to a given drug and highlight the potential mechanisms underlying anti-tumour responses. In view of this, once the efficacy of anti-PD-1 mAbs in MC38 had been established, the changes in the TME that were driving the observed differences amongst mAbs were investigated. To this end, immunophenotyping of tumour-infiltrating T cells and myeloid cells was performed. To achieve this, a similar treatment schedule to that in survival experiments was followed (Figure 4.15 A), but in this case tumours and spleens were harvested 24h after the last treatment dose of antibody.

As illustrated in Figure 4.15 B, a therapeutic effect on tumour growth was already evident at the time of tissue harvest. Anti-PD-1 mIgG1 and mIgG1-N297A (Figure 4.15 B,D,F) showed a small reduction in tumour size compared to the mIgG2a (E) or irrelevant control (C) groups, reflecting the results from the survival experiments. In line with the tumour size, tumour weight after harvesting was decreased in the mIgG1 and mIgG1-N297A anti-PD-1 groups compared to mIgG2a. Tumours from mice treated with irrelevant mAbs appeared to also show decreased weight compared to mIgG2a, but this was not statistically significant due to the spread of the data (Figure 4.15 G). Similarly, no differences amongst groups were observed in terms of spleen weight at the time of harvest (Figure 4.15 H).

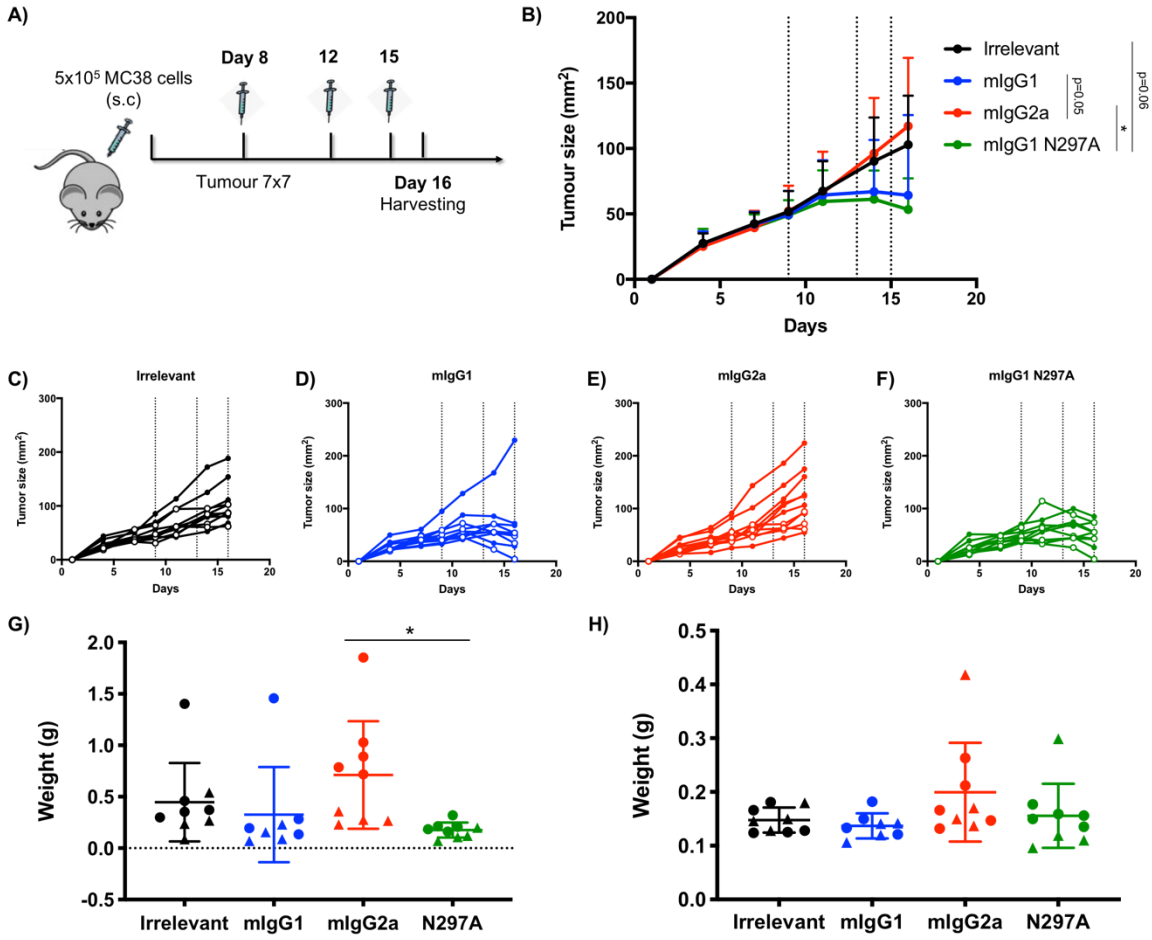

Figure 4.15 Immunophenotyping of MC38 tumours after anti-PD-1 therapy.
A) C57BL/6 mice were subcutaneously inoculated with 5x10^5 MC38 cells. When tumours reached 7x7 mm, mice received 3 Ip doses of 200 µg of irrelevant mAbs (AT10 mIgG1, mIgG2a and mIgG1-N297A) or anti-PD-1 mIgG1, mIgG2a and mIgG1-N297A mAbs. Tumours and spleens were harvested 24h after the last dose and processed for flow cytometry (see sections 2.7.5 and 2.8). B-F) Tumour growth curves showing the mean at each time point (B) or growth curves for each individual mice treated with irrelevant mAbs (C), anti-PD-1 mIgG1 (D), anti-PD-1 mIgG2a (E) and anti-PD-1 mIgG1-N297A (F). Tumour size was calculated as length x width and growth was monitored 3 times/week using calipers. G-H) Tumour (G) and spleen (H) weights after harvesting. Experiment performed twice, N=8-9 mice per group. Triangles represent values from the first replicate whilst circles correspond to the second. Bars represent mean ± S.D, *p<0.05 (One-way ANOVA).

4.5.1 T-cell phenotyping

As previously detailed, PD-1 is an inhibitory co-receptor largely expressed on activated T cells. The principal mechanism of action of PD-1 blocking mAbs is postulated to be the release of PD-1-mediated inhibition on effector T cells, although recent studies point to alternative mechanisms, such as blockade of the PD-1-mediated inhibition of macrophage phagocytosis (43). Hence, since T cells are the proposed target for anti-PD-1 mAbs, a panel of T-cell markers was developed to phenotype the T-cell response against MC38 tumours.

4.5.1.1 Tumour-infiltrating T cells

Once tumours had been digested into single cell suspensions, staining was performed as detailed in section 2.8 (Material and Methods) before analysis by flow cytometry. As a first step in the gating strategy (Figure 4.16), the marker CD45.2 was used to gate on immune cells and exclude any tumour cells. From CD45+ immune cells, T cells expressing CD8 and CD4 were then selected. Expression of the transcription factor FoxP3, which is key in the development and maintenance of Tregs (316), was used to distinguish this immunosuppressive sub-population (CD4+, FoxP3+) from effector CD4 T cells (CD4+, FoxP3-). For each of these three T-cell subsets, MFI and percentage of positive cells for each marker were calculated. Also, for each treatment group and tissue, isotype control values were then subtracted from active fluorochrome-labelled antibodies.

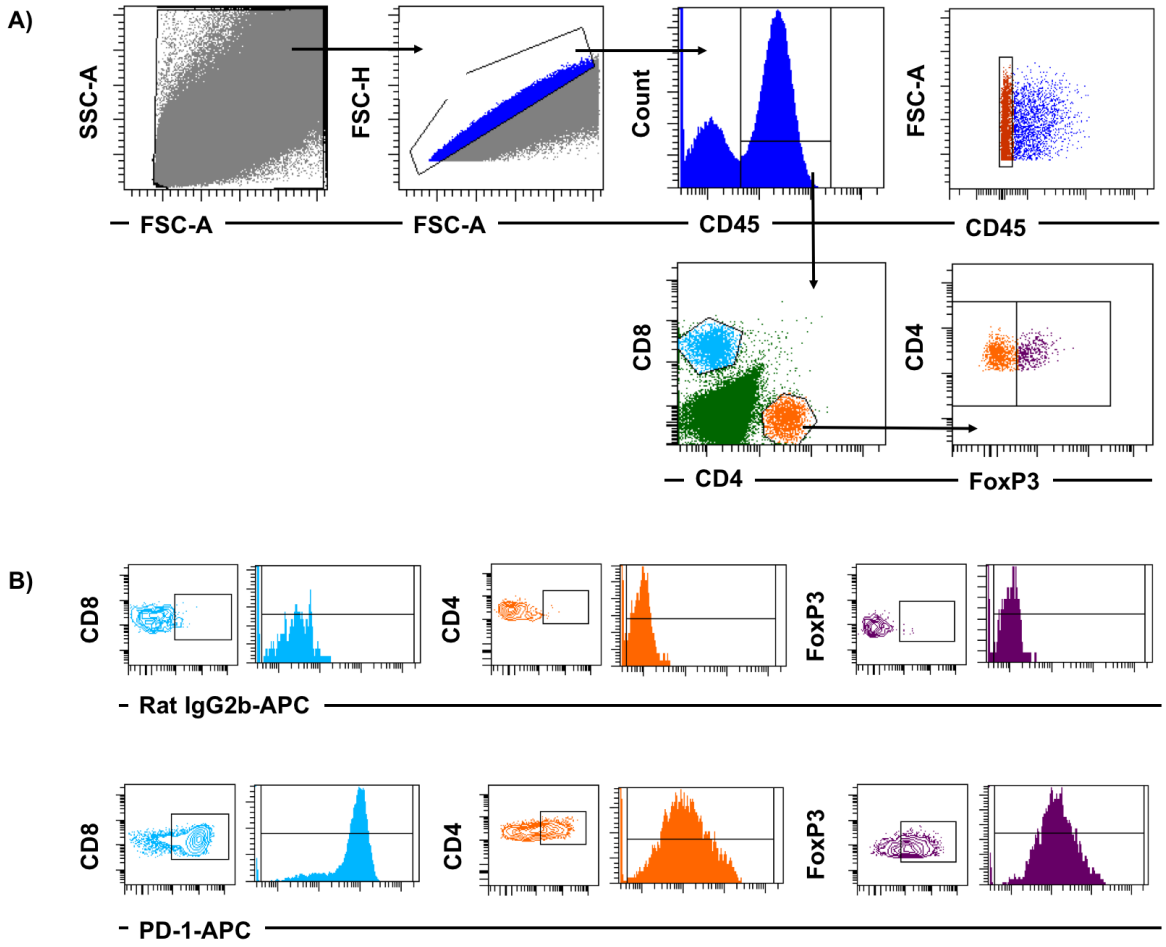

Figure 4.16 Gating strategy: Tumour-infiltrating T cells in MC38 tumours. Tumours were mechanically and enzymatically digested as detailed in 2.7.5, and single cell suspensions were obtained. Typically, 10^6 cells were stained with surface and intracellular markers (see 2.8) and samples were run on flow cytometry. A) Stained cells were acquired on flow cytometry. From all live cells (FSC-A–SSC-A), doublets were excluded and immune cells were gated according to their CD45 expression. From CD45+ cells, CD8+ and CD4+ T cells were gated. Within CD4+ cells, effector CD4 T cells were gated as FoxP3 negative, whilst Tregs were gated as FoxP3 positive. Tumour cells were gated as CD45 negative cells. B) Dot plots and histograms for each lymphocyte population showing the expression of PD-1. Positive cells were gated according to an isotype control (upper raw). Geometric mean of the whole population was calculated from the histogram plots, and isotype control values were subtracted. This strategy was followed for all markers assessed.

Of note, results showed that the number of immune infiltrates (CD45+), as a percentage of single live cells, was augmented in both anti-PD-1 mIgG1 and mIgG1-N297A groups compared to irrelevant and mIgG2a groups (Figure 4.17 A). Within these immune infiltrates, the percentage of Tregs and CD4 T cells remained similar across groups. However, there was an increase in the percentage of CD8 T cells in both mIgG1 and mIgG1-N297A groups, albeit more marked in the former group (Figure 4.17 B). Instead, treatment with IgG2a tended to decrease the percentage of CD8 T cells. It is important to highlight the difficulties of relying in cell percentage rather than absolute cell counts, as percentages will be strongly impacted by tumour size. Taking this into account, cell counts were inferred from the percentage of T cells obtained by FACS and the total cell count and tumour weight. Absolute cell counts indicated a clear trend towards increased CD8 T-cells by anti-PD-1 mIgG1 and mIgG1-N297A, whilst decreased CD8 T cells by mIgG2a (Figure 4.17 C), displaying the same pattern observed in cell percentages (B). Further to this, absolute cell counts were assessed within PD-1 positive cells, as these are the cell populations predicted to be most affected following anti-PD-1 mAb therapy. In this case, the number of CD8 TILs significantly reduced by mIgG2a compared to controls, as well as the number of PD-1+ Tregs (Figure 4.17 D). These demonstrated a clear depletion of PD-1+ TILs at the tumour site by anti-PD-1 mIgG2a.

Overall, these changes translated into a reduced CD8: Treg ratio in mice treated with anti-PD-1 mIgG2a compared to all other groups and a potential small increase in mIgG1 and mIgG1-N297A compared to controls (Figure 4.17 E). Remarkably, the baseline CD8: Treg ratio in mice treated with irrelevant controls was high (approximately 10; see Appendix A, Figure 6.10), which might be a contributing factor to the high sensitivity that this model displays to this immunotherapy (23).

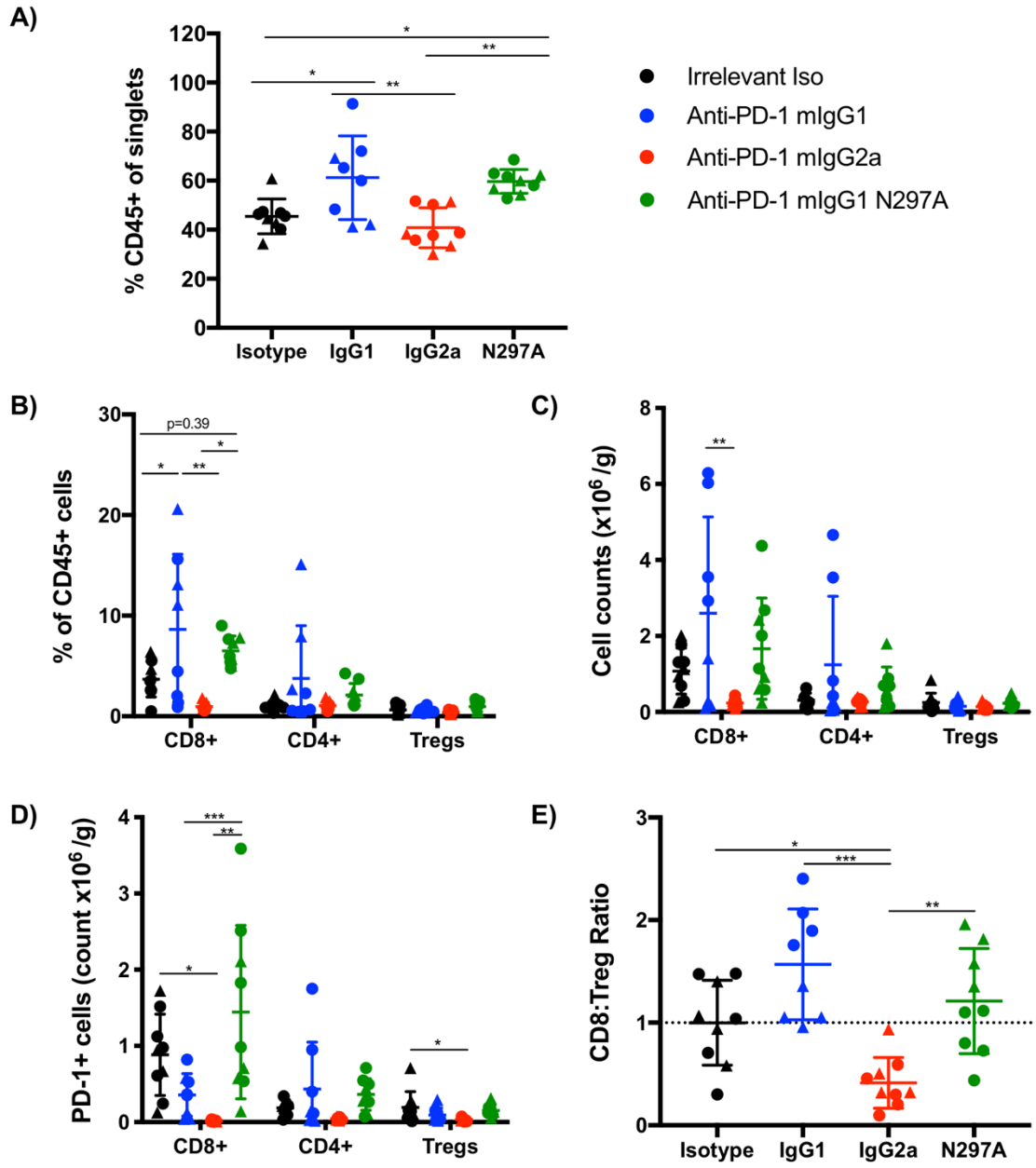

Figure 4.17 MC38 tumour-infiltrating immune cells after 3 doses of murine anti-PD-1 mAbs: T-cell populations.
A) Percentage of CD45 immune infiltrates out of the singlet gate. B) Percentage of CD8+, CD4+ (FoxP3-) and Tregs (CD4+ FoxP3+) out of CD45+ immune infiltrating cells. C) Total counts of CD8+, CD4+ and Tregs per tumour weight (g^{-1}). C) Total cell counts of PD-1+ cells within CD8+, CD4+ and Treg subsets per tumour weight (g^{-1}). E) Individual CD8: Treg ratios per mouse were obtained by dividing the percentage of CD8 T cells by the percentage of Tregs. Next, individual ratios were normalised to the average ratio of control mice in each independent experiment. Experiment performed twice, N=8-9 mice per group. Triangles correspond to the first experiment whilst circles correspond to the second. Total cell counts were calculated from the percentage obtained in FACS of each cell population and the total number of cell suspension counts, and then divided by tumour weight. Bars represent mean ± S.D, *p<0.05, **p<0.01 (One-way ANOVA).

In terms of TIL phenotyping, the most striking difference observed was the expression of PD-1. In control mice, the percentage of PD-1+ CD8 T cells was very high (approximately 80% on average), likely reflecting chronic activation due to prolonged antigen exposure (Figure 4.18 A). Likewise, this percentage remained high after treatment with anti-PD-1 mIgG1-N297A. However, it is important to note that these CD8 T cells expressed higher levels of PD-1 as illustrated by an increased PD-1 MFI value in the mIgG1-N297A group compared to control (Figure 4.18 B). Taking into account that the levels of PD-1 expression are associated to T-cell activation and exhaustion (34, 154), these results suggest that CD8 T cells in the mIgG1-N297A group could be more activated than controls. On the contrary, treatment with anti-PD-1 mIgG1 and mIgG2a mAbs decreased both the absolute number (Figure 4.17 D) and the percentage of PD-1+ CD8 T cells (Figure 4.18 A), as well as the level of PD-1 expression (Figure 4.18 B). Treatment with mIgG2a displayed the lowest expression of PD-1 (Figure 4.18 A). These differences amongst treatment groups observed on CD8 T cells were also mirrored on effector CD4 T cells and Tregs, with mIgG1-N297A showing the highest expression of PD-1; followed by control-treated cells; mIgG1-treated cells; and with mIgG2a-treated cells displaying almost null expression (Figure 4.18 A,B).

Numerous studies have postulated that PD-1 blockade may affect distinct T-cell subsets depending on their differentiation status (157-159). When the percentage of naïve, effector and central memory TILs was assessed according to CD62L and CD44 expression, no differences were found in the relative percentages of naïve or effector T cells across treatment groups (Figure 4.18 C,D). Effector T cells represented the majority of the TIL population, making up approximately 80% of TILs, whilst the percentage of naïve TILs was almost negligible. Importantly, the frequencies of CD8 and CD4 effector and central memory T cells were concordant with previous reports in MC38 TILs (315). In terms of central memory T cells, a reduction was found in CD8 memory T cells in the mIgG1-N297A group compared to controls (Figure 4.18 E). This could indicate that memory T cells are either recirculating to TDLN or they are undergoing intratumoural proliferation to give rise to more differentiated effector T cells. In this case, however, a rise in effector CD8 T cells would be expected alongside decreased central memory CD8 T cells.

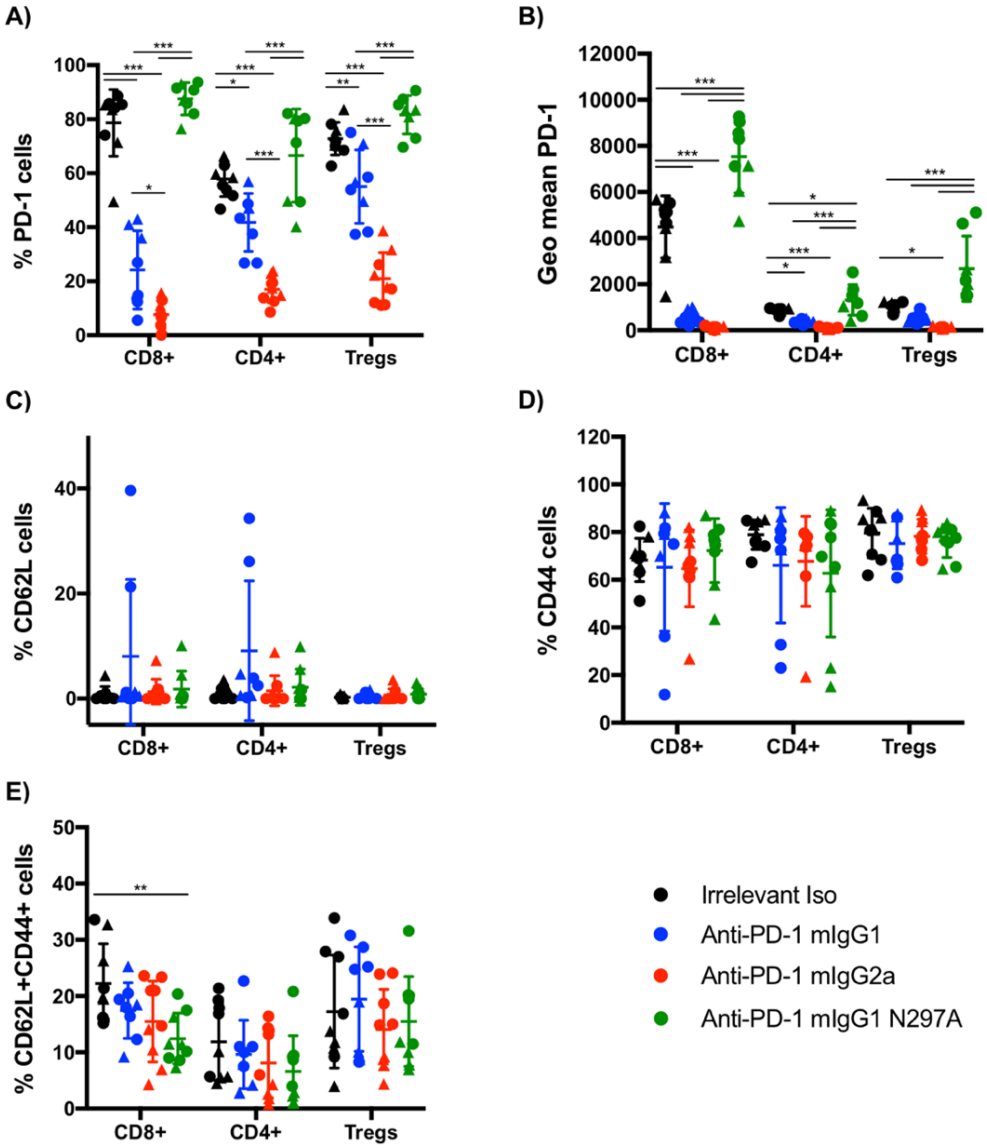

Figure 4.18 Phenotype of TILs in MC38 tumours after 3 doses of murine anti-PD-1 mAbs.
A-B) Expression of PD-1 in T-cell subsets shown as percentage of positive cells (A) or as MFI (B). C-E) Percentage of naïve (C), effector (D) and central memory (E) T cells in the tumour according to CD62L and CD44 staining. Experiment performed twice, N=8-9 mice per group. Triangles correspond to the first experiment whilst circles correspond to the second. Bars represent mean ± S.D, *p<0.05, **p<0.01, ***p<0.001 (One-way ANOVA).

Overall, these results indicated that both mIgG1 and mIgG1-N297A anti-PD-1 isotypes were able to trigger an immune response to MC38 tumours that led to increased immune infiltration and CD8 TILs. This immune response is likely responsible for the improved survival that these two antibodies showed (Figure 4.13). However, engagement of FcγRs by mIgG1 led to different expression of PD-1 between these two groups, with mIgG1-treated mice showing a reduction on PD-1 expression on TILs but mIgG1-N297A treated mice demonstrating a clear increase in expression levels.

4.5.1.2 T cells in spleen of MC38-bearing mice

In order to investigate the frequency and phenotype of T cells in the spleen, a similar gating strategy (Figure 4.19) was followed. Whilst some changes were seen in the spleens of MC38-bearing mice, the majority of the differences were restricted to the tumour. As shown in Figure 4.20, the relative proportions of lymphocytes in spleens remained generally constant, with only a slight increase in CD4 T cells after mIgG1-N297A anti-PD-1 treatment (A). Likewise, the CD8: Treg ratio remained constant across treatment groups (B). In relation to the phenotype, treatment with mIgG1-N297A mAb induced higher PD-1 expression on all T-cell subsets, but with a marked increase on Tregs (Figure 4.20 C,D). This effect could be interpreted to support that PD-1 blockade by mIgG1-N297A mAbs led to a systemic pro-inflammatory response that caused activation of T cells in the spleen as well as the tumour site. Finally, no differences were observed amongst T-cell phenotypes (Figure 4.20 E-G), where a large proportion of Tregs presented an effector phenotype, whilst approximately 40% of CD4 and CD8 T cells in spleens were naïve.

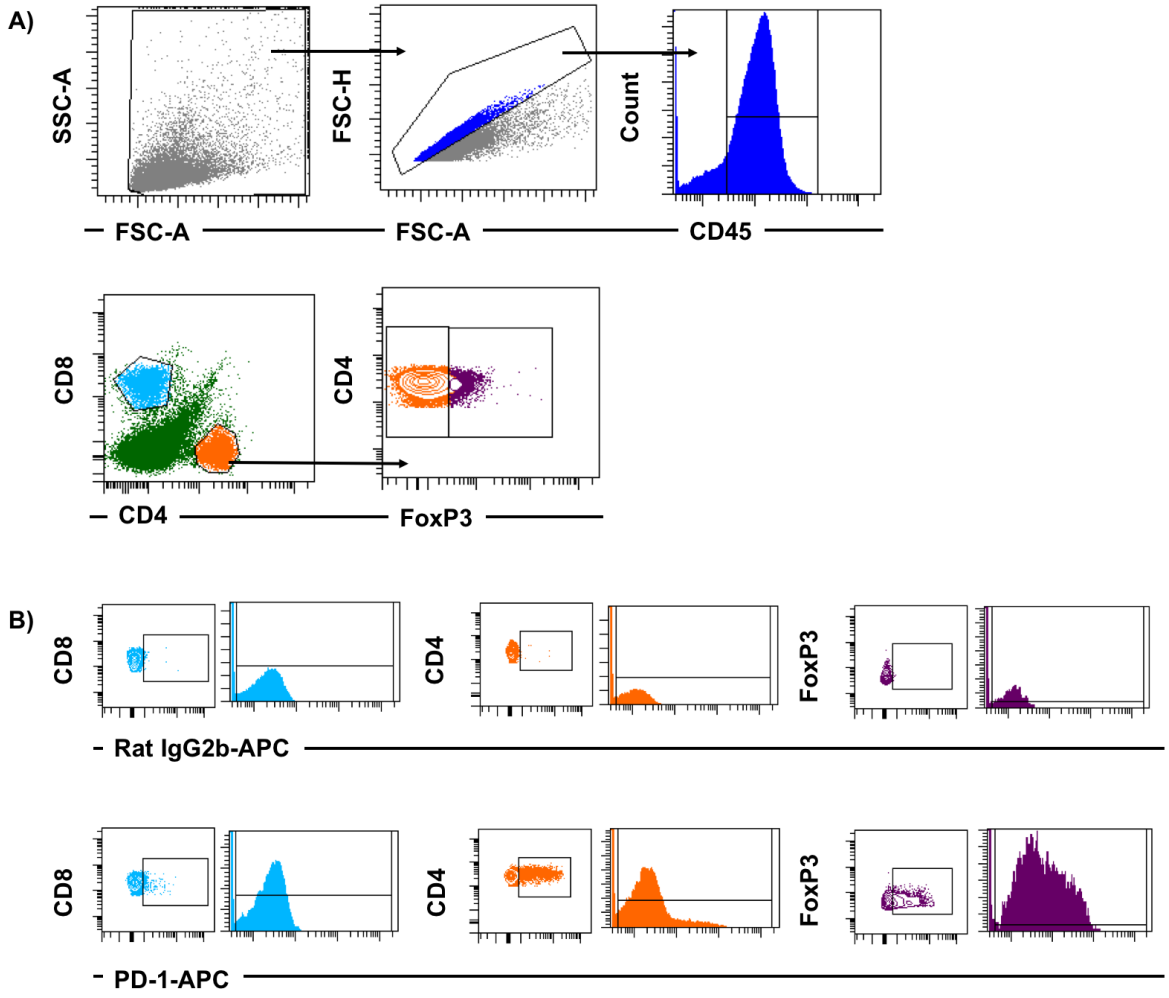

Figure 4.19 Gating strategy: T cells in spleen of MC38-bearing mice.
Spleens were mechanically digested as detailed in 2.7.5, and single cell suspensions were obtained. Typically, 10^6 cells were stained with surface and intracellular markers (see 2.8) and samples were run on flow cytometry. A) Stained cells were acquired on flow cytometry. From all live cells (FSC-A–SSC-A), doublets were excluded and immune cells were gated according to their CD45 expression. From CD45+ cells, CD8+ and CD4+ T cells were gated. Within CD4+ cells, effector CD4 T cells were gated as FoxP3 negative, whilst Tregs were gated as FoxP3 positive. B) Dot plots and histograms for each lymphocyte population -CD8+ in blue; CD4+ in orange; Tregs in purple- showing the expression of PD-1. Positive cells were gated according to an isotype control (upper raw). Geometric mean of the whole population was calculated from the histogram plots, and isotype control values were subtracted. This strategy was followed for all markers assessed.

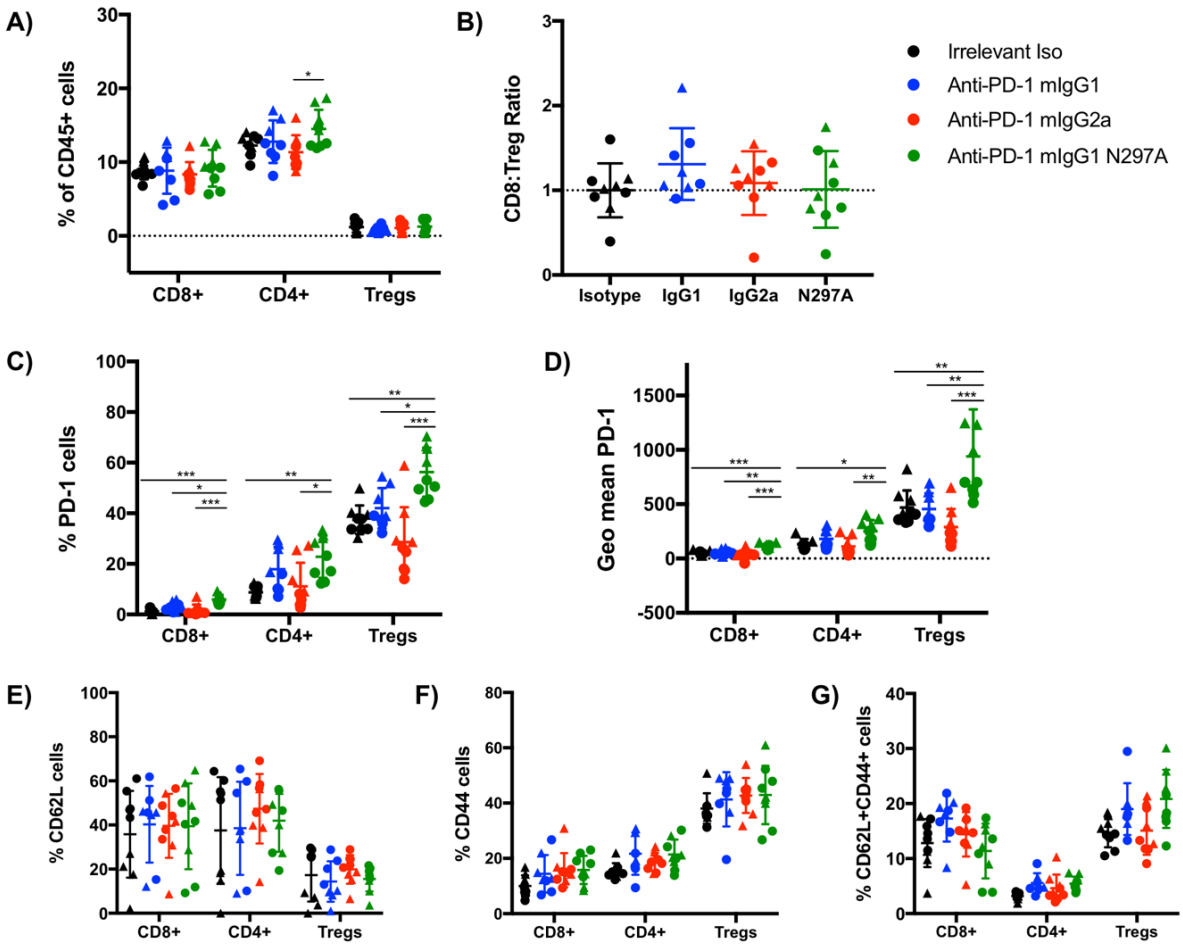

Figure 4.20 T-cell populations in spleens of MC38-bearing mice after 3 doses of murine anti-PD-1 mAbs.
A) Percentage of CD8+, CD4+ (FoxP3-) and Tregs (CD4+ FoxP3+) out of CD45+ cells. B) Individual CD8: Treg ratios per mouse were obtained by dividing the percentage of CD8 T cells by the percentage of Tregs. Next, individual ratios were normalised to the average ratio of control mice in each independent experiment. C-D) Expression of PD-1 in T-cell subsets shown as percentage of positive cells (C) or as MFI (D). E-G) Percentage of naïve (E), effector (E) and central memory (G) T cells in the tumour according to CD62L and CD44 staining. Experiment performed twice, N=8-9 mice per group. Triangles correspond to the first experiment whilst circles correspond to the second. Bars represent mean ± S.D, *p<0.05, **p<0.01, ***p<0.001 (One-way ANOVA).

4.5.2 Myeloid phenotyping

Tumour-infiltrating myeloid cells are a large component of the TME in most cancers. It is well documented that myeloid cells express activating and inhibitory FcγRs, the relative expression of which can give an insight of the activation state of a specific myeloid subset (121, 124, 125). Moreover, myeloid FcγRs at the TME are likely to be key to the different therapeutic effect of the three murine anti-PD-1 mAbs, and hence it was important to study their distribution in the TME. Similarly, several studies emphasised the important role of PD-L1 on host myeloid cells in

triggering PD-1-mediated inhibition of TILs (66-68). Therefore, the expression of FcγRs and PD-L1 on different myeloid cell populations in MC38 tumours was investigated.

Due to the high plasticity of this lineage, it is difficult to establish clear distinction between myeloid subsets. However, murine macrophages are usually characterised by high expression of F4/80 and CD11b, whilst other myeloid subsets are part of the CD11b-high but F4/80-low population. Hence, we followed this gating strategy and identified the F4/80+ CD11b+ population of macrophages after doublets had been excluded (Figure 4.21 A). From the CD11b+ F4/80-low population, neutrophils were defined by their high expression of Ly6G, whilst monocytes were gated as Ly6C high but Ly6G low. Activated DCs were gated as the population of cells that were CD11b+, F4/80-low, Ly6C/Ly6G negative, and which presented both high expression of CD11c and MHC-II (Figure 4.21 A). In both spleen and tumour, the percentage of positive cells and MFI was calculated for each marker respective to an isotype control as illustrate in Figure 4.21 B for PD-L1.

Results revealed that, overall, there was no differences in the percentage of CD11b+ myeloid infiltration amongst treatment groups (Figure 4.22 A), either in tumour or spleen. Within this broad CD11b+ myeloid population, the percentage of PD-L1+ cells increased in spleen in all anti-PD-1 treatment groups compared to controls, whilst there was only a minor rise in the mIgG1-N297A group in tumours (Figure 4.22 B). However, the levels of expression of PD-L1 were increased in the mIgG1-N297A group and tended towards an increase in the mIgG1 group (Figure 4.22 C), although not statistically significant. This up-regulation of PD-L1 in the tumour may indicate that these isotypes can induce an inflammatory response that activates myeloid cells, thereby up-regulating PD-L1. In agreement with this, PD-L1 expression was also increased in tumour cells after therapy with mIgG1 and mIgG1-N297A isotypes (Figure 4.22 D), which is likely due to the release of pro-inflammatory cytokines such as IFN-γ (29, 58, 59).

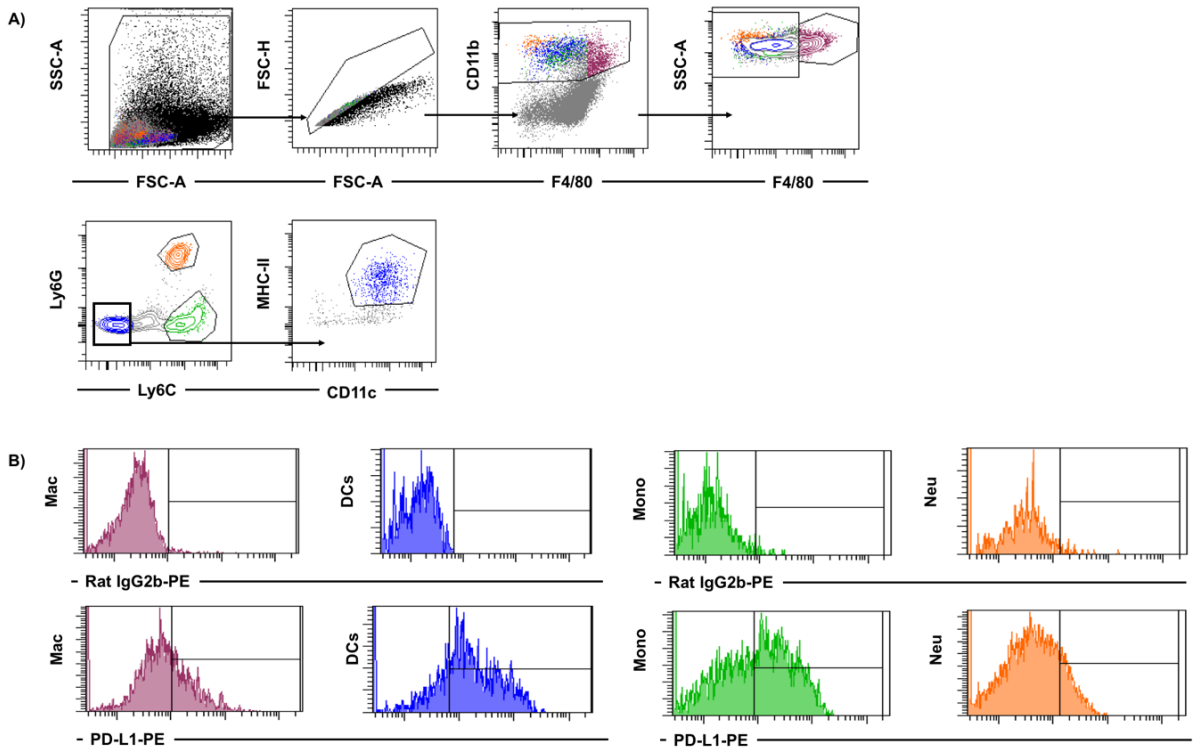

Figure 4.21 Gating strategy: Tumour-infiltrating myeloid populations in MC38 tumours.
Tumours were mechanically and enzymatically digested as detailed in 2.7.5, and single cell suspensions were obtained. Typically, 10^6 cells were stained with surface and intracellular markers (see 2.8) and samples were run on flow cytometry. A) Following doublet exclusion, live cells were gated according to CD11b and F4/80 expression. Tumour-infiltrating macrophages were gated as F4/80 high and CD11b high. Neutrophils, monocytes and DCs were gated from the CD11b high, F4/80 low population according to the expression of Ly6C, Ly6C, CD11c and MHC-II markers. Ly6C high and Ly6G high cells were gated as neutrophils, whilst Ly6Clow, Ly6G high were gated as monocytes. Gate for DCs was set as MHC-II high, CD11c high. B) Examples of histograms showing the expression of PD-L1 on macrophages (purple); DCs (blue); monocytes (green); and neutrophils (orange). Gates were set with an isotype control and subtracted to the sample values. This strategy was followed for all markers assessed.

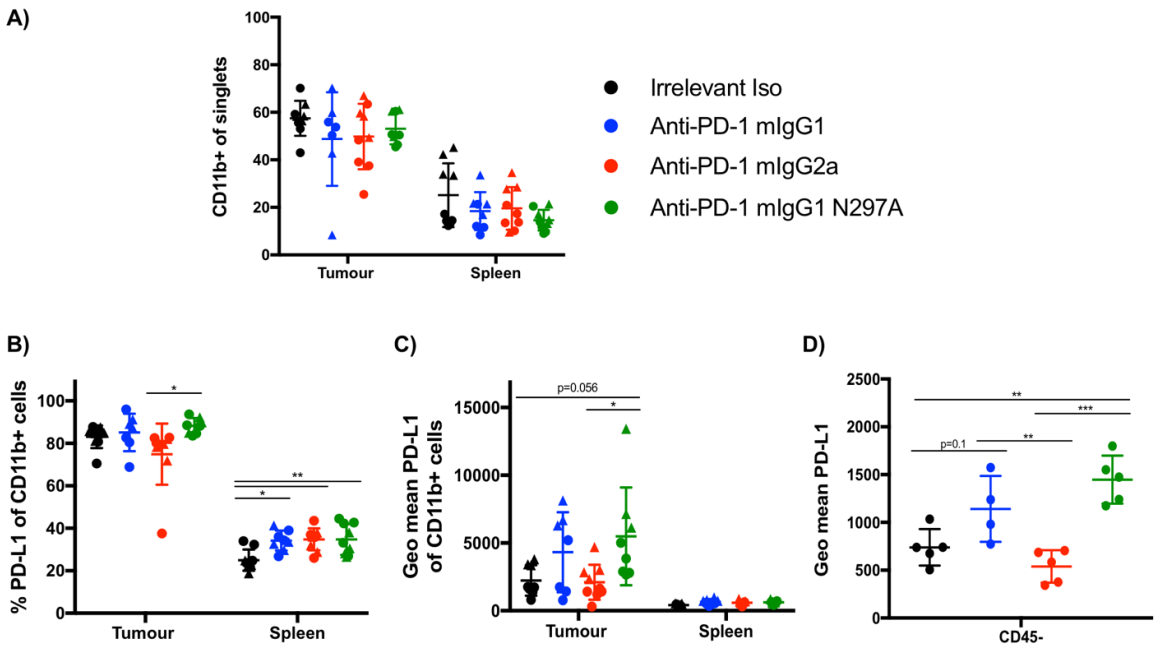

Figure 4.22 MC38 tumour-infiltrating CD11b+ cells after 3 doses of murine anti-PD-1 mAbs: PD-L1 expression.
A) Percentage of CD11b myeloid infiltrates out of the singlet gate in tumour and spleen. B-C) Expression of PD-L1 in CD11b+ cells shown as percentage of positive cells (B) or as MFI (C) in tumour and spleen. D) Expression of PD-L1 on tumour cells (CD45 negative) shown as MFI. Experiment performed twice, N=7-9 (A-C) or N=4-5 mice per group (D). Triangles correspond to the first experiment whilst circles correspond to the second. Bars represent mean ± S.D, *p<0.05, **p<0.01 (One-way ANOVA).

In terms of FcγR expression, almost 100% of CD11b+ cells expressed all four FcγRs (Figure 4.23 A). Similar to PD-L1, the expression of FcγRIV showed a clear trend towards increased levels in the mIgG1 and mIgG1-N297A groups compared to mIgG2a and controls (Figure 4.23 B,D). In particular, mIgG1-N297A appeared to induce the largest changes on FcγR expression relative to controls (D). Although the Fc region of irrelevant mAbs and anti-PD-1 mIgG2a could be binding to FcγRIV and blocking its detection, the levels of the activating FcγRI remained constant across treatment groups. This suggests that the decrease in FcγRIV might be a specific effect of the treatment and not due to non-specific binding, as this would affect both FcγRs for which mIgG2a has high binding affinity. Furthermore, calculation of the A/I ratio showed a decrease in the mIgG2a group compared to most of the other treatment groups (Figure 4.23 C), which was likely driven by the small increase in the inhibitory FcγRII (Figure 4.23 D). This might indicate that CD11b+ myeloid cells present a less activated phenotype after therapy with anti-PD-1 mIgG2a. Overall, higher expression of PD-L1 and activating FcγR were

observed in CD11b+ cells of mIgG1 and mIgG1-N297A anti-PD-1 groups, whilst mIgG2a-treated mice displayed a lower A/I ratio compared to controls. Taking into account the ability of IFN-γ to up-regulate activating FcγR expression, it is possible that the increase in both PDL1 and FcγRIV expression by anti-PD-1 mIgG1 and mIgG1-N297A is caused by an increase in the levels of this cytokine.

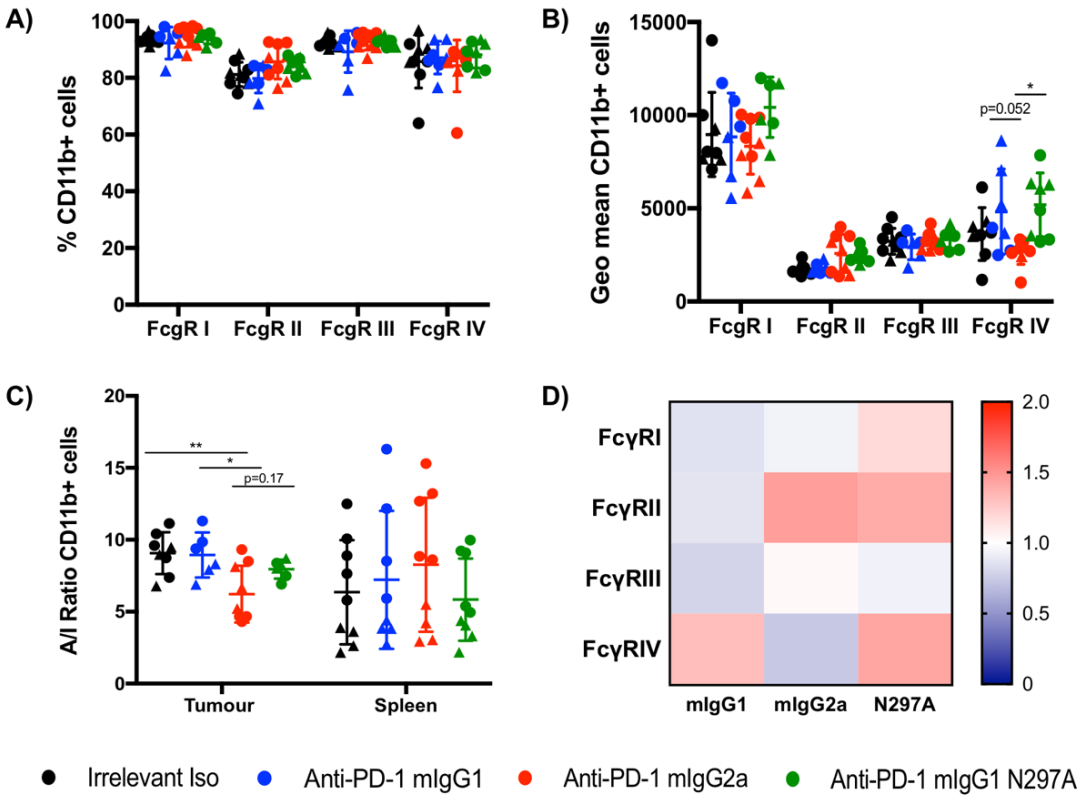

Figure 4.23 MC38 tumour-infiltrating CD11b+ cells after 3 doses of murine anti-PD-1 mAbs: FcγR expression.
A-B) Expression of FcγRs (I, II, III and IV) on CD11b+ myeloid infiltrates in tumour shown as percentage of positive cells (A) or as MFI (B). C) Ratio of activating to inhibitory (A/I) FcγRs on CD11b+ cells in tumour and spleen. The ratio was calculated by the sum of FcγRI, III and IV MFI divided by FcγRII MFI for each individual sample. D) Heat map indicating relative expression of FcγRs in treatment groups compared to controls. Ratios were calculated by dividing individual MFI values of every given marker to the average MFI value in the control group. Colours represent the mean ratio of all mice in a given group for each marker, where 1= no change; 1<downregulation; and 1>up-regulation relative to controls. Experiment performed twice, N=6-9 mice per group. Triangles correspond to the first experiment whilst circles correspond to the second. Bars represent mean ± S.D, *p<0.05, **p<0.01 (One-way ANOVA).

Next, the relative expression of PD-L1 and FcγRs across myeloid subpopulations was assessed, together with the frequency of each myeloid subtype. Analogous to the overall percentage of CD11b+ myeloid cells, the percentage of neutrophils,

monocytes, macrophages and DCs did not appear to change amongst treatment groups (Figure 4.24 A). Importantly, the percentage of CD11b infiltration and the relative proportion of tumour-associated macrophages were similar to previous reports in MC38 tumours (104). Both neutrophils and monocytes treated with anti-PD-1 mIgG1-N297A had increased expression of PD-L1 as percentage and MFI compared to mIgG2a and controls (Figure 4.24 B,C). Notably, macrophages displayed a trend towards increased levels of PD-L1 in both mIgG1 and mIgG1-N297A groups compared to mIgG2a and controls (Figure 4.24 C). Since macrophages comprised up to 80% of CD11b+ cells (Figure 4.24 A), changes in this subpopulation might be more biologically significant due to the large proportion of these cells in the TME. This up-regulation of PD-L1 on almost all myeloid subsets with mIgG1-N297A anti-PD-1 mAb (Figure 4.24) is in line with the overall findings on CD11b+ cells (Figure 4.22 C) and suggests that this isotype has a broad activating effect across all myeloid cells analysed here.

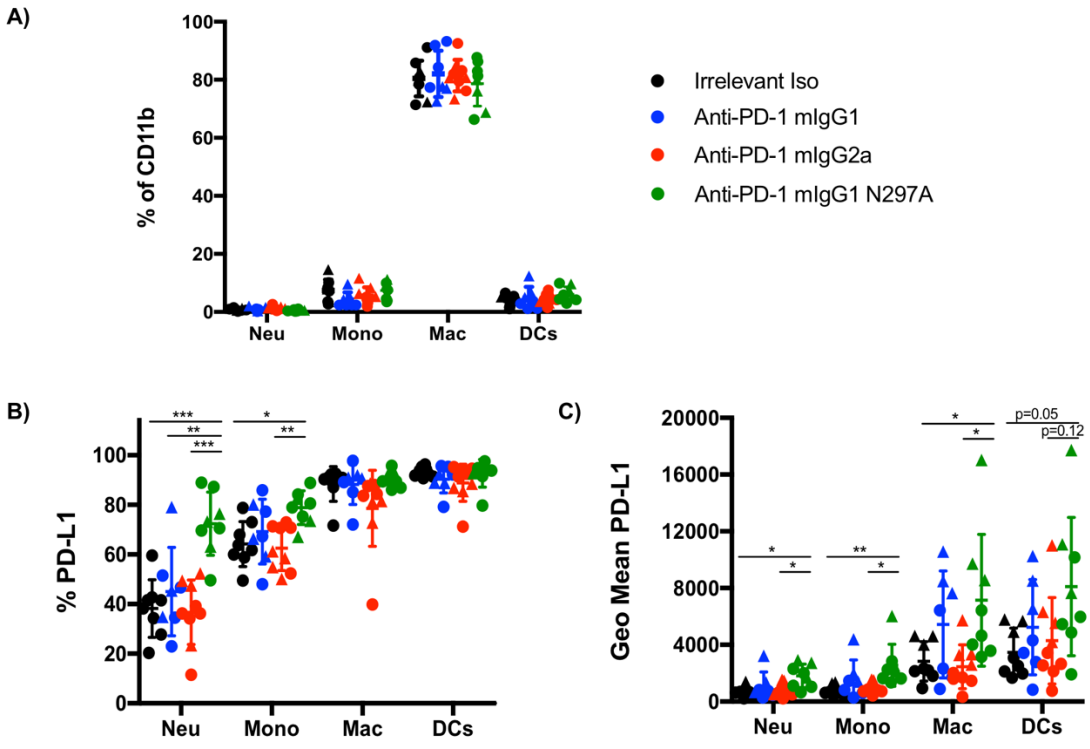

Figure 4.24 MC38 tumour-infiltrating myeloid populations after 3 doses of murine anti-PD-1 mAbs: PD-L1 expression.
A) Percentage of tumour-infiltrating myeloid populations out of CD11b+ gate. B-C) Expression of PD-L1 on tumour-infiltrating myeloid populations shown as percentage of positive cells (B) or as MFI (C). Experiment performed twice, N=6-9 mice per group. Triangles correspond to the first experiment whilst circles correspond to the second. Bars represent mean ± S.D, *p<0.05, **p<0.01, ***p<0.001 (One-way ANOVA).

To be able to distinguish subtler changes, the distribution of FcγRs in subpopulations of myeloid cells was also interrogated. Anti PD-1 mIgG1-N297A led to an up-regulation of activating FcγRI and IV in macrophages compared to controls and mIgG2a groups; however, it also induced a parallel up-regulation of FcγRII relative to controls (Figure 4.25 A). Whilst DCs, monocytes and neutrophils presented a similar patter to macrophages in terms of FcγRIV expression, an increase in FcγRI by mIgG1-N297A was only noted in DCs and monocytes (Figure 4.25 B-D). However, FcγRII was also up-regulated in these cells, similar to macrophages, albeit not significantly in all cases. Similar to mIgG1-N297A, mIgG1 isotype increased FcγRIV in macrophages, but this change was not recapitulated in other myeloid subsets. In contrast, administration of anti-PD-1 mIgG2a did not induce any changes relative to controls.

As mentioned before, it is important to acknowledge the potential confounding effect of the Fc region of irrelevant and anti-PD-1 mIgG1 and mIgG2a potentially blocking FcγR detection. If this was the case, due to their FcγR binding profile (Figure 3.2), mIgG1 would show decreased expression of FcγRII and III, whilst mIgG2a would likely reduce FcγRI and IV expression. Nevertheless, the levels of FcγRs were largely similar between anti-PD-1 mIgG1 and mIgG2a, therefore suggesting that the significant changes observed with mIgG1-N297A were caused by the blockade of PD-1 in vivo and not the lack of FcγR binding during the staining process.

Altogether, although there was a clear increase in activating FcγRs across myeloid subsets by mIgG1-N297A anti-PD-1 (Figure 4.25 D), the parallel increase in FcγRII probably reduced the overall A/I ratio, as it appeared to be similar in all treatment groups in CD11b+ cells (Figure 4.23 C). Furthermore, despite a similar increase in FcγRIV in macrophages, anti-PD-1 mIgG1 did not trigger changes in FcγR expression to the same extent of mIgG1-N297A, as evidenced by the summary heat map (Figure 4.25 D).

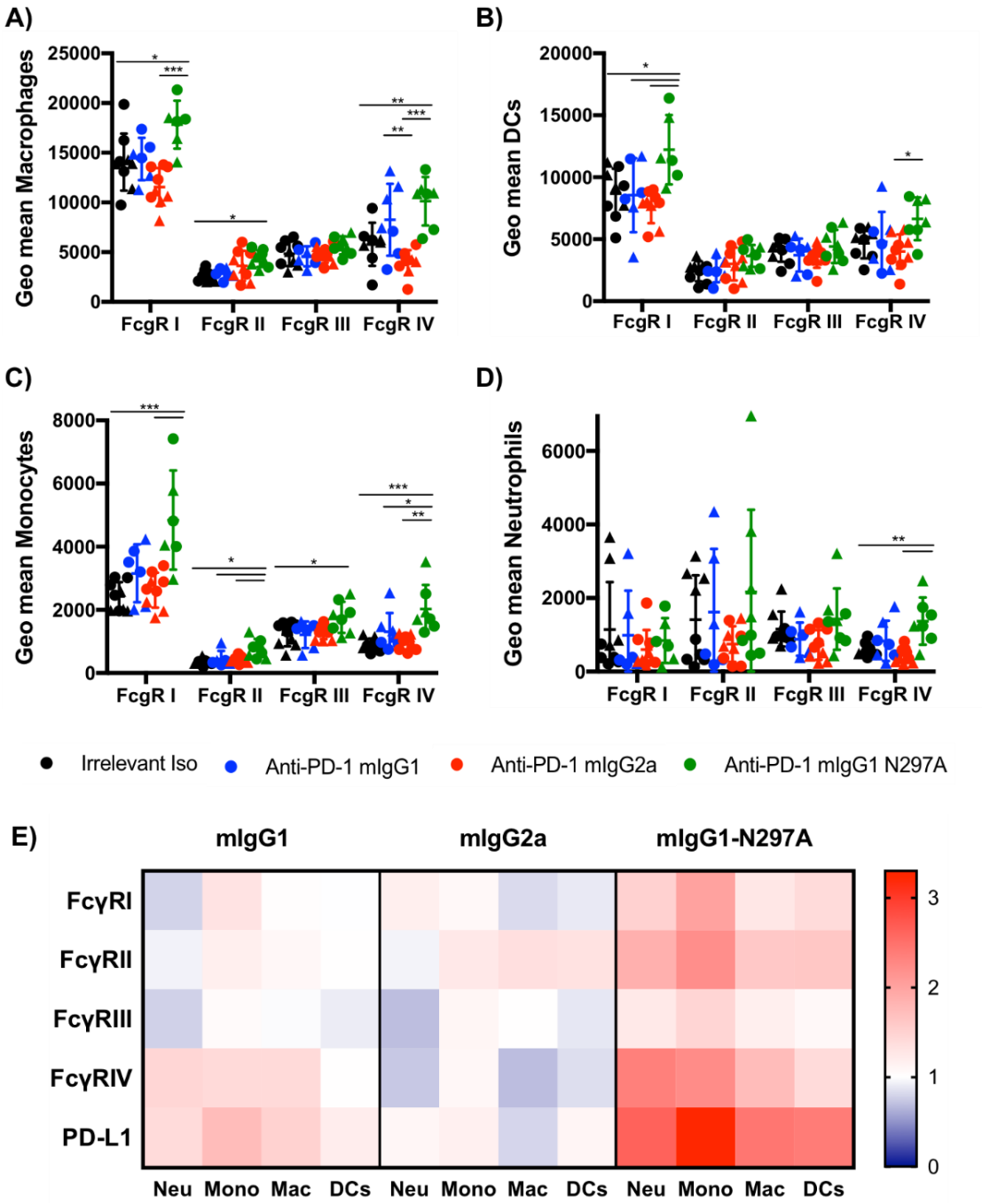

Figure 4.25 MC38 tumour-infiltrating myeloid populations after 3 doses of murine anti-PD-1 mAbs: FcγR expression.

Expression of FcγRs (I, II, III and IV) on tumour-infiltrating macrophages (A), DCs (B), monocytes (C) and neutrophils (D) shown as MFI. E) Heat map indicating relative expression of FcγRs in treatment groups compared to controls. Ratios were calculated by dividing individual MFI values of every given marker to the average MFI value in the control group. Colours represent the mean ratio of all mice in a given group for each marker, where 1= no change; 1<downregulation; and 1>up-regulation relative to controls. Experiment performed twice, N=6-9 mice per group. Triangles correspond to the first experiment whilst circles correspond to the second. Bars represent mean ± S.D, *p<0.05, **p<0.01, ***p<0.001 (One-way ANOVA).

To investigate the systemic effect of anti-PD-1 mAbs in myeloid phenotype, a similar analysis was performed in spleens of MC38-bearing mice (see Appendix A, Figure 6.12), but not many changes were observed. In spleen, neutrophils comprised the largest myeloid subpopulation, followed by monocytes, DCs and macrophages (see Appendix A, Figure 6.13 A). High levels of PD-L1 were found in both inflammatory and resident (CD11b-low) macrophages, with almost 100% of DCs expressing PD-L1 (see Appendix A, Figure 6.13 B,C). Overall, there were no clear differences across treatment groups in terms of PD-L1 or FcγR expression (see Appendix A, Figure 6.13, Figure 6.14, Figure 6.15), indicating that myeloid changes were restricted to the local TME.

4.6 Chapter discussion

4.6.1 OT-I and endogenous anti-OVA T-cell responses

The OT-I transfer model enabled the study of how different anti-PD-1 mAbs could alter the magnitude and kinetics of antigen-specific T-cell responses in vivo, without the presence of additional immunosuppressive factors. In terms of the expansion of Tet+ OT-I T cells, lack of FcγR engagement enhanced the ability of anti-PD-1 mIgG1-N297A to expand Tet+ percentages throughout the primary response (Figure 4.4). This agrees with previous studies where blockade of PD-L1 in early priming phases increased OT-I expansion and prevented T cells from becoming anergic (71). Notably, anti-PD-1 mIgG1 only showed a modest but significant increase in OT-I expansion at day 7 relative to controls, demonstrating an overall decrease in activity compared to mIgG1-N297A (Figure 4.4). In contrast, murine IgG2 tended to decrease the expansion of OT-I cells compared to irrelevant controls and treatment groups, albeit this was not statistically significant. This agrees with the previous study by Dahan R. et al., where binding of anti-PD-1 mAbs to activating FcγRs was shown to reduce the ability of this mAbs to augment T-cell responses in a tumour setting (104).

Up-regulation of PD-1 upon acute antigen exposure and co-stimulation is regarded as a marker of T-cell activation (34). In line with the enhanced Tet+ OT-I expansion, addition of anti-PD-1 mIgG1-N297A increased the expression of PD-1 in Tet+ CD8 T cells, whilst this effect was less clear with the other two anti-PD-1 mAbs (Figure 4.5 A). Despite the lack or little expansion of OT-I T cells by anti-PD-1 mIgG1 and mIgG2a, the presence of Tet+ CD8 T cells expressing medium to high levels of PD-1 could suggest that Tet+ T cells that persist in circulation are likely to remain activated regardless of their absolute number. Conversely, little changes in the relative frequencies of effector, naïve or central memory Tet+ CD8 T cells were observed across groups (Figure 4.6). Although the three anti-PD-1 mAbs induced an increase in the frequency of effector CD44+ Tet+ CD8 T cells by day 5, it is noteworthy that anti-PD-1 mIgG1-N297A displayed faster kinetics compared to the other two mAbs. Hence, within Tet+ CD8 T cells, the main differences across anti-PD-1 mAbs during the primary response to ovalbumin were found to be in the magnitude of T-cell expansion.

In the current work, it was also shown that 100 µg of anti-CD40 mAb, but not a lower dose of 10 µg, induced up-regulation of PD-1 on tetramer negative CD8 T

cells (Figure 4.5 B). This bystander activation of non-SIINFEKL, lower-affinity TCR clones by higher doses of CD40 agonists is likely induced by a more potent stimulation of APCs, which can lead to higher expression of MHC and co-stimulatory molecules together with a production of pro-inflammatory cytokines, thereby augmenting T-cell responses (76, 85). Interestingly, combination of low-dose anti-CD40 mAb (10 μg) with anti-PD-1 mIgG1-N297A increased the expression of PD-1 in tetramer negative CD8 T cells to a similar extent of the higher anti-CD40 mAb dose (100 μg) (Figure 4.5 B). In parallel, administration of mIgG1-N297A also increased the percentage of tetramer negative effector (CD44+) CD8 T cells at the peak of the response (days 5 and 7; Figure 4.7). This expansion of effector CD8 T cells was accompanied by a reduction in naïve T cells at the same time points, indicating that the priming of naïve T cells was driving the development and expansion of new effector CD8 T cells. In the context of cancer, effector CD8 T cells are potent mediators of tumour cytotoxicity and, in most cases, effective anti-tumour immunity is dependent on activated effector CD8 T-cell responses (152). Therefore, the increased frequency of these cells achieved by anti-PD-1 mIgG1-N297A could have important implications in cancer therapy. Overall, the observations that anti-PD-1 mIgG1-N297A enhanced effector CD8 T-cell responses and up-regulated PD-1 on tetramer negative T cells emphasised the capacity of this isotype to induce bystander activation of other lower-affinity T-cell clones.

The ultimate goal of cancer immunotherapy is to generate immunological memory to sustain tumour control and rejection. Owing to their modulation of T-cell activation, anti-PD-1 mAbs have the potential to induce immunological memory and enhance memory responses. In accordance, anti-PD-1 mIgG1-N297A prompted a strong memory response upon re-challenge with SIINFEKL peptide, with a clear expansion of Tet+ CD8 T cells (Figure 4.8). Despite a high level of variability across the two experimental replicates, mIgG1 showed a small expansion of memory Tet+ T cells at day 7, whilst the levels in the mIgG2a group were not significantly higher than those in control mice. Expression of PD-1 was similar in Tet+ and tetramer negative CD8 T cells across treatment groups. From this, it can be inferred that blockade of PD-1 by the different mAbs was the key factor driving changes during the primary response to ovalbumin, whereas memory responses were mainly driven by the magnitude of the initial primary response.

In these experiments, it is important to remember that a CD40 agonist was given as an adjuvant alongside PD-1 blockade to boost T-cell activation and up-regulate PD-1 expression on CD8 T cells. It is possible that anti-CD40 mAbs induced

activation of myeloid cells and other immune populations towards an inflammatory phenotype, with the secondary up-regulation of activating FcγRs. Despite a low A/I ratio, mIgG1 can still bind the activating FcγRIII (Figure 3.2) with low affinity. With the potential up-regulation of activating FcγRs on immune cells triggered by CD40 agonists, mIgG1 could lead to a small degree of deletion of activated, PD-1 expressing T cells through FcγRIII engagement, thereby triggering ADCC/ADCP. This is perhaps the reason why only a minimal but significant OT-I expansion was noted with this isotype compared to controls on day 7 (Figure 4.4 D). Even so, those expanded T cells that were not deleted presented an activated phenotype (CD44 expression and PD-1 up-regulation) and progressed to maintain a memory pool that in some animals resulted in an effective secondary response upon re-challenge (Figure 4.8). Because of the higher A/I ratio of mIgG2a, the deletion of OT-I T cells during the primary response was likely larger, thereby abolishing the formation of any immunological memory. Hence, the levels of OT-I expansion versus deletion by engaging activating FcγRs in the primary response might determine the ability to mount effective memory responses upon re-challenge. To confirm this, a similar OT-I transfer experiment could be performed in γ-chain and FcγRII knockout mice. If engagement of activating FcγRs was the cause for the decreased OT-I expansion observed by anti-PD-1 mIgG1, this mAb should display the same enhancement of OT-I responses as anti-PD-1 mIgG1-N297A in γ-chain knockout mice, which lack functional activating FcγRs. Similarly, anti-PD-1 mIgG2a would be predicted to also enhance OT-I expansion in γ-chain knockout mice. In contrast, mIgG1 should still lead to reduced OT-I expansion in FcγRII knockout mice compared to mIgG1-N297A due to the relative increase of A/I ratio caused by FcγRII removal (121, 133).

Furthermore, the increase in tetramer negative CD44+ CD8 T cells by anti-PD-1 mIgG1-N297A but not other isotypes could be a reflection of the overall increased level of activation in these mice, mainly driven by the enhanced Tet+ T-cell expansion. As such, increased T-cell responses from transferred, high affinity clones may lead to a pro-inflammatory environment that results in the activation and expansion of antigen-specific T cells reactive to low affinity epitopes. In the context of cancer, the presence of such a large population of high affinity T cells that mount strong inflammatory responses is rather unlikely. Therefore, it was important to assess the ability of mIgG1-N297A to enhance endogenous responses in the absence of transferred OT-I transgenic cells.

To test the ability of anti-PD-1 mAbs to enhance T-cell responses in a more physiological setting, a similar experiment to the OT-I transfer was performed in

the context of an endogenous response to ovalbumin. To make it comparable, the same doses of CD40 agonist were given in conjunction with anti-PD-1 mAbs. However, the low levels of expanded SIINFEKL-specific CD8 T cells during the primary response led to a weak memory response. This is likely because a minimum threshold of primary SIINFEKL-specific CD8 T-cell activation and expansion is required to develop and maintain memory T cells. Nevertheless, the results after initial challenge showed a comparable trend to those from the OT-I transfers. At the peak of the response, anti-PD-1 mIgG1-N297A had a similar enhancing effect, with increased SIINFEKL-specific CD8 T cells, PD-1 expression and potentially the percentage of tetramer negative effector T cells, relative to other treatment groups (Figure 4.10).

To investigate whether Tet+ CD8 T-cell expansion, which was less than 10% with the higher dose of anti-CD40 mAbs (100 μg), could be further boosted, anti-CD40 mAbs (100 μg) were combined with anti-PD-1 mIgG1-N297A. In this setting, a similar increment in T-cell expansion and PD-1 expression was found in both Tet+ and tetramer negative CD8 T cells with the addition of anti-PD-1 mAb (Figure 4.11, Figure 4.12). Interestingly, there was a clear induction of T-cell priming in naïve tetramer negative T cells by anti-PD-1 mIgG1-N297A, which led to increased CD44+ T cells throughout the primary response (Figure 4.12 D-F). This provided evidence that anti-PD-1 mIgG1-N297A could further enhance higher doses of anti-CD40 adjuvant in the context of an endogenous response to ovalbumin, inducing comparable changes in T-cell expansion and activation to those observed in the presence of high affinity-TCR OT-I cells.

Furthermore, these experiments served as a proof of concept that anti-PD-1 mIgG1-N297A can enhance endogenous immunity without adoptive T-cell transfer when combined with anti-CD40 mAbs. In a report where this combination was found to be effective in some preclinical cancer models, the proposed mechanism involved an IL-12/IFN-γ loop, whereby IFN-γ production by activated T cells after PD-1 blockade stimulated IL-12 secretion from DCs, which in turn licensed effector T cells to kill tumour cells. Agonistic anti-CD40 mAbs increased IL-12 production by DCs, leading to increased tumour-cell killing and long-term immunity (162). It is then possible that a similar loop might be driving the augmented expansion and activation of effector T cells in blood during both OT-I and endogenous responses to ovalbumin.

Overall, murine anti-PD-1 mIgG1-N297A proved to be the most effective isotype in boosting OT-I and endogenous T-cell responses. As well as expanding high-affinity

CD8 T-cell clones, this engineered anti-PD-1 isotype also broadened the response and activated other CD8 T-cell specificities. The differences observed amongst the three murine anti-PD-1 mAbs supported the Fc region as an important determinant in anti-PD-1 mAb efficacy. Therefore, the presence of similar differences was next investigated in an immunotherapy-sensitive tumour model.

4.6.2 Therapy in MC38 model

Despite the undeniable success of PD-1 blockade in human cancers, one of its main limitations revolves around the fact that it is only effective in a minority of tumour types that bear favourable characteristics. Likewise, some murine tumour models appear to be more responsive to immune modulation. The cell line MC38 is a well-characterised murine colorectal cancer model, widely used in cancer immunology thanks to its extensive immune infiltration and its sensitivity to immunotherapy. These characteristics made it an ideal candidate to assess therapeutic differences of monotherapy with anti-PD-1 mAbs.

First and most notable, a clear dichotomy in survival was found after PD-1 blockade. Both mIgG1 and mIgG1-N297A increased survival, with 66% of mice rejecting primary tumours and developing long-lasting immunity, as illustrated by the subsequent rejection of a tumour re-challenge. Conversely, anti-PD-1 mAbs completely lost their efficacy when delivered in the form of a mIgG2a isotype (Figure 4.13, Figure 4.14). These findings are partly in line with the reports by Dahan R. et al., where the Fc-null anti-PD-1 mIgG1-D265A isotype decreased tumour growth compared to an irrelevant isotype, similar to the current mIgG1-N297A mAb. However, Dahan R. et al did not demonstrate any clear differences in tumour growth between mIgG1 and mIgG2a (104). In contrast, in this current study, anti-PD-1 mIgG1 prevented tumour growth to the same extent as mIgG1-N297A, whereas the mIgG2a mAb had no therapeutic activity. Moreover, whilst no survival benefit was shown in the previous study (104), it was evident that both mIgG1 and mIgG1-N297A generated long-lasting anti-tumour immunity in the current work. Albeit discussed in the text, a detailed comparison between the results published by Dahan R. et al (104) and those in the current study was summarised in Table 4-1. Despite following similar treatment schedules, in the report by Dahan R. et al., the initial dose of MC38 cells was four times higher than in this current study, which could explain the differences observed.

Table 4-1 Comparison of current study vs Dahan R. et al.

	Dahan R. et al. (2015) (104)	**Current study**
Effect on survival	No significant difference between IgG1 vs IgG2a; IgG1 vs IgG1-D265A; or IgG2 vs IgG1-D265A. No cures shown.	Significant increase in survival with IgG1 and IgG1-N297A vs controls and IgG2a. Cures in 66% of mice in the two former groups.
Immunological memory	Not shown	Mice treated with IgG1 and IgG1-N297A able to reject re-challenge
Depletion of CD8 TILs by mIgG2a	Shown as % of CD45+ cells	Significant reduction of PD-1+ CD8 TILs as percentage and absolute numbers
Expression of PD-1 at the tumour	Decreased PD-1 (as %) with IgG1 and IgG2a vs controls	Decreased PD-1 (as % and MFI) with IgG1 and IgG2a vs controls
		Significant increase (as % and MFI) with IgG1-N297A vs controls
Expression of PD-1 (MFI) at the spleen	Not shown	Significant increase in PD-1 on all T-cell subsets, with Tregs showing the largest amount of PD-1 per cell
Functional data in vitro/ in vivo	No functional data shown	Comparable ability of engineered murine mAbs to block PD-1-mediated suppression
		Anti-PD-1 mIgG2a-mediated phagocytosis of primary activated CD8 T cells
Involvement of FcγRII	Neutral: Increased % of CD8 TILs with effector phenotype (CD107a+, CD69+) at the tumour with IgG1 vs control	Neutral: Increased % of CD8 TILs at the tumour with IgG1 vs control and improved survival by IgG1 equivalent to IgG1-N297A, indicating no detrimental effect of binding to FcγRII
	Detrimental: Small decrease in tumour volume in FcγRII$^{-/-}$ vs wilt type mice with rat IgG1 anti-PD-1 mAb, although IgG control in FcγRII$^{-/-}$ mice not shown	

The therapeutic response seen with mIgG1 and mIgG1-N297A mAbs was likely associated with the increase in CD45+ immune cells in the tumour bed (Figure 4.17 A). This increase was paralleled by an expansion of tumour-infiltrating CD8 T cells, which was particularly evident in the mIgG1 group but also with a clear trend in the

mIgG1-N297A group (Figure 4.17 A-C). With regards to mIgG2a, there was also a trend towards decreased CD8 TILs, but this was not statistically significant. In agreement with previous studies (104), the main conclusion that can be drawn is that while mIgG1 and mIgG1-N297A increased CD8 TILs, administration of mIgG2a seemed to reduce the numbers. Importantly, the assessment of absolute cell counts demonstrated deletion of PD-1 positive CD8 TILs and Tregs following therapy with anti-PD-1 mIgG2a but not mIgG1 or mIgG1-N297A (Figure 4.17 D). Although the reduction of total CD8 TILs by mIgG2a compared to controls was not statistically significant, this was due to the large variability in other treatment groups (Figure 4.17 C). Notably, the CD8: Treg ratio, which often correlates with therapeutic activity (23), decreased after therapy with anti-PD-1 mIgG2a (Figure 4.17 C), further suggesting that this isotype hinders the ability of PD-1 blockade to release T-cell activation. Noteworthy, the proportion of CD8 to Tregs was already high in the control group (see Appendix A, Figure 6.10 A), perhaps indicating that these tumours had favourable traits at baseline that rendered them more susceptible to PD-1 blockade.

In control mice, PD-1 was expressed on over 80% of CD8 TILs and at high levels, likely marking exhausted T cells. Anti-PD-1 mIgG1-N297A presented a similar high percentage of PD-1+ CD8 TILs, but with higher expression of PD-1 per cell (Figure 4.18). In the context of chronic antigen exposure, expression of PD-1 is often regarded as a marker of T-cell exhaustion due to its high expression on dysfunctional TILs. However, as mentioned previously, T-cell activation also leads to PD-1 up-regulation. Therefore, the further up-regulation of PD-1 by anti-PD-1 mIgG1-N297A could reflect activation of T cells secondary to PD-1 blockade. To discern between exhaustion and activation, expression of other inhibitory co-receptors such as LAG-3 and TIM-3 could have been assessed, as their co-expression with PD-1 has been characterised in exhausted TILs (317, 318). Nevertheless, the observed PD-1-high CD8 TILs were likely functional but required PD-1 blockade to release inhibition, as mIgG1-N297A led to a significant increase in survival. Further to this, recent reports argue that different pools of PD-1+ TILs exist based on the expression of transcription factors such as EOMES/T-bet (156) or Tcf1 (157, 158). Notably, a population of progenitor PD-1+Tcf1+ TILs can respond to PD-1 blockade and give rise to a subset of Tcf1 negative, PD-1-high TILs that bear effector function and can mediate tumour-cell killing (157, 158). As a possibility, the observed PD-1+ CD8 TILs in control mice may contain the progenitor population, which upon effective PD-1 blockade, can differentiate into potent effector TILs expressing higher levels of PD-1. To test this hypothesis, assessment

of the transcription factors T-bet, EOMES and Tcf1 could be carried out to establish the progenitor status or terminally differentiate phenotype of PD-1+ TILs in control mice and also following anti-PD-1 therapy with mIgG1-N297A.

In contrast, engagement of activating FcγRs by anti-PD-1 mIgG2a strongly reduced the percentage of PD-1+ CD8 TILs, consistent with previous studies (104). In view of the ability of this isotype to trigger phagocytosis in vitro (Figure 3.16), it is possible that PD-1+ TILs could also be phagocytosed in vivo by TAMs. Although the depletion of TILs through ADCC/ ADCP by other myeloid and NK populations (319) cannot be excluded, the large proportion of tumour-infiltrating macrophages of MC38 tumours (Figure 4.24 A) argues in favour of this hypothesis. Interestingly, anti-PD-1 mIgG1 increased CD8 TIL infiltration and survival similarly to mIgG1-N297A, but showed different TIL phenotype in terms of PD-1 expression. In contrast to the mIgG1-N297A mAb, mIgG1 clearly reduced PD-1 expression in TILs. Although mIgG1 can interact with the activating FcγRIII, which could lead to the preferential depletion of PD-1-high TILs similarly to mIgG2a, the observed increase of CD8 TILs and the rejection of tumours by mIgG1 might indicate that this effect is not the predominant one. Besides, previous work suggested that the inhibitory FcγRII could also be involved in reducing the efficacy of anti-PD-1 mAbs (104). In this scenario, engagement of FcγRII by mIgG1 could cause cross-linking of anti-PD-1 mAbs and induce PD-1 signalling, similarly to agonistic mAbs (133). As part of the signalling cascade, there is a negative loop whereby SHP2 dephosphorylates PD-1 cytoplasmic tail, destabilizing the PD-1-SHP2 complex (47). Although this could lead to PD-1 degradation and removal from the cell surface, PD-1 signal would also likely inhibit TCR/CD28 signals and reduce T-cell proliferation. However, the increment in CD8 TILs suggests perhaps that PD-1 signalling is not the main mechanism down-regulating PD-1 expression. Instead, FcγRII cross-linking could cause the internalisation of PD-1 in a similar way to which CTLA-4 co-internalises with CD80/86 after receptor binding (320).

Another plausible hypothesis is that engagement of FcγRII/III by anti-PD-1 mIgG1 could promote trogocytosis, whereby membrane fragments containing PD-1 could be transferred from T cells onto myeloid cells without compromising T-cell integrity. Anti-PD-1 mIgG2a could also trigger trogocytosis by engaging FcγRs, but the reduction of CD8 TILs observed herein and in previous reports (104) (Figure 4.17 B) would argue in favour of a type of trogocytisos that led to cell death, as opposed to mIgG1 mAbs. It is known that human and murine T cells and APCs can exchange molecules in a bidirectional manner via trogocytosis. Indeed, transfer of

PD-L1 from DCs or tumour cells to T cells was documented to occur and required antigen-specific recognition (321). In mAb therapy, anti-CD20 Rituximab has been shown to trigger trogocytosis via FcγR engagement, which reduced the surface levels of the target receptor (322). Taking into account that all murine FcγRs on macrophages can trigger trogocytosis (323), it is possible that selective binding to FcγRII/III on TAMs by anti-PD-1 mIgG1 leads to a reduction of PD-1 expression via trogocytosis.

Notably, a study by Arlacukas SP, et al. described that PD-1 negative TAMs acquired anti-PD-1 mAbs from the surface of T cells shortly after in vivo infusion, through a process that was dependent on FcγRII/III (324). Although the authors claimed that PD-1 remained on the surface of T cells after antibody capture, the high-affinity interaction between PD-1 and anti-PD-1 mAbs (293, 294) (Figure 3.5) suggests that this mechanism could likely lead to the physical disruption of the receptor too. Although decreased PD-1 expression did not appear to have any impact on the overall efficacy of anti-PD-1 mIgG1, it would be important to understand the mechanism behind this phenotype to assess potential implications in humans. Interestingly, an equivalent effect was observed with anti-CD25 rat IgG1 mAbs in vivo; whilst the percentage of intratumoural Tregs was not altered by anti-CD25 rat IgG1 mAbs, expression of the target receptor was largely reduced (309). Considering that rat IgG1 and mIgG1 have the same FcγR binding pattern by SPR (Figure 3.2), it could be hypothesised that mAbs with low A/I ratio may preferentially lead to the removal of the target receptor as opposed to causing depletion of the cells that express such receptor.

A similar pattern of PD-1 expression was observed in tumour-infiltrating CD4 T cells and Tregs, with higher levels in control and mIgG1-N297A groups and lower or absent expression in mIgG1 and mIgG2a, respectively (Figure 4.18 B). This proposes that anti-PD-1 mAbs affect all subsets of TILs despite the relatively higher PD-1 levels in CD8 T cells. Together with these changes, the increase in PD-1 on splenic Tregs by mIgG1-N297A could indicate that the potent activity of this isotype might also stimulate a suppressive Treg response, although no changes were noted in the frequency of these cells (Figure 4.20). In agreement, a recent study with 2 patients that presented hyperprogression following PD-1 blockade revealed a marked increase in proliferating effector Tregs. In vitro blockade of PD-1 increased proliferation and enhanced their suppressive capacity (170). Therefore, the parallel activation of suppressive Tregs by anti-PD-1 mIgG1-N297A could represent a resistance mechanism in non-responsive mice.

The interest on the role of myeloid cells in PD-1 blockade has been growing in the recent years, as they express both PD-L1 and PD-1, as well as FcγRs that can trigger antibody-dependent effector functions following administration of therapeutic mAbs (101). In MC38 tumours, around 50% of the tumour volume was comprised of CD11b+ myeloid cells, of which the majority expressed PD-L1 (Figure 4.22). This extensive expression of host-derived PD-L1 in the TME, together with the expression on cancer cells, supports the active role of PD-1 inhibition in these tumours. Also, the relatively low levels of PD-L1 in spleen demonstrate that tumour-specific factors sustain myeloid PD-L1 expression. Immune activation induced by anti-PD-1 mIgG1-N297A increased PD-L1 both in myeloid and tumour cells, which was likely driven by the release of IFN-γ and other inflammatory cues by activated T cells (325). To a lesser extent, mIgG1 tended to increase PD-L1 in a similar fashion to anti-PD-1 mIgG1-N297A. Although the intracellular production of IFN-γ by TILs was assessed ex vivo, no reliable data was obtained due to loss of fluorescent signal after in vitro stimulation. As an alternative approach to corroborate a potential increase in IFN-γ secretion, its quantification in whole tumour lysates could be evaluated, as opposed to intracellular expression in T cells.

In regards to FcγR expression, anti-PD-1 mIgG1-N297A broadly modulated myeloid phenotype, showing increased expression of mainly activating but also inhibitory FcγRs across myeloid subsets. In contrast, mIgG1 showed minimal up-regulation of FcγRIV on macrophages (Figure 4.22; Figure 4.25). The reduction of A/I ratio by mIgG2a at the tumour site (Figure 4.23 C) could suggests that myeloid cells bear a less activated phenotype compared to controls. This illustrates the profound effect that T-cell derived factors have on myeloid activation, as depletion of activated TILs by mIgG2a subsequently affected myeloid phenotype.

Although expression of PD-1 was not assessed in myeloid cells, other studies have shown that activated macrophages express PD-1, which has been associated with impaired phagocytic ability by TAMs in cancer (43). Considering the suppressive role of PD-1 also on myeloid precursor cells (44), blockade of PD-1 on TAMs by anti-PD-1 mAbs could enhance phagocytosis of tumour cells. Because of the sizable proportion of TAMs in MC38 tumours, enhancement of macrophage activity would arguably have a significant effect on anti-tumour responses. However, the percentage of macrophages was not altered by anti-PD-1 mIgG2a, suggesting that TILs remain the main target of anti-PD-1 mAbs.

To conclude, this chapter summarises the FcγR requirements for effective stimulation of T-cell responses and therapy by anti-PD-1 mAbs. Engagement of activating FcγR by mIgG2a decreased OT-I expansion and anti-tumour immunity against a sensitive model. Because of the clear reduction in PD-1+ TILs and the ability to trigger phagocytosis in vitro, mIgG2a may cause deletion of activated T cells that express high levels of PD-1, as summarised in Figure 4.26. On the other hand, abrogation of any FcγR binding by the Fc-null anti-PD-1 mIgG1-N297A variant enhanced CD8 T-cell expansion, T-cell activation and anti-tumour immunity. In this scenario, the N297A mutation enables anti-PD-1 mAbs to act as pure blockers. PD-1 is expressed in various cell types (i.e CD8 T cells, Tregs, macrophages, NK cells), and PD-1 blockade is likely to act on all of them. Although it could induce Treg expansion and function, the dominant presence of a PD-1+ CD8 population in MC38 tumours favours CD8 and CD4 effector T-cell activation, leading to effective and long-term anti-tumour immunity in almost 70% of mice bearing MC38 tumours.

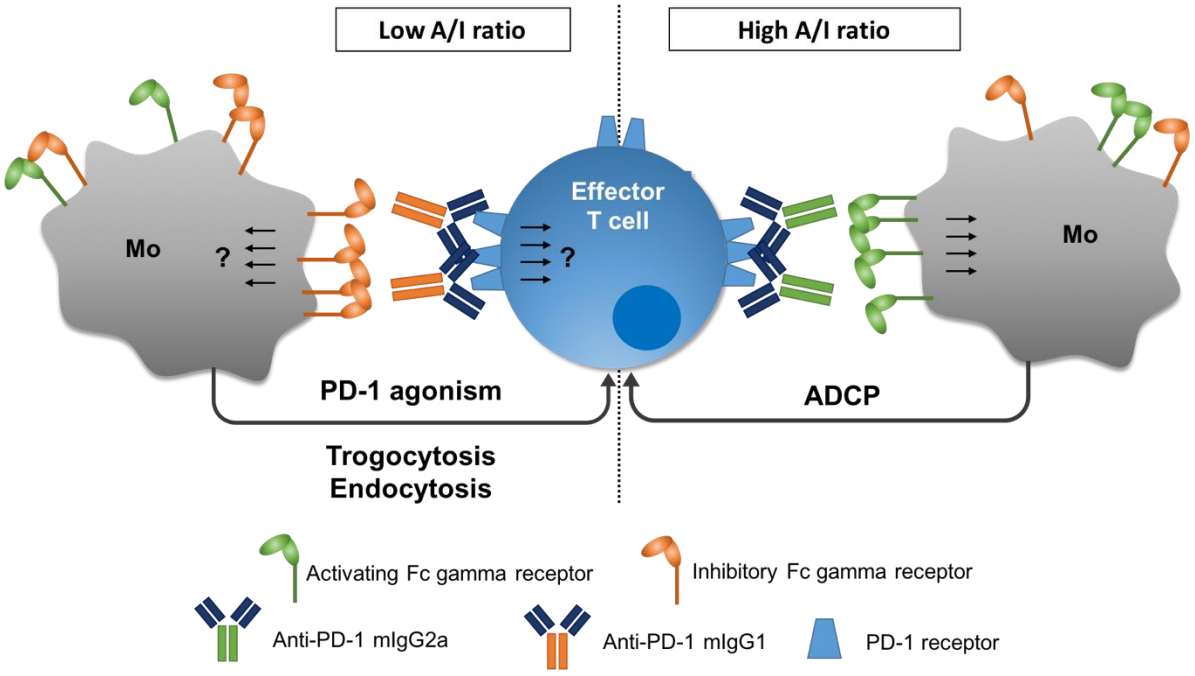

Figure 4.26 Potential effector mechanisms mediated by anti-PD-1 mAbs.
Summary of the different effector mechanisms that could take place depending on the expression of Fcγ Rs and anti-PD-1 isotype. In the context of a suppressive TME, with high Fcγ RII expression, mIgG1 may preferentially cause depletion of PD-1 receptor without compromising T-cell integrity via agonistic signalling, trogocytosis or endocytosis. In addition, cross-linking of Fcγ RII may down-regulate the effector state of myeloid populations. On the contrary, in the presence of pro-inflammatory cues and extensivee expression of activating Fcγ Rs, anti-PD-1 mAbs that engage Fcγ Rs (i.e mIgG2a and mIgG1) may preferentially trigger antibody-dependent effector mechanisms on myeloid effectors such as ADCP when, leading to PD-1+ T-cell depletion.

Finally, the role of FcγRII engagement in modulating anti-PD-1 mAbs is less clear. Whilst anti-PD-1 mIgG1 improved survival in MC38, it failed to consistently increase T-cell expansion in OT-I transfers and endogenous responses. As summarised in Figure 4.26, in the context of OT-I and endogenous responses, administration of anti-CD40 agonists and ovalbumin might lead to an increase in activating FcγRs and A/I ratio in myeloid subsets, thus favouring anti-PD-1 mIgG1 effector functions that may lead to the deletion of PD-1+ CD8 T cells. Conversely, the large expression of the inhibitory FcγRII (and hence low A/I ratio) at the TME (Figure 4.23) may favour trogocytosis or endocytosis of PD-1 following FcγRII cross-linking, thereby explaining the reduction on PD-1 expression in TILs by anti-PD-1 mIgG1. Analysis of the A/I ratio after ovalbumin and anti-CD40 mAb therapy in secondary lymphoid organs could help establish this hypothesis, allowing the comparison between A/I ratios in the different settings. However, the possibility that PD-1 signalling may lead to degradation or down-regulation of the receptor from the cell surface cannot be excluded either.

Furthermore, the overall changes in tumour-infiltrating myeloid cells observed after mIgG1-N297A therapy were recapitulated by mIgG1, but to a much lesser extent. Because of the expression of FcγRII on myeloid cells, mIgG1 could induce inhibitory signalling downstream of FcγRII, thereby dampening the activation status of myeloid cells. Otherwise, the increased activated and effector phenotype observed on OT-I cells and TILs by the mIgG1-N297A mAb could lead to a more pro-inflammatory environment, thereby driving more pronounced changes in surrounding immune cells compared to mIgG1. Regardless of the mechanism, Fc-null engineered anti-PD-1 mAbs were the most effective isotypes at mounting potent and long-lasting T-cell immunity.

Chapter 5: Therapeutic effect of anti-PD-1 mAbs in murine models of neuroblastoma

5.1 Chapter introduction

Over 50% of NB patients present with metastatic disease and large tumour burden at the time of diagnosis. Despite a very aggressive multi-modal treatment, outcomes for this high-risk NB group remain poor (232). Monoclonal antibodies targeting the TAA GD2 were approved as part of the maintenance therapy for high-risk NB; although 2-year EFS and OS were significantly improved, longer-term efficacy is less clear, and relapse rates are still high (189, 274). These facts highlight the need to investigate novel therapeutic strategies that can achieve long-lasting anti-tumour immunity in high-risk NB patients. To study the potential translation of anti-PD-1 therapy in preclinical models of NB, the murine neuroblastoma 9464D cell line was utilised. This model was established from spontaneous tumours that developed in TH-MYCN transgenic mice (235), where amplification of MYCN gene contributes to the transformation of neuroblasts in vivo, leading to neuroblastoma tumours that largely mirror human counterparts (235, 326). Whilst spontaneous tumours developed in TH-MYCN mice may recapitulate human tumours more closely, the incidence of tumours is low. Alternatively, subcutaneous injection of passaged 9464D cells is a practical way to test multiple therapeutic antibodies and combinations. Hence, the effect of antibody isotype in anti-PD-1 therapy was first investigated in 9464D tumours by assessing the impact of anti-PD-1 mAbs on survival and tumour growth, together with defining the phenotype of tumour-infiltrating immune cells following therapy. An initial study of the 9464D TME after anti-PD-1 therapy was conducted using the available parental rat IgG1 anti-PD-1 mAb and its deglycosylated variant. Following characterisation of the panel of murine anti-PD-1 isotypes (Chapter 3:), these mAbs were utilised in similar phenotypic experiments.

As summarised in the introduction (see Chapter 1 section 1.4.1), childhood cancers are poorly immunogenic and often display low or absent immune infiltration (187, 195-197). Perhaps not surprising given its immunologically ‘cold’ nature, clinical trials evaluating the use of checkpoint inhibitors as a monotherapy for NB revealed no significant efficacy (202, 214, 215). It is therefore anticipated that anti-PD-1 mAbs will achieve better therapeutic outcomes also in preclinical models as part of

combinatorial regimens. In view of this, in this chapter, clinically relevant combinations were also investigated in preclinical models. Specifically, therapeutic reagents that are already used for the treatment of NB (i.e anti-GD2 mAbs and chemotherapy) were tested in combination with anti-PD-1 mAbs.

5.2 Kinetics of PD-1/ PD-L1 expression in 9464D tumours

In some human cancers, expression of PD-L1 within the TME has been demonstrated to correlate with therapeutic response to anti-PD-1 therapy. However, expression of PD-L1 is very broad, being found on lymphocytes, myeloid and tumour cells within the TME. This has made it difficult to identify the relative contribution of each PD-L1+ cell type to tumour immune escape (67, 69, 327). Furthermore, due to the dynamic nature of PD-L1 expression, specific cell types within the TME might be regulated differently by environmental cues, leading to distinct PD-L1 expression patterns and kinetics (66). Therefore, the kinetics of expression of PD-1 and PD-L1 were investigated in the 9464D TME, as well as other molecules of interest that play a role in the immunogenicity of NB tumours, such as MHC-I and GD2. As mentioned in the introduction (see section 1.4.2.1.1), loss or down-regulation of MHC-I molecules is a common event in human NB, potentially resulting in impaired T-cell recognition but making tumour cells more susceptible to NK-mediated killing (11). Moreover, investigating the expression of GD2 by 9464D cells in vivo is important due to its nature as a TAA and also because of the conceivable therapeutic combination of anti-PD-1 and anti-GD2 mAbs (263, 265).

To study how these markers are regulated in the TME as the tumours develop, 9464D tumours were harvested at three different time points following subcutaneous inoculation. Lymphocytic populations and markers of interest were assessed when tumours were first palpable or at two different sizes (5x5 and 10x10 mm), using flow cytometry of disaggregated tumours as exemplified in Figure 5.1. The relative percentage of immune infiltrates out of the singlet gate ranged on average from 10 to 20%, but decreased as tumour progressed (Figure 5.2 B). In general, most lymphocyte populations did not change significantly as tumours progressed (Figure 5.2 B), although the relative percentage of CD8 and NK cells tended to be increased when tumours became larger. Notably, TILs only accounted for less than 10% of immune cells at the tumour site, highlighting the paucity of T-cell infiltrates.

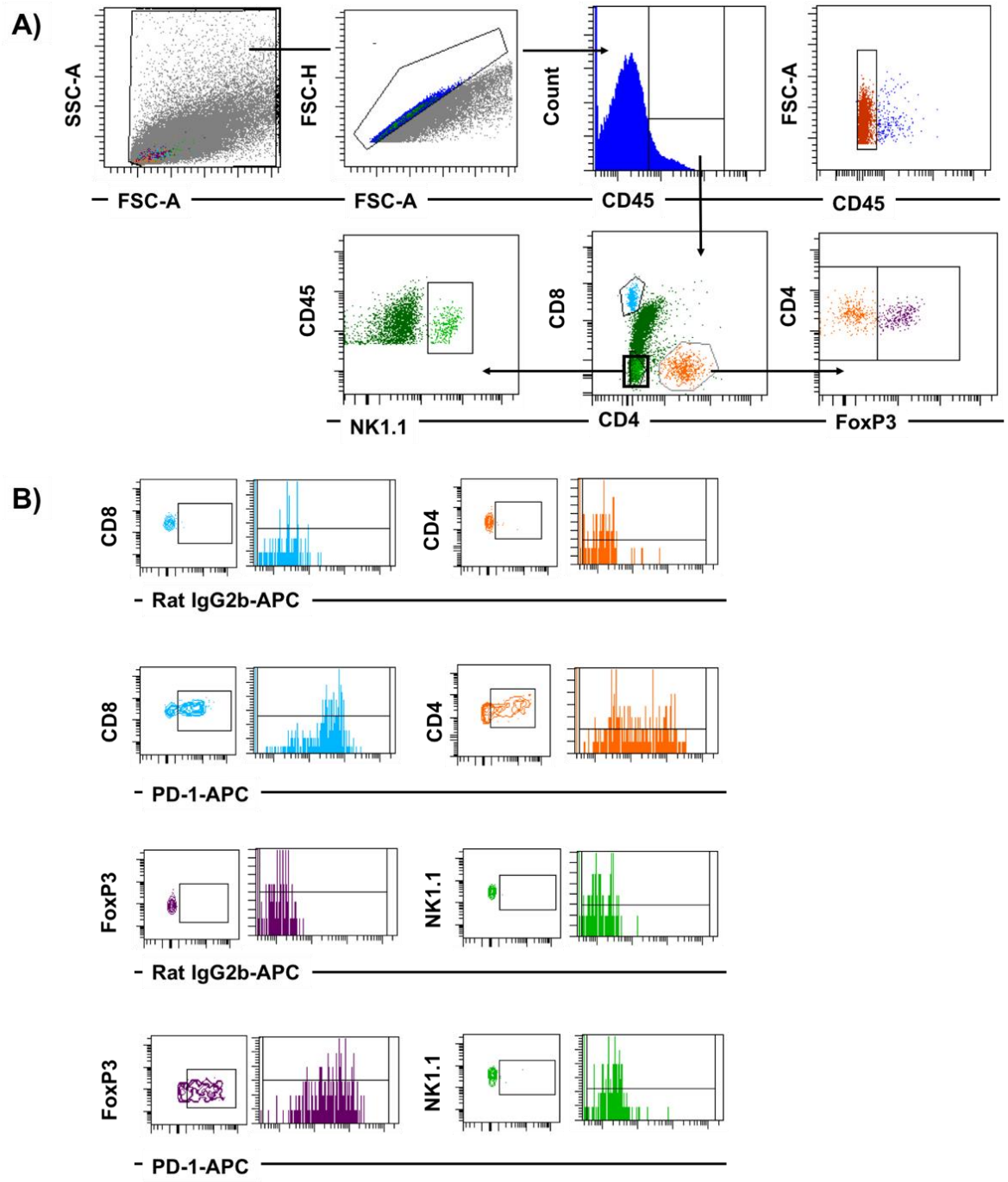

Figure 5.1 Gating strategy: Tumour-infiltrating T cells in 9464D tumours. Tumours were mechanically and enzymatically digested as detailed in 2.7.5, and single cell suspensions were obtained. Cells were stained with surface and intracellular markers (see 2.8) and samples were run on flow cytometry. A) Gating of T-cell populations. From all live cells (FSC-A–SSC-A), doublets were excluded and immune cells were gated according to their CD45 expression. Effector CD8 T cells, effector CD4 T cells (FoxP3-CD4+), Tregs (FoxP3+CD4+) and NK cells (CD8-CD4-CD3+NK1.1+) were gated from CD45+ cells. Tumour cells were gated as CD45- cells. B) Dot plots and histograms for each lymphocyte population showing the expression of PD-1. Positive cells were gated according to an isotype control. Geometric mean of the whole population was calculated from the histogram plots, and isotype control values were subtracted. This strategy was followed for all markers assessed.

No clear changes were detected in terms of PD-1 expression, which was present on CD8 T cells, CD4 T cells and Tregs from palpable to larger tumour sizes (Figure 5.2 C; Appendix B Figure 6.16 A). Yet, a small increase in PD-1 expression was observed on CD4 effectors and Tregs at the latest time point (Figure 5.2 C). Although NK cells have been reported to express PD-1 and to be able to respond to PD-1 blockade (328), no PD-1 expression was detected in 9464D-infiltrating NK cells. In contrast to PD-1, PD-L1 was present in all CD4, Tregs and NK cells (see Appendix B, Figure 6.16 B) and increased after tumours became 5x5 mm in all cells except CD8 T cells (Figure 5.2 D). High levels of MHC-I were also expressed by all lymphocyte populations within the TME (see Appendix B, Figure 6.16 C), with Tregs showing the highest levels (Figure 5.2 E).

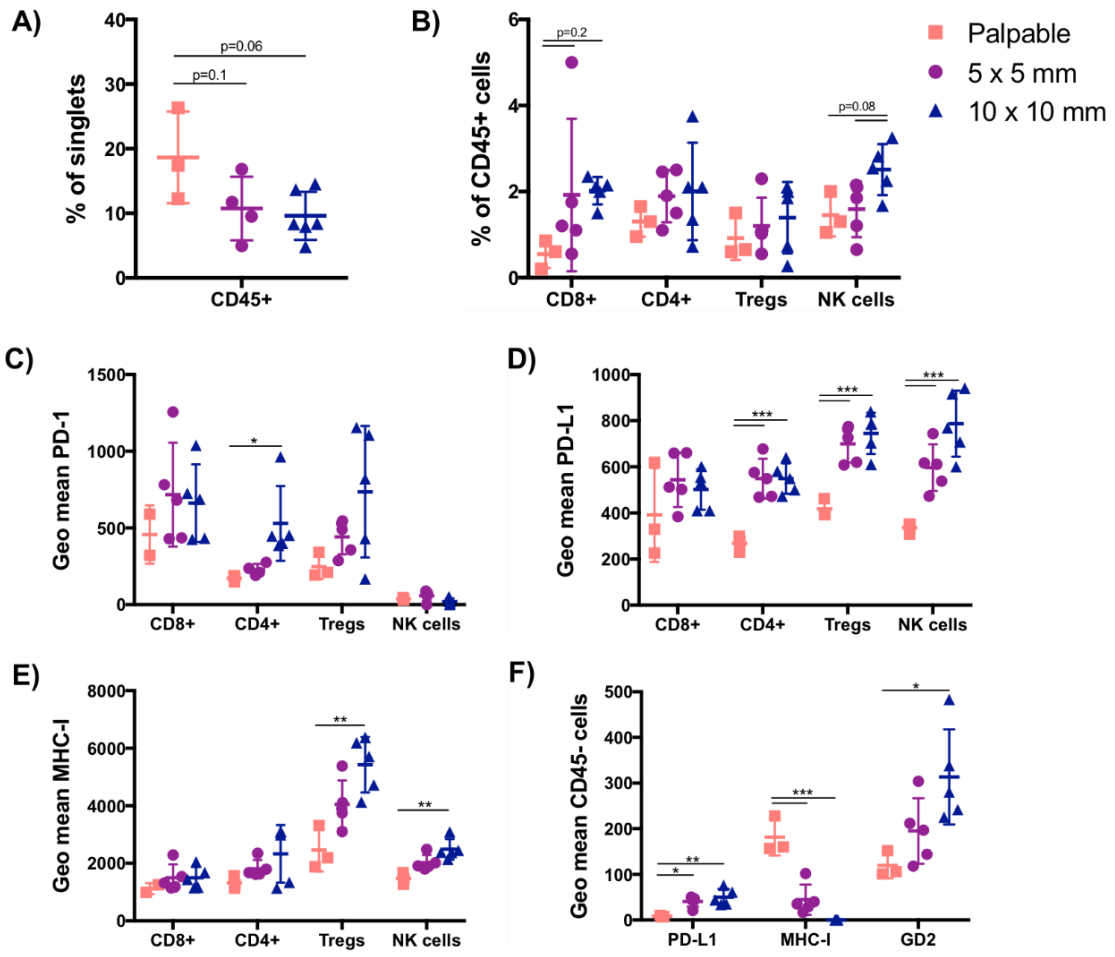

Figure 5.2 Kinetics of PD-1, PD-L1, MHC-I and GD2 expression in 9464D tumours.
A) Percentage of immune infiltrates (CD45+) out of singlets. B) TILs and NK cells as percentage of CD45+ immune infiltrating cells. C-E) Expression of PD-1 (C), PD-L1 (D) and MHC-I (E) by TILs and NK cells shown as geometric mean (MFI). F) Expression of PD-L1, MHC-I and GD2 on CD45 negative tumour cells shown as geometric mean (MFI). Experiment performed twice, N=3 or N=5 mice per group at palpable size or 5x5/10x10 mm, respectively. Bars represent mean ± S.D, *p<0.05, **p<0.01, ***p<0.001 (One-way ANOVA).

On the contrary, tumour cells (CD45 negative gated cells) displayed low level of expression of MHC-I molecules, which further decreased as tumours progressed (Figure 5.2 F). Levels of both GD2 and PD-L1 displayed a trend towards increased expression in tumour cells as tumours progressed, but the levels observed were low (Figure 5.2 F). In vitro, 9464D cells display low or absent GD2 expression (329), and therefore in vivo expression might be variable, particularly at small tumour sizes. In terms of PD-L1, the detection antibody and settings used were equivalent for T cells and tumour cells. Therefore, tumour cells expressed lower amounts of PD-L1 than T cells, but increased as tumour progressed (Figure 5.2 F). Nevertheless, tumour cells comprised the majority of the tumour mass, which supports that, despite the low PD-L1 expression, their potential impact on tumour evasion could be high.

Together with tumour cells, myeloid populations within the TME can contribute substantially to the inhibition of T-cell responses through PD-1/ PD-L1 (27, 143, 330). In view of this, a flow cytometry panel was optimised to assess the frequency and type of myeloid infiltration in 9464D tumours, as shown in Figure 5.3. There was a decrease in the overall percentage of myeloid infiltration (Figure 5.4 A) as tumour volume increased, but this might be reflective of the relative increase in the absolute numbers of tumour cells. Considering the small number of T cells out of CD45 and the similar percentage of immune infiltrates (CD45+; Figure 5.2 A,B) and myeloid cells (CD11b+; Figure 5.4 A), it is likely that the largest proportion of tumour-infiltrating immune cells in 9464D tumours correspond to myeloid infiltrates. This agrees with reports from human NB, where myeloid cells comprised the majority of immune infiltrating cells (196, 197).

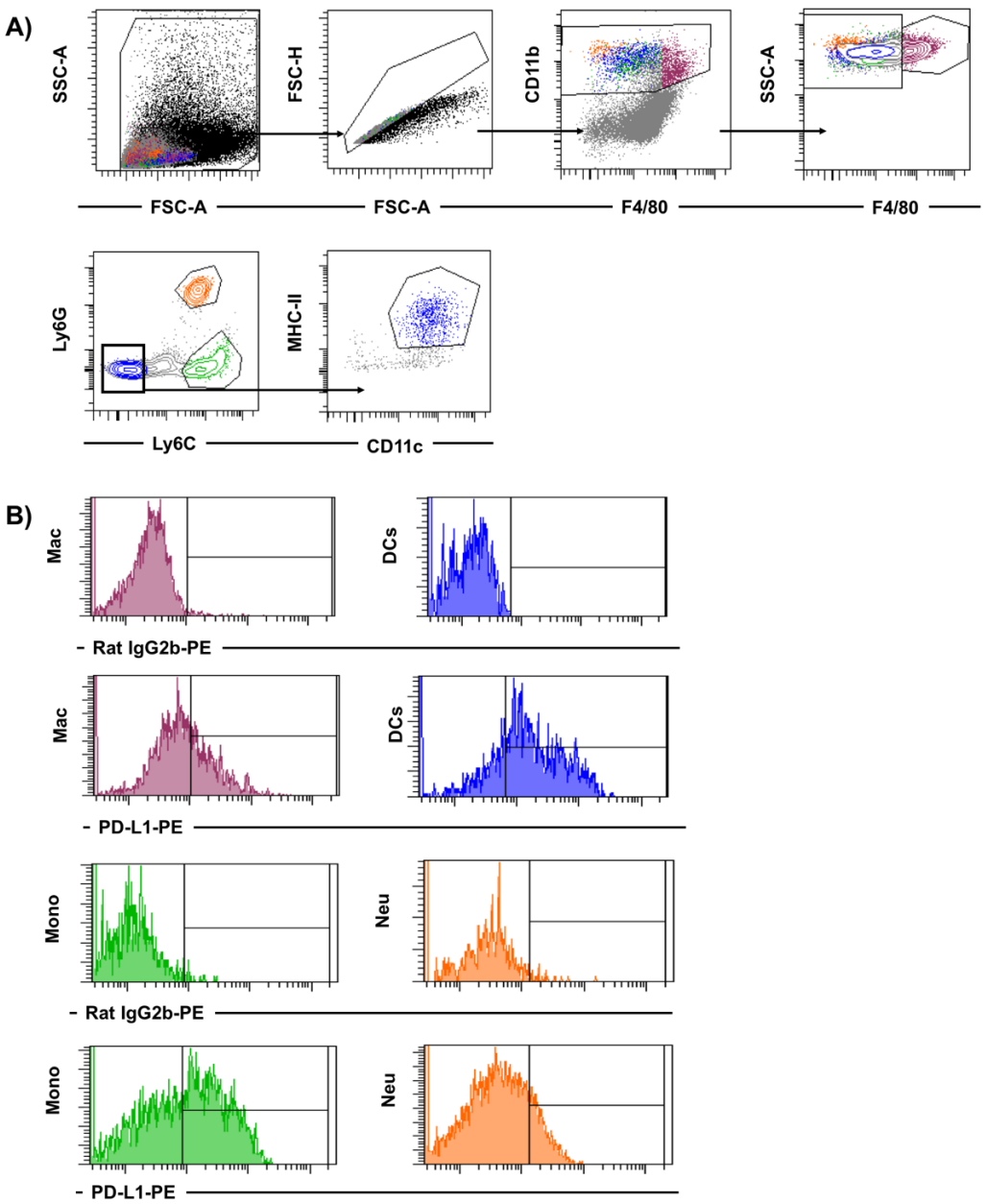

Figure 5.3 Gating strategy: Tumour-infiltrating myeloid populations in 9464D tumours.
Tumours were mechanically and enzymatically digested as detailed in 2.7.5, and single cell suspensions were obtained. Cells were stained with surface markers (see 2.8) and samples were run on flow cytometry. A) Following doublets exclusion, live cells were gated according to CD11b and F4/80 expression. Tumour-infiltrating macrophages were gated as F4/80 high and CD11b high. Neutrophils, monocytes and DCs were gated from the CD11b high, F4/80 low population according to their expression of Ly6C, Ly6C, CD11c and MHC-II markers as follows: neutrophils (Ly6C high, Ly6G high), monocytes (Ly6C low, Ly6G high) and DCs (Ly6C-, Ly6G-, MHC-II high, CD11c high). B) Examples of histograms showing the expression of PD-L1 on macrophages (purple); DCs (blue); monocytes (green); and neutrophils (orange). Gates were set according to an isotype control. Isotype values were subtracted to geo means for each population. This strategy was followed for all markers assessed.

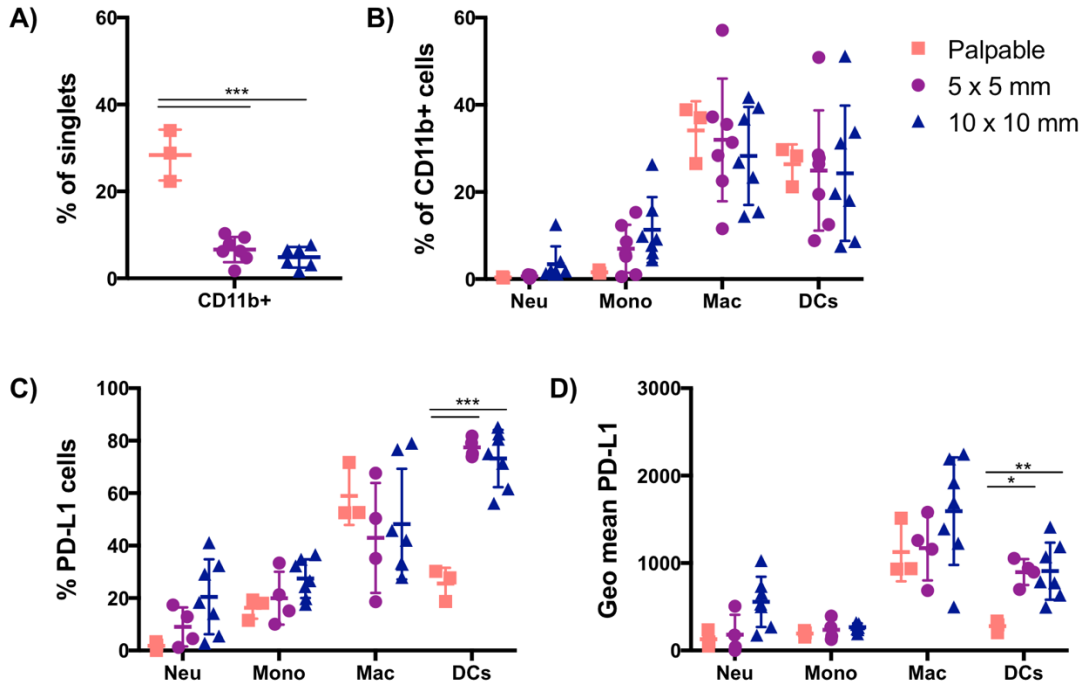

Figure 5.4 Kinetics of PD-L1 expression on myeloid populations in 9464D tumours.
A) Percentage of CD11b+ myeloid cells out of singlets. B) Percentage of tumour-infiltrating myeloid populations out of CD11b+ gate. C-D) Expression of PD-L1 in myeloid subsets shown as percentage of positive cells (C) or as MFI (D). Experiment performed twice, N=3-6 mice per group. Bars represent mean ± S.D, *p<0.05, **p<0.01, ***p<0.001 (One-way ANOVA).

The proportion of different myeloid subsets (Figure 5.4 B) did not vary across time points, with macrophages and DCs comprising the largest myeloid subpopulations. Similarly, macrophages and DCs expressed the highest levels of PD-L1 (Figure 5.4 C,D), which increased in DCs upon tumour growth. Overall, there was a paucity of TILs and myeloid infiltrates in 9464D tumours, with most immune subpopulations remaining stable as tumours progressed. Nevertheless, there was evidence of PD-1/ PD-L1 expression within the TME, as well as the TAA GD2.

5.3 Immunophenotyping of 9464D-bearing mice after therapy with wild-type rat IgG1 or deglycosylated anti-PD-1 mAbs

The presence of both PD-1 receptor and ligand within the 9464D TME supported the contention that the PD-1/ PD-L1 inhibitory axis may be active in the 9464D TME and that PD-1 blockade could potentially boost T-cell immunity in this tumour model. Initial studies in the group used the parental anti-PD-1 mAb (rat IgG1).

However, following later reports suggesting that engagement of FcγRs can be detrimental to the therapeutic activity of these mAbs (104, 324), enzymatic deglycosylation of the N-linked oligosaccharides was carried out to prevent any Fc-mediated effect of the parental mAb. In line with the earlier studies (104, 324), the deglycosylated (degly) anti-PD-1 mAb was found to have a small, yet significant increase in therapeutic activity on 9464D tumours compared to the parental rat IgG1 mAb (329). Hence, and as a starting point in the current work, immunophenotyping of 9464D tumours after treatment with either the parental rat IgG1 or degly mAbs was performed to investigate the differences behind the distinct therapeutic effects of the mAbs. Deglycosylation of rat IgG1 anti-PD-1 mAb was performed with PNGase F, which eliminates the carbohydrate chain at the C_{H2} domain of the heavy chain (331). Successful deglycosylation was confirmed as exemplified in Figure 5.5 prior to any in vivo experiment. In the presence of reducing buffer, there was a drop in the MW of the heavy chain in the degly mAb comparted to the parental version, which corresponded to the loss of the carbohydrate side chain attached to it. In the non-reducing conditions, both heavy and light chain remain linked by disulphide bonds, making it more difficult to certify the decreased MW.

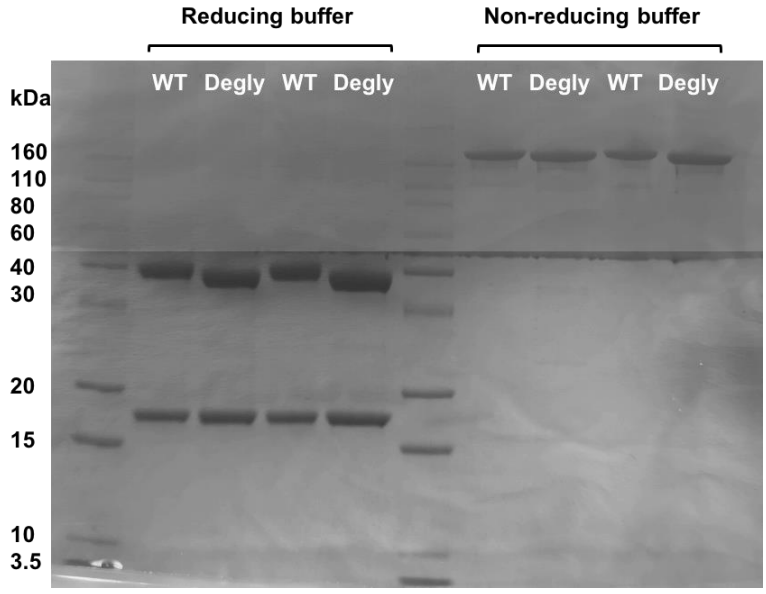

Figure 5.5 Confirmation of successful deglycosylation of parental EW1-9 mAb by SDS-gel PAGE.
Anti-PD-1 rat IgG1 was enzymatically deglycosylated with PNGase F overnight at 37°C. To confirm successful deglycosylation, 4 μg of wild-type (WT; first and third lanes of each reducing conditions) EW1-9 rat IgG1 and deglycosylated (Degly; second and fourth lanes) anti-PD-1 mAb was run in SDS-PAGE gels in non-reducing and reducing conditions (with the addition of DTT). Gels were incubated with Coomassie stain and destained overnight in a rocket with destaining buffer.

To study the phenotype of immune infiltrates in 9464D tumours in response to anti-PD-1 mAbs, gating strategies to identify T cell and myeloid populations were followed in the same way as previously shown (Figure 5.1, Figure 5.3). For the current experiment, mice inoculated with subcutaneous 9464D tumours were treated with a single dose of parental rat or degly anti-PD-1 mAbs when tumours reached 7x7 mm, and tumours and spleens were harvested 3 days later to allow for immune phenotypic changes to occur (Figure 5.6 A). No change in tumour (B) or spleen (C) weight was observed across treatment groups, nor in the relative percentage of effector CD8, CD4 or Tregs at the tumour site (D). As shown earlier, lymphocytes made up less than 1% of the total singlet gate, highlighting the low number of TILs in 9464D tumours.

In order to obtain a comprehensive picture of the nature of the immune response against 9464D tumours, a panel of T-cell markers was chosen, which included: activation markers (CD25, CD107a, Ki67, CD44); co-stimulatory receptors (4-1BB, OX40); markers of exhaustion (Tim-3, LAG-3); and transcription factors involved in the function and phenotype of T cells (T-bet, EOMES) (332). Despite the lack of changes in the overall percentage of TILs, some differences were observed with regards to their phenotype (Figure 5.6 E-H). First, around 80% of T cells expressed PD-1 in non-treated (PBS) mice (E), with CD8 T cells expressing the highest levels (F). The percentage of positive cells and level of expression was significantly decreased in the parental rat mAb group compared to controls (Figure 5.6 E,F). In contrast, the deglycosylated mAb showed an equally high expression of PD-1 compared to controls, which was also significantly higher than the parental rat group. Similarly, PD-1 expression on effector CD4 and Tregs was higher in controls and degly mAb groups compared to mice treated with the parental rat IgG1 (Figure 5.6 E,F).

In terms of the effector phenotype of these cells, there was a significantly larger percentage of effector CD8 and CD4 T cells that expressed the degranulation marker CD107a (333) in both anti-PD-1 mAb groups compared to controls, with a similar trend in Tregs (Figure 5.6 G). Likewise, the transcription factor EOMES, which contributes to the formation of memory CD8-T cell responses (332), was expressed in a larger percentage of CD8 T cells in both anti-PD-1 treatment groups compared to controls (Figure 5.6 H). These changes suggest that anti-PD-1 therapy could trigger effector phenotype and function in 9464D TILs.

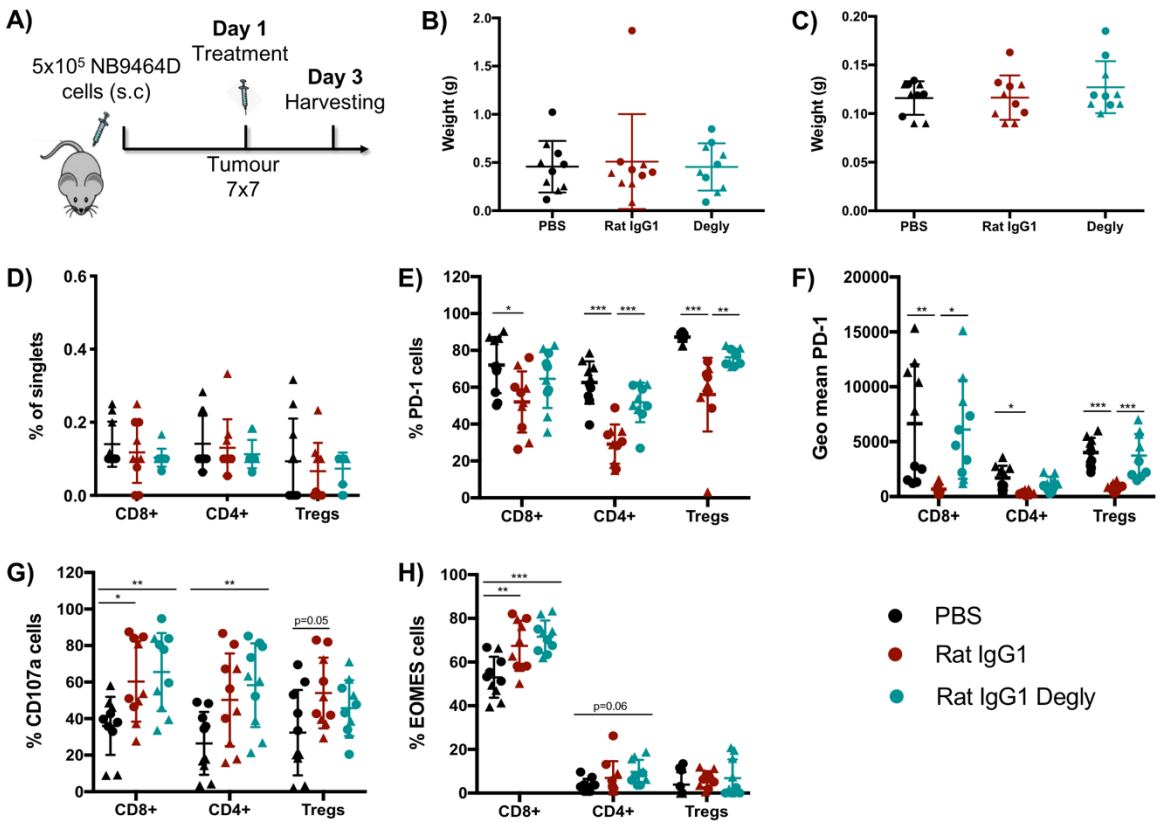

Figure 5.6 Phenotyping of TILs in 9464D tumours 3 days after therapy with anit-PD-1 rat IgG1 or degly.
A) C57BL/6 mice were subcutaneously inoculated with 5x10^5 9464D cells and tumour growth was monitored 3 times/week. When 9464D tumours reached 7x7 mm, mice were treated with 250 μg of rat IgG1 or degly anti-PD-1 mAbs. Tumours and spleens harvested after 3 days were processed and stained as detailed in sections 2.7.5 and 2.8, and acquired by flow cytometry. B-C) Tumour (B) and spleen (C) weights after harvest. D) Overall percentage of TILs. E-F) Percentage of positive (E) and MFI (F) of PD-1 in TILs. G-H) Percentage of CD107a (G) and EOMES (H) positive TILs. Experiment performed twice, N=5 mice per group and per experiment. Triangles represent values from the first replicate whilst circles correspond to the second one. Bars represent mean ± S.D, *p<0.05, **p<0.01, ***p<0.001 (One-way ANOVA).

Some markers were preferentially expressed on Tregs, and the level of expression did not change upon treatment with anti-PD-1 mAbs (see Appendix B, Figure 6.17 A-D, I-J). As expected due to its role in the maintenance of self-tolerance (19), expression of the IL-2 receptor α-chain CD25 was equivalently high in Tregs in all treatment groups (see Appendix B, Figure 6.17 C,D). Together with CD25, the co-stimulatory receptors 4-1BB and OX40 were also predominantly expressed on Tregs and almost absent in CD8 and CD4 effector T cells (see Appendix B, Figure 6.17 A,B, I,J), and did not change after anti-PD-1 therapy. Similarly, expression of the exhaustion markers Tim-3 and LAG-3 was not affected by anti-PD-1 mAbs. However, these markers were mainly present in CD8 T cells, with approximately 30% of these

expressing low levels of each receptor (see Appendix B, Figure 6.17 E-H). Likewise, no changes were noted in Ki67 expression (K), in the Th1-specific transcription factor T-bet (L) or the relative percentages of effector, naïve and central memory T cells, as determined by CD44 and CD62L surface expression (see Appendix B Figure 6.17 M-O).

In order to look at systemic responses, and compare these to the tumour-specific changes, an equivalent analysis of T-cell populations and phenotype was conducted in the spleens of 9464D-bearing mice. Following a similar gating strategy (see Appendix B, Figure 6.18), fewer differences across groups were observed in the spleen (see Appendix B, Figure 6.19), indicating that the majority of the changes were restricted to the tumour site. As such, the percentage of lymphocytes (Figure 5.7 A) remained constant across groups, and most of the activation and exhaustion markers had low or absent expression in the spleen (i.e LAG-3, Tim-3, EOMES, T-bet, 4-1BB) (see Appendix B, Figure 6.19). Nevertheless, a higher percentage of lymphocytes displayed an effector phenotype as characterised by CD44 expression in the degly mAb group (Figure 5.7 B), suggesting that this antibody induced systemic activation of T cells. In addition, there was a noticeable reduction of PD-1 on effector CD4 and Tregs following treatment with parental rat anti-PD-1, mirroring the results seen at the tumour site (Figure 5.7 C,D).

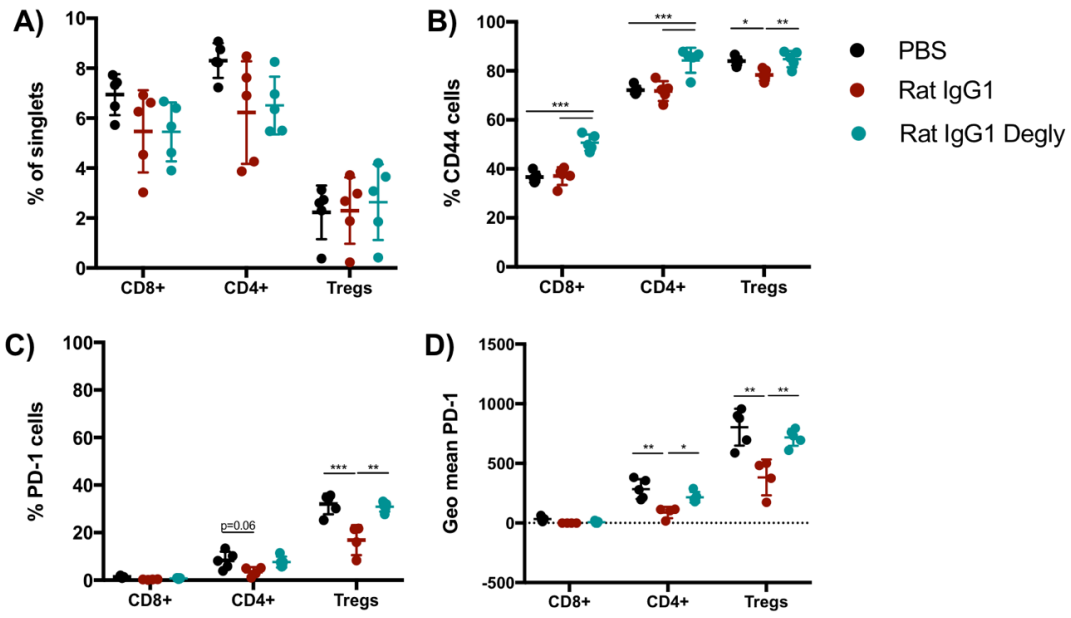

Figure 5.7 Phenotyping of T-cell populations in spleens of 9464D-bearing mice 3 days after therapy with anit-PD-1 rat IgG1 or degly.
A) Overall percentage of lymphocytes in spleen. B) Percentage of CD44 effector T cells. C-D) Percentage of PD-1 positive T cells (C) and MFI (D). Experiment performed once, N=5 mice per group. Bars represent mean ± S.D, *p<0.05, **p<0.01, ***p<0.001 (One-way ANOVA).

Next, the frequency and phenotype of myeloid cells following anti-PD-1 therapy was evaluated. For this, the previously described panel was utilised for the analysis of myeloid populations in the tumour (Figure 5.3) and spleen (see Appendix B, Figure 6.20) of 9464D tumour-bearing mice. Treatment with rat IgG1 or degly anti-PD-1 mAbs did not affect the overall percentage of myeloid subsets in the tumour site or at the spleen (Figure 5.8 A-D). Degly anti-PD-1 mAbs showed a trend towards increased PD-L1 expression in the majority of myeloid subsets in the TME (Figure 5.8 B,C), whilst both parental and degly mAbs increased the percentage of PD-L1+ macrophages at the spleen (E,F).

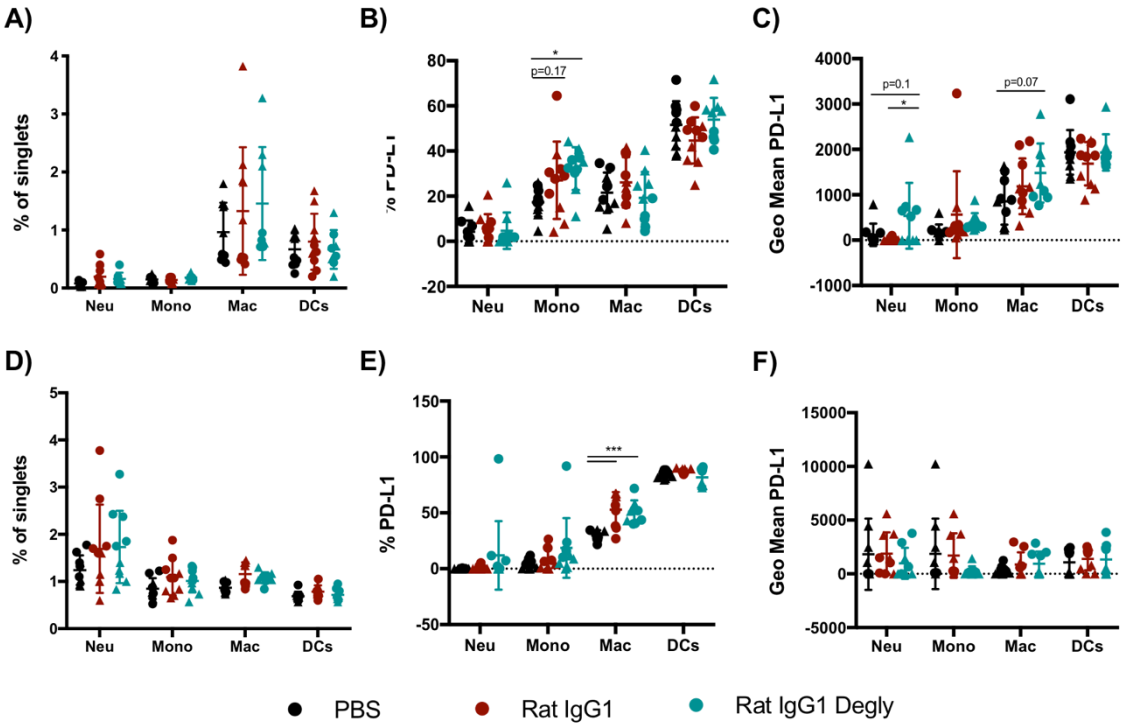

Figure 5.8 Myeloid populations in tumour and spleen of 9464D-bearing mice 3 days after therapy with anit-PD-1 rat IgG1 or degly.
A) Overall percentage of myeloid cells in tumour. B-C) Percentage of PD-L1 positive cells (B) and MFI (C) in tumour-infiltrating myeloid populations. D) Overall percentage of myeloid cells in spleen. E-F) Percentage of PD-L1 positive cells (E) and MFI (F) in spleens. Experiment performed twice, N=10 mice per group. Triangles represent values from the first replicate whilst circles correspond to the second one. Bars represent mean ± S.D, *p<0.05, ***p<0.001 (One-way ANOVA).

Overall, only minimal phenotypic differences were observed between parental rat IgG1 anti-PD-1 mAb and the degly variant, besides from the clear changes in PD-1 expression on TILs. In view of the treatment schedule followed, it is possible that a single dose of anti-PD-1 mAbs is not sufficient to sustain T-cell activation, thereby making it difficult to observe differences across treatment groups. Taking into consideration that myeloid modulation might likely occur secondary to T-cell

activation by anti-PD-1 mAbs, the lack of a clear effect on T cells might also explain the minimal myeloid changes. Therefore, these results highlight some potential changes in the 9464D TME following anti-PD-1 therapy, but differences across mAbs may become more evident with an alternative treatment schedule involving multiple doses over a longer period of time.

5.4 Effect of murine anti-PD-1 isotypes in 9464D model

5.4.1 Therapeutic effect in survival of 9464D model

Once it was established that the Fc region could influence the therapeutic and immunological effects of anti-PD-1 in NB, the Fc requirements were sought to be defined in more detail by using murine anti-PD-1 isotypes (mIgG1, mIgG2a and mIgG1-N297A), characterised in Chapter 3:. Notably, the use of rat mAbs in mouse models can lead to anti-rIgG responses, which may contribute to the faster clearance of mAbs and could limit the therapeutic efficacy of antibody therapy (334). This is of special importance when metronomic doses are used for prolonged periods of time. In addition, enzymatic deglycosylation of mAbs can reduce binding to FcγRs, but the degree of reduction is often influenced by IgG subclass (331). Therefore, utilising an engineered Fc-null variant and the two murine isotypes IgG1 and IgG2a, which bear low and high A/I ratio, respectively (112), offers a better system to assess effectiveness of anti-PD-1 mAbs in vivo.

To study the potential efficacy of murine anti-PD-1 isotypes as a monotherapy in 9464D tumours, mAbs were given either as a single dose (Figure 5.9 A) or on a weekly basis (Figure 5.10 A). An additional group was treated with two doses of degly anti-PD-1 mAb on days 1 and 4 as a comparison group, because previous work in the group suggested that this schedule had some therapeutic effect (329).

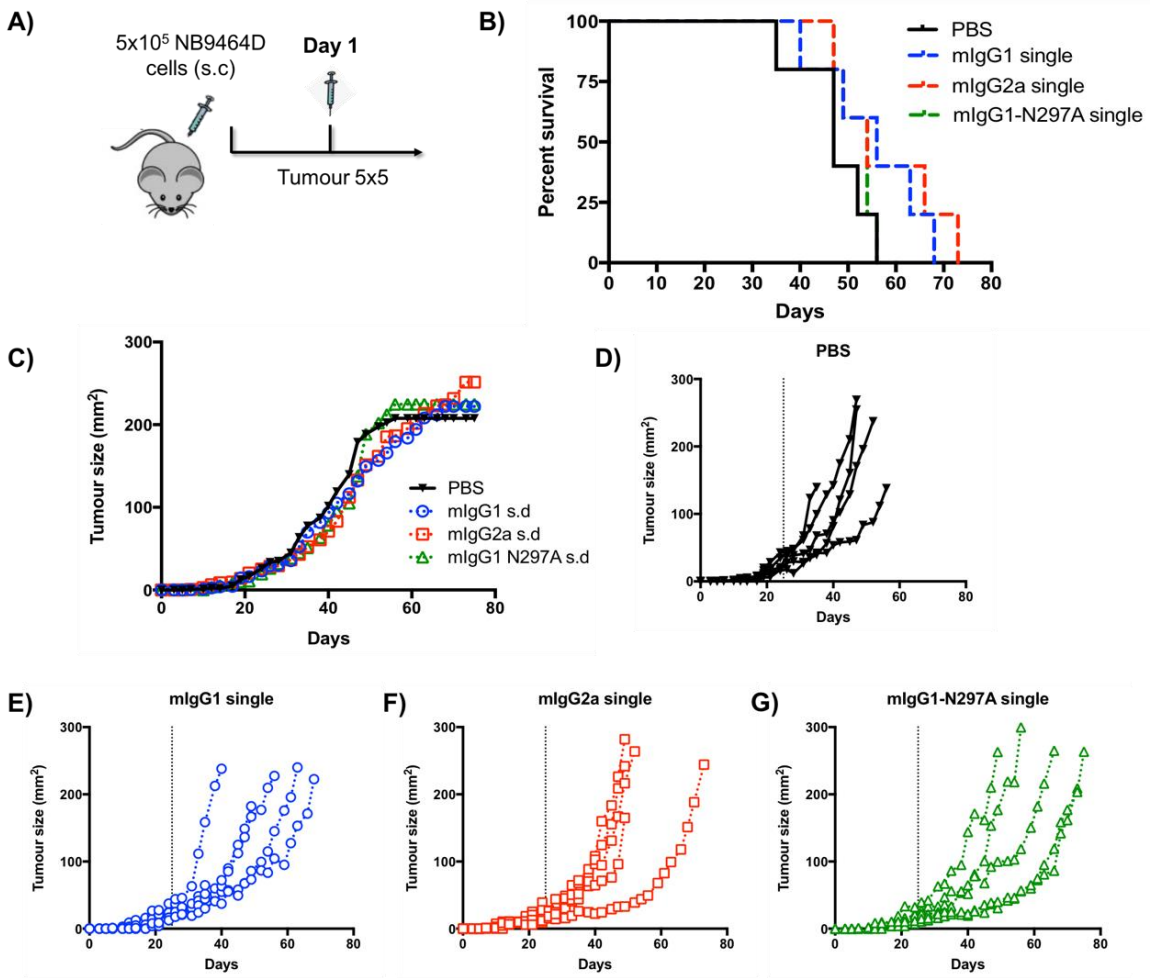

Figure 5.9 Monotherapy with anti-PD-1 mAbs in 9464D tumours: single doses. A) C57BL/6 mice were subcutaneously inoculated with 5x10^5 9464D cells and tumour growth was monitored 3 times/week. When tumours reached 5x5 mm, mice were treated Ip with PBS or a single dose (S.D) of 200 µg murine IgG1, IgG2a or IgG1-N297A anti-PD-1 mAbs. Animals were humanely culled when tumours reached 15x15 mm or if health was compromised. B) Kaplan-meier curves displaying the percentage of mice alive at each time point after tumour inoculation. C) Tumour growth curves showing the mean size per group. D-G) Individual tumour growth curves per group: PBS (D); mIgG1 (E); mIgG2a (F); and mIgG1-N297A (G). Experiment performed once, N=5 mice per group. Log-rank (Mantel-Cox) Test, n.s.

In regards to the anti-PD-1 mAb schedule, a single dose of murine mAbs did not provide any benefit in survival (Figure 5.9 B). Despite some spread in the individual tumour growth curves (Figure 5.9 D-G), no significant differences were observed in mean tumour size (C), indicating that a single dose of anti-PD-1 mAbs is not sufficient to alter therapeutic outcomes. Nevertheless, weekly dosage with anti-PD-1 mAbs elicited small but significant differences across isotypes (Figure 5.10). Despite not achieving statistical significance, 2 doses of degly mAb showed a trend towards decreased tumour size relative to controls (Figure 5.10 B-D), as anticipated. Amongst the murine mAbs, mIgG1 and the Fc engineered mIgG1-

N297A isotypes significantly increased survival compared to controls (Figure 5.10 B). These mAbs tended to decrease tumour size compared to controls at day 54 after tumour inoculation (C,D), albeit not statistically significant. However, a clear effect was observed with the individual growth curves, where 3/5 mice in each group displayed slower growth kinetics (Figure 5.10 F,H). In contrast, anti-PD-1 mIgG2a had no effect on survival or tumour growth (Figure 5.10 B-D). Although these effects were relatively modest, these results followed the same pattern to that observed in the responsive MC38 tumour model (Figure 4.13), further supporting the detrimental role of engaging activating FcγRs in anti-PD-1 therapy.

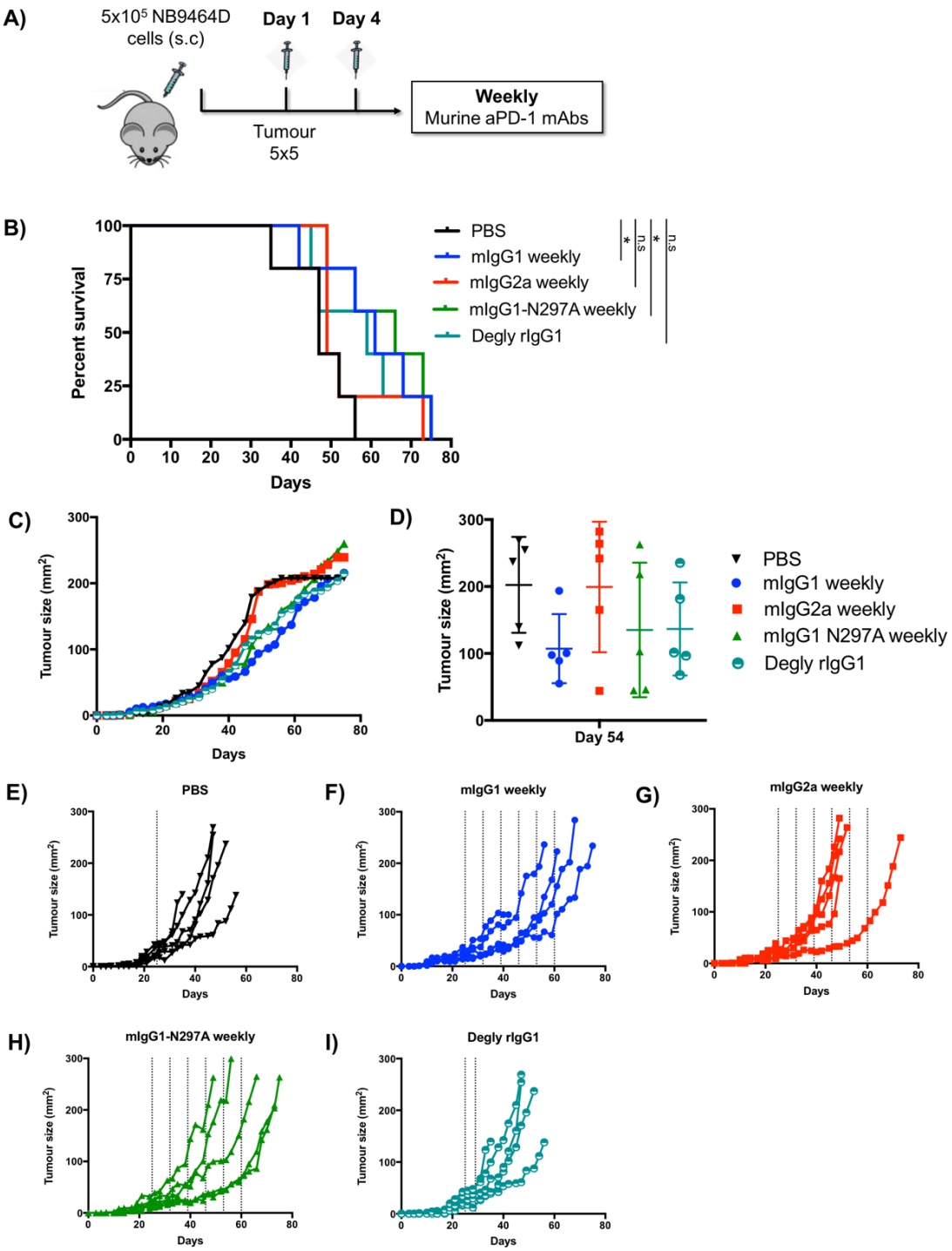

Figure 5.10 Monotherapy with anti-PD-1 mAbs in 9464D tumours: weekly schedule.
A) C57BL/6 mice were subcutaneously inoculated with 5x10^5 9464D cells and tumour growth was monitored 3 times/week. When tumours reached 5x5 mm, mice were treated Ip with PBS; two doses of 250 µg of degly anti-PD-1; or weekly dose of 200 µg of murine IgG1, IgG2a or IgG1-N297A isotypes. Animals were humanely culled when tumours reached 15x15 mm or if health was compromised. B) Kaplan-meier curves displaying the percentage of mice alive at each time point after tumour inoculation. C) Tumour growth curves showing the mean size per group. D) Tumour mean size on day 54 after tumour inoculation. E-I) Individual tumour growth curves per group: PBS (E); mIgG1 (F); mIgG2a (G); mIgG1-N297A (H); degly rat IgG1 (I). Experiment performed once, N=5 mice per group. Bars represent mean ± S.D. Log-rank (Mantel-Cox) Test, *p<0.05.

5.4.2 Immunophenotyping of 9464D-bearing mice after therapy with murine anti-PD-1 mAbs

As mentioned in section 5.3, repeated doses of anti-PD-1 mAbs might be required to induce prolonged immune activation and modulation of T cells and myeloid cells in 9464D tumour-bearing mice. Given the clear changes observed in the MC38 model (section 4.5), an equivalent treatment schedule was followed in the 9464D model with murine anti-PD-1 mAbs. In addition, this enabled the direct comparison of both models, providing an example of a responsive, highly immune-infiltrated tumour model such as MC38, with a less immune-infiltrated and responsive model such as 9464D.

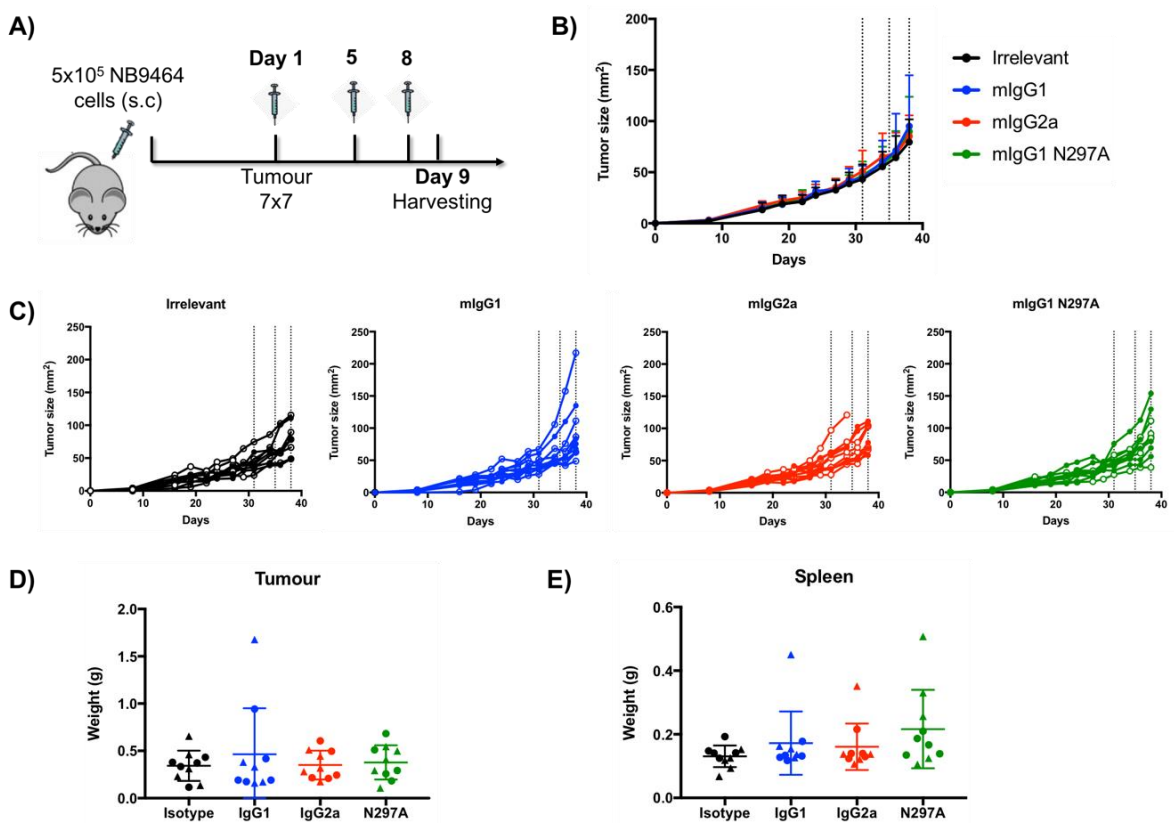

Figure 5.11 Immunophenotyping of 9464D tumours after anti-PD-1 therapy.
A) C57BL/6 mice were subcutaneously inoculated with 5x10^5 9464D cells. When tumours reached 7x7 mm, mice received 3 Ip doses of 200 µg of irrelevant mAbs (AT10 mIgG1, mIgG2a and mIgG1-N297A) or anti-PD-1 mIgG1, mIgG2a and mIgG1-N297A mAbs. Tumours and spleens were harvested 24h after the last dose and processed for flow cytometry (see sections 2.7.5 and 2.8). B-C) Tumour growth curves showing mean at each time point (B) or growth curves for each individual mice (C). Tumour size was calculated as length x width and growth was monitored 3 times/week using calipers. D-E) Tumour (D) and spleen (E) weights after harvesting. Experiment performed twice, N=10 mice per group. Triangles represent values from the first replicate whilst circles correspond to the second one. Bars represent mean ± S.D, (One-way ANOVA).

To this end, 9464D tumour-bearing mice were treated with three doses of anti-PD-1 mAbs when tumours reached 7x7 mm. Spleens and tumours were harvested one day after finishing therapy to study the effect of these mAbs (Figure 5.11 A); despite these treatments, tumour sizes were comparable across groups, resulting in equal tumour and spleen weights (Figure 5.11 B-E).

5.4.2.1 Lymphocyte populations

Similar to previous immunophenotyping studies, a gating strategy was followed to investigate the frequency and phenotype of lymphocytes at the tumour site (Figure 5.1) and at the spleen (see Appendix B, Figure 6.18) of 9464D tumour-bearing mice. Despite no changes in tumour weight, therapy with anti-PD-1 mIgG1-N297A significantly increased the percentage of CD45+ immune infiltrate in 9464D tumours compared to controls (Figure 5.12 A). As previously described, this infiltrate comprised only around 10% of the singlet gate, with effector T cells making up less than 10% of this immune infiltrate. Amongst CD45+ cells, mIgG1 and mIgG1-N297A mAbs showed a trend towards increased CD8 TILs compared to controls and the mIgG2a group (Figure 5.12 B), which was also noted when total cell counts were calculated (Figure 5.12 C) and likely reflected the proliferation of PD-1 positive CD8 TILs (Figure 5.12 D). Furthermore, mIgG1 also lead to a significant increase in CD4 effector T cells. No changes were seen in the relative percentage of Tregs and NK cells within 9464D tumours, nor in the CD8: Treg ratio (Figure 5.12 B,E) despite a clear trend towards decreased ratio by IgG2a compared to controls.

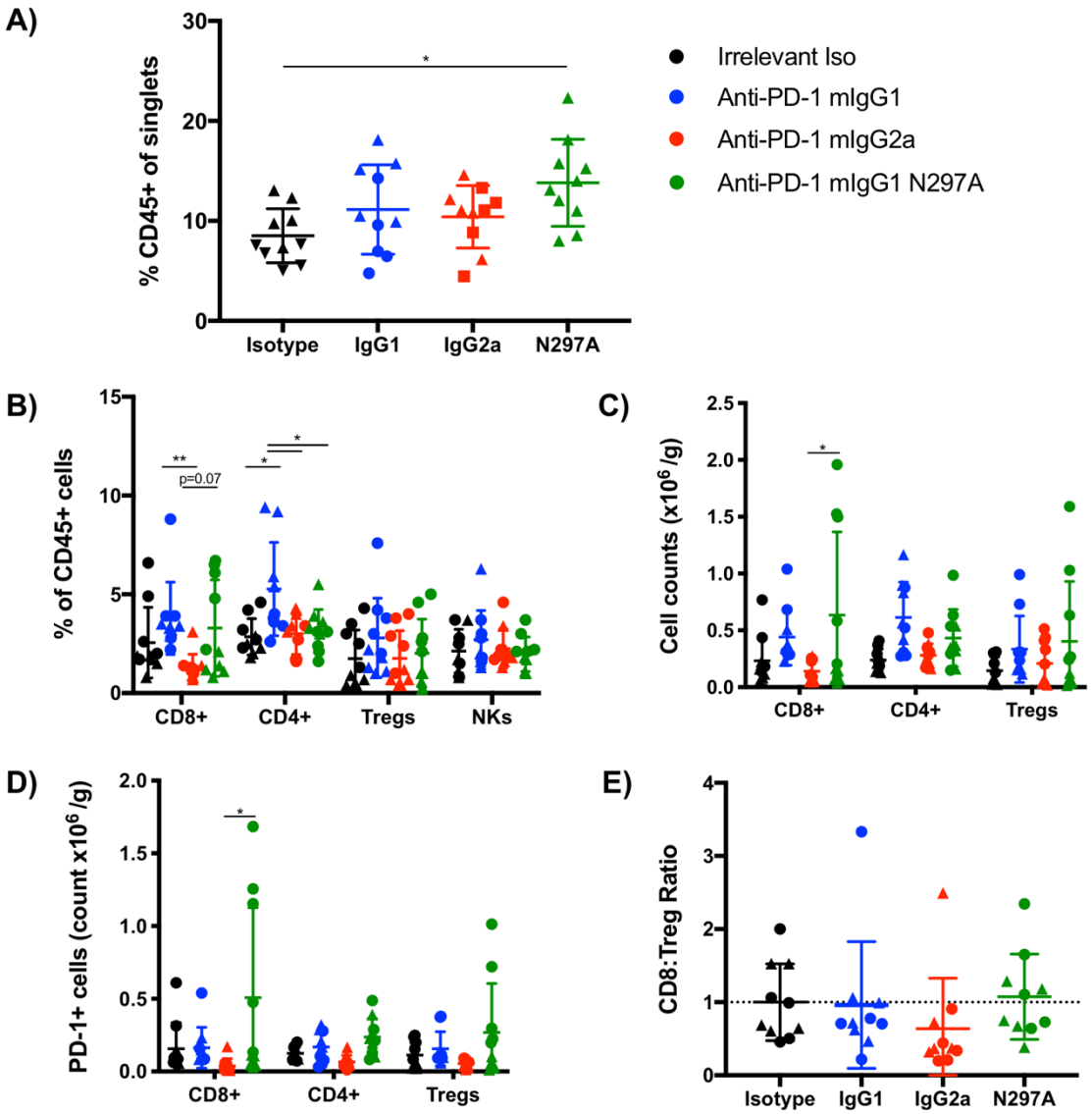

Figure 5.12 9464D tumour-infiltrating immune cells after 3 doses of murine anti-PD-1 mAbs: T-cell populations.
A) Percentage of CD45 immune infiltrates out of the singlet gate. B) Percentage of CD8+, CD4+ (FoxP3-), Tregs (CD4+ FoxP3+) and NK cells (CD4- CD8- NK1.1+) out of CD45+ immune infiltrating cells. C) Total counts of CD8+, CD4+ and Tregs per tumour weight (g^{-1}). C) Total cell counts of PD-1+ cells within CD8+, CD4+ and Treg subsets per tumour weight (g^{-1}). E) Individual CD8: Treg ratios per mouse were obtained by dividing the percentage of CD8 T cells by the percentage of Tregs. Next, individual ratios were normalised to the average ratio of control mice in each independent experiment. Experiment performed twice, N=8-9 mice per group. Triangles correspond to the first experiment whilst circles correspond to the second. Total cell counts were calculated from the percentage obtained in FACS of each cell population and the total number of cell suspension counts, and then divided by tumour weight.

Interestingly, PD-1 expression followed the same pattern observed in MC38 TILs following anti-PD-1 therapy (Figure 5.13 A,B). However, in this case, both effector CD8 and Tregs displayed the highest expression of PD-1. Minimal levels of PD-1 were noted on NK cells as seen in previous experiments. Notably, more than 60% of CD8 TILs in control mice expressed PD-1 at high levels, potentially reflecting their exhausted status (Figure 5.13 A,B) (153). This percentage remained high after treatment with mIgG1-N297A (A), and the relative expression of PD-1 per cell increased above controls (B). Treatment with this isotype also resulted in equivalent high levels of PD-1 on CD4 effectors, Tregs and NK cells compared to controls. On the other hand, mIgG1 and mIgG2a reduced PD-1 expression on TILs and NK cells (Figure 5.13 A,B). These differences indicate that murine anti-PD-1 mAbs elicit similar changes in PD-1 expression in both 9464D and MC38 models, despite their modest efficacy as a monotherapy in the former.

Further to the phenotype of TILs, the large majority of Tregs displayed an effector phenotype as characterised by CD44 expression, as well as approximately 70% of CD8 and CD4 T cells (Figure 5.13 C-E). Apart from a trend towards increased effector CD8 T cells by mIgG1-N297A (D), no changes were observed across treatment groups in the relative percentages of effector and central memory lymphocytes in the tumour.

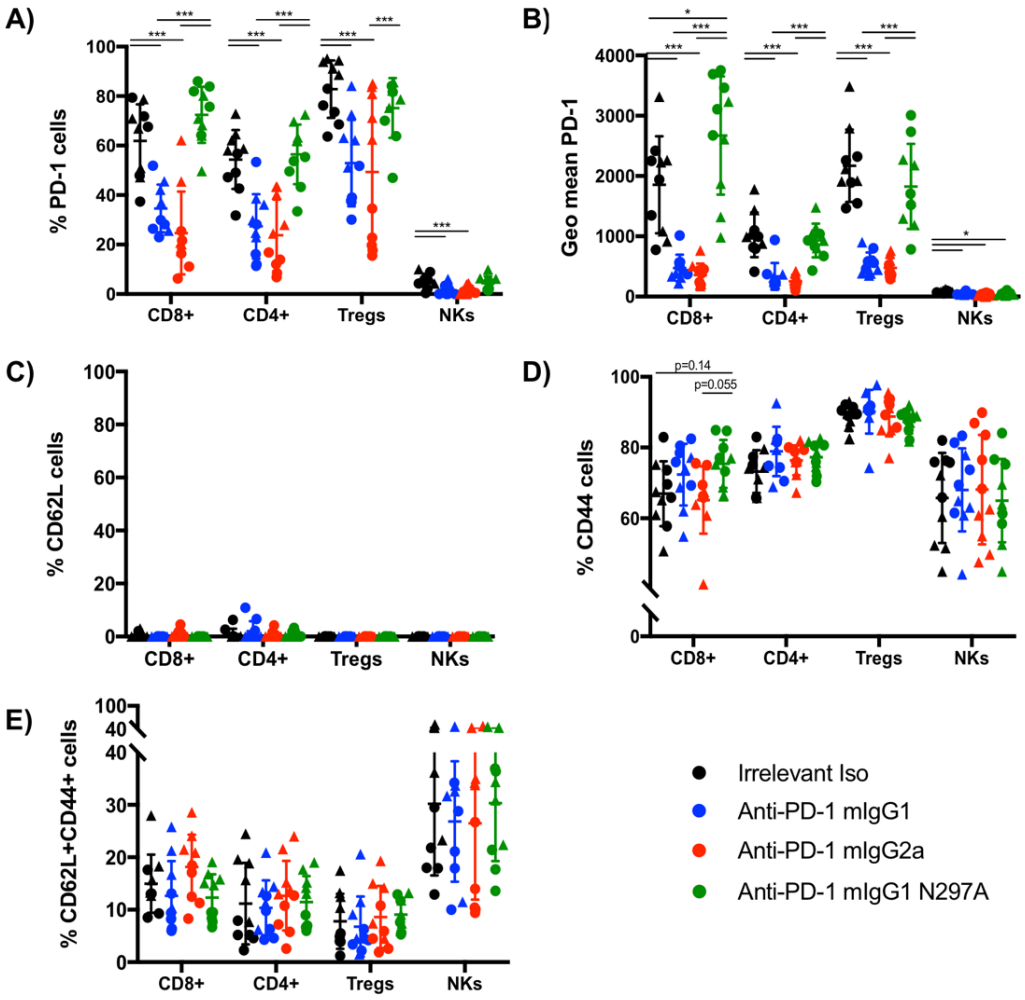

Figure 5.13 Phenotype of TILs in 9464D tumours after 3 doses of murine anti-PD-1 mAbs.
A-B) Expression of PD-1 in T-cell subsets and NK cells shown as percentage of positive cells (A) or as MFI (B). C-E) Percentage of naïve (C), effector (D) and central memory (E) lymphocytes in the tumour according to CD62L and CD44 staining. Experiment performed twice, N=10 mice per group. Triangles represent values from the first replicate whilst circles correspond to the second one. Bars represent mean ± S.D, *p<0.05, ***p<0.001 (One-way ANOVA).

In spleens of 94464D tumour-bearing mice, neither the percentages of lymphocytes or the CD8: Treg ratio was modified with anti-PD-1 therapy (Figure 5.14 A,B). However, mIgG1-N297A led to an overall increase in PD-1 expression on lymphocytes (Figure 5.14 C,D), suggestive of a systemic activation, which was also in agreement with the effect observed by degly rat anti-PD-1 mAb (Figure 5.7). In line with this up-regulation, the percentage of effector CD8 T cells also increased with mIgG1-N297A, together with a reduction in naïve CD4 T cells compared to controls (Figure 5.14 E,F).

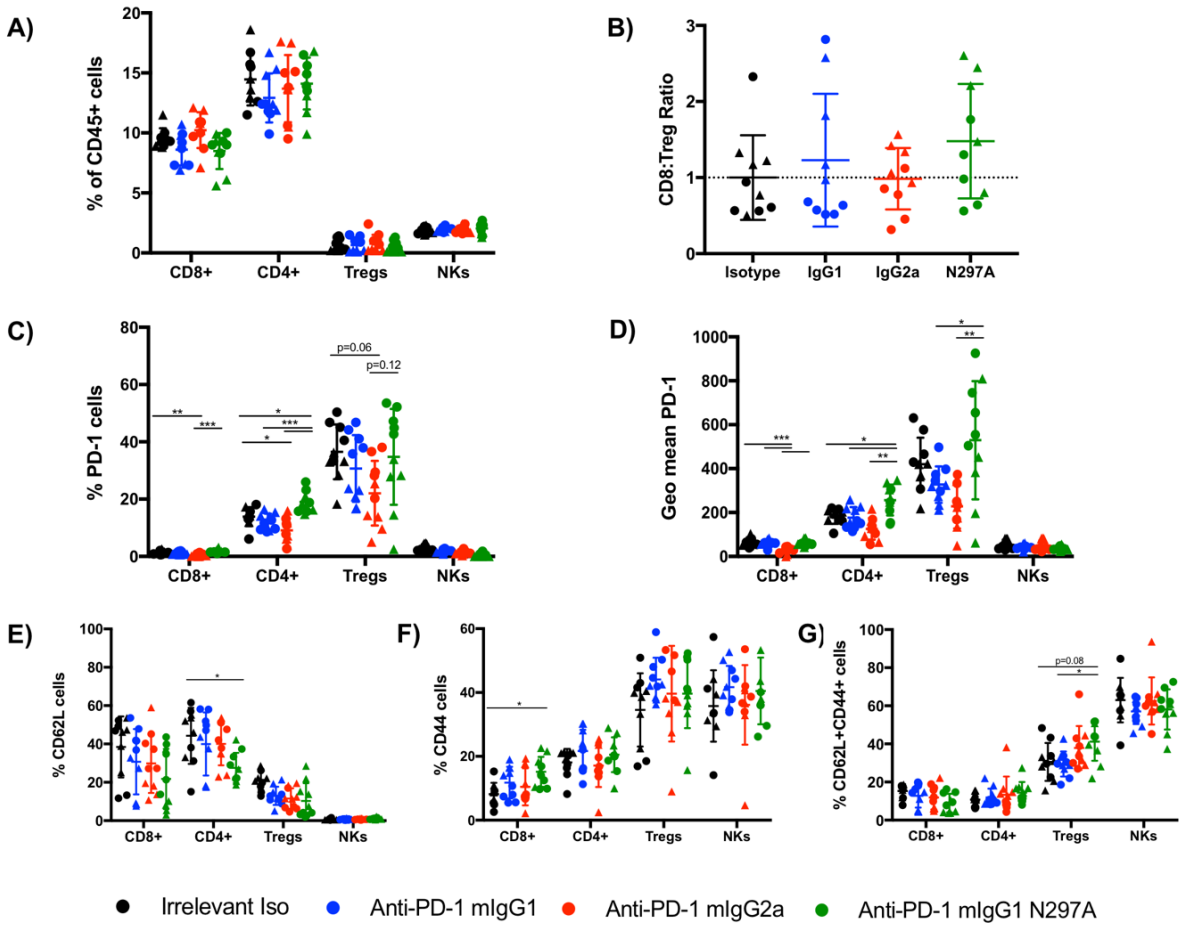

Figure 5.14 T-cell populations in spleens of 9464D-bearing mice after 3 doses of murine anti-PD-1 mAbs.
A) Percentage of CD8+, CD4+ (FoxP3-), Tregs (CD4+ FoxP3+) and NK cells (CD4- CD8- NK1.1+) out of CD45+ cells. B) Individual CD8: Treg ratios per mouse were obtained by dividing the percentage of CD8 T cells by the percentage of Tregs. Next, individual ratios were normalised to the average ratio of control mice in each independent experiment. C-D) Expression of PD-1 in lymphocytes shown as percentage of positive cells (C) or as MFI (D). E-G) Percentage of naïve (E), effector (E) and central memory (G) T cells according to CD62L and CD44 staining. Experiment performed twice, N=10 mice per group. Triangles represent values from the first replicate whilst circles correspond to the second one. Bars represent mean ± S.D, *p<0.05, **p<0.01, ***p<0.001 (One-way ANOVA).

5.4.2.2 Myeloid populations

The presence of tumour-infiltrating myeloid cells has been correlated with poor outcome in untreated NB patients (284), being found more abundantly in metastatic compared to localised tumours (335). Due to their potential role within the TME, a study of the frequency and phenotype of 9464D-infiltrating myeloid cells after murine anti-PD-1 mAbs was carried out following the same approach previously detailed in Figure 5.3 and Figure 6.20 (see Appendix B). Furthermore, owing to the important role of FcγRs in mAb therapy and their potentially negative

impact in anti-PD-1 therapy (104), a detailed study of FcγR expression in myeloid subsets was also included.

In 9464D tumours, CD11b+ myeloid infiltration accounted for approximately 10% of cells from the singlet gate in control mice (Figure 5.15 A). This percentage was increased by mIgG1-N297A, concordant with the observed increased CD45 immune infiltration (Figure 5.12 A). Only 30% of tumour-infiltrating CD11b+ cells expressed PD-L1 (Figure 5.15 B) both in control mice and after receiving anti-PD-1 therapy. Since PD-L1 can be up-regulated in myeloid cells under pro-inflammatory cues (Figure 3.10 C; (336)), the relatively low expression of PD-L1 could indicate that tumour-infiltrating myeloid cells are poorly activated in 9464D tumours. Moreover, PD-L1 levels remained unchanged in CD11b+ (Figure 5.12 C) and also tumour cells (D) across treatment groups after 3 doses of anti-PD-1 mAbs, suggesting that anti-PD-1 mAbs were unable to create a pro-inflammatory TME that could induce myeloid activation.

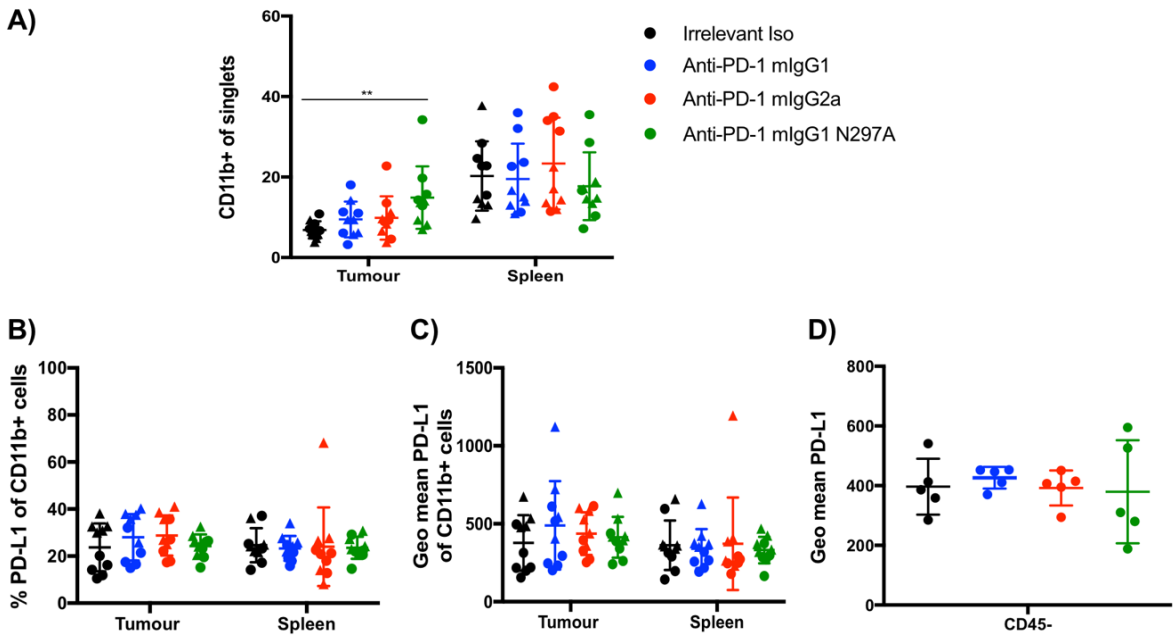

Figure 5.15 9464D tumour-infiltrating CD11b+ cells after 3 doses of murine anti-PD-1 mAbs: PD-L1 expression.
A) Percentage of CD11b myeloid infiltrates out of the singlet gate in tumour and spleen. B-C) Expression of PD-L1 in CD11b+ cells shown as percentage of positive cells (B) or as MFI (C) in tumour and spleen. D) Expression of PD-L1 on tumour cells (CD45 negative) shown as MFI. Experiment performed twice with N=10 (A-C) or once with N=5 mice per group (D). Triangles represent values from the first replicate whilst circles correspond to the second one. Bars represent mean ± S.D, **p<0.01 (One-way ANOVA).

In terms of FcγR expression, little changes were noted in specific receptors (Figure 5.16 A,B,D), with an overall decrease in all FcγR by mIgG1-N297A (D) compared to controls. However, this did not alter the ratio between activating and inhibitory FcγRs, as calculated by the A/I ratio (Figure 5.16 C), further indicating that anti-PD-1 mAbs did not lead to significant changes in myeloid phenotype.

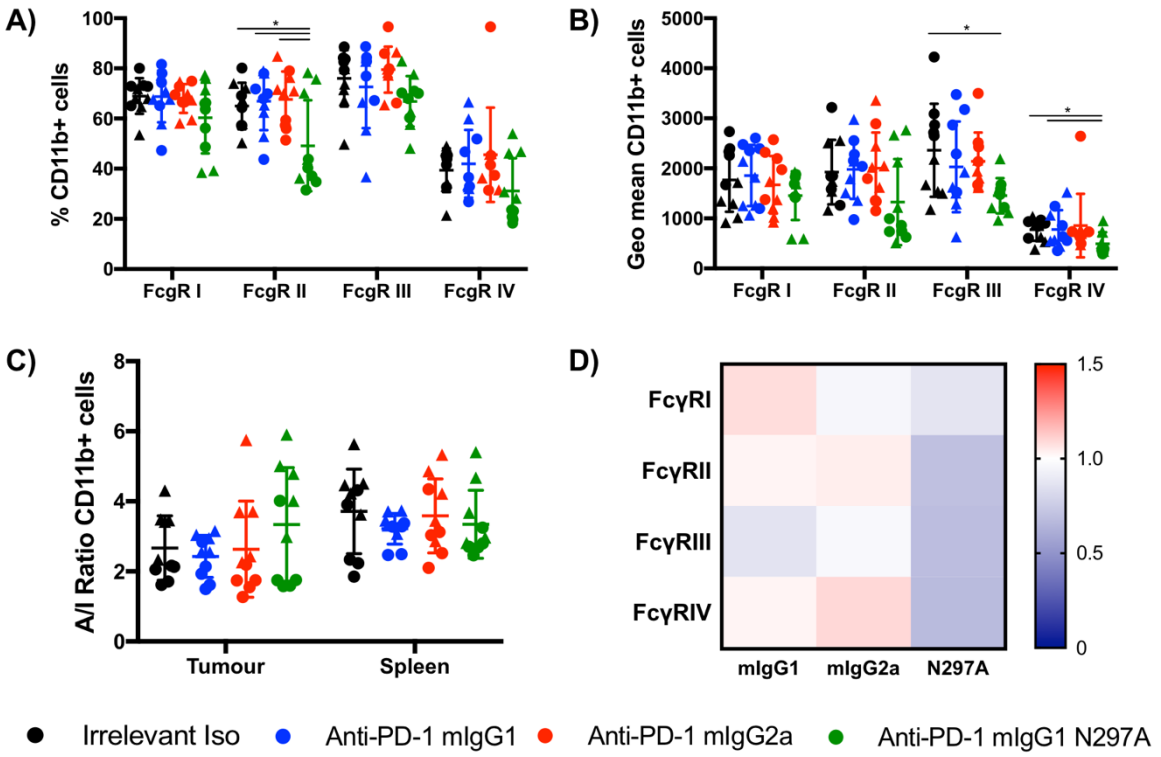

Figure 5.16 9464D tumour-infiltrating CD11b+ cells after 3 doses of murine anti-PD-1 mAbs: FcγR expression.
A-B) Expression of FcγRs (I, II, III and IV) on CD11b+ myeloid infiltrates in tumour shown as percentage of positive cells (A) or as MFI (B). C) Ratio of activating to inhibitory (A/I) FcγRs on CD11b+ cells in tumour and spleen. The ratio was calculated by the sum of FcγRI, III and IV MFIs divided by FcγRII MFI for each individual mouse. D) Heat map indicating relative expression of FcγRs in treatment groups compared to controls. Ratios were calculated by dividing individual MFI values of every given marker to the average MFI value in the control group. Colours represent the mean ratio of all mice in a given group for each marker, where 1= no change; 1<downregulation; and 1>up-regulation relative to controls. Experiment performed twice, N=10 mice per group. Triangles represent values from the first replicate whilst circles correspond to the second one. Bars represent mean ± S.D, *p<0.05, (One-way ANOVA).

In order to investigate in more detail the impact of murine anti-PD-1 isotypes in different populations of tumour-infiltrating myeloid cells, analysis of PD-L1 and FcγR expression was conducted in macrophages, DCs, monocytes and neutrophils. Amongst CD11b+ cells, macrophages and DCs accounted for the largest populations (Figure 5.17 A) and also expressed the highest levels of PD-L1 (B,C). However, anti-PD-1 mAbs did not lead to an increase in PD-L1 expression in any of the myeloid subsets (Figure 5.17 B,C).

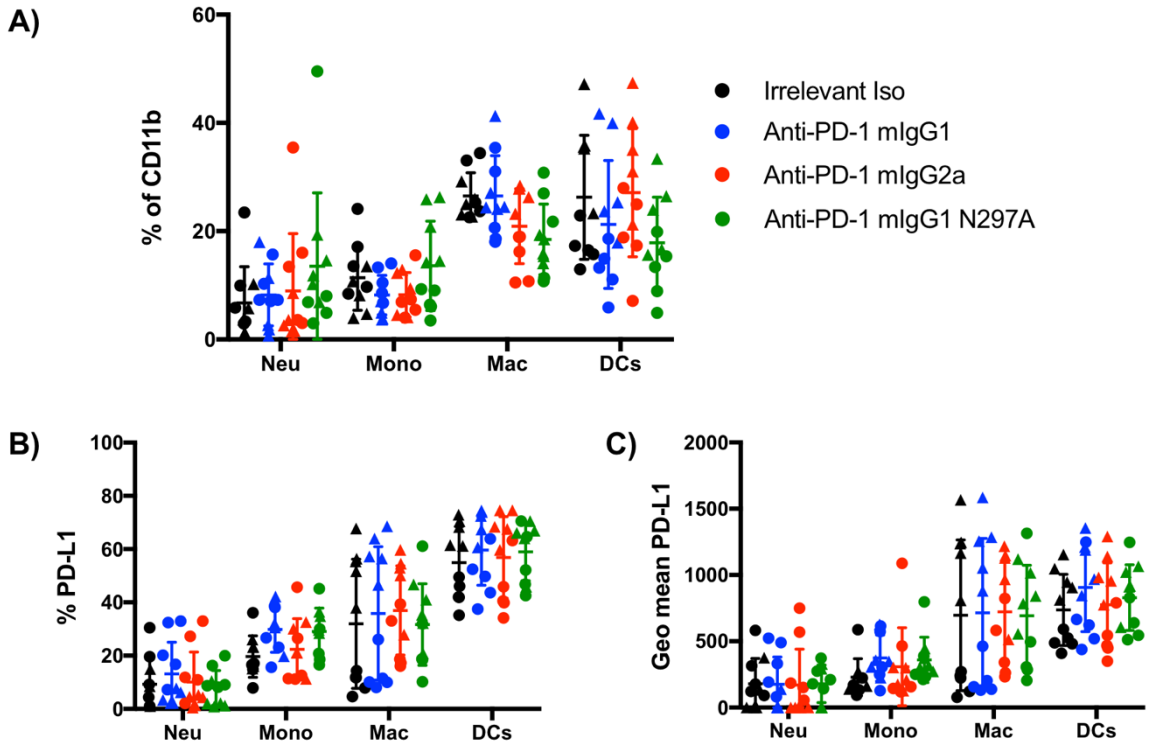

Figure 5.17 9464D tumour-infiltrating myeloid populations after 3 doses of murine anti-PD-1 mAbs: PD-L1 expression.
A) Percentage of tumour-infiltrating myeloid populations out of CD11b+ gate. B-C) Expression of PD-L1 on tumour-infiltrating myeloid populations shown as percentage of positive cells (B) or as MFI (C). Experiment performed twice, N=10 mice per group. Triangles represent values from the first replicate whilst circles correspond to the second one. Bars represent mean ± S.D, (One-way ANOVA).

Likewise, few changes were observed in FcγRs expression in the different subsets (Figure 5.18 A-D; Appendix B, Figure 6.22). Despite the lack of significant differences, mIgG1 and mIgG2a antibodies displayed similar expression patterns in relation to controls, with up-regulation of most FcγRs in neutrophils and monocytes but less in macrophages and DCs. On the contrary, therapy with mIgG1-N297A showed a trend towards decreased FcγR, particularly on macrophages and

DCs (Figure 5.18 E). In line with these, no significant differences were observed in myeloid cells in the spleen (see Appendix B, Figure 6.23, Figure 6.24).

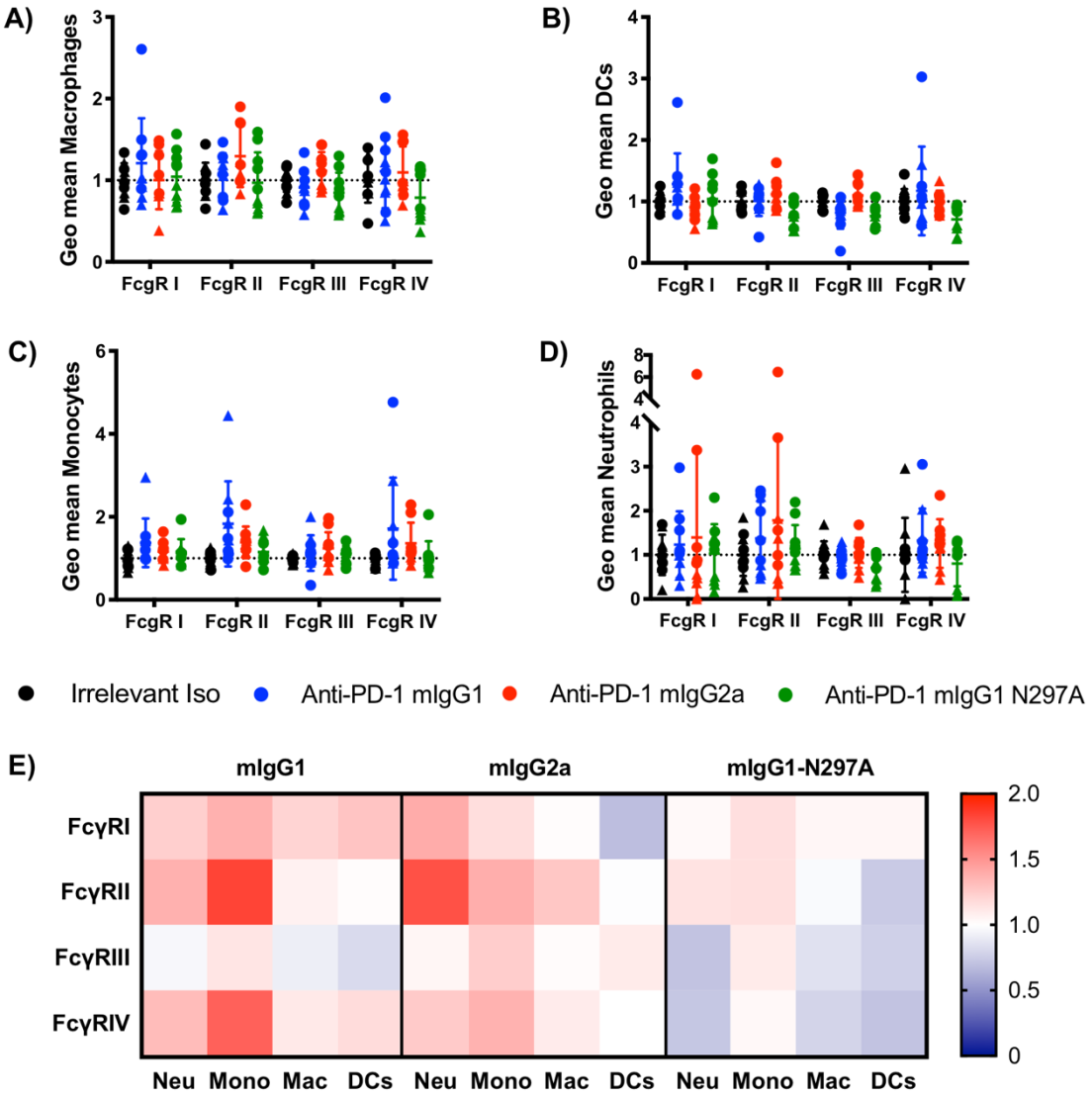

Figure 5.18 9464D tumour-infiltrating myeloid populations after 3 doses of murine anti-PD-1 mAbs: FcγR expression.
A-D) Expression of FcγRs (I, II, III and IV) on tumour-infiltrating macrophages (A), DCs (B), monocytes (C) and neutrophils (D) shown as MFI. Due to high variability between experimental replicates, results are shown as a fold-change of MFI relative to control mice within each experimental replicate. E) Heat map indicating relative expression of FcγRs in treatment groups compared to controls. Ratios were calculated by dividing individual MFI values of every given marker to the average MFI value in the control group. Colours represent the mean ratio of all mice in a given group for each marker, where 1= no change; 1<downregulation; and 1>up-regulation relative to controls. Experiment performed twice, N=10 mice per group. Triangles represent values from the first replicate whilst circles correspond to the second one. Bars represent mean ± S.D, *p<0.05, **p<0.01, (One-way ANOVA).

In general, 9464D TILs displayed a similar pattern to that in MC38 following PD-1 blockade in important aspects such as CD45 and CD8 infiltration, which were increased by IgG1 and particularly IgG1-N297A, together with PD-1 expression on CD8 TILs (increased by IgG1-N297A but decreased by IgG1 and IgG2a isotypes; Figure 5.19). However, these changes did not translate into tumour or myeloid modulation in 9464D, as opposed to MC38 tumours, which was particularly apparent for mIgG1-N297A. Although it cannot be defined whether the lack of myeloid modulation in 9464D is the cause of the limited improvement in survival, this fact is reflective of the therapeutic efficacy observed in MC38 but not in the 9464D model. Nevertheless, the increase in CD45 and CD8 TILs by mIgG1-N297A supports that this isotype might be eliciting a degree of immune activation, and offers the possibility that therapeutic outcomes could be improved when combined with other therapies.

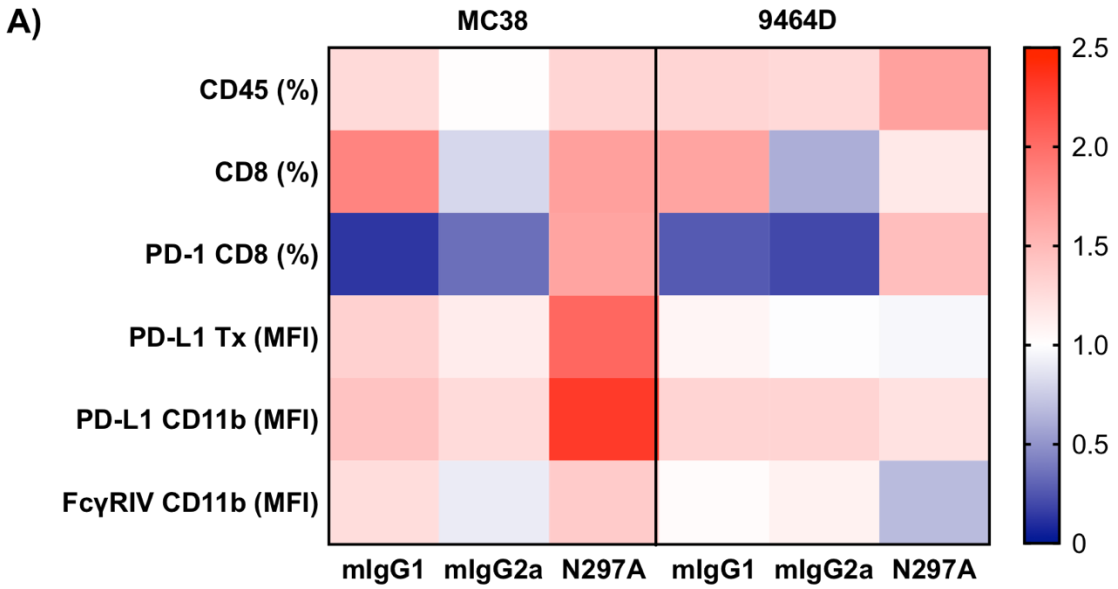

Figure 5.19 Summary figure of changes in MC38 and 9464D models after therapy with murine anti-PD-1 mAbs.
A) Summary heat map indicating relative expression of populations and markers in treatment groups compared to controls. Ratios were calculated by dividing individual MFI values/ percentages of every given marker to the average value in the control group. Colours represent the mean ratio of all mice in a given group for each marker, where 1= no change; 1<downregulation; and 1>up-regulation relative to controls. Markers include: percentage of CD45+, CD8+, CD8+PD-1+ cells; MFI of PD-L1 on tumour or CD11b+ cells; and MFI of FcγRIV on CD11b+ cells. Experiment performed twice, N=10 mice per group.

5.5 Combination therapy with anti-PD-1 mAbs in 9464D tumours

5.5.1 Combination of anti-PD-1 mAbs with anti-GD2 mAbs

The first immunotherapy to be approved by the FDA for the treatment of NB consists of mAbs targeting the TAA GD2 (189). These direct tumour-targeting mAbs are generally understood to rely on the recruitment and activation of FcγR-bearing immune cells to mediate efficient tumour cell killing (97). In particular, NK cells are the major immune cell postulated to trigger ADCC of NB cells following binding to anti-GD2 mAbs (266, 267, 270, 271). Importantly, an up-regulation of GD2 in 9464D tumour cells was observed as tumour progressed (Figure 5.2 E). Together with a concomitant down-regulation of MHC-I (see Figure 5.2 E), these traits may favour the susceptibility of cancer cells to NK cell-mediated killing. The subsequent release of pro-inflammatory mediators such as IFNs could induce MHC-I up-regulation on cancer cells and aid the recruitment of cytotoxic lymphocytes to the tumour bed (251, 337, 338). Hence, although NK cells displayed minimal PD-1 expression (Figure 5.2 B), anti-PD-1 mAbs could prevent T-cell exhaustion in this context, and synergise with anti-GD2 mAbs by supporting T-cell mediated killing of cancer cells (231). Taking this into account, the combination of anti-PD-1 mAbs with anti-GD2 mAbs was investigated in the 9464D model with the aim to improve the therapeutic outcomes seen with anti-PD-1 monotherapy.

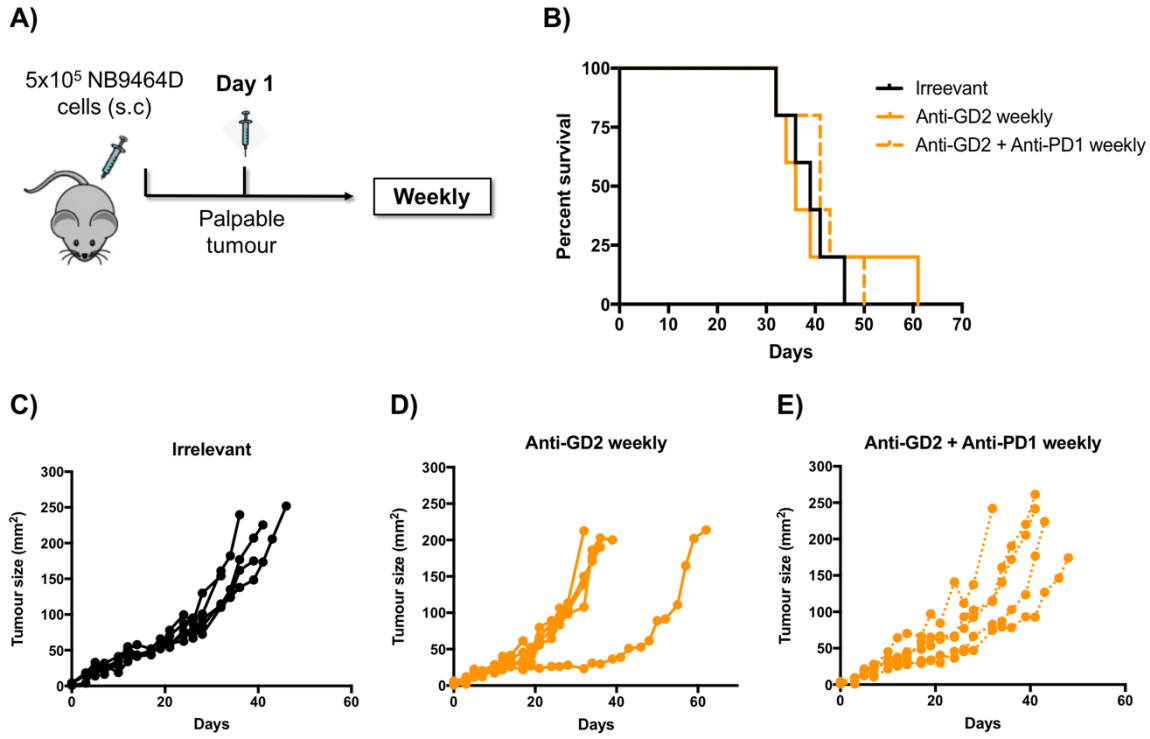

Figure 5.20 Combination of weekly anti-PD-1 mIgG1-N297A and anti-GD2 mAbs.
A) C57BL/6 mice were subcutaneously inoculated with 5x10^5 9464D cells and tumour growth was monitored 3 times/week. When tumours became palpable, mice were treated Ip with 200 µg of irrelevant mAbs; anti-GD2 mAbs; or anti-PD-1 mIgG1-N297A mAbs. Mice received the same weekly dose until tumours reached 15x15 mm, when they were humanely culled. B) Kaplan-meier curves displaying the percentage of mice alive at each time point after tumour inoculation. C-E) Individual tumour growth curves showing tumour size per group: irrelevant (C); anti-GD2 (D); or anti-GD2 plus anti-PD-1 mAbs (E). Experiment performed once, N=5 mice per group. Log-rank (Mantel-Cox) Test.

Based on the findings that mIgG1-N297A anti-PD-1 isotype had shown the most robust efficacy in both OT-I and MC38 settings (Figure 4.4, Figure 4.13), this isotype was selected to conduct initial combinatorial schedules in the 9464D model. Taking into consideration that anti-GD2 mAbs have been shown to be more effective in a setting of reduced tumour burden (189), therapy with anti-GD2 and mAbs was initiated when 9464D tumours became first palpable to maximise the potential benefit of these mAbs (Figure 5.20 A). Despite weekly administration of anti-GD2 mAbs, no benefit in survival was seen (Figure 5.20 B), with only one mouse displaying slower growth kinetics (D). Addition of anti-PD-1 mAb did not lead to improved survival (Figure 5.20 B,E). These results highlighted the need for alternative approaches that could further enhance anti-tumour immunity against 9464D tumours. Cyclophosphamide (CPM) is a chemotherapeutic agent commonly used in the treatment of human NB (232). Previous work in the group (329) as well

as other studies (339) propose that low doses of CPM can synergise with other forms of immunotherapy and improve therapeutic outcomes in NB models, whilst limiting the toxic side effects associated to higher doses of CPM. Furthermore, low-dose CPM was shown to synergise with anti-PD-1 mAbs and HPV16 E7 peptide vaccination to prolong survival in HPV16 E7+ lung carcinoma (Tc1) tumours (226). In light of these, CPM was considered as a valuable candidate to use in combination with anti-GD2 and anti-PD-1 mAbs in the treatment of 9464D tumours.

5.5.2 Effect of cyclophosphamide treatment

Cyclophosphamide is an alkylating agent that can cause direct cytotoxicity by the addition of alkyl groups to DNA, thereby inducing DNA damage and cell death (229). In humans and rodents, CPM requires in vivo conversion into 4-hydroxycyclophosphamide, its pharmacologically active form, which occurs in the liver. Thereafter, this metabolite can diffuse into the circulation and can be taken up by target cells, where it is converted into acrolein or phosphoramide mustard, which are the active products that facilitate cell death (229). Apart from its direct cytotoxicity, which is achieved at higher doses, CPM has been demonstrated to be an immune modulator at lower doses (340). In cancer, the main immunomodulatory effect of CPM is proposed to be mediated by the depletion of Tregs or attenuation of their function (340, 341). The greater susceptibility of Tregs to CPM is considered to be linked to their reduced capacity to detoxify CPM active metabolites due to lower ATP levels, and an intrinsic defect in DNA repair pathways compared to effector T-cell populations (229). Importantly, reduced number of tumour-infiltrating Tregs and high CD8: Treg ratio has been shown to correlate with better prognosis in several tumour types (23). Thus, the effect of CPM on Tregs may be of particular interest in the treatment of 9464D tumours, which present a relatively low CD8: Treg ratio (see Appendix B, Figure 6.21 A) compared to the immunotherapy-sensitive MC38 model (see Appendix A, Figure 6.10 A).

To elucidate if metronomic doses of CPM could have a therapeutic effect in 9464D tumours, a dose titration was performed. In humans, immune modulation by CPM is achieved at a dose of <8 mg/kg, whilst the equivalent dose in mice is thought to be <100 mg/kg (229). Therefore, doses up to 100 mg/kg were tested as single or weekly schedules. From previous observations in the group (329), single doses of 20 and 40 mg/kg were not anticipated to induce any survival benefit and so only a weekly schedule was investigated here. In addition, the higher doses of 80 and 100 mg/kg were administered as a single dose or in a weekly schedule (Figure 5.21).

Results showed that neither of the lower doses (20 and 40 mg/kg) impacted tumour growth, despite being given weekly (Figure 5.21 B,D,E). Likewise, a single dose of 80 and 100 mg/kg was not sufficient to induce a therapeutic effect (Figure 5.21 F,H); in fact, 3 out of 4 mice treated with 80 mg/kg reached humane end-point due to compromised health shortly after therapy. This effect could be caused by a rebound of Tregs proliferation and function, as the efficacy of metronomic CPM has been shown to be limited to a transient Treg depletion (341). Whilst a weekly dose of 100 mg/kg proved to be very efficacious at delaying and even stopping tumour growth, metronomic doses of 80 mg/kg CPM appeared to improve survival without fully inhibiting tumour growth (Figure 5.21 I-G). Despite the small number of mice in this group, this dose and schedule appeared to lengthen the therapeutic window, providing an opportunity for combination with anti-PD-1 and anti-GD2 mAbs.

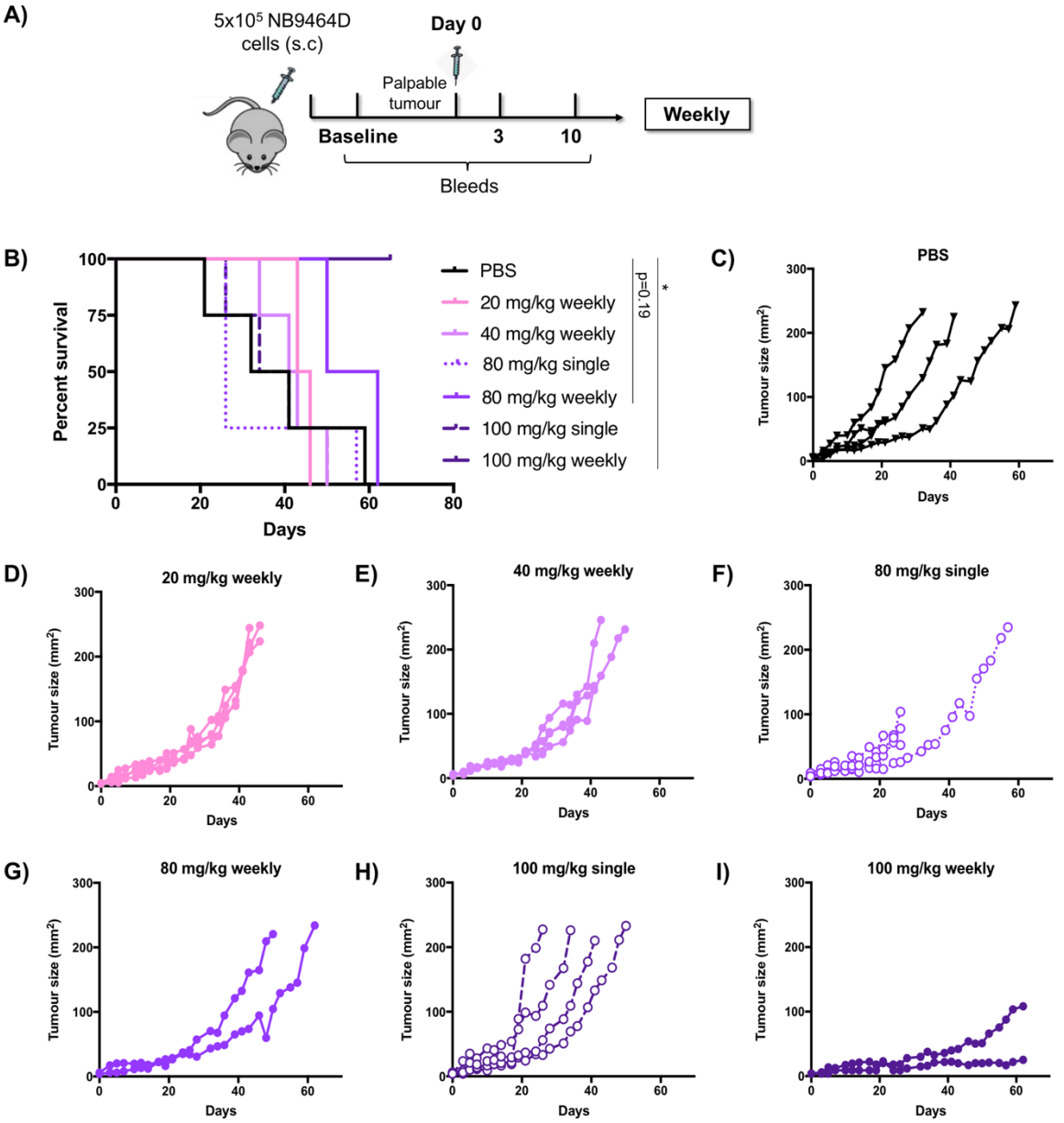

Figure 5.21 Monotherapy with cyclophosphamide: dose titration.
A) C57BL/6 mice were subcutaneously inoculated with 5x10^5 9464D cells and tumour growth was monitored 3 times/week. When tumours became palpable, mice were treated Ip with the appropriate dose of cyclophosphamide as a single dose or weekly; or with a single dose of PBS. Blood was withdrawn at baseline, day 3 and day 10 following therapy. Mice were humanely culled when tumours reached 15x15 mm or if health was compromised. B) Kaplan-meier curves displaying the percentage of mice alive at each time point after tumour inoculation. C-I) Individual tumour growth curves showing tumour size per group: PBS (C); 20 mg/kg CPM weekly (D); 40 mg/kg CPM weekly (E); 80 mg/kg CPM single dose (F); 80 mg/kg CPM weekly (G); 100 mg/kg CPM single dose (H); 100 mg/kg CPM weekly (I). Experiment performed once, N=2-4 mice per group. Log-rank (Mantel-Cox) Test, *p<0.05.

In mice, doses of CPM that are considered high (200 mg/kg) can induce general lymphodepletion in blood and peripheral organs (342). In view of this, serial bleeds were also performed to confirm that the chosen doses of CPM had no lymphodepleting effects on circulating lymphocytes (Figure 5.21 A). Bleeds were carried out at baseline and 3 or 10 days after CPM treatment to monitor total blood counts, as well as CD8 and CD4 counts (Figure 5.22). Overall, blood counts remained constant before and after therapy across CPM doses (Figure 5.23 A). Although a modest decrease was observed with the highest dose of 100 mg/kg, this did not reach statistical significance (A-B) likely due to the small numbers of mice.

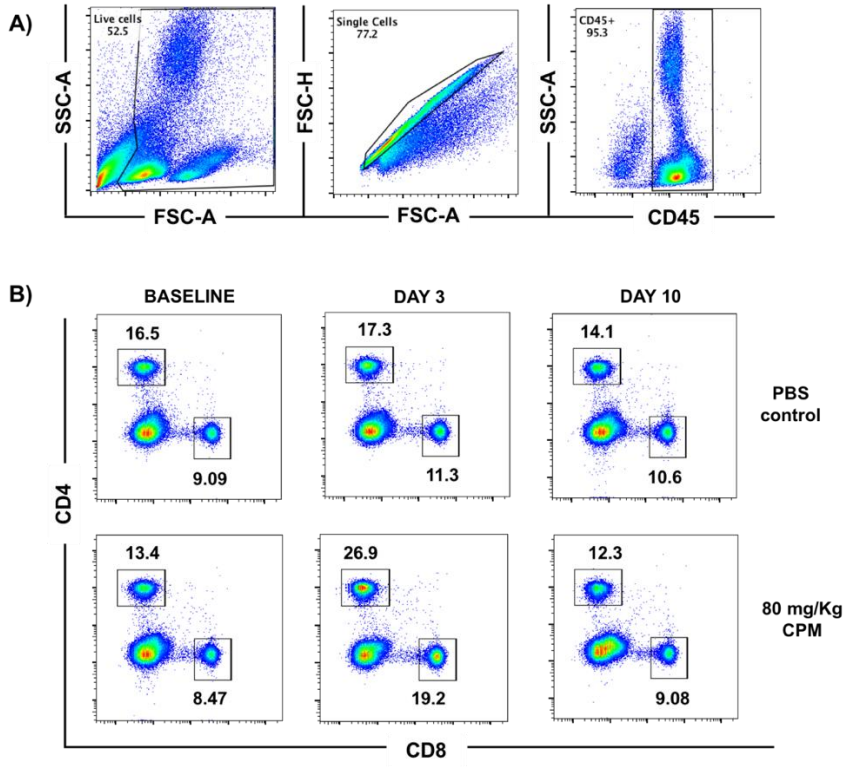

Figure 5.22 Gating strategy: blood counts.
Following tumour inoculation, mice were bled at baseline (before therapy), three and 10 days after therapy. Typically, 20 µl of blood were stained for 20 minutes at room temperature on the dark. A) Live and single were gated according to FSC-SSC. Circulating immune cells were gated according to their expression of CD45. B) Percentage of CD4+ and CD8+ T cells was calculated per mouse and per treatment group.

CD8 and CD4 blood counts displayed a similar trend to total counts (Figure 5.23 C-D), with no clear change compared to controls. In spite of this, percentages of CD8 and CD4 T cells increased at day 3 after the highest doses of CPM (E-F), as exemplified in Figure 5.22 B. Considering that absolute CD8 and CD4 counts remained stable (C-D), this suggests that higher doses of CPM can deplete another

immune population within the CD45+ gate, thus leading to an increase in relative percentage of lymphocytes but not overall counts. This could be caused by a depletion of B cells cells, which in another study were seen to decrease in spleens and lymph nodes after a single dose of 100 mg/kg CPM. Nevertheless, this effect was transient and percentages recovered by day 10 after therapy (Figure 5.23 E-F), similar to previous reports (341). Overall, whilst the highest dose of CPM (100 mg/kg) may lead to decreased blood counts, 80 mg/kg only displayed a transient deletion of circulating immune cells, but without a significantly diminished blood count.

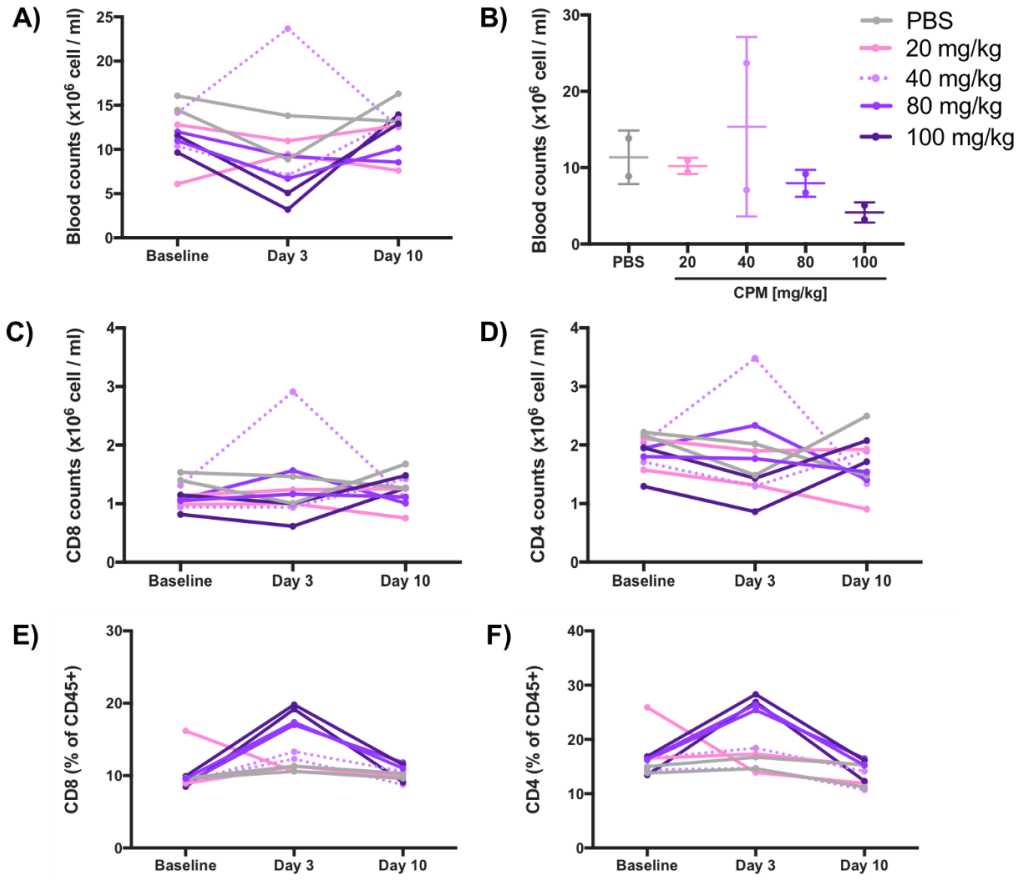

Figure 5.23 Blood counts after single doses of cyclophosphamide.
After blood withdrawal, total volume was measured using a calibrated pipette. A) To calculate total blood counts, the volume of heparin (5 µl) was subtracted to the total volume measured with the pipette. The subtracted volume was divided by the total volume to obtain the dilution factor specific for each sample, which was then multiplied by the number of counts obtained from the cell counter to obtain the total number of cells per ml of blood. B) Total blood counts on day 3. No statistical differences were reached amongst groups (One-way ANOVA). C-D) The percentage of CD8 and CD4 T cells obtained in flow cytometry was used to calculate the total counts of CD8 (C) and CD4 (D) T cells per ml of blood. E-F) Percentage of CD8 and CD4 T cells out of CD45+ gate. N=2 mice per group.

As mentioned previously, the main mechanism by which low doses of CPM aid to the generation of anti-tumour responses is through the depletion of intratumoural Tregs (340, 341). To confirm that a dose of 80 mg/kg CPM has an immunomodulatory effect on Tregs in 9464D-bearing mice, tumours and spleens were harvested 3 days after a single dose of CPM. In addition, to corroborate the transient effect of CPM, a second group of control and treated mice was harvested at day 10 after therapy.

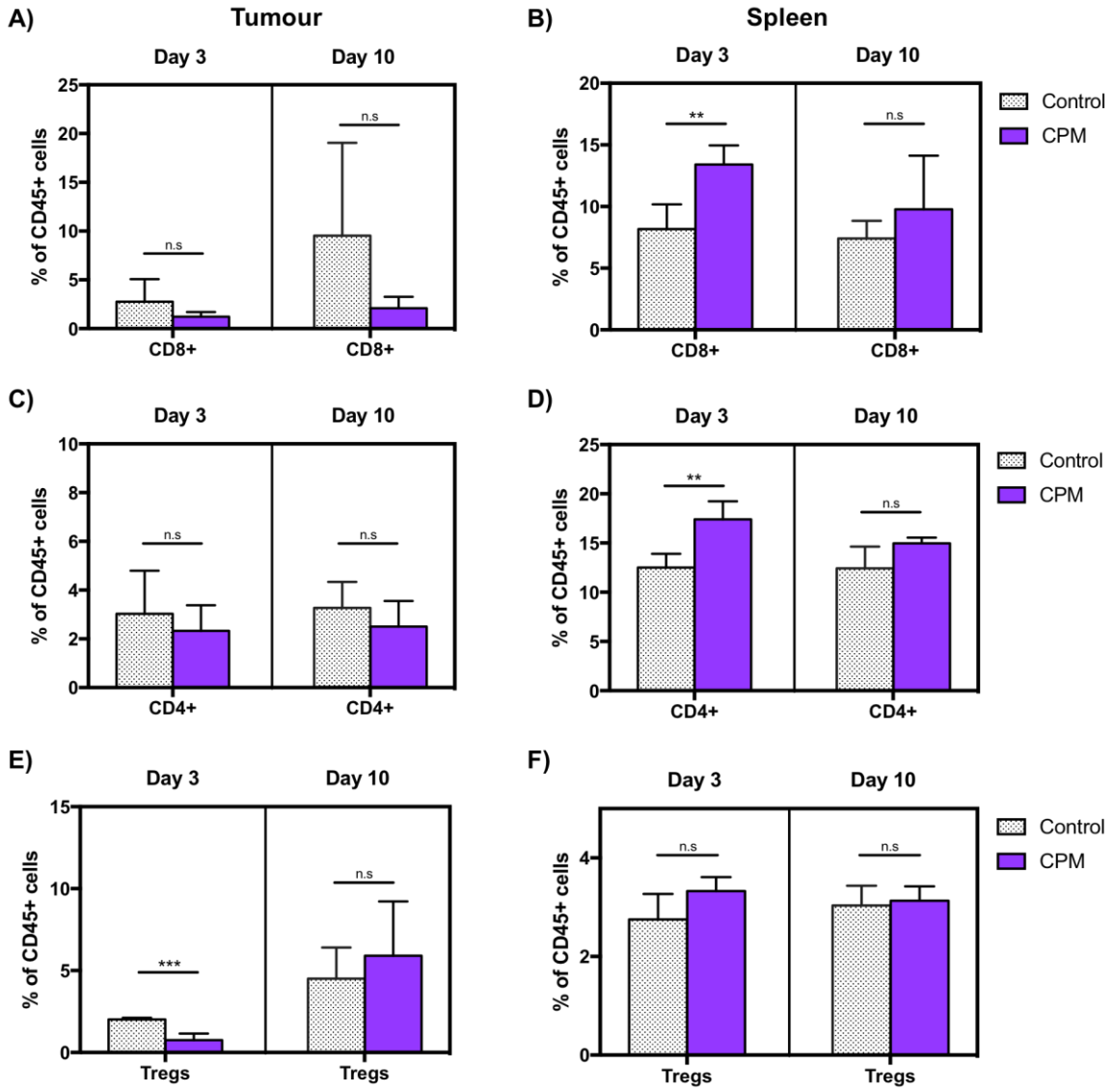

Figure 5.24 Lymphocyte populations following treatment with 80 mg/kg CPM. C57BL/6 mice were subcutaneously inoculated with $5x10^5$ 9464D cells. When tumours reached 7x7 mm, mice received one Ip with PBS or 80 mg/kg CPM. Tumours and spleens were harvested 3 or 10 days after treatment and processed for flow cytometry (see sections 2.7.5 and 2.8). Percentages of cells were calculated out of CD45+ cells. A-B) Percentage of CD8+ in tumour (A) and spleen (B). C-D) Percentage of CD4+ (FoxP3-) in tumour (C) and spleen (D). E-F) Percentage of Tregs (CD4+ FoxP3+) in tumour (E) and spleen (F). Experiment performed once, N=3-4 mice per group. Bars represent mean ± S.D, **p<0.01, ***p<0.001 (Unpaired Student T-Test).

At the tumour, CD8 or CD4 effector T cells were not significantly affected by CPM at either time-point, despite displaying a trend towards decreased percentages (Figure 5.24 A,C). On day 3, the percentage of both CD8 and CD4 T cell populations at the spleen increased compared to control mice (B,D), which paralleled the increase in relative percentages of these T-cell subsets observed in blood (Figure 5.23 E,F). As noted in the blood, this effect was transient and percentages stabilised by day 10 after CPM (Figure 5.24 B,D). On the contrary, there was a selective depletion of intratumoural Tregs at day 3 compared to controls (Figure 5.24 E). Although other reports have shown that 80 mg/kg CPM could also lead to Treg depletion in secondary lymphoid organs such as the spleen (341), the percentage of splenic Tregs in 9464D-bearing mice was not affected (Figure 5.24 F). Nevertheless, Treg levels were recovered 10 days post CPM, consistent with previous studies (341). In fact, there was a trend towards increased Treg percentages at day 10; this would argue in favour of the hypothesis that a rebound on Treg numbers and function following CPM-mediated depletion could promote tumour progression and compromise the health of mice, as observed in the survival experiment (Figure 5.21 F,H).

Taken together, these results suggest that selective intratumoural Treg depletion by 80 mg/kg CPM might be driving the delay in tumour growth observed in mice treated with a weekly schedule. In view of the therapeutic window achieved by weekly treatment with 80 mg/kg CPM and its reduced toxicity, this schedule was chosen to be tested in different combinatorial regimens to treat 9464D tumours.

5.5.3 Triple combination with anti-PD-1 mAbs, anti-GD2 mAbs and cyclophosphamide

With the aim of maximising anti-tumour responses against 9464D tumours, an alternative therapeutic schedule was tested, utilising a triple combination of CPM, anti-GD2 and anti-PD-1 mAbs. In more aggressive preclinical models of NB, anti-GD2 mAbs showed profound therapeutic activity when given in repeated doses at an early stage (231). This might indicate that multiple doses of these mAbs are required at earlier time points of the treatment schedule. Moreover, phenotypic changes in 9464D TILs were also observed following three doses of anti-PD-1 mAbs (Figure 5.12, Figure 5.13), Hence, to assess an effect on survival, three doses of both anti-PD-1 and anti-GD2 were administered at the start of the therapeutic schedule, following a similar timeline to that in the MC38 model. With regard to CPM, other studies (341) described that deletion of Tregs occurred as early as 24

hours after treatment, whilst complete recovery was evidenced by day 10 post CPM, similar to the current findings in this report (Figure 5.24). In light of these, the three doses of mAbs were administered within this therapeutic window to maximise NK and T-cell activation in the absence of suppressive Tregs (Figure 5.27 A). Aside from a treatment group that received a single administration of the full therapeutic dosage (Triple combo single), all other groups were treated weekly following the initial regimen. During these weekly doses, CPM was given three days prior to any therapeutic mAbs.

As shown in Figure 5.25, several therapeutic approaches appeared to delay tumour growth compared to controls. This was particularly marked in two mice treated with weekly anti-GD2 mAbs in combination with CPM (Figure 5.25 F) that showed stable disease for over 50 days. With respect to single arm groups, CPM displayed the biggest effect in decreasing tumour growth (Figure 5.25 A,E), followed by anti-GD2 mAbs, which showed a clear trend towards delaying tumour growth (Figure 5.25 A,C). In contrast, anti-PD-1 mAbs had no effect as a monotherapy (Figure 5.25 A,D). Despite not being statistically significant, monotherapy with anti-GD2 mAbs showed a trend towards decreased tumour volume compared to controls at early time points (Figure 5.26 A). Interestingly, dual therapy with anti-GD2 and anti-PD-1 mAbs appeared to be detrimental compared to anti-GD2 mAbs on their own, with 3 out of 4 mice showing rapid tumour progression (Figure 5.25 A). Nevertheless, neither monotherapy with anti-GD2, anti-PD-1 or dual therapy affected survival (Figure 5.27 B-D).

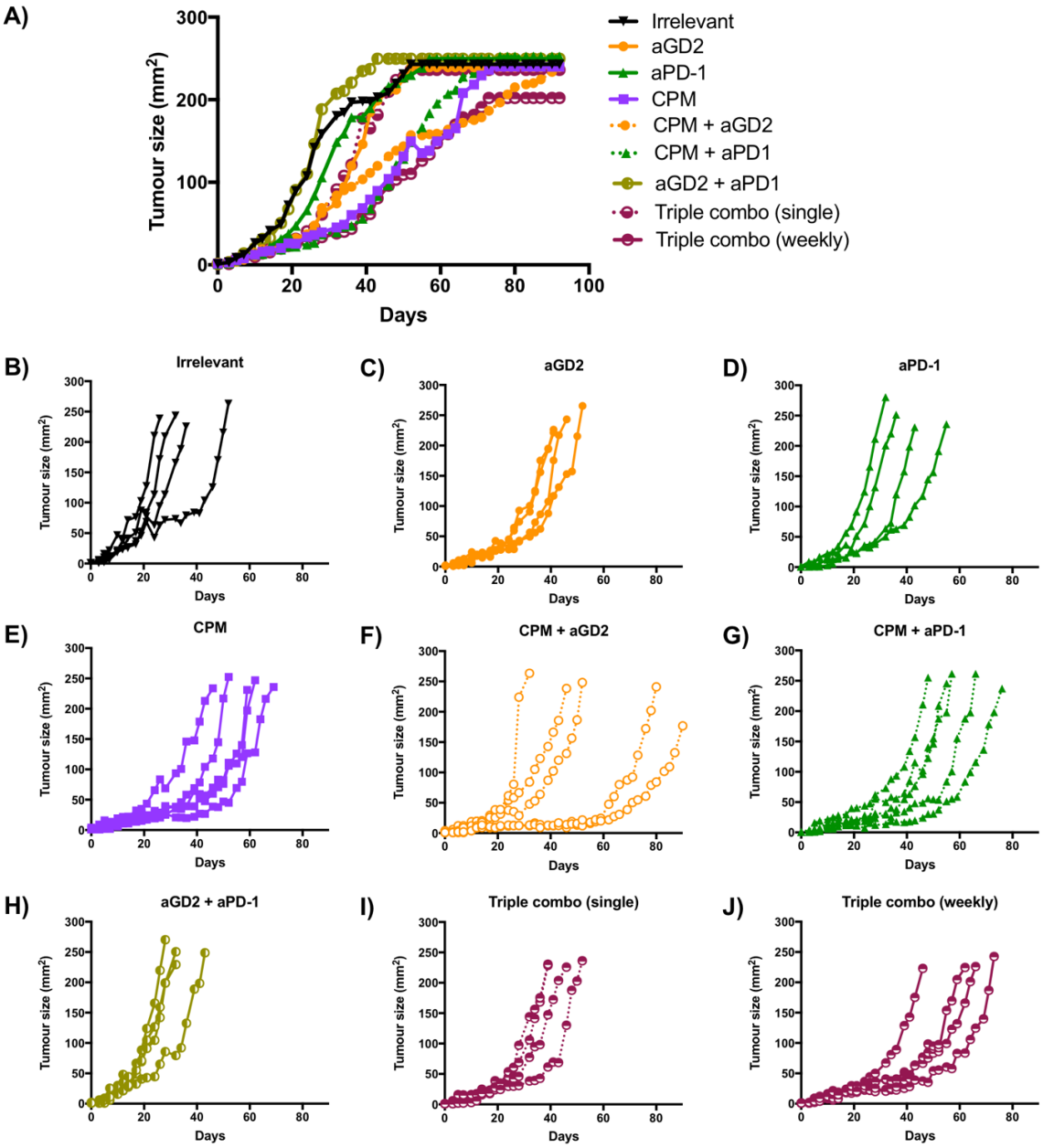

Figure 5.25 Growth curves after triple combination therapy in 9464D tumours. C57BL/6 mice were subcutaneously inoculated with $5x10^5$ 9464D cells and tumour growth was monitored 3 times/week. When tumours became palpable, mice were treated with PBS or 80 mg/kg CPM. Mice were treated 2, 4 and 7 days later with 200 µg of anti-GD2, anti-PD-1 mIgG1-N297A, both mAbs or irrelevant mAbs. According to treatment groups, mice were then administered PBS or CPM every Monday, followed by irrelevant or therapeutic mAbs every Thursday. All treatments were delivered Ip, with a typical dose of 200 µg of mAb. Mice were humanely culled when tumours reached 15x15 mm or if health was compromised. A) Tumour growth curves showing the mean size per group. B-J) Individual tumour growth curves per group: Irrelevant mAbs (B); anti-GD2 mAb weekly (C); anti-PD-1 mIgG1-N297A mAb weekly (D); CPM weekly (E); anti-GD2 + CPM weekly (F); anti-PD-1 + CPM weekly (G); anti-GD2 plus anti-PD-1 weekly (H); Triple combo of CPM, anti-GD2 and anti-PD-1 without weekly schedule (I); Triple combo of CPM, anti-GD2 and anti-PD-1 with weekly schedule (J). Experiment performed once, N=4-5 mice per group.

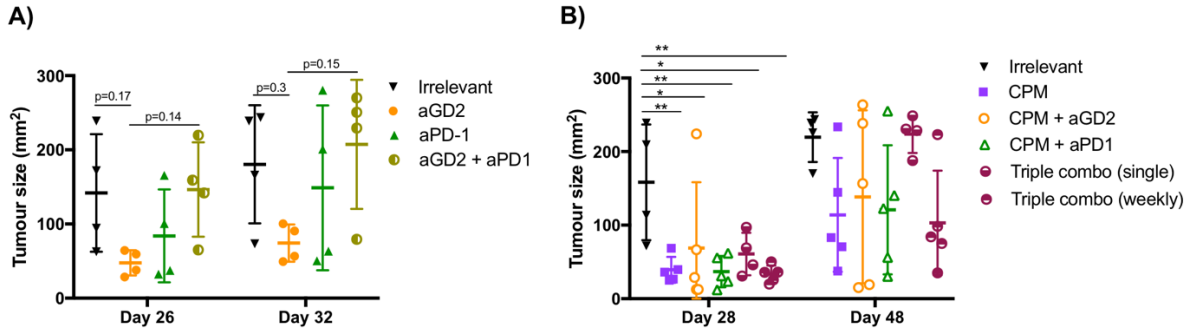

Figure 5.26 Comparison of tumour size at different time-points.
C57BL/6 mice were subcutaneously inoculated with $5x10^5$ 9464D cells and tumour growth was monitored 3 times/week. When tumours became palpable, mice were treated with PBS or 80 mg/kg CPM. Mice were treated 2, 4 and 7 days later with 200 µg of anti-GD2, anti-PD-1 mIgG1-N297A, both mAbs or irrelevant mAbs. According to treatment groups, mice were then administered PBS or CPM every Monday, followed by irrelevant or therapeutic mAbs every Thursday. All treatments were delivered Ip, with a typical dose of 200 µg of mAb. Mice were humanely culled when tumours reached 15x15 mm or if health was compromised. A) Tumour mean size on days 26 and 32 after tumour inoculation in controls, single mAb arms or upon combination of anti-GD2 and anti-PD-1 mAbs. B) Tumour mean size on days 28 and 48 after tumour inoculation in all groups containing CPM. Experiment performed once, N=4-5 mice per group. Bars represent mean ± S.D, *p<0.05, **p<0.01 (One-way ANOVA).

Amongst groups treated with CPM, a single administration of the therapeutic regimen decreased tumour volume compared to controls at day 28 after tumour inoculation (Figure 5.26 B). However, this did not translate into improved longer term survival (Figure 5.27 B,E). Combination of either weekly anti-GD2 or anti-PD-1 mAbs with CPM decreased tumour volume (Figure 5.26 B) and tended to increase survival (Figure 5.27 B-D) compared to non-treated controls. However, this effect was mostly driven by CPM administration, as the weekly CPM arm displayed reduced tumour growth (Figure 5.26 B) and increased survival (Figure 5.27 B,F) to a similar extent of dual combinations with anti-GD2 or anti-PD-1 mAbs. Likewise, mice treated with the triple combination in a weekly schedule showed reduced tumour growth (Figure 5.26 B) and increased survival (Figure 5.27 B,E,F), similar to weekly CPM alone.

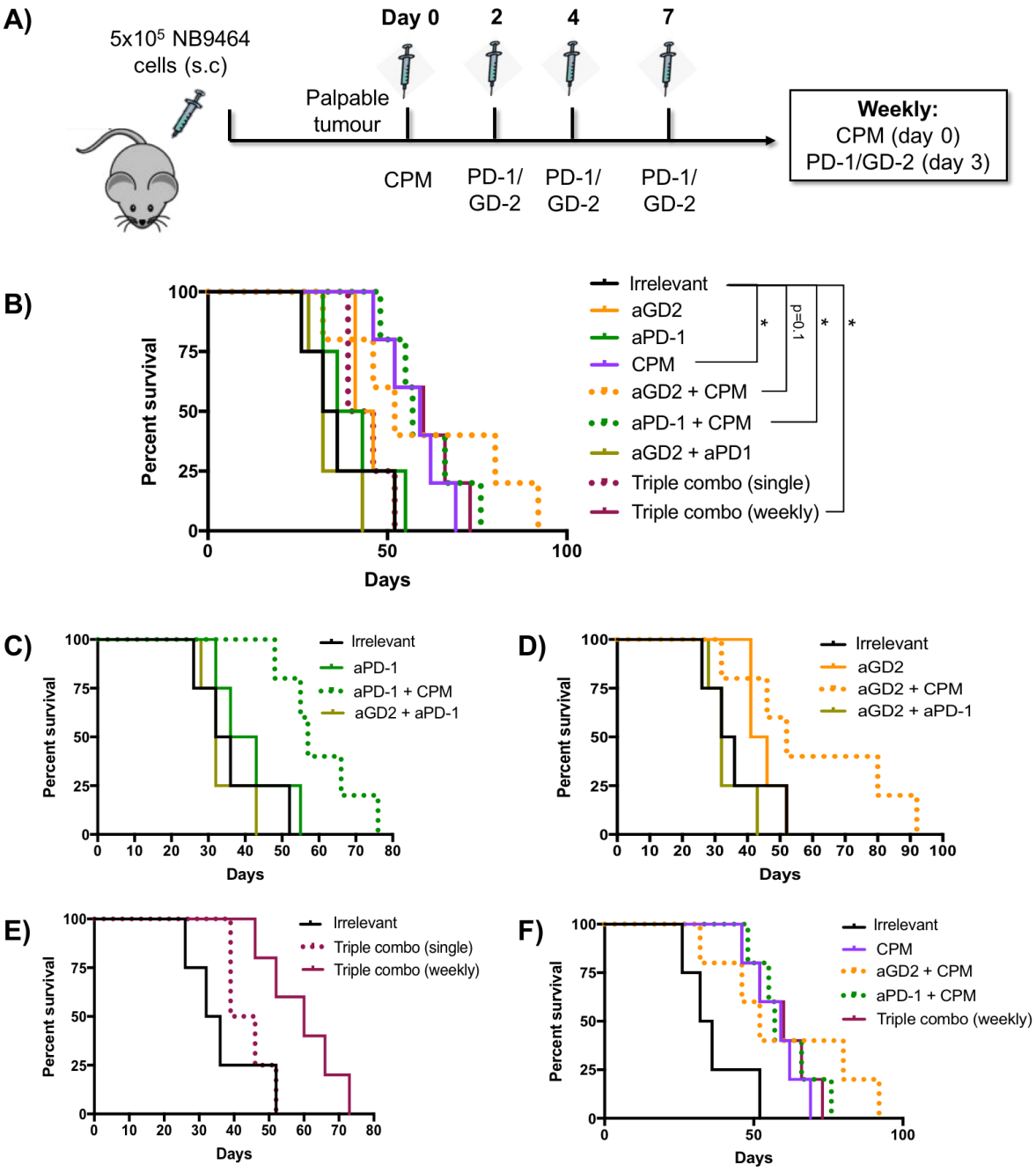

Figure 5.27 Triple combination therapy with cyclophosphamide, anti-PD-1 and anti-GD2 mAbs.
A) C57BL/6 mice were subcutaneously inoculated with 5x10^5 9464D cells and tumour growth was monitored. When tumours became palpable, mice were treated with PBS or 80 mg/kg CPM. Mice were treated 2, 4 and 7 days later with 200 µg of anti-GD2, anti-PD-1 mIgG1-N297A, both mAbs or irrelevant mAbs. According to treatment groups, mice were then administered PBS or CPM every Monday, followed by irrelevant or therapeutic mAbs every Thursday. All treatments were delivered Ip, with a typical dose of 200 µg of mAb. Mice were humanely culled when tumours reached 15x15 mm or if health was compromised. B-F) Kaplan-meier curves displaying the percentage of mice alive at each time point after tumour inoculation: all groups (B); anti-PD-1 groups (C); anti-GD2 groups (D); triple combinations (E); and CPM groups (F). Experiment performed once, N=4-5 mice per group. Log-rank (Mantel-Cox) Test, *p<0.05

Overall, the sub-curative metronomic dose of 80 mg/kg CPM provided sufficient therapeutic activity to delay tumour growth and improve survival compared to controls, but was insufficient to clear 9464D tumours. However, this could not be further enhanced with the addition of anti-PD-1 or anti-GD2 mAbs, potentially due to the low GD2 expression of 9464D cells in vivo. This suggested that these three therapies may not have a synergistic effect against 9464D tumours, and highlighted that alternative combinations should be considered for this model.

5.5.4 Modulation of anti-tumour responses by anti-GD2 plus anti-PD-1 mIgG1-N297A mAbs in 9464D-bearing mice

Despite the rationale behind the dual combination of anti-GD2 and anti-PD-1 mIgG1-N297A mAbs for neuroblastoma, this therapeutic approach tended towards a faster tumour growth compared to monotherapy with anti-PD-1 mIgG1-N297A and especially anti-GD2 mAbs (Figure 5.25 A; Figure 5.26 A). Albeit unexpected, hyperprogression following PD-1 blockade has been noted in 10-30% of patients in the clinic (169). A potential explanation has been linked to an increase in proliferating Tregs and their suppressive function by anti-PD-1 mAbs (170). To try and understand their contribution in tumour progression, the percentage and phenotype of Tregs was investigated in 9464D-bearing mice after dual therapy with anti-GD2 and anti-PD-1 mIgG1-N297A mAbs. Similar to other immunophenotyping experiments, 9464D-bearing mice were administered 3 doses of irrelevant or anti-GD2/PD-1 mAbs when tumours reached 7x7 mm, followed by harvest of tumours and spleens one day after the last dose.

As shown in Figure 5.28 A, dual combination of mAbs significantly increased CD8 TIL infiltration; although anti-PD-1 mIgG1-N297A had displayed a trend towards increased CD8 TILs in previous immunophenotypings (Figure 5.12 B), the effect was more clear when combined with anti-GD2 mAbs. This could be interpreted as a synergy between these two therapies, as anti-GD2 monotherapy did not alter CD8 TIL percentage (Figure 5.28 A). Whilst no differences were observed in the percentage of intratumoural Tregs between anti-GD2 monotherapy or combined therapy, dual anti-GD2/anti-PD-1 treatment might increase the percentage of this suppressive T-cell population in the spleen compared to monotherapy with anti-GD2 mAbs (Figure 5.28 B). Interestingly, the percentage of splenic CD4 T cells was also increased in the combination arm, which had not been observed with anti-PD-1 monotherapy (Figure 5.14 A). This expansion could perhaps translate into increased recruitment of CD4 T cells at the tumour site at later time points; taking

into account that multiple tolerogenic cues can be encountered at the TME, conversion of effector CD4 T cells into Tregs at the tumour bed could also occur.

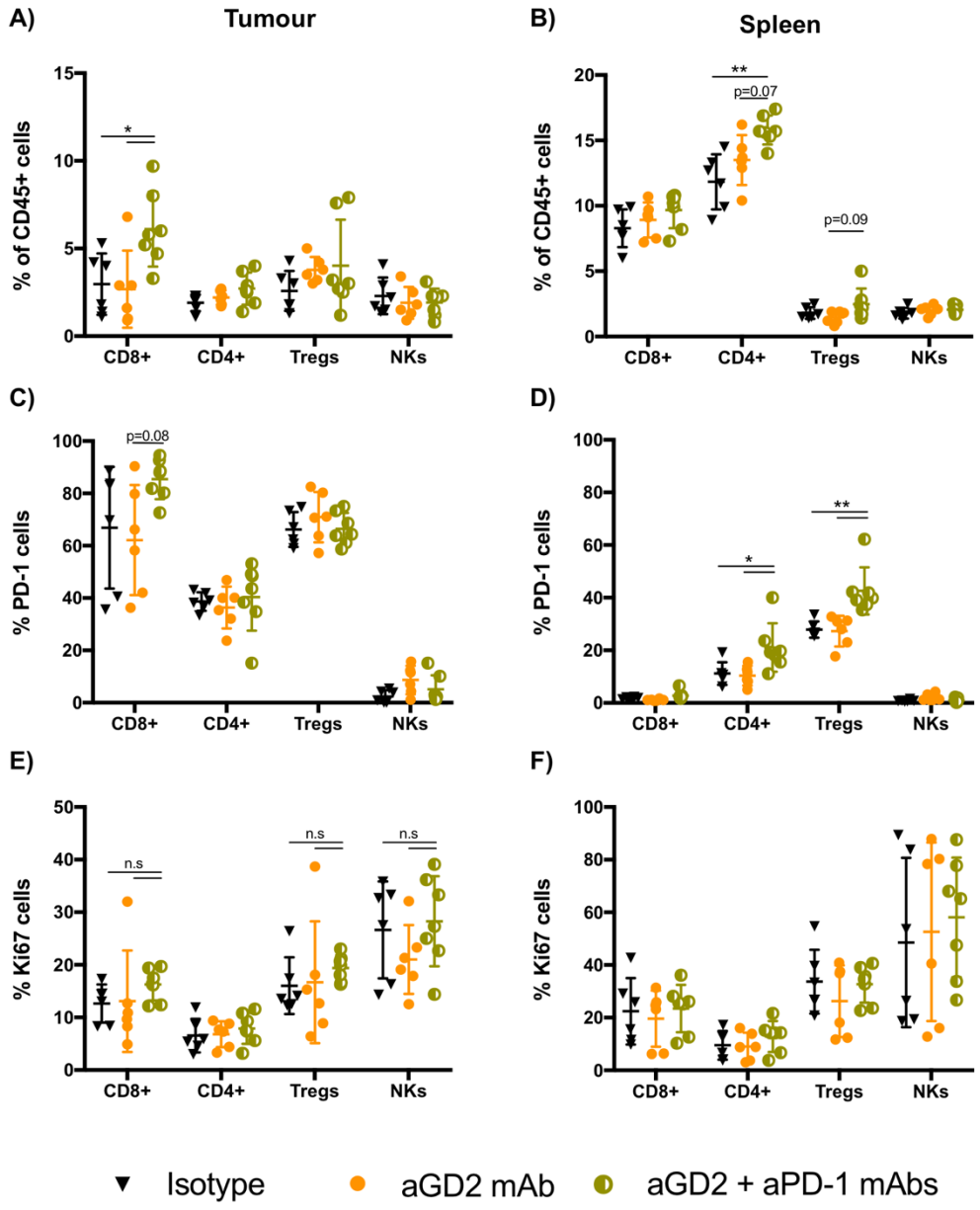

Figure 5.28 Lymphocyte populations in 9464D-bearing mice after therapy with anti-GD2 and anti-PD-1 mIgG1-N297A mAbs.
C57BL/6 mice were subcutaneously inoculated with $5x10^5$ 9464D cells. When tumours reached 7x7 mm, mice received 3 Ip doses of 200 µg of irrelevant mAbs (AT10 mIgG2a and mIgG1-N297A); 200 µg of anti-GD2 mAb alone; or 200 µg of anti-GD2 mAb plus 200 µg of anti-PD-1 mIgG1-N297A. Tumours and spleens were harvested 24h after the last dose and processed for flow cytometry (see sections 2.7.5 and 2.8). A-B) Percentage of CD8+, CD4+ (FoxP3-), Tregs (CD4+ FoxP3+) and NK cells (CD4- CD8- NK1.1+) out of CD45+ cells in tumour (A) and spleen (B) of 9464D-bearing mice. C-D) Expression of PD-1 in lymphocytes shown as percentage of positive cells in tumour (C) and spleen (D). E-F) Percentage of Ki67+ lymphocytes in tumour (E) and spleen (F). Experiment performed once, N=6/7 mice per group. Bars represent mean ± S.D, *p<0.05, **p<0.01, (One-way ANOVA).

Analogous to the results with anti-PD-1 monotherapy (Figure 5.13 A; Figure 5.14 C), the percentage of PD-1+ CD8 TILs, PD-1+ splenic CD4 effectors and Tregs was increased in the dual combination arm compared to controls and anti-GD2 monotherapy (Figure 5.28 C,D). When the percentage of proliferating, Ki67+ intratumoural Tregs was assessed, no statistically significant difference was found between anti-GD2 monotherapy and dual combination (Figure 5.28 E). Notably, this was due to a single (potentially outlier) sample in the monotherapy mAb group that presented a very high value. Therefore, there was a clear trend towards increased percentage of intratumural Ki67+ Tregs in 9464D tumours after dual therapy with anti-GD2/PD-1 mAbs. Furthermore, this effect was specific to the tumour site, as no differences were noted in the percentage of Ki67+ T cells at the spleen (Figure 5.28 F). Overall, the results presented herein were not conclusive, and a repeat of both survival and immunophenotyping experiments should be performed to ascertain the role of Tregs in decreasing anti-tumour immunity after anti-PD-1 therapy.

5.6 Therapeutic effect in transgenic TH-MYCN mice

One of the best characterised genetic abnormalities in human NB is the amplification of the protooncogene MYC-N, which occurs in 20-30% of tumours and correlates with advanced disease and poor prognosis (232, 234). The genetic alterations that lead to NB initiation are not yet clear; however, supporting evidence that MYC-N was involved in the tumorigenesis came from the development of transgenic mice that spontaneously developed NB tumours due to overexpression of Myc-N protein in neuroectodermal cells (235). Importantly, these murine tumours displayed critical similarities to human NB in that they arouse in abdomen and thorax; they presented similar histological characteristics and neural-specific traits; tumours showed secondary chromosomal gains and loses that are commonly observed in human NB; and they have high levels of the TAA GD2 (235). Therefore, transgenic mice bearing MYC-N amplification represent a valuable preclinical model to study potential therapeutic combinations for NB.

5.6.1 Anti-PD-1 mAbs in combination with anti-GD2 mAbs and cyclophosphamide in TH-MYCN mice

In order to establish the extent of therapeutic activity of anti-PD-1 therapy in this model, mice that presented with palpable TH-MYCN tumours were treated with a weekly dosage of anti-PD-1 mAbs as a monotherapy. TH-MYCN mice display more

T-cell infiltration compared to 9464D tumours (329), a priori suggesting that TH-MYCN could be more sensitive to monotherapy with anti-PD-1 mAbs. However, no benefit in survival was achieved (Figure 5.29 A), as mice reached humane end-point within 30 days after tumour presentation, similar to untreated controls (329). Besides T-cell infiltration, TH-MYCN tumours express a larger fraction of GD2+ cells compared to 9464D tumours (329). In spite of this, weekly anti-GD2 monotherapy was curative in only 1 out of 3 mice with no effect evident in the other 2 mice. Combination of both anti-PD-1 mIgG1-N297A and anti-GD2 mAbs also had limited effect in TH-MYCN tumours, with only 1 of 2 mice exhibiting extended survival but no cure (Figure 5.29 A). Therefore, despite some favourable traits, TH-MYCN tumours did not respond to dual mAb therapy.

As a result of their sensitivity to chemotherapy (329), the effect of a triple combination therapy with low doses of CPM and anti-PD-1/GD2 mAbs was investigated. To elucidate the best combinatorial regimen for TH-MYCN tumours, two doses of CPM were initially tested as single dose or in a weekly schedule. As displayed in Figure 5.29 B, both weekly schedules demonstrated a clear therapeutic activity in these tumours, inducing effective and durable anti-tumour responses. This highlights that TH-MYCN tumours are inherently more sensitive to CPM than 9464D tumours, and suggests that single doses of CPM might be sufficient in combination with anti-PD-1 and anti-GD2 mAbs to induce durable anti-tumour immunity. Previous work in the group (343) showed that a single dose of 40 mg/kg CPM was not curative in TH-MYCN tumour-bearing mice; however, combination with either anti-GD2 or anti-PD-1 mAbs provided effective anti-tumour immunity (Figure 5.29 B). Despite this success, we aimed to establish whether a triple combinatorial regimen with lower concentrations of CPM could also induce anti-tumour responses. Hence, the suboptimal dose of 20 mg/kg of CPM, which did not show any therapeutic effect as a monotherapy (Figure 5.29 B,C), was used. In this case, dual combination with anti-PD-1 mIgG1-N297A mAb had no benefit in survival, whilst combination with anti-GD2 mAbs led to 1 out of 2 cures. Due to time constrains of this project and limited availability of TH-MYCN mice developing tumours, the next obvious step with a triple therapy (20 mg/kg CPM plus anti-GD2 and anti-PD-1 mIgG1-N297A mAbs) could not be attempted.

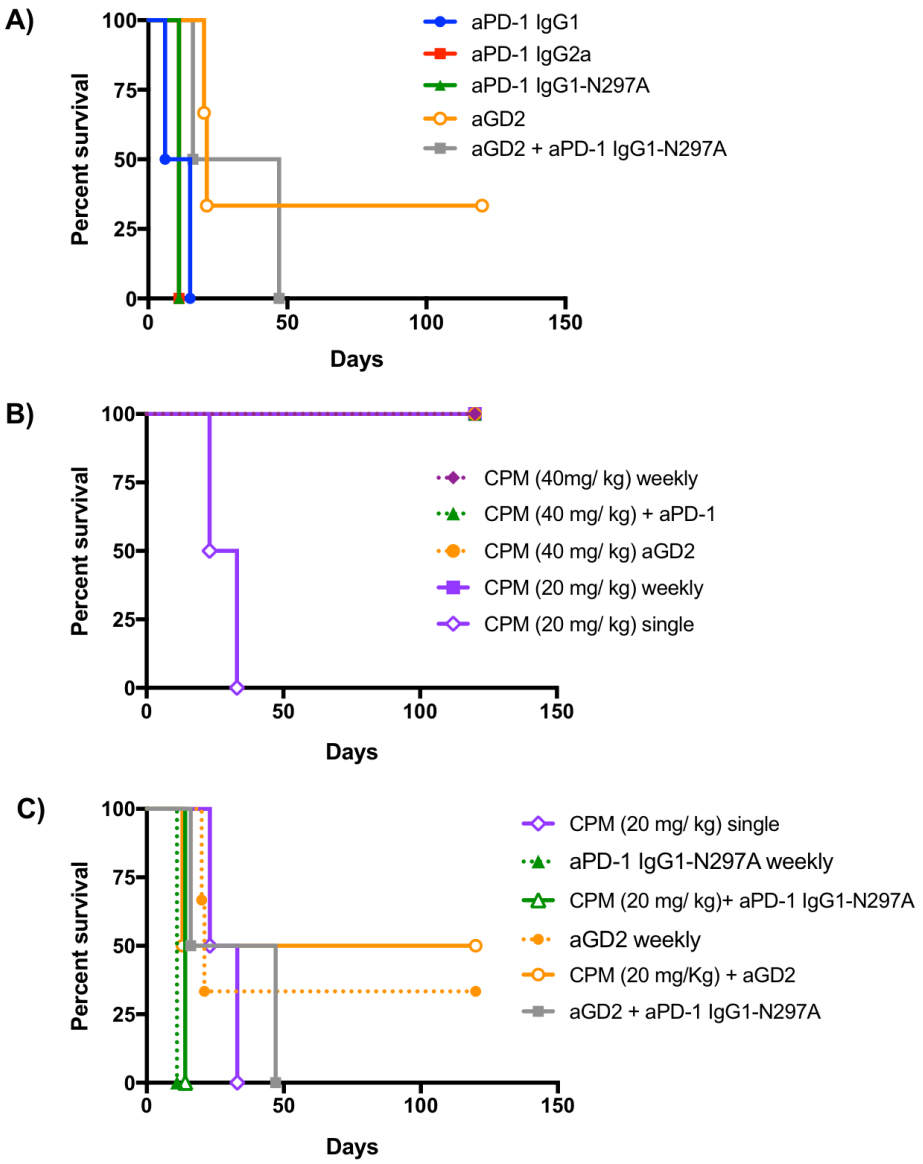

Figure 5.29 Survival analysis in transgenic TH-MYCN mice.
Upon tumour presentation (10 mm^2), heterozygous TH-MYCN were treated Ip with CPM (20 or 40 mg/kg), anti-PD-1 mAbs (200 µg), anti-GD2 mAb (200 µg) or a combination of the previous. Weekly schedules were administered for a period of 2 months. Mice were palpated twice a week by trained animal technicians to monitor tumour growth. In the case of tumour clearance, mice were monitored for another 2 months to look for the presence of secondary tumours. A) Mice were treated with anti-PD-1 mIgG1 weekly, N=2; anti-PD-1 mIgG2a weekly, N=1; anti-PD-1 mIgG1-N297A weekly, N=1; anti-GD2 mAb weekly, N=3; or anti-GD2 plus anti-PD-1 mIgG1-N297A mAbs on the following day, N=2. B) Mice were treated with CPM (40 mg/kg) weekly, N=3; a single dose of CPM (40 mg/kg) plus a single dose of anti-PD-1 mAb on the following day, N=1; a single dose of CPM (40 mg/kg) plus a single dose of anti-GD2 mAb on the same day, N=1; CPM (20 mg/kg) weekly, N=1; or a single dose of CPM (20 mg/kg), N=2. All treatments led to 100% cures except for 20 mg/ Kg CPM as a single dose. C) Mice were treated as mentioned above for the appropriate groups, or with a single dose of CPM (20 mg/kg) plus a single dose of anti-PD-1 mAb on the following day, N=1; or a single dose of CPM (20 mg/kg) plus a single dose of anti-GD2 mAb on the same day, N=2.

5.6.2 Phenotyping of transgenic TH-MYCN tumours

To investigate the lack of activity of anti-PD-1 mAbs as a monotherapy observed in TH-MYCN, phenotyping of tumour-infiltrating immune cells was performed in Myc-N tumours. As exemplified in Figure 5.30, the same gating strategy followed in 9464D tumours was used. In tumours harvested at ~10 mm^2, CD4 T cells comprised the largest lymphocyte population (Figure 5.31 A). Interestingly, the main lymphocyte population that expressed PD-1 within the TME was Tregs (Figure 5.31 C,D), which contrasted with the high expression found on CD8 TILs in 9464D tumours. The percentage of TILs and pattern of PD-1 expression was similar in end-point tumours (15x15 mm) that had progressed after CPM plus anti-PD-1 or anti-GD2 therapy, with CD8 and CD4 effector cells displaying negligible levels. Nevertheless, a trend towards increased PD-L1 expression on tumour cells was found in end-point tumours compared to non-treated (Figure 5.31 B), suggesting that these therapies could have induced an immune response that resulted in PD-L1 up-regulation in tumour cells, despite no improved survival. Although a limited number of TH-MYCN tumours were phenotyped, the preferential expression of PD-1 on Tregs could explain the inability of anti-PD-1 monotherapy to generate anti-tumour responses. In this setting, it is possible that depletion of Tregs by anti-PD-1 mIgG2a may be more beneficial than blockade of PD-1/PD-L1 interaction by the engineered Fc-null mAb as performed here.

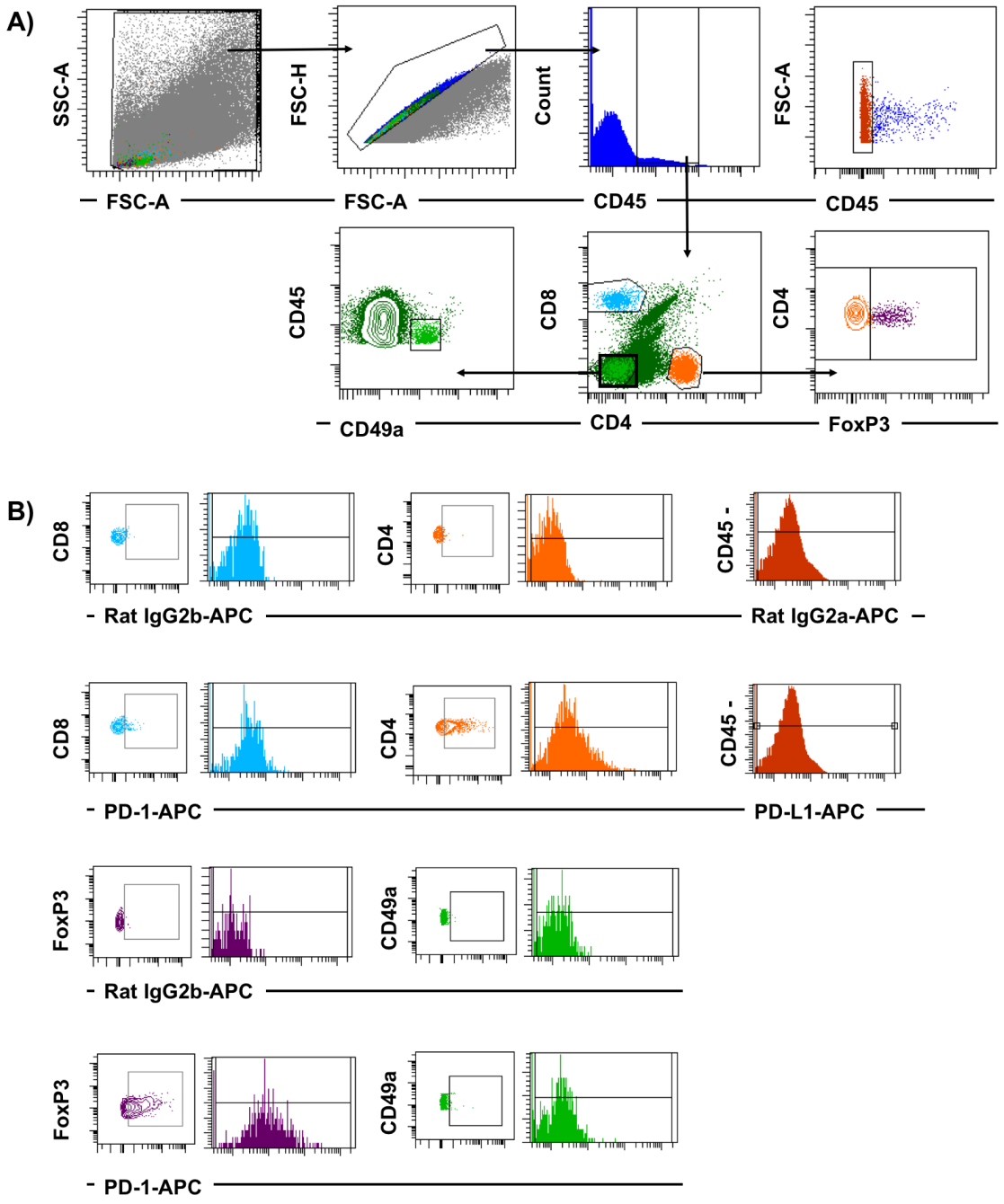

Figure 5.30 Gating strategy: Tumour-infiltrating lymphocytes in TH-MYCN tumours.
Following harvest, tumours were mechanically and enzymatically digested as detailed in 2.7.5, and single cell suspensions were obtained. Typically, 10^6 cells were stained with surface and intracellular markers (see 2.8) and samples were run on flow cytometry. A) Gating of T-cell populations. From all live cells (FSC-A–SSC-A), doublets were excluded and immune cells were gated according to their CD45 expression. Effector CD8 T cells, effector CD4 T cells (FoxP3-CD4+), Tregs (FoxP3+CD4+) and NK cells (CD8-CD4-CD3+CD49a+) were gated from CD45+ cells. Tumour cells were gated as CD45- cells. B) Dot plots and histograms for each lymphocyte population showing the expression of PD-1 or PD-L1. Positive cells were gated according to an isotype control. Geometric mean of the whole population was calculated from the histogram plots, and isotype control values were subtracted.

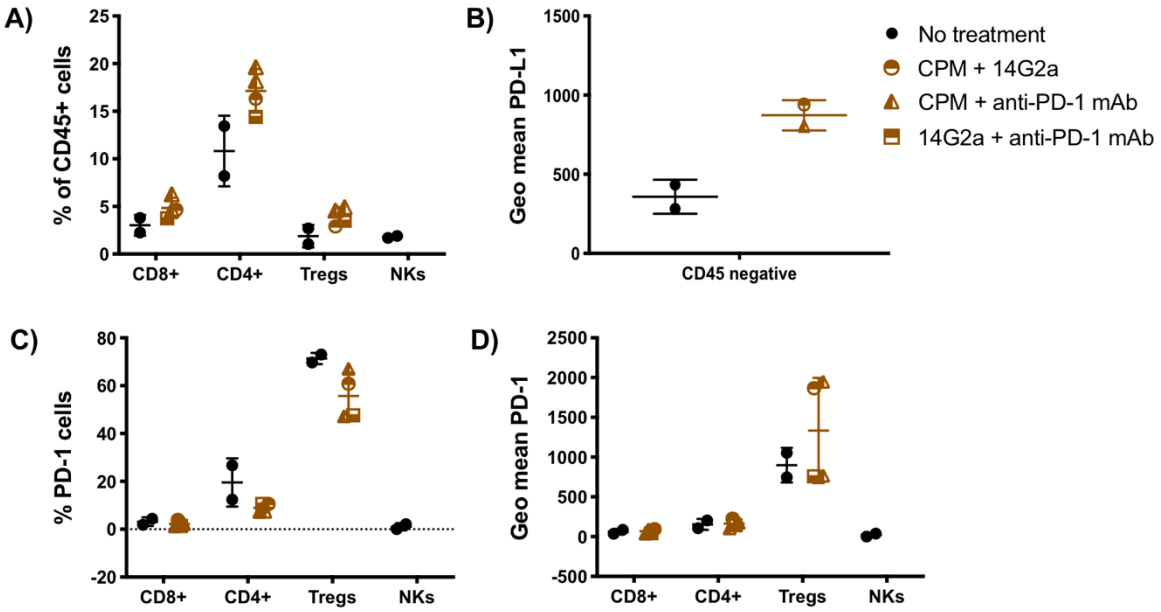

Figure 5.31 Phenotype of TILs in TH-MYCN tumours.
A) Percentage of lymphocytes out of CD45+ immune infiltrating cells. B) Expression of PD-L1 on tumour cells (MFI). C-D) Expression of PD-1 in T-cell subsets and NK cells shown as percentage of positive cells (C) or as MFI (D). N=2 non-treated mice and N=2-4 end-point mice after therapy with CPM, anti-GD2 or anti-PD-1 mAbs as described in legend. Bars represent mean ± S.D.

To obtain a more complete immune profile of the TH-MYCN TME, the frequency of myeloid infiltrates and the presence of PD-L1 were also investigated, as illustrated in Figure 5.32. Interestingly, the relative frequency of myeloid subsets differed from that in 9464D tumours. Neutrophils and monocytes were more abundant than MHC-II+ DCs and macrophages (Figure 5.33 A). Moreover, a large population of MHC-II negative DCs was detected in TH-MYCN tumours, perhaps representing a more immature DC subtype, which also expressed high levels of PD-L1 (Figure 5.33 B,C). Due to their potentially reduced expression of co-stimulatory molecules, the presence of such immature DCs could impair the priming of effective CD8 and CD4 T-cell responses, whilst promoting immune tolerance instead (344, 345). Therefore, together with the increased expression of PD-1 on Tregs, the higher proportion of immature DCs could contribute to the lack of activity of anti-PD-1 mAbs as a monotherapy in TH-MYCN tumours.

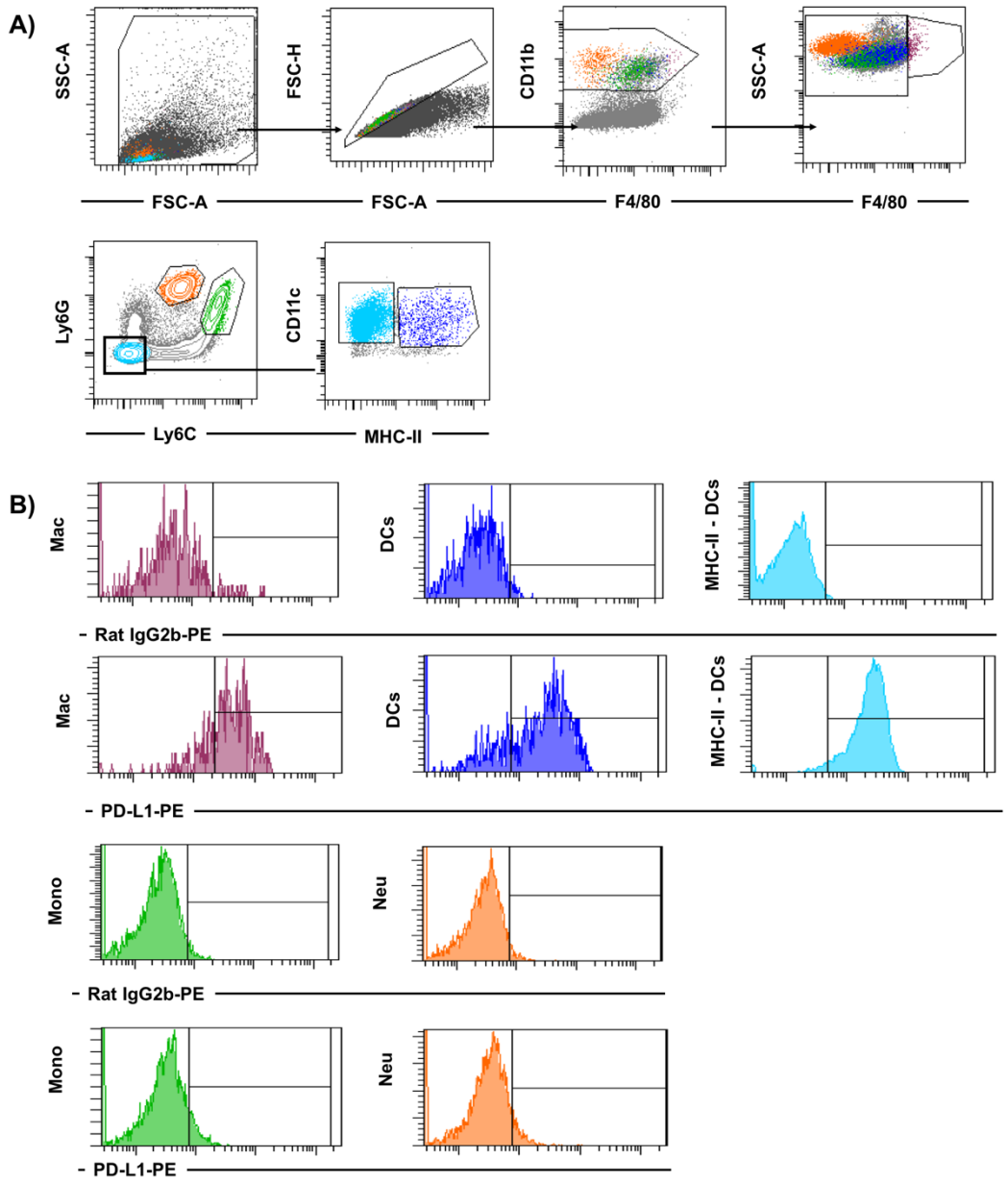

Figure 5.32 Gating strategy: Tumour-infiltrating myeloid populations in TH-MYCN tumours.
Following harvest, tumours were mechanically and enzymatically digested as detailed in 2.7.5, and single cell suspensions were obtained. Typically, 10^6 cells were stained with surface markers (see 2.8) and samples were run on flow cytometry. A) Following doublets exclusion, live cells were gated according to CD11b and F4/80 expression. Tumour-infiltrating macrophages were gated as F4/80 high and CD11b high. Neutrophils, monocytes and DCs were gated from the CD11b high, F4/80 low population according to their expression of Ly6C, Ly6C, CD11c and MHC-II markers as follows: neutrophils (Ly6C high, Ly6G high), monocytes (Ly6C low, Ly6G high), mature DCs (Ly6C-, Ly6G-, MHC-II high, CD11c high) and immature DCs (Ly6C-, Ly6G-, MHC-II low, CD11c high). B) Examples of histograms showing the expression of PD-L1 on macrophages (purple); DCs (blue); monocytes (green); and neutrophils (orange). Gates were set according to an isotype control. Isotype values were subtracted to geo means for each population.

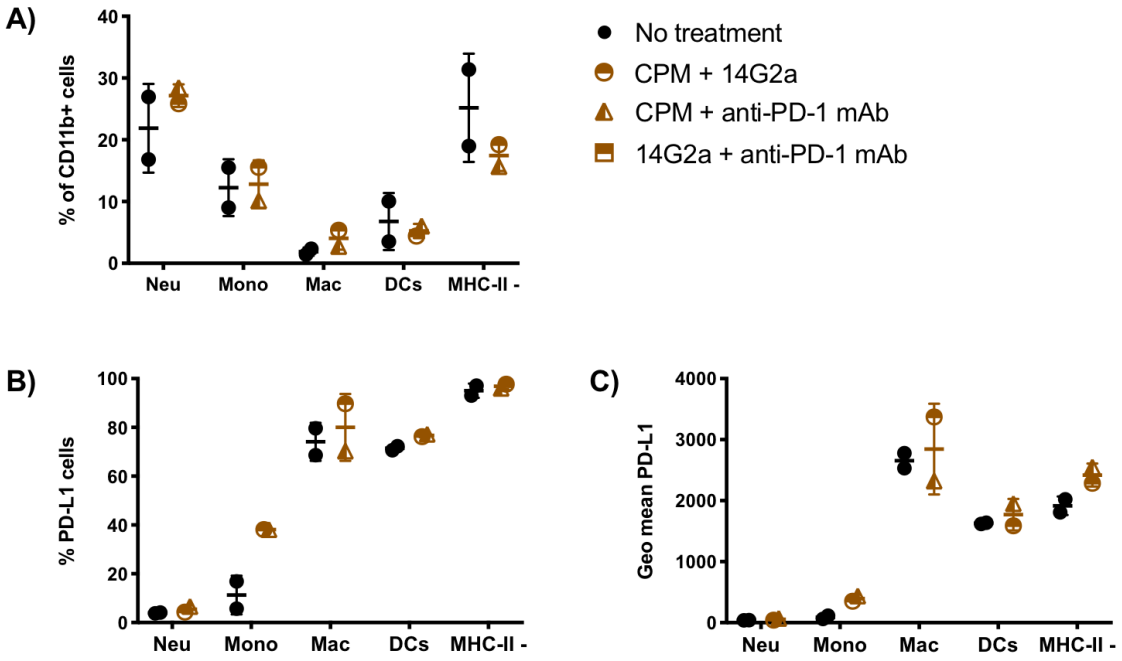

Figure 5.33 Phenotype of myeloid cells in TH-MYCN tumours.
A) Percentage of myeloid populations out of CD11b+ infiltrating cells. B-C) Expression of PD-L1 shown as percentage of positive cells (B) or as MFI (C). N=2 non-treated mice and N=2 end-point mice after therapy with CPM, anti-GD2 or anti-PD-1 mAbs as described in legend. Bars represent mean ± S.D.

5.7 Chapter discussion

PD-1 blockade has shown an unprecedented success in the treatment of some types of advanced solid cancers, such as melanoma and NSCLC (5). Response to PD-1 blockade has been linked to the degree of immunogenicity and immune contexture of each tumour. As such, tumours harbouring high mutational burden and large immune infiltrates are predicted to be more responsive, whilst poorly immunogenic tumours with little or no immune infiltration, which are often referred to as cold tumours, are predicted to be unresponsive. One of the main challenges that PD-1 blockade faces is its applicability in such cold tumours (194). As an example of cold tumours, childhood cancers bear on average a lower mutational burden than adult tumours, and generally have less immune infiltration (187, 191, 195-197). Due to these unfavourable traits, monotherapy with anti-PD-1 mAbs has proven to be ineffective in most childhood cancers, with the exception of HL and some highly mutated tumours like bMMRD glioblastoma (190, 202, 207, 208, 214, 215). Therefore, it is critical to understand the mechanisms driving this unresponsiveness and investigate ways to sensitise cold tumours to PD-1 blockade. By using preclinical models of NB, we have investigated the ability of anti-PD-1 mAbs to generate effective anti-tumour responses in cold tumours, either as a monotherapy or in a combinatorial regimen, as sought to further define the role of the Fc region in anti-PD-1 therapy.

Although PD-L1 expression in tumours cells is often a predictive biomarker of response (174), some studies suggest that this expression might be transient and linked to a transitory up-regulation of T-cell activation (66). In 9464D, tumour cells gained PD-L1 expression as tumour progressed, but this did not correlate with increased TILs (Figure 5.2). However, similar to a previous work using sarcoma tumours (66), expression of PD-L1 in myeloid subsets was high and constant throughout tumour growth. In addition, T cells also expressed PD-L1, which has been shown to inhibit neighbouring PD-1+ T cells and be able to polarise PD-1+ TAMs towards an immunosuppressive phenotype (69). Together with the presence of PD-1 in TILs even at a palpable size, these observations argued in favour of using anti-PD-1 mAbs to treat 9464D.

To gain a better picture of the overall differences that Fc engagement could induce in the 9464D TME, an initial immunophenotyping was performed after therapy with the parental rat anti-PD-1 mAb and its deglycosylated form. However, only a small number of changes were noted, such as the decreased expression of PD-1 on TILs

by rat IgG1 and an increase in CD107a and EOMES upon anti-PD-1 therapy (Figure 5.6). The limited number of differences was likely caused by the schedule used (single dosage and harvest 3 days later), but it could also be related to the fact that rat antibodies do not represent the ideal modality of mAbs to identify subtle phenotypic changes. Taking into account the enhancement of T-cell responses by murine IgG1 and IgG1-N297A anti-PD-1 mAbs described in Chapter 4 (Figure 4.4, Figure 4.10, Figure 4.13) and the differences observed in the MC38 TME, further immunophenotyping of 9464D tumours was performed using murine anti-PD-1 mAbs. This time, the same schedule followed for MC38 tumours was utilised, which included 3 doses of anti-PD-1 mAbs (on days 1, 5 and 8) after tumours reached 7x7 mm.

Tumour-infiltrating CD8 T cells are believed to be key to the efficacy of anti-PD-1 mAbs due to their effective targeting of tumour cells and their potent cytotoxic ability (346). In non-treated mice, over 60% of CD8 9464D TILs expressed PD-1 at a high level (Figure 5.13). The fact that it was almost absent in CD8 T cells in the spleen (Figure 5.14) suggested that high PD-1 expression is linked to chronic antigen exposure (153). Therapy with anti-PD-1 mIgG1-N297A increased the levels of PD-1 expression on CD8 TILs (Figure 5.13). Since the percentage of effector CD44+ CD8 TILs also tended to increase with the Fc-null mAb relative to controls (Figure 5.13), this rise in PD-1 expression perhaps correlates with a terminally differentiated phenotype of effector T cells (157, 158). Furthermore, both the increased myeloid infiltration at the tumour site (Figure 5.15) and the stimulation of effector CD8 T cells in spleens (Figure 5.14) also support the presence of a systemic pro-inflammatory response. Despite these changes, which generally recapitulated those seen in the MC38 model, weekly therapy with anti-PD-1 mIgG1-N297A showed a minimal increase in survival in 9464D tumours (Figure 5.10), albeit significant.

In terms of anti-PD-1 mIgG1 and mIgG2a, these isotypes reduced the percentage of PD-1+ cells at the TME (Figure 5.13) in a similar way to that in the MC38 model. Although no statistical difference was found in the percentage or absolute cell count of CD8 TILs between mIgG2a and controls (Figure 5.12), the preferential engagement of activating FcγR by mIgG2a could still cause the deletion of PD-1-expressing cells at the TME. On the contrary, mIgG1 displayed a trend towards increased CD8 TILs (Figure 5.12) and a significant improvement in survival when administered in a weekly schedule (Figure 5.10). As discussed in section 4.6.2, these facts infer that this isotype could lead to the removal of PD-1 from the cell

surface as opposed to causing the depletion of PD-1+ cells (322, 324). Of note, mIgG1 and rat IgG1 anti PD-1 mAbs, which had comparable FcγR binding patterns by SPR (Figure 3.2), displayed the same reduction in PD-1 levels in TILs in both MC38 and 9464D models. Likewise, both Fc-null degly rat IgG1 and murine IgG1-N297A displayed higher levels compared to their Fc-competent counterparts, highlighting the consistency of these changes across experiments and mAbs.

In contrast to MC38 tumours, no evident changes in myeloid cells across treatment groups were noted in 9464D tumours. At baseline, myeloid infiltrates in 9464D tumours exhibited less PD-L1-expressing cells (Figure 5.15, Figure 5.17) and a lower A/I ratio (Figure 5.16) compared to MC38 (Figure 4.22, Figure 4.24, Figure 4.23), suggestive of a less inflammatory TME (112, 122, 123, 336). Due to the important role that myeloid cells take in priming and re-activating effector T cells via antigen presentation (MHC-I/II), co-stimulatory molecules (i.e 4-1BB) and secretion of cytokines (i.e IL-12) (76, 86), their reduced activation within 9464D tumours could dampen T-cell mediated anti-tumour responses. Moreover, the anti-PD-1 mIgG1-N297A isotype lost its ability to induce up-regulation of myeloid markers in 9464D (Figure 5.16, Figure 5.18) as opposed to MC38 tumours (Figure 4.23, Figure 4.25), which could contribute to the minimal effect displayed in 9464D tumour growth.

Overall, the efficacy of the three anti-PD-1 isotypes in 9464D tumours followed a similar pattern to that in MC38, with mIgG1 and mIgG1-N297A mAbs displaying enhanced therapeutic activity compared to mIgG2a. Nevertheless, monotherapy with anti-PD-1 mAbs was curative in MC38 tumours, whilst a minimal improvement in survival was seen in the NB model. Since the phenotype of TILs was similar in both models, the difference in efficacy might be driven by the absolute numbers of immune cells, rather than the phenotype. Immune infiltration in 9464D tumours represented approximately 10% of all cells in control mice, with a CD8: Treg ratio of 2 on average (see Appendix B, Figure 6.21 A). The reduced immunogenicity of this model might be caused by the reduced mutational burden that these tumours carry compared to other NB models such as NXS2 (347) and which are more sensitive to immunotherapy (262, 329, 347). In contrast, almost 50% of all cells making up MC38 tumours were immune cells, with a baseline CD8: Treg ratio of approximately 10 in control mice (see Appendix A, Figure 6.10 A). Taking these differences into consideration, the disparity in therapeutic efficacy is not unexpected, as tumours that are rich in immune infiltrates and CD8 T cells are known to be more responsive to checkpoint blockade (23, 194). The small

percentage of immune infiltrates and low mutational burden of 9464D tumours, however, make them perhaps more representative of human tumours than other preclinical models like MC38 or NXS2. In agreement with the current findings, most studies in paediatric cancers, such as NB, report little or no efficacy of anti-PD-1 mAbs as a monotherapy (202, 214, 215). Nevertheless, the described changes in TILs, mainly by the Fc-null anti-PD-1 mAb, argue in favour of combining these mAbs with other therapies to enhance anti-tumour immunity against NB.

Similarly to human NB tumours (249-251), 9464D expression of MHC-I was low, and was further reduced as tumour progressed (Figure 5.2). Although this may provide a means of escape from T-cell mediated recognition, it is important to note that treatment with IFN-γ can largely up-regulate MHC-I expression in vitro in most NB cell lines, suggesting that this lack of MHC molecules might be reversible in vivo (251). Furthermore, tumour-infiltrating immune cells isolated from NB patients can be expanded ex vivo and produce Th1 cytokines (338), further supporting that T-cell responses could also take place in vivo. Besides, the reported low expression of MHC-I may also increase the susceptibility of neuroblastoma cells to NK-mediated targeting, as it was shown to occur in vitro (348). Taking into consideration that NK cells are postulated to be the primary immune cell responsible for the therapeutic activity of anti-GD2 mAbs (266, 267, 270, 271), low MHC-I expression could further enhance NK-cell effector mechanisms following anti-GD2 therapy. It is hence important to note that NK cells were present in 9464D tumours (Figure 5.12 B) and that 9464D cells expressed GD2 in vivo, thus becoming a potential target for anti-GD2 mAb-mediated NK-cell killing.

Tumour expression of PD-L1 has been shown to inhibit the function of intratumoural PD-1+ NK cells, the dysfunction of which could be reversed by PD-1 blockade (328). In 9464D tumours, NK cells displayed low levels of PD-1 (Figure 5.13 A,B), which might not be sufficient to observe an enhancement in NK-cell activity by PD-1 blockade. However, following ADCC of Lan-1 cells, lymphocytes were shown to up-regulate PD-1 in vitro, although the authors did not specifically discern between NK cells or T cells (231). Together with the concurrent up-regulation of PD-L1 on tumour and myeloid cells observed in vitro (231), it is likely that tumour cytotoxicity by NK cells is impaired by PD-1/ PD-L1 interactions, sensitising these cells to anti-PD-1 mAbs. In this scenario, PD-1 blockade could potentially increase NK-cell activation, favouring tumour cell killing and inducing a more pro-inflammatory TME that could lead to DC and T-cell recruitment (349).

Despite the rationale behind this combination, therapy with anti-GD2 and anti-PD-1 mAbs had no effect on 9464D growth (Figure 5.27). In the only study of such regimen in NB, a minor increase in ADCC in vitro by the addition of anti-PD-1 mAbs was found (231). Only a small but not significant additive effect was seen in a highly immunogenic in vivo model, where anti-GD2 monotherapy was already curative in the majority of mice (231). Together with the current results, these might suggest that both mAbs might not be sufficient to induce effective anti-tumour responses against NB. Dual targeting of GD2 and PD-1 appeared to show, in fact, the contrary effect. A trend towards increased tumour volume was noted compared to anti-GD2 monotherapy (Figure 5.26), suggesting that addition of anti-PD-1 therapy could potentially impair the efficacy of anti-GD2 mAbs. Intriguingly, a paradoxical clinical effect of PD-1 blockade has been characterised in 10-30% of patients with different tumour histologies (169). As described in Chapter 1 (section 1.3.2), hyperprogression defines a marked increase in tumour growth following anti-PD-1 therapy, which correlates with poorer outcome (169). In an attempt to explain these events, two studies proposed two distinct mechanisms. First, engagement of FcγR was found to be involved in HP (168); whilst the current study in MC38 tumours supports this hypothesis, it cannot explain the paradoxical increase in 9464D tumour volume because the Fc-null mIgG1-N297A isotype was utilised in that experiment.

On the other hand, a study by Kamada T. et al. showed that patients with advanced gastric cancer that presented HP after PD-1 blockade exhibited a marked increase in proliferating (Ki67+) effector Tregs in blood (170). Instead, patients without signs of HP had a reduction of these cells. Notably, PD-1 blockade enhanced Treg suppressive activity in vitro and increased proliferation of Tregs from healthy PBMCs (170). Despite the small number of patients in this study (n=2 HP; n=12 non-HP), it clearly highlights the potential augmentation of Treg activity by anti-PD-1 mAbs. In melanoma, although no differences in the percentage of intratumoural Tregs have been reported between responders and non-responders (350), studies described a correlation between increased peripheral Tregs with tumour progression and anti-PD-1 mAb resistance (351, 352). Taken together, these studies suggest that peripheral Treg activation and expansion by anti-PD-1 mAbs may conform a mechanism of resistance that could be shared across responsive and non-responsive tumours. Interestingly, the majority of tumour-infiltrating Tregs in 9464D (80%) and MC38 (70%) expressed PD-1; however, Tregs in 9464D tumours presented the same level of expression as CD8 TILs, whilst in MC38, Tregs displayed a largely reduced PD-1 expression (Figure 4.18, Figure 5.13) compared

to CD8 T cells. Therefore, it could be hypothesised that the degree of expression of PD-1 in tumour-infiltrating Tregs relative to CD8 T cells might be a determining factor in Treg-mediated resistance after PD-1 blockade. The importance of the relative target molecule expression between these two cell types has been previously demonstrated in anti-4-1BB mAbs, where the higher 4-1BB expression on Tregs rendered them more susceptible to anti-4-1BB IgG2a mediated depletion than effector CD8 T cells (133).

Moreover, Tregs were the lymphocyte population with the largest expression of PD-1 in the spleen (Figure 5.14). Thus, the inflammatory cues produced by innate immune cells within the TME after anti-GD2 therapy could recruit peripheral Tregs, which could be further activated by anti-PD-1 mAbs. In order to test this hypothesis, the frequency and phenotype of Tregs was assessed following anti-GD2/PD-1 dual therapy. Although no conclusive results were obtained, there was a trend towards increased CD4 and Treg expansion at the spleen with the dual combination compared to anti-GD2 monotherapy, which was accompanied by a potential increase in the percentage of intratumoural Ki67+ Tregs (Figure 5.28). These findings may support the role of peripheral Treg activation in driving therapeutic resistance; however, repeats of both survival and phenotyping experiments with the dual combination should be carried out, which should also include an assessment of Ki67 after monotherapy with anti-PD-1 mIgG1-N297A. Moreover, ex vivo suppression assays with peripheral Tregs could be performed to parallel the study by Kamada T. et al. (170).

In addition to the direct targeting of tumour cells, several therapeutic strategies focus on the repolarisation or deletion of suppressive populations within the TME. As mentioned previously, Tregs are key drivers of tumour development and growth due to their direct suppressive activity on effector T cells, but also because of their ability to induce and sustain additional tolerogenic myeloid populations within the TME (22). Selective depletion of Tregs by mAbs (133, 138) has been shown to enhance effective anti-tumour immunity and improve survival in several preclinical models. Alternatively, metronomic, low-dose CPM can also reduce levels of Tregs within the TME, peripheral blood and TDLNs (341). Given that NB is known to be sensitive to CPM, and this chemotherapeutic agent is frequently used in the treatment of NB patients (232), it offers a clinically relevant option to be combined with anti-PD-1 therapy for the depletion of Tregs. Furthermore, CPM showed a therapeutic dose-dependent effect on an aggressive in vivo model of NB (AgN2a) (339). In this study, vaccination with tumour lysate and CpG boosted the expansion

of effector memory T cells after CPM-mediated Treg depletion, achieving improved survival (339). In the current work, 9464D tumours presented a low CD8: Treg ratio (see Appendix B, Figure 6.21 A) compared to MC38 (see Appendix A, Figure 6.10 A), which has been associated with poor prognosis in multiple human cancers (23). Therefore, it was hypothesised that Treg depletion by metronomic CPM could increase the intratumoural CD8: Treg ratio and enhance T-cell effector function.

Interestingly, single administration of the triple combination with anti-PD-1 and anti-GD2 mAbs delayed tumour growth compared to controls (Figure 5.26). As a result of the toxicity observed in the dose escalation study with 80 mg/kg CPM (single dose) (Figure 5.21), a single arm group with 80 mg/kg CPM alone was not included in the triple combination experiment. It is therefore difficult to conclude whether the full triple combinatorial regimen can delay tumour growth and extend survival further than CPM alone. Nevertheless, no toxicity was noted in the triple schedule, indicating that addition of anti-PD-1 and/ or anti-GD2 mAbs had an effect in the overall response to therapy. Indeed, it has been shown that PD-1 blockade can prolong Treg deletion in spleen and tumour after a single CPM administration (226). Hence, it is likely that the toxicities after a single dose of 80 mg/kg CPM were associated with the recovery of Treg numbers and function (341), which could then be prevented by combination with anti-PD-1 mAbs. Consistent with this, there was a trend towards increased frequency of intratumoural Tregs 10 days post CPM compared to controls (Figure 5.24 E). Besides a repeat of this experiment, investigating the efficacy and immune-modulation of the three different murine anti-PD-1 isotypes in this triple schedule would give an important insight into the role of PD-1 blockade in the therapeutic combination and could help to better define the effect of anti-PD-1 isotype in 9464D tumours.

Due to the known transient effect of CPM on Treg proliferation and function, which was shown to last from 1 to 10 days after administration (341), a metronomic dosage was also tested. Despite being well tolerated, the initial effect of weekly CPM (80 mg/kg) was not significantly effective in 9464D tumours (Figure 5.21), but this pilot study only included 2 mice in that treatment group. In contrast, as part of the triple combination experiment, monotherapy with weekly CPM extended survival of mice bearing 9464D tumours (Figure 5.27). Unfortunately, this efficacy was not significantly enhanced by the combination with anti-PD-1 and anti-GD2 therapy or either type of mAbs alone.

The profound delay on tumour growth that metronomic, low doses of CPM alone displayed in 9464D tumours (Figure 5.21, Figure 5.27) could be explained by the

multiple effects that this drug has on both tumour and immune cells. As established in several studies, low-dose (80 mg/kg) CPM depleted intratumoural Tregs in 9464D tumours (Figure 5.24 E). Although Treg depletion has been postulated as its main immunomodulatory effect (341), the induction of immunogenic cell death (ICD) by CPM has also been described as an alternative mechanism of action by which these drugs can modulate anti-tumour immunity (223). Indeed, CPM was capable of inducing ICD of glioma cells in vivo (353) and stimulate apoptosis and HMGB1 release by EG7 cells in vitro (354). Therefore, to determine the contribution of ICD in CPM therapy, vaccination studies could be carried out. To this end, tumour challenge with live 9464D cells following previous vaccination with in vitro killed 9464D cells could help to establish whether CPM-induced ICD is implicated in anti-tumour immunity against NB in vivo (223).

Despite not achieving statistical significance compared to CPM monotherapy, 2 out of 5 mice treated with CPM and anti-GD2 mAbs (Figure 5.25) displayed a prolonged delay of tumour growth. Alternative dosing schedules could be attempted to optimise this combinatorial regimen, perhaps including daily doses of anti-GD2 mAbs for 5 days (231) and given simultaneously with the initial CPM dose. Although a repeat of this experiment would be necessary, this potential synergy is interesting, as it could be a relevant combination to enhance the long-term effects of anti-GD2 mAbs in NB patients (274). One possibility behind the mechanism of synergy of anti-GD2 mAbs with CPM could revolve around the modulation of the activation state of innate effector cells by CPM. As such, up-regulation of activating FcγRs on macrophages by low-dose CPM enhanced phagocytosis and synergised with direct tumour-targeting mAbs to clear metastatic breast cancer (311).

Alternatively, doxorubicin, another type of chemotherapy, has been reported to stimulate the production of type I IFNs from malignant cells, resulting in the release of the CXCR3 ligand, CXCL10. In this study, both ligand and receptor were essential for the therapeutic efficacy that doxorubicin presented in several tumour models (355). In a similar fashion to doxorubicin, low doses of CPM induced a type I IFN-response that augmented the expression of CXCR3 in tumour-reactive T cells in TDLNs (337). In another study, type I IFNs and expression of CXCR3 on NK cells were shown to be essential for the effective accumulation of NK cells at the tumour site and their anti-tumour activity (356, 357). Hence, increased NK-cell infiltration in 9464D tumours as a consequence of the type I IFN production and CXCR3 expression stimulated by CPM could lead to augmented ADCC by anti-GD2 mAbs. In agreement with this, orally administered CPM at low to medium doses increased

NK-cell infiltration in lymphoma and breast cancer models, thereby resulting in reduced tumour volume (228). To test this hypothesis, deletion of NK cells by anti-NK1.1 mAbs or the use of neutralising mAbs to type I IFNs could be used to delineate the role of these in the anti-tumour response.

Of note, CXCR3 was also necessary for an effective response to anti-PD-1 therapy in MC38 tumours (161). Although this finding could be used to infer that a similar synergy should occur between CPM and PD-1 blockade, therapeutic outcomes after anti-PD-1 therapy were dependent on the activation of CD8 effector TILs by intratumoural CD103+ DCs (161). The expression of CD103 and other activation markers (i.e CD40, CD80/86) were not investigated in 9464D-infiltrating DCs, but the rather cold and immunosuppressive environment of these tumours would argue against the presence of functionally activated DCs. Therefore, the limited frequency of CD8 TILs and activated DCs in 9464D tumours might be dampening the overall efficacy of the dual combination.

Overall, triple combination of CPM, anti-GD2 and anti-PD-1 was not sufficient to eradicate 9464D tumours. In a study by Voeller J. et al., the more immunogenic neuroblastoma NXS2 tumour model responded to dual radiotherapy and anti-GD2 immune-conjugates (anti-GD2 mAb-IL-2), whilst 9464D tumours remained unresponsive even with the addition of anti-CTLA-4 mAbs (347). Addition of anti-CD40 mAbs and danger signals (CpG) were required to sensitise 9464D tumours, leading to 100% cures (347). Therefore, this suggests that activation and maturation of myeloid cells within the TME is a key factor in determining 9464D responsiveness. This also implies that, due to the cold nature of 9464D tumours, immunostimulatory therapies such as anti-CD40 agonists might be required to generate effective anti-tumour immunity in this model. In line with this, combination of immunostimulatory STING-activating nanoparticles and anti-PD-L1 mAbs resulted in a strong therapeutic activity in 9464D tumours (286). Whilst STING agonists are capable of directly activating DCs and stimulating cross-presentation of TAA to CD8 T cells (358), they can also have a direct effect on STING+ tumour cells to induce the expression of IFN-stimulated genes and ICD, thereby causing an indirect activation of DCs (286). Therefore, STING agonists can lead to DC activation and CD8 T-cell infiltration in NB tumours, representing a very attractive approach that could synergise with PD-1 blockade.

Although the preclinical 9464D model provides a useful tool to study multiple combinatorial approaches, the spontaneous TH-MYCN transgenic model might be better to study the potential translation of immunotherapeutic mAbs in NB. Weekly

therapy with anti-GD2 mAbs increased overall survival and delayed tumour growth to a larger extent than in the 9464D model, likely owing to the higher expression of GD2 in TH-MYCN compared to 9464D tumours (329). Besides, similar to human NB (232), TH-MYCN tumours demonstrated to be highly sensitive to CPM, where a single dose of 40 mg/kg in combination with either anti-GD2 or anti-PD-1 mAbs was sufficient to prevent tumour growth (Figure 5.29). Nevertheless, monotherapy with the three anti-PD-1 mAbs had no therapeutic effect on TH-MYCN tumours, which could be due to the lack of PD-1 expression on effector CD8 and CD4 TILs (Figure 5.31). These low levels could be indicative of poor activation due to low antigenicity, suggesting that prior administration of direct tumour-targeting or immunostimulatory therapies might be required. For instance, in the event of immune activation after CPM or anti-GD2 treatment, PD-1 might be up-regulated in effector CD8 T cells, thereby sensitising these tumours to PD-1 blockade. In agreement with this, dual therapy with anti-PD-1 and anti-GD2 mAbs seemed to extend survival of TH-MYCN tumour-bearing mice. However, dual combination of anti-PD-1 IgG1-N297A and a sub-curative low-dose of CPM (20 mg/kg) did not delay tumour growth (Figure 5.29). Combination of anti-GD2 mAbs with CPM (20 mg/kg) improved survival and could potentially be curative in approximately 50% of mice. Nevertheless, it was sill insufficient to achieve complete cures in all mice. Hence, together with increasing the number of TH-MYCN mice treated with dual therapies, it would be interesting to determine whether a triple combination with a single administration of 20 mg/kg CPM, anti-GD2 mAb and anti-PD-1 N297A could lead to better overall survival than dual schedules in the TH-MYCN model.

Chapter 6: Discussion and future work

6.1 Discussion

Despite its unequivocal success, anti-PD-1 mAb therapy is at best effective in only approximately 30% of patients within a responsive tumour type (111). There are many potential reasons contributing to the lack of activity in non-responsive tumours, such as low T-cell infiltration and presence of immunosuppressive cell types within the TME (359). In addition, interactions between the Fc region of anti-PD-1 mAbs and FcγRs could comprise another mechanism that hinders the therapeutic activity of these mAbs (104, 165). Clinically approved PD-1 blocking mAbs Nivolumab and Pembrolizumab were initially designed to block ligand binding with minimal engagement of FcγRs. As such, these mAbs were generated as human and humanised IgG4-S228P antibodies, respectively, based on the lower ability of this isotype to mediate ADCC (360). Nevertheless, in the form of ICs, IgG4 antibodies retain the ability to engage both activating and inhibitory FcγRs (93). This implies that anti-PD-1 mAbs may be able to engage FcγRs in vivo following binding and opsonisation of PD-1-expressing T cells at the TME. Here, we took advantage of three murine isotypes bearing clearly distinct FcγR binding patterns to investigate how Fc: FcγR interactions could modulate the activity of anti-PD-1 mAbs.

In summary, results indicated that the Fc-null anti-PD-1 mIgG1-N297A was the most effective mAb at enhancing OT-I (Figure 4.4) and endogenous T-cell responses to ovalbumin (Figure 4.10) when given in combination with low doses of anti-CD40 agonists. This engineered isotype was able to induce activation and expansion of OT-I and endogenous T cells with a high-affinity TCR for ovalbumin (Figure 4.4; Figure 4.11), but more importantly, it may also lead to a bystander activation and expansion of low-affinity T-cell clones (Figure 4.7; Figure 4.12). It is possible that the activation of Th1 responses and effector CD8 T cells by anti-CD40 and anti-PD-1 mAbs favoured the production of pro-inflammatory cytokines such as IFN-γ and IL-12 (162, 361), thereby activating other T-cell specificities and broadening the immune response. Considering that loss of TAA represents an important immune escape mechanism exploited by cancer cells, activation of multiple tumour-reactive T-cell clones might prove beneficial for the overall anti-tumour response.

In line with these findings, anti-PD-1 mIgG1-N297A significantly improved survival compared to controls in mice bearing MC38 tumours (Figure 4.13). Increased immune cell infiltration (Figure 4.17) and myeloid activation (Figure 4.24; Figure 4.25) by this anti-PD-1 mAb resulted in long-term anti-tumour immunity (Figure 4.14). Notably, anti-PD-1 mIgG1 also generated effective and memory anti-tumour responses, but the degree of phenotypic changes in tumour-infiltrating myeloid cells was less than the mIgG1-N297A engineered isotype. The disparity between the lack of T-cell expansion in OT-I transfers and the improvement in survival in the MC38 model by anti-PD-1 mIgG1 might be related to a differential myeloid activation in both settings. Whilst it would be important to confirm experimentally, it is likely that vaccination with Ova (which contains LPS) and anti-CD40 mAbs results in an up-regulation of activating FcγRs on myeloid subsets in peripheral lymphoid organs. This pro-inflammatory environment might favour effector mechanisms (122, 123) of anti-PD-1 mIgG1, despite its relatively low A/I ratio, leading to PD1+ T-cell depletion. In contrast, the highly immunosuppressive TME of MC38 tumours and the extensive expression of FcγRII (Figure 4.23) might limit the effector functions of this isotype in this context. Alongside this, anti-PD-1 mIgG2a completely abrogated the therapeutic activity of PD-1 blockade in MC38 (Figure 4.13). This isotype demonstrated the ability to trigger phagocytosis of activated, PD-1+ T cells in vitro (Figure 3.16); therapy with anti-PD-1 mIgG2a tended to reduce the percentage of OT-I T cells (Figure 4.4) and significantly decreased the percentage of PD-1+ TILs in MC38 tumours (Figure 4.18), suggesting that phagocytosis of PD-1+ TILs also occurred in vivo.

In parallel to the study of the optimal anti-PD-1 mAb for cancer immunotherapy, the aim of the current work was to investigate the potential application of anti-PD-1 mAbs for the treatment of neuroblastoma. Using the murine neuroblastoma model 9464D, which has similar immune infiltration to human NB (329), we found that monotherapy with anti-PD-1 mAbs had little effect on tumour growth or survival. Nevertheless, a similar trend to that seen in the MC38 model towards improved survival with anti-PD-1 mIgG1 and mIgG1-N297A was noted (Figure 5.10), suggesting that the Fc requirements for anti-PD-1 mAbs are the same in responsive (i.e MC38) and non-responsive (i.e 9464D) tumours. Moreover, similar phenotypic changes in TILs were seen across anti-PD-1 isotypes in 9464D tumours (Figure 5.13) compared to MC38 (Figure 4.18), indicating that these mAbs were still able to modulate T-cell responses in non-responsive tumours. This further highlighted that the limiting factor for the therapeutic activity of these mAbs might be the magnitude of the T-cell response, which likely depends on the overall immune

infiltration of the tumours. As such, MC38 tumours had a larger percentage of immune infiltration and higher CD8: Treg ratio (Figure 4.17; Figure 6.10) compared to 9464D tumours (Figure 5.12; Figure 6.21).

Taking into account the small, yet significant, increase in immune cell infiltration caused by mIgG1-N297A treatment in 9464D model, and the clear effect of this mAb in OT-I and MC38 models, anti-PD-1 mIgG1-N297A was taken forward as the optimal isotype to be included in combinatorial regiments for 9464D tumours. In the clinic, tumour-targeting mAbs against GD2 were approved as part of the maintenance therapy (189), and therefore offered an attractive agent to combine with anti-PD-1 mAbs. Anti-GD2 mAbs are believed to kill tumour cells by engaging activating FcγRs in NK and myeloid cells (266, 267, 270, 271); owing to the potential immune activation that these mAbs could trigger, it was hypothesised that T cells recruited to the TME following anti-GD2 mAb therapy could be further boosted by anti-PD-1 mAbs (231, 349). However, in the schedules investigated herein, dual mAb therapy was insufficient to stop growth of 9464D tumours (Figure 5.20; Figure 5.27). As highlighted from the immune phenotyping experiments performed in 9464D-bearing mice, Tregs represented the same percentage of TILs as effector CD8 or CD4 T cells (Figure 5.12), which resulted in a low CD8: Treg ratio (Figure 6.21). Due to this large presence of Tregs within the 9464D TME, metronomic and low-dose CPM was included in the therapeutic regiment owing to the ability of this chemotherapy to reduce the frequency of intratumoural Tregs (340, 341). This triple combination approach also mirrored that of the MiNivAN trial (NCT02914405), which aims to improve long-term survival in patients with NB by combining Nivolumab, anti-GD2 mAbs and targeted molecular radiotherapy (131-I mIBG). Despite a triple combinatorial schedule being attempted, utilising anti-PD-1/GD2 mAbs and CPM, this did not show any therapeutic synergy (Figure 5.27), suggesting that alternative therapeutic approaches should be contemplated. In light of the low T-cell infiltration of 9464D tumours (Figure 5.12), immunostimulatory therapies that further boost immune activation and mobilisation might be required prior to checkpoint blockade in NB tumours.

It is important to remember that there is a range of cells within the TME that can participate in the interactions between PD-1 and PD-L1 (Figure 6.1). Together with PD-1, effector T cells have been reported to express PD-L1, which polarised PD-1+ macrophages towards an M2-like phenotype and inhibited neighbouring T cells (69). In agreement with this, tumour-derived factors such as TLR4, G-CSF or GM-CSF were shown to up-regulate PD-1 expression on myeloid cells, the ligation of

which inhibited their effector functions (43) and promoted the accumulation of MDSCs at the TME (44). In addition to myeloid and effector T cells, ligation of PD-1 on Tregs by PD-L1 was reported to participate in the induction and function of these cells (362). In fact, ligation of PD-1+ Tregs by PD-L1+ T cells led to a stronger suppression of cytokine secretion and proliferation of effector T cells than the direct ligation of PD-1 (363). As previously eluded to in section 5.7, it is not yet clear how PD-1 blockade can affect Treg function, either at the periphery or within the TME (170). Nevertheless, all these findings would argue in favour of blocking PD-1/ PD-L1 interactions within the TME to enhance effector T-cell and myeloid function, whilst reducing Treg suppression. Still, the relative frequency of these populations and their expression of PD-1/ PD-L1 might be a factor to consider when investigating differences between responsive and non-responsive tumours.

Despite being a powerful tool to study the FcγR involvement in PD-1 blockade in a preclinical setting, the engineered IgG1-N297A mAb might not be the optimal Fc-null variant in the human system. In previous studies, engineered human IgG1-N297A mAb showed no binding to low-affinity FcγRs in the form of ICs, but retained over 50% binding to the high-affinity receptor huFcγRI (331). Whilst human IgG4 cannot be engineered to present the N297A mutation, other mutations could be introduced to abrogate FcγR binding such as the human Fc-null variant IgG4-FALA (303). We therefore sought to study the translation of our findings into the human system by using huIgG4 and the engineered huIgG4-FALA anti-PD-1 isotypes in an in vitro proliferation assay (Figure 3.17), but further optimisation would be required to elucidate any differences between mAbs. Overall, and despite no direct translation of the N297A mutation into human IgG4, the engineered murine IgG1-N297A isotype utilised herein serves as an example of an engineered Fc-null mAb that can optimally block PD-1 without engaging FcγRs.

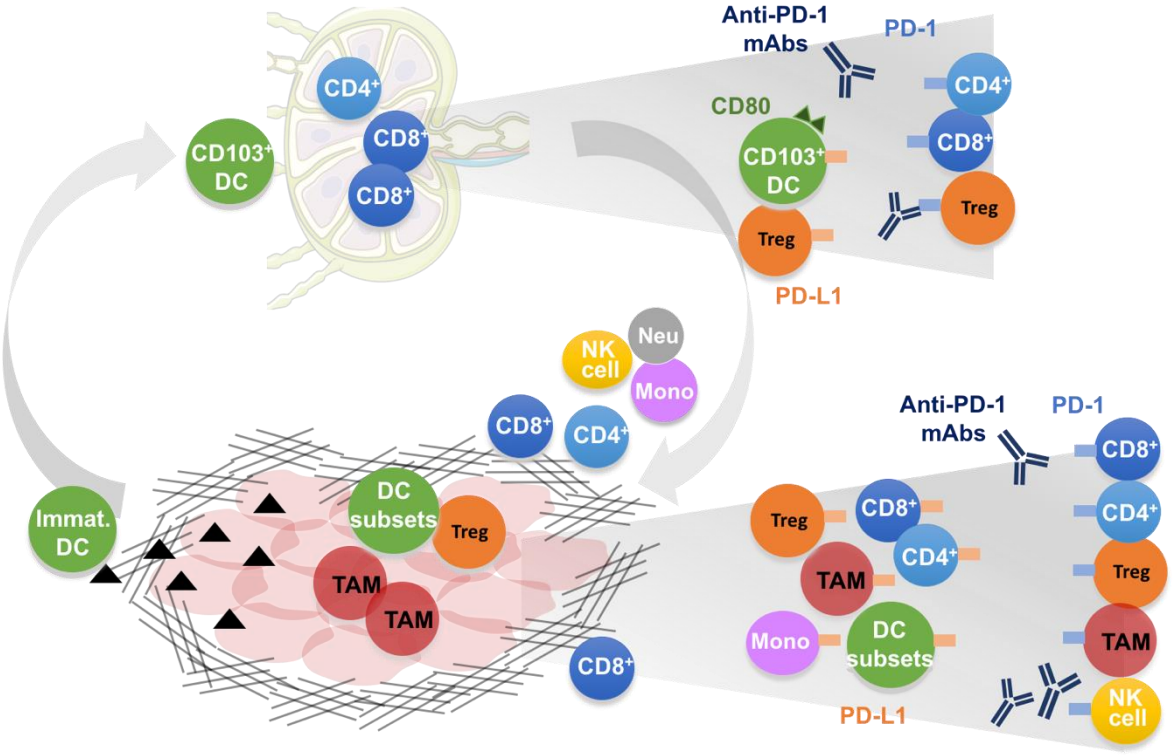

Figure 6.1 Complexity of PD-1: PD-L1 interactions in anti-tumour immunity. Following T-cell priming in lymph nodes, PD-1 is up-regulated on activated T cells and can hence engage its two ligands, PD-L1/2. During the early stage of the immune response, APCs and Tregs have been shown to express PD-L1. PD-1 up-regulation on T cells occurs shortly after T-cell activation, which suggests that PD-1-mediated inhibition could already occur at the priming phase. At the TME, both myeloid cells (macrophages, monocytes, DCs) and lymphocytes (CD8 and CD4 effectors, Tregs, NK cells) have been shown to express varying levels of PD-1. Expression of PD-L1 is also broad, being found on most immune cell types as well as tumour cells. Blockade of PD-1 is believed to act primarily by blocking its ligation on T cells, but recent studies highlight that this receptor also bears inhibitory function in myeloid cells and NK cells. The relative contribution of blocking PD-1 mediated inhibition in each cell type is not well defined, and will likely vary depending on the tumour type, frequency of different immune populations and prior therapeutic regimens. Nevertheless, it is important to consider all the possible PD-1: PD-L1 interactions within the TME to determine potential resistance mechanisms to anti-PD-1 therapy.

In conclusion, it has become clear that PD-1/ PD-L1 pathway and its therapeutic manipulation are more complex than that initially considered. Despite their success, the reasons behind the lack of therapeutic responses seen in certain cancers and patients are not yet well understood. Multiple layers of resistance to anti-PD-1 mAbs likely exist, and their relative dominance may depend on tumour type and microenvironment. As such, an immunologically cold tumour may offer a primary resistance due to the lack of antigenicity and T-cell infiltration. Successful combinatorial regimens that increase anti-tumour T-cell responses may also lead

to secondary resistance mechanisms that are likely shared with responsive tumour types. Some mechanisms are tumour-intrinsic, such as the loss of tumour antigens or acquired mutations that reduce sensitivity to immune cell killing; others may involve the expansion of immunosuppressive populations such as Tregs, thereby contributing to the overall tolerogenic polarisation of the TME; and in other cases, resistance might be related to the nature of the mAb isotype utilised and its engagement to FcγRs. Although the steps that lead to the former two groups of mechanisms are less known, thus making them more difficult to predict and tackle, engineering of anti-PD-1 mAbs into fully Fc-null isotypes could resolve the resistance associated to the Fc region of anti-PD-1 mAbs.

6.2 Future work

The key question remains of what impact FcγRII has on anti-PD-1 mAb therapy. Due to the different activity of anti-PD-1 mIgG1 in the OT-I and MC38 settings, it is possible that the overall relevance of engaging FcγRII depends on the relative expression of activating and inhibitory FcγRs. To explain the different activity in both systems, a first assessment of FcγR expression and A/I ratio in cells of the peripheral lymphoid organs could be performed in mice following anti-CD40 agonist plus ovalbumin therapy. This would enable the comparison of A/I ratios on both OT-I/ endogenous response and MC38 conditions. It is likely that myeloid cells display an activated phenotype following anti-CD40 agonist treatment with up-regulation of activating FcγR, which should be distinctive of the tumour-associated myeloid phenotype from MC38 tumours. In addition, an OT-I transfer experiment could be carried out in FcγRII$^{-/-}$ and γ-chain knock-out mice to confirm the impact of both types of FcγRs in anti-PD-1 mIgG1 compared to mIgG1-N297A therapy.

Considering the up-regulation of FcγRII under tolerogenic environments such as the TME, it is important to study all the potential mechanisms by which the interaction between anti-PD-1 mAbs and FcγRII could alter the therapeutic activity of these mAbs. As described in section 3.4 (see Chapter 3), we sought to test the hypothesis that PD-1 cross-linking by FcγRII engagement could trigger agonistic signals in activated T cells. To answer this, optimisation of both human and murine assays, as well the assessment of the phosphorylation status of intracellular mediators downstream the TCR and CD28 should be carried out.

Notably, anti-PD-1 mIgG1 led to reduced expression of PD-1 in vivo in both tumour models, but this was not associated with a decrease in overall number of TILs. The fact that a similar effect has been observed with CD25 and anti-CD25 rat IgG1 mAbs in another tumour model (309) suggests that these could be dependent on Fc: FcγRs interactions rather than the target molecule. Moreover, anti-PD-1 rat IgG2a mAbs were shown to be sequestered from the T-cell surface by FcγRII/III expressed on macrophages (324). Taking into consideration the well-described resistance mechanism of antibody trogocytosis or "shaving" (364, 365), it is conceivable that PD-1: anti-PD-1 mAb complexes could be trogocytosed from the T-cell surface following engagement with FcγRII/III on TAMs, thereby leading to loss of PD-1 expression. Alternatively, internalisation of mAbs in complex with their target molecule has been described for anti-CD20 mAbs, which would also lead to loss of PD-1 from the T-cell surface. To discern between these mechanisms, it would be interesting to label anti-PD-1 mIgG1 and mIgG1-N297A with AF-488 or 647 fluorochromes and perform quenching assays. These assays would provide a quantitative measurement of internalisation of labelled antibodies by utilising quenching anti-AF mAbs and determine the level of internalised fluorescence (366). Following this approach, previous studies in the group have been able to calculate the extent of receptor internalisation as well as the remaining CD20 molecules at the surface of anti-CD20-opsonised target cells following in vitro co-culture with macrophages, providing an indication of the degree of mAb shaving (367). Moreover, detection of anti-PD-1 labelled mAbs on macrophages could also be indicative of mAb sequestration by FcγRs on macrophages (364), which would further support the hypothesis of anti-PD-1 mAb mediated trogocytosis of PD-1.

In terms of anti-PD-1 mIgG2a, the ability of this mAb to trigger phagocytosis of activated T cells by macrophages was demonstrated in vitro. To further confirm the role of macrophage-mediated phagocytosis in the reduced therapeutic activity of this isotype in vivo, depletion of macrophages by liposome-encapsulated clodronate (368) or inhibition of phagocytosis by dynasore treatment (324) could be performed in the MC38 tumour model.

Finally, anti-PD-1 mAb therapy proved to be insufficient to generate effective anti-tumour responses in pre-clinical neuroblastoma models, either as a monotherapy or in combination with direct tumour-targeting anti-GD2 mAbs. Triple combination with atni-PD-1, anti-GD2 and CPM increased survival in 9464D tumours, but this was largely a result of the therapeutic effect that weekly CPM had on its own. Further optimisation of this triple combination could be attempted, perhaps by

increasing the number of doses of anti-GD2 mAb given at the start of the schedule, and by using single doses of CPM to limit its therapeutic effect as a monotherapy. Besides, this triple combination should be tested in TH-MYCN mice, as these tumours have higher expression of GD2 and hence might be more sensitive to the triple schedule. Alternatively, immunostimulatory therapies targeting myeloid cells, such as STING agonists or anti-CD40 mAbs, could help to establish a more pro-inflammatory TME and induce recruitment of effector T cells at the tumour site, the inhibition of which could in turn be blocked by therapy with anti-PD-1 mAbs. Overall, a more efficacious approach is needed in 9464D tumours to then confirm the role of anti-PD-1 isotype in the anti-tumour immunity against neuroblastoma. Nevertheless, considering the superior activity that anti-PD-1 mIgG1-N297A demonstrated in both OT-I/ endogenous response to ovalbumin and MC38 models, and the similar phenotypic changes induced in TILs in MC38 and 9464D models, it is predicted that an engineered Fc-null anti-PD-1 isotype will be the optimal mAb to enhance anti-tumour immunity in both responsive and non-responsive tumours.

Appendices

Appendix A

A.1 OT-I response after therapy with parental anti-PD-1 rat IgG1

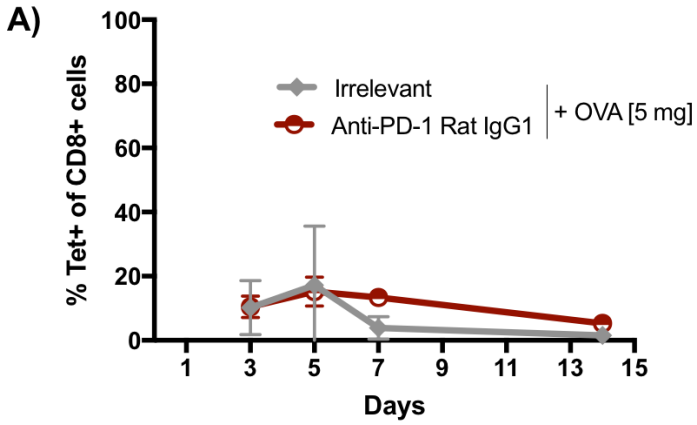

Figure 6.2 OT-I expansion following anti-PD-1 monotherapy.
A) Kinetics of OT-I expansion represented as tetramer+ CD8 T cells as a percentage of total CD8 T cells. A baseline dose of 5 mg ovalbumin was given in combination with 250 µg of irrelevant isotype (JG1.1A rat IgG1) or anti-PD-1 rat IgG1. Experiment performed once, N=4 mice per group. Bars represent mean ± S.D, (One-way ANOVA).

A.2 OT-I memory response

A.2.1 T-cell phenotype during memory responses

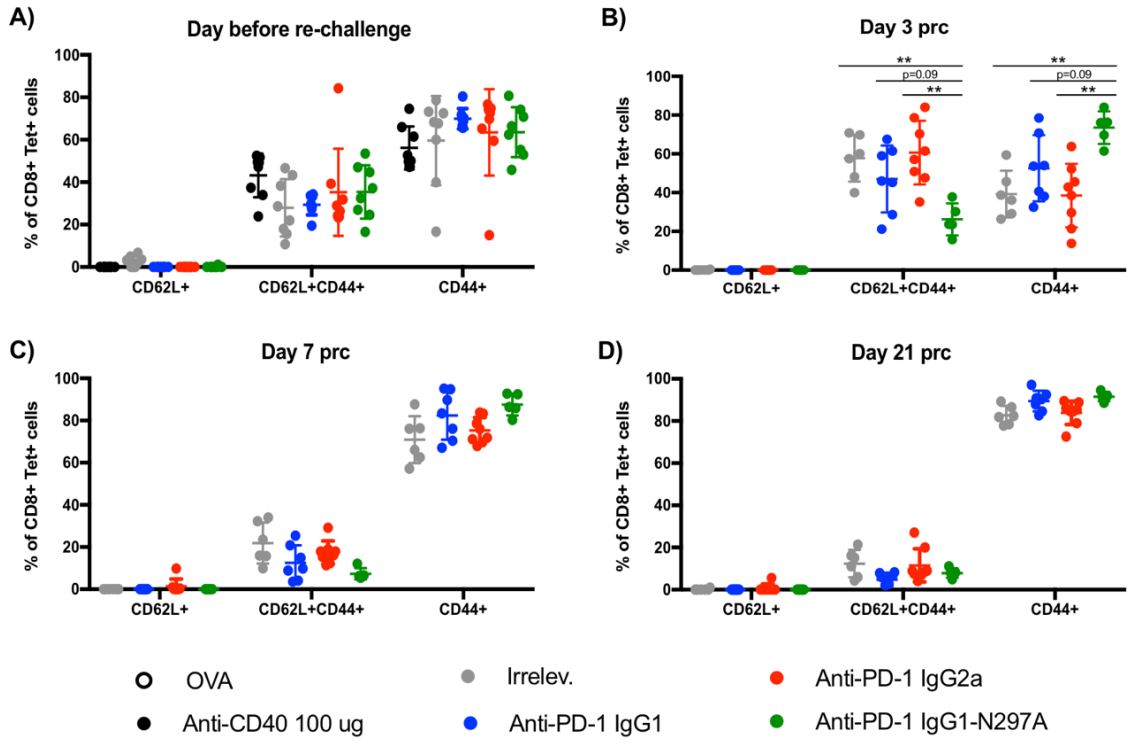

Figure 6.3 Phenotype of Tet+ OT-I T cells during the memory response. Graphs represent the percentage of naïve (CD62L+), effector (CD44+) and central memory (CD62L+CD44+) T cells within Tet+ CD8 T cells the day prior to the re-challenge (A) or on days 3 (B), 7 (C) and 21 (D) after re-challenge. Experiment performed twice, N=8 (A) or N=4-7 (B-D) mice per group. None of the mice treated with 100 µg of anti-CD40 mAb were able to be re-challenged due to persistent high levels of OT-I T cells. Bars represent mean ± S.D, **p<0.01, *p<0.5 (One-way ANOVA).

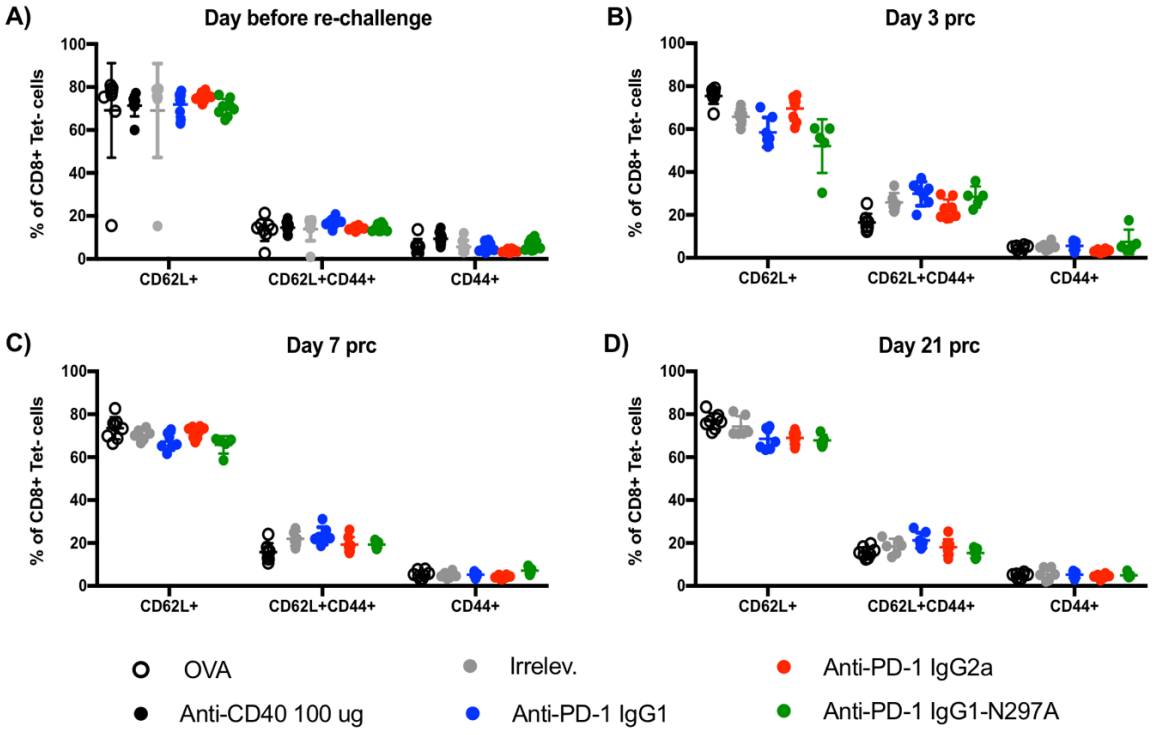

Figure 6.4 Phenotype of tetramer negative CD8 T cells during the memory response.
Graphs represent the percentage of naïve (CD62L+), effector (CD44+) and central memory (CD62L+CD44+) T cells within tetramer negative CD8 T cells the day prior to the re-challenge (A) or on days 3 (B), 7 (C) and 21 (D) after re-challenge. Experiment performed twice, N=8 (A) or N=4-7 (B-D) mice per group. None of the mice treated with 100 µg of anti-CD40 mAb were able to be re-challenged due to persistent high levels of OT-I T cells. Bars represent mean ± S.D.

A.3 Endogenous response

A.3.1 T-cell phenotype during the primary response

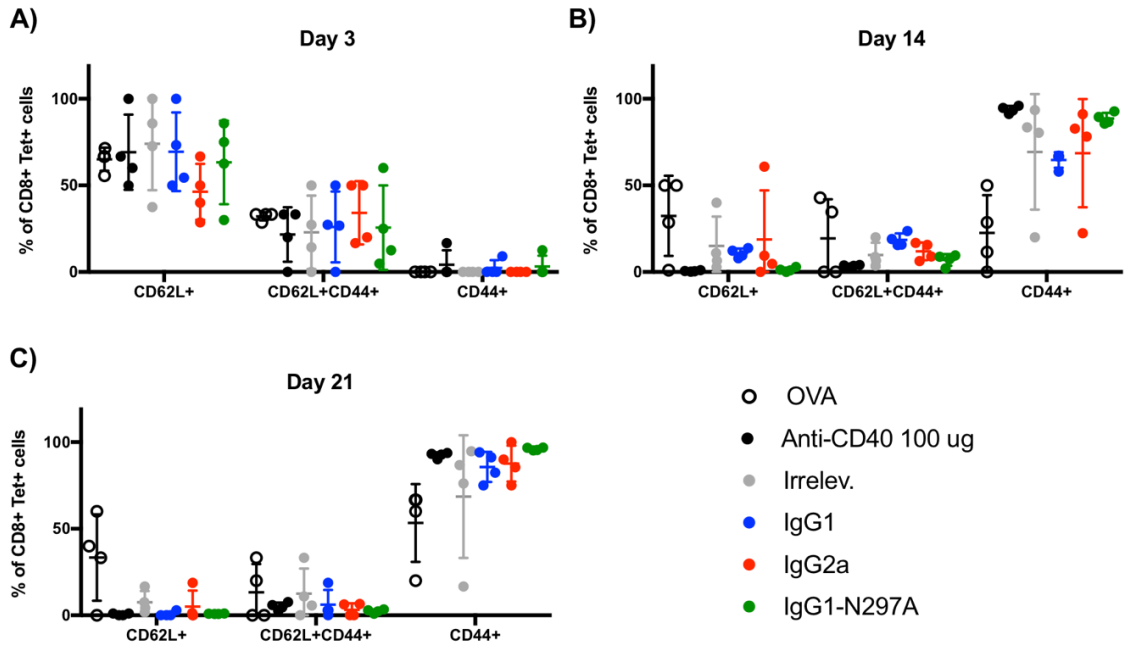

Figure 6.5 Phenotype of Tet+ CD8 T cells during an endogenous response to ovalbumin plus anti-PD-1 mAbs.
Graphs represent the percentage of naïve (CD62L+), effector (CD44+) and central memory (CD62L+CD44+) T cells within Tet+ CD8 T cells during the primary response on day 3 (A), day 14 (B) and day 21 (C). Mice were challenged with 5 mg of OVA alone or in combination with 100 µg of anti-CD40 mAb; 10 µg of anti-CD40 mAb or 10 µg of anti-CD40 mAb plus 250 µg of anti-PD-1 isotypes. Experiment performed once, N=4 mice per group. Bars represent mean ± S.D, p=n.s (One-way ANOVA).

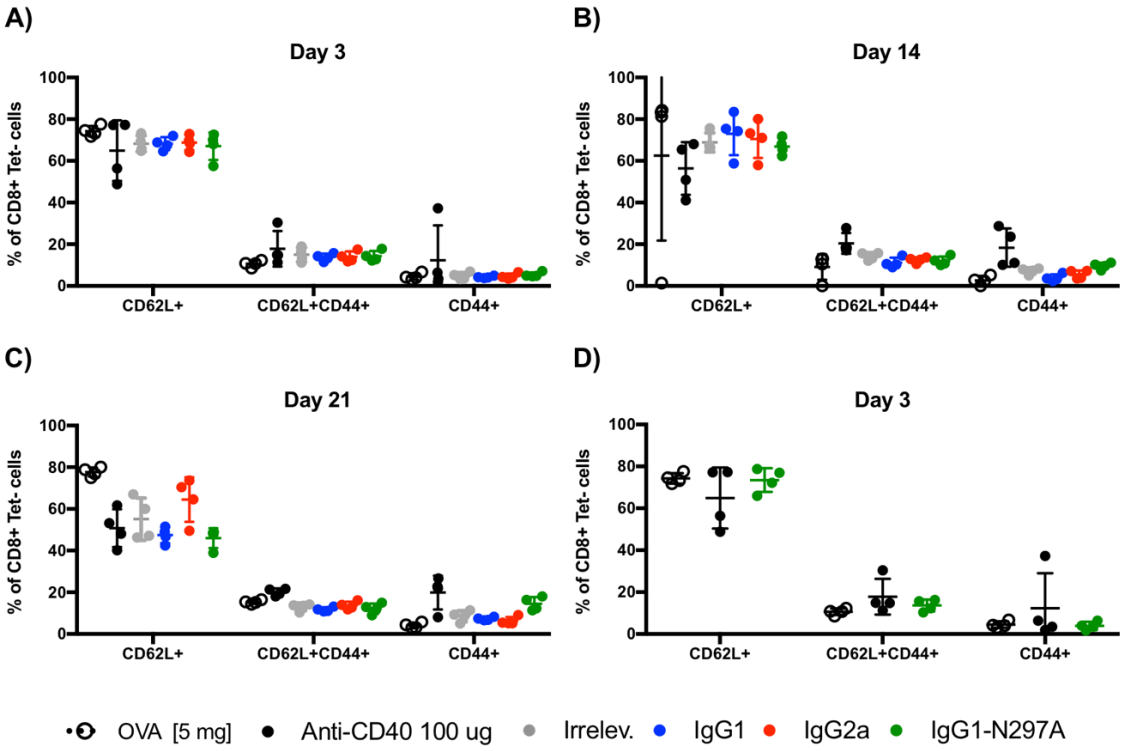

Figure 6.6 Phenotype of tetramer negative CD8 T cells during an endogenous response to ovalbumin plus anti-PD-1 mAbs.
Graphs represent the percentage of naïve (CD62L+), effector (CD44+) and central memory (CD62L+CD44+) T cells within Tet negative CD8 T cells during the primary response to ovalbumin. Mice were challenged with 5 mg of OVA alone or in combination with 100 µg of anti-CD40 mAb; 10 µg of anti-CD40 mAb or 10 µg of anti-CD40 mAb plus 250 µg of anti-PD-1 isotypes (A-C). Alternatively, mice were challenged with 5 mg of OVA alone or in combination with 100 µg of anti-CD40 mAb plus 250 µg of irrelevant mAb or anti-PD-1 mIgG1-N297A (D). Experiment performed once, N=4 mice per group. Bars represent mean ± S.D, p=n.s (One-way ANOVA).

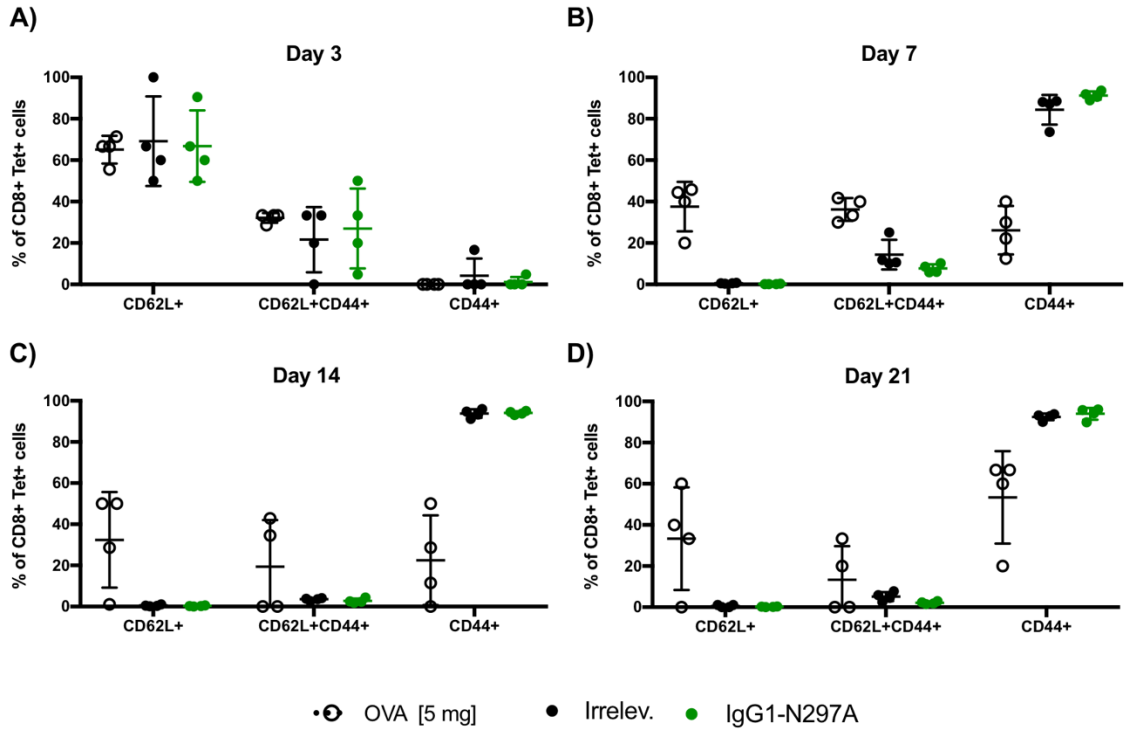

Figure 6.7 Phenotype of Tet+ CD8 T cells during an endogenous response to ovalbumin plus anti-PD-1 mIgG1-N297A.
Graphs represent the percentage of naïve (CD62L+), effector (CD44+) and central memory (CD62L+CD44+) T cells within Tet+ CD8 T cells during the primary response on days 3 (A), 7 (B), 14 (C) and 21 (D) after challenge. Mice were challenged with 5 mg of OVA alone or in combination with 100 µg of anti-CD40 mAb plus 250 µg of irrelevant mAb or anti-PD-1 mIgG1-N297A. Experiment performed once, N=4 mice per group. Bars represent mean ± S.D.

A.3.2 Memory responses after re-challenge

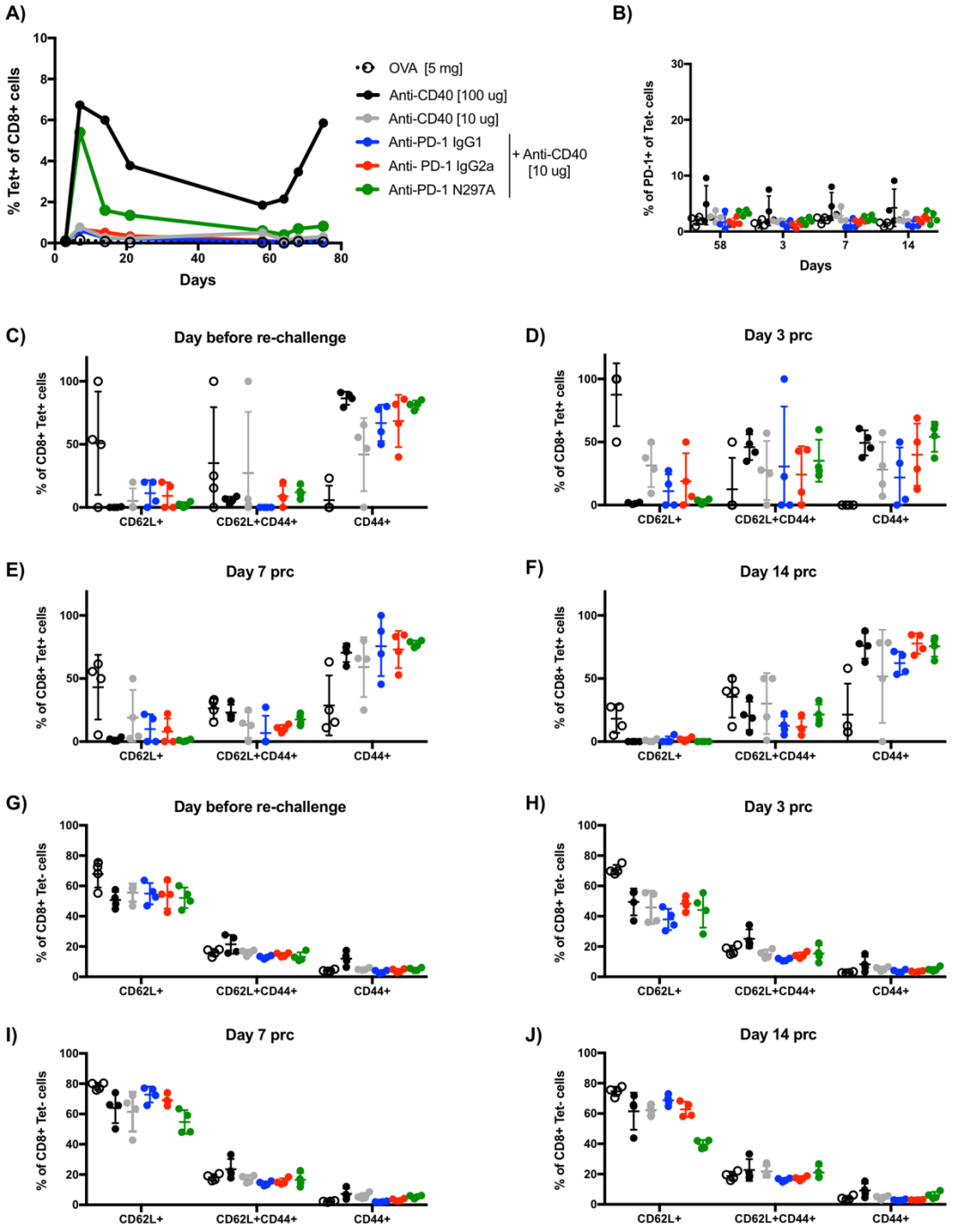

Figure 6.8 Endogenous response after re-challenge with SIINFEKL peptide. A) Kinetics of the endogenous response represented as percentage of Tet+ CD8 amongst all CD8 T cells at each time point. Re-challenged was performed with 30 nM SIINFEKL peptide IV on day 59 after initial challenge. Tail bleeds were carried out on the day before re-challenge and days 3, 7 and 14 after re-challenge. Due to the lack of T-cell expansion on anti-PD-1 mAb groups, the study was terminated on day 14 after re-challenge. B) Expression of PD-1 on Tet negative CD8 T cells shown as percentage of positive cells. Due to the lack of Tet+ expansion, expression of PD-1 in this subset could not be obtained accurately. C-J) Phenotype of Tet+ (C-F) and Tet negative (G-J) CD8 T cells prior to re-challenge (C,G) and on day 3 (D,H), day 7 (E,I) or day 14 (F,J) after re-challenge. Graphs represent the percentage of naïve (CD62L+), effector (CD44+) and central memory (CD62L+CD44+) T cells. Experiment performed once, N=4 mice per group. Bars represent mean ± S.D.

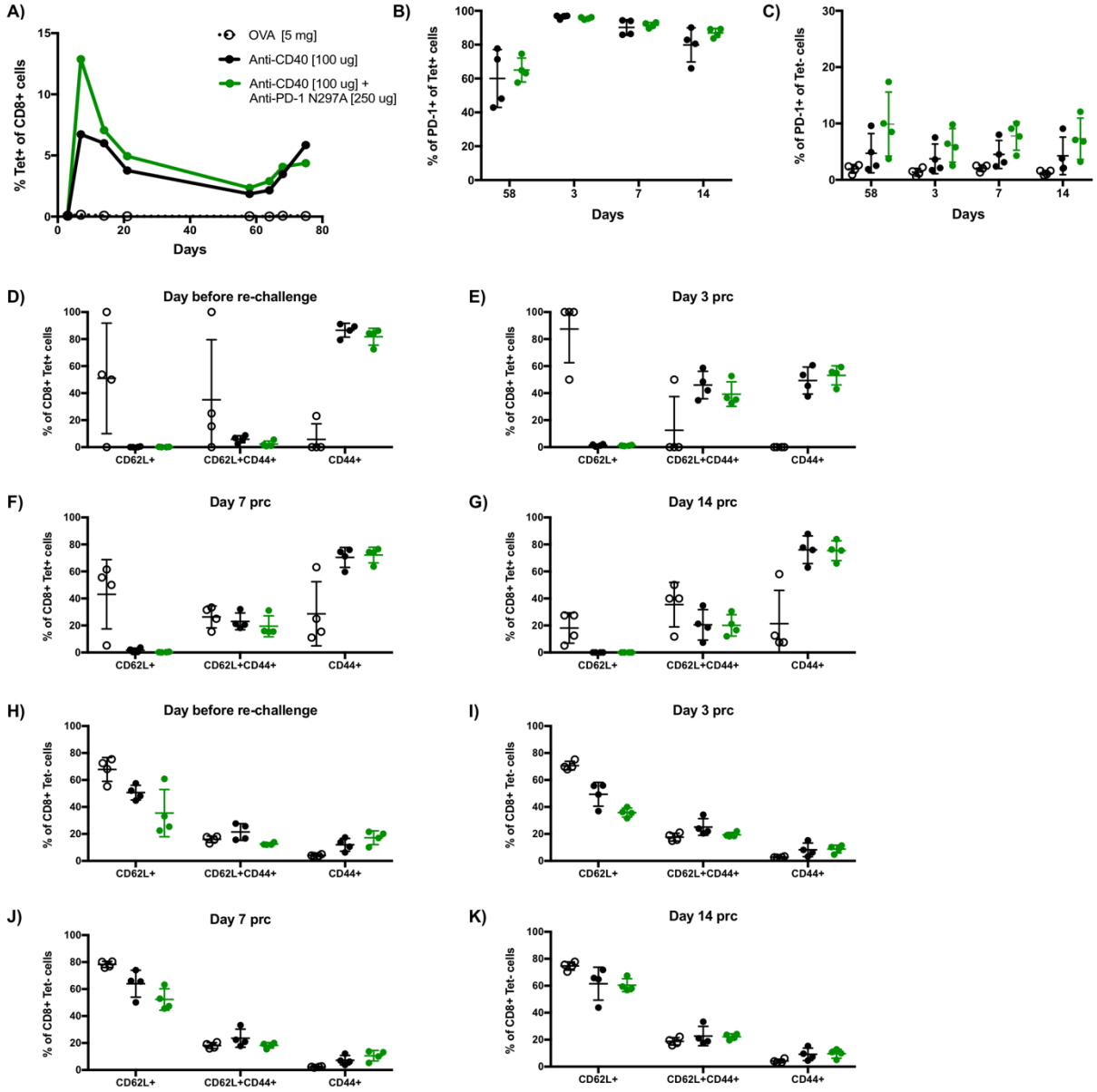

Figure 6.9 Enhancement of endogenous memory response after re-challenge with SIINFEKL peptide by anti-PD-1 mIgG1-N297A.

A) Kinetics of the endogenous response represented as percentage of Tet+ CD8 amongst all CD8 T cells at each time point. Re-challenged was performed with 30 nM SIINFEKL peptide IV on day 59 after initial challenge. Tail bleeds were carried out on the day before re-challenge and days 3, 7 and 14 after re-challenge. Due to the lack of T-cell expansion on anti-PD-1 mAb groups, the study was terminated on day 14 after re-challenge. B-C) Expression of PD-1 on Tet+ (B) and Tet negative (C) CD8 T cells shown as percentage of positive cells. Due to the lack of Tet+ expansion in OVA group, expression of PD-1 in this subset is not shown. D-K) Phenotype of Tet+ (D-G) and Tet negative (H-K) CD8 T cells prior to re-challenge (D,H) and on day 3 (E,I), day 7 (F,J) or day 14 (G,K) after re-challenge. Graphs represent the percentage of naïve (CD62L+), effector (CD44+) and central memory (CD62L+CD44+) T cells. Experiment performed once, N=4 mice per group. Bars represent mean ± S.D.

A.4 Immunophenotyping of MC38 tumours

A.4.1 Raw CD8: Treg ratio in tumour and spleen of MC38-bearing mice

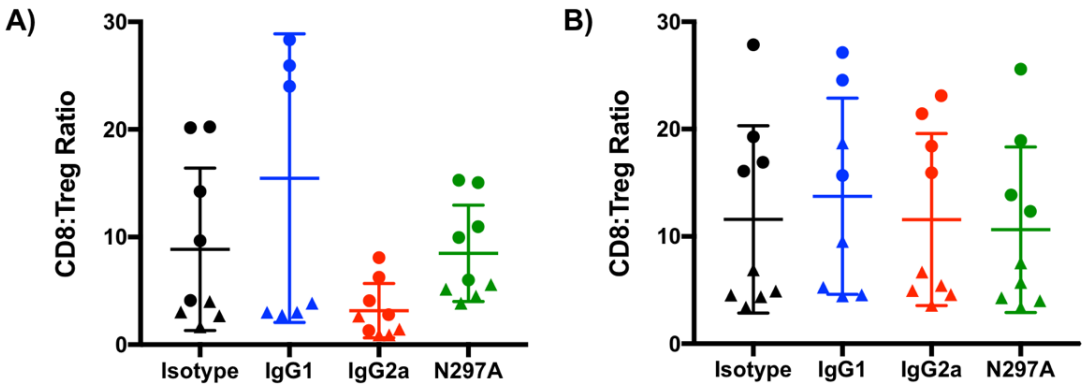

Figure 6.10 CD8: Treg ratio (raw numbers).
C57BL/6 mice were subcutaneously inoculated with $5x10^5$ MC38 cells. When tumours reached 7x7 mm, mice received 3 Ip doses of 200 µg of irrelevant mAbs (AT10 mIgG1, mIgG2a and mIgG1-N297A) or anti-PD-1 mIgG1, mIgG2a and mIgG1-N297A mAbs. Tumours and spleens were harvested 24h after the last dose and processed for flow cytometry (see sections 2.7.5 and 2.8). A-B) Raw CD8: Treg ratios in tumour (A) and spleen (B) were obtained by dividing the percentage of CD8 T cells by the percentage of Tregs per each individual mouse. Experiment performed twice, N=8-9 mice per group. Triangles correspond to the first experiment whilst circles correspond to the second. Bars represent mean ± S.D, (One-way ANOVA).

A.4.2 Tumour-infiltrating myeloid populations in of MC38-bearing mice

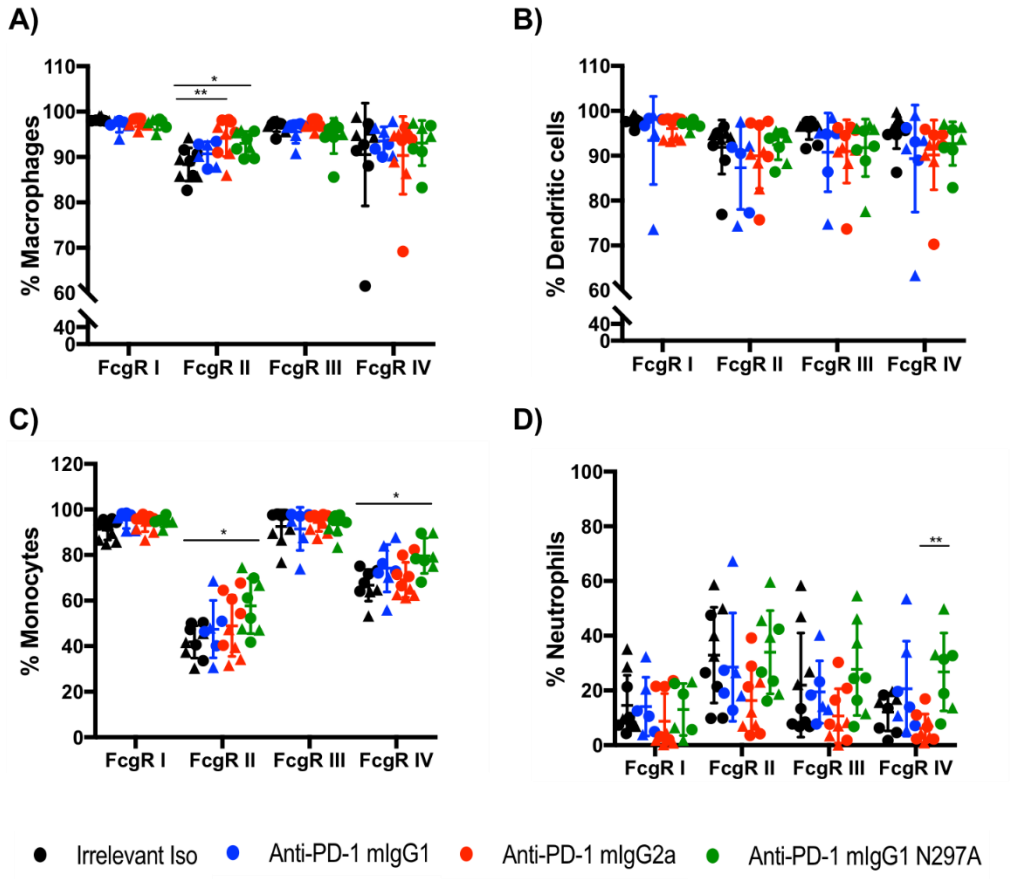

Figure 6.11 Tumour-infiltrating myeloid populations after therapy with murine anti-PD-1 isotypes: FcγR expression (2).
Expression of FcγRs (I, II, III and IV) on tumour-infiltrating macrophages (A), DCs (B), monocytes (C) and neutrophils (D) shown as percentage of positive cells. Experiment performed twice, N=8-9 mice per group. Triangles correspond to the first experiment whilst circles correspond to the second replicate. Bars represent mean ± S.D, *p<0.05, **p<0.01 (One-way ANOVA).

A.4.3 Myeloid populations in spleen of MC38-bearing mice

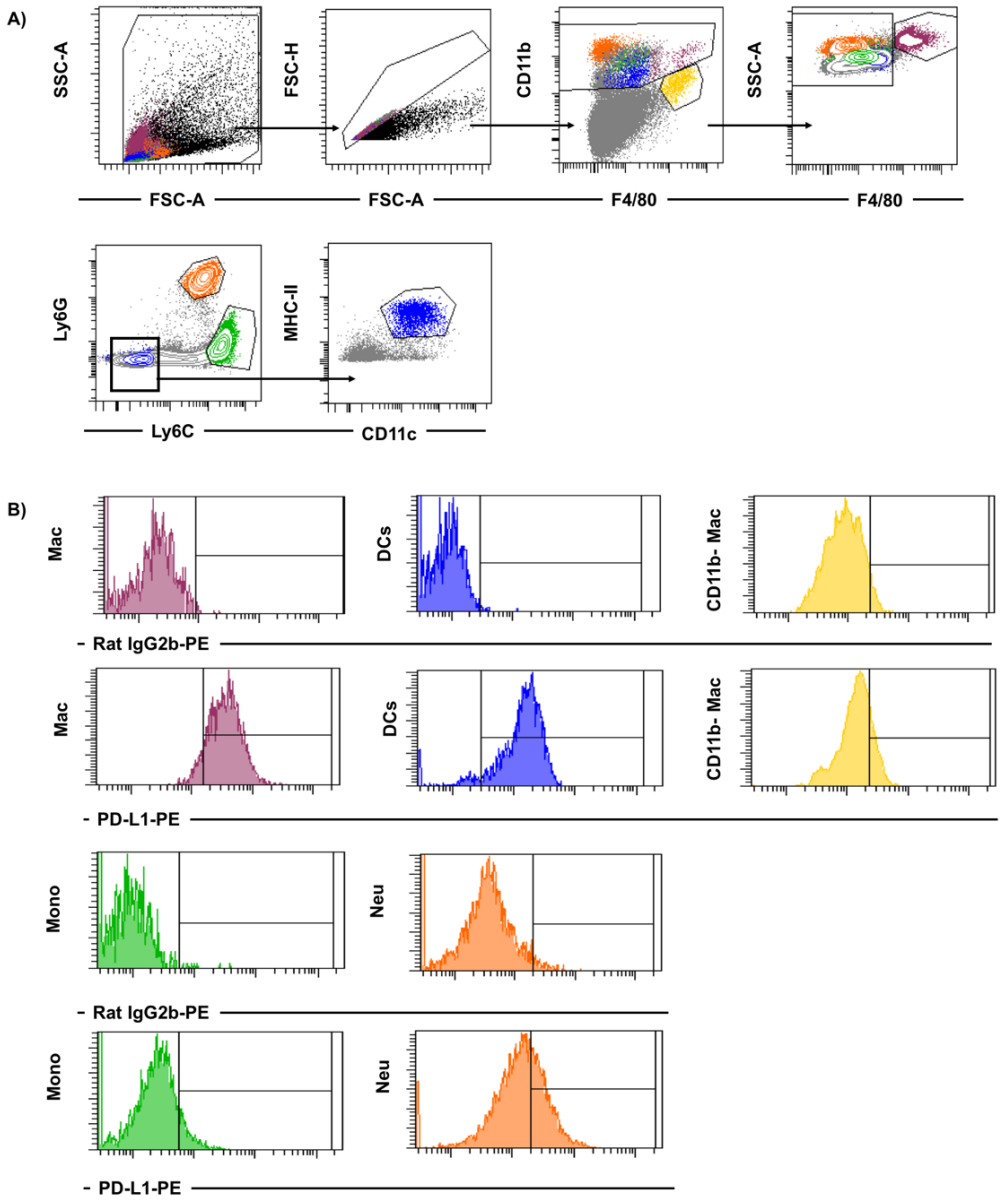

Figure 6.12 Gating strategy: Myeloid populations in spleen of MC38-bearing mice.
Spleens were mechanically digested as detailed in 2.7.5, and single cell suspensions were obtained. Typically, 10^6 cells were stained with surface and intracellular markers (see 2.8) and samples were run on flow cytometry. A) Following doublets exclusion, live cells were gated according to CD11b and F4/80 expression. Monocyte-derived macrophages were gated as F4/80 high and CD11b high, whilst tissue-resident, non-inflammatory macrophages were gated as CD11b low and F4/80 high. Neutrophils, monocytes and DCs were gated from the CD11b high, F4/80 low population according to the expression of Ly6C, Ly6C, CD11c and MHC-II markers. Ly6C high and Ly6G high cells were gated as neutrophils, whilst Ly6Clow, Ly6G high were gated as monocytes. Gate for DCs was set as MHC-II high, CD11c high. B) Examples of histograms showing the expression of PD-L1 on macrophages (purple); DCs (blue); CD11b- macrophages (yellow); monocytes (green); and neutrophils (orange). Gates were set with an isotype control and subtracted to the sample values. This strategy was followed for all markers assessed.

Appendix A

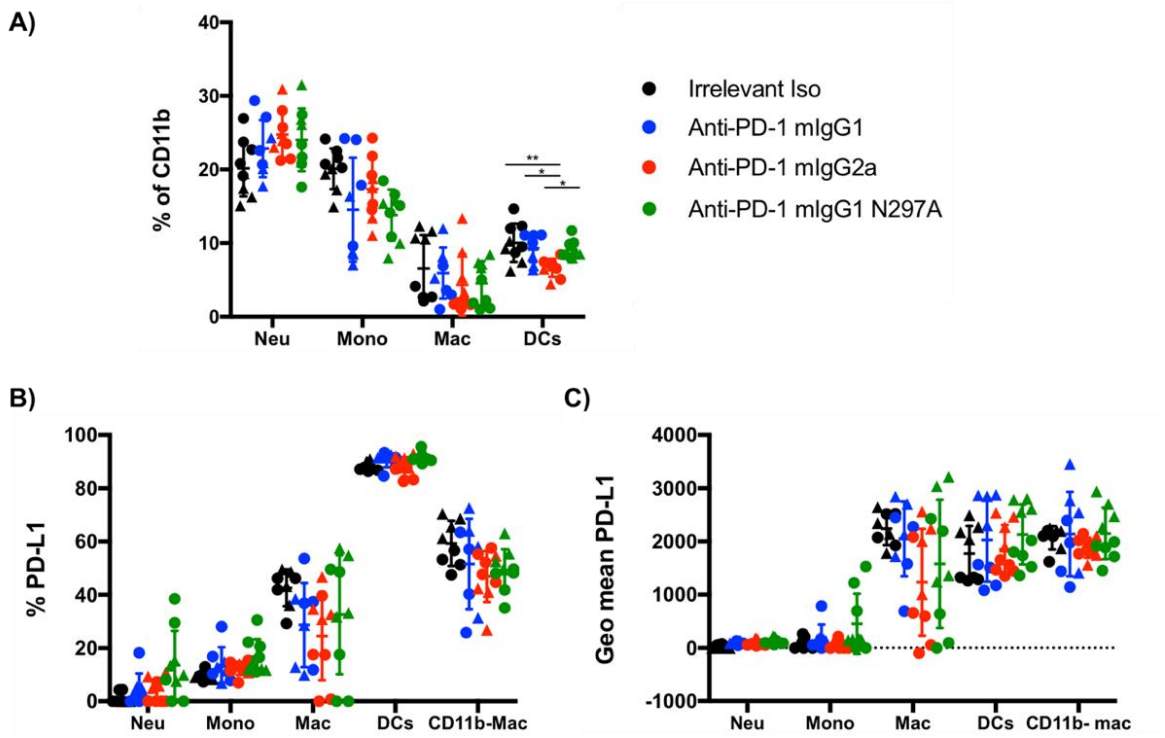

Figure 6.13 CD11b+ cells in spleens of MC38-bearing mice after therapy with murine anti-PD-1 isotypes: PD-L1 expression.
A) Percentage of myeloid populations out of CD11b+ gate in spleen. B-C) Expression of PD-L1 on myeloid populations shown as percentage of positive cells (B) or as MFI (C). Experiment performed twice, N=8-9 mice per group. Triangles correspond to the first experiment whilst circles correspond to the second replicate. Bars represent mean ± S.D, *p<0.05, **p<0.01 (One-way ANOVA).

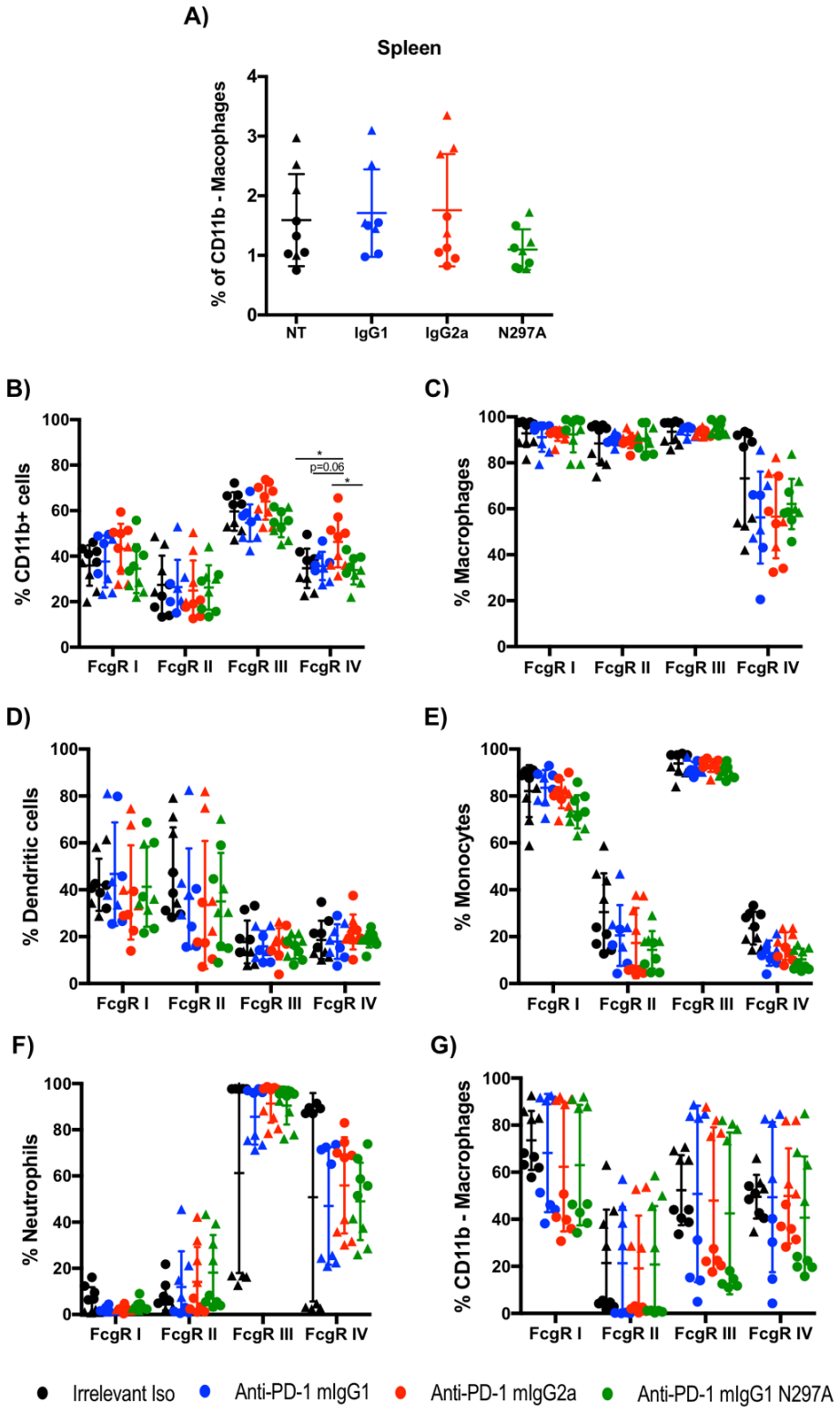

Figure 6.14 Myeloid cells in spleens of MC38-bearing mice after therapy with murine anti-PD-1 isotypes: FcγRs expression.
A) Percentage of CD11b low macrophages out of the singlet gate. B-G) Expression of FcγRs (I, II, III and IV) on myeloid infiltrates: CD11b+ cells (B), macrophages (C), DCs (D), monocytes (E), neutrophils (F) and CD11b negative macrophages (G) shown as percentage of positive cells. Experiment performed twice, N=8-9 mice per group. Triangles correspond to the first experiment whilst circles correspond to the second replicate. Bars represent mean ± S.D, *p<0.05 (One-way ANOVA).

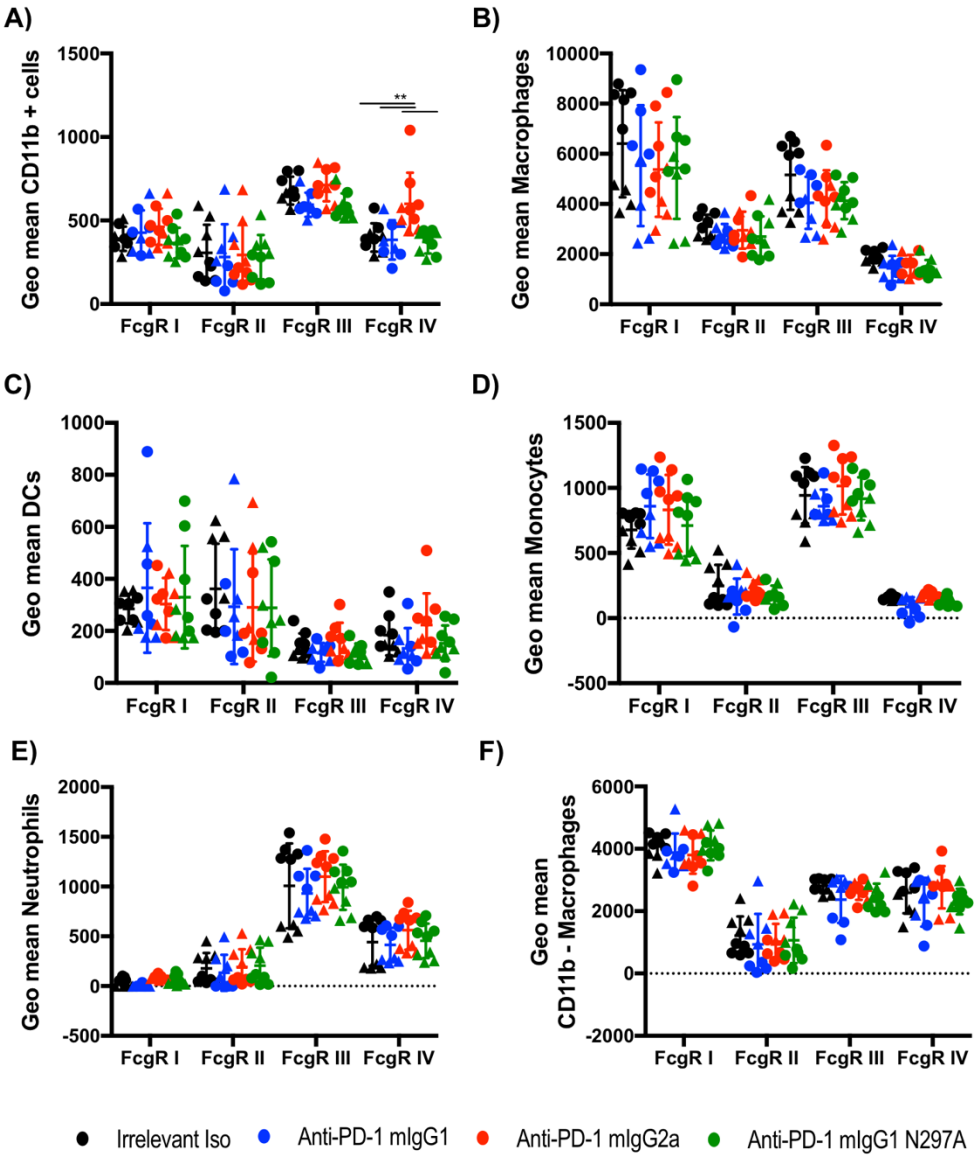

Figure 6.15 Myeloid cells in spleens of MC38-bearing mice after therapy with murine anti-PD-1 isotypes: FcγRs expression (2).
A-F) Expression of FcγRs (I, II, III and IV) on myeloid infiltrates: CD11b+ cells (A), macrophages (B), DCs (C), monocytes (D), neutrophils (E) and CD11b low macrophages (F) shown as MFI. Experiment performed twice, N=8-9 mice per group. Triangles correspond to the first experiment whilst circles correspond to the second replicate. Bars represent mean ± S.D, **p<0.01 (One-way ANOVA).

Appendix B

B.1 Kinetics of expression of immune markers in 9464D TILs

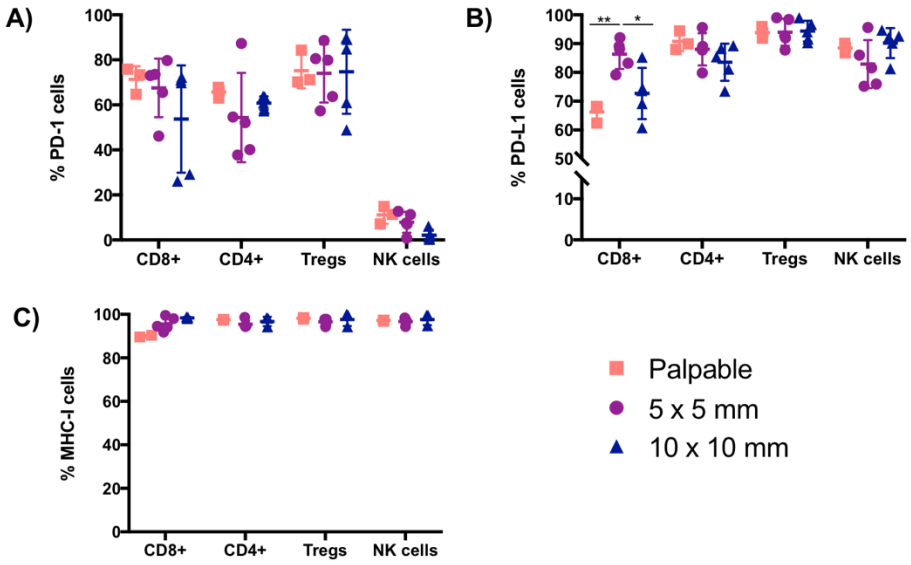

Figure 6.16 Kinetics of PD-1, PD-L1, MHC-I and GD2 expression (as %) in 9464D tumours.
A-C) Expression of PD-1 (A), PD-L1 (B) and MHC-I (C) by TILs and NK cells shown as percentage of the population. Experiment performed twice, N=3 or N=5 mice per group at palpable size or 5x5/10x10 mm, respectively. Bars represent mean ± S.D, *p<0.05, **p<0.01, (One-way ANOVA).

B.2 Immunophenotyping of 9464D tumours after therapy with rat IgG1 or deglycosylated anti-PD-1 mAbs

B.2.1 Phenotype of TILs in 9464D-bearing mice

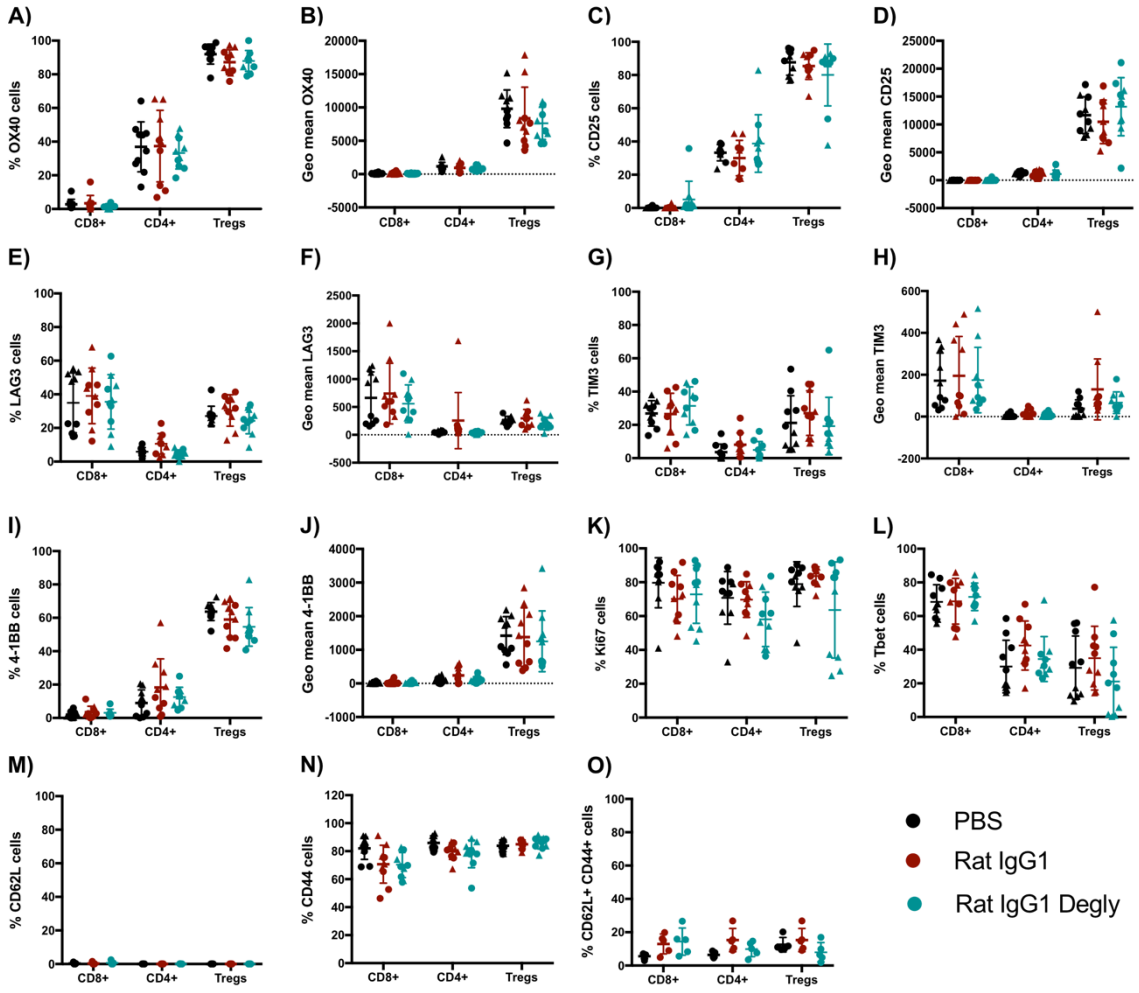

Figure 6.17 Phenotype of 9464D TILs 3 days after therapy with anti-PD-1 rat IgG1 or degly.
A-J) Expression of T-cell markers shown as percentage of positive cells or as MFI: OX40 (A-B), CD25 (C-D), LAG3 (E-F), TIM-3 (G-H), 4-1BB (I-J). K-L) Percentage of positive cells for the proliferation marker Ki67 (K) and the transcription factor Tbet (L). M-O) Percentage of naïve (M), effector (N) and central memory (O) TILs. Experiment performed twice, N=10 mice per group. Triangles correspond to the first experiment whilst circles correspond to the second replicate. Bars represent mean ± S.D.

B.2.2 Lymphocyte populations in spleen of 9464D-bearing mice

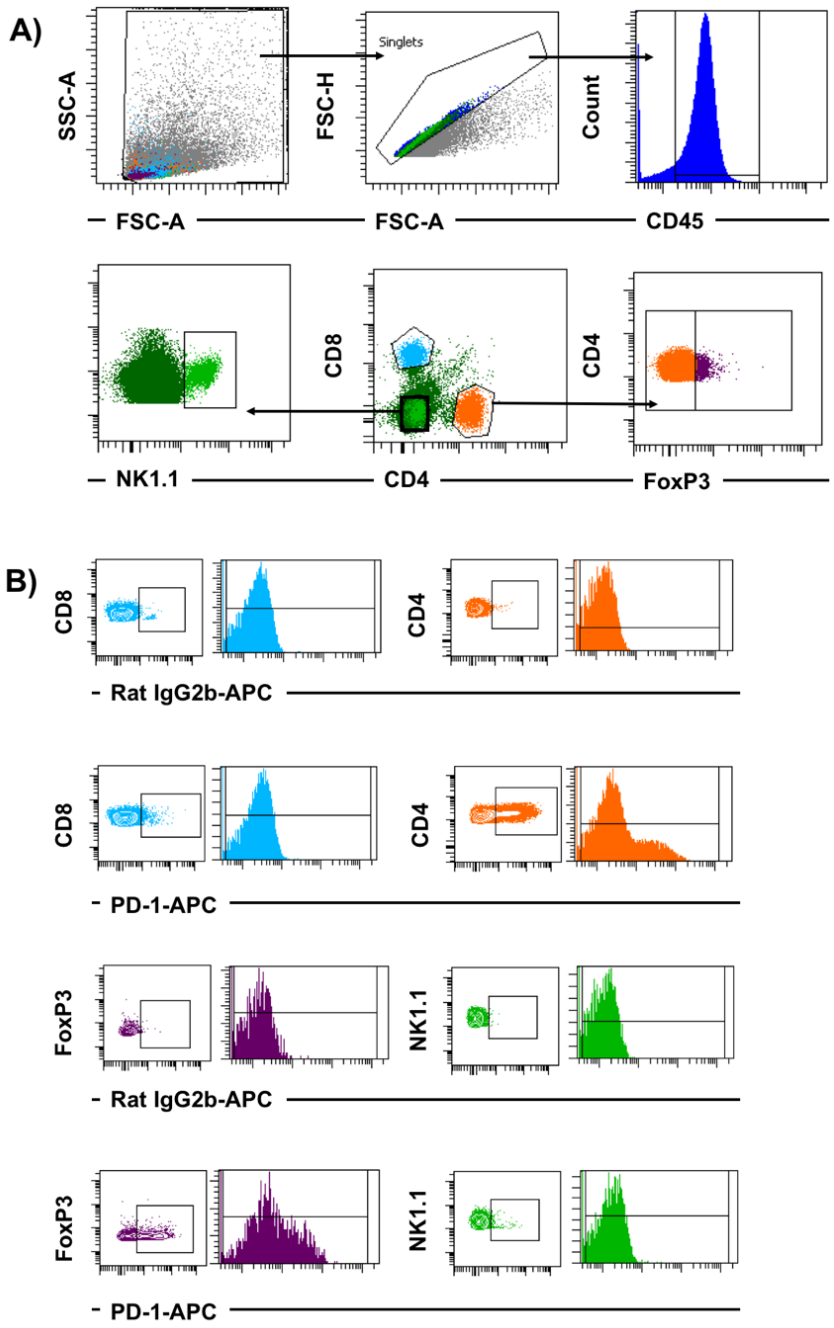

Figure 6.18 Gating strategy: T cells in spleen of 9464D-bearing mice.
Spleens were mechanically digested as detailed in 2.7.5, and single cell suspensions were obtained. Typically, 10^6 cells were stained with surface and intracellular markers (see 2.8) and samples were run on flow cytometryA) Gating of T-cell populations. From all live cells (FSC-A–SSC-A), doublets were excluded and immune cells were gated according to their CD45 expression. Effector CD8 T cells, effector CD4 T cells (FoxP3-CD4+), Tregs (FoxP3+CD4+) and NK cells (CD8-CD4-CD3+NK1.1+) were gated from CD45+ cells. B) Dot plots and histograms for each lymphocyte population showing the expression of PD-1. Positive cells were gated according to an isotype control. Geometric mean of the whole population was calculated from the histogram plots, and isotype control values were subtracted. This strategy was followed for all markers assessed.

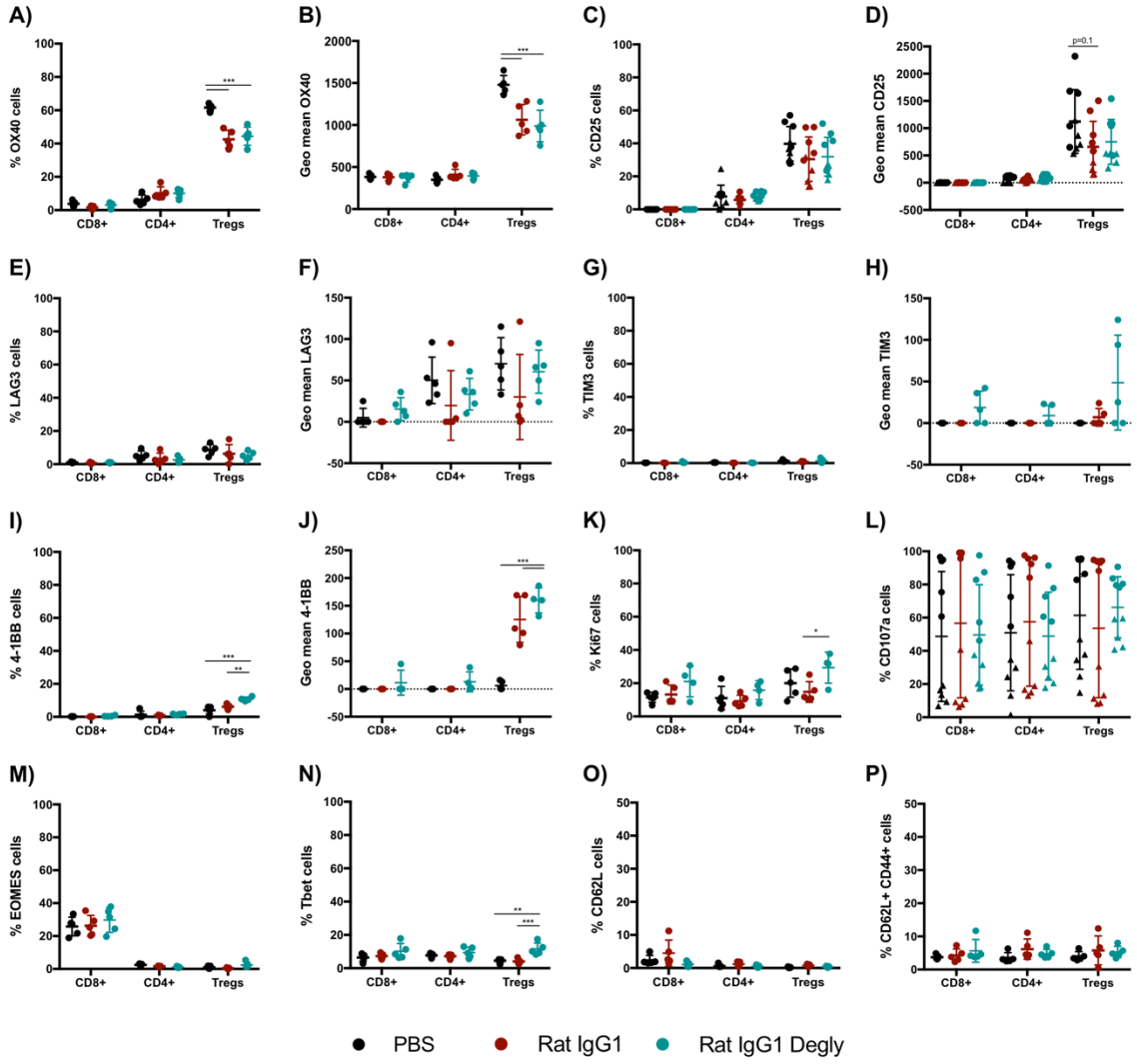

Figure 6.19 Phenotype of T cells in spleen of 9464D-bearing mice 3 days after therapy with anti-PD-1 rat IgG1 or degly..
A-J) Expression of T-cell markers shown as percentage of positive cells or as MFI: OX40 (A-B), CD25 (C-D), LAG3 (E-F), TIM-3 (G-H), 4-1BB (I-J). K-N) Percentage of positive cells for the proliferation marker Ki67 (K), the degranulation marker CD107a (L) and the transcription factors EOMES (M) and Tbet (N). O-P) Percentage of naïve (O) and central memory (P) T cells. Experiment performed twice, N=10 mice per group for CD25 and CD107a. Triangles correspond to the first experiment whilst circles correspond to the second replicate. Experiment performed once for the rest of markers, N=5 mice per group. Bars represent mean ± S.D, **p<0.01, ***p<0.001 (One-way ANOVA).

B.2.3 Myeloid populations in spleen of 9464D-bearing mice

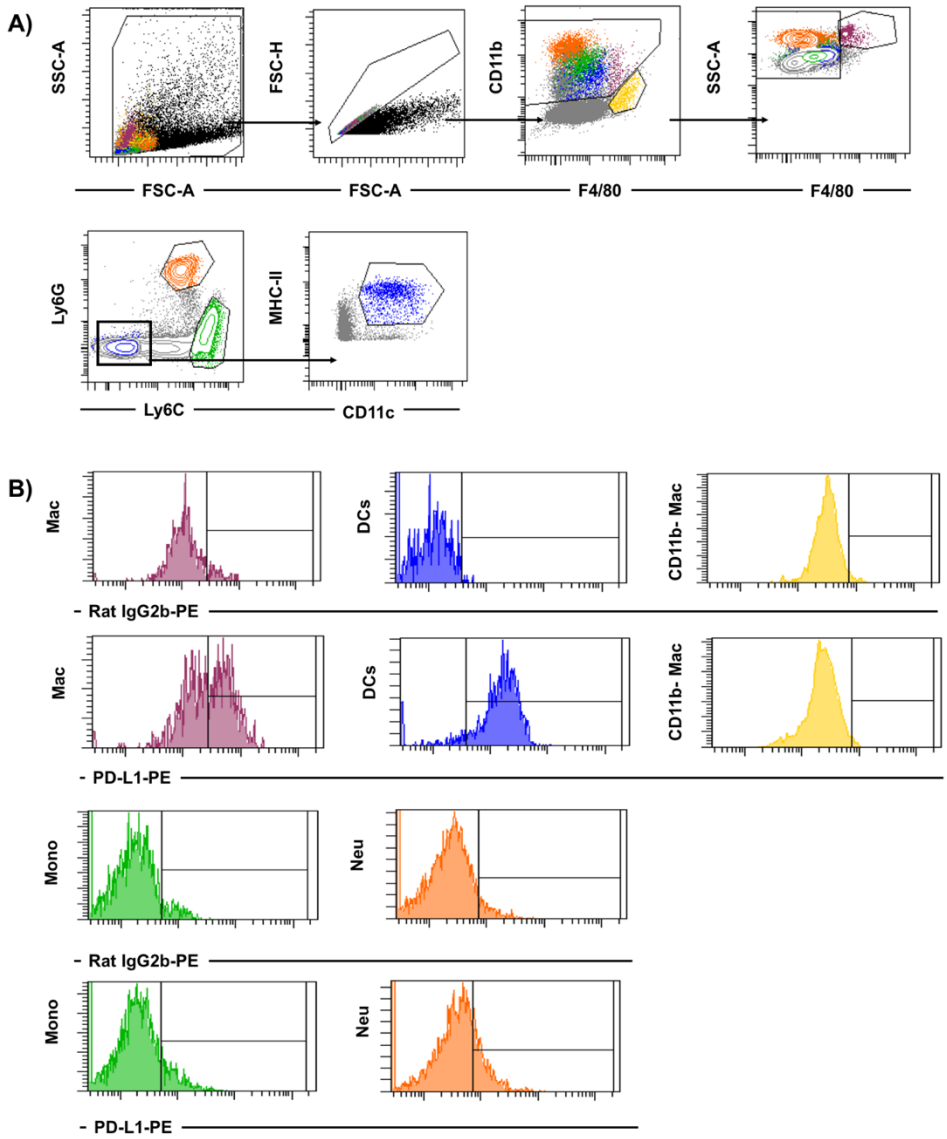

Figure 6.20 Gating strategy: Myeloid populations in spleen of 9464D-bearing mice.
Spleens were mechanically digested as detailed in 2.7.5, and single cell suspensions were obtained. Typically, 10^6 cells were stained with surface and intracellular markers (see 2.8) and samples were run on flow cytometry.. A) Following doublets exclusion, live cells were gated according to CD11b and F4/80 expression. Monocyte-derived macrophages were gated as F4/80 high, CD11b high, whilst tissue-resident, non-inflammatory macrophages were gated as CD11b low, F4/80 high. Neutrophils, monocytes and DCs were gated from the CD11b high, F4/80 low population according to their expression of Ly6C, Ly6C, CD11c and MHC-II markers as follows: neutrophils (Ly6C high, Ly6G high), monocytes (Ly6C low, Ly6G high) and DCs (Ly6C-, Ly6G-, MHC-II high, CD11c high). B) Examples of histograms showing the expression of PD-L1 on monocyte-derived macrophages (purple); tissue-resident macrophages (yellow); DCs (blue); monocytes (green); and neutrophils (orange). PD-L1 positive cells were gated according to an isotype control. Geometric mean of the whole population was calculated from the histogram plots, and isotype control values were subtracted.

B.3 Immunophenotyping of 9464D tumours after therapy with murine anti-PD-1 isotypes

B.3.1 Raw CD8: Treg ratio in tumour and spleen of 9464D-bearing mice

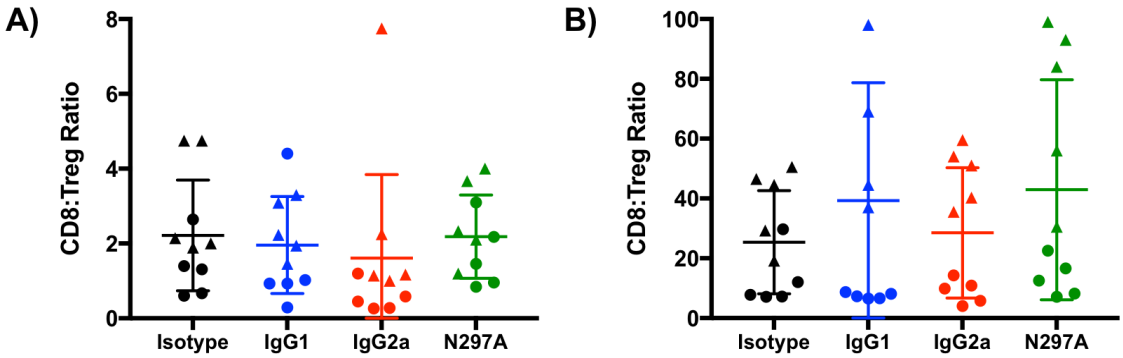

Figure 6.21 CD8: Treg ratio (raw numbers).
C57BL/6 mice were subcutaneously inoculated with $5x10^5$ 9464D cells. When tumours reached 7x7 mm, mice received 3 Ip doses of 200 µg of irrelevant mAbs (AT10 mIgG1, mIgG2a and mIgG1-N297A) or anti-PD-1 mIgG1, mIgG2a and mIgG1-N297A mAbs. Tumours and spleens were harvested 24h after the last dose and processed for flow cytometry (see sections 2.7.5 and 2.8). A-B) Raw CD8: Treg ratios in tumour (A) and spleen (B) were obtained by dividing the percentage of CD8 T cells by the percentage of Tregs per each individual mouse. Experiment performed twice, N=10 mice per group. Triangles correspond to the first experiment whilst circles correspond to the second. Bars represent mean ± S.D, (One-way ANOVA).

B.3.2 Tumour-infiltrating myeloid populations in of 9464D-bearing mice

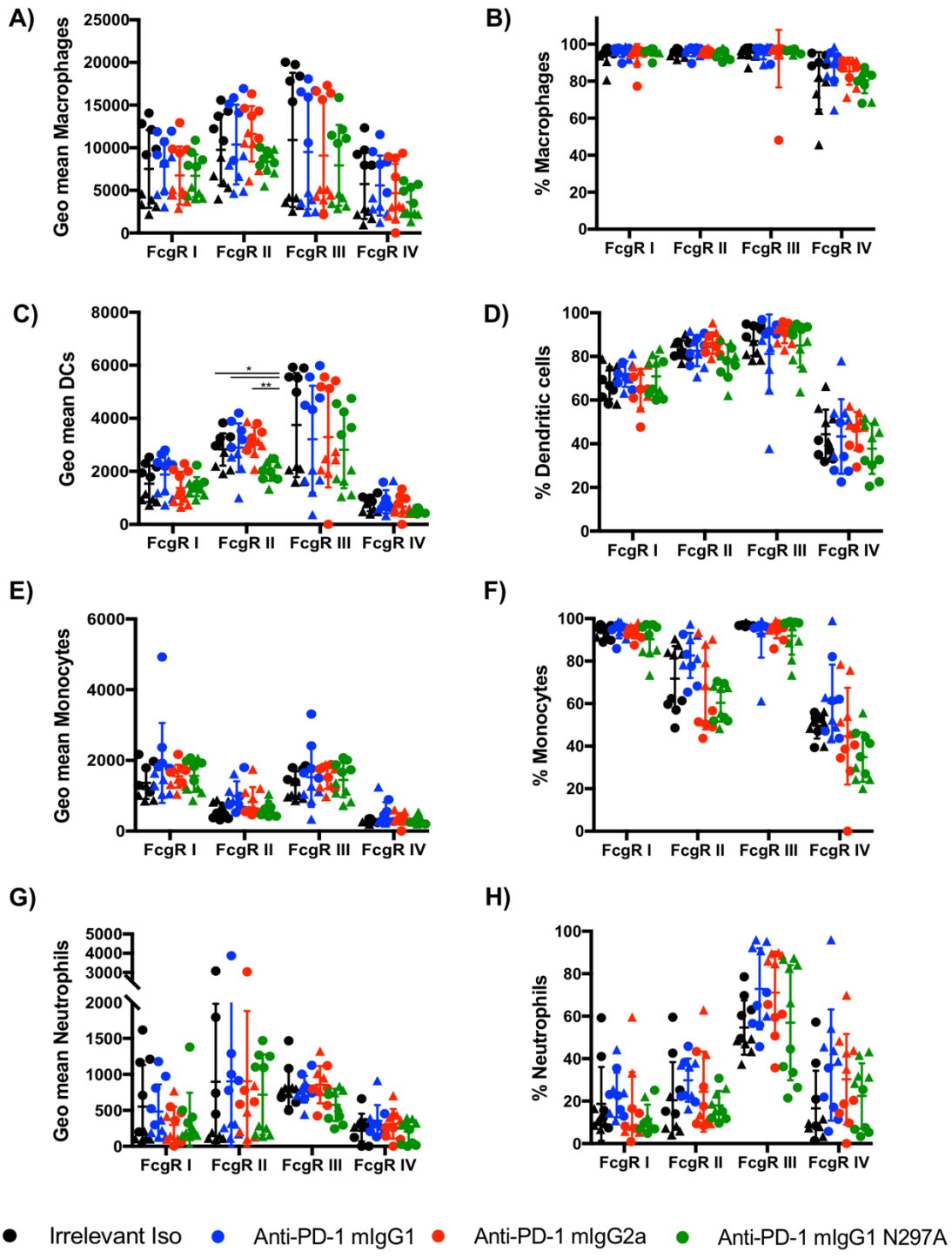

Figure 6.22 Tumour-infiltrating myeloid populations after therapy with murine anti-PD-1 isotypes: FcγR expression (2).
A-H) Expression of FcγRs (I, II, III and IV) on tumour-infiltrating macrophages (A,B), DCs (C,D), monocytes (E,F) and neutrophils (G,H) shown as MFI and percentage of positive cells. Experiment performed twice, N=10 mice per group. Triangles represent values from the first replicate whilst circles correspond to the second one. Bars represent mean ± S.D, (One-way ANOVA).

B.3.3 Myeloid populations in spleen of 9464D-bearing mice

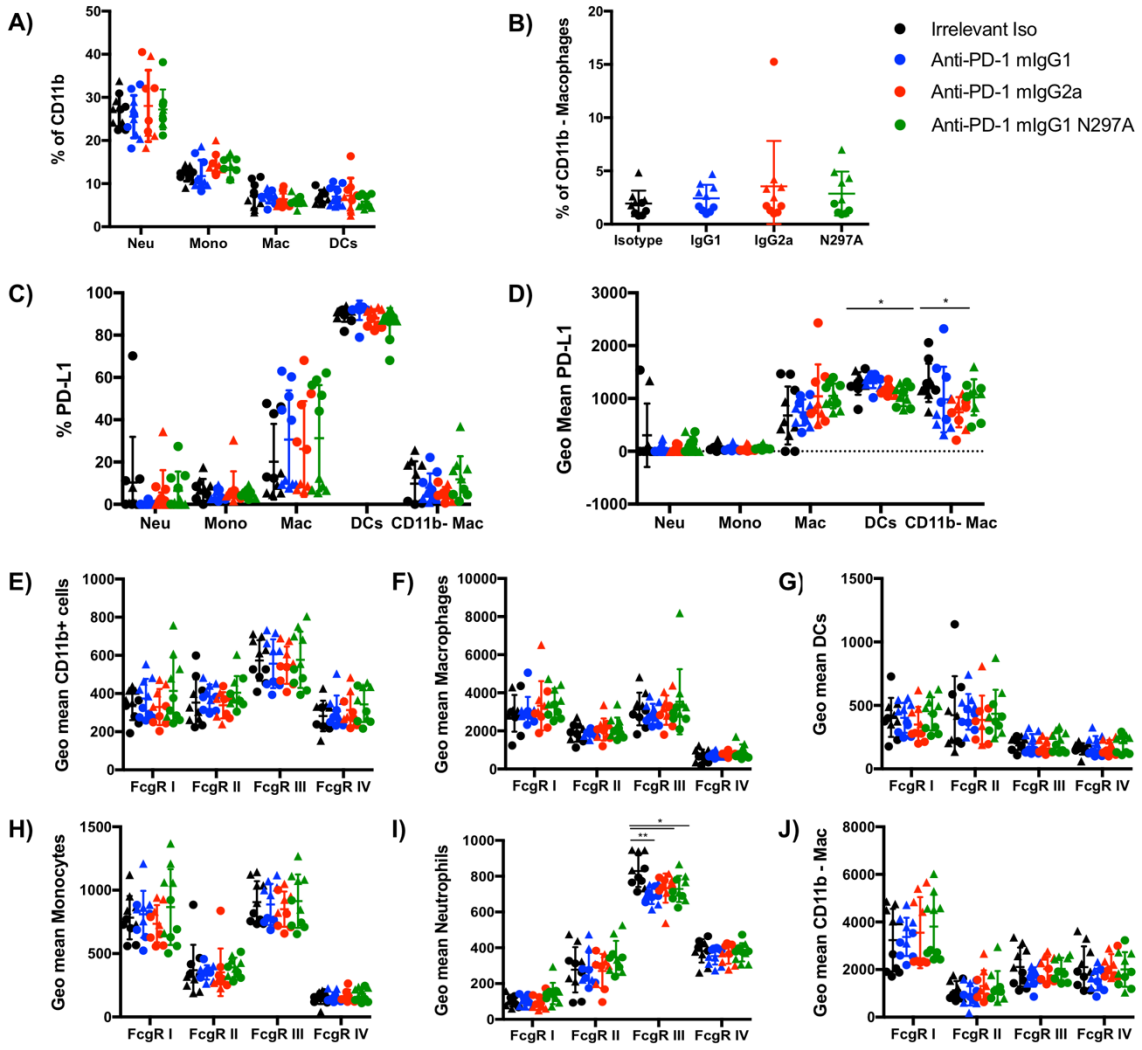

Figure 6.23 Myeloid cells in spleens of MC38-bearing mice after therapy with murine anti-PD-1 isotypes.
A) Percentage of myeloid populations out of CD11b+ gate in spleen. B) Percentage of CD11b low macrophages in spleen. C-D) Expression of PD-L1 on myeloid populations shown as percentage of positive cells (C) or as MFI (D). E-J) Expression of FcγRs (I, II, III and IV) on myeloid infiltrates: CD11b+ cells (E), macrophages (F), DCs (G), monocytes (H), neutrophils (I) and CD11b low macrophages (J) shown as MFI. Experiment performed twice, N=10 mice per group. Triangles represent values from the first replicate whilst circles correspond to the second one. Bars represent mean ± S.D, *p<0.05, **p<0.01 (One-way ANOVA).

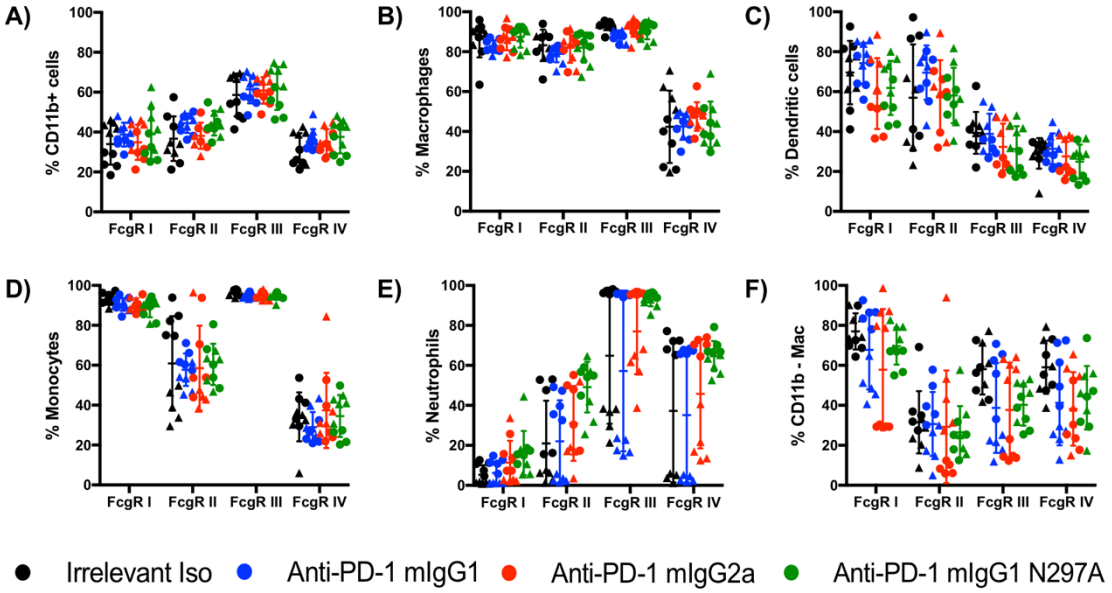

Figure 6.24 Myeloid cells in spleens of MC38-bearing mice after therapy with murine anti-PD-1 isotypes (2).
A-F) Expression of FcγRs (I, II, III and IV) on myeloid infiltrates: CD11b+ cells (A), macrophages (B), DCs (C), monocytes (D), neutrophils (E) and CD11b low macrophages (F) shown as percentage of positive cells. Experiment performed twice, N=10 mice per group. Triangles represent values from the first replicate whilst circles correspond to the second one. Bars represent mean ± S.D, (One-way ANOVA).

Glossary of Terms

List of References

Bibliography

1. World Health Organization: The Global Cancer Observatory. 2018 [Available from: https://gco.iarc.fr.

2. Hanahan D, Weinberg RA. The hallmarks of cancer. Cell. 2000;100:57-70.

3. Hanahan D, Weinberg RA. Hallmarks of cancer: the next generation. Cell. 2011;144(5):646-74.

4. Dunn GP, Bruce AT, Ikeda H, Old LJ, Schreiber RD. Cancer immunoediting : from immuno- surveillance to tumor escape. Nat Immunol. 2002;3:991-8.

5. Topalian SL, Hodi FS, Brahmer JR, Gettinger SN, Smith DC, McDermott DF, et al. Safety, activity, and immune correlates of anti-PD-1 antibody in cancer. N Engl J Med. 2012;366(26):2443-54.

6. Hamid O, Robert C, Daud A, Hodi FS, Hwu W-J, Kefford R, et al. Safety and tumor responses with Lambrolizumab (anti-PD-1) in melanoma. N Engl J Med. 2013;369:134-44.

7. Robert C, Schachter J, Long GV, Arance A, Grob JJ, Mortier L, et al. Pembrolizumab versus Ipilimumab in Advanced Melanoma. N Engl J Med. 2015;372:2521-32.

8. Ribas A, Hamid O, Daud A, Hodi FS, Wolchok JD, Kefford R, et al. Association of pembrolizumab with tumor response and survival among patients with advanced melanoma. Jama. 2016;315:1600-9.

9. Hodi FS, O'Day SJ, McDermott DF, Weber RW, Sosman JA, Haanen JB, et al. Improved survival with ipilimumab in patients with metastatic melanoma. N Engl J Med. 2010;363(8):711-23.

10. Abel AM, Yang C, Thakar MS, Malarkannan S. Natural Killer Cells: Development, Maturation, and Clinical Utilization. Front Immunol. 2018;9:1869.

11. Di Vito C, Mikulak J, Zaghi E, Pesce S, Marcenaro E, Mavilio D. NK cells to cure cancer. Semin Immunol. 2019;41:101272.

12. Zhu Y, Huang B, Shi J. Fas ligand and lytic granule differentially control cytotoxic dynamics of natural killer cell against cancer target. Oncotarget. 2016;7(30):47163-72.

13. Murphy K, Weaver C. Janeway's Immunobiology. . 9th Edition ed. New York, NY, USA: Taylor & Francis Group, LLC; 2016 1 March. 924 p.

14. Abbas AK, Murphy KM, Sher A. Functional diversity of helper T lymphocytes. Nature. 1996;383(6603):787-93.

15. Hirahara K, Nakayama T. CD4+ T-cell subsets in inflammatory diseases: beyond the Th1/Th2 paradigm. Int Immunol. 2016;28(4):163-71.

16. Galon J, Costes A, Sanchez-Cabo F, Kirilovsky A, Mlecnik B, Lagorce-Pagès C, et al. Type, density, and location of immune cells within human colorectal tumors predict clinical outcome. Science. 2006;313:1960-4.

17. Galon J, Mlecnik B, Bindea G, Angell HK, Berger A, Lagorce C, et al. Towards the introduction of the 'Immunoscore' in the classification of malignant tumours. J Pathol. 2014;232(2):199-209.

18. Gooden MJM, de Bock GH, Leffers N, Daemen T, Nijman HW. The prognostic influence of tumour-infiltrating lymphocytes in cancer: a systematic review with meta-analysis. Br J Cancer. 2011;105:93-103.

19. Sakaguchi S, Yamaguchi T, Nomura T, Ono M. Regulatory T Cells and Immune Tolerance. Cell. 2008;133:775-87.

20. Curiel TJ, Coukos G, Zou L, Alvarez X, Cheng P, Mottram P, et al. Specific recruitment of regulatory T cells in ovarian carcinoma fosters immune privilege and predicts reduced survival. Nat Med. 2004;10:942-9.

21. Spranger S, Spaapen RM, Zha Y, Williams J, Meng Y, Ha TT, et al. Up-regulation of PD-L1, IDO, and Tregs in the melanoma tumor microenvironment is driven by CD8+ T cells. Sci Transl Med. 2013;5(200):200ra116.

22. Zou W. Regulatory T cells, tumour immunity and immunotherapy. Nat Rev Immunol. 2006;6:295-307.

23. Shang B, Liu Y, Jiang SJ, Liu Y. Prognostic value of tumor-infiltrating FoxP3+ regulatory T cells in cancers: a systematic review and meta-analysis. Sci Rep. 2015;5:15179.

24. Kierdorf K, Prinz M, Geissmann F, Gomez Perdiguero E. Development and function of tissue resident macrophages in mice. Semin Immunol. 2015;27(6):369-78.

25. Movahedi K, Laoui D, Gysemans C, Baeten M, Stangé G, Van Bossche JD, et al. Different tumor microenvironments contain functionally distinct subsets of macrophages derived from Ly6C(high) monocytes. Cancer Res. 2010;70:5728-39.

26. De Palma M, Lewis CE. Macrophage regulation of tumor responses to anticancer therapies. Cancer Cell. 2013;23(3):277-86.

27. Bloch O, Crane CA, Kaur R, Safaee M, Rutkowski MJ, Parsa AT. Gliomas promote immunosuppression through induction of B7-H1 expression in tumor-associated macrophages. Clin Cancer Res. 2013;19:3165-75.

28. Wang X, Ni S, Chen Q, Ma L, Jiao Z, Wang C, et al. Bladder cancer cells induce immunosuppression of T cells by supporting PD-L1 expression in tumour macrophages partially through interleukin 10. Cell Biol Int. 2017;41:177-86.

29. Taube JM, Anders RA, Young GD, Xu H, Sharma R, Mcmiller TL, et al. Colocalization of inflammatory response with B7- h1 expression in human melanocytic lesions supports an adaptive resistance mechanism of immune escape. Sci Transl Med. 2012;4:127ra37.

30. Topalian SL, Drake CG, Pardoll DM. Targeting the PD-1/B7-H1(PD-L1) pathway to activate anti-tumor immunity. Curr Opin Immunol. 2012;24:207-12.

31. Andrews LP, Yano H, Vignali DAA. Inhibitory receptors and ligands beyond PD-1, PD-L1 and CTLA-4: breakthroughs or backups. Nat Immunol. 2019;20(11):1425-34.

32. Okazaki T, Maeda A, Nishimura H, Kurosaki T, Honjo T. PD-1 immunoreceptor inhibits B cell receptor-mediated signaling by recruiting src homology 2-domain-

containing tyrosine phosphatase 2 to phosphotyrosine. Proc Natl Acad Sci U S A. 2001;98(24):13866-71.

33. Parry RV, Chemnitz JM, Frauwirth Ka, Lanfranco AR, Braunstein I, Sumire V, et al. CTLA-4 and PD-1 Receptors Inhibit T-Cell Activation by Distinct Mechanisms CTLA-4 and PD-1 Receptors Inhibit T-Cell Activation by Distinct Mechanisms †. Mol Cell Biol. 2005;25:9543-53.

34. Agata Y, Kawasaki a, Nishimura H, Ishida Y, Tsubata T, Yagita H, et al. Expression of the PD-1 antigen on the surface of stimulated mouse T and B lymphocytes. Int Immunol. 1996;8:765-72.

35. Yoshida T, Jiang F, Honjo T, Okazaki T. PD-1 deficiency reveals various tissue-specific autoimmunity by H-2b and dose-dependent requirement of H-2g7 for diabetes in NOD mice. Proc Natl Acad Sci U S A. 2008;105(9):3533-8.

36. Wang J, Yoshida T, Nakaki F, Hiai H, Okazaki T, Honjo T. Establishment of NOD-Pdcd1-/- mice as an efficient animal model of type I diabetes. Proc Natl Acad Sci U S A. 2005;102(33):11823-8.

37. Nishimura H, Nose M, Hiai H, Minato N, Honjo T. Development of lupus-like autoimmune diseases by disruption of the PD-1 gene encoding an ITIM motif-carrying immunoreceptor. Immunity. 1999;11(2):141-51.

38. Keir ME, Liang SC, Guleria I, Latchman YE, Qipo A, Albacker LA, et al. Tissue expression of PD-L1 mediates peripheral T cell tolerance. J Exp Med. 2006;203(4):883-95.

39. Blank C, Brown I, Peterson AC, Spiotto M, Iwai Y, Honjo T, et al. PD-L1/B7H-1 inhibits the effector phase of tumor rejection by T cell receptor (TCR) transgenic CD8+ T cells. Cancer Res. 2004;64(3):1140-5.

40. Iwai Y, Ishida M, Tanaka Y, Okazaki T, Honjo T, Minato N. Involvement of PD-L1 on tumor cells in the escape from host immune system and tumor immunotherapy by PD-L1 blockade. Proc Natl Acad Sci U S A. 2002;99:12293-7.

41. Bally AP, Lu P, Tang Y, Austin JW, Scharer CD, Ahmed R, et al. NF-kappaB regulates PD-1 expression in macrophages. J Immunol. 2015;194(9):4545-54.

42. Yao S, Wang S, Zhu Y, Luo L, Zhu G, Flies S, et al. PD-1 on dendritic cells impedes innate immunity against bacterial infection. Blood. 2009;113(23):5811-8.

43. Gordon SR, Maute RL, Dulken BW, Hutter G, George BM, McCracken MN, et al. PD-1 expression by tumour-associated macrophages inhibits phagocytosis and tumour immunity. Nature. 2017;545:495-9.

44. Strauss L, Mahmoud MAA, Weaver JD, Tijaro-Ovalle NM, Christofides A, Wang Q, et al. Targeted deletion of PD-1 in myeloid cells induces antitumor immunity. Sci Immunol. 2020;5(43).

45. Sheppard KA, Fitz LJ, Lee JM, Benander C, George JA, Wooters J, et al. PD-1 inhibits T-cell receptor induced phosphorylation of the ZAP70/CD3?? signalosome and downstream signaling to PKC?? FEBS Letters. 2004;574:37-41.

46. Yokosuka T, Takamatsu M, Kobayashi-Imanishi W, Hashimoto-Tane A, Azuma M, Saito T. Programmed cell death 1 forms negative costimulatory microclusters that directly inhibit T cell receptor signaling by recruiting phosphatase SHP2. J Exp Med. 2012;209:1201-17.

47. Hui E, Cheung J, Zhu J, Su X, Taylor MJ, Wallweber HA, et al. T cell costimulatory receptor CD28 is a primary target for PD-1-mediated inhibition. Science. 2017;355:1428-33.

48. Chemnitz JM, Parry RV, Nichols KE, June CH, Riley JL. SHP-1 and SHP-2 associate with immunoreceptor tyrosine-based switch motif of programmed death 1 upon primary human T cell stimulation, but only receptor ligation prevents T cell activation. J Immunol. 2004;173(2):945-54.

49. Wei F, Zhong S, Ma Z, Kong H, Medvec A, Ahmed R, et al. Strength of PD-1 signaling differentially affects T-cell effector functions. Proc Natl Acad Sci U S A. 2013;110(27):E2480-9.

50. Ostrand-Rosenberg S, Horn LA, Haile ST. The programmed death-1 immune-suppressive pathway: barrier to antitumor immunity. J Immunol. 2014;193(8):3835-41.

51. Yamazaki T, Akiba H, Iwai H, Matsuda H, Aoki M, Tanno Y, et al. Expression of Programmed Death 1 Ligands by Murine T Cells and APC. J Immunol. 2002;169:5538-45.

52. Latchman YE, Liang SC, Wu Y, Chernova T, Sobel RA, Klemm M, et al. PD-L1-deficient mice show that PD-L1 on T cells, antigen-presenting cells, and host tissues negatively regulates T cells. Proc Natl Acad Sci U S A. 2004;101(29):10691-6.

53. Latchman Y, Wood CR, Chernova T, Chaudhary D, Borde M, Chernova I, et al. PD-L2 is a second ligand for PD-1 and inhibits T cell activation. Nat Immunol. 2001;2(3):261-8.

54. Eppihimer M, Gunn J, Freeman G, Greenfield E, Chernova T, Erikson J, et al. Expression and regulation of he PD-L1 immunohibitory molecule on microvascular endothelial cells. Microcirculation. 2002;9:133-45.

55. Seo SK, Seo HM, Jeong HY, Choi IW, Park YM, Yagita H, et al. Co-inhibitory role of T-cell-associated B7-H1 and B7-DC in the T-cell immune response. Immunol Lett. 2006;102:222-8.

56. Pfistershammer K, Klauser C, Pickl WF, Stockl J, Leitner J, Zlabinger G, et al. No evidence for dualism in function and receptors: PD-L2/B7-DC is an inhibitory regulator of human T cell activation. Eur J Immunol. 2006;36(5):1104-13.

57. Dong H, Strome SE, Salomao DR, Tamura H, Hirano F, Flies DB, et al. Tumor-associated B7-H1 promotes T-cell apoptosis: A potential mechanism of immune evasion. Nat Med. 2002;8:793-800.

58. Abiko K, Matsumura N, Hamanishi J, Horikawa N, Murakami R, Yamaguchi K, et al. IFN-γ from lymphocytes induces PD-L1 expression and promotes progression of ovarian cancer. Br J Cancer. 2015;112:1-9.

59. Kondo A, Yamashita T, Tamura H, al e. Interferon-gamma and tumor necrosis factor-kappa B induce an immunoinhibitory molecule, B7-H1, via nuclear factor-alfaB activation in blasts in myelodysplastic syndromes. Blood. 2010;116:1124-31.

60. Chen N, Fang W, Zhan J, Hong S, Tang Y, Kang S, et al. Upregulation of PD-L1 by EGFR activation mediates the immune escape in EGFR-driven NSCLC: Implication for optional immune targeted therapy for NSCLC patients with EGFR mutation. J Thorac Oncol. 2015;10:910-23.

61. Jiang X, Zhou J, Giobbie-Hurder A, Wargo J, Hodi FS. The activation of MAPK in melanoma cells resistant to BRAF inhibition promotes PD-L1 expression that is reversible by MEK and PI3K inhibition. Clinical Cancer Research. 2013;19:598-609.

62. Parsa AT, Waldron JS, Panner A, Crane CA, Parney IF, Barry JJ, et al. Loss of tumor suppressor PTEN function increases B7-H1 expression and immunoresistance in glioma. Nat Med. 2007;13(1):84-8.

63. Gowrishankar K, Gunatilake D, Gallagher SJ, Tiffen J, Rizos H, Hersey P. Inducible but not constitutive expression of PD-L1 in human melanoma cells is dependent on activation of NF-κB. PLoS ONE. 2015;10:e0123410.

64. Noman MZ, Desantis G, Janji B, Hasmim M, Karray S, Dessen P, et al. PD-L1 is a novel direct target of HIF-1alpha, and its blockade under hypoxia enhanced MDSC-mediated T cell activation. J Exp Med. 2014;211(5):781-90.

65. Lau J, Cheung J, Navarro A, Lianoglou S, Haley B, Totpal K, et al. Tumour and host cell PD-L1 is required to mediate suppression of anti-tumour immunity in mice. Nat Commun. 2017;8:14572.

66. Noguchi T, Ward JP, Gubin MM, Arthur CD, Lee SH, Hundal J, et al. Temporally Distinct PD-L1 Expression by Tumor and Host Cells Contributes to Immune Escape. Cancer Immunol Res. 2017;5:106-17.

67. Tang H, Liang Y, Anders RA, Taube JM, Qiu X, Mulgaonkar A, et al. PD-L1 on host cells is essential for PD-L1 blockade-mediated tumor regression. J Clin Invest. 2018;128(2):580-8.

68. Lin H, Wei S, Hurt EM, Green MD, Zhao L, Vatan L, et al. Host expression of PD-L1 determines efficacy of PD-L1 pathway blockade-mediated tumor regression. J Clin Invest. 2018;128(4):1708.

69. Diskin B, Adam S, Cassini MF, Sanchez G, Liria M, Aykut B, et al. PD-L1 engagement on T cells promotes self-tolerance and suppression of neighboring macrophages and effector T cells in cancer. Nat Immunol. 2020;21(4):442-54.

70. Park JJ, Omiya R, Matsumura Y, Sakoda Y, Kuramasu A, Augustine MM, et al. B7-H1/CD80 interaction is required for the induction and maintenance of peripheral T-cell tolerance. Blood. 2010;116(8):1291-8.

71. Tsushima F, Yao S, Shin T, Flies A, Flies S, Xu H, et al. Interaction between B7-H1 and PD-1 determines initiation and reversal of T-cell anergy. Blood. 2007;110(1):180-5.

72. Garcia-Bates TM, Palma ML, Shen C, Gambotto A, Macatangay BJC, Ferris RL, et al. Contrasting Roles of the PD-1 Signaling Pathway in Dendritic Cell-Mediated Induction and Regulation of HIV-1-Specific Effector T Cell Functions. J Virol. 2019;93(5).

73. Sugiura D, Maruhashi T, Okazaki IM, Shimizu K, Maeda TK, Takemoto T, et al. Restriction of PD-1 function by cis-PD-L1/CD80 interactions is required for optimal T cell responses. Science. 2019;364(6440):558-66.

74. Mayoux M, Roller A, Pulko V, Sammicheli S, Chen S, Sum E, et al. Dendritic cells dictate responses to PD-L1 blockade cancer immunotherapy. Sci Transl Med. 2020;12(534).

75. Zhao Y, Lee CK, Lin CH, Gassen RB, Xu X, Huang Z, et al. PD-L1:CD80 Cis-Heterodimer Triggers the Co-stimulatory Receptor CD28 While Repressing the Inhibitory PD-1 and CTLA-4 Pathways. Immunity. 2019;51(6):1059-73 e9.

76. Banchereau J, Steinman RM. Dendritic cells and the control of immunity. Nature. 1998;392(6673):245-52.

77. Embgenbroich M, Burgdorf S. Current Concepts of Antigen Cross-Presentation. Front Immunol. 2018;9:1643.

78. Hildner K, Edelson BT, Purtha WE, Diamond M, Matsushita H, Kohyama M, et al. Batf3 deficiency reveals a critical role for CD8alpha+ dendritic cells in cytotoxic T cell immunity. Science. 2008;322(5904):1097-100.

79. Salmon H, Idoyaga J, Rahman A, Leboeuf M, Remark R, Jordan S, et al. Expansion and Activation of CD103(+) Dendritic Cell Progenitors at the Tumor Site Enhances Tumor Responses to Therapeutic PD-L1 and BRAF Inhibition. Immunity. 2016;44(4):924-38.

80. Wang RF, Miyahara Y, Wang HY. Toll-like receptors and immune regulation: implications for cancer therapy. Oncogene. 2008;27(2):181-9.

81. Moynagh PN. TLR signalling and activation of IRFs: revisiting old friends from the NF-kappaB pathway. Trends Immunol. 2005;26(9):469-76.

82. Barber GN. STING: infection, inflammation and cancer. Nat Rev Immunol. 2015;15(12):760-70.

83. Forster R, Davalos-Misslitz AC, Rot A. CCR7 and its ligands: balancing immunity and tolerance. Nat Rev Immunol. 2008;8(5):362-71.

84. Young JW, Koulova L, Soergel SA, Clark EA, Steinman RM, Dupont B. The B7/BB1 antigen provides one of several costimulatory signals for the activation of CD4+ T lymphocytes by human blood dendritic cells in vitro. J Clin Invest. 1992;90(1):229-37.

85. Cella M, Scheidegger D, Palmer-Lehmann K, Lane P, Lanzavecchia A, Alber G. Ligation of CD40 on dendritic cells triggers production of high levels of interleukin-12 and enhances T cell stimulatory capacity: T-T help via APC activation. J Exp Med. 1996;184(2):747-52.

86. Macatonia SE, Hosken NA, Litton M, Vieira P, Hsieh CS, Culpepper JA, et al. Dendritic cells produce IL-12 and direct the development of Th1 cells from naive CD4+ T cells. J Immunol. 1995;154(10):5071-9.

87. Pham TH, Baluk P, Xu Y, Grigorova I, Bankovich AJ, Pappu R, et al. Lymphatic endothelial cell sphingosine kinase activity is required for lymphocyte egress and lymphatic patterning. J Exp Med. 2010;207(1):17-27.

88. Groom JR, Luster AD. CXCR3 in T cell function. Exp Cell Res. 2011;317(5):620-31.

89. Mills CD, Lenz LL, Harris RA. A Breakthrough: Macrophage-Directed Cancer Immunotherapy. Cancer Res. 2016;76(3):513-6.

90. Golstein P, Griffiths GM. An early history of T cell-mediated cytotoxicity. Nat Rev Immunol. 2018;18(8):527-35.

91. Gray JC, Kohler JA. Immunotherapy for neuroblastoma: turning promise into reality. Pediatr Blood Cancer. 2009;53(6):931-40.

92. Vidarsson G, Dekkers G, Rispens T. IgG subclasses and allotypes: from structure to effector functions. Front Immunol. 2014;5:520.

93. Bruhns P, Iannascoli B, England P, Mancardi DA, Fernandez N, Jorieux S, et al. Specificity and affinity of human Fcgamma receptors and their polymorphic variants for human IgG subclasses. Blood. 2009;113(16):3716-25.

94. Pincetic A, Bournazos S, DiLillo DJ, Maamary J, Wang TT, Dahan R, et al. Type I and type II Fc receptors regulate innate and adaptive immunity. Nat Immunol. 2014;15(8):707-16.

95. Tao MH, Morrison SL. Studies of aglycosylated chimeric mouse-human IgG. Role of carbohydrate in the structure and effector functions mediated by the human IgG constant region. J Immunol. 1989;143(8):2595-601.

96. Arduin E, Arora S, Bamert PR, Kuiper T, Popp S, Geisse S, et al. Highly reduced binding to high and low affinity mouse Fc gamma receptors by L234A/L235A and N297A Fc mutations engineered into mouse IgG2a. Mol Immunol. 2015;63(2):456-63.

97. Marshall MJE, Stopforth RJ, Cragg MS. Therapeutic antibodies: What have we learnt from targeting CD20 and where are we going? Front Immunol. 2017;8:1245.

98. Alduaij W, Ivanov A, Honeychurch J, Cheadle EJ, Potluri S, Lim SH, et al. Novel type II anti-CD20 monoclonal antibody (GA101) evokes homotypic adhesion and actin-dependent, lysosome-mediated cell death in B-cell malignancies. Blood. 2011;117(17):4519-29.

99. Xu Y, Szalai AJ, Zhou T, Zinn KR, Chaudhuri TR, Li X, et al. Fc gamma Rs modulate cytotoxicity of anti-Fas antibodies: implications for agonistic antibody-based therapeutics. J Immunol. 2003;171(2):562-8.

100. Wilson NS, Yang B, Yang A, Loeser S, Marsters S, Lawrence D, et al. An Fcgamma receptor-dependent mechanism drives antibody-mediated target-receptor signaling in cancer cells. Cancer Cell. 2011;19(1):101-13.

101. Nimmerjahn F, Ravetch JV. Fcγ receptors as regulators of immune responses. Nat Rev Immunol. 2008;8:34-47.

102. Abès R, Gélizé E, Fridman WH, Teillaud JL. Long-lasting antitumor protection by anti-CD20 antibody through cellular immune response. Blood. 2010;116:926-34.

103. DiLillo DJ, Ravetch JV. Differential Fc-receptor engagement drives an anti-tumor vaccinal effect. Cell. 2015;161:1035-45.

104. Dahan R, Sega E, Engelhardt J, Selby M, Korman Alan JJ, Ravetch Jeffrey VV. FcγRs Modulate the Anti-tumor Activity of Antibodies Targeting the PD-1/PD-L1 Axis. Cancer Cell. 2015;28:285-95.

105. Buchan SL, Dou L, Remer M, Booth SG, Dunn SN, Lai C, et al. Antibodies to Costimulatory Receptor 4-1BB Enhance Anti-tumor Immunity via T Regulatory Cell Depletion and Promotion of CD8 T Cell Effector Function. Immunity. 2018;49(5):958-70.e7.

106. Turaj AH, Hussain K, Cox KL, Rose-Zerilli MJJ, Testa J, Dahal LN, et al. Antibody Tumor Targeting Is Enhanced by CD27 Agonists through Myeloid Recruitment. Cancer Cell. 2017;32(6):777-91 e6.

107. Willoughby JE, Kerr JP, Rogel A, Taraban VY, Buchan SL, Johnson PWM, et al. Differential Impact of CD27 and 4-1BB Costimulation on Effector and Memory CD8 T Cell Generation following Peptide Immunization. J Immunol. 2014;193:244-51.

108. Gough MJ, Ruby CE, Redmond WL, Dhungel B, Brown A, Weinberg AD. OX40 agonist therapy enhances CD8 infiltration and decreases immune suppression in the tumor. Cancer Res. 2008;68:5206-15.

109. French RR, Chan HTC, Tutt AL, Glennie MJ. CD40 antibody evokes a cytotoxic T-cell response that eradicates lymphoma and bypasses T-cell help. Nat Med. 1999;5:548-53.

110. Van Kooten G, Banchereau J. CD40-CD40 ligand. J Leukoc Biol. 2000;67:2-17.

111. Alsaab HO, Sau S, Alzhrani R, Tatiparti K, Bhise K, Kashaw SK, et al. PD-1 and PD-L1 Checkpoint Signaling Inhibition for Cancer Immunotherapy: Mechanism, Combinations, and Clinical Outcome. Front Pharmacol. 2017;8:561.

112. Nimmerjahn F, Ravetch JV. Divergent immunoglobulin g subclass activity through selective Fc receptor binding. Sci Rep. 2005;310:1510-2.

113. Cassel DL, Keller MA, Surrey S, Schwartz E, Schreiber AD, Rappaport EF, et al. Differential expression of Fc gamma RIIA, Fc gamma RIIB and Fc gamma RIIC in hematopoietic cells: analysis of transcripts. Mol Immunol. 1993;30(5):451-60.

114. Metes D, Ernst LK, Chambers WH, Sulica A, Herberman RB, Morel PA. Expression of functional CD32 molecules on human NK cells is determined by an allelic polymorphism of the FcgammaRIIC gene. Blood. 1998;91(7):2369-80.

115. Warmerdam PA, Nabben NM, van de Graaf SA, van de Winkel JG, Capel PJ. The human low affinity immunoglobulin G Fc receptor IIC gene is a result of an unequal crossover event. J Biol Chem. 1993;268(10):7346-9.

116. Nimmerjahn F, Bruhns P, Horiuchi K, Ravetch JV. FcγRIV: A novel FcR with distinct IgG subclass specificity. Immunity. 2005;23:41-51.

117. Tutt AL, James S, Laversin SA, Tipton TR, Ashton-Key M, French RR, et al. Development and Characterization of Monoclonal Antibodies Specific for Mouse and Human Fcgamma Receptors. J Immunol. 2015;195(11):5503-16.

118. García-García E, Rosales C. Signal transduction during Fc receptor-mediated phagocytosis. J Leukoc Biol. 2002;72:1092-108.

119. Brandsma AM, Hogarth PM, Nimmerjahn F, Leusen JH. Clarifying the Confusion between Cytokine and Fc Receptor "Common Gamma Chain". Immunity. 2016;45(2):225-6.

120. Ravetch JV, Lanier LL. Immune inhibitory receptors. Science. 2000;290:84-9.

121. Clynes R, Maizes JS, Guinamard R, Ono M, Takai T, Ravetch JV. Modulation of Immune Complex–induced Inflammation In Vivo by the Coordinate Expression of Activation and Inhibitory Fc Receptors. J Exp Med. 1999;189:179-85.

122. Guyre PM, Morganelli PM, Miller R. Recombinant immune interferon increases immunoglobulin G Fc receptors on cultured human mononuclear phagocytes. J Clin Invest. 1983;72:393-7.

123. Okayama Y, Kirshenbaum AS, Metcalfe DD. Expression of a Functional High-Affinity IgG Receptor, FcγRI, on Human Mast Cells: Up-Regulation by IFN-γ. J Immunol. 2000;164:4332-9.

124. Tridandapani S, Wardrop R, Baran CP, Wang Y, Opalek JM, Caligiuri MA, et al. TGF-beta 1 suppresses [correction of supresses] myeloid Fc gamma receptor function by regulating the expression and function of the common gamma-subunit. J Immunol. 2003;170:4572-7.

125. te Velde AA, Huijbens RJ, de Vries JE, Figdor CG. IL-4 decreases Fc gamma R membrane expression and Fc gamma R-mediated cytotoxic activity of human monocytes. J Immunol. 1990;144:3046-51.

126. Pricop L, Redecha P, Teillaud J-L, Frey J, Fridman WH, Sautes-Fridman C, et al. Differential Modulation of Stimulatory and Inhibitory Fc Receptors on Human Monocytes by Th1 and Th2 Cytokines. J Immunol. 2001;166:531-7.

127. Fanger NA, Voigtlaender D, Liu C, Swink S, Wardwell K, Fisher J, et al. Characterization of expression, cytokine regulation, and effector function of the high affinity IgG receptor Fc gamma RI (CD64) expressed on human blood dendritic cells. J Immunol. 1997;158:3090-8.

128. Hussain K, Hargreaves CE, Roghanian A, Oldham RJ, Chan HT, Mockridge CI, et al. Upregulation of FcgammaRIIb on monocytes is necessary to promote the superagonist activity of TGN1412. Blood. 2015;125(1):102-10.

129. Shi Y, Fan X, Deng H, Brezski RJ, Rycyzyn M, Jordan RE, et al. Trastuzumab Triggers Phagocytic Killing of High HER2 Cancer Cells In Vitro and In Vivo by Interaction with Fcγ Receptors on Macrophages. J Immunol. 2015;194:4379-86.

130. Minard-Colin V, Xiu Y, Poe JC, Horikawa M, Magro CM, Hamaguchi Y, et al. Lymphoma depletion during CD20 immunotherapy in mice is mediated by macrophage FcγRI, FcγRIII, and FcγRIV. Blood. 2008;112:1205-13.

131. White AL, Chan HTC, Roghanian A, French RR, Mockridge CI, Tutt AL, et al. Interaction with Fc RIIB Is Critical for the Agonistic Activity of Anti-CD40 Monoclonal Antibody. The Journal of Immunology. 2011;187:1754-63.

132. Li F, Ravetch JV. Inhibitory Fcg receptor engagement drives adjuvant and anti-tumor activities of agonistic CD40 antibodies. Science. 2011;333:1030-4.

133. Buchan SL, Dou L, Remer M, Booth SG, Dunn SN, Lai C, et al. Antibodies to Costimulatory Receptor 4-1BB Enhance Anti-tumor Immunity via T Regulatory Cell Depletion and Promotion of CD8 T Cell Effector Function. Immunity. 2018;49(5):958-70 e7.

134. Bulliard Y, Jolicoeur R, Zhang J, Dranoff G, Wilson NS, Brogdon JL. OX40 engagement depletes intratumoral Tregs via activating FcγRs, leading to antitumor efficacy. Immunol Cell Biol. 2014;92:475-80.

135. Selby MJ, Engelhardt JJ, Quigley M, Henning KA, Chen T, Srinivasan M, et al. Anti-CTLA-4 Antibodies of IgG2a Isotype Enhance Antitumor Activity through Reduction of Intratumoral Regulatory T Cells. Cancer Immunol Res. 2013;1:32-42.

136. Simpson TR, Li F, Montalvo-Ortiz W, Sepulveda MA, Bergerhoff K, Arce F, et al. Fc-dependent depletion of tumor-infiltrating regulatory T cells co-defines the efficacy of anti-CTLA-4 therapy against melanoma. J Exp Med. 2013;210(9):1695-710.

137. Romano E, Kusio-Kobialka M, Foukas PG, Baumgaertner P, Meyer C, Ballabeni P, et al. Ipilimumab-dependent cell-mediated cytotoxicity of regulatory T cells ex vivo by nonclassical monocytes in melanoma patients. Proc Natl Acad Sci U S A. 2015;112:6140-5.

138. Arce Vargas F, Furness AJS, Litchfield K, Joshi K, Rosenthal R, Ghorani E, et al. Fc Effector Function Contributes to the Activity of Human Anti-CTLA-4 Antibodies. Cancer Cell. 2018;33(4):649-63 e4.

139. Hirano F, Kaneko K, Tamura H, Dong H, Wang S, Ichikawa M, et al. Blockade of B7-H1 and PD-1 by monoclonal antibodies potentiates cancer therapeutic immunity. Cancer Res. 2005;65:1089-96.

140. Ahrends T, Bąbała N, Xiao Y, Yagita H, van Eenennaam H, Borst J. CD27 Agonism Plus PD-1 Blockade Recapitulates CD4+ T-cell Help in Therapeutic Anticancer Vaccination. Cancer Res. 2016;76:2921-31.

141. Zaretsky JM, Garcia-Diaz A, Shin DS, Escuin-Ordinas H, Hugo W, Hu-Lieskovan S, et al. Mutations Associated with Acquired Resistance to PD-1 Blockade in Melanoma. N Engl J Med. 2016;375:819-29.

142. Memarnejadian A, Meilleur CE, Shaler CR, Khazaie K, Bennink JR, Schell TD, et al. PD-1 Blockade Promotes Epitope Spreading in Anticancer CD8 + T Cell Responses by Preventing Fratricidal Death of Subdominant Clones To Relieve Immunodomination. J Immunol. 2017;199:3348-59.

143. Brown JA, Dorfman DM, Ma F-RF-R, Sullivan EL, Munoz O, Wood CR, et al. Blockade of programmed death-1 ligands on dendritic cells enhances T cell activation and cytokine production. J Immunol. 2003;170:1257-66.

144. Wang W, Lau R, Yu D, Zhu W, Korman A, Weber J. PD1 blockade reverses the suppression of melanoma antigen-specific CTL by CD4+CD25Hi regulatory T cells. Int Immunol. 2009;21(9):1065-77.

145. Robert C, Long GV, Brady B, Dutriaux C, Maio M, Mortier L, et al. Nivolumab in Previously Untreated Melanoma without BRAF Mutation. N Engl J Med. 2015;372:320-30.

146. Brahmer JR. PD-1-targeted immunotherapy: recent clinical findings. Clin Adv Hematol Oncol. 2012;10(10):674-5.

147. Migden MR, Rischin D, Schmults CD, Guminski A, Hauschild A, Lewis KD, et al. PD-1 Blockade with Cemiplimab in Advanced Cutaneous Squamous-Cell Carcinoma. N Engl J Med. 2018;379(4):341-51.

148. Shi Y, Su H, Song Y, Jiang W, Sun X, Qian W, et al. Safety and activity of sintilimab in patients with relapsed or refractory classical Hodgkin lymphoma (ORIENT-1): a multicentre, single-arm, phase 2 trial. Lancet Haematol. 2019;6(1):e12-e9.

149. Chang SS. Re: Efficacy and Safety of Durvalumab in Locally Advanced or Metastatic Urothelial Carcinoma: Updated Results from a Phase 1/2 Open-Label Study. J Urol. 2018;199(5):1110-2.

150. Joseph J, Zobniw C, Davis J, Anderson J, Trinh VA. Avelumab: A Review of Its Application in Metastatic Merkel Cell Carcinoma. Ann Pharmacother. 2018;52(9):928-35.

151. Joshi NS, Cui W, Chandele A, Lee HK, Urso DR, Hagman J, et al. Inflammation directs memory precursor and short-lived effector CD8(+) T cell fates via the graded expression of T-bet transcription factor. Immunity. 2007;27(2):281-95.

152. Kaech SM, Wherry EJ, Ahmed R. Effector and memory T-cell differentiation: implications for vaccine development. Nat Rev Immunol. 2002;2(4):251-62.

153. Wherry EJ, Kurachi M. Molecular and cellular insights into T cell exhaustion. Nature Reviews Immunology. 2015;15:486-99.

154. Overcoming T cell exhaustion in infection and cancer, (2015).

155. Utzschneider DT, Legat A, Fuertes Marraco SA, Carrie L, Luescher I, Speiser DE, et al. T cells maintain an exhausted phenotype after antigen withdrawal and population reexpansion. Nat Immunol. 2013;14(6):603-10.

156. Paley MA, Kroy DC, Odorizzi PM, Johnnidis JB, Dolfi DV, Barnett BE, et al. Progenitor and terminal subsets of CD8+ T cells cooperate to contain chronic viral infection. Science. 2012;338:1220-5.

157. Im SJ, Hashimoto M, Gerner MY, Lee J, Kissick HT, Burger MC, et al. Defining CD8(+) T cells that provide the proliferative burst after PD-1 therapy. Nature. 2016;537:417-21.

158. Siddiqui I, Schaeuble K, Chennupati V, Fuertes Marraco SA, Calderon-Copete S, Pais Ferreira D, et al. Intratumoral Tcf1(+)PD-1(+)CD8(+) T Cells with Stem-like Properties Promote Tumor Control in Response to Vaccination and Checkpoint Blockade Immunotherapy. Immunity. 2019;50(1):195-211 e10.

159. Miller BC, Sen DR, Al Abosy R, Bi K, Virkud YV, LaFleur MW, et al. Subsets of exhausted CD8(+) T cells differentially mediate tumor control and respond to checkpoint blockade. Nat Immunol. 2019;20(3):326-36.

160. Wu TD, Madireddi S, de Almeida PE, Banchereau R, Chen YJ, Chitre AS, et al. Peripheral T cell expansion predicts tumour infiltration and clinical response. Nature. 2020;579(7798):274-8.

161. Chow MT, Ozga AJ, Servis RL, Frederick DT, Lo JA, Fisher DE, et al. Intratumoral Activity of the CXCR3 Chemokine System Is Required for the Efficacy of Anti-PD-1 Therapy. Immunity. 2019;50(6):1498-512 e5.

162. Garris CS, Arlauckas SP, Kohler RH, Trefny MP, Garren S, Piot C, et al. Successful Anti-PD-1 Cancer Immunotherapy Requires T Cell-Dendritic Cell Crosstalk Involving the Cytokines IFN-gamma and IL-12. Immunity. 2018;49(6):1148-61 e7.

163. Silva JP, Vetterlein O, Jose J, Peters S, Kirby H. The S228P mutation prevents in vivo and in vitro IgG4 Fab-arm exchange as demonstrated using a combination of novel quantitative immunoassays and physiological matrix preparation. J Biol Chem. 2015;290(9):5462-9.

164. Isaacs JD, Wing MG, Greenwood JD, Hazleman BL, Hale G, Waldmann H. A therapeutic human IgG4 monoclonal antibody that depletes target cells in humans. Clin Exp Immunol. 1996;106(3):427-33.

165. Zhang T, Song X, Xu L, Ma J, Zhang Y, Gong W, et al. The binding of an anti-PD-1 antibody to FcgammaRIota has a profound impact on its biological functions. Cancer Immunol Immunother. 2018;67(7):1079-90.

166. Lee A, Keam SJ. Tislelizumab: First Approval. Drugs. 2020;80(6):617-24.

167. Schlothauer T, Herter S, Koller CF, Grau-Richards S, Steinhart V, Spick C, et al. Novel human IgG1 and IgG4 Fc-engineered antibodies with completely abolished immune effector functions. Protein Eng Des Sel. 2016;29(10):457-66.

168. Lo Russo G, Moro M, Sommariva M, Cancila V, Boeri M, Centonze G, et al. Antibody-Fc/FcR Interaction on Macrophages as a Mechanism for Hyperprogressive Disease in Non-small Cell Lung Cancer Subsequent to PD-1/PD-L1 Blockade. Clin Cancer Res. 2019;25(3):989-99.

169. Adashek JJ, Subbiah IM, Matos I, Garralda E, Menta AK, Ganeshan DM, et al. Hyperprogression and Immunotherapy: Fact, Fiction, or Alternative Fact? Trends Cancer. 2020;6(3):181-91.

170. Kamada T, Togashi Y, Tay C, Ha D, Sasaki A, Nakamura Y, et al. PD-1(+) regulatory T cells amplified by PD-1 blockade promote hyperprogression of cancer. Proc Natl Acad Sci U S A. 2019;116(20):9999-10008.

171. Boyerinas B, Jochems C, Fantini M, Heery CR, Gulley JL, Tsang KY, et al. Antibody-Dependent Cellular Cytotoxicity Activity of a Novel Anti-PD-L1 Antibody Avelumab (MSB0010718C) on Human Tumor Cells. Cancer Immunol Res. 2015;3(10):1148-57.

172. Goletz C, Lischke T, Harnack U, Schiele P, Danielczyk A, Ruhmann J, et al. Glyco-Engineered Anti-Human Programmed Death-Ligand 1 Antibody Mediates Stronger CD8 T Cell Activation Than Its Normal Glycosylated and Non-Glycosylated Counterparts. Front Immunol. 2018;9:1614.

173. Sow HS, Benonisson H, Breukel C, Visser R, Verhagen O, Bentlage AEH, et al. FcgammaR interaction is not required for effective anti-PD-L1 immunotherapy but can add additional benefit depending on the tumor model. Int J Cancer. 2019;144(2):345-54.

174. Patel SP, Kurzrock R. PD-L1 Expression as a Predictive Biomarker in Cancer Immunotherapy. Mol Cancer Ther. 2015;14(4):847-56.

175. Kleinovink JW, Marijt KA, Schoonderwoerd MJA, van Hall T, Ossendorp F, Fransen MF. PD-L1 expression on malignant cells is no prerequisite for checkpoint therapy. Oncoimmunology. 2017;6(4):e1294299.

176. Lee HH, Wang YN, Xia W, Chen CH, Rau KM, Ye L, et al. Removal of N-Linked Glycosylation Enhances PD-L1 Detection and Predicts Anti-PD-1/PD-L1 Therapeutic Efficacy. Cancer Cell. 2019;36(2):168-78 e4.

177. Snyder A, Makarov V, Merghoub T, Yuan J, Zaretsky JM, Desrichard A, et al. Genetic Basis for Clinical Response to CTLA-4 Blockade in Melanoma. N Engl J Med. 2014;371:2189-99.

178. Rizvi NA, Hellmann MD, Snyder A, Kvistborg P, Makarov V, Havel JJ, et al. Mutational landscape determines sensitivity to PD-1 blockade in non – small cell lung cancer. Sci Rep. 2015;348:124-9.

179. Le DT, Uram JN, Wang H, Bartlett BR, Kemberling H, Eyring AD, et al. PD-1 Blockade in Tumors with Mismatch-Repair Deficiency. N Engl J Med. 2015;372:2509-20.

180. Anagnostou V, Smith KN, Forde PM, Niknafs N, Bhattacharya R, White J, et al. Evolution of neoantigen landscape during immune checkpoint blockade in non-small cell lung cancer. Cancer Discov. 2017;7:264-76.

181. Fridman WH, Zitvogel L, Sautes-Fridman C, Kroemer G. The immune contexture in cancer prognosis and treatment. Nat Rev Clin Oncol. 2017;14(12):717-34.

182. Tumeh PC, Harview CL, Yearley JH, Shintaku IP, Taylor EJM, Robert L, et al. PD-1 blockade induces responses by inhibiting adaptive immune resistance. Nature. 2014;515:568-71.

183. Children's cancer statistics | Cancer Research UK 2018 [Available from: https://www.cancerresearchuk.org/health-professional/cancer-statistics/childrens-cancers.

184. Oeffinger KC, Mertens AC, Sklar CA, Kawashima T, Hudson MM, Meadows AT, et al. Chronic Health Conditions in Adult Survivors of Childhood Cancer. N Engl J Med. 2006;355:1572-82.

185. DePinho RA. The age of cancer. Nature. 2000;408:248-54.

186. Ma X, Liu Y, Liu Y, Alexandrov LB, Edmonson MN, Gawad C, et al. Pan-cancer genome and transcriptome analyses of 1,699 paediatric leukaemias and solid tumours. Nature. 2018;555:371-6.

187. Gröbner SN, Worst BC, Weischenfeldt J, Buchhalter I, Kleinheinz K, Rudneva VA, et al. The landscape of genomic alterations across childhood cancers. Nature. 2018;555:321-7.

188. Maude SL, Frey N, Shaw PA, Aplenc R, Barrett DM, Bunin NJ, et al. Chimeric Antigen Receptor T Cells for Sustained Remissions in Leukemia. N Engl J Med. 2014;371:1507-17.

189. Yu AL, Gilman AL, Ozkaynak MF, London WB, Kreissman SG, Chen HX, et al. Anti-GD2 Antibody with GM-CSF, Interleukin-2, and Isotretinoin for Neuroblastoma. N Engl J Med. 2010;363:1324-34.

190. Bouffet E, Larouche V, Campbell BB, Merico D, De Borja R, Aronson M, et al. Immune checkpoint inhibition for hypermutant glioblastoma multiforme resulting from germline biallelic mismatch repair deficiency. J Clin Oncol. 2016;34:2206-11.

191. Downing JR, Wilson RK, Zhang J, Mardis ER, Pui CH, Ding L, et al. The pediatric cancer genome project. Nat Genetics. 2012;44:619-22.

192. Alexandrov LB, Nik-Zainal S, Wedge DC, Aparicio SA, Behjati S, Biankin AV, et al. Signatures of mutational processes in human cancer. Nature. 2013;500(7463):415-21.

193. Wein L, Luen SJ, Savas P, Salgado R, Loi S. Checkpoint blockade in the treatment of breast cancer: current status and future directions. Br J Cancer. 2018;119(1):4-11.

194. Bonaventura P, Shekarian T, Alcazer V, Valladeau-Guilemond J, Valsesia-Wittmann S, Amigorena S, et al. Cold Tumors: A Therapeutic Challenge for Immunotherapy. Front Immunol. 2019;10:168.

195. Aoki T, Hino M, Koh K, Kyushiki M, Kishimoto H, Arakawa Y, et al. Low Frequency of Programmed Death Ligand 1 Expression in Pediatric Cancers. Pediatr Blood Cancer. 2016;63:1461-4.

196. Vakkila J, Jaffe R, Michelow M, Lotze MT. Pediatric cancers are infiltrated predominantly by macrophages and contain a paucity of dendritic cells: a major nosologic difference with adult tumors. Clin Cancer Res. 2006;12(7 Pt 1):2049-54.

197. Rivoltini L, Arienti F, Orazi A, Cefalo G, Gasparini M, Gambacorti-Passerini C, et al. Phenotypic and functional analysis of lymphocytes infiltrating paediatric tumours, with a characterization of the tumour phenotype. Cancer Immunol Immun. 1992;34:241-51.

198. Majzner RG, Simon JS, Grosso JF, Martinez D, Pawel BR, Santi M, et al. Assessment of programmed death-ligand 1 expression and tumor-associated immune cells in pediatric cancer tissues. Cancer. 2017;123(19):3807-15.

199. Chowdhury F, Dunn SN, Simon M, Mellows T, Ashton-Key M, Gray JC. PD-L1 and CD8+ PD1+ lymphocytes exist as targets in the pediatric tumor microenvironment for immunomodulatory therapy. Oncoimmunology. 2015;4(10):e1029701-1 - 8.

200. van Erp AEM, Versleijen-Jonkers YMH, Hillebrandt-Roeffen MHS, van Houdt L, Gorris MAJ, van Dam LS, et al. Expression and clinical association of programmed cell death-1, programmed death-ligand-1 and CD8(+) lymphocytes in primary sarcomas is subtype dependent. Oncotarget. 2017;8(41):71371-84.

201. Spurny C, Kailayangiri S, Jamitzky S, Altvater B, Wardelmann E, Dirksen U, et al. Programmed cell death ligand 1 (PD-L1) expression is not a predominant feature in Ewing sarcomas. Pediatr Blood Cancer. 2018;65:1-8.

202. Blumenthal DT, Yalon M, Vainer GW, Lossos A, Yust S, Tzach L, et al. Pembrolizumab: first experience with recurrent primary central nervous system (CNS) tumors. J Neurooncol. 2016;129:453-60.

203. Geoerger B, Kang HJ, Yalon-Oren M, Marshall LV, Vezina C, Pappo AS, et al. Phase 1/2 KEYNOTE-051 study of pembrolizumab (pembro) in pediatric patients (pts) with advanced melanoma or a PD-L1+ advanced, relapsed, or refractory solid tumor or lymphoma. J Clin Oncol. 2017;35:10525.

204. Davis KL, Fox E, Reid JM, Liu X, Minard CG, Weigel B, et al. ADVL1412: Initial results of a phase I/II study of nivolumab and ipilimumab in pediatric patients with relapsed/refractory solid tumors—A COG study. J Clin Oncol. 2017;35:10526.

205. Ansell SM, Lesokhin AM, Borrello I, Halwani A, Scott EC, Gutierrez M, et al. PD-1 Blockade with Nivolumab in Relapsed or Refractory Hodgkin's Lymphoma. N Engl J Med. 2015;372:311-9.

206. Armand P, Shipp MA, Ribrag V, Michot JM, Zinzani PL, Kuruvilla J, et al. Programmed death-1 blockade with pembrolizumab in patients with classical hodgkin lymphoma after brentuximab vedotin failure. J Clin Oncol. 2016;34:3733-9.

207. Younes A, Santoro A, Shipp M, Zinzani PL, Timmerman JM, Ansell S, et al. Nivolumab for classical Hodgkin's lymphoma after failure of both autologous stem-

cell transplantation and brentuximab vedotin: a multicentre, multicohort, single-arm phase 2 trial. Lancet Oncol. 2016;17(9):1283-94.

208. Chen R, Zinzani PL, Fanale MA, Armand P, Johnson NA, Brice P, et al. Phase II Study of the Efficacy and Safety of Pembrolizumab for Relapsed/Refractory Classic Hodgkin Lymphoma. J Clin Oncol. 2017;35(19):2125-32.

209. Roemer MG, Advani RH, Ligon AH, Natkunam Y, Redd RA, Homer H, et al. PD-L1 and PD-L2 Genetic Alterations Define Classical Hodgkin Lymphoma and Predict Outcome. J Clin Oncol. 2016;34(23):2690-7.

210. Chen BJ, Chapuy B, Ouyang J, Sun HH, Roemer MG, Xu ML, et al. PD-L1 expression is characteristic of a subset of aggressive B-cell lymphomas and virus-associated malignancies. Clin Cancer Res. 2013;19(13):3462-73.

211. Menter T, Bodmer-Haecki A, Dirnhofer S, Tzankov A. Evaluation of the diagnostic and prognostic value of PDL1 expression in Hodgkin and B-cell lymphomas. Hum Pathol. 2016;54:17-24.

212. Naumann-Bartsch N, Stachel D, Chada M, Fritscher T, Rompel O, Haller F, et al. Nivolumab As Salvage Therapy in Pediatric Patients with Relapsed and Refractory Lymphomas. Blood. 2016;128.

213. Rigaud C, Abbou S, Minard-Colin V, Geoerger B, Scoazec JY, Vassal G, et al. Efficacy of nivolumab in a patient with systemic refractory ALK+ anaplastic large cell lymphoma. Pediatr Blood Cancer. 2018;65(4).

214. Davis KL, Fox E, Merchant MS, Reid JM, Kudgus RA, Liu X, et al. Nivolumab in children and young adults with relapsed or refractory solid tumours or lymphoma (ADVL1412): a multicentre, open-label, single-arm, phase 1-2 trial. Lancet Oncol. 2020;21(4):541-50.

215. Geoerger B, Kang HJ, Yalon-Oren M, Marshall LV, Vezina C, Pappo A, et al. Pembrolizumab in paediatric patients with advanced melanoma or a PD-L1-positive, advanced, relapsed, or refractory solid tumour or lymphoma (KEYNOTE-051): interim analysis of an open-label, single-arm, phase 1-2 trial. Lancet Oncol. 2020;21(1):121-33.

216. Shlien A, Campbell BB, De Borja R, Alexandrov LB, Merico D, Wedge D, et al. Combined hereditary and somatic mutations of replication error repair genes result in rapid onset of ultra-hypermutated cancers. Nat Genetics. 2015;47:257-62.

217. McCaughan GJ, Fulham MJ, Mahar A, Soper J, Hong AM, Stalley PD, et al. Programmed cell death-1 blockade in recurrent disseminated Ewing sarcoma. J Hematol Oncol. 2016;9(1):48.

218. Dovedi SJ, Lipowska-Bhalla G, Beers SA, Cheadle EJ, Mu L, Glennie MJ, et al. Antitumor Efficacy of Radiation plus Immunotherapy Depends upon Dendritic Cell Activation of Effector CD8+ T Cells. Cancer Immunol Res. 2016;4(7):621-30.

219. Ferris RL, Lenz HJ, Trotta AM, García-Foncillas J, Schulten J, Audhuy F, et al. Rationale for combination of therapeutic antibodies targeting tumor cells and immune checkpoint receptors: Harnessing innate and adaptive immunity through IgG1 isotype immune effector stimulation. Cancer Treat Rev. 2018;63:48-60.

220. Chung HS, Higgins GR, Siegel SE, Seeger RC. Abnormalities of the immune system in children with neuroblastoma related to the neoplasm and chemotherapy. J Pediatr. 1977;90(4):548-54.

221. Mackall CL, Fleisher TA, Brown MR, Andrich MP, Chen CC, Feuerstein IM, et al. Age, thymopoiesis, and CD4+ T-lymphocyte regeneration after intensive chemotherapy. N Engl J Med. 1995;332(3):143-9.

222. Nowak AK, Lake RA, Marzo AL, Scott B, Heath WR, Collins EJ, et al. Induction of tumor cell apoptosis in vivo increases tumor antigen cross-presentation, cross-priming rather than cross-tolerizing host tumor-specific CD8 T cells. J Immunol. 2003;170(10):4905-13.

223. Galluzzi L, Buque A, Kepp O, Zitvogel L, Kroemer G. Immunogenic cell death in cancer and infectious disease. Nat Rev Immunol. 2017;17(2):97-111.

224. Rizvi NA, Hellmann MD, Brahmer JR, Juergens RA, Borghaei H, Gettinger S, et al. Nivolumab in Combination With Platinum-Based Doublet Chemotherapy for First-Line Treatment of Advanced Non-Small-Cell Lung Cancer. J Clin Oncol. 2016;34(25):2969-79.

225. Pfirschke C, Engblom C, Rickelt S, Cortez-Retamozo V, Garris C, Pucci F, et al. Immunogenic Chemotherapy Sensitizes Tumors to Checkpoint Blockade Therapy. Immunity. 2016;44:343-54.

226. Mkrtichyan M, Najjar YG, Raulfs EC, Abdalla MY, Samara R, Rotem-Yehudar R, et al. Anti-PD-1 synergizes with cyclophosphamide to induce potent anti-tumor vaccine effects through novel mechanisms. Eur J Immunol. 2011;41(10):2977-86.

227. Peng J, Hamanishi J, Matsumura N, Abiko K, Murat K, Baba T, et al. Chemotherapy Induces Programmed Cell Death-Ligand 1 Overexpression via the Nuclear Factor-kappaB to Foster an Immunosuppressive Tumor Microenvironment in Ovarian Cancer. Cancer Res. 2015;75(23):5034-45.

228. Orecchioni S, Talarico G, Labanca V, Calleri A, Mancuso P, Bertolini F. Vinorelbine, cyclophosphamide and 5-FU effects on the circulating and intratumoural landscape of immune cells improve anti-PD-L1 efficacy in preclinical models of breast cancer and lymphoma. Br J Cancer. 2018;118(10):1329-36.

229. Madondo MT, Quinn M, Plebanski M. Low dose cyclophosphamide: Mechanisms of T cell modulation. Cancer Treat Rev. 2016;42:3-9.

230. Lee DW, Kochenderfer JN, Stetler-Stevenson M, Cui YK, Delbrook C, Feldman SA, et al. T cells expressing CD19 chimeric antigen receptors for acute lymphoblastic leukaemia in children and young adults: A phase 1 dose-escalation trial. Lancet. 2015;385:517-28.

231. Siebert N, Zumpe M, Juttner M, Troschke-Meurer S, Lode HN. PD-1 blockade augments anti-neuroblastoma immune response induced by anti-GD2 antibody ch14.18/CHO. Oncoimmunology. 2017;6(10):e1343775.

232. Maris JM, Hogarty MD, Bagatell R, Cohn SL. Seminar Neuroblastoma. Lancet. 2007;369:2106-20.

233. Goto S, Umehara S, Gerbing RB, Stram DO, Brodeur GM, Seeger RC, et al. Histopathology (International Neuroblastoma Pathology Classification) and MYCN status in patients with peripheral neuroblastic tumors. Cancer. 2001;92:2699-708.

234. Brodeur GM. Neuroblastoma: Biological insights into a clinical enigma. Nat Rev Cancer. 2003;3:203-16.

235. Weiss WA, Aldape K, Mohapatra G, Feuerstein BG, Bishop JM. Targeted expression of MYCN causes neuroblastoma in transgenic mice. EMBO. 1997;16:2985-95.

236. Janoueix-Lerosey I, Lequin D, Brugieres L, Ribeiro A, de Pontual L, Combaret V, et al. Somatic and germline activating mutations of the ALK kinase receptor in neuroblastoma. Nature. 2008;455(7215):967-70.

237. Zhu S, Lee JS, Guo F, Shin J, Perez-Atayde AR, Kutok JL, et al. Activated ALK collaborates with MYCN in neuroblastoma pathogenesis. Cancer Cell. 2012;21(3):362-73.

238. Matthay KK, Maris JM, Schleiermacher G, Nakagawara A, Mackall CL, Diller L, et al. Neuroblastoma. Nat Rev Dis Primers. 2016;2:16078.

239. Pearson AD, Pinkerton CR, Lewis IJ, Imeson J, Ellershaw C, Machin D, et al. High-dose rapid and standard induction chemotherapy for patients aged over 1 year with stage 4 neuroblastoma: a randomised trial. Lancet Oncol. 2008;9(3):247-56.

240. Hellström I, Hellström K. Demonstration of cell-bound and humoral immunity against neuroblastoma cells. Proc Natl Acad Sci U S A. 1968;60:1231-8.

241. Rimoldi D, Romero P, Carrel S. The human melanoma antigen-encoding gene, MAGE-1, is expressed by other tumour cells of neuroectodermal origin such as glioblastomas and neuroblastomas. Int J Cancer. 1993;54:527-8.

242. Corrias MV, Scaruffi P, Occhino M, De Bernardi B, Tonini GP, Pistoia V. Expression of MAGE-1, MAGE-3 and MART-1 genes in neuroblastoma. Int J Cancer. 1996;69:403-7.

243. Ishida H, Matsumura T, Salgaller ML, Ohmizono Y, Kadono Y, Sawada T. MAGE-1 and MAGE-3 or-6 expression in neuroblastoma-related pediatric solid tumors. Int J Cancer. 1996;69:375-80.

244. Sarkar AK, Nuchtern JG. Lysis of MYCN-amplified neuroblastoma cells by MYCN peptide-specific cytotoxic T lymphocytes. Cancer Res. 2000;60:1908-13.

245. Huebener N, Fest S, Hilt K, Schramm A, Eggert A, Durmus T, et al. Xenogeneic immunization with human tyrosine hydroxylase DNA vaccines suppresses growth of established neuroblastoma. Mol Cancer Ther. 2009;8:2392-401.

246. Adida C, Berrebi D, Peuchmaur M, Reyes-Mugica M, Altieri DC. Anti-apoptosis gene, survivin, and prognosis of neuroblastoma. Lancet. 1998;351:882-3.

247. Coughlin CM, Fleming MD, Carroll RG, Pawel BR, Hogarty MD, Shan X, et al. Immunosurveillance and survivin-specific T-cell immunity in children with high-risk neuroblastoma. J Clin Oncol. 2006;24:5725-34.

248. Fest S, Huebener N, Bleeke M, Durmus T, Stermann A, Woehler A, et al. Survivin minigene DNA vaccination is effective against neuroblastoma. Int J Cancer. 2009;125:104-14.

249. Wolfl M, Jungbluth AA, Garrido F, Cabrera T, Meyen-Southard S, Spitz R, et al. Expression of MHC class I, MHC class II, and cancer germline antigens in neuroblastoma. Cancer Immunol Immunother. 2005;54(4):400-6.

250. Lampson LA, Fisher CA, Whelan JP. Striking paucity of HLA-A, B, C and beta 2-microglobulin on human neuroblastoma cell lines. J Immunol. 1983;130(5):2471-8.

251. Corrias MV, Occhino M, Croce M, De Ambrosis A, Pistillo MP, Bocca P, et al. Lack of HLA-class I antigens in human neuroblastoma cells: analysis of its relationship to TAP and tapasin expression. Tissue Antigens. 2001;57(2):110-7.

252. Raffaghello L, Prigione I, Airoldi I, Camoriano M, Levreri I, Gambini C, et al. Downregulation and/or Release of NKG2D Ligands as Immune Evasion Strategy of Human Neuroblastoma. Neoplasia. 2004;6:558-68.

253. Groh V, Wu J, Yee C, Spies T. Tumour-derived soluble MIC ligands impair expression of NKG2D and T-cell activation. Nature. 2002;419:734-8.

254. Zhen Z, Guo X, Liao R, Yang K, Ye L, You Z. Involvement of IL-10 and TGF-beta in HLA-E-mediated neuroblastoma migration and invasion. Oncotarget. 2016;7(28):44340-9.

255. Morandi F, Ferretti E, Castriconi R, Dondero A, Petretto A, Bottino C, et al. Soluble HLA-G dampens CD94/NKG2A expression and function and differentially modulates chemotaxis and cytokine and chemokine secretion in CD56bright and CD56dim NK cells. Blood. 2011;118(22):5840-50.

256. Katie Pearson CT, Piku Basu, Francis Mussai, Giorgia Santilli, Arturo Sala, John Anderson. Functionally active myeloid derived suppressor cells (MDSCs) are found within the blood of patients with neuroblastoma: PH013. Pediatric Blood &amp. 2012;59:1055.

257. Johnson BD, Jing W, Orentas RJ. CD25+ regulatory T cell inhibition enhances vaccine-induced immunity to neuroblastoma. J Immunother. 2007;30(2):203-14.

258. Castriconi R, Dondero A, Augugliaro R, Cantoni C, Carnemolla B, Sementa AR, et al. Identification of 4Ig-B7-H3 as a neuroblastoma-associated molecule that exerts a protective role from an NK cell-mediated lysis. Proc Natl Acad Sci U S A. 2004;101(34):12640-5.

259. Dondero A, Pastorino F, Della Chiesa M, Corrias MV, Morandi F, Pistoia V, et al. PD-L1 expression in metastatic neuroblastoma as an additional mechanism for limiting immune surveillance. Oncoimmunology. 2016;5:e1064578.

260. Airoldi I, Lualdi S, Bruno S, Raffaghello L, Occhino M, Gambini C, et al. Expression of costimulatory molecules in human neuroblastoma. Evidence that CD40+ neuroblastoma cells undergo apoptosis following interaction with CD40L. Br J Cancer. 2003;88(10):1527-36.

261. Walker SR, Redlinger RE, Jr., Barksdale EM, Jr. Neuroblastoma-induced inhibition of dendritic cell IL-12 production via abrogation of CD40 expression. J Pediatr Surg. 2005;40(1):244-9; discussion 9-50.

262. Williams EL, Dunn SN, James S, Johnson PW, Cragg MS, Glennie MJ, et al. Immunomodulatory monoclonal antibodies combined with peptide vaccination provide potent immunotherapy in an aggressive murine neuroblastoma model. Clin Cancer Res. 2013;19:3545-55.

263. Honsik CJ, Jung G, Reisfeld RA. Lymphokine-activated killer cells targeted by monoclonal antibodies to the disialogangliosides GD2 and GD3 specifically lyse human tumor cells of neuroectodermal origin. Proc Natl Acad Sci U S A. 1986;83:7893-7.

264. Modak S, Cheung N-KV. Disialoganglioside Directed Immunotherapy of Neuroblastoma. Cancer Invest. 2007;25:67-77.

265. Wu ZL, Schwartz E, Seeger R, Ladisch S. Expression of GD2 ganglioside by untreated primary human neuroblastomas. Cancer Res. 1986;46(1):440-3.

266. Mujoo K, Cheresh DA, Yang HM, Reisfeld RA. Disialoganglioside GD2 on human neuroblastoma cells: target antigen for monoclonal antibody-mediated cytolysis and suppression of tumor growth. Cancer Res. 1987;47(4):1098-104.

267. Mujoo K, Kipps TJ, Yang HM, Cheresh DA, Wargalla U, Sander DJ, et al. Functional properties and effect on growth suppression of human neuroblastoma tumors by isotype switch variants of monoclonal antiganglioside GD2 antibody 14.18. Cancer Res. 1989;49(11):2857-61.

268. Murray JL, Cunningham JE, Brewer H, Mujoo K, Zukiwski AA, Podoloff DA, et al. Phase I trial of murine monoclonal antibody 14G2a administered by prolonged intravenous infusion in patients with neuroectodermal tumors. J Clin Oncol. 1994;12(1):184-93.

269. Mueller BM, Romerdahl CA, Gillies SD, Reisfeld RA. Enhancement of antibody-dependent cytotoxicity with a chimeric anti-GD2 antibody. J Immunol. 1990;144(4):1382-6.

270. Zeng Y, Fest S, Kunert R, Katinger H, Pistoia V, Michon J, et al. Anti-neuroblastoma effect of ch14.18 antibody produced in CHO cells is mediated by NK-cells in mice. Mol Immunol. 2005;42(11):1311-9.

271. Barker E, Mueller BM, Handgretinger R, Herter M, Yu AL, Reisfeld RA. Effect of a chimeric anti-ganglioside GD2 antibody on cell-mediated lysis of human neuroblastoma cells. Cancer Res. 1991;51(1):144-9.

272. Ladenstein R, Potschger U, Valteau-Couanet D, Luksch R, Castel V, Yaniv I, et al. Interleukin 2 with anti-GD2 antibody ch14.18/CHO (dinutuximab beta) in patients with high-risk neuroblastoma (HR-NBL1/SIOPEN): a multicentre, randomised, phase 3 trial. Lancet Oncol. 2018;19(12):1617-29.

273. Sorkin LS, Otto M, Baldwin WM, 3rd, Vail E, Gillies SD, Handgretinger R, et al. Anti-GD(2) with an FC point mutation reduces complement fixation and decreases antibody-induced allodynia. Pain. 2010;149(1):135-42.

274. Diaz R, McCracken F. Premeeting briefing: Dinutuximab for treating high-risk neuroblastoma. National Institute for health and care excellence (NICE); 2015.

275. Tran HC, Wan Z, Sheard MA, Sun J, Jackson JR, Malvar J, et al. TGFbetaR1 Blockade with Galunisertib (LY2157299) Enhances Anti-Neuroblastoma Activity of the Anti-GD2 Antibody Dinutuximab (ch14.18) with Natural Killer Cells. Clin Cancer Res. 2017;23(3):804-13.

276. Kowalczyk A, Gil M, Horwacik I, Odrowaz Z, Kozbor D, Rokita H. The GD2-specific 14G2a monoclonal antibody induces apoptosis and enhances cytotoxicity of chemotherapeutic drugs in IMR-32 human neuroblastoma cells. Cancer Lett. 2009;281:171-82.

277. Faraj S, Bahri M, Fougeray S, El Roz A, Fleurence J, Veziers J, et al. Neuroblastoma chemotherapy can be augmented by immunotargeting O-acetyl-GD2 tumor-associated ganglioside. Oncoimmunology. 2017;7(1):e1373232.

278. Neal ZC, Imboden M, Rakhmilevich AL, Kim KM, Hank JA, Surfus J, et al. NXS2 murine neuroblastomas express increased levels of MHC class I antigens upon recurrence following NK-dependent immunotherapy. Cancer Immunol Immunother. 2004;53(1):41-52.

279. Zuo S, Sho M, Sawai T, Kanehiro H, Maeda K, Yoshida M, et al. Potential role of the PD-L1 expression and tumor-infiltrating lymphocytes on neuroblastoma. Pediatr Surg Int. 2020;36(2):137-43.

280. Melaiu O, Mina M, Chierici M, Boldrini R, Jurman G, Romania P, et al. PD-L1 Is a Therapeutic Target of the Bromodomain Inhibitor JQ1 and, Combined with HLA Class I, a Promising Prognostic Biomarker in Neuroblastoma. Clin Cancer Res. 2017;23(15):4462-72.

281. Boes M, Meyer-Wentrup F. TLR3 triggering regulates PD-L1 (CD274) expression in human neuroblastoma cells. Cancer Lett. 2015;361(1):49-56.

282. Srinivasan P, Wu X, Basu M, Rossi C, Sandler AD. PD-L1 checkpoint inhibition and anti-CTLA-4 whole tumor cell vaccination counter adaptive immune resistance: A mouse neuroblastoma model that mimics human disease. PLoS One. 2018;15(1):e1002497.

283. Rigo V, Emionite L, Daga A, Astigiano S, Corrias MV, Quintarelli C, et al. Combined immunotherapy with anti-PDL-1/PD-1 and anti-CD4 antibodies cures syngeneic disseminated neuroblastoma. Sci Rep. 2017;7(1):14049.

284. Mao Y, Eissler N, Blanc KL, Johnsen JI, Kogner P, Kiessling R. Targeting Suppressive Myeloid Cells Potentiates Checkpoint Inhibitors to Control Spontaneous Neuroblastoma. Clin Cancer Res. 2016;22(15):3849-59.

285. Eissler N, Mao Y, Brodin D, Reutersward P, Andersson Svahn H, Johnsen JI, et al. Regulation of myeloid cells by activated T cells determines the efficacy of PD-1 blockade. Oncoimmunology. 2016;5(12):e1232222.

286. Wang-Bishop L, Wehbe M, Shae D, James J, Hacker BC, Garland K, et al. Potent STING activation stimulates immunogenic cell death to enhance antitumor immunity in neuroblastoma. J Immunother Cancer. 2020;8(1).

287. Beauford SS, Kumari A, Garnett-Benson C. Ionizing radiation modulates the phenotype and function of human CD4+ induced regulatory T cells. BMC Immunol. 2020;21(1):18.

288. Hogquist KA, Jameson SC, Heath WR, Howard JL, Bevan MJ, Carbone FR. T cell receptor antagonist peptides induce positive selection. Cell. 1994;76(1):17-27.

289. Tomida M, Yamamoto-Yamaguchi Y, Hozumi M. Purification of a factor inducing differentiation of mouse myeloid leukemic M1 cells from conditioned medium of mouse fibroblast L929 cells. J Biol Chem. 1984;259(17):10978-82.

290. De Crescenzo G, Boucher C, Durocher Y, Jolicoeur M. Kinetic characterization by surface plasmon resonance-based biosensors: Principle and emerging trends. Cell Mol Bioeng 2008;1(4):204-15.

291. Cooper MA, Williams DH. Kinetic analysis of antibody-antigen interactions at a supported lipid monolayer. Anal Biochem. 1999;276(1):36-47.

292. Edelman GM, Cunningham BA, Gall WE, Gottlieb PD, Rutishauser U, Waxdal MJ. The covalent structure of an entire gammaG immunoglobulin molecule. Proc Natl Acad Sci U S A. 1969;63(1):78-85.

293. Zak KM, Grudnik P, Magiera K, Domling A, Dubin G, Holak TA. Structural Biology of the Immune Checkpoint Receptor PD-1 and Its Ligands PD-L1/PD-L2. Structure. 2017;25(8):1163-74.

294. Tan S, Zhang H, Chai Y, Song H, Tong Z, Wang Q, et al. An unexpected N-terminal loop in PD-1 dominates binding by nivolumab. Nat Commun. 2017;8:14369.

295. Van Wauwe JP, De Mey JR, Goossens JG. OKT3: a monoclonal anti-human T lymphocyte antibody with potent mitogenic properties. J Immunol. 1980;124(6):2708-13.

296. Leo O, Foo M, Sachs DH, Samelson LE, Bluestone JA. Identification of a monoclonal antibody specific for a murine T3 polypeptide. Proc Natl Acad Sci U S A. 1987;84(5):1374-8.

297. van Lier RA, Brouwer M, Rebel VI, van Noesel CJ, Aarden LA. Immobilized anti-CD3 monoclonal antibodies induce accessory cell-independent lymphokine production, proliferation and helper activity in human T lymphocytes. Immunology. 1989;68(1):45-50.

298. Ding L, Linsley PS, Huang LY, Germain RN, Shevach EM. IL-10 inhibits macrophage costimulatory activity by selectively inhibiting the up-regulation of B7 expression. J Immunol. 1993;151(3):1224-34.

299. Cunnick J, Kaur P, Cho Y, Groffen J, Heisterkamp N. Use of bone marrow-derived macrophages to model murine innate immune responses. J Immunol Methods. 2006;311(1-2):96-105.

300. Austyn JM, Gordon S. F4/80, a monoclonal antibody directed specifically against the mouse macrophage. Eur J Immunol. 1981;11(10):805-15.

301. Burke B, Sumner S, Maitland N, Lewis CE. Macrophages in gene therapy: cellular delivery vehicles and in vivo targets. J Leukoc Biol. 2002;72(3):417-28.

302. Gül N, Babes L, Siegmund K, Korthouwer R, Bögels M, Braster R, et al. Macrophages eliminate circulating tumor cells after monoclonal antibody therapy. J Clin Invest. 2014;124:812-23.

303. Xu D, Alegre ML, Varga SS, Rothermel AL, Collins AM, Pulito VL, et al. In vitro characterization of five humanized OKT3 effector function variant antibodies. Cell Immunol. 2000;200(1):16-26.

304. Lazar-Molnar E, Yan Q, Cao E, Ramagopal U, Nathenson SG, Almo SC. Crystal structure of the complex between programmed death-1 (PD-1) and its ligand PD-L2. Proc Natl Acad Sci U S A. 2008;105(30):10483-8.

305. Ghetie V, Popov S, Borvak J, Radu C, Matesoi D, Medesan C, et al. Increasing the serum persistence of an IgG fragment by random mutagenesis. Nat Biotechnol. 1997;15(7):637-40.

306. Dashivets T, Thomann M, Rueger P, Knaupp A, Buchner J, Schlothauer T. Multi-Angle Effector Function Analysis of Human Monoclonal IgG Glycovariants. PLoS One. 2015;10(12):e0143520.

307. Liu L, Stadheim A, Hamuro L, Pittman T, Wang W, Zha D, et al. Pharmacokinetics of IgG1 monoclonal antibodies produced in humanized Pichia pastoris with specific glycoforms: a comparative study with CHO produced materials. Biologicals. 2011;39(4):205-10.

308. Leabman MK, Meng YG, Kelley RF, DeForge LE, Cowan KJ, Iyer S. Effects of altered FcgammaR binding on antibody pharmacokinetics in cynomolgus monkeys. MAbs. 2013;5(6):896-903.

309. Arce Vargas F, Furness AJS, Solomon I, Joshi K, Mekkaoui L, Lesko MH, et al. Fc-Optimized Anti-CD25 Depletes Tumor-Infiltrating Regulatory T Cells and Synergizes with PD-1 Blockade to Eradicate Established Tumors. Immunity. 2017;46(4):577-86.

310. Romer PS, Berr S, Avota E, Na SY, Battaglia M, ten Berge I, et al. Preculture of PBMCs at high cell density increases sensitivity of T-cell responses, revealing cytokine release by CD28 superagonist TGN1412. Blood. 2011;118(26):6772-82.

311. Roghanian A, Hu G, Fraser C, Singh M, Foxall RB, Meyer MJ, et al. Cyclophosphamide Enhances Cancer Antibody Immunotherapy in the Resistant Bone Marrow Niche by Modulating Macrophage FcgammaR Expression. Cancer Immunol Res. 2019;7(11):1876-90.

312. Liu Y, Song C, Shen F, Zhang J, Song SW. IGFBP2 promotes immunosuppression associated with its mesenchymal induction and FcgammaRIIB phosphorylation in glioblastoma. PLoS One. 2019;14(9):e0222999.

313. Badovinac VP, Haring JS, Harty JT. Initial T cell receptor transgenic cell precursor frequency dictates critical aspects of the CD8(+) T cell response to infection. Immunity. 2007;26(6):827-41.

314. Zippelius A, Schreiner J, Herzig P, Muller P. Induced PD-L1 expression mediates acquired resistance to agonistic anti-CD40 treatment. Cancer Immunol Res. 2015;3(3):236-44.

315. Ngiow SF, Young A, Jacquelot N, Yamazaki T, Enot D, Zitvogel L, et al. A Threshold Level of Intratumor CD8+ T-cell PD1 Expression Dictates Therapeutic Response to Anti-PD1. Cancer Res. 2015;75(18):3800-11.

316. Hori S, Sakaguchi S. Foxp3: a critical regulator of the development and function of regulatory T cells. Microbes Infect. 2004;6(8):745-51.

317. Anderson AC, Joller N, Kuchroo VK. Lag-3, Tim-3, and TIGIT: Co-inhibitory Receptors with Specialized Functions in Immune Regulation. Immunity. 2016;44(5):989-1004.

318. Yang ZZ, Kim HJ, Villasboas JC, Chen YP, Price-Troska T, Jalali S, et al. Expression of LAG-3 defines exhaustion of intratumoral PD-1(+) T cells and correlates with poor outcome in follicular lymphoma. Oncotarget. 2017;8(37):61425-39.

319. Knudson KM, Hicks KC, Ozawa Y, Schlom J, Gameiro SR. Functional and mechanistic advantage of the use of a bifunctional anti-PD-L1/IL-15 superagonist. J Immunother Cancer. 2020;8(1).

320. Qureshi OS, Zheng Y, Nakamura K, Attridge K, Manzotti C, Schmidt EM, et al. Trans-endocytosis of CD80 and CD86: a molecular basis for the cell-extrinsic function of CTLA-4. Science. 2011;332(6029):600-3.

321. Gary R, Voelkl S, Palmisano R, Ullrich E, Bosch JJ, Mackensen A. Antigen-specific transfer of functional programmed death ligand 1 from human APCs onto CD8+ T cells via trogocytosis. J Immunol. 2012;188(2):744-52.

322. Daubeuf S, Lindorfer MA, Taylor RP, Joly E, Hudrisier D. The direction of plasma membrane exchange between lymphocytes and accessory cells by trogocytosis is influenced by the nature of the accessory cell. J Immunol. 2010;184(4):1897-908.

323. Boross P, Jansen JH, Pastula A, van der Poel CE, Leusen JH. Both activating and inhibitory Fc gamma receptors mediate rituximab-induced trogocytosis of CD20 in mice. Immunol Lett. 2012;143(1):44-52.

324. Arlauckas SP, Garris CS, Kohler RH, Kitaoka M, Cuccarese MF, Yang KS, et al. In vivo imaging reveals a tumor-associated macrophage-mediated resistance pathway in anti-PD-1 therapy. Sci Transl Med. 2017;9(389).

325. Loke P, Allison JP. PD-L1 and PD-L2 are differentially regulated by Th1 and Th2 cells. Proc Natl Acad Sci U S A. 2003;100(9):5336-41.

326. Rasmuson A, Segerstrom L, Nethander M, Finnman J, Elfman LH, Javanmardi N, et al. Tumor development, growth characteristics and spectrum of genetic aberrations in the TH-MYCN mouse model of neuroblastoma. PLoS One. 2012;7(12):e51297.

327. Juneja VR, McGuire KA, Manguso RT, LaFleur MW, Collins N, Haining WN, et al. PD-L1 on tumor cells is sufficient for immune evasion in immunogenic tumors and inhibits CD8 T cell cytotoxicity. J Exp Med. 2017;214:895-904.

328. Trefny MP, Kaiser M, Stanczak MA, Herzig P, Savic S, Wiese M, et al. PD-1(+) natural killer cells in human non-small cell lung cancer can be activated by PD-1/PD-L1 blockade. Cancer Immunol Immunother. 2020;69(8):1505-17.

329. Webb ER. Combination of immunomodulatory cyclophosphamide with anti-PD-1 monoclonal antibody therapy to improve survival in preclinical models of neuroblastoma. . University of Southampton Research Repository (ePrints Soton): University of Southampton; 2018.

330. Kuang D-M, Zhao Q, Peng C, Xu J, Zhang J-P, Wu C, et al. Activated monocytes in peritumoral stroma of hepatocellular carcinoma foster immune privilege and disease progression through PD-L1. J Exp Med. 2009;206:1327-37.

331. Lux A, Yu X, Scanlan CN, Nimmerjahn F. Impact of immune complex size and glycosylation on IgG binding to human FcgammaRs. J Immunol. 2013;190(8):4315-23.

332. Kaech SM, Cui W. Transcriptional control of effector and memory CD8+ T cell differentiation. Nat Rev Immunol. 2012;12(11):749-61.

333. Peters PJ, Borst J, Oorschot V, Fukuda M, Krahenbuhl O, Tschopp J, et al. Cytotoxic T lymphocyte granules are secretory lysosomes, containing both perforin and granzymes. J Exp Med. 1991;173(5):1099-109.

334. Jaffers GJ, Fuller TC, Cosimi AB, Russell PS, Winn HJ, Colvin RB. Monoclonal antibody therapy. Anti-idiotypic and non-anti-idiotypic antibodies to OKT3 arising despite intense immunosuppression. Transplantation. 1986;41(5):572-8.

335. Asgharzadeh S, Salo JA, Ji L, Oberthuer A, Fischer M, Berthold F, et al. Clinical significance of tumor-associated inflammatory cells in metastatic neuroblastoma. J Clin Oncol. 2012;30(28):3525-32.

336. Hartley G, Regan D, Guth A, Dow S. Regulation of PD-L1 expression on murine tumor-associated monocytes and macrophages by locally produced TNF-alpha. Cancer Immunol Immunother. 2017;66(4):523-35.

337. Hanoteau A, Henin C, Svec D, Bisilliat Donnet C, Denanglaire S, Colau D, et al. Cyclophosphamide treatment regulates the balance of functional/exhausted tumor-specific CD8(+) T cells. Oncoimmunology. 2017;6(8):e1318234.

338. Facchetti P, Prigione I, Ghiotto F, Tasso P, Garaventa A, Pistoia V. Functional and molecular characterization of tumour-infiltrating lymphocytes and clones thereof from a major-histocompatibility-complex-negative human tumour: neuroblastoma. Cancer Immunol Immunother. 1996;42(3):170-8.

339. Gershan JA, Barr KM, Weber JJ, Jing W, Johnson BD. Immune modulating effects of cyclophosphamide and treatment with tumor lysate/CpG synergize to eliminate murine neuroblastoma. J Immunother Cancer. 2015;3:24.

340. Motoyoshi Y, Kaminoda K, Saitoh O, Hamasaki K, Nakao K, Ishii N, et al. Different mechanisms for anti-tumor effects of low- and high-dose cyclophosphamide. Oncol Rep. 2006;16(1):141-6.

341. Lutsiak ME, Semnani RT, De Pascalis R, Kashmiri SV, Schlom J, Sabzevari H. Inhibition of CD4(+)25+ T regulatory cell function implicated in enhanced immune response by low-dose cyclophosphamide. Blood. 2005;105(7):2862-8.

342. Salem ML, Diaz-Montero CM, Al-Khami AA, El-Naggar SA, Naga O, Montero AJ, et al. Recovery from cyclophosphamide-induced lymphopenia results in expansion of immature dendritic cells which can mediate enhanced prime-boost vaccination antitumor responses in vivo when stimulated with the TLR3 agonist poly(I:C). J Immunol. 2009;182(4):2030-40.

343. Wareham C. Exploring the efficacy of anti-GD2 and anti-4-1BB monoclonal antibody therapy for the treatment of neuroblastoma. . University of Southampton Research Repository (ePrints Soton): University of Southampton 2014.

344. Wang W, Li J, Wu K, Azhati B, Rexiati M. Culture and Identification of Mouse Bone Marrow-Derived Dendritic Cells and Their Capability to Induce T Lymphocyte Proliferation. Med Sci Monit. 2016;22:244-50.

345. Delamarre L, Holcombe H, Mellman I. Presentation of exogenous antigens on major histocompatibility complex (MHC) class I and MHC class II molecules is differentially regulated during dendritic cell maturation. J Exp Med. 2003;198(1):111-22.

346. The prognostic influence of tumour-infiltrating lymphocytes in cancer: A systematic review with meta-analysis, (2011).

347. Voeller J, Erbe AK, Slowinski J, Rasmussen K, Carlson PM, Hoefges A, et al. Combined innate and adaptive immunotherapy overcomes resistance of immunologically cold syngeneic murine neuroblastoma to checkpoint inhibition. J Immunother Cancer. 2019;7(1):344.

348. Main EK, Lampson LA, Hart MK, Kornbluth J, Wilson DB. Human neuroblastoma cell lines are susceptible to lysis by natural killer cells but not by cytotoxic T lymphocytes. J Immunol. 1985;135(1):242-6.

349. Allen F, Bobanga ID, Rauhe P, Barkauskas D, Teich N, Tong C, et al. CCL3 augments tumor rejection and enhances CD8(+) T cell infiltration through NK and

CD103(+) dendritic cell recruitment via IFNgamma. Oncoimmunology. 2018;7(3):e1393598.

350. Ribas A, Shin DS, Zaretsky J, Frederiksen J, Cornish A, Avramis E, et al. PD-1 Blockade Expands Intratumoral Memory T Cells. Cancer Immunol Res. 2016;4:194-203.

351. Weber JS, Kudchadkar RR, Yu B, Gallenstein D, Horak CE, Inzunza HD, et al. Safety, efficacy, and biomarkers of nivolumab with vaccine in ipilimumab-refractory or -naive melanoma. J Clin Oncol. 2013;31(34):4311-8.

352. Gibney GT, Kudchadkar RR, DeConti RC, Thebeau MS, Czupryn MP, Tetteh L, et al. Safety, correlative markers, and clinical results of adjuvant nivolumab in combination with vaccine in resected high-risk metastatic melanoma. Clin Cancer Res. 2015;21(4):712-20.

353. Du B, Waxman DJ. Medium dose intermittent cyclophosphamide induces immunogenic cell death and cancer cell autonomous type I interferon production in glioma models. Cancer Lett. 2020;470:170-80.

354. Schiavoni G, Sistigu A, Valentini M, Mattei F, Sestili P, Spadaro F, et al. Cyclophosphamide synergizes with type I interferons through systemic dendritic cell reactivation and induction of immunogenic tumor apoptosis. Cancer Res. 2011;71(3):768-78.

355. Sistigu A, Yamazaki T, Vacchelli E, Chaba K, Enot DP, Adam J, et al. Cancer cell-autonomous contribution of type I interferon signaling to the efficacy of chemotherapy. Nat Med. 2014;20(11):1301-9.

356. Wendel M, Galani IE, Suri-Payer E, Cerwenka A. Natural killer cell accumulation in tumors is dependent on IFN-gamma and CXCR3 ligands. Cancer Res. 2008;68(20):8437-45.

357. Swann JB, Hayakawa Y, Zerafa N, Sheehan KC, Scott B, Schreiber RD, et al. Type I IFN contributes to NK cell homeostasis, activation, and antitumor function. J Immunol. 2007;178(12):7540-9.

358. Wang H, Hu S, Chen X, Shi H, Chen C, Sun L, et al. cGAS is essential for the antitumor effect of immune checkpoint blockade. Proc Natl Acad Sci U S A. 2017;114(7):1637-42.

359. Topalian SL, Taube JM, Anders RA, Pardoll DM. Mechanism-driven biomarkers to guide immune checkpoint blockade in cancer therapy. Nat Rev Cancer. 2016;16:275-87.

360. Brüggemann M, Williams GT, Bindon CI, Clark MR, Walker MR, Jefferis R, et al. Comparison of the effector functions of human immunoglobulins using a matched set of chimeric antibodies. J Exp Med. 1987;166:1351-61.

361. Martinez-Usatorre A, Donda A, Zehn D, Romero P. PD-1 Blockade Unleashes Effector Potential of Both High- and Low-Affinity Tumor-Infiltrating T Cells. J Immunol. 2018;201(2):792-803.

362. Francisco LM, Salinas VH, Brown KE, Vanguri VK, Freeman GJ, Kuchroo VK, et al. PD-L1 regulates the development, maintenance, and function of induced regulatory T cells. J Exp Med. 2009;206(13):3015-29.

363. Park HJ, Park JS, Jeong YH, Son J, Ban YH, Lee BH, et al. PD-1 upregulated on regulatory T cells during chronic virus infection enhances the suppression of CD8+

T cell immune response via the interaction with PD-L1 expressed on CD8+ T cells. J Immunol. 2015;194(12):5801-11.

364. Beum PV, Kennedy AD, Williams ME, Lindorfer MA, Taylor RP. The shaving reaction: rituximab/CD20 complexes are removed from mantle cell lymphoma and chronic lymphocytic leukemia cells by THP-1 monocytes. J Immunol. 2006;176(4):2600-9.

365. Beers SA, French RR, Chan HT, Lim SH, Jarrett TC, Vidal RM, et al. Antigenic modulation limits the efficacy of anti-CD20 antibodies: implications for antibody selection. Blood. 2010;115(25):5191-201.

366. Liao-Chan S, Daine-Matsuoka B, Heald N, Wong T, Lin T, Cai AG, et al. Quantitative assessment of antibody internalization with novel monoclonal antibodies against Alexa fluorophores. PLoS One. 2015;10(4):e0124708.

367. Dahal LN, Huang CY, Stopforth RJ, Mead A, Chan K, Bowater JX, et al. Shaving Is an Epiphenomenon of Type I and II Anti-CD20-Mediated Phagocytosis, whereas Antigenic Modulation Limits Type I Monoclonal Antibody Efficacy. J Immunol. 2018;201(4):1211-21.

368. Biewenga J, van der Ende MB, Krist LF, Borst A, Ghufron M, van Rooijen N. Macrophage depletion in the rat after intraperitoneal administration of liposome-encapsulated clodronate: depletion kinetics and accelerated repopulation of peritoneal and omental macrophages by administration of Freund's adjuvant. Cell Tissue Res. 1995;280(1):189-96.